

High Voltage Overhead
Transmission Line
Electromagnetics
Volume I

Copyright © 2015 by Robert G. Olsen

ISBN: 978-1507848043

All rights reserved. No part of this publication may be reproduced, distributed, or transmitted in any form or by any means, including photocopying, recording, or other electronic or mechanical methods, without the prior written permission of the publisher, except in the case of brief quotations embodied in critical reviews and certain other noncommercial uses permitted by copyright law. For permission requests, write to the publisher, addressed “Attention: Permissions Coordinator,” at the address below.

Robert G. Olsen, Professor of Electrical Engineering
School of Electrical Engineering and Computer Science
Washington State University, Pullman, WA 99164-2753

Quantity sales. Special discounts are available on quantity purchases by corporations, associations, and others. For details, contact the publisher at the address above.

Printed in the United States of America

Preface

Most books written for students in the area of power engineering emphasize either the physics or design of energy conversion machines, the operation of the power system or (more recently) power electronics. In each of these cases, the transmission and distribution system is either neglected or treated relatively simply (e.g., as an inductor in a one line representation of a balanced system). Some books do discuss the transmission and distribution system more carefully, such as the Westinghouse Transmission and Distribution Book, The EPRI AC Transmission Line Reference Book – 200 kV and Above, and the Southwire Overhead Conductor Manual. These are now difficult to find or are priced out of the range of students. There does not appear to be a manuscript that summarizes what we know about the electromagnetics of the transmission and distribution system. This text is designed to fill that void.

One text that did inspire this one is entitled, “Transmission and Distribution of Electrical Energy” authored by the late Walter L. Weeks of Purdue University. Unfortunately, it was published in 1981, available only briefly and is now difficult to find. Since this author has not been able to find anything to replace that text, the present text will cover much of the same material, but will also extend the theory beyond what was covered by that excellent book.

There are two purposes for this manuscript. The first is to examine the electromagnetic theory behind many of the calculations relevant to the design of high voltage power lines. These include electromagnetic propagation on wires above the earth, corona onset calculations, electrostatic fields near insulators and electromagnetic induction effects between high voltage transmission lines and other systems that share the right of way. This portion of the book can be used as the basis for further research in these areas. Sections of the book that require more advanced theory are indicated by a ◀ and can be skipped by the reader who is not interested in research. Following these sections (if necessary) are short introductions that provide a summary of the ideas introduced in the more advanced section.

The second purpose is to show how the more general theory reduces to the theory commonly used by practicing engineers. Mastering this material will result in a better understanding of the limitations of the simplified theory of transmission lines that is often presented in power systems courses. As an adjunct to this, some practical aspects of designing high voltage transmission lines will be discussed. These include discussions of transmission line ampacity and sag calculations, a general approach to the selection of insulators and the physics behind switching surges and their consequences.

Given that the title has the word “overhead” in it, the book’s focus is on overhead transmission lines. Nevertheless, there are places where underground transmission lines will be mentioned to contrast them with overhead transmission lines. One example would be the significantly different capacitance per unit length that places severe limits on the length of underground (but not overhead) alternating current transmission lines.

It is assumed that the reader has had an undergraduate course in electromagnetic theory although a graduate course in electromagnetic would provide better preparation. Since some of the techniques introduced in the book use theory that is beyond that covered in an undergraduate course, there is a chapter designed to cover some of these more advanced topics as well as appendices that supplement material in the text as needed.

The fundamental approach taken here is to consider power transmission lines to be waveguides that direct energy along the wave guiding structure. This will become evident in the way that the analysis is presented here; it is valid for all frequencies from 0 (i.e., DC) to nearly optical. Although most applications for power transmission lines require an understanding of their behavior at “low frequencies,” there are some special cases for which transmission lines must be treated at high frequency. The models introduced in this text are general enough to allow the analysis of transmission lines at these higher frequencies.

Another (and very important) aspect of the approach to the book is the assumption that the ultimate measure of a theory’s usefulness is successful comparison to measurement. Theory is a very valuable tool for providing insight into the operation of electric power transmission systems and because it is generally significantly less expensive to perform calculations than to conduct an experiment. But, if there is no confidence that an experiment (that can be defined and, in principle conducted) will produce the same results as the theory predicts, the value of the theory is (at best) severely diminished and (at worst) negligible. Because of this assumption, a chapter on measurements has been written and experiments designed to validate theory are discussed.

On Notation

Explicit field points will generally be indicated by unprimed rectangular coordinates. Continuously distributed sources of electromagnetic fields will be indicated by primed rectangular coordinates. Discrete sources of electromagnetic fields will generally be indicated by numerically subscripted rectangular coordinates where “n” is the number of the source. Given these designations, a z directed line source (discrete in x and y, but continuous in z) will be indicated by the coordinates.

In the special cases for one or two sources at the same height above the earth (assumed here in the $y = 0$ plane), the heights may be indicated as (single source) and (two sources at equal heights) while the locations along the x axis are (two sources with a total separation of d).

Given that many of the operations are conducted in the spatial Fourier transform domain, the three transform domain coordinates corresponding to are x , y , and z respectively. Since many operations are carried out in the k domain, transformed variables in this domain are indicated by a “tilde” above the variable in addition to the explicit functional dependence upon ω , for example. Phasor quantities are indicated by a “hat” above the variable in addition to the explicit functional dependence upon the radian frequency, for example.

Table of Contents

◀ Topics marked with this symbol are more advanced and need not be covered by all readers

Chapter 1 – Introduction to High Voltage Electric Power Transmission

- 1.1 Wireless vs. Wired Power Transmissios (9)
- 1.2 Power Transmission Line Basics (14)
- 1.3 Complex Power Flow in simple Transmission System (25)
- 1.4 Unbalanced Single Phase Transmission Lines with Reactive Effects (37)
- 1.5 Why is Three Phase Power Used? (43)
- 1.6 On Increasing the Capacity of Power Transmission Lines (46)
- 1.7 Alternative Transmission Line Systems (49)
- 1.8 Conclusion (51)
- 1.9 Problems (52)
- 1.10 References (57)

Chapter 2 - Real High Voltage Overhead Transmission Lines and Physical Approximations Prior to Analysis

- 2.1 Introduction (59)
- 2.2 Brief Description of Real High Voltage Overhead Power Transmission Line (59)
- 2.3 Services that share the right-of-way (80)
- 2.4 Environmental issues (85)
- 2.5 Rationale for Physical Assumptions and the “Gold Standard.” (92)
- 2.6 Brief Review of Real Overhead Power Transmission Line Construction (94)
- 2.7 Summary of the Physical Approximations Generally Made Before Analysis (97)
- 2.8 Comments on the Validity of Solutions Based on Simplifying Physical Approximations (98)
- 2.9 Survey of the Techniques that Extend Solutions to More General Problems (100)
- 2.10 “Rules of Thumb” for Minimizing the Effect of Physical Approximations on Accuracy (106)
- 2.11 Problems (110)
- 2.12 References (116)

Chapter 3 - Brief Overview of Electromagnetic Field Theory

- 3.1 Maxwell's Equations (121)
- 3.2 Constitutive Relationships for Dielectric and Conducting Materials (126)
- 3.3 The Wave Equation - Frequency Domain **(129)**
- 3.4 Boundary Conditions (130)
- 3.5 Poynting's Theorem in the Frequency Domain ◀ (131)
- 3.6 The Uniqueness Theorem – Frequency Domain ◀ (133)
- 3.7 Electromagnetic Potentials ◀ (137)
- 3.8 Reciprocity Theory ◀ (142)
- 3.9 Problems (150)
- 3.10 References (152)

Chapter 4 – Propagation on an Infinitely Long Single Conductor Transmission Line above Homogeneous Earth.

- 4.1 Introduction (154)
- 4.2 Setting up an Integral Equation for Conductor Current with Series Voltage and External Field Sources ◀ (157)
- 4.3 Formal Solution to the Integral Equation for Conductor Current with Series Voltage and External Field Sources ◀ (161)
- 4.4 The Axial Electric Field of a Propagating Horizontal Current above Earth ◀ (162)
- 4.5 Exact Modal Equation and General Expression for Current ◀ (175)
- 4.6 Derivation of the low-frequency Carson approximation (181)
- 4.7 Equivalent Transmission Line Theory (190)
- 4.8 Circuit Equivalents for Short Power Lines (195)
- 4.9 Limiting Case for DC lines (197)
- 4.10 Lumped Element Devices along Lines – Line Compensation (197)
- 4.11 Problems (211)
- 4.12 References (216)

Chapter 5 – Electromagnetic Fields Surrounding an Infinitely Long Single Conductor Transmission Line above Homogeneous Earth.

- 5.1 Introduction (219)
- 5.2 Hertz Potential Coefficients Above and in the Earth ◀ (220)
- 5.3 General Expressions for the Electric and Magnetic Fields at Arbitrary Frequency ◀ (222)
- 5.4 Low Frequency Approximations for the Electric and Magnetic Fields (228)

- 5.5 Capacitance and Inductance Per Unit Length of a Conductor Over Earth (244)
- 5.6 Justification for Electrostatics (246)
- 5.7 Problems (247)
- 5.8 References (249)

Chapter 6 – Brief Overview of Numerical Techniques for Electrostatics

- 6.1 Introduction (250)
- 6.2 Analytical Solutions (253)
- 6.3 Numerical Solutions (274)
- 6.4 Problems (287)
- 6.5 References (291)

Chapter 7 – Propagation on an Infinitely Long Multiconductor Transmission Line above Homogeneous Earth.

- 7.1 The Balanced Two Wire Line – Arbitrary Frequency (293)
- 7.2 The Balanced Two Wire Line – Low Frequency (299)
- 7.3 Examples of Coupling to Multiconductor Transmission Lines (315)
- 7.4 The Unbalanced Two Wire Line – Low Frequency (344)
- 7.5 The General Multiconductor Case – Low Frequency (349)
- 7.6 Symmetrical Components (360)
- 7.7 Per-Unit Length Parameters for an “Equivalent Symmetric” Transmission Line (364)
- 7.8 Currents in the Space Domain (368)
- 7.9 The Single Line Approximation and Calculation of the Individual Currents (369)
- 7.10 Comparison of the Single Line and General methods for Calculating of Phase currents (370)
- 7.11 Extension to conductor bundles (372)
- 7.12 Problems (376)
- 7.13 References (380)

Appendix A – Wireless vs. Wired Transmission (383)

Appendix B – Round Wire Impedance (386)

Appendix C - Essentials of Complex Variable Theory (391)

Appendix D – Carson Integral and Series Derivation (404)

Index (418)

Chapter I

Introduction to High Voltage Electric Power Transmission

1.1 Wireless vs. Wired Power Transmission

Since the topic of this manuscript is power transmission “electromagnetics,” it is instructive to note that energy can be transported from one location to another using electromagnetic fields without the use of wires between the two locations. In fact, small amounts of power are routinely transferred over long distances from a transmitter to a receiver without the use of wires in all types of communication systems. The key phrase here is “small amounts” because in communication systems only a tiny fraction of the power transmitted is recovered by the receiver. This “inefficiency” is acceptable for communication systems but not acceptable for the transport of large amounts of energy. In fact, generally efficiencies on the order of 90% or better are required for systems designed to transport large amounts of energy.

It is often pointed out that Nikola Tesla pursued “wireless” power transmission in the 1890’s. While it is true that Tesla’s plans called for no human-made or installed wires to be introduced between transmitter and receiver, his proposals involved using natural conductors (i.e., the earth and/or the ionized atmosphere) that spanned the distance between the source and the load (Anderson 1992). Hence, it is not clear whether his proposals should or should not be properly referred to as “wireless.”

Recently, there has been renewed interest in wireless power transfer and a number of devices for this purpose have been introduced into the market (Karalis et. al. 2008). These systems have, however, been restricted to relatively short distances and small rates of energy transfer. A good discussion of wireless power transfer through this “magnetic resonance coupling” mechanism can be found in a paper by Cannon, Hoburg, Stancil, and Goldstein (2009). It is shown there that it is very difficult to achieve the efficiencies generally expected of high voltage overhead transmission lines (i.e., 90 – 95%) with wireless power transfer systems.

Given the waveguide approach to power transmission lines used in this text, it is perhaps useful to provide a short comparison between wireless and wired transmission of energy for long distances. Consider first, wireless power transmission. The simplest source of electromagnetic fields is an electric dipole antenna (a short element of length (h) and electric current (I)

driven by a voltage source at its center) as shown by the arrow in Figure 1.1.1. The electromagnetic fields of this dipole antenna in free space are

$$H_\phi = \frac{Ih}{4\pi} e^{-jk_0 r} \left(\frac{jk_0}{r} + \frac{1}{r^2} \right) \sin\theta \quad (1.1.1)$$

$$E_r = \frac{j\eta_0 Ih}{2\pi k_0} e^{-jk_0 r} \left(\frac{jk_0}{r^2} + \frac{1}{r^3} \right) \cos\theta \quad (1.1.2)$$

$$E_\theta = -j \frac{\eta_0 Ih}{4\pi k_0} e^{-jk_0 r} \left(-\frac{k_0^2}{r} + \frac{jk_0}{r^2} + \frac{1}{r^3} \right) \sin\theta \quad (1.1.3)$$

Where ϵ_0 and μ_0 are respectively the permittivity and permeability of free space, $k_0 = \omega\sqrt{\mu_0\epsilon_0} = 2\pi/\lambda$ where ω is the radian frequency of the source and λ is its wavelength and $\eta_0 = \sqrt{\mu_0/\epsilon_0}$ is the impedance of free space¹.

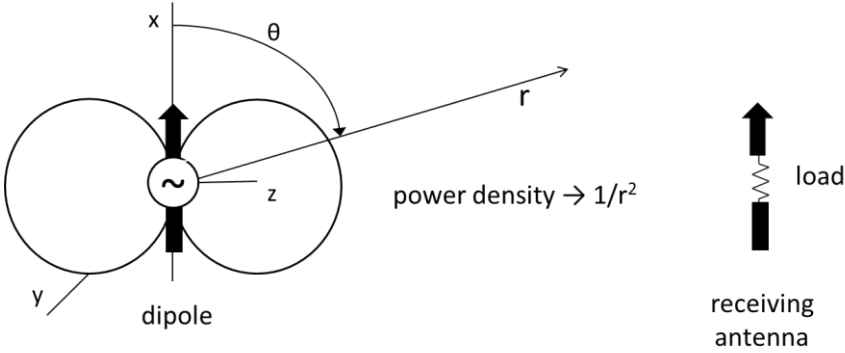


Fig. 1.1.1. Geometry for explaining energy transfer efficiency in wireless power transfer.

At a distance from the dipole large compared to the wavelength (i.e., the “far field”), these fields reduce to

$$H_\phi \cong \frac{jk_0 Ih}{4\pi r} \sin\theta e^{-jk_0 r} \quad (1.1.4)$$

$$E_\theta \cong \frac{j\eta_0 k_0 Ih}{4\pi r} \sin\theta e^{-jk_0 r} = \eta_0 H_\phi \quad (1.1.5)$$

A graphic of the field pattern from this dipole is shown in Figure 1.1.1.

To the right and left of the dipole are circles that indicate (by the distance from the center of the dipole to the far edge of the circle) the relative “far field” amplitude of the electromagnetic fields emitted in that direction (i.e.

¹ The coordinate system used here for the dipole is a bit nonstandard, but its utility will be evident later. It is oriented in the x direction and θ is defined with respect to the x axis. Further, the magnetic field (in the ϕ direction is in the yz plane with $\phi = 0$ along the y axis.

proportional to $\sin \theta$). Thus, it can be observed that a dipole generates electromagnetic “far” fields in all directions except directly above and below it and that these fields are greatest to the right and left. It turns out that since the emitted power is spread out over (almost) all space and since space is considered lossless, the power density (i.e., watts/m²) must decay inversely with the area of a sphere (i.e., $4\pi r^2$) that is centered on the dipole² in order that the total power passing through the sphere is constant. Thus, the power density in any given direction decays algebraically and is proportional to³ $1/r^2$. In some cases, “gain” can be added to these systems to enhance the amplitude of the power density in certain directions but the decay is still $1/r^2$ because the power still spreads out in all directions (albeit with a different spatial distribution). Unfortunately, at low frequencies it is very difficult (if not impossible) to achieve much gain by modifying the directivity of a source; doing this requires that the source be comparable in size to a wavelength ($\lambda = 3 \times 10^8 / f(\text{Hz})$ where f is the frequency of the source). Hence this is not an option for power transmission systems that operate at low frequencies since the wavelength at 60 Hz is 5000 km.

Now, the power emitted in a certain direction can be transferred from the electromagnetic fields to a “receiving antenna” as also shown in Fig. 1.1.1. But, the receiving antenna is roughly of the same size as the source dipole and because of the $1/r^2$ decay and the related fact that its ability to gather emitted energy is roughly limited to that which it physically intercepts, the receiving system extracts only a small fraction of the energy emitted by the source dipole⁴. More specifically for an electrically short dipole receiving antenna with an assumed uniform current distribution and oriented as shown in Fig. 1.1.1, the maximum power that can be received by a receiver that is conjugate matched to the antenna is equal to

$$P_{\max} = \frac{h^2}{4R_a} |E_{inc}|^2 \quad (1.1.6)$$

where R_a is the input resistance⁵ of the antenna (Weeks, 1968). Using the last term of (1.1.3) since it is dominant for $k_0 r \ll 1$,

$$P_{\max}^{wireless}(r) = \frac{f^2 \pi^2 10^{-14} I^2 h^4}{r^6 R_a} \quad (1.1.7)$$

² In the far field, the magnitude of the power density is equal to $E_\theta H_\phi$. More will be said about power density in Chapter 3.

³ It turns out that the power density from this dipole decays as $1/r^2$ even when the far field condition is not satisfied.

⁴ “Matching” can maximize the amount of energy retrieved, but cannot overcome the fact that the fields decay as $1/r^2$.

⁵ The resistance R_a is left unspecified here because the interest is only to compare the wireless and wired cases. More information about can be found in Weeks (1968).

since $\theta = \pi/2$ for the geometry of Fig. 1.1.1 and f is the frequency in Hz. For typical values of parameters, the power received can be shown to be very small fraction of the power emitted and not appropriate for power systems that require efficiencies as close to 100% efficient as possible.

As an aside, it is interesting to note that a method for (reasonably efficient) wireless energy transport at high frequency has been proposed. This involves the conversion of power generated by photovoltaic cells in space to microwave frequencies for transmission to the earth (Flournoy 2011). One of the reasons for using microwave frequencies is that the wavelength is much smaller and hence a very narrow electromagnetic beam can be used. The fact that this beam is so narrow significantly improves the overall efficiency of the system.

There is an alternative to the wireless system shown in Fig. 1.1.1 that is “wired” and results in a much smaller loss of energy (and hence significantly greater efficiency). The idea is to use some kind of a structure (e.g., two wires near the dipole as shown in Fig. 1.1.2) that extends from the dipole to the place where the energy is transported (i.e., the receiver). If the dipole is “close” to the wires, it is capacitively coupled to the wires and it turns out that most of the energy emitted by the dipole is “captured” by the pair of wires and “guided” to the place where it will be extracted and used (Olsen and Aburwein, 1980). Such a structure is called a “waveguide” (or a transmission line) because even if the pair of wires changes direction, the energy will still follow the new direction of the wires (hence the word “waveguide”). There is no longer the $1/r^2$ attenuation because the electromagnetic fields are confined to the vicinity of the wires. However, because any material used to make the waveguide is electrically lossy (e.g., resistance in a wire) there will be attenuation that (since the loss is proportional to the incident power) corresponds to exponential decay with a decay constant α . Nevertheless, if the wires are lossless enough, then this decay can be much less than the geometric loss associated with wireless transmission and (hence) “wired” transmission is more efficient than wireless transmission. A more explicit proof of this can be found in Appendix A.

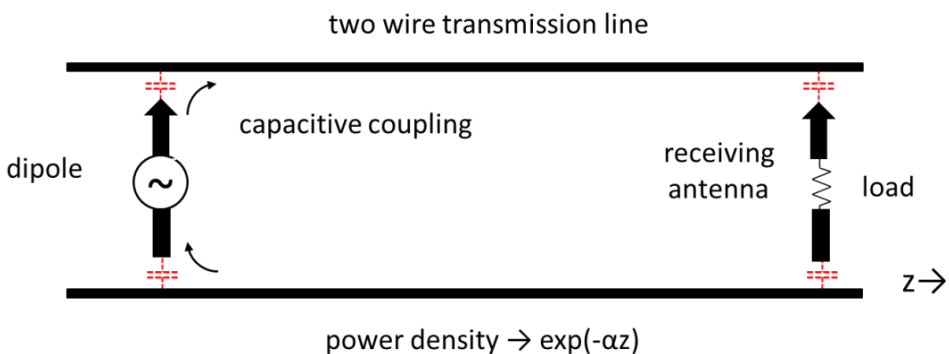


Fig. 1.1.2. Geometry for explaining energy transfer efficiency in capacitively coupled, “wired” power transfer.

Using the result from A.8 of Appendix A, the incident electric field at a distance r from the source dipole is

$$E_{inc} = \eta_0 H_{inc} = -\frac{240Ih}{d^2 \ln(d/a)} e^{-j\gamma_a r} \quad (1.1.8)$$

where d is the spacing between the wires and a is the radius of each wire. Given this result,

$$P_{max}^{wired}(r) = \frac{h^2}{4R_a} |E_{inc}|^2 = \frac{(120)^2 I^2 h^4}{d^4 \ln^2(d/a) R_a} e^{-2|\text{Im}(\gamma_a)|r} \quad (1.1.9)$$

The ratio of P_{max}^{wired} to $P_{max}^{wireless}$ is then

$$\frac{P_{max}^{wired}(r)}{P_{max}^{wireless}(r)} = \frac{(1.2)^2 10^{18} r^6}{\pi^2 f^2 d^4 \ln^2(d/a)} e^{-2|\text{Im}(\gamma_a)|r} \quad (1.1.10)$$

For realistic distances, this is generally a huge number because $2|\text{Im}(\gamma_a)|r$ is generally much less than 1 and indicates that wireless transmission at typical power transmission frequencies is just not viable.

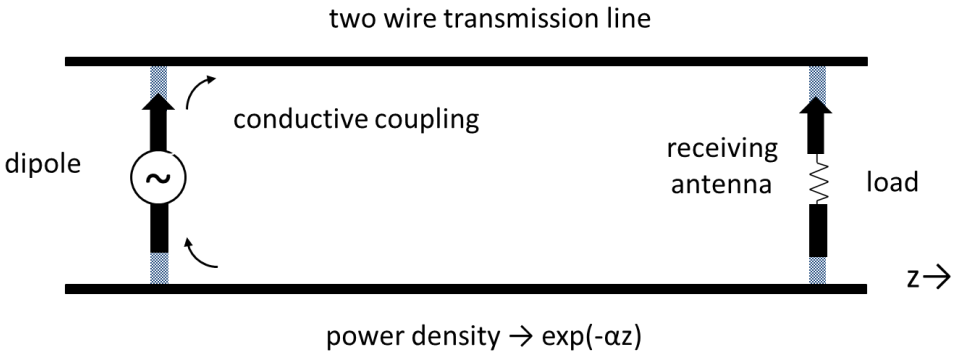


Fig. 1.1.3. Geometry for explaining energy transfer efficiency in conductively coupled, “wired” power transfer.

At low frequencies, this relatively much more efficient transmission line system is the reason why most power transmission is “wired” rather than “wireless.” Note that the system shown in Fig. 1.1.2 can be made even more efficient if the dipole and receiver are conductively coupled (i.e., “connected”) to the two wire transmission line as shown in Fig. 1.1.3. This process eliminates the relatively inefficient low frequency capacitive coupling and represents a close approximation to a simple realistic low frequency power line.

In summary, except for the microwave system discussed above, it does not appear that wireless transmission of energy will be a major competitor to power lines for efficient long distance power transfer in the foreseeable future. For this reason, emphasis will be placed on power transmission lines for the remainder of the manuscript.

1.2 Power Transmission Line Basics

Introduction

The purpose of this manuscript is to describe techniques to analyze the electromagnetic fields associated with high voltage overhead power transmission lines. As a preliminary to this exercise, an introduction is given here to simple power transmission systems and to some of the reasons why they are designed and built as they are.

The goals for the transmission system planner are to provide a reliable, efficient, safe and cost effective source of electric power with known characteristics (i.e. voltage, amplitude and waveshape) throughout the system. The system should supply sufficient electric energy to meet the needs of the public, private and commercial sectors of society and should be as environmentally benign and aesthetically pleasing as possible with minimal interaction with other legitimate systems that share the transmission line right-of-way. The integration of these goals into the design of the system will be evident in the remainder of this manuscript.

Simple transmission lines

From the time that electricity was first generated for commercial purposes, it was necessary to use it at a different location from that where it was generated. This was done by connecting wires between the generator of electricity and the device that was using the power (i.e., the load) as shown in Fig. 1.2.1. For this discussion, the load will be assumed to behave like a pure resistor; this condition will be relaxed in subsequent sections. This system is a simple representation of what is called in the power industry a “single phase” transmission line. In this system there is a single voltage source which generates a waveform that is sinusoidal in shape with a given “single” phase angle; hence the name “single phase.” This characteristic distinguishes this transmission line from the more complicated multiphase systems (e.g., three phase transmission lines) that will be discussed later in this chapter and which contain at least two sinusoidal voltage sources with distinct phase angles.

The behavior of the transmission system depends not only on the characteristics of the conductors, but on the nature of the generator and load as well. More specifically, one important characteristic of the generator is its

voltage ($v_g(t)$) that can (as mentioned earlier) be assumed to be sinusoidal in time and described mathematically in (1.2.1)⁶.

$$v_g(t) = V_p \cos(2\pi ft + \alpha) \quad (1.2.1)$$

Here V_p is the zero to peak amplitude in volts, f is the frequency in Hertz (Hz) and a is the phase angle in radians (e.g., one time t at which the maximum voltage occurs is $t = -a/(2\pi f)$). Note that the “direct current” case is the limiting case for which the frequency $f \rightarrow 0$ and $a = 0$ radians. A plot of a typical sinusoidal voltage is shown in Fig. 1.2.2. Here, $V_p = 1$ kilovolt (kV), the frequency (f) is 160 Hz and the phase angle (α) is $-\pi/2$ radians.

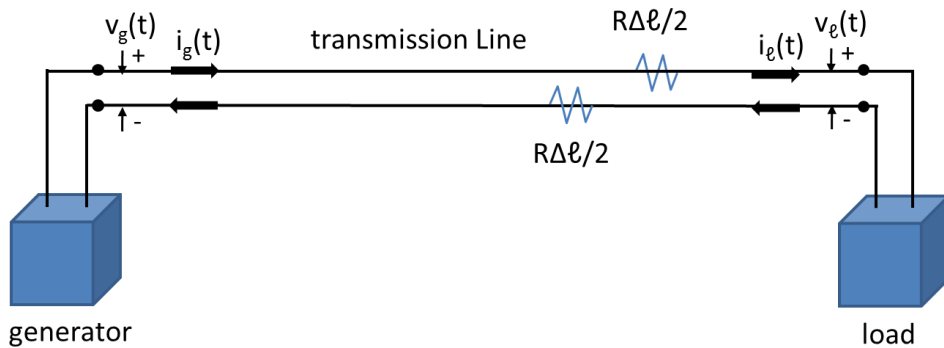


Fig. 1.2.1. Simple generator, load and transmission system.

The choice of frequency does make a difference. For example, it will be shown later that the power transfer across a short transmission line with fixed voltages at each end is inversely proportional to frequency. Thus, lower frequencies are preferred. But the use of too low a frequency causes unanticipated consequences such as flickering of lights and a requirement for more, heavy magnetic material in devices such as transformers. Through the early days of electric power systems, a variety of frequencies between $16 \frac{2}{3}$ Hz and $133 \frac{1}{3}$ Hz were used although eventually the frequency for alternating current (AC) systems (i.e., those that use sinusoidally time-varying voltages and currents) was standardized on either 50 or 60 Hz in different parts of the world (Electrical Science 2009). Direct current (DC) systems are still used in some circumstances and (as mentioned above) can be represented by (1.2.1) with $f = 0$ and $a = 0$.

⁶ A sinusoid has the property that its wave shape is unaltered if used in a power system that generally contains “reactive” elements such as lumped capacitors, lumped inductances and distributed parameter transmission lines.

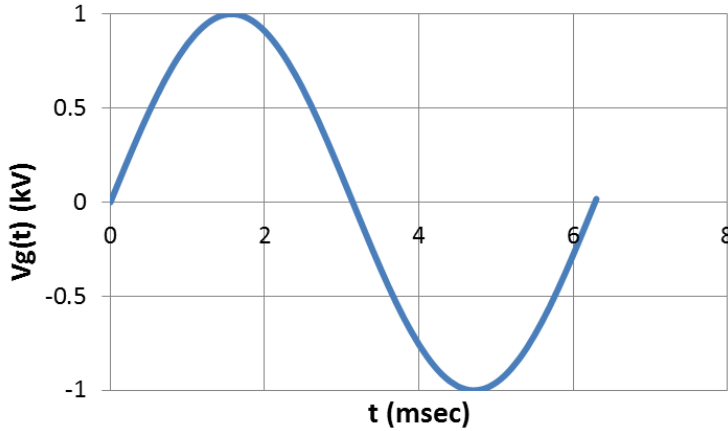


Fig. 1.2.2. Generator voltage with $V_p = 1$ kV, $f = 160$ Hz and $a = -\pi/2$

To this day, voltage levels for different parts of the power system are less standardized. In fact, significantly different voltage levels are used both in the transmission (i.e., generally higher than approximately 80 kV) and distribution (i.e., generally lower than approximately 50 kV) portions of the system in different parts of the world. Transmission lines with voltages between these two levels are often referred to as sub-transmission. For the case of sinusoidal voltages,

$$V_{rms} = \frac{V_p}{\sqrt{2}} \quad (1.2.3)$$

In most power systems analysis, the time varying voltage is represented as a “phasor” quantity with an amplitude (usually, but not always the rms voltage) and a phase expressed in degrees or radians. Such a voltage (with phase expressed in radians) is written as

$$\hat{V} = V_{rms} e^{j\alpha} \quad (1.2.4)$$

where the carat $\hat{}$ indicates a phasor quantity and α is given in radians. The phase in degrees $= 180\alpha/\pi$. A similar result can be found for sinusoidally time varying currents.

The time varying voltage can be recovered from the phasor voltage (i.e. 1.2.4) using

$$\begin{aligned} v(t) &= \sqrt{2}V_{rms} \operatorname{Re}(e^{j(2\pi ft + \alpha)}) \\ &= \sqrt{2}V_{rms} \operatorname{Re}(\cos(2\pi ft + \alpha) + j \sin(2\pi ft + \alpha)) \\ &= \sqrt{2}V_{rms} \cos(2\pi ft + \alpha) \end{aligned} \quad (1.2.5)$$

where $\text{Re}(\cdot)$ means “real part of” and Euler’s identity (i.e., $e^{ax} = \cos(ax) + j\sin(ax)$) can be used to convert the exponential to explicit sinusoidal or co-sinusoidal form. Note that the last expression in (1.2.5) is identical to (1.2.1). For completeness, the current at any point in the system can be represented as

$$i(t) = \sqrt{2}I_{\ell rms} \cos(2\pi ft + \alpha) \quad (1.2.6)$$

where I_{rms} is the rms amplitude of the current and α is the phase angle in radians⁷.

The wires in Fig. 1.2.1 are called the transmission line and the most relevant parameters here are the voltage ($v_g(t)$) between the wires at the generator, the current ($i_g(t)$) that travels from the generator down one wire through the load and returns on the other wire, the voltage ($v_\ell(t)$) between the wires at the load and the current ($i_\ell(t)$) through the “load⁸.” The resistance of each wire is $(R\Delta\ell/2)$ where $R/2$ is the resistance per unit length of each wire and $\Delta\ell$ is the length of the transmission line. Note that for this simple example, the effects of capacitance and inductance have been ignored in order that some fundamental characteristics of power transmission systems not be obfuscated by too much complexity. These will be introduced later.

The reason for the use of higher voltage levels

One of the issues that arose early in the age of electric power is that of increasing the efficiency of transmitting power from generator to load. The imperfect efficiency is primarily due to the fact that some power is lost as heat in the wires during the process of moving it from one place to another. This issue can be studied in the following way using the assumptions $V_{grms} \cong V_{\ell rms}$ (i.e., low loss) and $I_{grms} \cong I_{\ell rms}$ (i.e., capacitive effects ignored). Using the circuit in Fig. 1.2.1, the average power lost (P_{lost}) in the process of transmitting power from the generator to the load is⁹

$$P_{lost} \cong 2I_{grms}^2 R\Delta\ell/2 = \frac{2P_{gavg}^2}{V_{grms}^2} R\Delta\ell/2 \quad (1.2.7)$$

As a fraction of the transmitted power (i.e., (1.2.7) divided by P_{gavg}), the power loss can be written as

$$\frac{P_{lost}}{P_{gavg}} \cong \frac{2P_{gavg}}{V_{grms}^2} R\Delta\ell/2 \quad (1.2.8)$$

⁷ Since the load is assumed to be resistive, the phase angle of the current is the same as that of the voltage. This will not be true in general.

⁸ Since capacitive effects have been ignored, the generator current and the load current will be identical

⁹ Note that the “2” in this result is because there is loss in each of the two conductors.

Hence, for a given transmitted power (P_{avg}), the fractional power lost (i.e., P_{lost} / P_{avg}) can be reduced by either reducing the electrical resistance of the conductors or increasing the voltage between the wires. Consider first, reducing the resistance. The resistance per unit length of a wire of circular cross section at very low frequencies is

$$R / 2 = \frac{\rho}{\pi a^2} \tag{1.2.9}$$

where ρ is the resistivity of the conductor material and a is the radius of the wire. The resistivity ρ can only be changed by using a different material for the wire and (given the common materials available) cannot be changed very much. Further, if the material is changed, the goal would more likely be to reduce wire weight for mechanical reasons or cost (such as replacing copper with aluminum as has been done historically) and this might actually increase the resistivity. Increasing the radius “ a ” is possible, but there is a limit to how much this can be done because both wire weight and cost are proportional to the cross sectional area of the wire (and hence to a^2). Thus, the better of these two candidates for reducing relative losses (and hence improving efficiency) is to increase the voltage between the wires.

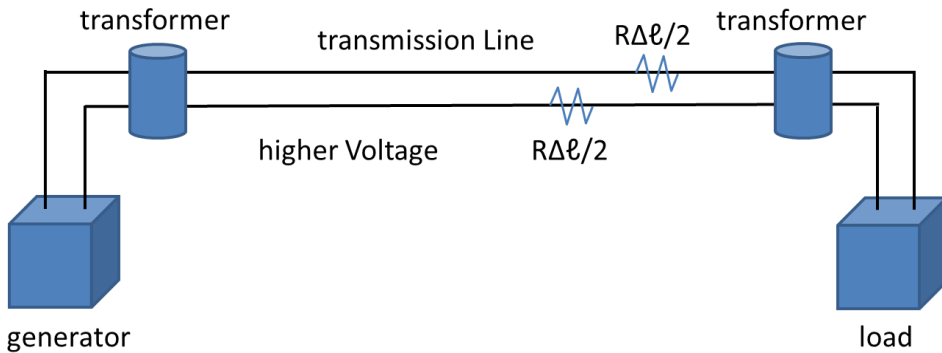


Fig. 1.2.3. The use of transformers to increase the voltage on a transmission line.

In this context, it is interesting to note that in the earliest part of the “electrical age,” there was a well-known and well publicized argument over the appropriateness of using direct current (DC) or alternating current (AC) systems for distributing electrical energy (McNichol 2006). Over time the clear winner was AC because it was much easier to change voltage levels on different parts of the system (in order to reduce losses) using transformers than with any technique that could be used for DC systems¹⁰. It should be noted that the physical basis for transformers is magnetic induction based on Faraday’s law that requires a time varying magnetic field. Hence transformers

¹⁰ At present, power electronics has made it more feasible to change voltage levels at DC.

do not work for DC systems. For an AC system, transformers are used as shown in Fig. 1.2.3¹¹.

As discussed above, these higher voltages were desirable because transmission lines operate more efficiently at higher voltages. Clearly, for a fixed power flow, the higher the voltage, the smaller the losses as a fraction of the power flow. The resulting economic benefits are clear.

As a side note (and as will be demonstrated in more detail later), it is known that the resistance of typical power line conductors increases with frequency due to the “skin effect.” This factor would tend to favor DC over AC systems. But, the reduced resistive losses for DC transmission are usually (but not always) offset by the energy lost in converting from AC to DC and vice versa unless the transmission lines are very long and the cost of these voltage conversions can be averaged over a large distance.

Also as mentioned above, it was necessary to introduce a transformer that raises the voltage to a higher level to implement these higher voltage transmission lines¹². Of course, these also introduce some losses into the system, but usually at an acceptable level. As a final note, even though higher voltages were recognized to result in more efficient transmission systems, there are upper limits to voltages used in power equipment at the generator and load due to insulation limitations and safety issues.

More realistic transmission line model

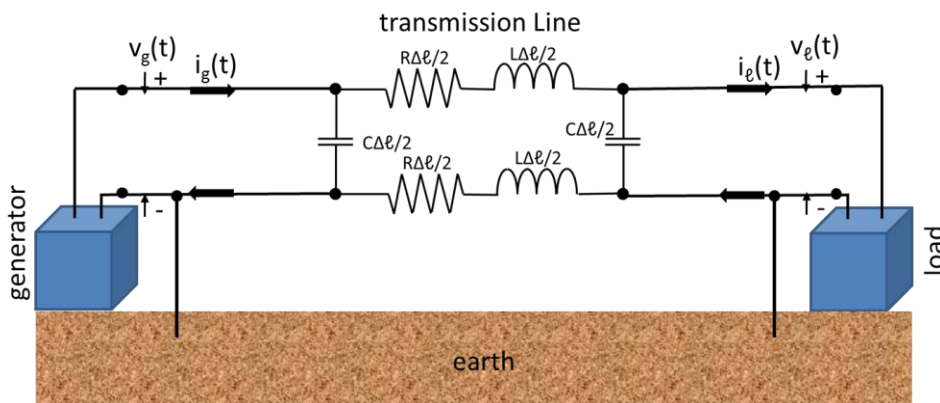


Fig. 1.2.4. A more appropriate model for an AC transmission line system

While the simple model for the transmission line used to this point (i.e., wires with resistance and a purely resistive load) is adequate for illustrating the

¹¹ Note that it is necessary to have a transformer because neither generators nor loads can operate at arbitrary large voltages. Transformers also introduce additional losses into the system and have power capacity limits.

¹² On real power systems, there are more than two voltage levels for a number of reasons. Portions of the system that operate at voltages greater than about 80,000 volts are called transmission lines while those at less than this are called distribution lines.

points that have been made, it is overly simplistic for the AC systems that are most commonly used. There are two fundamental reasons for this. First, the current at the generator will not in general be the same as the current at the load due to currents that flow through capacitance between the wires. Second, the resistance of the transmission line conductors will be augmented by a series inductive reactance that causes additional voltage drops between the two ends of the transmission line. If the transmission line is electrically short, these effects can be represented by lumped impedances as illustrated here in Fig 1.2.4. More specifically, R , C and L^{13} represent the resistance, capacitance and inductance per unit length respectively while $\Delta\ell$ is the length of the transmission line. If the transmission line is longer, then they must be treated as distributed parameters (Weeks 1981). More will be said about this topic later. Finally, the assumption made earlier that the load is purely resistive will be relaxed here. In general, it will have a resistive and a reactive part.

Fig. 1.2.4 illustrates a more reasonable lumped circuit model for the transmission line. It consists of distributed capacitance between the wires and distributed inductance along the transmission line in addition to the distributed wire resistance modelled earlier. One consequence of allowing these reactive elements in the transmission line model as well as the load is that voltages and currents, in addition to having different amplitudes throughout the system also have different phases. One specific consequence of this is that voltages across and currents through any circuit element in the system will, in general, have different amplitudes and phases. This can be illustrated in as shown in Fig. 1.2.5.

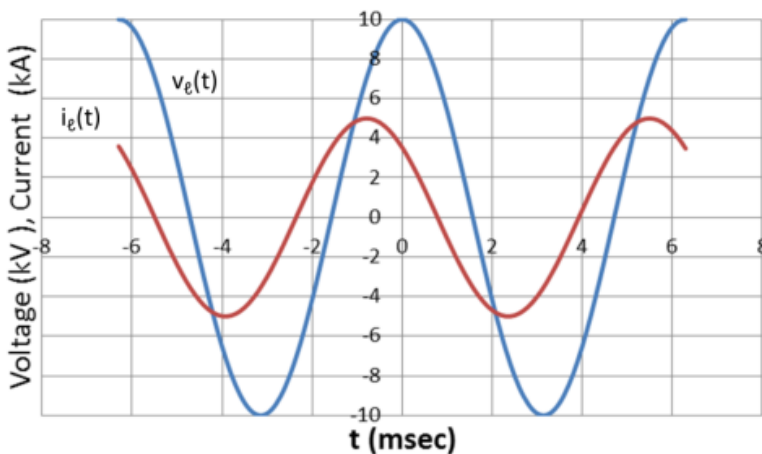


Fig. 1.2.5. Load voltage and current with peak values $V_{lp} = \sqrt{2}V_{rms} = 10$ kV and $I_{lp} = \sqrt{2}I_{rms} = 5$ kA. $f = 160$ Hz, $a = 0$ and $\theta = \pi/4$. The current “leads” the voltage by $\pi/4$ radians or 45 degrees.

¹³ These parameters combine the effects of both wires

More specifically, the sinusoidal voltage across and current through a load can be written respectively as¹⁴

$$v_\ell(t) = \sqrt{2}V_{\ell rms} \cos(2\pi ft) \quad (1.2.10)$$

and

$$i_\ell(t) = \sqrt{2}I_{\ell rms} \cos(2\pi ft + \theta) \quad (1.2.11)$$

where it has been assumed that the phase angles of the voltage and current are zero and θ radians respectively and that both are written in terms of their rms amplitudes. Note that **if the angle θ is a positive number, the current is said to “lead” the voltage** because the current peak occurs before the voltage peak as shown in Fig. 1.2.5. Similarly, **if the angle θ is a negative number, the current is said to “lag” the voltage.**

The importance of reactive elements

A cursory examination of Fig. 1.2.4 does not reveal the full significance of the inductive and capacitive elements yet. Hence, this topic will be examined here more carefully in the frequency domain.

Inductance

A “very short” transmission line is shown in Fig. 1.2.6. Typically, the capacitance can be neglected in this case since its impedance is inversely proportional to the line length $\Delta\ell$ and the inductive impedance¹⁵ is large compared to the series resistance of the transmission line connecting two voltage generators (usually called generator busses).

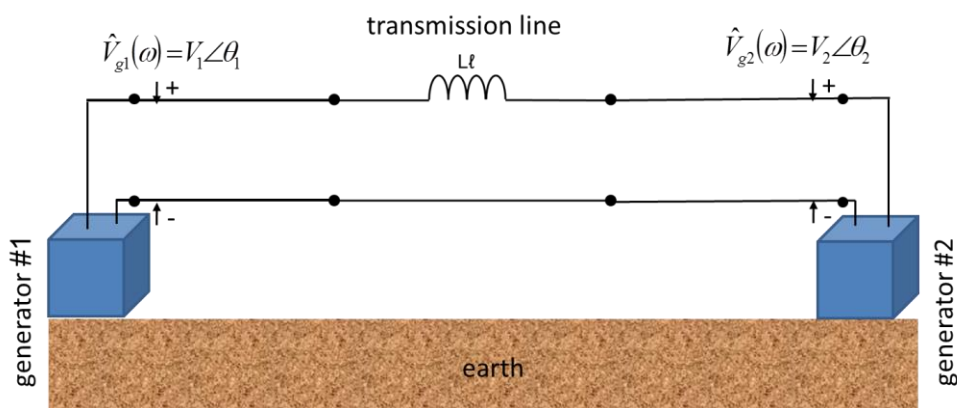


Fig. 1.2.6. Two generator busses connected by a short transmission line.

¹⁴ The phase angle of the voltage across the load end is not equal to the phase angle of the generator. Without loss of generality, α in (1.2.1) is set equal to 0 to get (1.2.10).

¹⁵ Note in this case that the inductances in both wires of the transmission line shown in Fig. 1.2.4 have been combined into one and placed into the upper wire. This will not affect the results here.

Clearly, if there is current through the transmission line, there will be a voltage drop across the transmission line. One consequence of this is that both the amplitude and phase of the generator and load voltages are different. It will be shown later that since the voltage drop is proportional to the current, the current and hence the power (since it is proportional to current) that can flow from one generator to another is limited. This is, perhaps the most significant effect of the inductive reactance. More will be said about this shortly when power flow is quantified.

Capacitance

Consider next a short “open circuited” transmission line connected to a voltage generator as shown in Fig. 1.2.7. In this case, relatively little current flows and inductive effects can be neglected. It would be tempting to simply say that the current entering this transmission line was zero because the transmission line is open circuited. But, if this assumption is made, an important characteristic of these transmission lines will be missed. It is more appropriate in this case to consider the “hidden” capacitance per unit length of the transmission line as illustrated in Fig. 1.2.8.

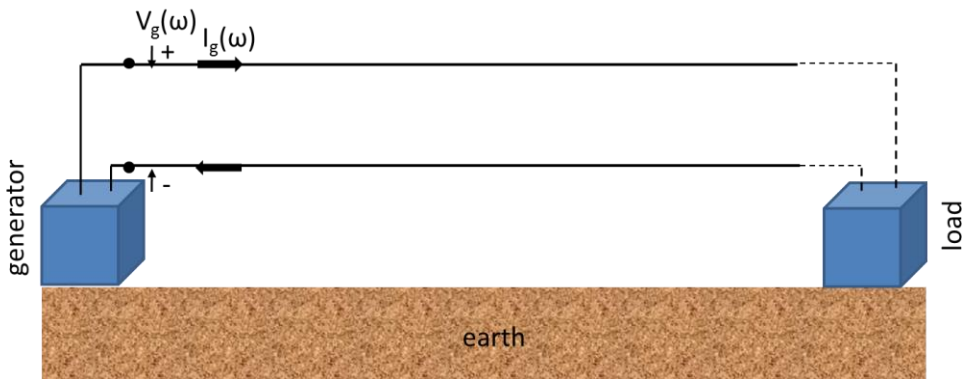


Fig. 1.2.7. A short, “open circuited” transmission line connected to a generator.

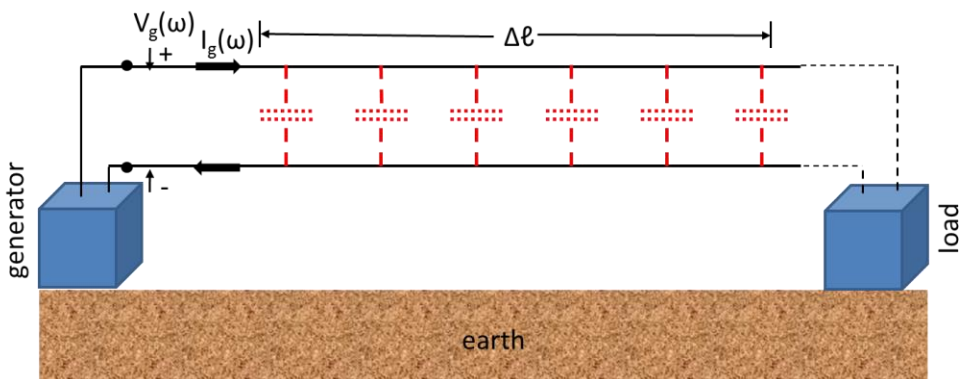


Fig. 1.2.8. A short, “open circuited” transmission line of length Δl connected to a generator with “hidden” capacitance shown.

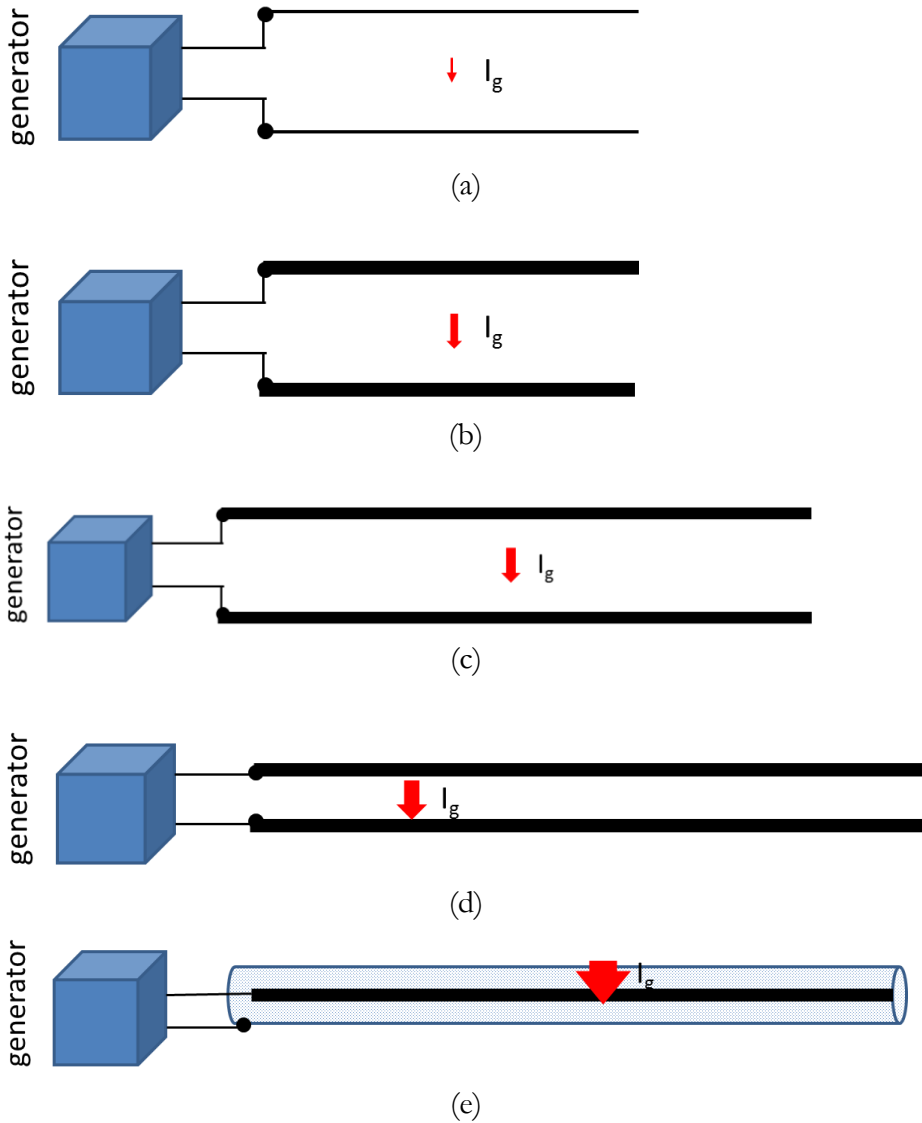


Fig. 1.2.9. Sequence of open circuited transmission lines with increasing capacitive current illustrated by the size of the red arrow a) thin widely spaced short wires, b) thick widely spaced short wires, c) thick widely spaced long wires, d) thick, closely spaced long wires, e) coaxial, closely spaced long wires with a solid dielectric.

For AC systems, the current flowing into the transmission line is

$$\hat{I}_g(\omega) = j\omega c \Delta \ell \hat{V}_g(\omega) \quad (1.2.12)$$

where c and $\Delta \ell$ are the capacitance per unit length and length of the transmission line respectively.

Now, in many cases for traditionally designed overhead transmission lines, this current is small enough to be neglected. But, the issue is important

enough in some cases that a further examination will be given here. Consider the sequence of transmission lines shown in Fig. 1.2.9. In each, the amplitude of the current that flows from line to line is indicated by the size of the red arrow.

As shown in Fig. 1.2.9a, electrically short (typically less than 100 km) traditionally designed transmission lines have very small capacitive current, but if the length is increased, the capacitive current increases as shown in Fig. 1.2.9b. If “thin” wires are replaced by thicker wires (such as conductor bundles) as shown in Fig. 1.2.9c, the capacitive current increases. Closer spacing (such as for compact lines) results in a further increase in capacitive current as illustrated in Fig. 1.2.9d. Finally, as shown in Fig. 1.2.9e, the use of a coaxial geometry with inner and outer conductors separated by a solid dielectric (such as for an underground cable) results in an even larger capacitive current.

It is illustrative to consider the capacitance per unit length of a typical underground cable used for power transmission. It would be

$$c = \frac{2\pi\epsilon_r\epsilon_0}{\ln(b/a)} \text{ F/m} \quad (1.2.13)$$

where ϵ_r is the relative dielectric constant of the dielectric insulation and a and b are the inner and outer radii of the cable respectively. For typical parameter values (i.e., $\epsilon_r = 3$, $b/a = 4$), $c \cong 0.12\mu\text{F}/\text{km}$. Using this value for the capacitance per unit length, the magnitude of the generator current is

$$|\hat{I}_g| / (|\hat{V}_g| \Delta\ell) = 2\pi f c \cong 0.045 \text{ Amps}/(\text{km} - \text{kV}) \quad (1.2.14)$$

For short, low voltage cables this current is relatively small (e.g., 4.5 A for a 10 kV, 10 km cable). However, for long, high voltage cables the current can be significant (e.g., 450 A for a 100 kV, 100 km cable). This current is comparable to the total current carried by the cables to the load. Capacitive currents this large present a serious problem for the power system in part because they result in losses even under no load conditions.

These capacitive currents and the associated losses are a significant part of the reason why it is reasonable to use short low voltage underground cables for residential distribution but not to replace long high voltage overhead transmission lines. In fact, whenever long high voltage underground cables are needed (such as for undersea applications), they are operated at DC to eliminate capacitive currents.

1.3 Complex Power Flow in Simple Transmission Systems

Introduction

Using 1.2.10 and 1.2.11, the time averaged power¹⁶ absorbed by a load is defined as

$$\begin{aligned}
 P_{\ell avg} &= \frac{1}{T} \int_0^T v_{\ell}(t) i_{\ell}(t) dt = \frac{\omega}{\pi} V_{\ell rms} I_{\ell rms} \int_0^{\frac{2\pi}{\omega}} \cos(\omega t) \cos(\omega t + \theta) dt \\
 &= \frac{\omega}{2\pi} V_{\ell rms} I_{\ell rms} \int_0^{\frac{2\pi}{\omega}} [\cos\theta + \cos(2\omega t + \theta)] dt \\
 &= \frac{\omega}{2\pi} V_{\ell rms} I_{\ell rms} \int_0^{\frac{2\pi}{\omega}} [\cos\theta(1 + \cos(2\omega t)) + \sin\theta \sin(2\omega t)] dt \\
 &= V_{\ell rms} I_{\ell rms} \cos\theta
 \end{aligned} \tag{1.3.1}$$

where $T = 2\pi/\omega$ is the period of the voltage and current.

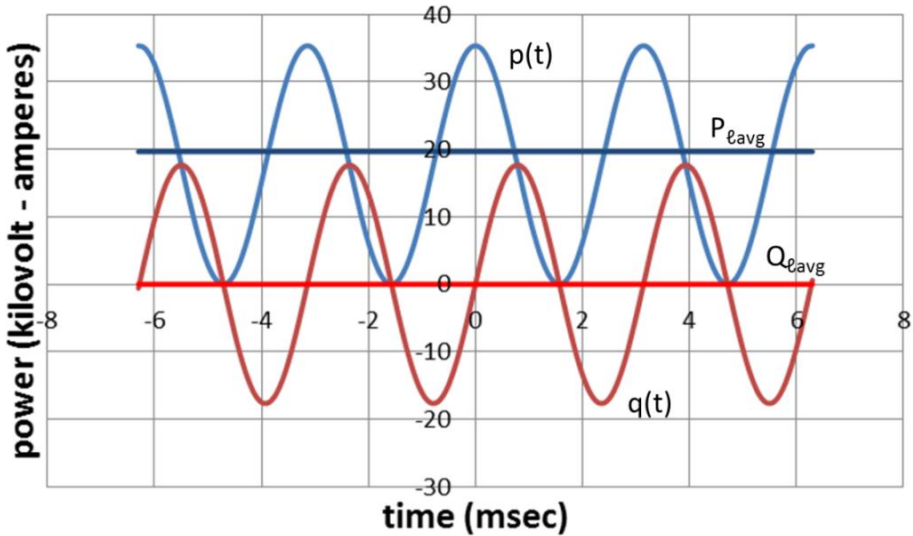


Fig. 1.3.1. Plots of $p_{\ell}(t)$ and $q_{\ell}(t)$ for the parameters of Fig. 1.2.5

Before moving on, it is instructive to plot the parameter

$$s_{\ell}(t) = p_{\ell}(t) + q_{\ell}(t) = v_{\ell}(t) i_{\ell}(t) \tag{1.3.2}$$

¹⁶ Averaged over one period of the sinusoidal waveform

for the assumed sinusoidal voltages and currents in (1.3.1).

Here, from (1.3.1)

$$p_\ell(t) = V_{\ell rms} I_{\ell rms} [\cos\theta(1 + \cos(2\omega t))] \quad (1.3.3)$$

and

$$q_\ell(t) = V_{\ell rms} I_{\ell rms} [\sin\theta \sin(2\omega t)] \quad (1.3.4)$$

$p_\ell(t)$ and $q_\ell(t)$ correspond to the first and second terms in the integrand for the last integral of (1.3.1). These two terms are plotted in Fig. 1.3.1 for the same parameters as given in Fig. 1.2.5.

It is clear that $p_\ell(t) \geq 0$ and the dark blue horizontal line in Fig. 1.3.1 corresponds to the time averaged power absorbed by the load. This term represents the time varying real power absorbed by the load with an average value of $V_{\ell rms} I_{\ell rms} \cos\theta$ as shown in the light blue line. But another important component of the power is the time varying term $q_\ell(t)$. This term is in quadrature with $p_\ell(t)$ and is alternatively positive and negative with a time average of zero. It represents energy that is alternatively being stored in and returned from the reactive (i.e., inductive and capacitive energy storing) parts of the load. While its time average is zero, it is an important component of the electrical activity within the system. For positive values of θ , its peak amplitude multiplied by the time varying term is¹⁷

$$q_\ell(t) = -Q \sin(2\omega t) \quad (1.3.5)$$

where

$$Q = -V_{\ell rms} I_{\ell rms} \sin\theta \quad (1.3.6)$$

turns out to be an important parameter for power load flow studies. Hence to fully capture the electrical response of the load in phasor analysis, it will become necessary to define “complex power” as described next and to use the imaginary part (i.e., Q) to characterize the energy storage capacity of a load.

It is very useful at this point to consider the power calculation using phasors. To this end, the phasor versions of (1.2.10) and (1.2.11) are respectively

$$\hat{V}_\ell = V_{\ell rms} \quad (1.3.7)$$

¹⁷ The minus sign is used to be consistent with the definition of Q in the phasor analysis

and

$$\hat{I}_\ell = I_{\ell rms} e^{j\theta} \quad (1.3.8)$$

If (1.3.7) is multiplied by the complex conjugate (denoted by the superscript “*”) of (1.3.8), the following result is obtained.

$$\begin{aligned} S &= P_{\ell avg} + jQ_\ell = \hat{V}_\ell \hat{I}_\ell^* = V_{\ell rms} I_{\ell rms} e^{-j\theta} \\ &= V_{\ell rms} I_{\ell rms} (\cos\theta - j \sin\theta) = |S|(\cos\theta - j \sin\theta) \end{aligned} \quad (1.3.9)$$

where S is defined as the “**complex power**” and its magnitude $|S| = V_{\ell rms} I_{\ell rms}$ is defined as the “**apparent power.**” Clearly, the real part of (1.3.9) is equal to the time averaged power absorbed by the load. Hence

$$P_{\ell avg} = \text{Re}(\hat{V}_\ell \hat{I}_\ell^*) = V_{\ell rms} I_{\ell rms} \cos\theta \quad (1.3.10)$$

But, there is additional information in (1.3.9) that will be useful for the analysis of power systems. More specifically,

$$Q_\ell = \text{Im}(\hat{V}_\ell \hat{I}_\ell^*) = -V_{\ell rms} I_{\ell rms} \sin\theta \quad (1.3.11)$$

where Q is called the “reactive power.” This is the term described above as the peak value of “out of phase power” defined in the last section.

To illustrate how this concept can be useful, consider a load that is a capacitor. In this case, for the voltage across the load given by (1.3.7), the current through the capacitor is

$$\hat{I}_\ell = j\omega CV_{\ell rms} = \omega CV_{\ell rms} e^{j\pi/2} \quad (1.3.12)$$

and the “reactive power” is

$$Q = \text{Im}(\hat{V}_\ell \hat{I}_\ell^*) = \text{Im}(\omega CV_{\ell rms}^2 (\cos(\pi/2) - j \sin(\pi/2))) = -\omega CV_{\ell rms}^2 \quad (1.3.13)$$

Since Q is a measure of the reactive power “absorbed” by the load and is a negative number, it is said that a **capacitor “supplies” reactive power to a network.** Similarly, an **inductor absorbs reactive power from a network.**

Complex power is conserved

If radiation is ignored, the sum of the complex power supplied by the independent sources (all at the same frequency) in a power network equals the sum of the complex power absorbed by all other branches of the network (Bergen, 1986). This property is a direct result of Poynting’s

theorem that will be introduced in Chapter 3. One implication of this property is that if reactive power is absorbed somewhere in the system, then it must have been generated somewhere else in the system. In some cases, reactive power is purposely generated close to where it is absorbed in order to avoid losses and voltage differences due to the flow of reactive power. This can be done by installing devices such as capacitor banks and static voltage ampere reactive (VAR) compensators.

Power factor

A final concept related to this is “power factor” which is defined as the ratio between real power and the apparent power in a circuit element.

$$\text{Power factor} = \frac{P}{V_{\text{rms}} I_{\text{rms}}} \quad (1.3.14)$$

Power factors are usually stated as “leading” or “lagging” to indicate the positive or negative sign of Q respectively (i.e., the sign of the phase angle of current with respect to voltage). A capacitor has a “leading” power factor and an inductor a “lagging” power factor.

Why introduce the concept of “complex power?”

It is, in principle, possible to solve for the currents and voltages in any power system network in the same way that circuits are analyzed in textbooks used for linear circuit analysis courses (or distributed parameter analysis if necessary). Techniques that could be used for this include mesh and nodal analysis with subsequent solution of large sets of linear equations for the currents or voltages respectively. However, quantities in a power system that are easily specified do not easily lend themselves to such analysis nor does the analysis provide as much insight as alternative techniques. More specifically, it is much more meaningful to specify complex power either supplied by a generator or absorbed by a load¹⁸ and/or phasor voltage at a generator terminal than load impedance, and source voltage or current. As a result, an alternative set of equations known as “power flow” equations are set up and solved. While these equations are more amenable to the type of data available and result in more insight, they are nonlinear equations that are (in general) solved iteratively.

¹⁸ Part of the reason that complex power is specified is that there are voltage regulators on the distribution side of the power system that adjust the transformer ratio up and down in order to keep the distribution voltage constant as the transmission bus voltage changes. Hence, as long as the number of devices connected to the power system is the same, the complex power required stays constant as the transmission bus voltage changes. Another is that the object of the system is to deliver power, hence this is the desired variable. For this reason, system planners (who use load flow studies) specify increases in required load (i.e., power) than current.

A simple example using these equations is given here. Consider the power system shown in Fig. 1.3.2 that consists of a single generator of known phasor voltage \hat{V}_g connected through a transmission line (modeled as a pi network with admittances Y_{gg} , Y_{gl} and Y_{ll}) to a load which absorbs a specified amount of power S_ℓ . The derivation begins with the writing of Kirchoff's current law at each node (usually called a bus in power engineering terminology). The results are

$$\hat{I}_g = Y_{gg} \hat{V}_g + Y_{gl} (\hat{V}_g - \hat{V}_\ell) \quad (1.3.15)$$

and

$$\hat{I}_\ell = -Y_{ll} \hat{V}_\ell - Y_{gl} (\hat{V}_g - \hat{V}_\ell) \quad (1.3.16)$$

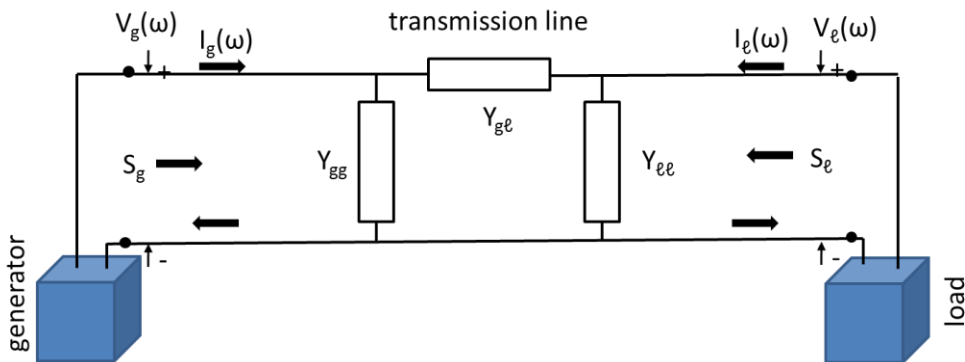


Fig. 1.3.2. Simple power system to be modeled with power flow equations.

The power supplied by the generator and by the load are respectively

$$S_g = P_g + jQ_g = \hat{V}_g \hat{I}_g^* = (Y_{gg}^* + Y_{gl}^*) |\hat{V}_g|^2 - Y_{gl}^* \hat{V}_g \hat{V}_\ell^* \quad (1.3.17)$$

and

$$S_\ell = P_\ell + jQ_\ell = \hat{V}_\ell \hat{I}_\ell^* = -(Y_{ll}^* + Y_{gl}^*) |\hat{V}_\ell|^2 + Y_{gl}^* \hat{V}_\ell \hat{V}_g^* \quad (1.3.18)$$

If it is now assumed that the generator voltage is known (and typically set to 1 for per-unit analysis) and the (complex) power (S_ℓ) “absorbed” by the load is known, then (1.3.17) and (1.3.18) form a set of nonlinear equations that can be solved for the voltage at the load ($\hat{V}_\ell(\omega)$) and the generator complex power (S_g)¹⁹. These equations are:

¹⁹ The assumption that the generator bus voltage is known but the power is not is equivalent to assuming that this generator bus is a “swing bus” (Bergen, 1986). This type of bus is required in order that the total complex power of the system be conserved.

$$S_g = P_g + jQ_g = (Y_{gg}^* + Y_{g\ell}^*) - Y_{g\ell}^* \hat{V}_\ell^*(\omega) \quad (1.3.19)$$

and

$$S_\ell = P_\ell + jQ_\ell = -\left(Y_{\ell\ell}^* + Y_{g\ell}^*\right) \left|\hat{V}_\ell(\omega)\right|^2 + Y_{g\ell}^* \hat{V}_\ell^*(\omega) \quad (1.3.20)$$

But, it should be noted that a natural consequence of using these equations is that the power is assumed complex and hence includes both real and reactive power.

Clearly, this methodology can be (and has been) extended to the case for which there are multiple generator and load busses²⁰. This extension can be found in many power system analysis texts (Bergen, 1986).

It turns out that reactive power is important for several reasons. One is that losses in the system occur whether the power transmitted is real or reactive. Since real power is the only kind that can result in real work, it is necessary to minimize reactive power in order to minimize losses. In addition, the flow of reactive power is associated with differences in voltages at different parts of the system (as will be shown here and again later in Chapter 4). Hence, minimizing reactive power flow generally results in more uniform distribution of voltage throughout the power system.

Power flow example (short transmission line- generators at each end)

Consider again the simple power system shown in Fig. 1.2.6. The power that flows from Generator 1 to Generator 2 (S_{12}) can be found using (1.3.18) with S_ℓ , V_g , V_ℓ and $Y_{g\ell}$ replaced by S_{12} , V_{g1} , V_{g2} and $j\omega L\Delta\ell$ respectively. The result is

$$P_{12} = \text{Re}(S_{12}) = \text{Re}\left(\frac{\hat{V}_{g2}(V_{g1}^* - \hat{V}_{g2}^*)}{-j\omega L\Delta\ell}\right) = \frac{|\hat{V}_{g1}||\hat{V}_{g2}|}{\omega L\Delta\ell} \sin(\theta_1 - \theta_2) \quad (1.3.21)$$

and

$$\begin{aligned} Q_{12} = \text{Im}(S_{12}) &= \text{Im}\left(\frac{\hat{V}_{g2}(V_{g1}^* - \hat{V}_{g2}^*)}{-j\omega L\Delta\ell}\right) \\ &= \frac{|\hat{V}_{g2}|}{\omega L\Delta\ell} \left(|\hat{V}_{g1}| \cos(\theta_1 - \theta_2) - |\hat{V}_{g2}|\right) \end{aligned} \quad (1.3.22)$$

In most cases the phase angles of the voltages at the two ends are not too different (i.e., $|\theta_1 - \theta_2| \ll 1$). As a result, (1.2.41) and (1.2.42) can be written

²⁰ Other generator buses have the property that real power and voltage magnitude are specified.

in a form that provides insight into the relationship between voltage and power in a power system. They are:

$$P_{12} \cong \frac{|\hat{V}_{g1}| |\hat{V}_{g2}|}{\omega L \Delta \ell} (\theta_1 - \theta_2) \quad (1.3.23)$$

and

$$Q_{12} \cong \frac{|\hat{V}_{g2}|}{\omega L \Delta \ell} (|\hat{V}_{g1}| - |\hat{V}_{g2}|) \quad (1.3.24)$$

Clearly, the flow of real power between two generator busses is related to the phase angle of the voltages at the two busses. Since there are limitations on the voltage angle difference related to system stability (to be discussed further in Chapters 4 and 8), the inductance of a short transmission line limits the amount of power that can be transferred from one end of the transmission line to the other. But, in addition, it should be clear that the flow of reactive power results in differences between the amplitudes of the two bus voltages. Because it is important to keep the voltages in a power system as uniform as possible, it is clear that attention needs to be paid to reactive power flow. **In summary, real power flow is related to differences in voltage phase angles while reactive power flow is related to differences in voltage amplitude.**

Power flow example (short transmission line – passive load)

In this section, the power flow equations given in (1.3.19) and (1.3.20) will be applied to a simple, but well-known problem in electrical engineering circuits; that of calculating the power transferred to a load from a voltage source behind fixed impedance²¹. The difference is that the terminology and approach used will be that of a load flow program. The problem is illustrated in Fig. 1.3.3. Here the generator bus has a sinusoidal voltage with fixed rms amplitude (here set equal to 1) and is connected to a very simple electrically short transmission line modelled as a series inductor. The transmission line is, in turn, connected to a load that could be considered as a simple impedance, but that is instead characterized by specified real and reactive powers rather than a specified impedance value. Hence the complex power S_ℓ in (1.3.19) becomes $P_\ell + jQ_\ell$.

²¹ If the fixed impedance is a resistor, the load is a resistor, and the goal is to determine the maximum power transferred to the load, this is the problem used to prove the maximum power transfer theorem.

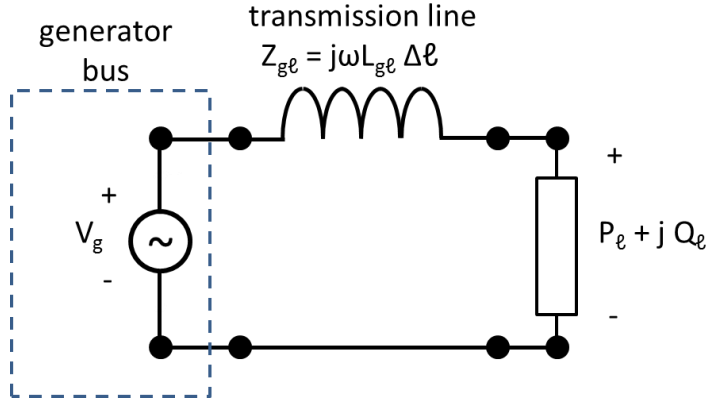


Fig. 1.3.3. Determining the power flow to an arbitrary load through a short transmission line

Using these assumptions and equating real and imaginary parts separately, the nonlinear power flow equation (1.3.20) reduces to

$$\omega L_{g\ell} \Delta \ell P_{\ell} = -\hat{V}_{\ell i} \quad (1.3.25)$$

and

$$\omega L_{g\ell} \Delta \ell Q_{\ell} + |\hat{V}_{\ell}|^2 = \hat{V}_{\ell r} \quad (1.3.26)$$

where $\hat{V}_{\ell} = V_{\ell r} + jV_{\ell i}$. If (1.3.25) and (1.3.26) are each squared and added, the result is

$$\begin{aligned} \hat{V}_{\ell r}^2 + \hat{V}_{\ell i}^2 &= |\hat{V}_{\ell}|^2 \\ &= (\omega L_{g\ell} \Delta \ell P_{\ell})^2 + |\hat{V}_{\ell}|^4 + 2\omega L_{g\ell} \Delta \ell Q_{\ell} |\hat{V}_{\ell}|^2 + (\omega L_{g\ell} \Delta \ell Q_{\ell})^2 \end{aligned} \quad (1.3.27)$$

This can be put in standard quadratic form as

$$|\hat{V}_{\ell}|^4 + (2\omega L_{g\ell} \Delta \ell Q_{\ell} - 1) |\hat{V}_{\ell}|^2 + (\omega L_{g\ell} \Delta \ell)^2 (P_{\ell}^2 + Q_{\ell}^2) \quad (1.3.28)$$

(1.3.28) can be solved using the standard quadratic formula as

$$|\hat{V}_{\ell}|^2 = \frac{1 - 2\omega L_{g\ell} \Delta \ell Q_{\ell} \pm \sqrt{1 - 4\omega L_{g\ell} \Delta \ell Q_{\ell} - 4(\omega L_{g\ell} \Delta \ell)^2 P_{\ell}^2}}{2} \quad (1.3.29)$$

This is the formula for a parabola, but this may be made more clear by considering the standard parabolic form

$$(y - y')^2 = -2p(x - x') \quad (1.3.30)$$

where the nose of the parabola is at (x', y') , the parabola opening faces toward negative x and its directrix is at $(x' - p/2)$. In this form, (1.3.28) becomes

$$\left[|\hat{V}_\ell|^2 - \frac{(1 - 2\omega L_{g\ell} \Delta \ell Q_\ell)}{2} \right]^2 = -(\omega L_{g\ell} \Delta \ell) \left[P_\ell^2 - \frac{(1 - 4\omega L_{g\ell} \Delta \ell Q_\ell)}{4(\omega L_{g\ell} \Delta \ell)^2} \right] \quad (1.3.31)$$

and the coordinates of the “nose” of the parabola (in the coordinates $(P_\ell, |\hat{V}_\ell|^2)$) are at

$$\left[\frac{(1 - 4\omega L_{g\ell} \Delta \ell Q_\ell)}{4(\omega L_{g\ell} \Delta \ell)^2}, \frac{(1 - 2\omega L_{g\ell} \Delta \ell Q_\ell)}{2} \right]. \quad (1.3.32)$$

Further, the points of intersection with the $|\hat{V}_\ell|^2$ axis (i.e. $P_\ell^2 = 0$) are

$$|\hat{V}_\ell|^2 = \frac{(1 - 2\omega L_{g\ell} \Delta \ell Q_\ell)}{2} \pm \frac{\sqrt{1 - 4\omega L_{g\ell} \Delta \ell Q_\ell}}{2} \quad (1.3.33)$$

At this point, the special case $Q_\ell = 0$ will be considered. In this case, the nose of the parabola is at

$$\left[\frac{1}{4(\omega L_{g\ell} \Delta \ell)^2}, \frac{1}{2} \right] \quad (1.3.34)$$

and the points of intersection with the $|\hat{V}_\ell|^2$ axis are $|\hat{V}_\ell|^2 = 1$ and 0. If (as is usually done) the parabola is plotted in the coordinates $(P_\ell, |\hat{V}_\ell|^2)$ (i.e., the square root of each coordinate) then it looks like shown in Fig. 1.3.4.

The first thing to notice is that the power absorbed by the load has a maximum value. This result ($P_{\ell \max} = 1/(2\omega L_{g\ell} \Delta \ell)$) is consistent with the fact that a voltage source in series with fixed impedance can only deliver a finite amount of power. Second, because (1.3.28) is nonlinear, there are in some cases (i.e., $P_\ell \leq 1/(2\omega L_{g\ell} \Delta \ell)$) multiple solutions for load voltage given load power and in other cases no solutions (i.e., $P_\ell > 1/(2\omega L_{g\ell} \Delta \ell)$). In the case for multiple solutions, the solution relevant to the problem under consideration must be selected carefully to be consistent with the physics of the problem.

Third, if it is assumed that the correct solution is the one for which the load voltage $\hat{V}_\ell = \hat{V}_g = 1$ when $P_\ell = 0$, then it is clear that as the power absorbed by the load is increased, the load voltage decreases. This is consistent with the general property that power flow in transmission systems results in (or from) differences in source and load voltage that the power system designer should control. Fourth, in this simple model, if the power demanded by the load (e.g., the load resistance is reduced below $R_\ell = \omega L_{g\ell} \Delta \ell$) is increased beyond its maximum possible value, the actual power will decrease and the solution for the voltage will revert to the lower portion of the curve. Under these conditions, the voltage can be said to “collapse” to a very small value. While the behavior of a real power system is much more complicated due to stability issues, the existence of (for example) protection systems and the fact that “voltage collapse” is not entirely well defined, situations have occurred for which the system voltage is not stable. These situations are referred to as voltage collapses and have led to widespread system blackouts.

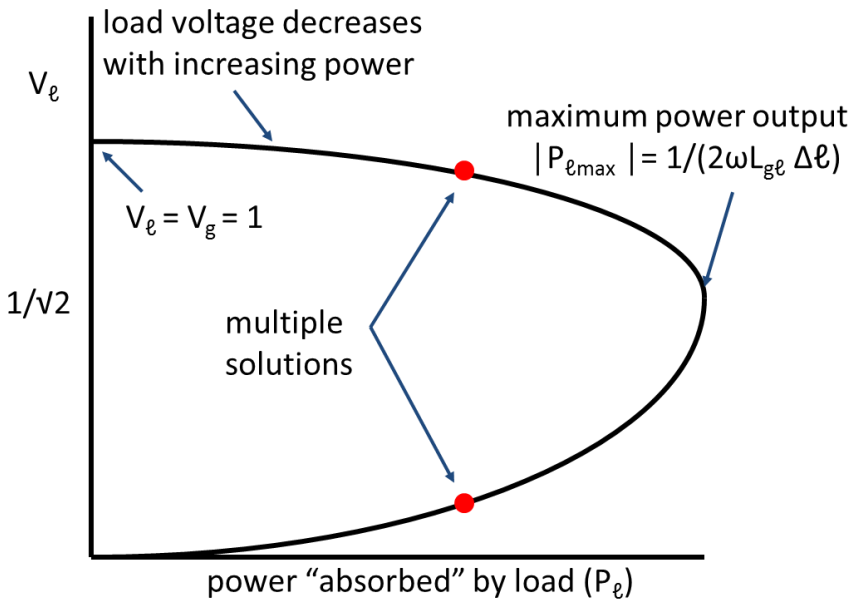


Fig. 1.3.4. Solving the load flow problem for a generator and resistive load connected by an inductive transmission line

To complete this derivation, the complex power supplied by the generator will be computed using (1.3.19) for the special case $P_{\ell \max} = 1/(2\omega L_{g\ell} \Delta \ell)$. In this case $\hat{V}_{\ell r} = -\hat{V}_{\ell i} = 1/2$ and (1.3.19) becomes

$$S_g = \frac{j}{\omega L_{g\ell} \Delta \ell} (1 - (1/2 + j/2)) = \frac{1}{2\omega L_{g\ell} \Delta \ell} (1 - j) \quad (1.3.35)$$

where the complex power absorbed by the transmission line is

$$S_{trans\ line} = Y_{g\ell} |\hat{V}_g - \hat{V}_\ell|^2 = -\frac{j}{\omega L_{g\ell} \Delta\ell} |1 - (1/2 - j/2)|^2 = -\frac{j}{2\omega L_{g\ell} \Delta\ell} \quad (1.3.36)$$

Complex power is conserved because the real plus reactive power supplied by the generator is equal to the real power absorbed by the load plus the reactive power absorbed by the transmission line.

Finally, it is worth noting that this circuit is similar to the one used in circuits courses to prove the “maximum power transfer” theorem. Conclusions should not be made about power systems based on that model because “maximum power transfer” is generally not the optimum condition for operating a power system. Rather it is more correct to either maximize the efficiency of the system which is done by minimizing the losses within the system or to achieve an acceptable degree of voltage uniformity over the system.

“Thinking” Reactive Power

To illustrate the utility of thinking in terms of complex power, the results in Fig. 1.3.4 will be extended to the case for which a portion of the load is characterized by reactive power, Q_ℓ . This may be accomplished in a variety of ways. First, it could be that the load is simply reactive. Second, it could be that either a “shunt” inductor or capacitor is placed in parallel with the load for some purpose (e.g., to cause an increase or reduction in voltage). Third, this reactance could be a model for the natural capacitance of a transmission line long enough to require parallel capacitances to appropriately model it²².

Again, the coordinates of the “nose” of the parabola in $(P_\ell, |\hat{V}_\ell|)$ coordinates are at

$$\left[\frac{\sqrt{1 - 4\omega L_{g\ell} \Delta\ell Q_\ell}}{2\omega L_{g\ell} \Delta\ell}, \frac{\sqrt{1 - 2\omega L_{g\ell} \Delta\ell Q_\ell}}{\sqrt{2}} \right] \quad (1.3.37)$$

If $4\omega L_{g\ell} \Delta\ell Q_\ell \ll 1$, then after using a one term Taylor series to expand the square roots above, these coordinates become

$$\left[\frac{1}{2\omega L_{g\ell} \Delta\ell} - Q_\ell, \frac{1}{\sqrt{2}} - \frac{\omega L_{g\ell} \Delta\ell Q_\ell}{\sqrt{2}} \right] \quad (1.3.38)$$

²² In this case, the capacitance of the transmission line on the generator end has no influence on the fixed generator voltage although reactive power must be absorbed somewhere in the system to match the amount supplied by this capacitance.

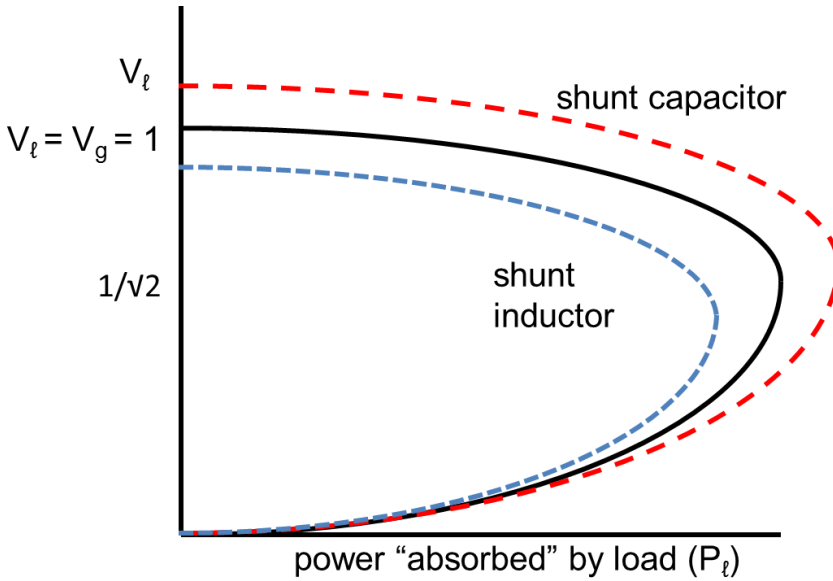


Fig. 1.3.5. Effect of injecting or absorbing reactive power at the load

If the reactive element is capacitive (i.e. $Q_\ell < 0$), then the nose of the curve is moved to the right by an amount Q_ℓ which means that more power is available at the load. This is illustrated in Fig. 1.3.5. Using the same Taylor series approximation, the points of intersection with the $|\hat{V}_\ell|$ axis (i.e. $P_\ell = 0$) are

$$|\hat{V}_\ell|^2 = 0 \quad \text{and} \quad 1 - 2\omega L_{g\ell} \Delta\ell Q_\ell \quad (1.3.39)$$

Clearly, “injecting reactive power” at the load has an impact on the voltage there. If, for example, the voltage at the load is too small, a shunt capacitor can be added to increase the voltage to a desired level. If, on the other hand, P_ℓ is small and the voltage is too high due to the capacitance of the line (i.e., the Ferranti effect), then a shunt inductor (i.e. a shunt reactor) can be added to reduce the voltage to an appropriate level. The Ferranti effect will be discussed further in Chapter 4. A photograph of a shunt reactor will be given in Chapter 2 and shunt capacitors and inductors (i.e., shunt reactors) will be analyzed in Chapter 4.

1.4 Unbalanced Single Phase Transmission Lines with Reactive Effects

Introduction

The simple transmission line models considered earlier are useful for illustrating properties of transmission lines such as the origin of transmission line losses, the reason why power systems are more efficient if they utilize higher transmission voltages and the importance of reactive elements. However, a more sophisticated model must be used to illustrate issues related to the fact that power transmission lines are operated in the presence of the earth and often have parts that are connected to earth. A model of a single phase transmission line above earth with one wire grounded is shown in Fig. 1.4.1.

In this figure, one of the wires is connected to earth at each end of the transmission line. This connection allows some of the current to flow in the earth so that in addition to unequal voltages at the ends, the wire currents will no longer generally be equal and opposite. In addition, there may be capacitances between the wires and other objects such as the earth that are not shown in the figure and that can result in further current imbalances. Finally, the circuit parameters that define the transmission line (i.e. R , L and C) are affected by the presence of the earth. This subject will be considered in Chapter 4. Details of the connections to the earth will be considered in Chapter 13.

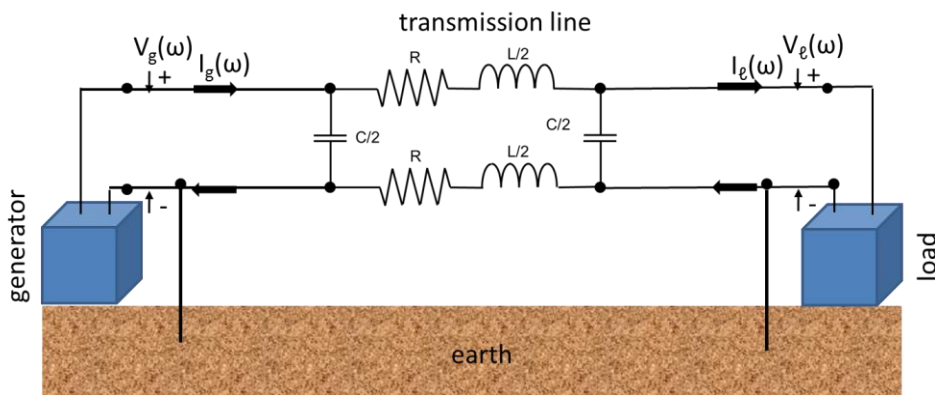


Fig. 1.4.1. Model of a short single phase power transmission line with earth connections shown

The importance of grounding

Current paths and current continuity (hidden paths)

Having observed that currents through “hidden capacitances” can be important, it is useful to consider the set of all possible paths for current. In Fig. 1.4.2, several current “paths” are indicated that may not have been

obvious initially. These include capacitive paths between conductors and between conductors and ground. In addition, current may flow from the generator and/or load to the earth. In some cases, the generator and/or load are bonded to their housing which is, in turn grounded. In others the generator and/or load are intentionally insulated from the housing and hence the ground. But, if this is the situation, there is still capacitive coupling from the generator and/or load to the housing and ground. The only difference is that the connection to ground is now of much higher impedance. In either case there are ground currents as shown in the figure.

Once all current paths have been identified “current continuity” can be invoked. This restriction is a direct result of Maxwell’s equations as will be shown in Chapter 3. As an example, the current continuity calculation must be applied to all currents flowing in and out of the generator in Fig. 1.4.2. Clearly, in this figure some current flows as displacement or ‘capacitive’ current through “hidden” circuit elements to earth or other conductors that are not explicitly part of the circuit diagram as it returns to the generator as shown. Other current may flow in the earth through either intentional or unintentional grounds.

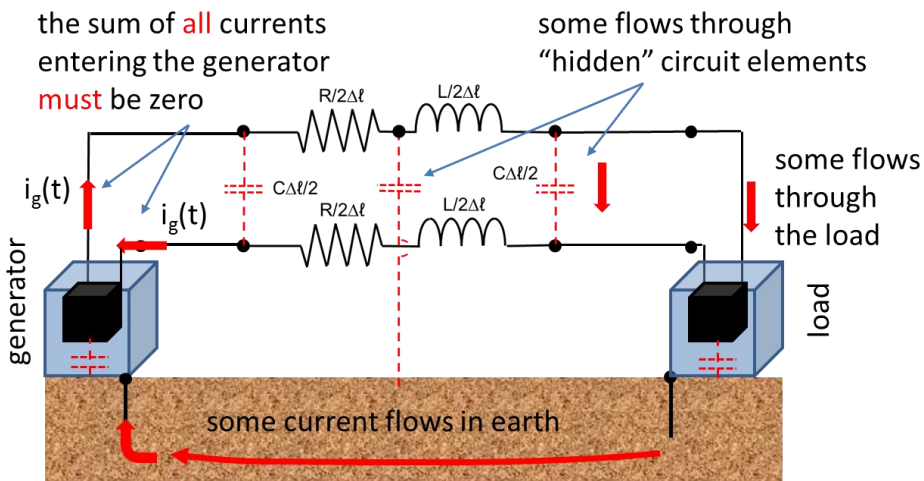


Fig. 1.4.2. Current paths and current continuity

On the definition of voltage with respect to ground (there must be a reference point)

Before moving to a consideration of grounding systems, it is useful to point out that whenever a voltage is given (especially with respect to ground), its description should include the two points between which it is defined. One should never say, “the voltage at point A is” because the reference location is then ambiguous. Rather, the voltage should be described as the “voltage between A and B” or “voltage at A with respect to B” as shown in Fig. 1.4.3. It may seem that this is not a problem, but it becomes an issue especially in describing grounding conditions as shown in Chapter 13.

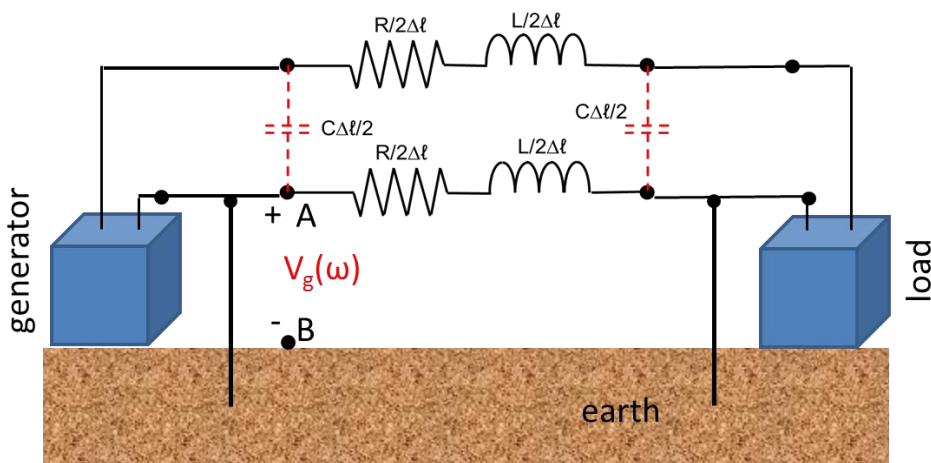


Fig. 1.4.3. Correct method for defining a voltage
Impact of imperfect ground (the earth is NOT an equipotential)

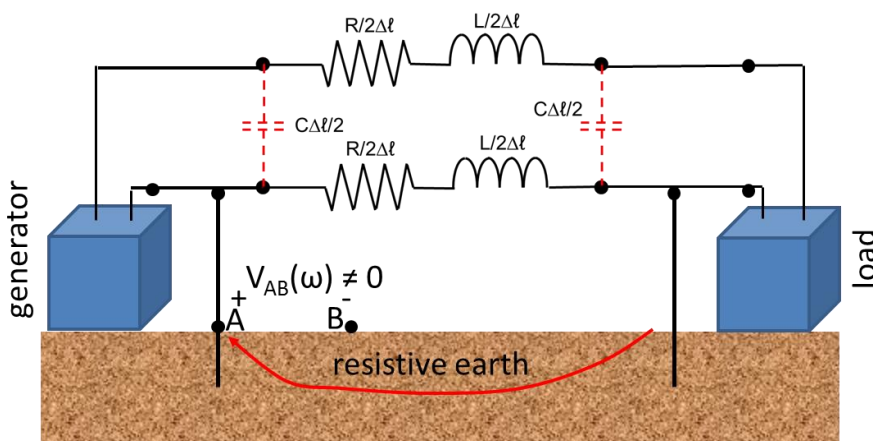


Fig. 1.4.4. Illustration of why the earth is NOT an equipotential

Having defined voltage carefully, it is important to remember that the earth is **NOT** an equipotential surface. In fact, it cannot be an equipotential surface because, if current flows through the earth and the earth is not a perfect conductor, then there must be voltage between different points on the earth as shown in Fig. 1.4.4 (i.e., $V_{AB}(\omega)$ is **NOT** equal to zero if there is current flowing in the earth) between points A and B.

Grounded vs. ungrounded systems (there is no such thing as an ungrounded system)

An important topic to consider is, “why power systems are ‘grounded.’” To begin the answer to this question, it should be noted that actually all power systems are grounded (whether explicitly as shown in Figs. 1.2.9 and 1.2.16 - 17 or not as discussed earlier). A system that is not explicitly grounded is illustrated in Fig. 1.4.5.

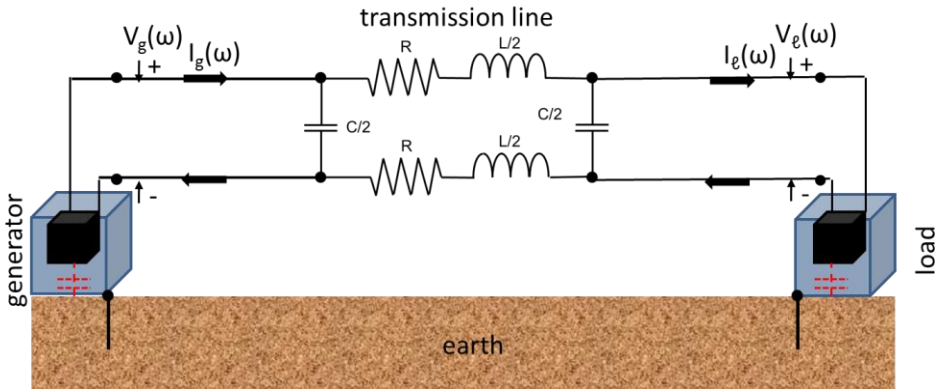


Fig. 1.4.5. Illustration of how “isolated” electrical systems are “grounded” through capacitance to earth through the generator and load cases.

As shown in this figure, even if an attempt is made to isolate the power system from the earth, there is a path for currents to the earth through the hidden capacitances between (for example) the generator and its housing which may sit on the earth. Hence no electrical system is ungrounded. Rather, the only question to ask is whether the system is grounded through a high impedance (as shown in Fig. 1.4.5) or a low impedance explicit ground (as shown in Fig. 1.4.1). The difference between these two types of grounds can be dramatic especially during fault (i.e., unintentional grounding of some point in the power system) conditions as will be illustrated next.

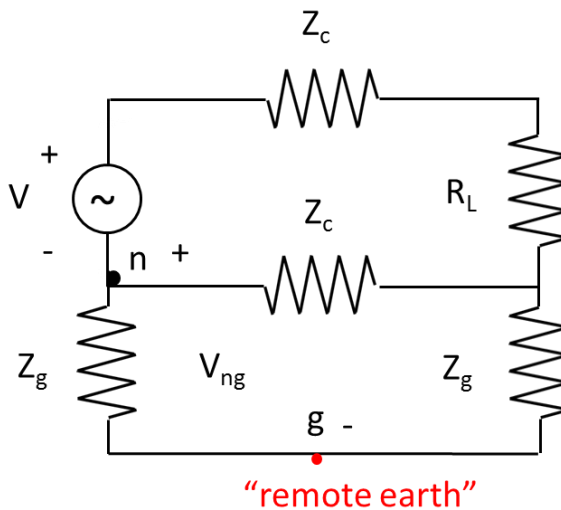


Fig. 1.4.6. A simple power system used for calculating neutral to ground voltage under normal operating conditions

This point about the impact of grounding impedance is important enough that a more detailed explanation is warranted. Fig. 1.4.6 shows a very simple power system which consists of a voltage generator, a two wire (i.e., a phase and a neutral conductor) transmission line with a series impedance Z_c for

each conductor and a load R_L at the end. The neutral conductor is grounded at each end through equal impedances Z_g . In this configuration the system is in normal operation. It can be shown that if $|Z_c| \ll |Z_g|, R_L$ (a reasonable assumption for normal operation)

$$|V_{ng}| \cong |VZ_c / (2R_L)| \ll V \quad (1.4.1)$$

where V_{ng} is the voltage from the neutral conductor to a point on the earth “far” from the ground connection called “remote earth.”

Hence, under normal conditions and independent of whether the grounding impedance is high or low as long as, $|Z_c| \ll |Z_g|, R_L$ the voltage between the generator neutral and remote earth (i.e., center of the power line – more will be said about “remote earth” in Chapter 13) is very small compared to source voltage and the issues related to personnel safety or neutral conductor insulation breakdown would be minimal.

If, however, this system is analyzed under fault conditions, a different situation exists. Consider the situation shown in Fig. 1.4.7a. Here, the phase conductor is inadvertently grounded (for simplicity through an impedance to ground of Z_f) and the neutral to remote earth ground voltage is calculated. If it is assumed that $|Z_c| \ll |Z_g|, R_L, |Z_f|$, then Z_c can be ignored in Fig. 1.4.7a resulting in the circuit shown in Fig. 1.4.7b. In this case, the voltage between neutral and ground can be written as

$$|V_{ng}| \cong |VZ_g / (Z_g + 2Z_f)| \quad (1.4.2)$$

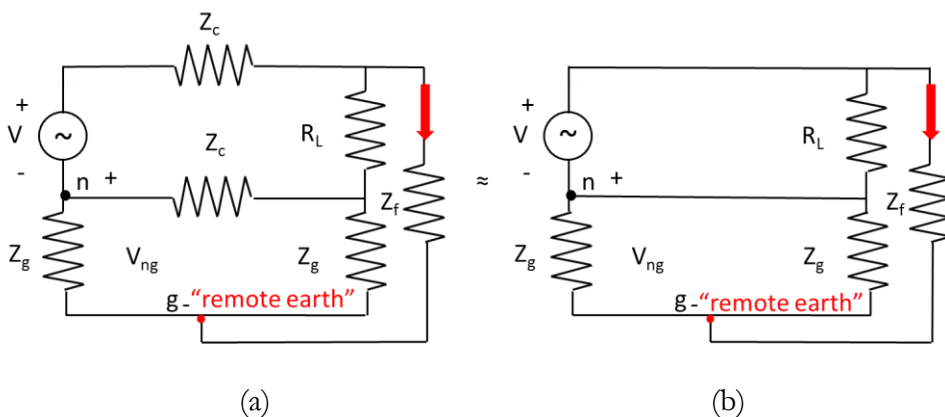


Fig. 1.4.7. A simple power system used for calculating neutral to ground voltage under fault conditions with a low impedance ground

If $|Z_g / 2| \ll |Z_f|$, the neutral to ground voltage is relatively low and issues related to personnel safety or neutral conductor insulation breakdown would

be minimal. The case for a high impedance ground is significantly different, however. If, $|Z_g/2| \gg |Z_f|$, then

$$|V_{ng}| \cong |V| \quad (1.4.3)$$

This means that this “ungrounded” (i.e., high impedance grounded) systems may experience neutral to ground voltages that could be hazardous to personnel and/or high enough to damage the insulation on the neutral conductor. This exercise illustrates why intentional grounding is important for most transmission systems.

Thevenin Equivalent Circuits (they are handy)

As an aside, Thevenin equivalent circuits are very handy for analyzing electric power transmission systems (assuming that linearity can be assumed). Fig. 1.4.8 shows how a complicated power transmission system can be represented as a simple Thevenin equivalent circuit.

Here, the Thevenin equivalent can be used to determine the effect of the entire system on a device (or person) connected between terminals A and B. Later in the text, methods for determining the parameters of the Thevenin equivalent will be discussed.

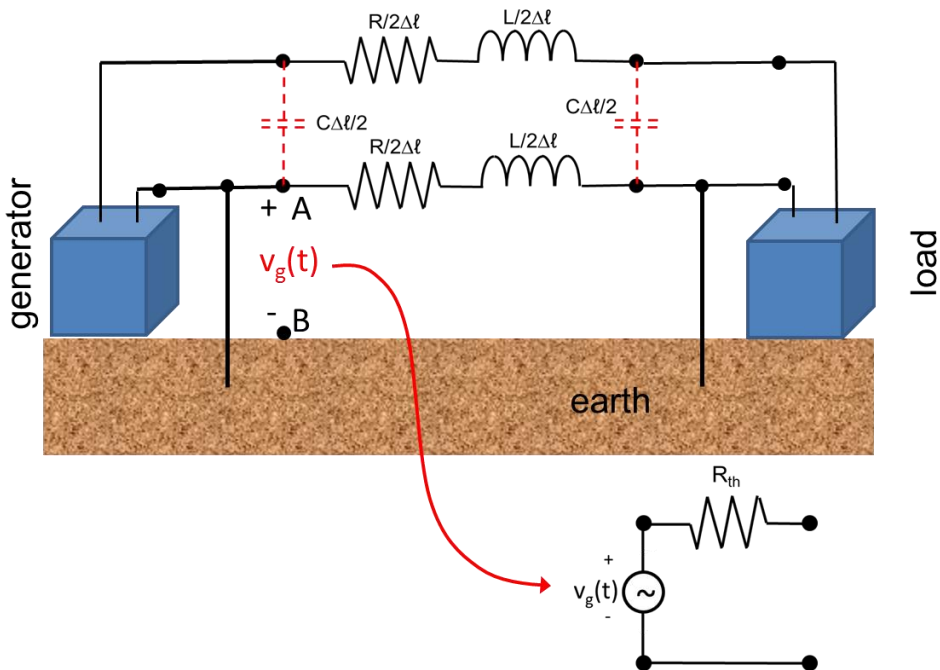


Fig. 1.4.8. Replacing an entire transmission system at terminals A and B by a Thevenin equivalent circuit

1.5 Why is Three Phase Power Used?

An early development in power systems related to improving efficiency was the advent of three phase transmission lines. To understand why, consider the superposition of three separate “single phase” systems with equal loads as shown in Fig. 1.5.1. For simplicity, the loads will be assumed to be resistances and inductive/capacitive effects are ignored. Here the voltage sources \hat{V}_a, \hat{V}_b and \hat{V}_c represent the generator for each circuit, $R\Delta\ell/2$ is the resistance of each wire where $R/2$ is the resistance per unit length and $\Delta\ell$ is the wire length and “ R_L ” represents the resistance of the load for each circuit.

Each of the circuits has a loss

$$P_{lost(n)} = \frac{2(R\Delta\ell/2)V_n}{(R_L + 2R\Delta\ell/2)} \quad (1.5.1)$$

where $n = a, b$ or c for a total loss of

$$P_{lost}^{3,\phi} = \frac{3R\Delta\ell V_n}{(R_L + 2R\Delta\ell/2)} \quad (1.5.2)$$

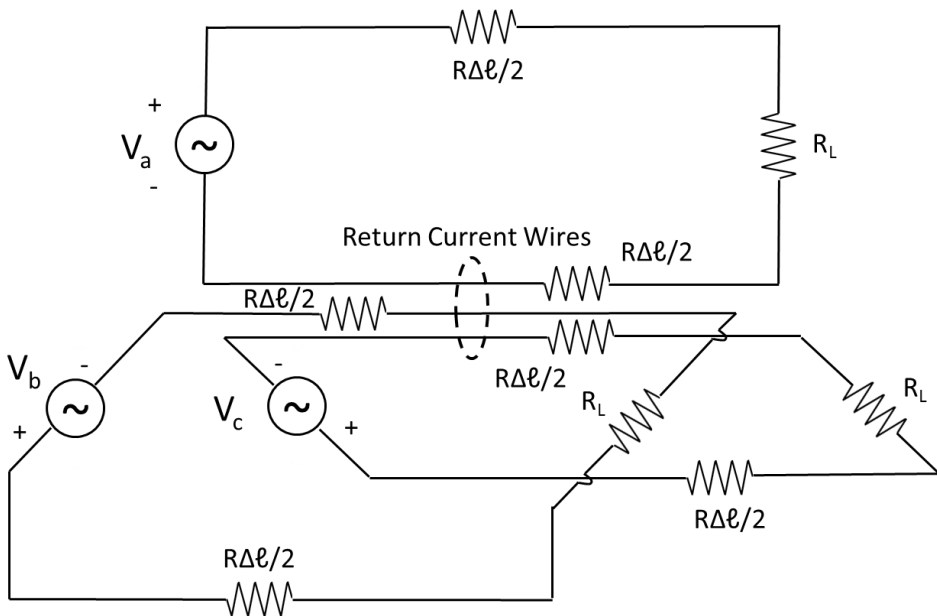


Fig. 1.5.1. Superposition of three identical single phase circuits

In each of the three circuits the current (expressed as a phasor) is equal to

$$\hat{I}_n = \frac{\hat{V}_n}{(R_L + 2R\Delta\ell/2)} \quad (1.5.3)$$

where n is a , b or c . The collective current in the set of three return current wires is

$$\hat{I} = \frac{\hat{V}_a + \hat{V}_b + \hat{V}_c}{(R_L + 2R\Delta\ell/2)} \quad (1.5.4)$$

If $\hat{V}_a + \hat{V}_b + \hat{V}_c = 0$, then the total current through the three wires is zero. Given this, if the ends of the wires are connected together there is no net voltage drop across this set of wires because there is no total current. Since there is no current through this set of “return current” wires they could be eliminated as shown in Fig. 1.5.2²³. The effect of this is to eliminate the need for these three wires and hence their cost. In addition, the resistive losses in these three wires are eliminated and, hence, the efficiency of the system is approximately doubled since there is loss in only three wires rather than six. The loss in the three-phase case is

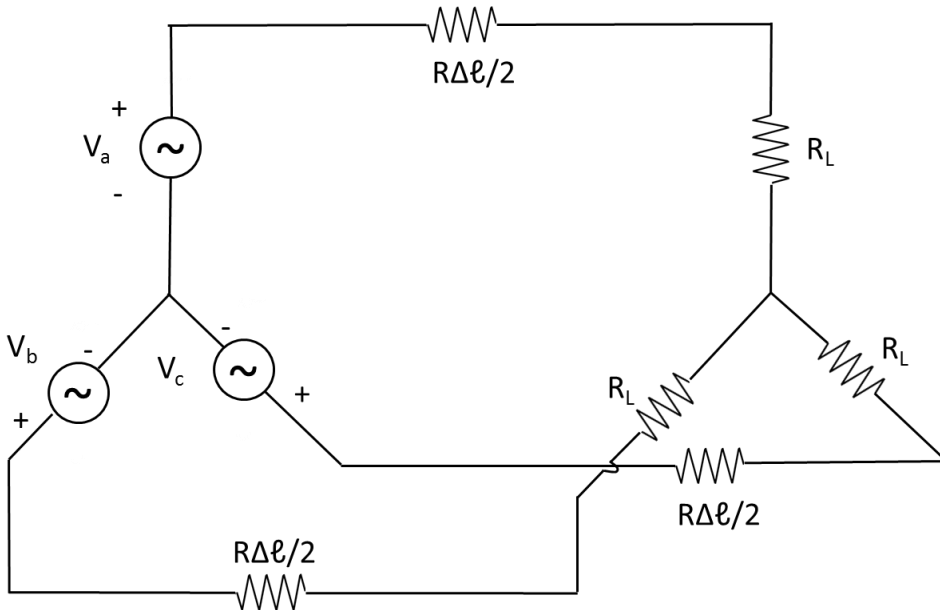


Fig. 1.5.2. Three phase system “wye” connected system with return (neutral) wires eliminated

²³ This type of connection is called a “wye” connection because the generator and load connections look like the letter Y. Another common connection for generator and load is the delta or Δ connection for which the connections look like a Δ and there is no return wire.

$$P_{lost}^{3\phi} = \frac{1.5R\Delta\ell V_n}{(R_L + R\Delta\ell/2)} \quad (1.5.5)$$

Such a system is constructed generally using

$$\hat{V}_a = Ve^{j0}, \quad \hat{V}_b = Ve^{-j2\pi/3}, \quad \hat{V}_c = Ve^{j2\pi/3} \quad (1.5.6)$$

so that $\hat{V}_a + \hat{V}_b + \hat{V}_c = 0$. There are other reasons why three phase systems are used including the fact that three-phase connected generators and motors have a constant power output in time and the fact that three phase components such as transformers can be constructed more economically than three single phase components. Further, these advantages are not limited to three phase systems. But, this subject is beyond the scope of this discussion (Bergen 1986).

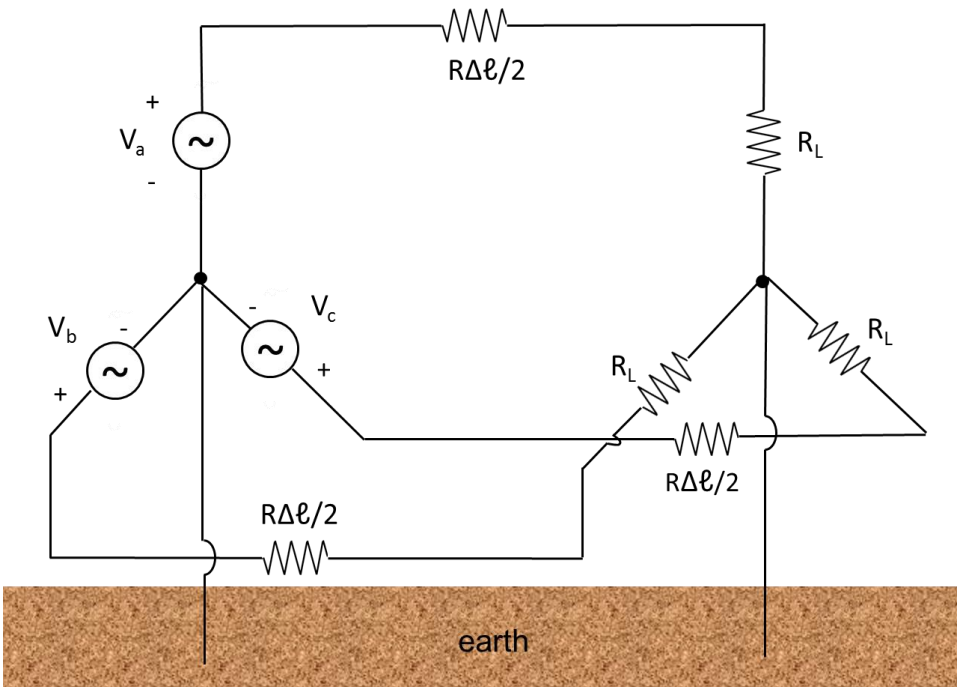


Fig. 1.5.3. Three-phase grounded “wye” connected system

Practical three-phase systems are grounded to the earth at the center of each “wye” as shown in Fig 1.5.3. This kind of a connection is used because the power system is almost never completely balanced (especially during unbalanced fault conditions) and grounding in this way carries unbalanced currents to ground and hence, enhances safety and system recovery.

As a final note, transmission lines (e.g., a 500 kV transmission line) are usually identified by their line to line voltage. The relationship between line to line and line to ground voltage is

$$|\hat{V}_{ll}| = \sqrt{3}|\hat{V}_a| \quad (1.5.7)$$

The reason for the square root of 3 term can be illustrated by referring to the phasor diagram of the voltages associated with a three phase system in Fig. 1.5.4. Here the three phase voltages in (1.5.6) are plotted. The line to line voltage between phases A and B which is the phasor difference between \hat{V}_a and \hat{V}_b is also shown

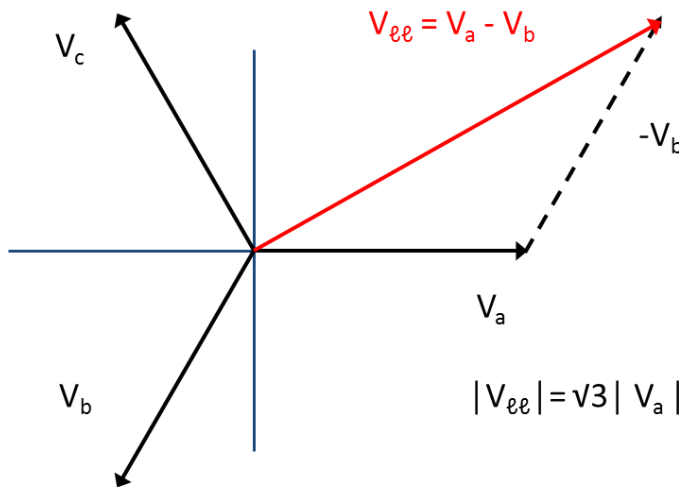


Fig. 1.5.4. Phasor diagram of the voltages on a three phase system

1.6 On Increasing the Capacity of Power Transmission Lines

Introduction

It is known that the power transferred through a power transmission line is proportional to some current and some voltage. Earlier in this chapter, it was shown that in order to realize efficient power transmission over long distances, the voltage of a transmission line should be increased rather than its current. It is also generally true, that higher voltage transmission lines have greater capacity for transferring electric power. Hence, the most important approach to increasing the power capacity of transmission lines is that of developing techniques for building transmission lines at higher voltages. This will be covered in the next section. Following that will be a

brief introduction to techniques for increasing the capacity of transmission lines to handle electric current.

Voltage limitations on high voltage transmission systems and their solutions

In the twentieth century as electric power became more ubiquitous, a trend continued towards the use of even higher voltages for power transmission over long distances, again because of the desire to improve the efficiency of power transfer and to transfer more power. Before, these higher voltage lines could be used practically however, it was necessary to solve problems related to the use of high voltage on these transmission lines. To be complete, there is a short section about techniques that have been used to increase the current handling capacity of high voltage transmission lines.

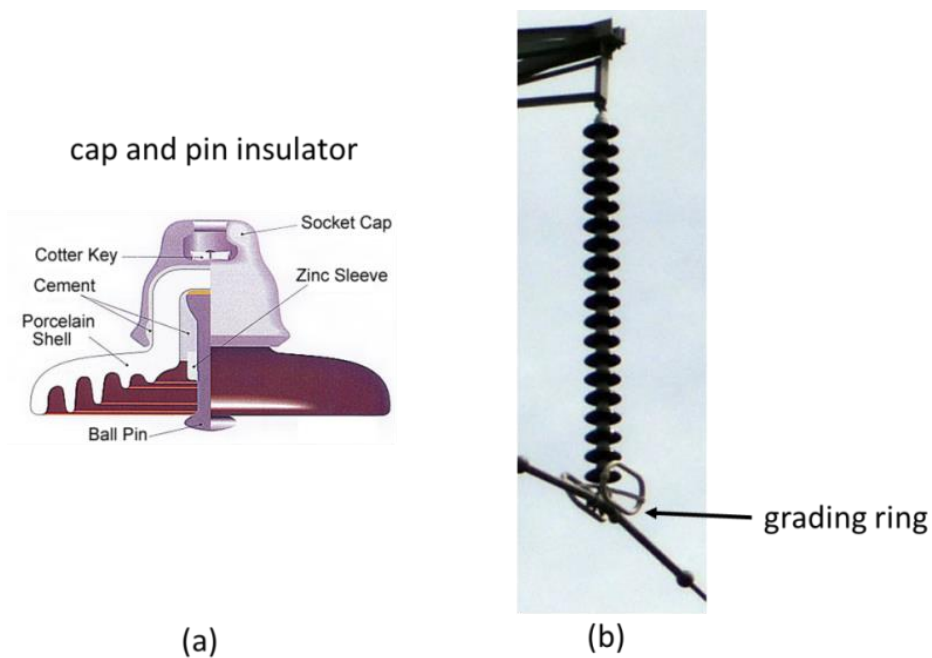


Fig. 1.6.1. a) Single cap and pin insulator b) String of cap and pin Insulators used on a high voltage transmission line. The hardware at the bottom end is a pair of grading rings that will be discussed in more detail later. (photo courtesy R. Aho - BPA)

The two most important of these solutions were the development of insulators appropriate for high voltage applications and the design of conductors and hardware suitable for managing corona effects on power lines (Maruvada 2000). The key development in insulation design was the development of the cap and pin suspension insulator which is further discussed by Mills (1979) and Creager and Justin (1927) and shown in Fig. 1.6.1. The individual unit is shown in Fig. 1.6.1a while a sting of units is shown in Fig. 1.6.1b. Also visible near the end of the string of insulators is a “ring” structure often called either a “grading” ring or a “corona” ring. The

primary purpose of this hardware is to distribute the power frequency electric field near the conductor end of the insulator more evenly (i.e., to “grade” it) so that the insulation strength is more nearly proportional to the number of insulator units in the string. A positive side effect (and part of the solution to the corona issue) is that these rings can also act to reduce corona (i.e., partial electric discharge in air near high voltage conductors and hardware). Corona occurs because the electric field near these conductors is large enough to cause ionization of the air and results in power loss as well as audible and electromagnetic noise (see Figs. 1.6.2 and 1.6.3). More information about this can be found in Chapters 8 and 9. Another aspect of the solution to the corona problem was the development of “bundled” conductors as will be visible in the photographs of power line conductors in the next section. While some aspects of corona will be covered in this manuscript the subject is covered more completely in (Maruvada, 2000). A negative side effect of grading rings is that they reduce the insulation strength for impulsive voltages (EPRI 1982).



Fig. 1.6.2. The white spots at the tips of the attachment hardware are corona discharges. (courtesy B. Clairmont – EPRI)



Fig. 1.6.3. The white spots are corona discharges randomly located along a conductor energized to high voltage

To be complete, it should be noted that there are also limitations on the current carrying capacity of these transmission lines such as excessive conductor sag and temperature. These will be discussed in more detail later in Chapter 8.

Current limitations on high voltage transmission systems and their solutions

While voltage issues were the primary limitation on the development of high voltage transmission lines, increasing current limits can be another way to increase the power handling capability of high voltage transmission lines. Many of these issues will be covered in much more detail in Chapter 8. However a short summary is included here. The primary issue that limits current carried by high voltage power lines is that the current causes heating of the conductors and if excessive, this in turn leads to stretching and hence unsafe sagging of conductors and shorter lives for conductors and other components such as splices. This issue can be mitigated primarily in two ways. First, reducing the resistance of the conductors by using conductors with larger diameters results in less heat dissipation and a higher current capacity. Second, the use of different materials for conductor core strength material results in reduced stretching for a given temperature. Other remedies include closer monitoring of weather conditions to determine conditions under which higher currents can be tolerated without violating standards on maximum sag. Having said this, the power handling capacity of very long high voltage overhead transmission lines is often limited by other issues such as system stability. In these cases, replacement of conductors does not result in increased current capacity since the current can never get large enough to be of concern without violating other limits such as those related to stability.

1.7 Alternative Transmission Line Systems

Introduction

As mentioned earlier, there are many types of high voltage transmission lines. Some are modifications of the standard single circuit three phase transmission line such as “double circuit,” “compact,” “low sag conducting,” “high surge impedance loading” and “low reactance” each designed to mitigate against some disadvantage of conventional high voltage transmission lines. Each of these will be considered in some detail later in this manuscript. However, there are other designs that are more radical than those just mentioned. Two of these are introduced in the following sections and will be discussed further in Chapter 8.

High voltage direct current (HVDC)



Fig. 1.7.1. Transmission line structure for the HVDC Pacific Intertie. (courtesy R. Aho, BPA)

It was mentioned earlier that during the beginnings of electric power, direct current (DC) systems were one of the competing technologies for power transmission (Bahrman 2008). Alternating current (AC) systems prevailed primarily because transformers made it relatively easy to change from one voltage level to another in order to reduce energy losses associated with transmission. However, as also mentioned earlier, the electrical resistance of a conductor at DC is lower than that of the same conductor at AC. Hence, even through the cost (both in terms of dollars and losses) of converting AC to DC and vice versa is high, economics may favor DC lines if the line is long enough. Since the 1950's some long DC transmission lines have been constructed such as the Dalles, OR to Los Angeles, CA Pacific Intertie shown in Fig. 1.7.1. The fact that there are only two power carrying conductors should be noted. The other two conductors are shield wires.

For overhead transmission lines, HVDC has the advantages of lower line losses due to a smaller resistance per unit length and the removal of stability related load limits for long transmission lines (and hence larger power transfer on a given corridor). In addition, while cables are not the specific subject of this manuscript, DC technology is exclusively used for long underwater cables due to the large capacitive currents that flow in unloaded AC cables.

High phase order transmission



Fig. 1.7.2. Experimental six-phase power system tower. (Courtesy J. R. Stewart)

Three phase transmission lines are not the only transmission lines that have been studied and or constructed in the past. In fact high phase order (e.g., six or twelve phase) transmission lines have been considered as an alternative (Grant and Stewart 1984). While it is difficult to determine exactly what is the best way to compare these to traditional three phase transmission lines (e.g., voltage, number of phases, conductor size, right of way width, environmental criteria, and phase spacing), the principal advantages of high phase order lines are: a) They can provide the same power transfer (thermal or surge impedance) capability as three phase lines, on a smaller right of way, for the same electric field and audible noise criteria, with smaller structures and reduced overall cost and b) They can provide higher power transfer-on a given right of way than three phase, for the same electric field and noise criteria. A photograph of a six phase line can be found in Fig. 1.7.2.

1.8 Conclusion

It should be clear that the design of high voltage, overhead power lines is a complicated process. In the following chapter, an overview of real high voltage overhead power lines will be given in order that the reader understand the hardware that is used to build these lines. At the end of the

discussion is a list of simplifying physical assumptions that must be made before realistic mathematical models of the electromagnetic fields of these power lines can be developed.

1.9 Problems

P1.1. Of the three following possibilities, what is the fundamental reason why wireless power transmission is not generally used for transporting bulk power?

- Not as efficient as wired transmission
- More expensive than wire transmission
- Frequency spectrum not available for wireless transmission

P1.2. Assume a simplistic model for an antenna that radiates power equally in all directions. Hence the radiated power density is $P_{rad} = \frac{P_{gen}}{4\pi r^2}$ Watts/m².

If, equally simplistically, it can be assumed that a receiving antenna captures an amount of power (P_{rec}) equal to the incident power density multiplied by the area of the receiving antenna, calculate the efficiency (i.e., $\frac{P_{rec}}{P_{gen}} \times 100$ %)

of a wireless power transmission system for a receiving antenna with an area of 100 m² over a distance of 1000 meters. Compare this to the efficiency of a 1000 meter long “wired” system that connects a 10 kV rms 60 Hz voltage source to a purely resistive 1 Mw load with copper wire of 5 mm diameter (assume no skin effect). At room temperature, the resistivity of copper is 1.68×10^{-8} Ω-m. Hint: use the power flow equation 1.3.17 with V_l assumed to be real because the load power is real and there are no reactive elements.

P1.3. How much weight can you save if you replace a copper conductor with an aluminum conductor of the same total dc resistance and length? (The density of copper and aluminum are 8960 kg/m³ and 2700 kg/m³, respectively. At room temperature, the resistivity of copper and aluminum are 1.68×10^{-8} Ω-m and 2.82×10^{-8} Ω-m, respectively.)

P1.4. Calculate the RMS value of the square and triangular waves shown in Figure P1.9.4

P1.5. You are given the phasor voltage $\hat{V} = 120e^{-j\pi/6}$. If the frequency is 60 Hz, calculate the voltage in the time domain.

P1.6. Why are 50/60 Hz the most common frequencies for power systems around the world?

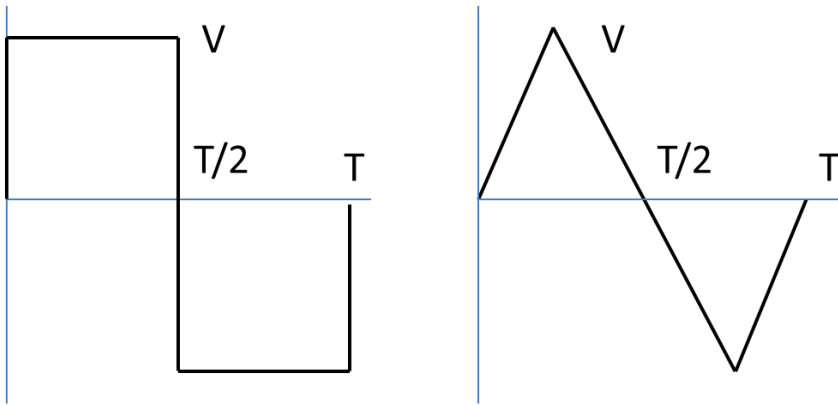


Fig. P1.4. Square and Triangular Waves

P1.7. You are given a simple single phase transmission line of length 100 km and made of aluminum wire with a radius of 1.0 cm. The resistivity of aluminum at room temperature is $2.82 \times 10^{-8} \Omega\text{-m}$. Assume that inductive effects can be neglected and that there is no skin effect.

- What is the resistance of each wire?
- If the voltage of the generator is 10 kV and the power absorbed by the load (purely resistive) is 1 MW, what is the efficiency of the system?
- Repeat for a generator voltage of 100 kV.
- Hint: start with the power flow equation 1.3.17.

P1.8. Historically, what fundamental advantage did AC have that resulted in a mostly AC transmission and distribution system rather than a DC one?

P1.10. You are given that the inductance per unit length of a two wire 100 kV, 100 km AC transmission line is

$$L \cong \frac{\mu_0}{\pi} \ln\left(\frac{d}{a}\right) \text{ Henries/m}$$

where d is the spacing between the wires and a is the wire radius. Assuming that $d = 3 \text{ m}$, $a = 2 \text{ cm}$ and the frequency is 60 Hz, show that resistive effects can be ignored compared to the inductive effects if the wires are made of aluminum. Find conditions for which capacitive effects can also be ignored given

$$C \cong \frac{\pi\epsilon_0}{\ln\left(\frac{d}{a}\right)} \text{ Farads per meter}$$

P1.11. Suppose $s_\ell(t) = p_\ell(t) + q_\ell(t) = v_\ell(t)i_\ell(t)$ and

$$v_\ell(t) = \sqrt{2}V_{\ell rms} \cos(2\pi ft) \quad i_\ell(t) = \sqrt{2}I_{\ell rms} \cos(2\pi ft + \theta)$$

What is the most important distinguishing characteristic between $p_\ell(t)$ and $q_\ell(t)$?

P1.12 Is the current (green) in Fig. P1.12 leading or lagging the voltage (blue)? By how much?

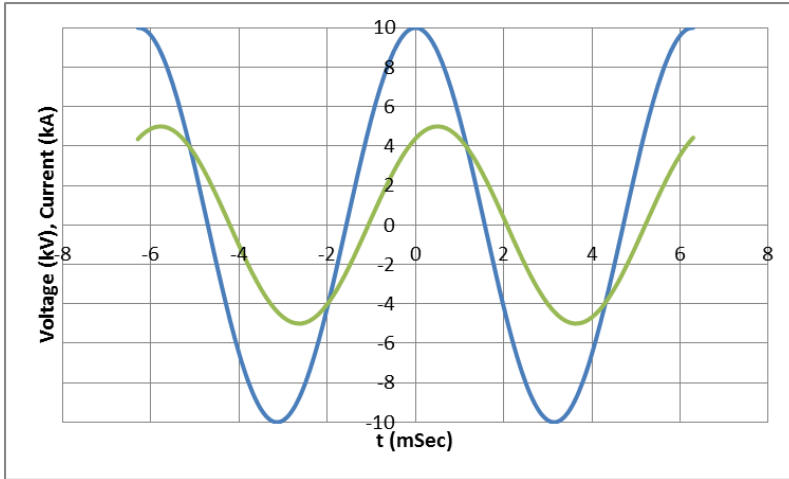


Fig. P1.12. Voltage across and current through a load.

P1.13. Assuming that complex power is conserved, what is the reactive power supplied to (or by) each of the circuit elements (including the generator) in the following circuit. $V_g = 100$ kV and $P_\ell + jQ_\ell = 1$ MW + j 0.2 kVAr.

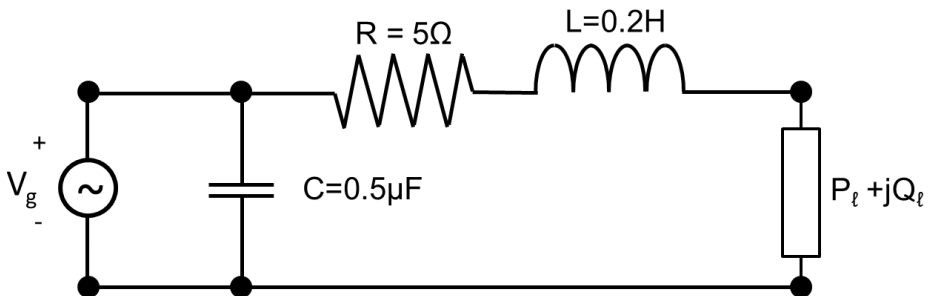


Fig. P1.13. Power System for problem P1.13

P1.14. Using the power flow equation, 1.3.23, the fact that the total inductance of a short transmission line is 0.2 H and the fact that the voltage at generator 2 is 100kV, how much reactive power (in kVAr) can flow across the transmission line with less than a 10% voltage drop between generator and load? What can be done to reduce this voltage drop?

P1.15. Given the list below, identify which are the valid attributes of power flow equations?

- a. Nonlinear
- b. Linear
- c. Multiple solutions
- d. Unique solutions

P1.16. If positive reactive power is injected into a power network, what happens at (and near) that point ?

- a. voltage increases
- b. voltage decreases
- c. phase changes
- d. the system is more efficient

P1.17. In a simple two bus power system with bus voltages $V_1 e^{j\theta_1}$ and $V_2 e^{j\theta_2}$ connected by a transmission line that can be modelled as an inductor, the real and reactive power flows follow which of the following

- a. $P_{12} \propto (\theta_1 - \theta_2)$ $Q_{12} \propto |V_1| - |V_2|$
- b. $P_{12} \propto (\theta_1 - \theta_2)$ $Q_{12} \propto (\theta_1 - \theta_2)$
- c. $P_{12} \propto |V_1| - |V_2|$ $Q_{12} \propto (\theta_1 - \theta_2)$
- d. $P_{12} \propto |V_1| - |V_2|$ $Q_{12} \propto |V_1| - |V_2|$

P1.18. Explain why the earth cannot be considered an equipotential surface.

P1.19. Which of the following is an appropriate way to define a voltage? Indicate all that apply.

- a. The voltage at point A is ...
- b. The voltage between points A and B is
- c. The voltage at A with respect to B is
- d. all of the above

P1.20. You are given a cable with capacitance per unit length $c = \frac{2\pi\epsilon_r\epsilon_0}{\ln(b/a)}$

F/m. The outer and inner radii of the cable are $b = 10$ cm and $a = 2$ cm while the relative dielectric constant of the dielectric is $\epsilon_r = 3.0$. Calculate the reactive power supplied to the system by a 10 km long, 230 kV single phase cable. Assume that the frequency of operation is 60 Hz. Compare this to a similar cable that is 1 km long and is operated at 13.8 kV.

P1.21. What is the maximum power that can be supplied to the load by the system shown below in Fig. P1.21 if the load is resistive (i.e., $Q_\ell = 0$)? Explain what happens to the maximum power output if Q_ℓ is added. Note that Q_ℓ can be positive or negative.

P1.22. What is the primary reason that three phase systems are used? Is this property unique to three phase systems? What about systems that are $n \times 3$ phase?

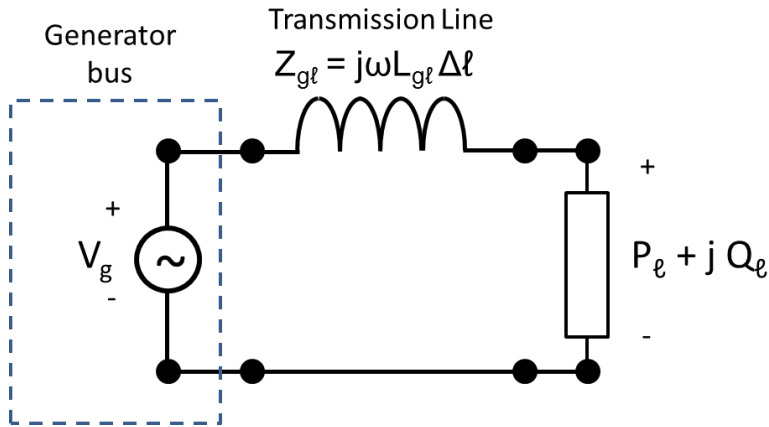


Fig. P1.21. Simple Power System

P1.23. Show that the power output (in time) for a balanced three phase system in Fig. P1.26 is independent of time. Show that this does not happen for a two phase system.

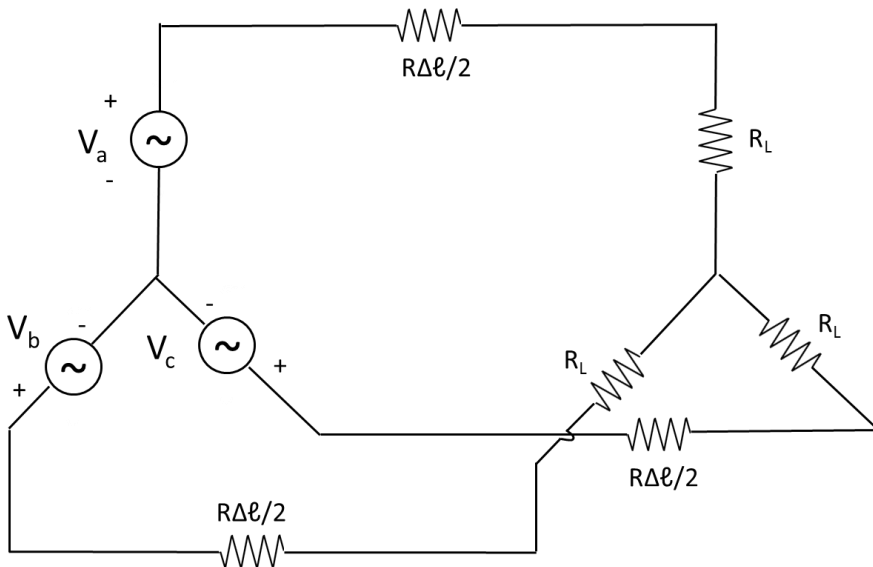


Fig. P1.23. Balanced Three Phase Power System

P1.24. Under what conditions is it possible to eliminate the neutral conductor of a Y connected 3 phase system?

P1.25. What are the key problems that have placed limits the amount of power that can be carried by a high voltage transmission line?

1.10 References

Anderson, L. I., Ed. 1992. *Nikola Tesla on His Work with Alternating Currents and their Application to Wireless Telegraphy, Telephony, and Transmission of Power*. Twenty-First Century Books. Minneapolis.

M. P. Bahrman. 2008. "HVDC Transmission Overview." *IEEE Transmission and Distribution Conference and Exposition, Chicago, IL*. pp. 1-7.

Bergen, A. R. 1986. *Power System Analysis*. Prentice Hall. Englewood Cliffs, NJ

Cannon, B. L., J. F. Hoburg, D. D. Stancil, and S. C. Goldstein. 2009. "Magnetic Resonant Coupling as a Potential Means for Wireless Power Transfer to Multiple Small Receivers." *IEEE Transactions on Power Electronics*, Vol. 24. pp. 1819-1825. July.

Creager, W.P., and J.D. Justin. 1927. *Hydro-Electric Handbook*. John Wiley and Sons. New York.

Electrical Science. 2009. <http://electrical-science.blogspot.com/2009/12/history-of-power-frequency.html>

EPRI. 1982. *Transmission Line Reference Book: 345 kV and Above/ Second Edition*, Electric Power Research Institute. Palo Alto, California.

Flournoy, D.M. 2011. *Solar Power Satellites*. Springer. New York.

Grant, I.S. and J. R. Stewart. 1984. "Mechanical And Electrical Characteristics of EHV High Phase Order Overhead Transmission." *IEEE Transactions on Power Apparatus and Systems*. Vol. PAS-103. pp. 3379-3385. November.

Karalis, A., J. D. Joannopoulos and M. Soljacic. 2008. "Efficient Wireless Non-Radiative Mid-Range Energy Transfer." *Annals of Physics*. Vol. 323. pp. 34-48.

Maruvada, P. S. 2000. *Corona Performance of High-Voltage Transmission Lines*. Research Studies Press Ltd. Baldock, Hertfordshire, England.

McNichol, T. 2006. *AC/DC: the Savage Tale of the First Standards War*. John Wiley and Sons. New York.

Mills, B. 1970. *Porcelain Insulators and How They Grew*, (privately published). available from ABE Books (subsidiary of Amazon.com).

Olsen, R. G. and A. Aburwein. 1980. "Current Induced on a Pair of Wires Above Earth by a Vertical Electric Dipole for Grazing Angles of Incidence." *Radio Science*, Vol. 15. pp. 733–742. July-August.

Peterson, H. A. 1952. *Transients in Power Systems*." Dover. New York.

Weeks, W. L. 1968. *Antenna Engineering*. McGraw Hill. New York.

Weeks, W. L. 1981. *Transmission and Distribution of Electrical Energy*. Harper and Rowe. New York.

Chapter II

Real High Voltage Overhead Transmission Lines and Physical Approximations Prior to Analysis

2.1 Introduction

In this chapter, a description of real high voltage overhead power transmission lines and their associated components will be given. Special attention will be paid to the differences between these and the idealized transmission lines that are usually analyzed. For example, in most cases, the fact that power line conductors sag between towers is ignored and the towers used to suspend the conductors above ground are ignored. Hence, it is important to understand the differences between the electrical behavior of real high voltage overhead power transmission lines and the idealizations that are mathematically analyzed and, even more important, to understand when these differences result in significant inaccuracies. Later in this chapter, the issue of inaccuracies introduced by these approximations as well as some ideas for overcoming these inaccuracies (when necessary) will be discussed.

2.2 Brief Description of Real High Voltage Overhead Power Transmission Lines

Transmission vs. distribution

On power systems the higher voltage overhead power lines are usually referred to as “transmission lines” and the lower voltage power lines referred to as “distribution lines.” The transition between these two is usually between 50 kV and 80 kV. In this manuscript, emphasis will be placed on the higher voltage overhead “transmission lines.” An example of a three phase high voltage alternating current (AC) overhead transmission line is shown in Fig. 2.2.1. It is clear from this photograph that transmission line components include conductors, towers, insulators and other hardware. These and more will be discussed in the following sections.

Conductors, conductor bundles, and shield wires

Early lower voltage power transmission lines used solid (usually copper) conductors. Copper was initially selected because of its relatively low resistivity compared to other common conducting materials. But, eventually there was an almost complete switch to the use of aluminum conductor

because, while its resistivity is nearly 60% higher than copper, its density is only 30% that of copper. Hence for a given weight per unit length (according to (1.2.9)) the resistance per unit length of aluminum conductor is roughly half that of a copper conductor. As the diameter of conductors was made larger, most conductors were constructed from “strands” of wire for mechanical reasons (primarily flexibility) as shown schematically in Fig. 2.2.2. This is still the case today.

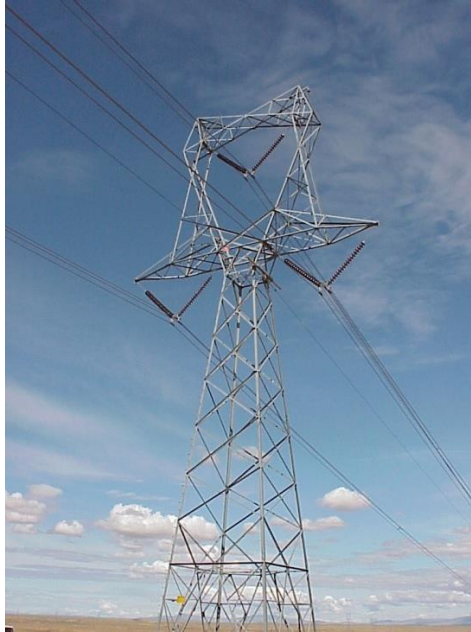


Fig. 2.2.1. A typical high voltage transmission line on steel towers. (courtesy BPA)

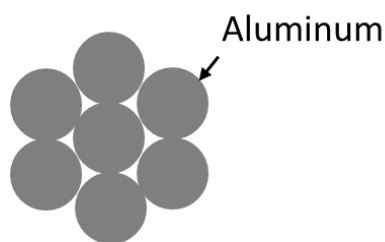


Fig. 2.2.2. An example cross section of a stranded all aluminum conductor (AAC) with 7 strands

In addition to resistance per unit length, two other important design criteria for conductors are their mechanical and thermal properties. The mechanical properties are important because conductors must be strong enough to suspend their own weight over long spans between towers as well as to sustain forces due to high winds that cause additional stress on the conductor. In cold climates, accumulated ice and snow augments the

conductor weight (see Section 2.4). All of these factors must be accounted for in the design. The thermal properties are important since the power dissipated in the conductor's resistance by the large currents that pass through them is converted into heat that raises the temperature of the conductors. This, in turn, causes two problems. First, most conductors expand in length as temperature rises. This causes the conductors to sag and, if large enough, to cause flashovers to objects under the line and/or potentially unsafe conditions for humans under the line. Ultimately this problem limits the power flow on many (but not all) transmission lines²⁴. Second, the material properties of the conductor may be changed permanently by the heating. Aluminum, for example, can be annealed and (as a result) may lose its strength over time if it becomes too hot for too long a time (Thrash, et. al. 2007).

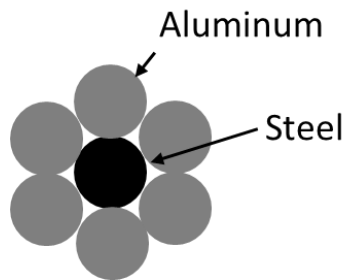


Fig. 2.2.3. An aluminum conductor steel reinforced (ACSR) conductor

It was recognized early that (for typical power line conductors carrying AC current) the current flows mostly near the outside surface (or “skin”) of the conductor (This effect is called the skin effect and will be discussed in Chapter 4 and Appendix B). Thus, it is possible to use a strong, but higher resistance material in the “core” of the conductor and a lower resistance material with less desirable mechanical properties on the outside without significantly sacrificing either the mechanical or electrical properties of the conductor. Such a conductor is shown schematically in Fig. 2.2.3. This conductor uses a steel inner core for strength and an aluminum outer shell for low resistance. Such a conductor is called an aluminum conductor steel reinforced (ACSR) conductor.

A photograph of the cross-section of an ACSR conductor with many strands is shown in Fig. 2.2.4. In this photo, the smaller diameter darker colored strands near the center are steel for strength and the larger diameter lighter colored strands are aluminum for lower resistance. More recently, conductors with different core material to reduce sag have been developed.

²⁴ Other factors that limit power flow are system stability (generally for long lines) and voltage regulation (generally for lines of medium length) (Maruvada ,2000).



Fig. 2.2.4. Cross sectional view of a stranded aluminum conductor steel reinforced (ACSR) conductor (courtesy R. Aho, BPA). Note that the rubber coating is here only for the purpose of holding the sample together. Conductors in service will generally not have this coating.

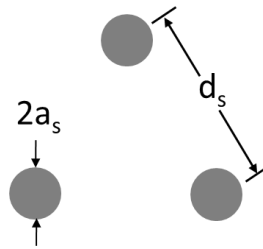


Fig. 2.2.5. Cross-sectional view of a three subconductor bundle

The higher the voltage, the more likely that a single conductor will be replaced by a “conductor bundle” as shown in Figs. 2.2.5 and 2.2.6. These bundles consist of several parallel subconductors (each of which is stranded) and are used (as will be illustrated later in the manuscript) to control corona by reducing the electric field at its surface compared to that for a single conductor of the same weight per unit length. The use of bundles also reduces the inductance per unit length of a transmission line and sometimes is the primary reason why they are incorporated into a design.

Although not evident from Fig. 2.2.6, conductor bundles always involve some spacer hardware to maintain the designed spacing between subconductors at all points between towers, especially during wind. One example of spacer hardware for a four conductor bundle is shown in Fig. 2.2.7.



Fig. 2.2.6. A three conductor bundle on a 500 kV line

In many locations around the world, lightning is a significant cause of transmission line outages. In these cases, utilities often install “overhead

shield wires” above the phase conductors as shown in Fig. 2.2.8 that are usually (but not always) connected to ground at each tower (Eriksson 1987). In some cases a small gap between shield wire and ground is purposely used to reduce losses during normal operating conditions but to allow the higher voltages during faults and lightning strikes to flashover the gap and hence ground the shield wire during these conditions. The purpose of these shield wires is to divert lightning away from the phase conductors and to ground it through the towers and their grounding systems to reduce the probability of a flashover to a phase conductor and a subsequent outage. They also conduct fault current during system faults and are useful for detecting faults. At power frequencies, they are often included in an analysis of the electric field near power lines (they are assumed to have a potential of 0 at power frequency because of grounding at each tower and the fact that the spacing between towers is a small fraction of a wavelength²⁵), but ignored for magnetic field calculations because relatively little current is induced on these wires under normal operating conditions. At significantly higher frequencies, such simple analysis may not be possible because the spacing between towers becomes a significant fraction of a wavelength. In fact, at some frequencies in the hundreds of kilohertz to low Megahertz range, sections of grounded shield wire may become resonant and have a noticeable effect on the electromagnetic fields from broadcast stations (Madge and Jones, 1986).

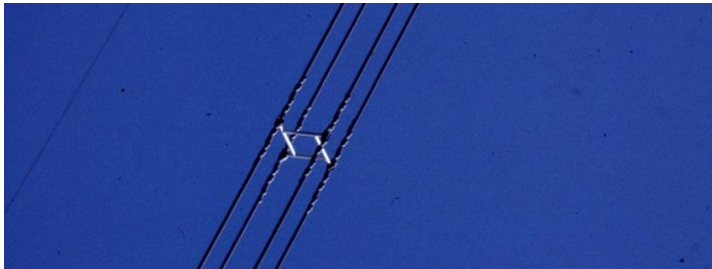


Fig. 2.2.7. Typical spacer hardware on a four conductor 765 kV bundle. (courtesy J.R. Stewart)

Finally, there are a number of different ways that the phase conductors can be configured in space. The specific configuration shown in Fig. 2.2.1 is a “single circuit” (i.e., a single set of three phase conductors) “delta” configured line because the phase conductors are arranged in a Δ arrangement (in the cross section of the transmission line) with two phases at one lower height and one centered above them. But, the phase conductors could also be arranged in a “horizontal” configuration (i.e., all at the same height above the ground) as illustrated later in Fig. 2.2.10 or as a “vertical” configuration for which each conductor is at the same horizontal location but one above the other at different heights. It is also common to see two

²⁵ Wavelength (λ) is defined as 300,000 km divided by the frequency in Hertz. At 60 Hz, the wavelength is 5,000 km and much larger than typical spacing between towers.

circuits on a single tower (i.e., a “double circuit” configuration) as shown in Fig. 2.2.9. The reasons for the different configurations include (but are not restricted to) maximizing the power transfer through a fixed right-of-way, balancing currents, minimizing the cost of construction, reducing the line inductance and aesthetics.



Fig. 2.2.8. Overhead shield wires visible at the tops of the two poles. (courtesy J.R. Stewart)



Fig. 2.2.9. Double circuit transmission line. (courtesy R. Aho, BPA)

Towers

In order to operate at high voltages, transmission line conductors must be supported in space and effectively isolated from the earth and the public so that very little or none of the current can “leak” into the earth and that electrical safety standards for the public are satisfied. This is accomplished by using towers such as the one shown in Fig. 2.2.1 to suspend the conductors above the earth. These towers can be constructed of steel (as

shown in Fig. 2.2.1), wood (as shown in Fig. 2.2.10), concrete or other material. The conductors are suspended in the air with insulators that are mechanically strong but which have very high electrical resistance. The towers and their foundations must be strong enough to both suspend the conductors in air as well as to avoid failure in the harshest of environmental conditions (e.g., rain, snow, conductor ice and wind during hurricanes or tornados) during the expected lifetime of the tower. This civil engineering problem is an entire field in itself and is discussed extensively in standards (IEEE 2001, ASCE 1991).

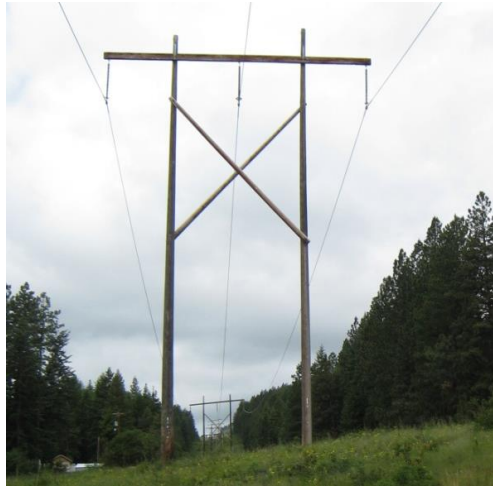


Fig. 2.2.10. A wood pole tower with vertical suspension insulators



Fig. 2.2.11. A dead end tower that is stronger and does not allow conductor movement parallel to the transmission line direction

Since this manuscript is designed primarily for electrical engineers, it should be mentioned that there will always be conflicts between the design requirements of the civil engineers who design towers and the electrical engineers who design the insulators and the conductors. Compromises are often necessary. Finally, it should be mentioned that transmission line towers are grounded to provide protection of the system during faults and lightning. More will be said about this in Chapter 13.

Different kinds of towers are used along a transmission line in part because transmission lines are designed in sections with each end terminated by a structure that does not allow movement of the conductors parallel to the direction of the line (i.e., mechanical ends of the line section). Mechanically separate sections such as these are terminated by “dead-end” towers at the ends as shown in Fig. 2.2.11. Generally, these dead end towers will be stronger and the insulators positioned horizontally as shown in the figure. Between the dead end structures, the towers are typically “suspension” towers such as shown in Fig. 2.2.10 that allow movement of the conductors both parallel to and perpendicular to the transmission line direction. Suspension towers are used when possible because they are less expensive. However, they cannot be used for arbitrarily long sections of the transmission line because the mechanical failure of one suspension tower can cause adjacent towers to fail as well in what is called a “cascading failure.” The use of dead-end towers tends to limit the extent of cascading failures (CIGRE 2012).



Fig. 2.2.12. Transmission line tower with line post insulators. These do not allow movement of the conductors in any direction. Hence, clearances between conductors and the tower can be smaller.

Another type of tower (a Vee string tower) is illustrated in Fig. 2.2.1 for which the conductors can move parallel to but not perpendicular to the

direction of the transmission line. Finally, some towers use “post” insulators as shown in Fig. 2.2.12 that do not allow either horizontal or vertical movement at the structure. Such restrictions on conductor movement generally allow smaller clearances between conductors and towers, but generate stricter mechanical requirements for the insulators.

Insulators and insulator contamination

Some towers (e.g., wooden towers) provide partial electrical insulation of the conductors from the earth, but even these must be augmented by devices called insulators that provide the bulk of the electrical insulation. Suspension insulators such as the ones that connect tower to conductor as shown in Figs. 2.2.13 are designed for this purpose. These are referred to as “suspension” insulators because they are suspended vertically and carry the weight of the conductor directly but do not provide mechanical support in any other direction. Care must be taken in the design so that insulator characteristics and clearances between conductors and conductors at other voltages or grounded structures are sufficient to withstand voltage surges and lightning even during wind conditions²⁶ as well as to provide sufficient working space and protection of the public (EPRI 1982; Kuffel and Zaengl 1984).

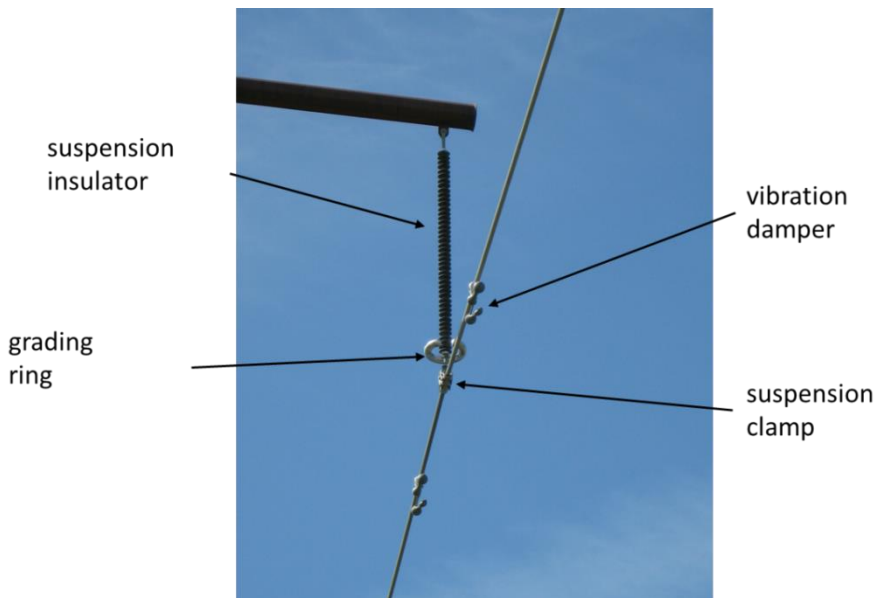


Fig. 2.2.13. Close-up of a suspension insulator with a grading ring and suspension clamp at its bottom. Also shown on the conductor at short distances in both directions away from the attachment point are vibration dampers

²⁶ Wind is accounted for differently for power frequency and switching surge voltages. In the former, the maximum expected swing is used while in the latter, statistical calculations are done since the probability of a simultaneous switching surge and maximum wind swing is very small.

Historically, insulators have been constructed from glass or porcelain, but in earlier days, the designs for such insulators were not sufficient to withstand the desired higher voltages. As discussed in Chapter 1, a fundamental improvement that allowed higher voltages to be used was the cap and pin suspension insulator that allowed individual insulators to be “stacked” together to be able to withstand higher voltages. More recently, polymer insulators have been used and other materials have been considered, but issues about brittle fracture and lack of live-line work methods have caused some utilities to return to porcelain cap and pin suspension insulators. Again, insulation is an area of engineering in itself and has been covered extensively in (EPRI 1982, RUS-USDA 2005). One of the most important topics covered in these references is that overhead transmission lines are exposed to the environment. As a result, insulators can become contaminated with, for example, salt from the sea, chemicals from industrial effluents and automobile exhaust. When combined with water, these contaminants can form conducting layers on the insulators. Hence, (over time) the insulator’s capability to provide the necessary insulation level can be compromised. In fact, it has been shown that insulators (usually due to contamination) are responsible for nearly 70% of the line outages and over 50% of the line maintenance costs (Gorur, 2012). For this reason, insulators are often selected while taking into account the particular environment in which they will be used. In some cases special insulators with semi-conducting coatings designed to be heated by leakage current and keep the insulators dry (and hence reduce the problem of insulator caused outages) are used. In some cases, insulators in severely contaminated environments are periodically washed.

Another issue to note with transmission line insulators is that they may incorporate additional hardware such as the grading rings shown in Fig. 2.1.13 near the bottom of the insulator. The purpose of this grading ring is to more evenly distribute the electric field along the length of the insulator and hence produce an insulation strength that is more nearly proportional to the number of insulator discs in the string. A positive side effect of this is that the electric field is reduced near places where it otherwise may be strong enough to produce corona. A negative side effect is that the critical flashover voltage during fault events may be reduced. The other hardware shown in Figure 2.2.13 on the conductor a short distance away from the insulator is a vibration damper designed to reduce Aeolian vibration.

Conductor sag, direction changes and transpositions

Another characteristic of real overhead transmission lines is that the power line conductors are not horizontal (i.e., they sag under their own weight between towers) as shown in Fig. 2.2.14. This sag is an important design consideration for utilities because the amount of sag is dependent on conductor temperature which (in turn) depends on weather conditions and the amount of current flowing on the line. In fact, there is usually a

maximum allowed conductor sag because of public safety issues and this can, in turn, limit the maximum power flow for that transmission line. The conductor sag also raises questions about the accuracy of electromagnetic field calculations that are based on the assumption of horizontal conductors. An introduction to methods used to calculate sag will be given later in Chapter 8 (House and Tuttle, 1959).



Fig. 2.2.14. A sagging conductor. (courtesy BPA)



Fig. 2.2.15. A “heavy angle” structure at a change in the transmission line direction.
(courtesy J.R. Stewart)

Also, as mentioned earlier, transmission lines are constructed in sections with “heavy angle” or “dead-end” towers at the ends of each section. One

reason for this is to allow transmission lines to change direction as illustrated in Fig. 2.2.15²⁷. It is clear from this figure, that special mechanical design is needed for these structures to ensure mechanical stability. Again, changes in direction such as this beg questions about the accuracy of electromagnetic field calculations that assume infinitely long horizontal parallel conductors.

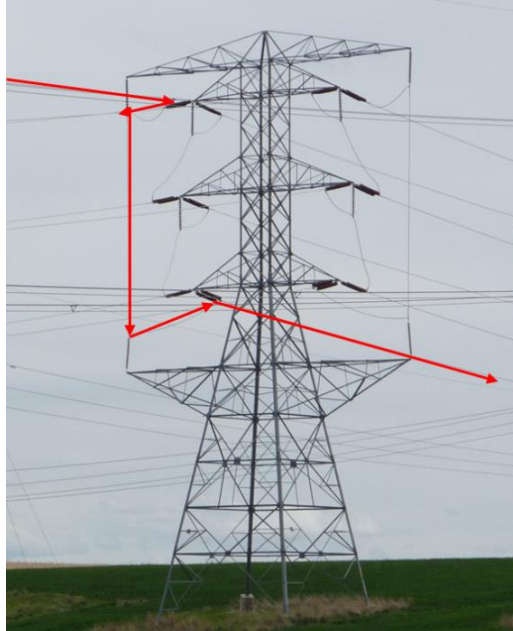


Fig. 2.2.16. A transposition tower designed to reposition the phase conductors on the transmission line in order to balance the currents on long transmission lines (courtesy R. Aho BPA)

Another type of tower that is occasionally seen on long high voltage transmission lines is a “transposition” tower such as the one shown in Fig. 2.2.16. Here, the positions of the three phase conductors with respect to earth are shifted in order to preserve the balance (i.e., relative magnitude and specified 120 degree separation of electrical phasing) of the phase conductor currents as much as possible. Here, the red arrowed line traces the repositioning of an upper phase conductor to the lower position on the tower. It will be shown in Chapter 7 that current balance is lost due to the lack of symmetry of the transmission line conductor configuration and occurs both at the beginning of and continuously along the transmission line.

Terrain, vegetation and river crossings

A further complication is that transmission lines pass through terrain that is not horizontal as illustrated in Fig. 2.2.17. Such realities not only create problems for transmission line designers, but also generate questions about

²⁷ Others are the end of the line, at major crossings such as rivers and at periodic intervals for long lines

the accuracy of electromagnetic field calculations based on the assumption of a horizontal homogeneous earth.



Fig. 2.2.17. An example of a transmission passing through hilly territory



Fig. 2.2.18. Flashover to vegetation from a power line. Although this photo is from a lower voltage distribution line, it illustrates the point that vegetation can cause faults. (courtesy C. Gellings, EPRI)

It is clear in Fig. 2.2.15 that vegetation often grows under transmission lines. Since living vegetation is a reasonably good conductor, it may (given enough time) grow close enough to one or more conductors to cause an arc to ground (i.e., a flashover). Fig. 2.2.18 is a photo of a flashover between vegetation and a power line conductor. Although this particular photo was

taken of a lower voltage distribution line, the same phenomenon occurs on higher voltage transmission lines and has (historically) been responsible for flashovers that have led to system failures. Another related issue is the relatively high electric fields at the tips of vegetation near a high voltage transmission line. These higher electric fields can result in corona from tips of vegetation. For these reasons, utilities have aggressive programs to monitor and control vegetation under transmission lines.

Finally, another feature of transmission line construction is crossings of long distances such as rivers that often require special towers on either side due to the length of the spans. One example is shown in Fig. 2.2.19.



Fig. 2.2.19. River crossing that requires special towers for long spans. (courtesy R. Aho, BPA)

Hardware mounted on a conductor

Many different pieces of hardware are found on transmission line structures and conductors. This topic will be introduced here because these may (in some cases) cause corona and, if so, it may be necessary to either calculate electric fields in their vicinity while developing designs to reduce corona or to do special laboratory testing to evaluate corona performance (Kuffel, et. al. 2001).

The first type of hardware to be discussed here is the hardware used to attach conductors to insulators. Varieties of such hardware can be found in Figs. 2.2.11 and 2.2.13. A view from underneath of the kind of hardware sometimes used at a dead-end tower is shown in Fig. 2.2.20. Somewhat unusual in this photo is the “barrel shaped” object in the upper left-hand corner which is a “wave trap” for a power line carrier communication system. Signals from these systems are used to monitor and control substations from a remote location. Wave traps are signal blocking devices installed in series with one or more of the phases on the transmission line at a tap point to prevent the signal from following the tap line.



Fig. 2.2.20. Transmission Line Hardware. (courtesy R. Aho, BPA)

In Fig. 2.2.21, a close up view of a conductor suspension clamp is shown. Along with the clamp is a section of “armor rod” that surrounds the conductor and is often used to provide mechanical support for the conductor at tower attachment points as shown.



Fig. 2.2.21. A suspension clamp and armor rod used to connect a conductor to a suspension insulator. (courtesy R. Aho, BPA)

Another type of hardware is a splice between sections of conductors that are placed during construction when the conductor on one reel ends and must be connected to the conductor on a new reel of conductor to form a continuous conductor. These are also inserted when the conductor has broken for some reason and the break has been repaired with one or more splices. A close-up view of a splice on a transmission line is shown in Fig. 2.2.22. Generally, splices do not have a large effect on the electric fields of the conductor, but they may have a relatively large resistance if the contact is not good enough and hence, becomes excessively heated.

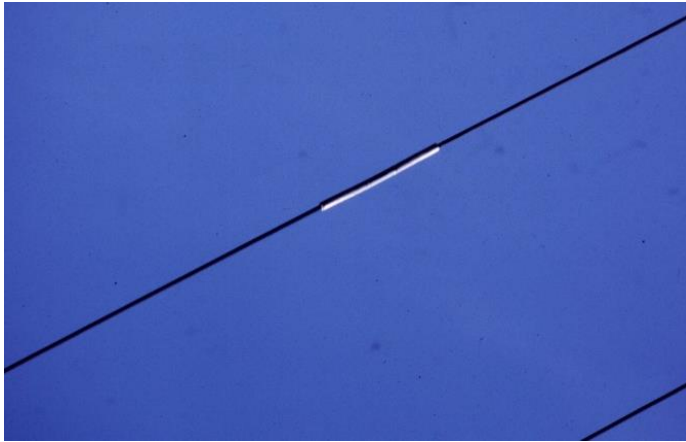


Fig. 2.2.22. A splice on a transmission line conductor. (courtesy J.R. Stewart)



Fig. 2.2.23. Marker ball on power line conductor near an airport.

Near airports or along long river or valley crossings, there is a concern that power line conductors may not be visible to pilots. In order to ensure that the power lines are visible, marker balls are often placed on the conductors. An example is shown in Fig. 2.2.23.

Marker balls are also often used when power lines cross large distances such as over a river where conductors are high and may not be as visible as illustrated in Fig. 2.2.20. Clearly, the marker ball is more visible from a distance than the conductors. As with other hardware on the transmission line, care must be taken to design these so that the effect of corona is minimized.

Power line conductors often experience wind-induced conductor motion such as Aeolian vibration, swinging or “galloping” that can limit the performance and/or lifetime of the transmission line. A variety of devices have been installed on transmission line conductors to reduce the motion

and hence to minimize its effects on transmission line performance. One example is the damper to reduce Aeolian vibration shown on the conductor a short distance away from the insulator in Fig. 2.2.13. Other devices have been developed to reduce galloping (Akagi et. al. 2002).

Finally, another form of hardware found on power lines is environmental control hardware. For example, the “cover” placed over the insulator junction in Fig. 2.2.24 is designed to protect birds from exposure to potentially lethal voltages and currents. Other examples of similar hardware can be found on transmission line systems.



Fig. 2.2.24. Bird control hardware. (courtesy A. Stewart, EDM Intl.)

Grounding of towers

In order to protect the power system and surrounding areas from excessive voltages during faults and lightning strikes, grounds are often provided at towers (IEEE 2000). These are designed to have a low enough resistance to ground that unbalanced currents occurring during faults and currents due to lightning strikes do not cause hazardous voltages to which personnel near the tower are exposed. This is important since the lightning trip out rate is very sensitive to grounding resistance. Although these grounds are generally mostly below the ground and hence, not visible, connections to them are. These include (if the towers are not metallic) the wires that connect shield wires (if any) to the bottom of the structure as well as the connections from this wire to the buried ground. An example of a connection to ground is shown in Fig. 2.2.25. An example of a grounding system to which the ground wire in Fig. 2.2.25 might be connected is shown with a top schematic view of a tower and ground in Fig. 2.2.26. The mesh at each tower leg is below the ground and consists of fat stranded wire often augmented by vertical ground rods.



Fig. 2.2.25. Wire connection to tower ground. (courtesy N. Mullen, BPA)

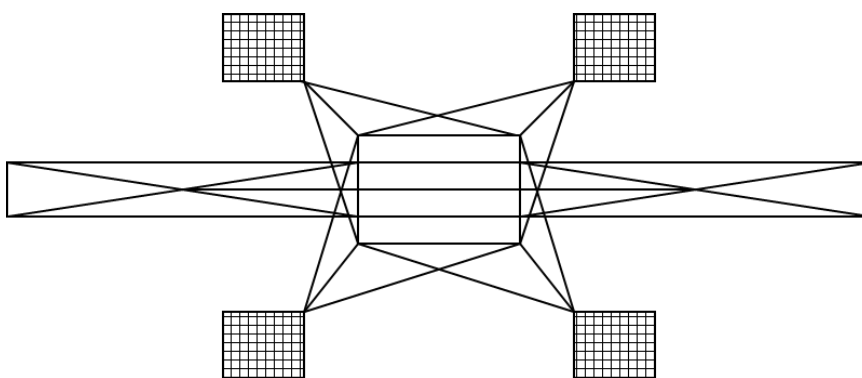


Fig. 2.2.26. Schematic view (from above) of a tower and grounding system that consists of 4 metallic meshes below ground, one connected to each leg of the tower.

Lumped parameter devices along or at the ends of the transmission line

Introduction

Another issue along transmission lines is that there may be lumped parameter devices along it or at its ends that are needed to increase power transfer or to ensure efficient and/or reliable operation of the transmission system. More specific information will be given about several of these devices in Chapter 4 after some foundational theory is introduced. Here, a brief introduction to each will be given.

Series capacitors

One example of a lumped parameter device is a series capacitor as shown in Fig. 2.2.27. These capacitors are placed there because the amount of power that can be transmitted through an electrically short power transmission line is limited by the inductive reactance of the line and this reactance is proportional to the length of the line. The reactance of the series capacitors is designed to (at least partially) cancel the inductive reactance and hence increase the power handling capability of the line. They also can be used to compensate for voltage variations along the line during light loading conditions.



Fig 2.2.27. Series capacitors along a 500 kV transmission line. (courtesy J. Hildreth, BPA)

Surge arresters

Another device that can be found either along its length or at the ends of a transmission line is a surge or lightning arrester such as shown in Figs. 2.2.28 (line arrester) and 2.2.29 (substation arrester). These are nonlinear devices designed to limit the overvoltages on power lines during transients due to lightning strikes and switching events. Surge arresters in substations are nearly universal, but many utilities choose not to use line arresters since they may not be needed or due to maintenance and/or economic issues.



Fig. 2.2.28. Three line surge arresters installed along a transmission line, each connected from an individual phase to ground. <http://www.liveline.co.za/high-voltage-surge.php>
Note one disc missing on the leftmost insulator



Fig. 2.2.29. Three single phase surge arresters installed in a substation. (courtesy of BPA)

Shunt reactors



Fig. 2.2.30. A three phase shunt reactor installed in a substation. (courtesy BPA)

Another device that is relevant to the operation of high voltage transmission line is a shunt reactor as shown in Fig. 2.2.30. These can be used to compensate the capacitive reactive power of (especially long higher voltage) transmission lines (especially during lightly loaded conditions), reduce system-frequency overvoltages when a sudden load drop occurs or there is

no load and to improve the stability and efficiency of the energy transmission.

Circuit breakers

Another device that is found at the ends of high voltage transmission line is a circuit breaker as shown in Fig. 2.2.31. These are used to separate the line from the remainder of the transmission system during maintenance or to clear faults. Operation of these devices is controlled by relays designed to detect faults and to proscribe appropriate action.



Fig. 2.2.31. A three phase circuit breaker installed in a substation.

Transformers

The final device illustrated here in Fig 2.2.32 is a three phase power transformer. As mentioned earlier, the purpose of these is to change the voltage level of whatever is connected to each end of a transmission line (e.g., a generator, another transmission line or the distribution system) to the desired voltage level for transmission line. The purpose is to transmit power more efficiently over long distances by using the highest reasonable transmission line voltage.



Fig. 2.2.32. Three phase 230 kV – 115 kV power transformer. (courtesy BPA)

2.3 Services that Share the Right of Way

Introduction

Given the increasing density of both population and buildings, long uninterrupted corridors of land are not as readily available as they once were. Because of this, other services that need these corridors (e.g., railroads, pipelines and optical communication systems) often share or request to share a right-of-way with a power transmission line. When this happens, there is always a question about the compatibility between these systems that is related to the electromagnetic field environment of the power line.

Railroads

The railroad/power line corridor shown in Fig. 2.3.1 is an example (AAR/EEI 1977;IEC 2003) of a railroad and high voltage transmission line that share a right-of-way. In cases like this, the potential exists for interference between the power line and the railroad crossing guard system shown due to inductive coupling with the track signaling circuit as well as other signaling and communication systems. In addition, there will be concerns about personnel safety both during normal operation and during fault conditions. More about these issues can be found in Chapter 10.



Fig. 2.3.1. A railroad and a power line that share a corridor. (courtesy B. Cramer)

Pipelines

A second service that commonly shares power line rights-of-way is pipelines (usually underground) as shown in Fig. 2.3.2 (Bonds 1999; CEA 1994). In cases such as this, there are concerns that voltages induced on the pipeline

can cause electrical shock hazards, ignition of gas in case of leaks, corrosion at locations for which the pipeline is above ground or damage to insulating flanges designed to electrically isolate sections for cathodic protection. Such interference can occur because while the pipelines are buried, the earth is transparent to the transmission line's magnetic fields. More about these issues can be found in Chapter 10.



Fig. 2.3.2. Although not evident because most pipelines are buried, there is a buried pipeline to the left of the transmission line in this photo. (courtesy, J. Dabkowski)

Optical fiber communication



Fig. 2.3.3. Optical fibers inside of an optical ground wire (OPGW).
[http://www.aflglobal.com/Products/Fiber-Optic-Cable/OPGW/HexaCore-Cable/HexaCore-Optical-Ground-Wire-\(OPGW\).aspx](http://www.aflglobal.com/Products/Fiber-Optic-Cable/OPGW/HexaCore-Cable/HexaCore-Optical-Ground-Wire-(OPGW).aspx)

In recent years, many utilities have installed optical fiber communication systems on their transmission systems. In some cases, optical fibers are placed within shield or “ground” wires. Such shield wires are called optical ground wires (OPGW). Lightning and large fault currents are the biggest threats to these (Austin 1984; Zischank and Weisinger 1997).

A photo of an OPGW cable is shown in Fig. 2.3.3. Here it is shown that the fibers are placed at the center of the cable and hence designed to be protected from lightning by the outside wires. Despite this design, lightning strokes with the right characteristics can damage these shield wires.

Another type of system is an “all dielectric self-supporting” (ADSS) cable that is generally suspended somewhere beneath the phase conductors such as shown in Fig. 2.3.4 (the cable that turns in this figure is ADSS). Threats to these include dry band arcing and corona on attachment hardware (Carter and Waldron 1992; Tuominen and Olsen 2000). The former is controlled by careful placement of the cable and the latter by devices placed on the cable such as the “corona coil” shown in Fig. 2.3.5. Again, the issue of compatibility between high voltage transmission lines and ADSS cable is considered in more detail in Chapter 10.

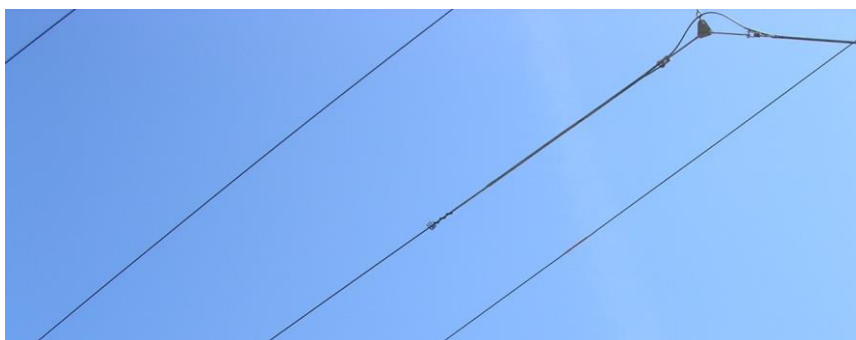


Fig. 2.3.4. An ADSS communications cable below three phase conductors. It is the second conductor from the bottom in the figure (i.e., the one that changes direction).

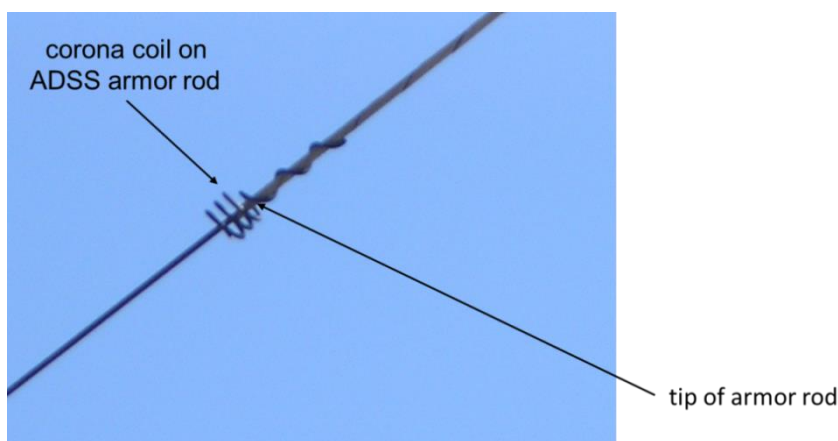


Fig. 2.3.5. A “corona coil” placed on an ADSS cable to reduce corona activity near the tip of the armor rod.

Wireless communication

Another service that is more commonly found to share transmission line facilities is wireless communications base stations such as the one shown in

Fig. 2.3.6. Such locations are desirable for wireless companies since they can install antennas on existing towers. Here, several antennas have been placed on a transmission line tower and the RF electronics and switching equipment is placed in a small building at the base of the tower. It has been shown that the power frequency electromagnetic fields can interfere with the operation of instruments used to measure the radio frequency (RF) fields and that common grounding systems can cause unintended voltage pulses on distribution systems during faults (Olsen and Yamazaki 2005).

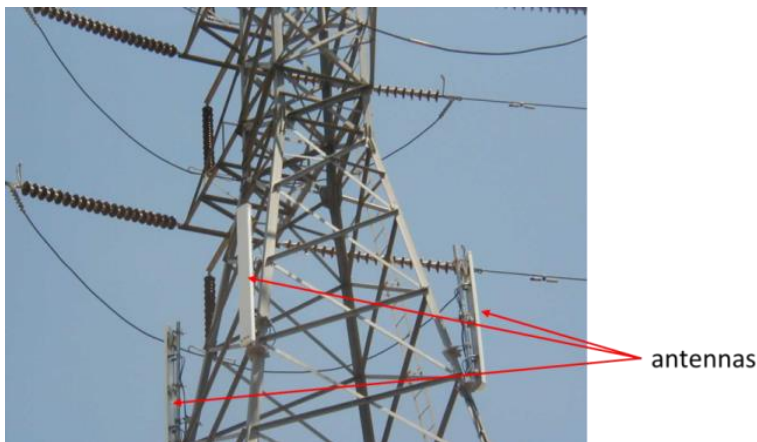


Fig. 2.3.6. Wireless communications antennas on transmission line tower (courtesy R. Tell)



Fig. 2.3.7. Transmission line with nearby AM transmitting antennas in background. (courtesy T. Osborn, BPA)

AM broadcast stations such as the one shown in the background of Fig. 2.3.7 radiate electromagnetic fields that can interact with the transmission line system. One consequence is that re-radiated electromagnetic fields from the transmission system can cause deviations in the legally required radiation pattern of the broadcast antenna (Madge and Jones 1986). Another is that

the radiated fields can cause significant high radio frequency (RF) voltages on transmission line conductors especially when they are being installed. Without some care taken in work practices, these can lead to RF burns to exposed workers (Olsen et. al. 2011).

Distribution underbuild



Fig. 2.3.8. Distribution underbuild.

Next, it is often true that distribution lines share towers with transmission lines as shown in Fig. 2.3.8. This is often called, “distribution underbuild.” In these cases, care must be taken that the National Electric Safety Code is satisfied and that excessive voltages are not induced on the distribution lines during faults (IEEE 2002).

Human occupancy

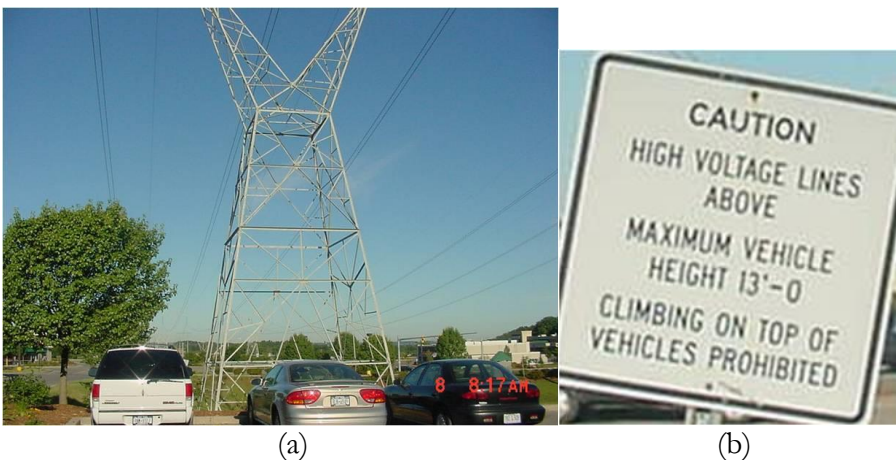


Fig. 2.3.9. (a) Power line over a parking lot. (b) warning sign. (courtesy M. Tuominen, BPA)



Fig. 2.3.10. Non permitted structure constructed near transmission line. (courtesy R. Aho)

Power lines often are constructed near other facilities and can cause potential safety issues. One example is a power line constructed over a parking lot as shown in Fig. 2.3.9a. Here, the electric fields from the power line cause voltages to be induced on the cars and, hence shocks to people when they touch the cars (EPRI 1982). This must be managed as (for example) indicated by the warning sign illustrated in Fig. 2.3.9b. Another is the occasional construction of non-permitted structures such as the playhouse shown in Fig. 2.3.10²⁸. Clearly, these are of concern to electric utilities and can present true safety hazards.

Other compatibility issues

Finally, while not explicitly covered here, there are issues with a variety of other systems that share the right-of-way. These include irrigation systems, GPS navigation devices using VLF augmentation and broadband over the power line (BPL) communication issues (Olsen and Heins 1998; Silva and Whitney 2002; Tengdin 1987; Tesche, et. al. 2003, Galli et. al. 2011).

2.4 Environmental Issues

Introduction

All of the above photographs and nearly all of the discussion relate to power transmission lines in reasonably good weather conditions. But, power lines are outdoors and hence subject to a wide variety of weather conditions. These cause everything from ice on conductors that leads to excessive sag, corona in rain and snow that generates electromagnetic interference, to resistive leakage on insulators caused by contamination plus moisture that

²⁸ This structure was later removed at the request of the local utility

can lead to failure, to lightning strikes that may cause line failure to icing of conductors that can cause excessive sag. These issues and many others must be accounted for in designing power transmission lines.

Ice and snow



Fig. 2.4.1. Iced insulators after a snowstorm resulting in tower failure. (courtesy BPA)

Examples of power lines in ice and snow are shown in Figs. 2.4.1. – 2.4.2 It is clear from Fig. 2.4.1 that snow can cause tower failure as well as insulator failure during melting and from Fig. 2.4.2 that ice loading on conductors can cause excessive sagging of conductors.



Fig. 2.4.2. Iced conductors in a winter storm that caused conductors to sag. (courtesy BPA)

Rain

In rain, water drops form on conductors and hydrophobic insulators such as the one shown Fig. 2.4.3. On conductors, these drops lead to a significant increase in corona activity and hence to electromagnetic interference and audible noise as shown in Fig. 2.4.4. Water on contaminated insulators can

lead to flashover and insulator failure. (RUS – USDA, 2005). In addition, water on non-ceramic insulators can cause material degradation and premature failure (Phillips et. al., 1999).



Fig. 2.4.3. Rain on a transmission line insulator. (<http://www.bing.com/images/>)

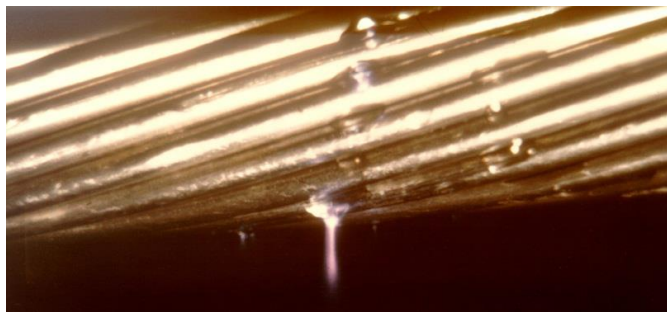


Fig. 2.4.4. Corona discharge on a rain droplet on an energized transmission line conductor (courtesy EPRI)

Lightning

Lightning strikes to transmission lines and currents induced by nearby lightning such as that shown in Fig. 2.4.5 are common. If transmission lines are not properly designed these strikes and induced currents can lead to trip out of the transmission line as well as cause safety hazards to personnel who are near transmission line towers. More about how lightning models can be used to calculate lightning induced currents on transmission lines and how injected lightning currents propagate on transmission lines can be found in Chapter 7.



Fig. 2.4.5. Lightning near a transmission line.

<http://ts3.mm.bing.net/th?id=H.4580600666718958&pid=1.7&w=121&h=138&c=>

Wind



Fig. 2.4.6. Conductor galloping in wind <http://i.ytimg.com/vi/IfhfsjFG0jo/0.jpg>

During windy conditions, Aeolian vibrations, galloping and conductor swinging can occur. An example of galloping in wind is shown in Fig. 2.4.6. Aeolian vibrations are caused by the interaction of aerodynamic forces generated as the wind blows across the conductor with the conductor's natural mechanical vibration frequency (Lu et. al. 2007). This wind induced vibration can cause cracks on the conductors due to fatigue particularly where the conductors are fastened to the insulators by means of clamps. This kind of vibration can be minimized by the use of dampers clamped to

the conductor as shown in Fig. 2.2.13. When the conductor vibrates, the weights dissipate the vibrational energy. Gallop vibrations are low frequency, high amplitude vibrations and can result in breaking of the conductor or flashover if the conductors come too close to each other during oscillations (Fu, 2012). Swinging is the result of steady forces on the conductors that push them in the direction of the wind. The major impact of this phenomenon is to require larger clearances between the conductor and either towers or other conducting structures (IEEE 2002).

Fire

Fire near a power line such as shown in Fig. 2.4.7 can affect its performance since fire causes a significant amount of ionized particles in the air that affect its conductivity and hence its ability to withstand the high electric fields in its vicinity (Fonseca et. al. 1990).



Fig. 2.4.7. A fire near a high voltage transmission line. (courtesy of BPA)

In addition to the direct effect of fires on high voltage transmission, it is known that under certain environmental conditions (e.g., moisture after prolonged dry spell) fires can be started on wood poles that support high voltage transmission lines (Lusk and Mak, 1976).

Geomagnetic induced currents

Quasi-DC electric currents are created in the ionosphere by solar activity in space. During severe solar weather, these currents can be large enough to cause visible colored light (aurora borealis) such as shown in Fig. 2.4.8 and (more importantly for power engineers) can cause induced currents in power lines that can (among other things) cause transformer cores to saturate and generate unwanted harmonics on the system. Further information about

these currents along with a method for calculating them can be found in Chapter 7.



Fig. 2.4.8. Aurora near power line. http://images.nationalgeographic.com/wpf/media-live/photos/000/244/cache/northern-lights-solar-flare-power-line_24418_600x450.jpg

Landslides, earthquakes, volcanoes, and windblown material

Landslides and Earthquakes can have a dramatic effect on transmission and distribution lines. As indicated in Figs. 2.4.9 and 2.4.10, towers may collapse resulting in line outages.



Fig. 2.4.9. Landslide damage to a power line. The Exponent Telegram <http://www.theet.com>. Staff photo by Darlene J. Swiger

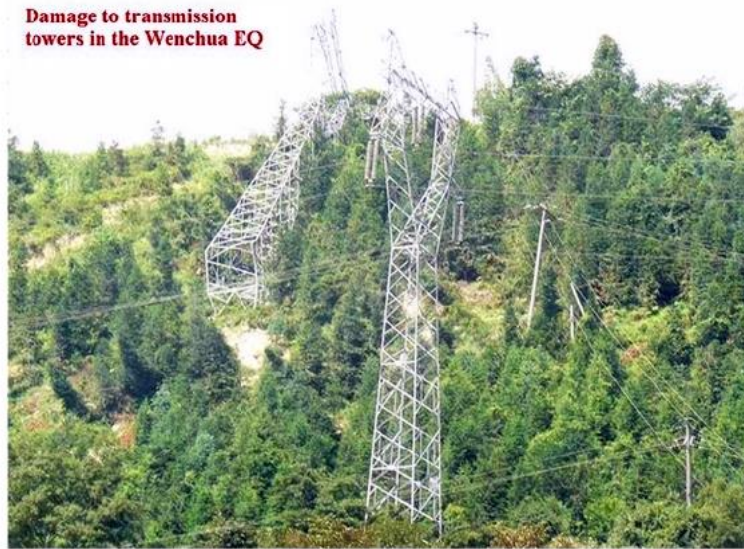


Fig. 2.4.10. Earthquake damage to transmission line towers.
<http://www.hindawi.com/journals/mpe/2013/829415/fig1/>

The fall of volcanic ash as illustrated in Fig. 2.4.11 can also have a negative impact on the operation of overhead transmission lines (Wardman et. al., 2012). More specifically, it may (in the presence of moisture such as rain) lead to insulator flashover, as well as to increased corona activity (e.g., audible noise and radio interference and mechanical damage to moving parts).



Fig. 2.4.11. Volcanic ash that can impact the operation of high voltage transmission lines.
http://skywalker.cochise.edu/wellerr/students/Los-Alamos/earthquake_files/image001.gif

In addition to volcanic ash, a variety of other solid material can be carried by the wind. This can include dust that is either conductive by itself or conductive when wet. An example of windblown material (i.e., tumbleweeds) common in the western United States in a substation is shown in Fig. 2.4.12. Other examples could be sand and dust (Yu et. al. 2006).



Fig. 2.4.12. Windblown tumbleweeds in a substation. (Courtesy of BPA)

2.5 Rationale for Physical Assumptions and the “Gold Standard”

It should be clear at this point that real power lines are quite complicated structures. Hence, before reasonably simple mathematical models can be developed, simplifying physical assumptions must be made. That is the subject of this section.

As mentioned briefly in the Foreword to this text, **mathematical analysis of physical systems is useful for one of two reasons:**

- To **provide insight** into the dependence of measurable quantities of interest on certain parameters (e.g., the fact that the 60 Hz electric field usually decays laterally away from a power line as the inverse of the distance squared can easily be understood by appealing to mathematical analysis)
- To **eliminate the need for** setting up and performing (often very time consuming and expensive) **experiments**.

However, as also mentioned in the Foreword, **no theory is useful at all unless it is validated** well enough for the user to have confidence that it can be used to predict the results of some experiment that is well specified and can (in principle) be performed. Hence, ultimately, measurements are

usually the “gold standard” by which any theory is validated. It is, of course, recognized that no measurement is completely accurate and that this issue should be noted and used in the determination about whether measurement and theory agree. Also, in some cases, “gold standard” could refer to an exact closed form solution to a canonical problem.

The overall purpose of this text, then, is to introduce mathematical analysis techniques to study the electrical design and operation of high voltage overhead transmission lines. Of specific interest is the calculation of measurable quantities used to characterize overhead transmission lines such as the distribution of voltage and current along the lines as well as the electromagnetic fields associated with them. These can be used, for example, to determine how the power flow along a specific transmission line can be maximized, or to determine if the operation of a transmission line is compatible with another system that occupies the right-of-way. The mathematical analysis is used to develop appropriate relationships between these measurable quantities and specified physical parameters (e.g., conductor locations and sizes, materials used and earth electrical properties). Each of these measurable quantities is then used to characterize the operation of these transmission lines.

The first purpose of this portion of the chapter is to summarize the characteristics of real transmission lines that were discussed in more detail earlier. This is done in Section 2.6. Given the fact that the geometries and other relevant electrical properties of real transmission lines are very complicated, it should be clear that **numerous physical approximations to real transmission lines must be made before an “idealized” problem is realized** for which realistic mathematical analysis can be attempted. This leads, then, to the second purpose of this portion of the chapter; to identify the physical approximations that are usually made to the real physical problem prior to mathematical analysis of idealized problems. This is done in Section 2.7.

It will be shown in subsequent chapters that, in many cases, exact closed form solutions for the measurable quantities associated with these idealized problems can be found. However, it is also shown that simple (and often sufficiently accurate) approximate solutions for these same variables can be found. In developing these approximate solutions, it is usually possible (as will be done in this text) to identify conditions under which the simple approximate solutions to the idealized physical problem are valid.

It is, however, usually not as easy to characterize the differences between solutions for the real and idealized high voltage overhead transmission lines. When attempted, it is usually done in one of two ways. First, in some cases, the idealized problem can be modified in some way (e.g., use of a two layer earth rather than a single layer earth) that still allows for an exact solution. A comparison of the solutions to the original (i.e., “idealized”) and modified problems can be used to determine the conditions under which the simplified geometry is acceptable. In this case, the modified problem is the

“gold standard.” If not acceptable, the solutions to the modified problem can be used to provide more accurate solutions. Several examples of such modified problems are given in this chapter. A second method is to compare theoretical solutions to careful measurements made on the original system for which physical approximations have (obviously) not been made. In this case, measurements are the “gold standard.”

As much as is practical, care will be taken in this text to quantify the range of errors that have been introduced by making both physical and mathematical approximations. It is important to understand when the differences between real and idealized transmission lines either are not important or result in significant inaccuracies for calculations using idealized transmission lines. Some initial comments on this topic are given in Section 2.8.

Next, a survey of some techniques that have been used in the past to relax the physical assumptions made in the initial canonical problem described in Section 2.7 is given in Section 2.9. Solutions to these problems can be used in two ways. First, and as mentioned earlier, by comparing solutions of physically modified problems with those of unmodified problems, it may be possible to validate the former. For example, it can be shown (in most cases) by using the solutions to single conductor over a two layered earth that the 60 Hz. electric field just above the earth’s surface is essentially insensitive to the specific assumed vertical distribution of earth conductivity. Hence, a single layered earth model is adequate. In fact, it is quite accurate in this case to assume that the earth is perfectly conducting. Second, if it is shown that the modified problem produces significantly different results than the unmodified problem, it should be clear that the solution to the modified problem should be used. For example, it can be shown that a two layer earth model is necessary for many calculations of subsurface electric field that relate to substation grounding problems (Meliopoulos, Webb and Joy, 1981).

Finally, a number of simple techniques are described that can be used to estimate when solutions for idealized transmission lines are satisfactory. Last, a summary of “rules of thumb” often used for identifying parameters to be used in simple models of transmission lines is given.

2.6 Brief Review of Real Overhead Power Transmission Line Construction

Most real power transmission lines consist of multiple parallel “phase” conductors (that may consist of two or more subconductors) energized to the rated line voltage and (in many but not all cases) periodically grounded shield wires above the phase conductors. The phase conductors (or subconductors) usually consist of many “strands” of wire wound together in a cable and hence do not have a smooth surface. The (usually three or more) phase conductors and shield wires (collectively called a power transmission

line) are located above the earth. Each transmission line extends over a finite distance between two end points (usually substations). In nearly all cases, the horizontal orientation (e.g., east, south etc.) and the elevation of the power line is not the same all along the entire distance. In addition, the orientation with respect to the vertical also changes along its length since the terrain over which the line passes can be hilly or even mountainous. Finally, vegetation above the earth may be important. It may interfere with the operation of the transmission line as it grows taller and/or may also influence the electric fields near the earth's surface.

The electrical properties of the earth below the transmission line are usually inhomogeneous both as a function of depth as well as position along the length of the transmission line (e.g., the permeability and conductivity of the earth vary with soil type as well as between land and water). In some relatively rare cases (such as near iron ore deposits) the earth may be magnetic. If the electrical current density induced in the earth by the power line is large enough (such as near a grounding electrode during a fault), the earth may also exhibit non-linear properties caused (in part) by excessive ohmic heating. The author is not aware of any model (relevant to power lines) in which the earth is (or needs to be) assumed to be anisotropic.

The conductors of the transmission line are suspended in the air by structures (e.g., towers) that may be constructed of wood, steel or some other material. Steel towers and shield wires are generally connected to a grounding electrode. Towers are of several types including the "suspension" towers, "dead end" towers and transposition towers described earlier in this chapter. Insulators are used to mechanically connect to and electrically separate the phase conductors from the structure (and the earth) while shield wires are (usually) connected to the structure and to a grounding electrode buried in the earth. Because the conductors are suspended only at the points where they are attached to insulators that are in turn connected to towers, they "sag" between towers. The specific amount of sag can vary quite a bit since with time since it is a function of the amount of current on the line (through ohmic heat generation in the conductors) and local weather conditions in addition to the conductor weight per unit length, the mechanical properties of the conductor material and the tension to which the conductor is installed.

Located along the power line and connected to it are a variety of pieces of hardware including insulators and tower attachment hardware, splices between sections of conductor, devices to control mechanical vibration, devices to protect animals and birds and devices to provide warning to airplanes and others of the power line's existence. These may be supplemented by lumped elements such as series capacitors and surge arresters designed to limit the voltage during surges. Also, towers may play host to devices such as wireless communication antennas or aircraft warning lights. Finally, the path followed by the transmission line may be shared by other power lines (on the same or separate structures) or another service such as a railroad, a pipeline or communication line. In some cases (such as

optical fiber cables) the transmission line towers may be shared. The presence of the transmission line and its associated electromagnetic fields may lead to interference between it and any one of these services.

An example of a transmission line that illustrates several of these characteristics of real transmission lines is given in Fig. 2.6.1. Shown in this photograph is a double circuit transmission line with sagging phase conductors and multiply grounded shield wires that is located over irregular terrain, that changes direction and is located near another transmission line on separate structures. Further, there are trees near the right of way that can affect the electromagnetic fields associated with the transmission line. Steel towers distort the electric field near them and insulators affect the electric fields in their vicinity. Finally, in the distance is an AM broadcast antenna (visible slightly to the left of the closest tower) that may cause significant radio frequency electromagnetic fields in the vicinity of the transmission line.



Fig. 2.6.1. Real power line that will shortly be modeled using simplifying physical assumptions (courtesy R. A. Tell)

In summary, the typical power line is a “messy” system. Mathematical analysis of the exact system appears to be almost impossible. For this reason, physical approximations are made and it is important to consider the consequences of making these approximations. It is probably, for example, not reasonable in most cases to carry out calculations to four significant

figures after the earth has been assumed to be perfectly flat and conductor sag has been ignored. The use of either mathematical or physical experiments to either increase confidence in the final results or to “calibrate” them so that they can be used for calculations on real systems is another important topic.

2.7 Summary of the Physical Approximations Generally Made Before Analysis

To analyze typical real transmission lines, numerous physical approximations must be made before a canonical²⁹ mathematical problem can be obtained. These approximations are:

- The earth is assumed to be flat, homogeneous, linear, isotropic and (usually) non-magnetic
- Towers and insulators are simply ignored
- Stranded conductors are approximated as smooth homogeneous conductors and conductor bundles may be approximated as smooth conductors of some “equivalent radius”
- The phase conductors are assumed to be perfectly horizontal, straight and infinitely long (i.e., transmission line terminations, transpositions, conductor sag, changes in direction and altitude changes are ignored).
- The shield wires are often (but not always) ignored.
- All hardware connected to the system is ignored.
- Any systems that share the right-of-way with the transmission line are ignored.

A diagram of a simple idealized and mathematically tractable power line for which all of the above approximations have been made is shown in Fig. 2.7.1. This can be contrasted to the real transmission line that is shown in Fig. 2.6.1. Clearly there are differences between the idealized and real power lines. Given this, it is important to understand the relationships between the calculations made using the idealized line and measurements on the real line.

²⁹ Here, canonical is taken to mean a problem for which it is possible to develop a mathematically exact solution in closed form (i.e., it is not necessary to use a numerical method to develop the formal solution). Note that it still may be necessary to use numerical methods to evaluate the formal solution.

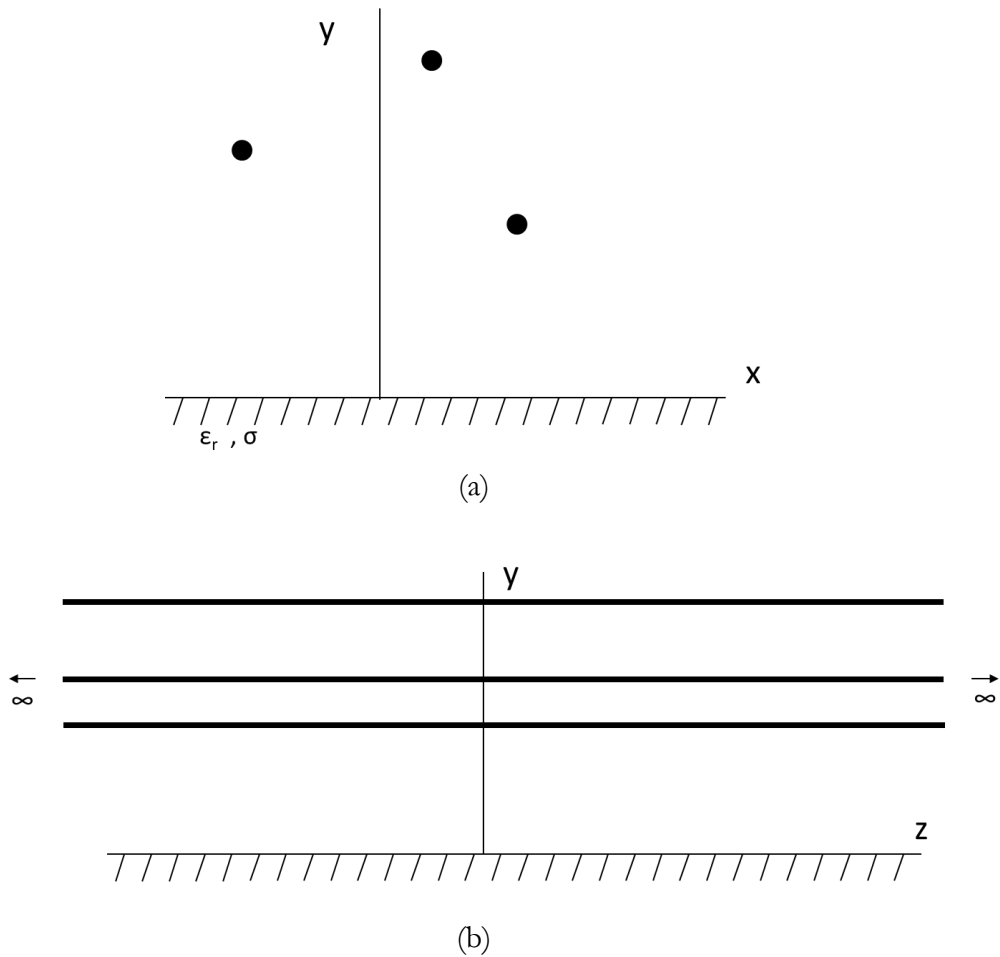


Fig. 2.7.1. Idealized geometry of a power line used for analysis. (a) cross sectional view, (b) side view

2.8 Comments on the Validity of Solutions Based on Simplifying Physical Approximations

Ultimately the reason why a theory is constructed and used to calculate predictions of voltages, currents, electromagnetic fields etc. is to eliminate (or severely restrict) the need to conduct an extensive set of (generally very expensive) measurements. However, as mentioned earlier, unless there is confidence that 1) there is a well-defined transmission line system on which measurements could have been done to generate equivalent results and 2) the calculations are actually “equivalent” to measurements that could have been done on this system, there is no reason to pursue the theory. It is imperative that calculations be understood in terms of an experiment that could have

been done and that there is confidence that the results are the same (within certain accuracy limits) to those that would have been measured.

Again, the most important test of a theory is the comparison of it to careful measurements. This is certainly true for the case of calculations based on power transmission line models similar to those discussed in the last section. Whether this comparison is successful may depend on the specific variable calculated, the number and type of additional mathematical approximations made in obtaining the solution, the range of parameters over which the variable is computed and the accuracy of the measurement. For example, if one is only interested in the voltage and current at the ends of a transmission line at power frequency, the results of making the approximations in Section 2.7 are generally adequate. The same calculation method, may, however, not be appropriate for calculating voltage and current on a dc transmission line (especially in the monopolar mode) because the portion of the series impedance due to the earth is affected by earth electrical properties deep in the earth that may not be modeled properly. In addition, the simplifying assumptions in Section 2.7 are clearly not good enough for calculating the electric field near a tower because the tower has a significant influence on the electric field near it and cannot be neglected.

As mentioned earlier, the idea of a “gold standard” to which all calculations will be compared is often raised. Sometimes this may refer to a very carefully controlled and conducted experiment. Other times it may refer to an exact mathematical solution to a problem for which physical approximations have been made. In any case, the term “gold standard” always refers to a solution to a problem that is well defined and for which there is great confidence in the accuracy of its results. In many cases, problems are solved that do not have an exact solution, but the gold standard is used to validate the solution to the more general problem when parameters are selected for which it is directly comparable to the “gold standard.” For example, one might compare the results for the magnetic field of a sagging conductor with those for a perfectly horizontal conductor in the special case for which the sag is assumed to be zero. A successful comparison of these two solutions is a necessary but not sufficient proof that the general solution is correct. Nevertheless such comparisons are very useful tools. In summary, whenever possible a “gold standard” should be used to establish the validity of a new calculation.

An interesting example of how measurement can guide theory occurs in the history of radio noise theory development. From the beginning, it was assumed that the (approximately 1 MHz) electric and magnetic fields associated with radio noise could be calculated using the same theory as used to calculate the (nearly static) 60 Hz electric and magnetic fields. One characteristic of these fields is that they decay as one over the distance squared laterally away from the transmission line. Unfortunately, measurements showed that the radio noise fields decayed at a rate smaller than one over the distance squared. It was not until a more sophisticated theory that more

accurately accounted for the earth's finite conductivity was used that comparisons of theoretical and measured lateral radio noise profiles came into agreement.

2.9 Survey of the Techniques that Extend Solutions to More General Problems

New research is often suggested by recognizing that approximations made in existing work restrict the applicability of theory derived using those approximations. Thus, a new problem is often identified by relaxing one or more of the assumptions and solving the modified problem. For example, the conditions under which the use of a single layer earth is satisfactory can be identified by studying a two layer earth model. The same two layered earth model can be used in cases for which it is necessary to achieve reasonable accuracy. In the following subsections, several problems like this will be described.

Two layered earth

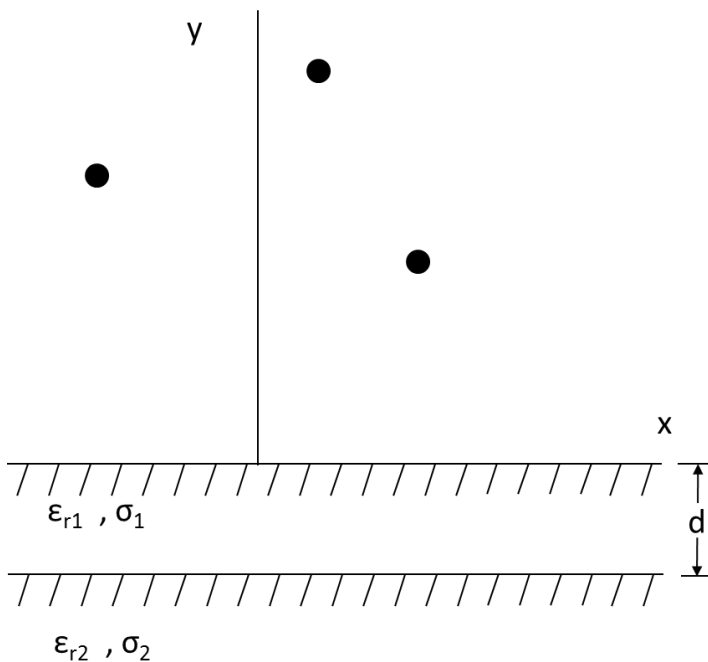
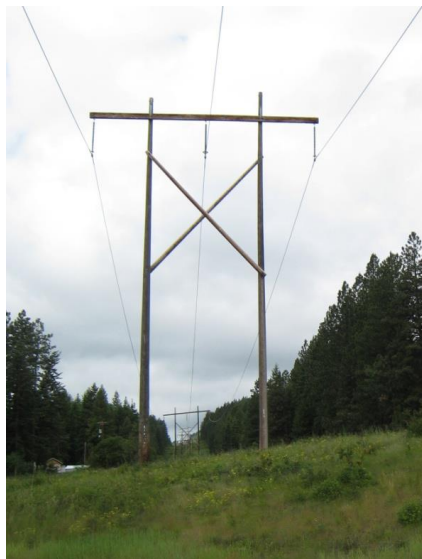


Fig. 2.9.1. Power line over a two layered earth.

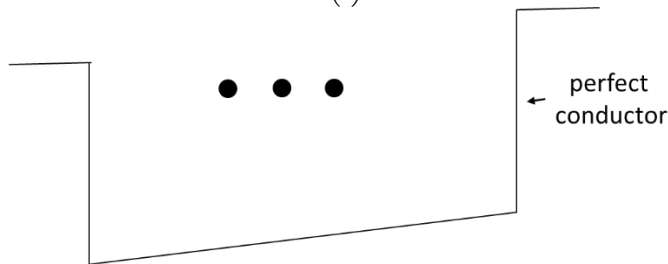
As mentioned briefly above it is usually assumed that the earth is a single layer homogeneous medium. Whether this is sufficient for any situation may be studied by considering the two layered earth model shown in Fig. 2.9.1

(Anderson, 1976). In this figure the homogeneous earth that was earlier characterized by permittivity and conductivity ϵ_r and σ respectively had been replaced by an inhomogeneous two layered earth with the first layer of thickness d characterized by permittivity and conductivity ϵ_{r1} and σ_1 over a second infinitely thick layer of earth characterized by permittivity and conductivity ϵ_{r2} and σ_2 . Based on these studies, it can be shown that a single layer earth model may not be appropriate for problems related to calculating earth losses or dc transmission or geomagnetic induced currents. In these cases the problem defined in Fig. 2.7.1a can be used as an alternative to that shown in Fig. 2.9.1.

Effect of terrain and vegetation on electric field calculations



(a)



(b)

Fig. 2.9.2. Calculation of power line electric fields near non horizontal terrain with trees at the edge of the right of way a) the real transmission line b) the approximate model for electrostatic calculations.

It has been found that the problem shown in Fig. 2.7.1 cannot be used to accurately examine the electric fields in space surrounding the power line in

Fig. 2.9.2a because the land is not horizontal and trees at the edges of the “right-of-way” can be good conductors at power frequencies. Hence, the flat earth assumption is not valid. Instead the problem shown in Fig. 2.9.2b could be used for the purpose of studying the effect of vertical trees at the edge of the right-of-way (Simpson and Brice, 1987). This problem could be done using a numerical method to solve electrostatic equations for the electric field as discussed in Chapter 6. Note that if vegetation can be assumed of uniform height over the right-of-way, the effect of vegetation growth over time can be studied by reducing the height of the conductors.

It should be noted that it is not necessary to perform a similar calculation for magnetic fields. This is because (as will be shown later) the earth (or vegetation such as trees) has little effect on the magnetic fields of a 50/60 Hz transmission line and can usually be ignored.

Effect of conductor sag on magnetic fields

There have been instances for which it is important to know the magnetic field of a sagging conductor more precisely than is available by assuming the conductors to be purely horizontal and infinitely long. In this case, the geometry shown in Fig. 2.9.3 can be used to replace the geometry shown in Fig. 2.7.1b (Mamishev, Nevels and Russell, 1996). The first use of this problem is to validate the use of horizontal conductors when this is permissible. For example, the further the calculation or measurement point is from the transmission line, the more reasonable it is to use infinitely long horizontal conductors as long as the calculation point is not near to a change in direction of the transmission line. When more precision is needed, the method used to solve this problem is to divide the conductors into short segments and to calculate the total magnetic field by superimposing the magnetic fields of each of these segments.

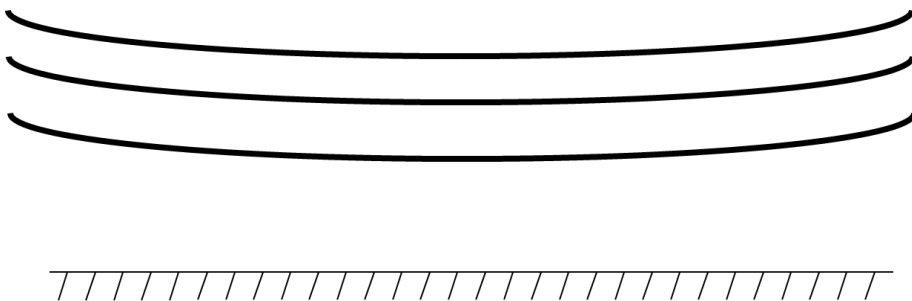


Fig. 2.9.3. Power line with sagging conductors

Electric fields near a bundled conductor

As will be shown later in Chapter 4, a bundled conductor (i.e., two or more subconductors) is usually approximated as a single equivalent conductor. But there are times (e.g., calculating the surface electric field needed for

electromagnetic interference calculations when it is necessary to know the electric fields on the surface of individual subconductors. In these cases, the problem shown in Fig. 2.9.4 can be solved (Sarma, M.P. and W. Janischewskyj 1969).

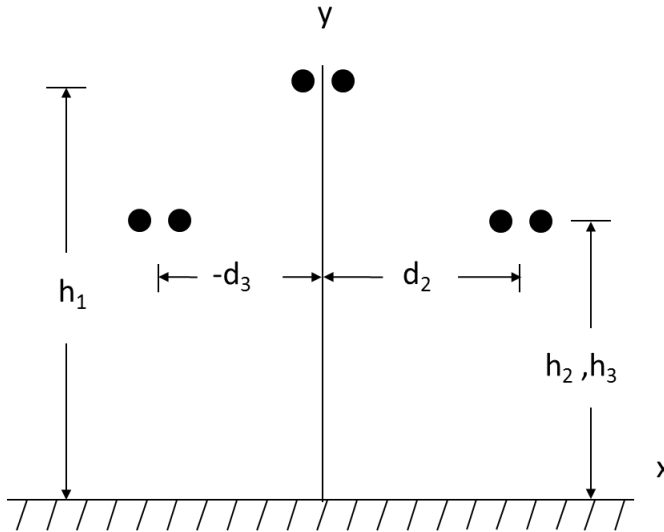


Fig. 2.9.4. A power line with conductor bundles shown explicitly.

Effect of a tower on the electric field

In some cases, it is important to be able to calculate the electric field near a tower. In that case, a simple model such as that shown in Fig 2.9.5 can be used (Olsen, 1999). This problem shown is an example of a very crude model for a tower window, but one that can be solved analytically if the toroid is far from the earth compared to its diameter. More about this problem can be found in Chapter 6.

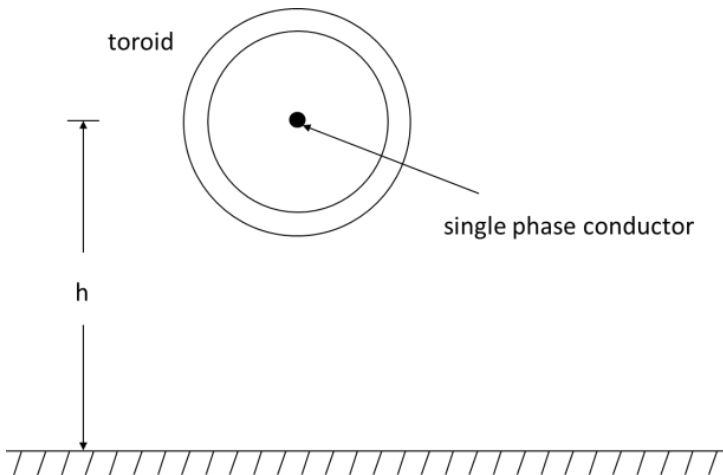


Fig. 2.9.5. Simple model of a tower window that allows analytic calculation of perturbed electric fields for a single conductor transmission line above earth

The effect of tower geometries much more complicated than the one shown in Fig. 2.9.5 can be analyzed using the numerical electrostatics techniques described in Chapter 6. An example of a method for determining the electric field to which the worker on the tower in Fig 2.9.6 is exposed is given by Olsen et. al. (2007).

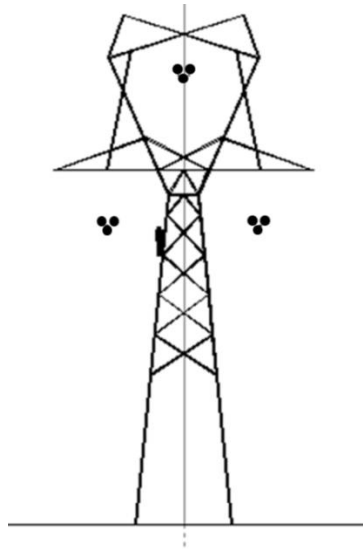


Fig. 2.9.6. Tower model used to calculate the electric field to which a worker (shown on the left side of the tower) is exposed when climbing a tower.

Use of lumped circuits as approximations

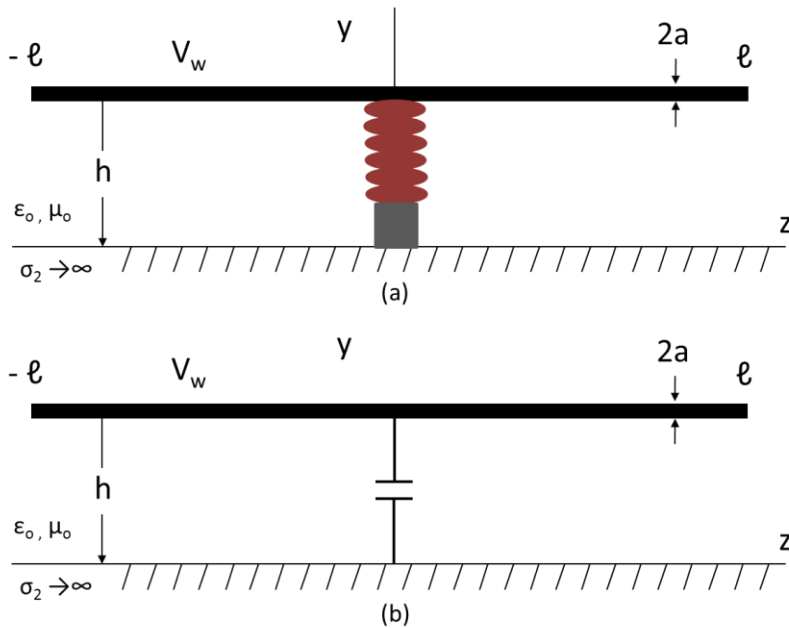


Fig. 2.9.7. Insulator supporting a conductor above ground a) explicit insulator b) equivalent capacitor useful for calculating the currents and voltages along a conductor with multiple insulators.

In many cases, hardware of complex geometry is approximated by a circuit element in order to calculate the current and voltages along a transmission line. For example, the insulator geometry shown in Fig. 2.9.7a can (for purposes of calculating its effect on the voltage and current along the transmission line) be replaced by the capacitor in Fig. 2.9.7b. Using this kind of an approximation allows more complex problems to be solved.

Three dimensional electrostatic fields

Three dimensional methods have been used to evaluate the electrostatic fields near attachment hardware in order to understand why corona occurs there. As described in Chapter 5, these problems are often solved by defining small region of space and solving electrostatic equations using numerical methods. This technique is illustrated in Fig 2.9.8. Here, the space within the shaded region in Fig 2.9.8a is excised and the electric field found by solving the problem shown in Fig. 2.9.8b. There are (as described in Chapter 6) several techniques including the boundary element method, the charge simulation method, the finite difference method, the Monte Carlo method and the finite element method that have been used for this purpose.

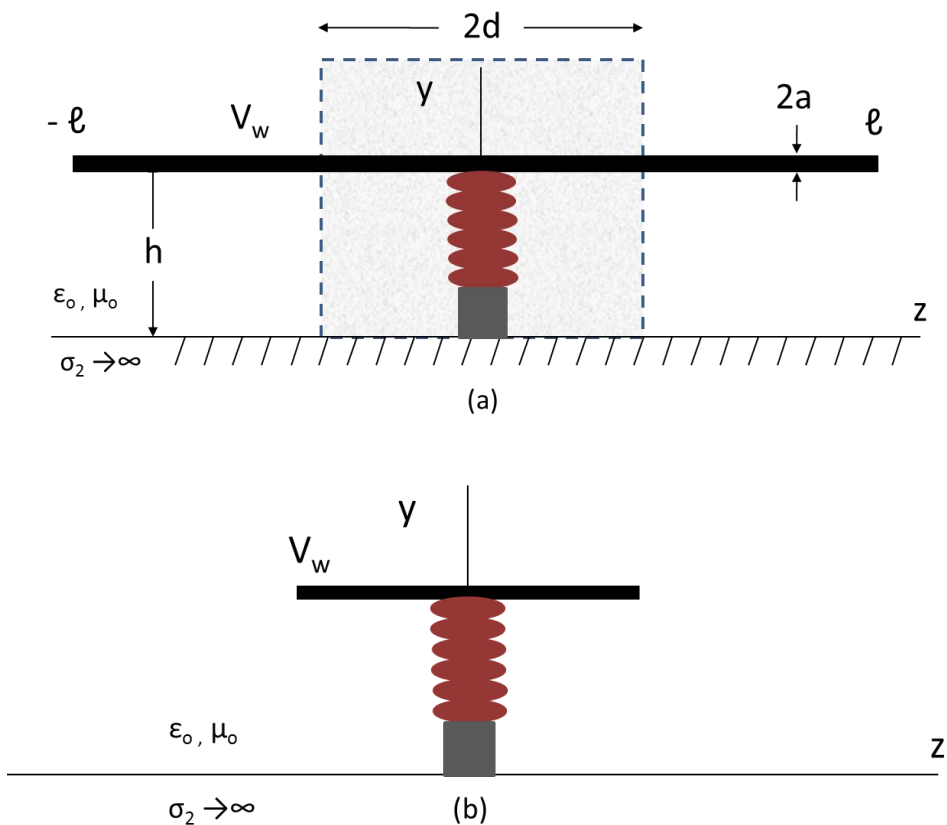


Fig. 2.9.8. a) original problem b) problem to be solved with electrostatic theory and numerical methods.

2.10 “Rules of Thumb” for Minimizing the Effect of Physical Approximations on Accuracy

Effect of finite length and corners

One of the most useful tools for evaluating the effect of physical approximations is the expression for the magnetic field of a finite length wire carrying a current I . Consider the geometry shown in Fig. 2.10.1. Here, the total length of the current can be written as

$$\ell = r \left(\frac{1}{\tan \theta_1} + \frac{1}{\tan \theta_2} \right) \quad (2.10.1)$$

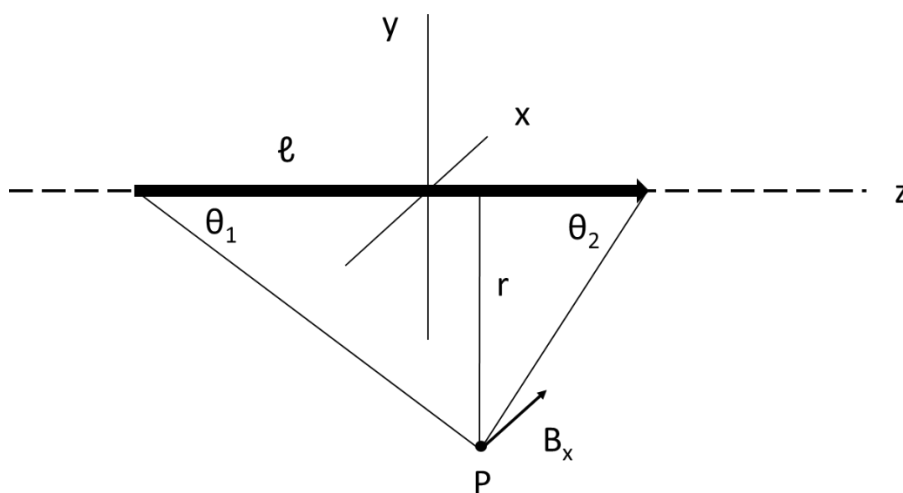


Fig. 2.10.1. Geometry for calculating the magnetic field from a uniform current of magnitude I of finite length. For this figure, it is assumed that the calculation point “P” is in the yz plane.

The magnetic field from this finite length of current (in the yz plane for $y < 0$) is

$$B_x = \frac{\mu_0 I}{4\pi r} [\cos \theta_1 + \cos \theta_2] \quad (2.10.2)$$

It should be clear that as θ_1 and θ_2 approach 0, (2.10.2) approaches

$$B_x = \frac{\mu_0 I}{2\pi r} \quad (2.10.3)$$

which is the magnetic field of an infinite line of current. Given this result, the percentage error in the magnetic field calculation (i.e., by approximating a finite length wire by an infinitely long wire) is

$$E(\%) = 100[1 - 0.5(\cos\theta_1 + \cos\theta_2)] \quad (2.10.4)$$

As an example, the error made if the length of the wire is 20 times the distance from the wire and the field point is halfway between the ends of the wire is approximately 0.5%. But, if the field point is at the end of the wire, the error is about 50%! (2.10.4) can be used to estimate the error made in magnetic field³⁰ calculations near ends of transmission lines.

A similar calculation can be made for wires that turn a 90 degree corner. Consider the geometry shown in Fig. 2.10.2

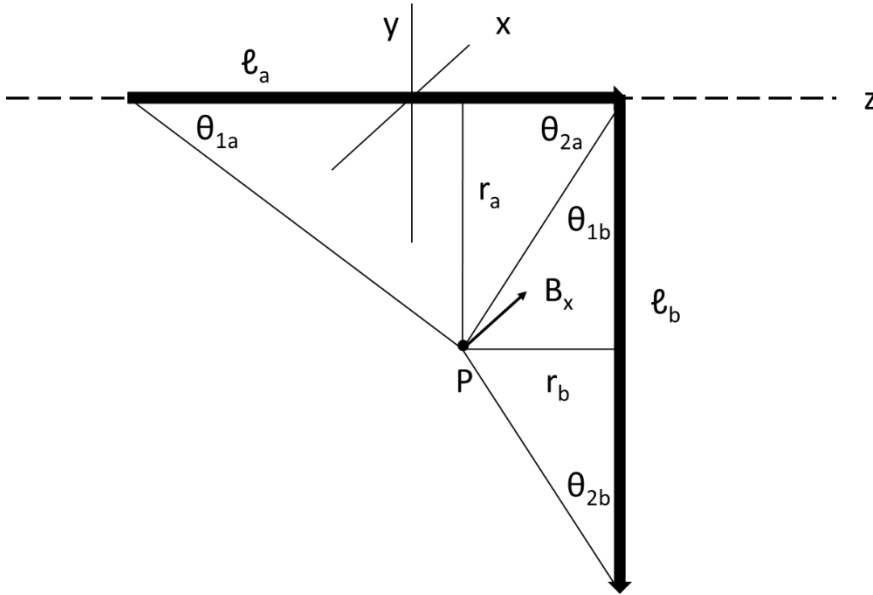


Fig. 2.10.2. Geometry for calculating the magnetic field from a uniform current of magnitude I of finite length along with a second wire at a 90 degree angle. For this figure, it is assumed that the wires and the calculation point "P" are in the yz plane.

In this case, the magnetic field (B_x) can be calculated by summing the contribution from each segment of the wire. The result is

$$B_x = \frac{\mu_0 I}{4\pi} \left\{ \frac{1}{r_a} [\cos\theta_{1a} + \cos\theta_{2a}] + \frac{1}{r_b} [\cos\theta_{1b} + \cos\theta_{2b}] \right\} \quad (2.10.5)$$

where $\theta_{1a} + \theta_{1b} = \pi/2$.

As an example, consider a case for which the field point is midway along wire "a" in Fig. 2.10.2 at a distance from the wire of r_a and that the length of

³⁰ (2.10.4) is not explicitly for electric field calculations because the charge distribution is not uniform near the wire's end, it is reasonable to use it to estimate error for electric field as long as it is recognized that the estimate is crude.

each wire is $10 r_a$. In this case, it can be shown that the error made in assuming that wire “a” is infinitely long and neglecting the effect of wire “b” is approximately 10%.

Effect of conductor sag on field measurements

An approximation to the error made by ignoring the effect of sag in calculating magnetic fields can be estimated by considering the geometry shown in Fig. 2.10.3. Here a sagging transmission line conductor is approximated by a set of three finite length current carrying wires. As an example, suppose that $h = r_b/3$ and that the length of each wire is $2r_b$. Given this, it can be shown that the error in approximating the magnetic field of the system shown in Fig. 2.10.3 at $P = r_b$ can be approximated by 5%.

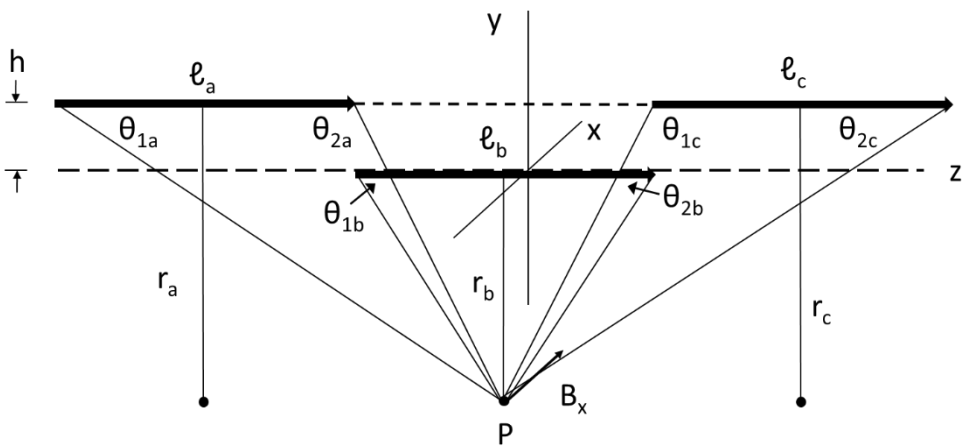


Fig. 2.10.3. Geometry for calculating the magnetic field from a uniform current of magnitude I of finite length with additional currents at each end a distance h above the center wire. For this figure, it is assumed that the wires and the calculation point “P” are in the yz plane.

Effect of conductor sag on transmission line distributed parameters

The most important parameters used to describe the propagation of power frequency voltages and currents on high voltage transmission lines are inductance and capacitance per unit length. It will be shown later in this manuscript that the inductance per unit length (at least for balanced transmission line currents) is largely unaffected by the presence of the earth because (unless the earth is magnetic) it is essentially transparent to magnetic fields at power frequencies. Hence, it is reasonable to specify the average height of each transmission line conductor when calculating the inductance per unit length because the choice has little effect on the inductance calculation. Capacitance per unit length, however, is dependent on the conductor height because the earth can be considered a perfect conductor

for electric field calculations at power frequencies. But, it is found that the dependence on height appears in logarithmic terms similar to

$$\ln(2h/a)$$

where h is the height of a conductor above earth and a is its radius. For a typical conductor radius of 1 centimeter and height of 15 meters, a 30% increase in conductor height causes less than a 4% change in the parameter. This issue is further minimized by the fact that for balanced voltages, the proximity of other conductors is more important than the effect of the earth. Given these observations, it is again, reasonable to use average height of a transmission line conductor when calculating capacitance per unit length.

The capacitive effect of a tower

In principle, the towers add additional lumped capacitance to the system parameters. However, it is generally found that (at power frequencies) this excess capacitance can be ignored. More details about this issue can be found in Section 6.2.

Rule of thumb for electric field measurements when steel towers exist

Generally, electric field measurements directly under the transmission line are made as far from a tower as possible and, hence usually at midspan. As a rule of thumb, it is probably reasonable to make measurements at least 4-5 tower window diameters from the tower if the measurements are to be compared to calculations that neglect towers. To calculate the electric fields at midpoint and close to the transmission line, the transmission line conductors are modeled as infinitely long and located at the minimum conductor height. In these cases, it is found reasonable to ignore the effect of the towers. For field points further away from the transmission line, the assumption that the conductors are at the average height will generally produce better results.

Rule of thumb for magnetic field measurements

There are fewer problems with comparing calculated and measured magnetic field results at power frequencies since towers have only a minimal influence on these magnetic fields. Nevertheless, magnetic field measurements are usually made near midspan. For field points close to the transmission line, predictions are more accurate if the conductor height is selected to be the minimum conductor height. Further from the transmission line, it is reasonable to use the average conductor height, although calculations further away from the field point are less sensitive to conductor height than those close to the transmission line.

Rule of thumb for electromagnetic interference measurements

Since electromagnetic interference³¹ (EMI) fields are generated by random corona pulses with a frequency spectra that extend well above tens of MHz, this is one of the few problems for which a high voltage transmission line is “operated” at significantly higher frequencies than those for which it was designed. At these frequencies, one might easily assume that the results are more sensitive to physical approximations. In fact, as stated above, the earth is assumed to be flat and homogeneous, the conductors are assumed to be infinite and horizontal, conductor sag has been ignored, the corona activity has been assumed to be nearly uniformly distributed along the conductors, and that the effect of towers has been ignored. Nevertheless it has been found that these physical approximations do not lead to predicted EMI levels that deviate significantly from measured values of EMI at field points relatively close to the transmission line. For these calculations, it is generally assumed that the conductors are at their “average height” (Olsen et. al. 1992), that the measurements are made at midspan and that the terrain is reasonably flat. In addition, measurements are generally made at a significant distance (5 – 10 km) from a substation in order that reflections from the substation be attenuated enough to be ignored.

One difference at higher frequencies is important enough to mention. As 50/60 Hz, the earth can be considered a perfect conductor for electric field calculations and to be transparent for magnetic field calculations. This is no longer true at EMI frequencies especially for field points that are at least a significant fraction of a wavelength³² away from the transmission line. Here it is found that the rate of decay of the EMI field away from the transmission line is affected in a noticeable way by the earth conductivity. In these cases, simpler models that either ignore the earth or equate it to a perfect conductor do not produce satisfactory results (Olsen, 1998).

2.11 Problems

P2.1 A balanced two wire transmission line above the earth is shown in Fig. P2.1. The capacitance per unit length for the balanced (i.e., equal and opposite) voltage case is

$$C = \frac{2\pi\epsilon_0}{\ln\left(\frac{2hd}{as}\right)} \quad \text{Farads/m} \quad (\text{P2.1})$$

³¹ Historically these fields were called “radio noise” fields.

³² At 1 MHz, the wavelength (λ) is 300 meters and a “significant fraction” of a wavelength might be $\lambda/10 = 30$ m.

where $s = \sqrt{d^2 + (2h)^2}$. For $a = 2$ cm, $d = 5$ meters and $h = 10, 20$ and 30 meters, calculate the capacitance of these wires above the earth. Assume that the frequency is 60 Hz and the earth conductivity is assumed to be infinite. Comment on the difference between these results and then about the effect of sag and varying earth height along a transmission line path on inductance per unit length

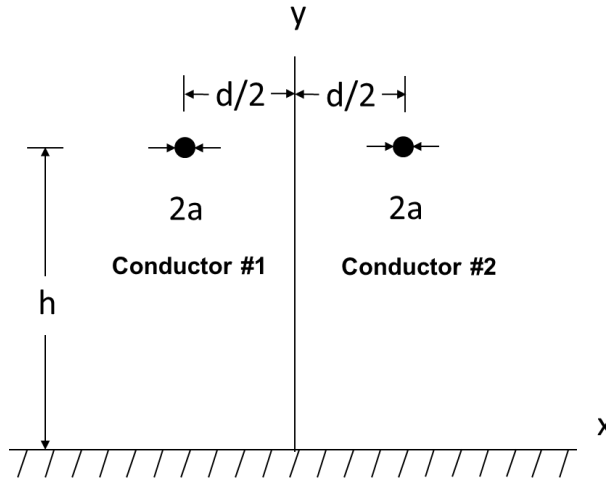


Fig. P2.1. A balanced two conductor transmission line above earth

P2.2. Consider one possible reason for using spacers along the bundled conductors of a transmission line. In SI units, the magnetic force per unit length between the two conductors can be calculated using the formula

$$F = \frac{\mu_0 I_1 I_2}{2\pi d} \quad \text{Newtons/m} \quad (\text{P2.2})$$

where the force pulls the conductors together if I_1 and I_2 have the same sign. Clearly, if the force is large enough, the conductor spacing may not be as large as the design value. a) Calculate the force between two wires separated by a distance $d = 0.457$ meters (18 inches) and carrying identical 500 A currents. Compare this force with the force of gravity per unit length on the conductors if the conductors are made of aluminum and have a radius of 2 cm. The density of aluminum is 2700 kg/m^3 and the acceleration of gravity is 9.8 N/kg . Comment on the relative size of the two forces. b) does anything change if the currents are each 5000 A during a fault event?

P2.3. a) Calculate the resistance per unit length of the solid conductor shown below in Fig. P2.3. It has aluminum on the outside and steel on the inside and the resistivity of these are 2.62×10^{-8} and $1.0 \times 10^{-7} \text{ } \Omega\text{-m}$ respectively. b) Using a simplified version of the skin effect, assume that all of the current

flows in the aluminum, how much would this change the resistance per unit length?

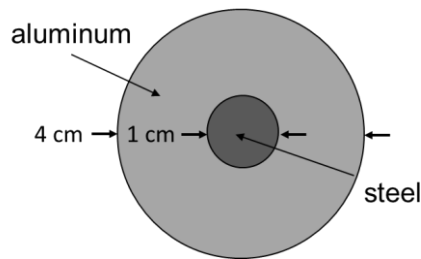


Fig. P2.3. A solid steel core surrounded by a solid aluminum conductor

P2.4. Why are typical transmission line conductors stranded?

P2.5. What is the purpose for using conductor bundles? Identify the appropriate reasons from the list below

- a. Lower inductance
- b. Reduced capacitance
- c. Increased corona onset voltage for a given weight per unit length
- d. All of the above

P2.6. What is the purpose of installing shield wires? Are they grounded at each tower?

P2.7. What are the reasons why someone might consider using post insulators? Select from the following list

- a. Reduced weight
- b. Reduced conductor movement
- c. Reduced phase to phase spacing for a compact line
- d. All of the above

P2.8. Why are grading rings used? Identify appropriate reasons from the list below.

- a. Minimization of corona on hardware
- b. Reduction of damage to non-ceramic insulators due to water drop corona
- c. Results in a more uniform voltage distribution along an insulator string
- d. All of the above

P2.9. What can be done in very high contamination areas to improve insulator performance?

- a. Use insulators with resistive coatings that carry current and cause moisture to dry
- b. Periodic washing of insulators
- c. Use of different materials that do not attract contamination.
- d. All of the above

- P2.10. What is the purpose of marker balls on transmission line conductors?
- P2.11. Identify different types of conductor movement from the list below. Describe each
- aeolian vibration
 - galloping
 - swinging
 - hydrostatic vibration
 - all of the above
- P2.12. Why are towers grounded?
- P2.13. What are vibration dampers? For what purpose are they installed on transmission line conductors?
- P2.14. What is the difference between a dead end tower and a suspension tower?
- P2.15. You are given a 2 meter long, 3 cm radius cylinder of wet wood with a conductivity of 10^{-3} S/m. Calculate the total resistance of the cylinder. Calculate how much power is dissipated in this wood if it is placed between two conductors with a voltage difference of 100 kV. Based on your answer, what do you think might happen if a tree branch falls across pair of conductors with a voltage difference of 100 kV rms? Given your answer, why are electrical utilities concerned about the growth of vegetation near transmission lines?
- P2.16. What can happen when an insulator is exposed to the environment? How and why does its performance change?
- P2.17. Why does conductor sag change with time? Why are there limits to the amount of sag that can be accepted?
- P2.18. Why are transposition towers used on long transmission lines by some utilities?
- P2.19. Name several kinds of hardware used on high voltage overhead transmission lines. Explain the purpose of each.
- P2.20. What is the purpose of installing series capacitors along a high voltage transmission line? Under what conditions would you expect to find them used?

P2.21. What is the purpose of installing shunt reactors along a high voltage transmission line? Under what conditions would you expect to find them used.

P2.22. What is the purpose of installing surge arresters either in substations or along a high voltage transmission line? Under what conditions would you expect to find them used.

P2.23. Why are most conductors made of a steel core with aluminum outer strands?

P2.24. In (a) – (e) is a list of services that could share the right-of-way with an overhead transmission line. In (f) – (n) is a list of compatibility issues which are possible consequences of sharing the right-of-way with at least one of these services. Identify which consequences can be identified with which services.

- a. ADSS optical fiber
- b. Railroads
- c. Pipelines
- d. Wireless communication antennas
- e. AM broadcast towers
- f. Interference with signaling
- g. Dry band arcing
- h. Shocks to personnel
- i. Ignition of gas leaks
- j. Minimize corona on armor rod
- k. Corrosion
- l. RF burns
- m. Shocks from vehicles
- n. Distortion of radiation patterns

P2.25. In (a) – (f) is a list of environmental issues that affect the performance of an overhead transmission line. In (g) – (l) is a list of consequences which may accompany at least one of these environmental issues. Identify which consequences can be identified with which environmental issue.

- a. Ice
- b. Rain
- c. lightning
- d. wind
- e. geomagnetic storms
- f. volcanoes
- g. excessive conductor motion
- h. excessive conductor sag
- i. excessive corona
- j. flashover

- k. additional contamination
- l. quasi-dc current induction

P2.26. What effect might rain have on a transmission line? How (if at all) does this affect the design and/or maintenance of the transmission line?

P2.27. What effect might lightning have on a power line? How (if at all) does this affect the design and/or maintenance of the transmission line?

P2.28. What might a fire under a transmission line cause? Why? How (if at all) does this affect the design and/or maintenance of the transmission line?

P2.29. Why would a utility be concerned about vegetation management? How (if at all) does this affect the design and/or maintenance of the transmission line?

P2.30. What is geomagnetic induced current and under what conditions might you expect to see its effects? What effects might you expect?

P2.31. What is meant by the term, “gold standard?”

P2.32. Explain why mathematical analysis of transmission lines is used?

P2.33. List the physical approximations that are usually made to high voltage transmission lines prior to analysis?

P2.34. Describe some methods by which a physical approximation to a transmission line prior to analysis could be validated?

P2.35. What precautions should one use to be certain that electric field measurements made under a transmission line can be appropriately compared to electric field calculations carried out with two dimensional methods?

P2.36. What are “rules of thumb?”

P2.37. Examine transmission lines in the area where you live. Identify some of the hardware that is generally ignored in the analysis of propagation characteristics as presented in this manuscript. What impact might this hardware have on the propagation analysis if it was not ignored? How do you think you could account for these effects if necessary?

P2.38. Consider an infinitely long single conductor power line in free space carrying a current of 1000 Amps as shown in Fig. P2.1.1 below (note that the infinitely long conductor prior to sag follows the dashed line). a) Calculate

the magnetic field (B_x) at the point P a distance 20 meters below the conductor. b) To simulate sag, a 20 meter length of the conductor is now moved 5 meters below the rest of the conductor as shown. For this configuration, calculate the magnetic field (B_x) at point P and compare the results with part a.

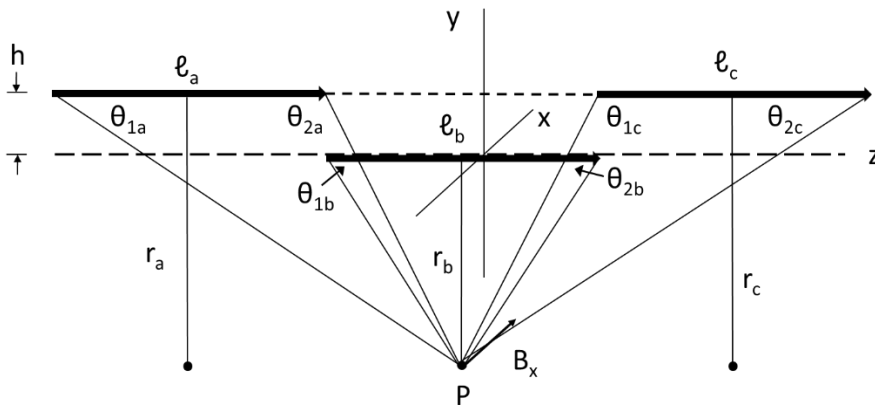


Fig. P2.38. A single conductor power line with and without sag.

P2.39. Evaluate the magnetic field of a 90 degree bend in an infinitely long single conductor power line carrying a current of 1000 A as shown in Fig. P2.39? At any distance that is 10 meters from the closest conductor, where is the magnetic field the largest?

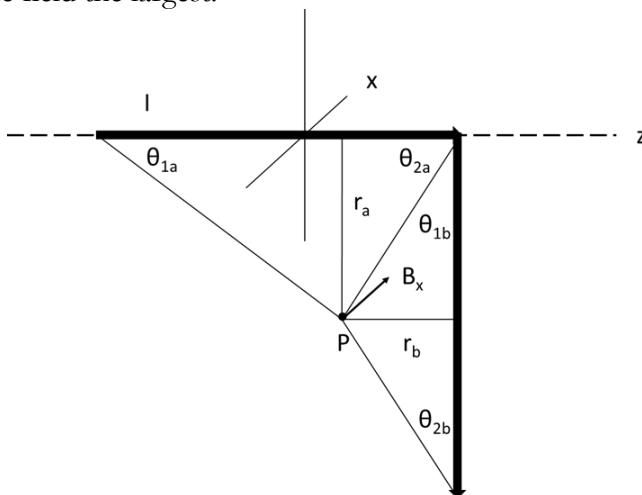


Fig. P2.39. A single conductor power line with a 90 degree.

2.12 References

AAR/EEI. 1977. "Principles and Practices for Inductive Coordination of Electric Supply and Railroad Communication/Signal Systems." Report of the

Joint Committee of the AAR and EEI on Inductive Coordination. September.

Akagi, Y., S. Koyama, H. Ohta, H. Nishizawa, Y. Nagata and T. Oka. 2002. "Development of Anti-galloping Device for UHV Transmission Line." *IEEE/PES [Transmission and Distribution Conference and Exhibition Asia Pacific](#)*. Vol. 3. pp. 2158 – 2161. October.

Anderson, C. III. 1976. "Mutual Impedances for Parallel Wires Over a Two-Layer Earth," *IEEE Transactions on Communications*. Vol. 24-2. pp. 222-. February.

ASCE. 1991. "Guidelines for Electrical Transmission Structural Loading," American Society of Civil Engineers Manuals and Reports on Engineering Practice No. 24, New York.

Austin, K. A. et. al. 1984. "Optical Communications using Overhead Power Transmission Lines." *CIGRE Paper No. 35-04*.

Bonds, R.W. 1999. "The Effect of Overhead AC Power Lines Paralleling Ductile Iron Pipelines." Ductile Iron Pipe Research Association, Birmingham, Alabama.

Carter, C. N. and M.A. Waldron. 1992. "Mathematical Model of Dry-Band Arcing on Self-Supporting, All-Dielectric, Optical Cables Strung on Overhead Power Lines." *IEE Proceedings-C*. Vol. 139. pp. 185-196. May.

CEA. 1994. "[Powerline Ground Fault Effects on Pipelines](#)." Canadian Electricity Association (Former name: Canadian Electrical Association) Technical Report 239 T 817.

CIGRE. 2012. "Mechanical Security of Overhead Lines - Containing Cascading Failures and Mitigating their Effects." CIGRE Technical Brochure No 515. October.

Eriksson, A.J. 1987. "The Incidence of Lightning Strikes to Power Lines." *IEEE Transactions on Power Delivery*. Vol. PWRD-2. pp. 859-870. July.

Fonseca, J. R., A. L. Tan, V. Monassi, W. S. Junqueira, R. P. Silva, L. A. R. Assuncao, and M. O. C. Melo. 1990. "Effects of Agricultural Fires on the Performance of Overhead Transmission Lines." *IEEE Transactions on Power Delivery*. Vol. PWRD-5. pp. 687-694. April.

Fu, G., L. Wang, Z. Guan, L. Hou, X. Meng and M. MacAlpine. 2012. "Simulations of the Controlling Effect of Interphase Spacers on Conductor

Galloping,” *IEEE Transactions on Dielectrics and Electrical Insulation*. Vol. DIEL-19. pp. 1325 – 1334. August.

Galli, S., A Scaglione and Z. Wang. 2011. “For the Grid and Through the Grid: The Role of Power Line Communications in the Smart Grid.” *Proceedings of the IEEE*. Vol. 99. pp. 998- 1027. June.

Giao, T.N.; Sarma, M.P. 1972, “[Effect of a Two-Layer Earth on the Electric Field Near HVDC Ground Electrodes.](#)” *IEEE Transactions on Power Apparatus and Systems*. Vol. PAS-91. pp. 2356 – 2365.

Gorur, R. 2012. Private Communication.

House, H. E. and P. D. Tuttle. 1959. “Current Carrying Capacity of ACSR.” *AIEE Transactions*. Vol. 77. pp. 1169-1177. Feb.

IEC. 2003. “Railway Applications - Electromagnetic Compatibility - Part 1: General.” IEC Standard 62236-1. April.

IEEE. 2000. “IEEE Guide for Safety in AC Substation Grounding.” IEEE Standard 80. IEEE, New York.

IEEE. 2001. "IEEE Guide for Transmission Structure Foundation Design and Testing," IEEE Standard 691. IEEE, New York.

IEEE. 2002. “National Electric Safety Code,” IEEE Standard C2. IEEE, New York.

Kuffel, E. and W. S. Zaengl. 1984. *High Voltage Engineering: Foundations*. Pergamon Press. Oxford.

Kuffel, J, Z. Li, V. Chartier, S. Grzybowski, J. Vandermaar and B. Gunasekaran 2001. "Round Robin Investigation of a Corona Test Procedure Based on Gradient Calibrating Spheres.” *Proceedings of the 12th International Symposium on High Voltage Engineering (ISH'2001), Bangalore, India*. Vol. 5. pp. 1130-1133.

Madge, R. C. and Jones, D. E. 1986. "Effect of Power Lines on AM Radio Broadcast Radiation Patterns." *IEEE Transactions on Power Delivery*. Vol.PWRD-1. pp.163-168. April.

Lu, M.L., J. K. Chan. 2007. “An Efficient Algorithm for Aeolian Vibration of Single Conductor with Multiple Dampers.” *IEEE Transactions on Power Apparatus and Systems*. Vol. PAS-95. pp. 621 – 629. March/April.

Lusk, G. Z. and S. T. Mak. 1976. "Wood Pole Fires: Their Cause and Potential Effects." *IEEE Transactions on Power Delivery*. Vol. PWRD-22. pp. 1822 – 1829. July.

Mamshiev, A.V., R. D. Nevels, and B. D. Russell. 1996. "[Effects of Conductor Sag on Spatial Distribution of Power Line Magnetic Field.](#)" *IEEE Transactions on Power Delivery*. Vol. PWRD-11. pp. 1571 – 1576.

Meliopoulos, A. P., R. P. Webb and E. B. Joy. 1981, "Analysis of Grounding Systems," *IEEE Transactions on Power Apparatus and Systems*. Vol. PAS-100. pp. 1039 - 1048. March.

Olsen, R. G, S.D. Schennum and V.L. Chartier. 1992. "Comparison of Several Methods for Calculating Power Line Electromagnetic Interference Levels and Calibration with Long-Term Data," *IEEE Transactions on Power Delivery*. Vol. PWRD-7. pp. 903–913. April.

Olsen, R. G. and G.L. Heins. 1998. "A Study of the Electromagnetic Compatibility of High Voltage Transmission Lines and the Guidance of Center Pivot Irrigation Units with Cornering Systems." *IEEE Transactions on Power Delivery*. Vol. PWRD-13, pp. 1230-1237. October.

Olsen, R. G. 1999. "An Improved Model for the Electromagnetic Compatibility of All Dielectric Self Supporting Fiber Optic Cable and High Voltage Power Lines," *IEEE Transactions on Electromagnetic Compatibility*, Vol. 41. pp. 180 – 192. August.

Olsen R. G. and K. Yamazaki. 2005. "The Interaction between ELF Electric Fields and RF Survey Meters: Theory and Experiment." *IEEE Transactions on Electromagnetic Compatibility*. Vol. EMC-47. pp. 86-96. February.

Olsen, R. G., R. A. Tell, and H. K. Westby, 2007, "Interaction Between Power Frequency Electric Fields and RF Survey Meters: Test Protocol and Evaluation of Commercial Meters," *IEEE Transactions on Power Delivery*. Vol. PWRD-22. pp. 2508 – 2516. October.

Olsen, R. G., R. A. Tell and J. Schneider. 2011. "Radiofrequency Burns in the Power System Workplace," *IEEE Transactions on Power Delivery*. Vol. PWRD-26. pp. 352-359. January.

Phillips, A. J., D. J. Childs and H. M. Schneider. 1999. "Aging of Non-Ceramic Insulators Due to Corona from Water Drops." *IEEE Transactions on Power Delivery*. Vol. PWRD-14. pp. 1081 – 1089. July.

RUS-USDA. 2005. "Design Manual for High Voltage Transmission." Rural Utilities Service, US Department of Agriculture RUS Bulletin 1724-200.

Sarma, M.P. and W. Janischewskyj. 1969. "[Electrostatic Field of a System of Parallel Cylindrical Conductors.](#)" *IEEE Transactions on Power Apparatus and Systems*. Vol. PAS-88. pp. 1069 – 1079.

Silva, J. M. and B. Whitney. 2002. "Evaluation of the Potential for Power Line Carrier (PLC) to Interfere with Use of the Nationwide Differential GPS Network." *IEEE Transactions on Power Delivery*. Vol. PWRD-17. pp. 349-352. April.

Simpson, T.L. and C.W. Brice. 1987. "Moment Method Analysis of the Electric Field under EHV Transmission Lines." *IEEE Transactions on Power Delivery*. Vol. PWRD-2. pp. 1264-1270. October.

Tengdin, J. T. 1987. "Distribution Line Carrier Communications – An Historical Perspective." *IEEE Transactions on Power Delivery*. Vol. PWRD-2. pp. 321-329. April.

Tesche, F. M., B.A. Renz, R.M. Hayes, and R.G. Olsen. 2003. "Development and Use of a Multiconductor Line Model for PLC Assessments," *Proceedings of the 15th International Zurich Symposium on EMC*. February.

Thrash, R. G., A. Murrah, M. Lancaster and K. Knuckles, eds. 2007. *Overhead Conductor Manual (2nd Ed.)*. Southwire, Co., Carolton, GA,

Tuominen, M. W. and R.G. Olsen. 2000. "Electrical Design of All-Dielectric Self-Supporting Optical Fiber Cable." *IEEE Transactions on Power Delivery*. Vol. PWRD-15. pp. 940-947. July.

Wardman, J. B., T. M. Wilson, P. S. Bodger, J. W. Cole and D. M. Johnston. 2012. "Investigating the Electrical Conductivity of Volcanic Ash and its Effect on the HV Transmission Systems." *Physics and Chemistry of the Earth, Parts A/B/C*. Vol. 45–46. pp. 128-145.

Yu. Z., Z. Peng, P.Liu, and X. Wu. 2006. "The Influence of Charged Sand Particles on the External Insulation Performance of Composite Insulators in Sandstorm Condition." *8th International Conference on Properties and applications of Dielectric Materials*, pp. 542-545.

Zischank, W. and J. Wiesinger. 1997. "Damages to Optical Ground Wires Caused by Lightning," *Proceedings of the 10th International Symposium on High Voltage Engineering*, Montreal, Quebec.

Chapter III

Brief Overview of Relevant Electromagnetic Theory

3.1 Maxwell's Equations

Differential form - time domain

Electromagnetic theory is based on solutions to Maxwell's equations, a set of coupled partial differential equations in the electric and magnetic fields. In the time domain, these equations can be written (Harrington, 2001)

$$\nabla_x \bar{E} + \frac{\partial \bar{B}}{\partial t} = 0, \quad \text{Faraday's Law} \quad (3.1.1)$$

$$\nabla_x \bar{H} - \frac{\partial \bar{D}}{\partial t} = J, \quad \text{Ampere's Law} \quad (3.1.2)$$

$$\nabla \bullet \bar{B} = 0 \quad (3.1.3)$$

$$\nabla \bullet \bar{D} = \rho \quad \text{Gauss' Law} \quad (3.1.4)$$

where $\nabla_x \bar{Q}$ and $\nabla \bullet \bar{Q}$ are the curl and divergence operator, respectively, that will be defined more carefully shortly. These equations are often supplemented by the continuity equation (i.e., a mathematical statement that charge is conserved)

$$\nabla \bullet \bar{J} = -\frac{\partial \rho}{\partial t} \quad (3.1.5)$$

It is possible to derive this equation by taking the divergence of (3.1.2), using the vector identity

$$\nabla \bullet \nabla_x \bar{Q} = 0 \quad (3.1.6)$$

which holds for mathematically well behaved (Harrington 1961) vector fields³³ and inserting (3.1.4) into the result.

The variables in (3.1.1) – (3.1.4) are all functions of x, y, z and t and are defined as:

$$\begin{aligned} \bar{E} & - \text{Electric field strength (a vector field)} \\ \bar{D} & - \text{Electric flux density (a vector field)} \\ \bar{H} & - \text{Magnetic field strength (a vector field)} \\ \bar{B} & - \text{Magnetic flux density (a vector field)} \\ \bar{J} & - \text{Electric current density (a vector field)} \\ \rho & - \text{Electric charge density (a scalar field)} \end{aligned}$$

Fully written out, a vector field looks (in rectangular coordinates) like

$$\bar{E}(x, y, z, t) = E_x(x, y, z, t)\bar{a}_x + E_y(x, y, z, t)\bar{a}_y + E_z(x, y, z, t)\bar{a}_z \quad (3.1.7)$$

where the \bar{a}_x, \bar{a}_y and \bar{a}_z are respectively unit vectors in the x, y and z directions. It is clear that each vector field contains three unknown scalar fields and that each of these may independently vary in both space and time.

A scalar field (for example, charge density) can be written as

$$\rho(x, y, z, t) \quad (3.1.8)$$

The curl and divergence operators can be written in rectangular coordinates respectively as

$$\text{Curl}(\bar{Q}) = \nabla \times \bar{Q} = \det \begin{vmatrix} \bar{a}_x & \bar{a}_y & \bar{a}_z \\ \frac{\partial}{\partial x} & \frac{\partial}{\partial y} & \frac{\partial}{\partial z} \\ Q_x & Q_y & Q_z \end{vmatrix} \quad (3.1.9)$$

and

$$\text{Divergence}(\bar{Q}) = \nabla \cdot \bar{Q} = \frac{\partial Q_x}{\partial x} + \frac{\partial Q_y}{\partial y} + \frac{\partial Q_z}{\partial z} \quad (3.1.10)$$

Clearly, the result of a “curl” operation on a vector field is another vector field while the result of a “divergence” operation on a vector field is a scalar field. Formulas for these operations in other coordinate systems are available in most electromagnetic textbooks.

³³ Generally this entails conditions on the continuity of the vector function \bar{Q} and its derivatives. More specific information can be found in books by Stratton (1941 – Section 8.13) and Dudley (1994).

It is useful to note (Stratton 1941) that if conservation of charge (i.e., (3.1.5)) is assumed then only (3.1.1) and (3.1.2) of Maxwell's equations are independent since (3.1.3) and (3.1.4) can be derived from (3.1.1), (3.1.2) and (3.1.5) if (3.1.6) is invoked. Given the number of unknowns, further conditions must be imposed before unique solutions to Maxwell's equations can be found³⁴. The additional relationships needed to accomplish this relate to the interaction of electric and magnetic fields with materials on a macroscopic level and will be discussed in Section 3.2. One important property of these materials is linearity which will be discussed further in Section 3.2 and which will be assumed in the following discussion of time harmonic fields.

Differential form - frequency (phasor) domain

If all materials are linear, then it is possible to assume that all sources (and hence all fields) vary in time as $\exp(j\omega t)$ where $\omega = 2\pi f$ is the radian frequency and f is the frequency in Hertz. If this is done, then Maxwell's equations become (Harrington, 2001).

$$\nabla \times \hat{\mathbf{E}} + j\omega \hat{\mathbf{B}} = \mathbf{0}, \quad \text{Faraday's Law} \quad (3.1.11)$$

$$\nabla \times \hat{\mathbf{H}} - j\omega \hat{\mathbf{D}} = \hat{\mathbf{J}}, \quad \text{Ampere's Law} \quad (3.1.12)$$

$$\nabla \cdot \hat{\mathbf{B}} = 0 \quad (3.1.13)$$

$$\nabla \cdot \hat{\mathbf{D}} = \hat{\rho} \quad \text{Gauss' Law} \quad (3.1.14)$$

$$\nabla \cdot \hat{\mathbf{J}} = -j\omega \hat{\rho} \quad \text{Continuity equation} \quad (3.1.15)$$

where it is assumed that the magnitude of the field is its RMS value equal to the peak value divided by $\sqrt{2}$ for a sinusoidal field. Thus, for example, $\hat{\mathbf{E}} = \hat{\mathbf{E}}(x, y, z, \omega)$ is now a "phasor" quantity indicated by a "carat" (i.e., $\hat{\mathbf{a}}$) over the variable from which the time harmonic solution in the time domain can be found as

$$\bar{\mathbf{E}}(x, y, z, t) = \sqrt{2} \operatorname{Re}(\hat{\mathbf{E}}(x, y, z, \omega) e^{j\omega t}) \quad (3.1.15)$$

In the time harmonic case, equations (3.1.13) and (3.1.14) can be obtained from (3.1.11) and (3.1.12) respectively by taking the divergence of each, using the identity (3.1.6) and then (3.1.15). Thus, only (3.1.11), (3.1.12) and (3.1.15)

³⁴ Conditions for uniqueness will be discussed in Section 3.6

are needed in the time harmonic case and if the region is sourceless, then only (3.1.11) and (3.1.12) are needed.

Integral form - time domain

The first Maxwell's equation can also be written in integral form by integrating (3.1.1) over some surface "S"

$$\iint_S \nabla \times \bar{E} \cdot d\bar{s} = -\frac{\partial}{\partial t} \iint_S \bar{B} \cdot d\bar{s}, \quad (3.1.17)$$

where it has been assumed that the functions are well behaved enough to allow the order of the derivative and integral to be interchanged and that $d\bar{s}$ is an oriented differential element of the area "S" with its direction normal to "S."

Next, Stokes theorem (Stratton 1941)

$$\iint_S \nabla \times \bar{Q} \cdot d\bar{s} = \oint_C \bar{Q} \cdot d\bar{l} \quad (3.1.18)$$

is applied to (3.1.16) where "C" is a contour that forms the boundary of S as shown in Fig. 3.1.1. The positive side of the surface S (the normal is directed outward to this side) is related to the positive direction of circulation on contour C by the right hand rule convention; with fingers following the direction of C, the thumb points in the direction of the normal to S.

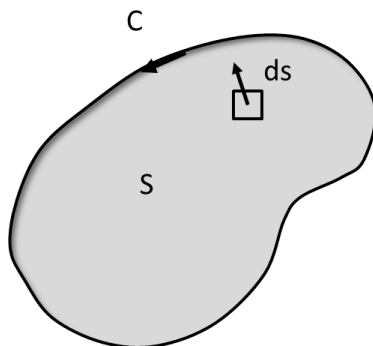


Fig. 3.1.1. Definition of Geometry for Stokes Theorem. Note that the positive sense of the contour C is "counterclockwise" and the positive side of the surface (shaded) is the top of the paper. This is consistent with the right hand rule described above.

Using (3.1.18), (3.1.17) becomes

$$\oint_C \bar{E} \cdot d\bar{l} = -\frac{\partial}{\partial t} \iint_S \bar{B} \cdot d\bar{s}, \quad (3.1.19)$$

which is the integral form of Faraday's law.

Similarly (3.1.2) can be integrated and rewritten as

$$\oint_C \bar{H} \cdot d\bar{l} = \iint_S \left(\bar{J} + \frac{\partial}{\partial t} \bar{D} \right) \cdot d\bar{s}, \quad (3.1.20)$$

which is the integral form of Ampere's law.

Next, if (3.1.4) is integrated over some volume "V" it becomes

$$\iiint_V \nabla \cdot \bar{D} dv = \iiint_V \rho dv \quad (3.1.21)$$

If next, the divergence law (Balanis 1989)

$$\iiint_V \nabla \cdot \bar{Q} dv = \oiint_S \bar{Q} \cdot d\bar{s} \quad (3.1.22)$$

is applied, then (3.1.21) becomes

$$\oiint_S \bar{D} \cdot d\bar{s} = \iiint_V \rho dv \quad (3.1.23)$$

which is the integral form of Gauss' law. Here, S is the closed surface that surrounds V and $d\bar{s}$ is the outward normal at any point on S.

Similarly (3.1.3) can be integrated over a volume in space and the divergence law used to get

$$\oiint_S \bar{B} \cdot d\bar{s} = 0 \quad (3.1.24)$$

Finally, the continuity equation can be integrated over a volume and the divergence law used to get

$$\oiint_S \bar{J} \cdot d\bar{s} = -\frac{\partial}{\partial t} \iiint_V \rho dv \quad (3.1.25)$$

Integral form - frequency (phasor) domain

Frequency domain forms of Faraday's law (3.1.19), Ampere's law (3.1.20) and the continuity equation (3.1.25) can be developed by simply substituting $j\omega$ for the time derivative to get respectively

$$\oint_C \hat{\bar{E}} \cdot d\bar{l} = -j\omega \iint_S \hat{\bar{B}} \cdot d\bar{s}, \quad (3.1.26)$$

$$\oint_C \hat{H} \cdot d\bar{l} = \iint_S (\hat{J} + j\omega\hat{D}) \cdot d\bar{s}, \quad (3.1.27)$$

$$\oiint_S \hat{J} \cdot d\bar{s} = -\frac{\partial}{\partial t} \iiint_V \hat{\rho} dv \quad (3.1.28)$$

Here, the field and source variables become phasors.

3.2 Constitutive Relationships for Dielectric and Conducting Materials

As mentioned earlier, before unique solutions to Maxwell's equations can be found, it is necessary to specify relationships between \bar{D} and \bar{E} , \bar{B} and \bar{H} and \bar{J} and \bar{E} . These are called constitutive relationships and characterize the materials in which the fields exist.

In free space, the relationships are simply

$$\bar{D} = \varepsilon_0 \bar{E} \quad (3.2.1)$$

$$\bar{B} = \mu_0 \bar{H} \quad (3.2.2)$$

$$\bar{J} = 0 \quad (3.2.3)$$

where ε_0 and μ_0 are the permittivity (dielectric constant) and permeability of free space respectively.

In more complex media, it is convenient to augment the electric and magnetic flux densities by electric polarization $\bar{P}(\bar{E})$ and magnetization $\bar{M}(\bar{H})$ vectors respectively. These account for the influence of the materials and are defined as:

$$\bar{D} = \varepsilon_0 \bar{E} + \bar{P}(\bar{E}) \quad (3.2.4)$$

$$\bar{B} = \mu_0 (\bar{H} + \bar{M}(\bar{H})) \quad (3.2.5)$$

Finally, the electric current \bar{J} can be separated into an impressed source current \bar{J}_0 and a current that is dependent on the local electric field $\bar{J}(\bar{E})$ as

$$\bar{J} = \bar{J}_0 + \bar{J}(\bar{E}) \quad (3.2.6)$$

Given (3.2.4) and (3.2.5), Maxwell's equations can be rewritten as

$$\nabla_x \bar{E} + \frac{\partial \bar{B}}{\partial t} = 0, \quad \text{Faraday's Law} \quad (3.2.7)$$

$$\begin{aligned} \nabla_x \bar{B} - \varepsilon_0 \mu_0 \frac{\partial \bar{E}}{\partial t} = \\ \mu_0 \left(\bar{J}_0 + \bar{J}(\bar{E}) + \frac{\partial \bar{P}(\bar{E})}{\partial t} + \nabla_x \bar{M}(\bar{H}) \right) \end{aligned} \quad \text{Ampere's Law} \quad (3.2.8)$$

$$\nabla \cdot \bar{B} = 0 \quad (3.2.9)$$

$$\nabla \cdot \bar{E} = \frac{1}{\varepsilon_0} (\rho - \nabla \cdot \bar{P}(\bar{E})) \quad \text{Gauss' Law} \quad (3.2.10)$$

Written in this way, it is clear that the “material” can be treated as a source (albeit a dependent source) of electric and magnetic fields. In the next paragraph, the dependence of these sources on the local electric and magnetic field will be examined further.

In matter that is “linear³⁵,” then it is possible to write the following relationships between these quantities (Harrington 1961)

$$\bar{D} = \varepsilon \bar{E} + \varepsilon_1 \frac{\partial \bar{E}}{\partial t} + \varepsilon_2 \frac{\partial^2 \bar{E}}{\partial t^2} + \dots \quad (3.2.11)$$

$$\bar{B} = \mu \bar{H} + \mu_1 \frac{\partial \bar{H}}{\partial t} + \mu_2 \frac{\partial^2 \bar{H}}{\partial t^2} + \dots \quad (3.2.12)$$

and

$$\bar{J} = \sigma \bar{E} + \sigma_1 \frac{\partial \bar{E}}{\partial t} + \sigma_2 \frac{\partial^2 \bar{E}}{\partial t^2} + \dots \quad (3.2.13)$$

where the permittivity (ε_i), permeability (μ_i) and conductivity (σ_i) coefficients are (in general) tensors (indicates an anisotropic material) and functions of space coordinates (indicates an inhomogeneous material). In general, the time derivatives must be included because of losses and inertia in real material (Balanis 1989).

³⁵ Linearity means that if two sets of fields (\bar{E}_1, \bar{H}_1) and (\bar{E}_2, \bar{H}_2) are separately solutions of Maxwell's equations and the constitutive relationships, then so is $(\bar{E}_1 + \bar{E}_2, \bar{H}_1 + \bar{H}_2)$. If a material is non-linear, the right hand sides of (3.2.1) – (3.2.3) would be non-linear functions of the field amplitudes. In this text, it is appropriate to model nearly all materials as linear. One exception is the case for which a very large current is injected into the earth such as in a grounding system during a fault.

Since the materials are considered to be linear, (3.2.1) – (3.2.3) can be simplified in the time harmonic case (i.e., $\exp(j\omega t)$) time variation assumed) to

$$\hat{D} = \varepsilon \hat{E} + j\omega \varepsilon_1 \hat{E} - \omega^2 \varepsilon_2 \hat{E} + \dots = \varepsilon(\omega) \hat{E} \quad (3.2.14)$$

$$\hat{B} = \mu \hat{H} + j\omega \mu_1 \hat{H} - \omega^2 \mu_2 \hat{H} + \dots = \mu(\omega) \hat{H} \quad (3.2.15)$$

and

$$\hat{J} = \sigma \hat{E} + j\omega \sigma_1 \hat{E} - \omega^2 \sigma_2 \hat{E} + \dots = \sigma(\omega) \hat{E} \quad (3.2.16)$$

The terms $\varepsilon(\omega)$, $\mu(\omega)$ and $\sigma(\omega)$ are complex functions of ω and represent the frequency dependence of the permittivity, permeability and conductivity respectively. Recall that each of these could still be a tensor (anisotropic material) and a function of spatial coordinates (inhomogeneous material).

Many materials have relatively simple behavior. They are linear, homogeneous, isotropic materials. In addition, the higher order coefficients in (3.2.14) – (3.2.16) are zero. Hence, for such “simple materials” (3.2.14) – (3.2.16) reduce to

$$\hat{D} = \varepsilon \hat{E} = \varepsilon_0 \varepsilon_r \hat{E} \quad (3.2.17)$$

$$\hat{B} = \mu \hat{H} = \mu_0 \mu_r \hat{H} \quad (3.2.18)$$

and

$$\hat{J} = \sigma \hat{E} \quad (3.2.19)$$

where ε_r (relative permittivity or relative dielectric constant), μ_r (relative permeability) and σ are scalar constants that characterize the material.

Often, in the frequency domain the effects of permittivity and conductivity are combined since according to (3.1.13)

$$\nabla \times \hat{H} = j\omega \varepsilon \hat{E} + \sigma \hat{E} = (\sigma + j\omega \varepsilon) \hat{E} = j\omega (\varepsilon - j\sigma/\omega) \hat{E} \quad (3.2.20)$$

where the term $(\sigma + j\omega \varepsilon)$ is often called the “complex conductivity” of the material or alternatively the term $(\varepsilon - j\sigma/\omega)$ is called the “complex permittivity” of the material.

3.3 The Wave Equation - Frequency Domain

Consider Faraday's and Ampere's laws in the phasor domain as given respectively by (3.1.11) and (3.1.12). If the "curl" operation is applied to Faraday's law then

$$\nabla_x \nabla_x \hat{\mathbf{E}} + j\omega \nabla_x \hat{\mathbf{B}} = 0 \quad (3.3.1)$$

If now, it is assumed that $\hat{\mathbf{B}} = \mu \hat{\mathbf{H}}$ as in (3.2.18) where μ represents a homogeneous medium, and (3.1.12) is substituted into (3.3.1) where $\hat{\mathbf{D}} = \epsilon \hat{\mathbf{E}}$ as in (3.2.17), then

$$\nabla_x \nabla_x \hat{\mathbf{E}} - \omega^2 \mu \epsilon \hat{\mathbf{E}} = -j\omega \mu \hat{\mathbf{J}} \quad (3.3.2)$$

Now, the vector identity

$$\nabla_x \nabla_x \hat{\mathbf{E}} = \nabla(\nabla \cdot \hat{\mathbf{E}}) - \nabla^2 \hat{\mathbf{E}} \quad (3.3.3)$$

is applied. If the region of interest has no free charge and ϵ also represents a homogeneous medium, then (3.1.13) can be used to obtain

$$\nabla^2 \hat{\mathbf{E}} + \omega^2 \hat{\mu} \hat{\epsilon} \hat{\mathbf{E}} = j\omega \hat{\mu} \hat{\mathbf{J}} \quad (3.3.4)$$

(3.3.4) is the wave equation for the electric field in a homogeneous medium. If the current is assumed to consist of a source current $\hat{\mathbf{J}}_0$ and an ohmic current characterized by (3.2.3) then (3.3.4) can be written as

$$\nabla^2 \hat{\mathbf{E}} + \omega^2 \mu(\epsilon - j\sigma/\omega) \hat{\mathbf{E}} = j\omega \mu \hat{\mathbf{J}}_0 \quad (3.3.5)$$

It is interesting to note that (in rectangular coordinates only)

$$\nabla^2 \hat{\mathbf{Q}} = \nabla^2(\hat{\mathbf{Q}}_x \bar{a}_x + \hat{\mathbf{Q}}_y \bar{a}_y + \hat{\mathbf{Q}}_z \bar{a}_z) = \bar{a}_x \nabla^2 \hat{\mathbf{Q}}_x + \bar{a}_y \nabla^2 \hat{\mathbf{Q}}_y + \bar{a}_z \nabla^2 \hat{\mathbf{Q}}_z \quad (3.3.6)$$

In a similar way, the wave equation for the magnetic field can be found as

$$\nabla^2 \hat{\mathbf{H}} + \omega^2 \mu(\epsilon - j\sigma/\omega) \hat{\mathbf{H}} = -\nabla_x \hat{\mathbf{J}}_0 \quad (3.3.7)$$

where again, (3.3.6) can be used in rectangular coordinates.

3.4 Boundary Conditions

The boundary conditions discussed below can be derived by applying the integral forms of Maxwells equations to either a “pillbox” that spans two different materials (for surface integral) or a rectangular contour that spans two different materials (for line integral). These derivations are included in many textbooks such as Balanis (1989).

The general conditions that the electric and magnetic fields must satisfy at any boundary between two lossy dielectric materials are:

$$\bar{n}_1 \bullet (\bar{D}_1 - \bar{D}_2) = \rho_s \text{ (surface charge)} \quad (3.4.1)$$

$$\bar{n}_1 \times (\bar{H}_1 - \bar{H}_2) = \bar{J}_s \text{ (surface current)} \quad (3.4.2)$$

$$\bar{n}_1 \bullet (\bar{B}_1 - \bar{B}_2) = 0 \quad (3.4.3)$$

$$\bar{n}_1 \times (\bar{E}_1 - \bar{E}_2) = 0 \quad (3.4.4)$$

where the geometry (including the definition of \bar{n}_1) is shown in Fig. 3.4.1. On boundaries between two lossy dielectrics (with finite conductivity), $\rho_s = J_s = 0$ (Balanis 1989).

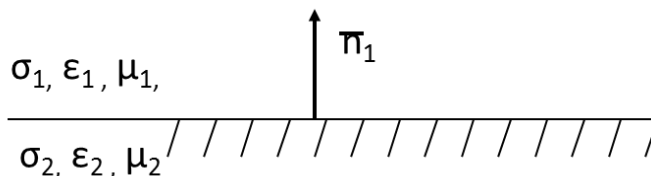


Fig. 3.4.1. Definition of normal vector for boundary conditions.

At a perfectly conducting boundary (i.e., region 2 in Fig 3.4.1 is a perfect conductor for which $\sigma_2 \rightarrow \infty$)

$$\bar{n}_1 \bullet \bar{D}_1 = \rho_s \text{ (surface charge)} \quad (3.4.5)$$

$$\bar{n}_1 \times \bar{H}_1 = \bar{J}_s \text{ (surface current)} \quad (3.4.6)$$

$$\bar{n}_1 \bullet \bar{B}_1 = 0 \quad (3.4.7)$$

$$\bar{n}_1 \times \bar{E}_1 = 0 \quad (3.4.8)$$

3.5 Poynting's Theorem in the Frequency Domain ◀

The derivation of Poynting's Theorem begins with the two Maxwell curl equations for time harmonic electromagnetic fields from (3.1.11) and (3.1.12) (Harrington, 2001; Balanis, 1989).

$$\nabla \times \hat{\mathbf{E}} = -j\omega\mu\hat{\mathbf{H}} \quad (3.5.1)$$

$$\nabla \times \hat{\mathbf{H}} = \hat{\mathbf{J}}_0 + \sigma\hat{\mathbf{E}} + j\omega\varepsilon\hat{\mathbf{E}} \quad (3.5.2)$$

where ε , μ and σ are assumed to be real scalar functions of position and frequency, the current in (3.5.2) has been separated into an impressed "source" current ($\hat{\mathbf{J}}_0$) and an ohmic "bulk" current ($\sigma\hat{\mathbf{E}}$). The next step is to dot multiply (3.5.1) by $\hat{\mathbf{H}}^*$ (where * indicates the complex conjugate) and the complex conjugate of (3.5.2) by $\hat{\mathbf{E}}$. The results are

$$\hat{\mathbf{H}}^* \cdot \nabla \times \hat{\mathbf{E}} = -j\omega\mu\hat{\mathbf{H}} \cdot \hat{\mathbf{H}}^* \quad (3.5.3)$$

$$\hat{\mathbf{E}} \cdot \nabla \times \hat{\mathbf{H}}^* = \hat{\mathbf{E}} \cdot \hat{\mathbf{J}}_0^* + \sigma\hat{\mathbf{E}} \cdot \hat{\mathbf{E}}^* - j\omega\varepsilon\hat{\mathbf{E}} \cdot \hat{\mathbf{E}}^* \quad (3.5.4)$$

(3.5.3) can now be subtracted from (3.5.4) to get

$$\begin{aligned} \hat{\mathbf{E}} \cdot \nabla \times \hat{\mathbf{H}}^* - \hat{\mathbf{H}}^* \cdot \nabla \times \hat{\mathbf{E}} = \\ \hat{\mathbf{E}} \cdot \hat{\mathbf{J}}_0^* + \sigma\hat{\mathbf{E}} \cdot \hat{\mathbf{E}}^* - j\omega\varepsilon\hat{\mathbf{E}} \cdot \hat{\mathbf{E}}^* + j\omega\mu\hat{\mathbf{H}} \cdot \hat{\mathbf{H}}^* \end{aligned} \quad (3.5.5)$$

Using the vector identity

$$\nabla \cdot (\bar{\mathbf{Q}}_1 \times \bar{\mathbf{Q}}_2) = \bar{\mathbf{Q}}_2 \cdot \nabla \times \bar{\mathbf{Q}}_1 - \bar{\mathbf{Q}}_1 \cdot \nabla \times \bar{\mathbf{Q}}_2, \quad (3.5.6)$$

(3.5.6) becomes

$$\begin{aligned} -\nabla \cdot (\hat{\mathbf{E}} \times \hat{\mathbf{H}}^*) = \\ \hat{\mathbf{E}} \cdot \hat{\mathbf{J}}_0^* + \sigma\hat{\mathbf{E}} \cdot \hat{\mathbf{E}}^* + j2\omega \left(\frac{1}{2} \mu \hat{\mathbf{H}} \cdot \hat{\mathbf{H}}^* - \frac{1}{2} \varepsilon \hat{\mathbf{E}} \cdot \hat{\mathbf{E}}^* \right) \end{aligned} \quad (3.5.7)$$

For time-harmonic fields, this represents the conservation of energy equation in differential form. Integrating (3.5.7) and applying the divergence theorem

$$\oiint_S \bar{Q} \cdot d\bar{s} = \iiint_V \nabla \cdot \bar{Q} dv \quad (3.5.8)$$

where V is the volume bounded by the surface S as shown in Fig. 3.5.1 yields

$$\begin{aligned} - \iiint_V \hat{E} \cdot \hat{J}_0^* dv &= \oiint_S (\hat{E} \times \hat{H}^*) \cdot d\bar{s} + \iiint_V \sigma \hat{E} \cdot \hat{E}^* dv \\ &+ j2\omega \iiint_V \left(\frac{1}{2} \mu \hat{H} \cdot \hat{H}^* - \frac{1}{2} \epsilon \hat{E} \cdot \hat{E}^* \right) dv \end{aligned} \quad (3.5.9)$$

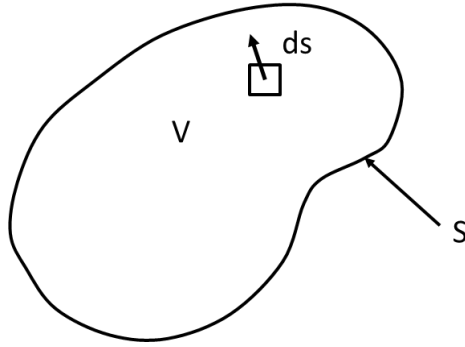


Fig. 3.5.1. Region V (bounded by the closed surface S) that may contain a continuously inhomogeneous material (i.e., no discontinuities in material parameters).

Here

$$P_s = - \iiint_V \hat{E} \cdot \hat{J}_0^* dv \quad (3.5.10)$$

is the complex power supplied to the volume V (Watts)

$$P_e = \oiint_S (\hat{E} \times \hat{H}^*) \cdot d\bar{s} \quad (3.5.11)$$

is the complex power leaving the volume V through S (Watts)

$$P_d = \iiint_V \sigma \hat{E} \cdot \hat{E}^* dv \quad (3.5.12)$$

is the real power dissipated inside the volume V (Watts)

$$W_m = \iiint_V \left(\frac{1}{2} \mu \hat{H} \cdot \hat{H}^* \right) dv \quad (3.5.13)$$

is the time averaged magnetic energy stored in V (Joules)

$$W_e = \iiint_V \left(\frac{1}{2} \hat{\epsilon} \hat{\mathbf{E}} \bullet \hat{\mathbf{E}}^* \right) dv \quad (3.5.14)$$

is the time averaged electric energy stored in V (Joules) so that Poynting's theorem can be written as

$$P_s = P_e + P_d + j2\omega(W_m - W_e) \quad (3.5.15)$$

where, as stated earlier, it is assumed in (3.5.10) - (3.5.14) that $\bar{\mathbf{E}}$ and $\bar{\mathbf{H}}$ are written in terms of "RMS" values. This result is a statement of conservation of energy although the interpretation of specific terms has been a subject of controversy (Wen et. al 2000). Nevertheless, the interpretation of the term

$$P_e = \text{Re} \left[\oint_S \left(\hat{\mathbf{E}} x \hat{\mathbf{H}}^* \right) \bullet d\bar{s} \right] \text{ Watts} \quad (3.5.16)$$

which will be used in this manuscript is clear. It represents the is the time averaged real power leaving the volume V and passing through the surface S.

3.6 The Uniqueness Theorem – Frequency Domain



To understand how boundary conditions interact with Maxwell's equations, it is necessary to consider the uniqueness theorem (Harrington 2001; Balanis, 1989). In this section, materials that are linear (because of the time-harmonic assumption) and isotropic (since based on Poynting's theorem) but possibly continuously inhomogeneous in a region V surrounded by a boundary S will be considered. The volume is shown in Fig. 3.5.1.

Since the problem will be limited to the time harmonic (i.e., $\exp(j\omega t)$) case, Poynting's theorem can be used as the starting point here and is

$$\oint_S \hat{\mathbf{E}} x \hat{\mathbf{H}}^* \bullet ds + \iiint_V \left(\hat{\mathbf{E}} \bullet \hat{\mathbf{J}}_0^* + (\sigma - j\omega\epsilon) \hat{\mathbf{E}} \bullet \hat{\mathbf{E}}^* + (j\omega\mu) \hat{\mathbf{H}} \bullet \hat{\mathbf{H}}^* \right) dv = 0 \quad (3.6.1)$$

To study uniqueness, it is first assumed that there are two sets of solutions within V. They are:

$$\left(\hat{\mathbf{E}}_a, \hat{\mathbf{H}}_a \right) \quad \text{and} \quad \left(\hat{\mathbf{E}}_b, \hat{\mathbf{H}}_b \right).$$

Now since it has been assumed that all material within V is linear, the difference between solution sets “a” and “b” must also be a solution. This “third” solution is written as

$$\left(\hat{\delta E}, \hat{\delta H} \right)$$

where

$$\hat{\delta E} = \hat{E}_a - \hat{E}_b \quad \text{and} \quad \hat{\delta H} = \hat{H}_a - \hat{H}_b.$$

Note that since the source of the “a” and “b” fields is the same, $\hat{J}_{0a} - \hat{J}_{0b} = 0$. If the difference fields are now used in Poynting’s theorem, then

$$\oiint_S \hat{\delta E} \times \hat{\delta H}^* \cdot \bar{n} ds + \iiint_V \left((\sigma - j\omega\epsilon) \left| \hat{\delta E} \right|^2 + (j\omega\mu) \left| \hat{\delta H} \right|^2 \right) dv = 0 \quad (3.6.2)$$

where

$$\left| \hat{\delta E} \right|^2 = \hat{\delta E} \cdot \hat{\delta E}^* \quad \text{and} \quad \left| \hat{\delta H} \right|^2 = \hat{\delta H} \cdot \hat{\delta H}^*.$$

At this point, it is possible to look for conditions under which the surface integral in (3.6.2) becomes zero. If these are found, then the volume integral must also be zero. As long as $\sigma \neq 0$, then this implies that $\hat{\delta E} = \hat{\delta H} = 0$ everywhere within the volume V. This implies that if a set of fields (\bar{E}, \bar{H}) satisfies Maxwell’s equations (used in setting up Poynting’s theorem) and satisfies some conditions on the surface S, then there can be only one solution throughout V because any two separate solutions must be equal everywhere within V.

Now, the specific conditions for which the surface integral in (3.6.2) is equal to zero will be determined. Let $\bar{n} \times \hat{E}_a = \bar{n} \times \hat{E}_b$ on S (i.e., the tangential component of E is known on the surface S and hence must be the same for all solutions “a” and “b”). The integrand of the surface integral is

$$\hat{\delta E} \times \hat{\delta H} \cdot \bar{n} dS \quad (3.6.3)$$

If the difference fields are written explicitly in terms of tangential and normal components as

$$\hat{\delta E} = \hat{\delta E}_t \bar{a}_t + \left(\hat{\delta E} \cdot \bar{n} \right) \bar{n} \quad (3.6.4)$$

$$\hat{\delta H} = \hat{\delta H}_t \bar{a}_t + \left(\hat{\delta H} \cdot \bar{n} \right) \bar{n}, \quad (3.6.5)$$

Then (3.6.3) reduces to

$$\hat{\delta}\hat{E}_t \times \hat{\delta}\hat{H}_t \cdot \hat{n} dS \quad (3.6.6)$$

Clearly if either the tangential E field or the tangential H field is known everywhere on S then $\hat{n} \times \hat{E}_a = \hat{n} \times \hat{E}_b$, $\hat{\delta}\hat{E}_t$ or $\hat{\delta}\hat{H}_t = 0$ on S and the surface integral in (3.6.2) is zero. Given this, as stated above, the E and H fields everywhere within V must be unique and uniqueness is proven.

Next, it is useful to expand this theorem to the case for which V is divided into two parts and the boundary coincides with a step jump in the values of at least one material parameter. Consider the volume shown below in Fig. 3.6.1

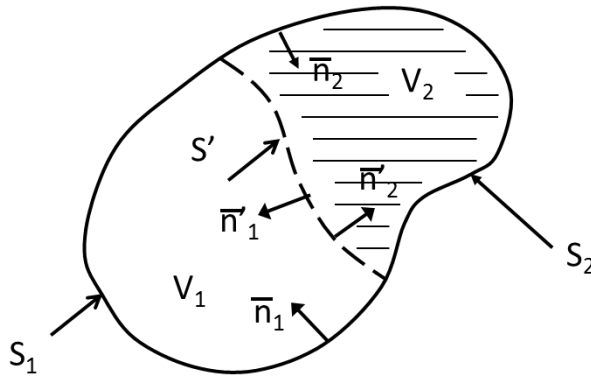


Fig. 3.6.1. Regions V_1 and V_2 (bounded by S_1 and S_2) that each contains a continuously inhomogeneous material except on S' where there is a discontinuity in at least one material parameters.

The approach to the proof here by assuming the following sets of solutions.

$$\text{Volume 1 - } \left(\hat{E}_{1a}, \hat{H}_{1a} \right) \text{ and } \left(\hat{E}_{1b}, \hat{H}_{1b} \right)$$

$$\text{Volume 2 - } \left(\hat{E}_{2a}, \hat{H}_{2a} \right) \text{ and } \left(\hat{E}_{2b}, \hat{H}_{2b} \right)$$

Again, by linearity,

$$\left(\hat{\delta}\hat{E}_1, \hat{\delta}\hat{H}_1 \right) \text{ is a valid solution set in volume 1 and}$$

$$\left(\hat{\delta}\hat{E}_2, \hat{\delta}\hat{H}_2 \right) \text{ is a valid solution set in volume 2.}$$

If now, Poynting's theorem is applied in both Volume 1 and Volume 2, the result is

$$\iint_{S_1} \hat{\mathbf{E}}_1 x \hat{\mathbf{H}}_1^* \cdot \bar{\mathbf{n}}_1 ds + \iint_{S'} \hat{\mathbf{E}}_1 x \hat{\mathbf{H}}_1^* \cdot \bar{\mathbf{n}}_1 ds + \iiint_{V_1} \left((\sigma_1 - j\omega\epsilon_1) \left| \hat{\mathbf{E}}_1 \right|^2 + (j\omega\mu_1) \left| \hat{\mathbf{H}}_1 \right|^2 \right) dv = 0 \quad (3.6.7)$$

$$\iint_{S_2} \hat{\mathbf{E}}_2 x \hat{\mathbf{H}}_2^* \cdot \bar{\mathbf{n}}_2 ds + \iint_{S'} \hat{\mathbf{E}}_2 x \hat{\mathbf{H}}_2^* \cdot \bar{\mathbf{n}}_1 ds + \iiint_{V_2} \left((\sigma_2 - j\omega\epsilon_2) \left| \hat{\mathbf{E}}_2 \right|^2 + (j\omega\mu_2) \left| \hat{\mathbf{H}}_2 \right|^2 \right) dv = 0 \quad (3.6.8)$$

Now, given that either $\bar{\mathbf{n}}x\hat{\mathbf{E}}$ or $\bar{\mathbf{n}}x\hat{\mathbf{H}}$ is assumed known on S_1 and S_2 , the integrals over S_1 and S_2 go to zero as in the first case. To examine the remaining terms, the two equations will be added to get (noting that $\bar{\mathbf{n}}_1 = -\bar{\mathbf{n}}_2$ on S')

$$\iint_{S'} \left(\hat{\mathbf{E}}_1 x \hat{\mathbf{H}}_1^* - \hat{\mathbf{E}}_2 x \hat{\mathbf{H}}_2^* \right) \cdot \bar{\mathbf{n}}_1 ds + \sum_{i=1}^2 \iiint_{V_i} \left((\sigma_i - j\omega\epsilon_i) \left| \hat{\mathbf{E}}_i \right|^2 + (j\omega\mu_i) \left| \hat{\mathbf{H}}_i \right|^2 \right) dv = 0 \quad (3.6.9)$$

Suppose next that on S'

$$\begin{aligned} \bar{\mathbf{n}}x\hat{\mathbf{E}}_{1a} &= \bar{\mathbf{n}}x\hat{\mathbf{E}}_{2a}, & \bar{\mathbf{n}}x\hat{\mathbf{E}}_{1b} &= \bar{\mathbf{n}}x\hat{\mathbf{E}}_{2b} \quad \text{and} \\ \bar{\mathbf{n}}x\hat{\mathbf{H}}_{1a} &= \bar{\mathbf{n}}x\hat{\mathbf{H}}_{2a}, & \bar{\mathbf{n}}x\hat{\mathbf{H}}_{1b} &= \bar{\mathbf{n}}x\hat{\mathbf{H}}_{2b} \end{aligned}$$

Then,

$$\bar{\mathbf{n}}x\hat{\mathbf{E}}_1 = \bar{\mathbf{n}}x\hat{\mathbf{E}}_2 \quad \text{and} \quad \bar{\mathbf{n}}x\hat{\mathbf{H}}_1 = \bar{\mathbf{n}}x\hat{\mathbf{H}}_2$$

In this case, the integral over S' portion of (3.6.9) goes to zero and by the same arguments used previously \mathbf{E} and \mathbf{H} are unique with V_1 and V_2 .

Note that the condition imposed on the fields on S' is the different from the condition on S_1 and S_2 . On S' it is NOT assumed that $\bar{\mathbf{n}}x\hat{\mathbf{E}}$ or $\bar{\mathbf{n}}x\hat{\mathbf{H}}$ is known. Rather, it is assumed that the DISCONTINUITY (usually = 0 which means that the component of the field is continuous) of both $\bar{\mathbf{n}}x\hat{\mathbf{E}}$ and $\bar{\mathbf{n}}x\hat{\mathbf{H}}$ IS KNOWN across S' .

In summary, the boundary conditions that result in a unique solution to Maxwell's equations are

$$\bar{\mathbf{n}}x\hat{\mathbf{E}} \quad \text{or} \quad \bar{\mathbf{n}}x\hat{\mathbf{H}} \quad \text{is known on } S_1 \text{ and } S_2 \quad (3.6.10)$$

$$\bar{\mathbf{n}}x\left(\hat{\mathbf{E}}_1 - \hat{\mathbf{E}}_2\right) \quad \text{and} \quad \bar{\mathbf{n}}x\left(\hat{\mathbf{H}}_1 - \hat{\mathbf{H}}_2\right) \quad \text{are known on } S' \quad (3.6.11)$$

Infinitely large regions

Suppose that volume V becomes all space. If this happens, then a boundary condition must be applied at infinity in order to prove uniqueness since it can be shown that the fields may not go to zero fast enough for the integral on the infinite surface to be zero. If there is even a small amount of lossy material filling the space, the fields decay away from the sources (assumed to be contained in a finite volume) exponentially and the field can be said to be zero on the infinite interface. Thus, uniqueness conditions are satisfied. If the region is not lossy, however, then it can be shown that uniqueness holds if the fields behave as

$$\lim_{r \rightarrow \infty} r \left(\frac{\partial \psi}{\partial r} + jk\psi \right) = 0 \quad (3.6.12)$$

as the infinite surface is approached. Here ψ represents the radial variation of either E or H and k is the propagation constant as the infinite surface is approached. This condition is called the “radiation condition” (Stratton 1941).

Edge conditions

Before completing the discussion of the uniqueness theorem, it is necessary to point out that the proof of the uniqueness theorem depends on the convergence of the two integrals on the right side of (3.6.2). This places some restrictions on the fields primarily at sharp edges of the geometry. Fields may diverge, but not so rapidly that the volume integral doesn't converge. These additional constraints on the fields are known as “edge conditions” (Hurd, 1976).

3.7 Electromagnetic Potentials ◀

In sourceless space, Maxwell's equations can be written as

$$\nabla \times \bar{E} + \frac{\partial \bar{B}}{\partial t} = 0, \quad \text{Faraday's Law} \quad (3.7.1)$$

$$\nabla \times \bar{H} - \frac{\partial \bar{D}}{\partial t} = 0, \quad \text{Ampere's Law} \quad (3.7.2)$$

$$\nabla \cdot \bar{B} = 0 \quad (3.7.3)$$

$$\nabla \cdot \bar{D} = 0 \quad \text{Gauss' Law} \quad (3.7.4)$$

According to the Helmholtz theorem (Collin, 1991) any well behaved vector field (\bar{Q}) satisfies

$$\bar{Q}(x, y, z) = \nabla x \left\{ \iiint_V \frac{\nabla' x \bar{Q}}{4\pi|r-r'|} dv' + \iint_S \frac{\bar{Q} x \bar{n}}{4\pi|r-r'|} ds' \right\} - \nabla \left\{ \iiint_V \frac{\nabla' \cdot \bar{Q}}{4\pi|r-r'|} dv' + \iint_S \frac{\bar{Q} \cdot \bar{n}}{4\pi|r-r'|} ds' \right\} \quad (3.7.5)$$

where V is any volume and S is its boundary and $|r-r'|$ is the source field point distance (in rectangular coordinates)

$$|r-r'| = \sqrt{(x-x')^2 + (y-y')^2 + (z-z')^2}$$

Now, if V is assumed to be all space, then

$$\bar{Q}(x, y, z) = \nabla x \left\{ \iiint_{all\ space} \frac{\nabla' x \bar{Q}}{4\pi|r-r'|} dv' \right\} - \nabla \left\{ \iiint_{all\ space} \frac{\nabla' \cdot \bar{Q}}{4\pi|r-r'|} dv' \right\} \quad (3.7.6)$$

Next, since $\nabla \cdot \bar{B} = 0$ everywhere from (3.7.3) above,

$$\bar{B} = \nabla x \bar{A} \quad \text{where} \quad \bar{A} = \bar{A}_0 - \nabla \psi \quad (3.7.7)$$

and

$$\bar{A}_0 = \iiint_{all\ space} \frac{\nabla' x \bar{B}}{4\pi|r-r'|} dv' \quad (3.7.8)$$

where ψ is any scalar field since $\nabla x(\nabla \psi) = 0$ by vector identity.

Next, using (3.7.1)

$$\nabla x \bar{E} + \frac{\partial}{\partial t} (\nabla x \bar{A}) = 0$$

or

$$\nabla x \left(\bar{E} + \frac{\partial \bar{A}}{\partial t} \right) = \nabla x \left(\bar{E} + \frac{\partial \bar{A}_0}{\partial t} \right) = 0 \quad (3.7.9)$$

since, again, $\nabla x(\nabla(\psi)) = 0$.

If, next, the field $\bar{E} + \frac{\partial \bar{A}_0}{\partial t}$ is inserted into the Helmholtz theorem (3.7.6), then

$$\bar{E} + \frac{\partial \bar{A}_0}{\partial t} = -\nabla \phi \quad (3.7.10)$$

where

$$\phi = \phi_0 + \frac{\partial \psi}{\partial t} \quad (3.7.11)$$

$$\phi_0 = \iiint_{\text{all space}} \frac{\nabla' \cdot \left(\bar{E} + \frac{\partial \bar{A}_0}{\partial t} \right)}{4\pi|r-r'|} dv' \quad (3.7.12)$$

Again, $\frac{\partial \psi}{\partial t}$ can be added because it is known that $\nabla x(\nabla(\psi)) = 0$.

Next, from (3.2.4) (for a simple linear medium)

$$\bar{D} = \varepsilon_0 \bar{E} + \bar{P}(\bar{E}) = \varepsilon_0 \varepsilon_r \bar{E} + \bar{P}_0 \quad (3.7.13)$$

where \bar{D} includes the not only the displacement (free space) contribution and that of the linearly polarizable charges in the dielectric, but also impressed (i.e., source) polarization \bar{P}_0 , the impressed electric dipole moment per unit volume. Thus³⁶,

$$\bar{D} = -\varepsilon_0 \varepsilon_r \left(\nabla \phi + \frac{\partial \bar{A}}{\partial t} \right) \bar{E} + \bar{P}_0 \quad (3.7.14)$$

and if

$$\bar{B} = \mu_0 \mu_r \bar{H},$$

then

$$\bar{H} = \frac{1}{\mu_0 \mu_r} \nabla x \bar{A}$$

Using these results in (3.7.2) and (3.7.4) yields

$$\nabla x \nabla x \bar{A} + \mu \varepsilon \left(\nabla \left(\frac{\partial \phi}{\partial t} \right) + \frac{\partial^2 \bar{A}}{\partial t^2} \right) = \mu \frac{\partial \bar{P}_0}{\partial t} \quad (3.7.15)$$

where

$$\varepsilon = \varepsilon_0 \varepsilon_r \text{ and } \mu = \mu_0 \mu_r$$

and

³⁶ Here ψ has been set to zero without loss of generality. Hence \bar{A} and \bar{A}_0 are identical

$$-\varepsilon \left(\nabla^2 \phi + \nabla \cdot \frac{\partial \bar{A}}{\partial t} \right) + \nabla \cdot \bar{P}_0 = 0 \quad (3.7.16)$$

At this point, it can be recognized that only $\nabla_x \bar{A}$ has been specified. But, according to the Helmholtz theorem, \bar{A} is not fully specified until $\nabla \cdot \bar{A}$ is specified. Thus, it may be said (for convenience) that

$$\nabla \cdot \bar{A} + \mu \varepsilon \frac{\partial \phi}{\partial t} = 0 \quad (3.7.17)$$

Hence, (3.7.15) becomes

$$\nabla_x \nabla_x \bar{A} - \nabla (\nabla \cdot \bar{A}) + \mu \varepsilon \frac{\partial^2 \bar{A}}{\partial t^2} = \mu \frac{\partial \bar{P}_0}{\partial t}$$

or

$$\nabla^2 \bar{A} - \mu \varepsilon \frac{\partial^2 \bar{A}}{\partial t^2} = -\mu \frac{\partial \bar{P}_0}{\partial t} \quad (3.7.18)$$

where (only in rectangular coordinates)

$$\nabla^2 \bar{A} \equiv (\nabla^2 A_x) \bar{a}_x + (\nabla^2 A_y) \bar{a}_y + (\nabla^2 A_z) \bar{a}_z \quad (3.7.19)$$

This equation defines the “electric vector potential.”

(3.7.16) now reduces to

$$\left(\nabla^2 \phi - \mu \varepsilon \frac{\partial^2 \bar{A}}{\partial t^2} \right) = \frac{1}{\varepsilon} \nabla \cdot \bar{P}_0 \quad (3.7.20)$$

By superposition, another solution to the homogeneous Maxwell equations may be added to \bar{A} and ϕ . To do this, the following can be written

$$\bar{D} = -\nabla_x \bar{A}^* \quad (3.7.21)$$

$$\bar{B} = \mu_0 \bar{H} + \mu_0 \bar{M}(\bar{H}) = \mu_0 \mu_r \bar{H} + \mu_0 \hat{M}_0 \quad (3.7.22)$$

where \bar{M}_0 is the magnetic moment per unit volume for simple magnetic material.

The resulting equation for the “magnetic vector potential” is

$$\nabla^2 \bar{A}^* - \mu \varepsilon \frac{\partial^2 \bar{A}^*}{\partial t^2} = -\mu_0 \varepsilon \frac{\partial \bar{M}_0}{\partial t} \quad (3.7.23)$$

with a similar equation for ϕ^*

$$\left(\nabla^2 \phi^* - \mu \varepsilon \frac{\partial^2 \phi^*}{\partial t^2} \right) = \frac{1}{\mu_0} \nabla \bullet \bar{M}_0 \quad (3.7.24)$$

Now in the sinusoidal steady state, it is only necessary to solve for \bar{A} and \bar{A}^* since ϕ and ϕ^* can be derived from them.

Next, the Hertz electric and magnetic potentials ($\bar{\Pi}$ and $\bar{\Pi}^*$ respectively) can be defined. These are:

$$\bar{A} = \mu \varepsilon \frac{\partial \bar{\Pi}}{\partial t} \quad (3.7.25)$$

and

$$\bar{A}^* = \mu \varepsilon \frac{\partial \bar{\Pi}^*}{\partial t}. \quad (3.7.26)$$

The wave equations for $\bar{\Pi}$ and $\bar{\Pi}^*$ become

$$\nabla^2 \bar{\Pi} - \mu \varepsilon \frac{\partial^2 \bar{\Pi}}{\partial t^2} = -\frac{1}{\varepsilon} \bar{P}_0 \quad (3.7.27)$$

and

$$\nabla^2 \bar{\Pi}^* - \mu \varepsilon \frac{\partial^2 \bar{\Pi}^*}{\partial t^2} = -\frac{1}{\mu_r} \bar{M}_0 \quad (3.7.28)$$

where

$$\phi = -\nabla \bullet \bar{\Pi} \quad \text{and} \quad \phi^* = -\nabla \bullet \bar{\Pi}^*.$$

Thus,

$$\bar{E} = \nabla \nabla \bullet \bar{\Pi} - \mu \varepsilon \frac{\partial^2 \bar{\Pi}}{\partial t^2} - \mu \nabla x \frac{\partial \bar{\Pi}^*}{\partial t} \quad (3.7.29)$$

and

$$\bar{H} = \nabla \nabla \bullet \bar{\Pi}^* - \mu \varepsilon \frac{\partial^2 \bar{\Pi}^*}{\partial t^2} + \varepsilon \nabla x \frac{\partial \bar{\Pi}}{\partial t} \quad (3.7.30)$$

For the time harmonic case

$$\nabla^2 \bar{\Pi} + \omega^2 \mu \varepsilon \bar{\Pi} = -\frac{1}{\varepsilon} \bar{P}_0 \quad (3.7.31)$$

and

$$\nabla^2 \bar{\Pi}^* + \omega^2 \mu \varepsilon \frac{\partial^2 \bar{\Pi}^*}{\partial t^2} = -\frac{1}{\mu_r} \bar{M}_0 \quad (3.7.32)$$

where $\phi = -\nabla \cdot \bar{\Pi}$ and $\phi^* = -\nabla \cdot \bar{\Pi}^*$. Thus, (3.7.29) and (3.7.30) can be written as

$$\bar{E} = \nabla \nabla \cdot \bar{\Pi} - \omega^2 \mu \varepsilon \bar{\Pi} - j \omega \mu \nabla x \bar{\Pi}^* \quad (3.7.29)$$

and

$$\bar{H} = \nabla \nabla \cdot \bar{\Pi}^* - \omega^2 \mu \varepsilon \bar{\Pi}^* + j \omega \varepsilon \nabla x \bar{\Pi} \quad (3.7.30)$$

3.8 Reciprocity Theory ◀

Electromagnetic reciprocity

The study of reciprocity theory begins with Faraday's and Amperes laws in time harmonic form from (3.1.11) with $\hat{B} = \mu_0 (\hat{H} + \hat{M}_0)$ and (3.1.12) with $\hat{D} = \varepsilon \hat{E}$ and $\hat{J} = \sigma \hat{E} + \hat{J}_0$ that are repeated here as (3.8.1) and (3.8.2) respectively (Harrington, 2001; Balanis, 1989)

$$\nabla x \hat{E} + j \omega \mu \hat{H} = \hat{M}_0, \quad (3.8.1)$$

where \bar{M}_0 is an impressed magnetization and

$$\nabla x \hat{H} - j \omega \varepsilon \left(1 - \frac{\sigma}{j \omega}\right) \hat{E} = \hat{J}_0, \quad (3.8.2)$$

where the source currents are designated as \hat{J}_0 and separated from the conduction currents $\hat{J}_c = \sigma \bar{E}$ and that

$$\hat{B} = \mu(x, y, z) \hat{H}, \quad \hat{D} = \varepsilon(x, y, z) \hat{E} \quad \text{and} \quad \hat{J}_c = \sigma(x, y, z) \hat{E}$$

These two equations are next applied to a linear and isotropic, but generally inhomogeneous region in space as shown in Fig. 3.8.1. Each region in the figure could represent a different material with position dependent conducting, dielectric and magnetic properties.

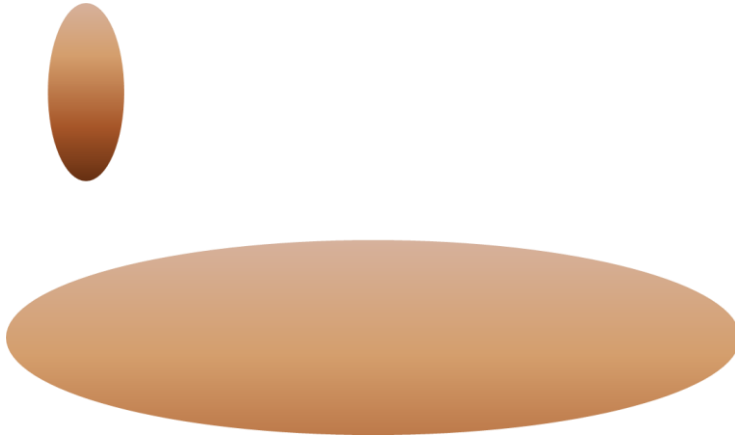


Fig. 3.8.1. The inhomogeneous region to which the reciprocity theorem applies.

Next, some distribution of electric and magnetic sources is inserted in the region as shown in Fig. 3.8.2. Maxwell's equations in this case become

$$\nabla \times \hat{E}_a + j\omega\mu\hat{H}_a = \hat{M}_{0a}, \quad (3.8.3)$$

$$\nabla \times \hat{H}_a - j\omega\epsilon\hat{E}_a - \sigma\hat{E}_a = \hat{J}_{0a}, \quad (3.8.4)$$

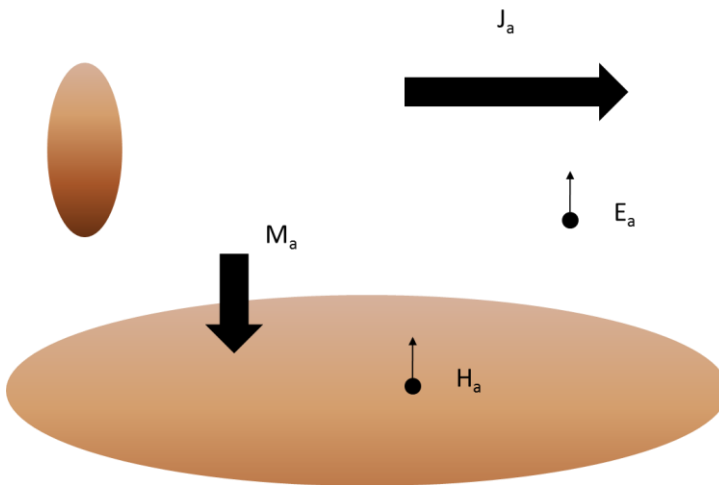


Fig. 3.8.2 The inhomogeneous region to which the reciprocity theorem applies with "a" sources and field points.

Similarly, it is possible to place a different set of sources and field points in the same region as shown in Fig. 3.8.3.

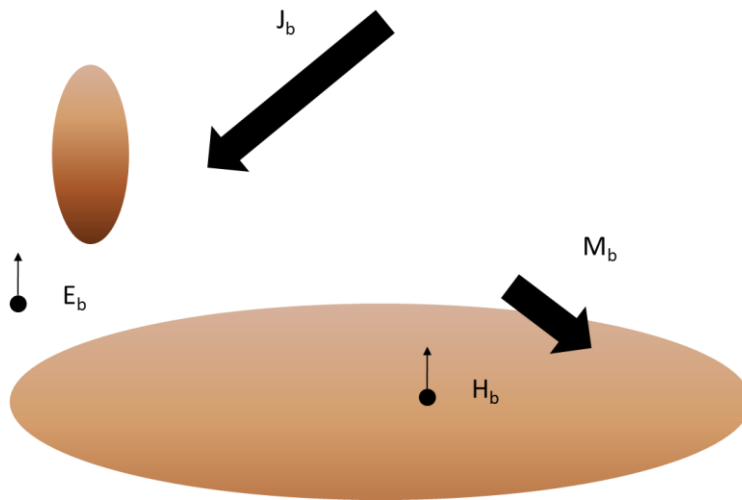


Fig. 3.8.3. The inhomogeneous region to which the reciprocity theorem applies with “b” sources and field points.

Maxwell’s equations in this case become

$$\nabla_x \hat{E}_b + j\omega\mu\hat{H}_b = \hat{M}_{0b}, \quad (3.8.5)$$

$$\nabla_x \hat{H}_b - j\omega\varepsilon\hat{E}_b - \sigma\hat{E}_b = \hat{J}_{0b}, \quad (3.8.6)$$

It is very important to note that, since both sets of sources (i.e., “a” and “b”) are in the same medium, the terms μ , ε , and σ are identical in both sets of equations. The next step in deriving the reciprocity theorem is to dot multiply (3.8.3) by \bar{H}_b , (3.8.4) by \bar{E}_b , (3.8.5) by \bar{H}_a and (3.8.6) by \bar{E}_a . The result is

$$\hat{H}_b \bullet \nabla_x \hat{E}_a + j\omega\mu\hat{H}_b \bullet \hat{H}_a = \hat{H}_b \bullet \hat{M}_{0a}, \quad (3.8.7)$$

$$\hat{E}_b \bullet \nabla_x \hat{H}_a - j\omega\varepsilon\hat{E}_b \bullet \hat{E}_a - \sigma\hat{E}_b \bullet \hat{E}_a = \hat{E}_b \bullet \hat{J}_{0a}, \quad (3.8.8)$$

$$\hat{H}_a \bullet \nabla_x \hat{E}_b + j\omega\mu\hat{H}_a \bullet \hat{H}_b = \hat{H}_a \bullet \hat{M}_{0b}, \quad (3.8.9)$$

$$\hat{E}_a \bullet \nabla_x \hat{H}_b - j\omega\varepsilon\hat{E}_a \bullet \hat{E}_b - \sigma\hat{E}_a \bullet \hat{E}_b = \hat{E}_a \bullet \hat{J}_{0b}, \quad (3.8.10)$$

If now, (3.8.7) and (3.8.8) are added together and (3.8.9) and (3.8.10) subtracted from this result, then

$$\begin{aligned} & \hat{E}_b \bullet \nabla x \hat{H}_a - \hat{E}_a \bullet \nabla x \hat{H}_b + \hat{H}_b \bullet \nabla x \hat{E}_a - \hat{H}_a \bullet \nabla x \hat{E}_b \\ & = \hat{H}_b \bullet \hat{M}_{0a} - \hat{H}_a \bullet \hat{M}_{0b} + \hat{E}_b \bullet \hat{J}_{0a} - \hat{E}_a \bullet \hat{J}_{0b} \end{aligned} \quad (3.8.11)$$

Note that all of the terms that contain material properties cancel because the material properties are the same for both the “a” and “b” problems. Next, by vector identity

$$(3.8.12)$$

$$\hat{E}_b \bullet \nabla x \hat{H}_a - \hat{E}_a \bullet \nabla x \hat{H}_b + \hat{H}_b \bullet \nabla x \hat{E}_a - \hat{H}_a \bullet \nabla x \hat{E}_b = \nabla \bullet \left(\hat{E}_a x \hat{H}_b - \hat{E}_b x \hat{H}_a \right)$$

Hence, if (3.8.11) is integrated over all space and the divergence law (i.e., 3.1.21) is applied,

$$\begin{aligned} & \iiint_{all\ space} \nabla \bullet \left(\hat{E}_a x \hat{H}_b - \hat{E}_b x \hat{H}_a \right) dv = \\ & \iiint_{all\ space} \left(\hat{H}_b \bullet \hat{M}_{0a} - \hat{H}_a \bullet \hat{M}_{0b} + \hat{E}_b \bullet \hat{J}_{0a} - \hat{E}_a \bullet \hat{J}_{0b} \right) dv \end{aligned} \quad (3.8.13)$$

and

$$\begin{aligned} & \oint_{S_\infty} \left(\hat{E}_a x \hat{H}_b - \hat{E}_b x \hat{H}_a \right) \bullet d\bar{s} = \\ & \iiint_{all\ space} \left(\hat{H}_b \bullet \hat{M}_{0a} - \hat{H}_a \bullet \hat{M}_{0b} + \hat{E}_b \bullet \hat{J}_{0a} - \hat{E}_a \bullet \hat{J}_{0b} \right) dv \end{aligned} \quad (3.8.14)$$

where S_∞ is the infinite boundary. If \bar{E} and \bar{H} decay rapidly enough that the integral over $S_\infty = 0$, then (3.8.14) becomes

$$\iiint_{all\ space} \left(\hat{H}_b \bullet \hat{M}_{0a} - \hat{H}_a \bullet \hat{M}_{0b} + \hat{E}_b \bullet \hat{J}_{0a} - \hat{E}_a \bullet \hat{J}_{0b} \right) dv = 0 \quad (3.8.15)$$

In the form that will be used here, M is set equal to zero, so that

$$\iiint_{all\ space} \left(\hat{E}_b \bullet \hat{J}_{0a} \right) dv = \iiint_{all\ space} \left(\hat{E}_a \bullet \hat{J}_{0b} \right) dv \quad (3.8.16)$$

Clearly, the only places that the integrands are not zero are where the source currents for either problem “*a*” or “*b*” are located. For currents that exist only along a line, (3.8.16) can be rewritten as (Weeks, 1968)

$$\int_{ca} \hat{\mathbf{E}}_b \cdot \hat{\mathbf{I}}_{0a} dl = \int_{cb} \hat{\mathbf{E}}_a \cdot \hat{\mathbf{I}}_{0b} dl \quad (3.8.17)$$

where “*ca*” and “*cb*” represent the lines on which sources I_{sa} and I_{sb} lie.

Application to circuit theory

As an example, consider the environment shown in Fig. 3.8.4 which is designed to look like that of a simple electrical circuit.

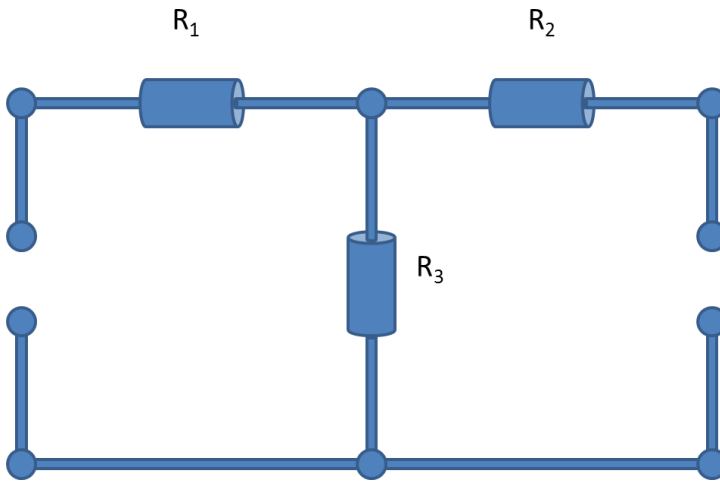


Fig. 3.8.4. The environment of a simple electrical circuit.

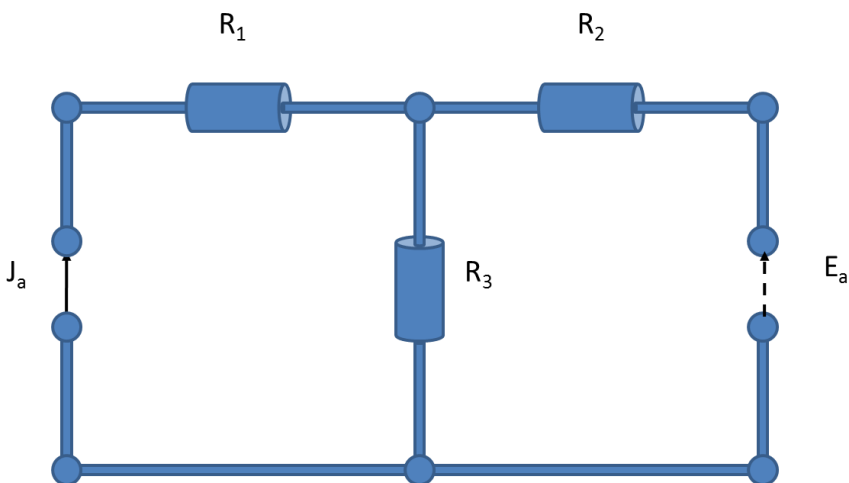


Fig. 3.8.5. The environment of a simple electrical circuit with a source at the left terminals.

As shown in Fig. 3.8.6, a current source placed between the two terminals on the right hand side of the circuit (problem “b”) causes an electric field everywhere, but most specifically between the terminals on the left hand side of the circuit where the problem “a” current was placed earlier.

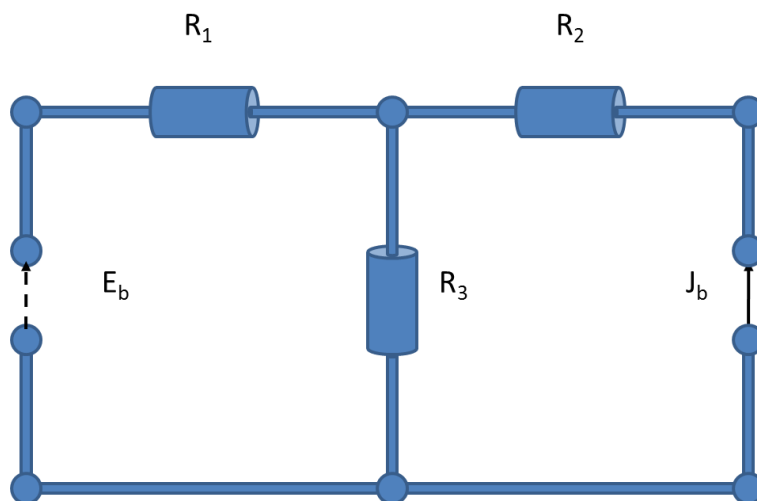


Fig. 3.8.6. The environment of a simple electrical circuit with a source at the left terminals.

If 3.8.16 is now applied to problems “a” and “b” shown in Figs. 3.8.5 and 3.8.6 respectively, the result is

$$\hat{I}_a \int_1^2 \hat{E}_b dl = -\hat{I}_a \hat{V}_{b12} = \hat{I}_b \int_1^2 \hat{E}_a dl = -\hat{I}_b \hat{V}_{a12} \quad (3.8.18)$$

This is the familiar reciprocity theorem from circuit theory, but derived from electromagnetic theory. Note that there are no frequency restrictions on this except that the terminals over which the voltage is defined must be close compared to a wavelength. Further, the only restrictions on the geometry are that the material be linear and isotropic.

Electrostatic reciprocity

Reciprocity can also be formulated using electrostatic theory (Smythe, 1968). The geometry that will be assumed is the same as shown in Fig. 3.8.1. The first “a” problem that will be considered next is shown in Fig. 3.8.7. Here a charge distribution ρ_a is placed in the region which causes a potential distribution V_a in the region. Similarly, for the “b” problem, a charge distribution ρ_b is placed in the region which causes a potential distribution V_b in the region. This problem is shown in Fig. 3.8.8.

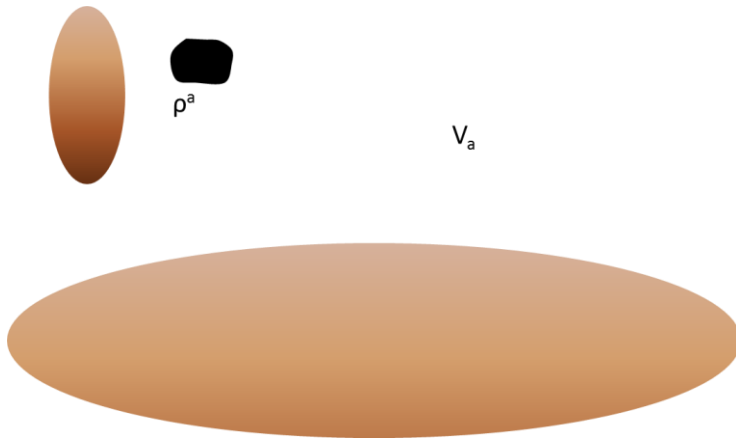


Fig. 3.8.7. The inhomogeneous region to which the reciprocity theorem applies with “a” sources and field points.

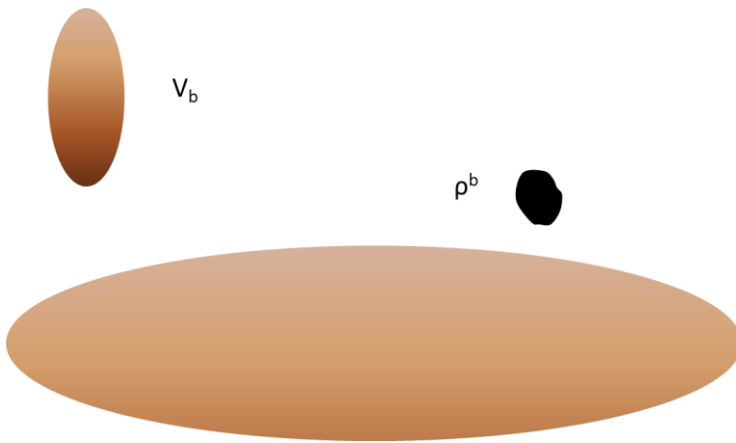


Fig. 3.8.8. The inhomogeneous region to which the reciprocity theorem applies with “a” sources and field points.

The governing equations for the electrostatics problem above with the “a” sources are:

$$\nabla \cdot \bar{D}_a = \rho_a \quad (3.8.19)$$

and

$$\bar{E}_a = -\nabla \phi_a \quad (3.8.20)$$

Similarly, the governing equations for the same problem but with the “b” sources are:

$$\nabla \cdot \bar{D}_b = \rho_b \quad (3.8.21)$$

and

$$\bar{E}_b = -\nabla\phi_b \quad (3.8.22)$$

If now, (3.8.19) is multiplied by ϕ_b , (3.8.21) is multiplied by ϕ_a and the two results are subtracted, the following result is obtained

$$\phi_b\nabla\bullet\bar{D}_a - \phi_a\nabla\bullet\bar{D}_b = \phi_b\rho_a - \phi_a\rho_b \quad (3.8.23)$$

but, by the vector identity

$$\phi\nabla\bullet\bar{D} = \nabla\bullet(\phi\bar{D}) - \bar{D}\bullet\nabla\phi \quad (3.8.24)$$

(3.8.23) can be converted into

$$\nabla\bullet(\phi_b\bar{D}_a) - \nabla\bullet(\phi_a\bar{D}_b) - \bar{D}_a\bullet\nabla\phi_b + \bar{D}_b\bullet\nabla\phi_a = \phi_b\rho_a - \phi_a\rho_b \quad (3.8.25)$$

Next, (3.8.20) and (3.8.22) can be used along with the relation $\bar{D} = \varepsilon E$ to obtain

$$\begin{aligned} \nabla\bullet(\phi_b\bar{D}_a) - \nabla\bullet(\phi_a\bar{D}_b) + \varepsilon\bar{E}_a\bullet\bar{E}_b - \varepsilon\bar{E}_b\bullet\bar{E}_a &= \phi_b\rho_a - \phi_a\rho_b \quad \text{or} \\ \nabla\bullet(\phi_b\bar{D}_a) - \nabla\bullet(\phi_a\bar{D}_b) &= \phi_b\rho_a - \phi_a\rho_b \end{aligned} \quad (3.8.26)$$

where the two center terms cancel because the environment is the same for the “a” and “b” problems. If, now, (3.8.26) is integrated over a volume V

$$\iiint_V (\nabla\bullet(\phi_b\bar{D}_a) - \nabla\bullet(\phi_a\bar{D}_b)) dv = \iiint_V (\phi_b\rho_a - \phi_a\rho_b) dv \quad (3.8.27)$$

Finally, an application of the divergence theorem

$$\iiint_V \nabla\bullet\bar{A} dv = \oiint_S \bar{A}\bullet d\bar{s} \quad (3.8.28)$$

results in

$$\oiint_S (\phi_b\bar{D}_a - \phi_a\bar{D}_b)\bullet d\bar{s} = \iiint_V (\phi_b\rho_a - \phi_a\rho_b) dv \quad (3.8.29)$$

If S is expanded to include all space and the surface integral goes to zero, then

$$\iiint_V (\phi_b\rho_a - \phi_a\rho_b) dv = 0 \quad (3.8.30)$$

which is the desired result.

3.9 Problems

P3.1. Based on the Maxwell's equations listed in (3.1.1) – (3.1.4) and the vector identity of (3.1.6), derive the continuity equation as given by (3.1.5). (Briefly explain the physical meaning of the continuity equation.)

P3.2. The time-harmonic electric field inside a source-free, homogeneous, isotropic, and linear medium is given by (in Cartesian Coordinates and assume the time variation term is $e^{j\omega t}$)

$$\hat{\mathbf{E}} = \bar{a}_y \hat{E}_0 \sin\left(\frac{\pi}{\alpha} xy\right) e^{-j\beta z} \quad (\text{P3.2a})$$

where E_0 , a , and β are all constants. Given the permittivity of the medium, ϵ (Farads/m), the electric flux density D (Coulombs/m²) can be found by

$$\hat{\mathbf{D}} = \epsilon \hat{\mathbf{E}} \quad (\text{P3.2b})$$

In the medium, by using the Maxwell's equations, determine: (a) the electric charge density ρ (Coulombs/m³), (b) the magnetic field H (A/m) given that the permeability of the medium is μ (Henries/m) and the magnetic flux density $B = \mu H$.

P3.3. Derive the wave equation for the magnetic field as given by (3.3.6). Assume the region of interest has, respectively, the permittivity and permeability of ϵ and μ , neither of which is a function of position.

P3.4. Consider an interface between two source-free (no free charges) media, shown in Fig. P3.4, both of which have finite conductivity. Media 1 and 2 are characterized by the constitutive parameters $\epsilon_1, \mu_1, \sigma_1$ and $\epsilon_2, \mu_2, \sigma_2$, respectively. Show that the tangential electric fields across the interface are continuous ($E_{1t} = E_{2t}$) by applying the integral form of Faraday's law given in (3.1.18). (Note: the “= 0” on the most right hand side of (3.1.16), (3.1.18), and (3.1.19) should be removed.) Hint: choose a rectangular box as shown in Fig. 1 and apply Faraday's law on the box. The integral of the \mathbf{B} field can be reduced to zero if the height Δh of the box is small enough.

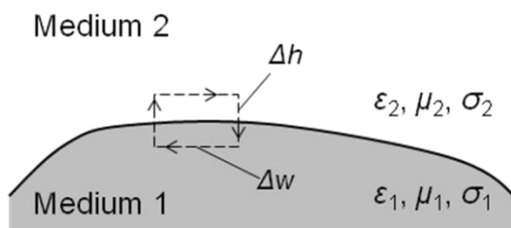


Fig. P3.4. A source-free interface between two media

P3.5. Suppose there is a current I (A, rms value) flowing through a long straight resistance cylinder, which has radius of a (m) and conductivity of σ (S/m). Choose the axis of the cylinder to be the z -axis and the x - y plane coincides with one of its cross-sections, as shown in Fig. P3.5. Now only consider a segment of length L (m) of this cylinder. Assume the current is evenly distributed over the cross-section of the cylinder. Determine:

- the electric and magnetic fields on the circumferential surface of the cylinder and the directions of them; (Hint: the electric field can be determined by the current density in the cylinder, $\bar{J}_c = \sigma \bar{E}$.)
- the power dissipated in the cylinder ($P_s = -\iiint_V \hat{E} \bullet \hat{J}_i^* dv$);
- the Poynting vector (including the magnitude and direction) and the power exiting (or entering) the circumferential surface of the cylinder ($P_e = \oint_S (\hat{E} \times \hat{H}^*) \bullet d\bar{s}$).
- Compare the results from (b) and (c).

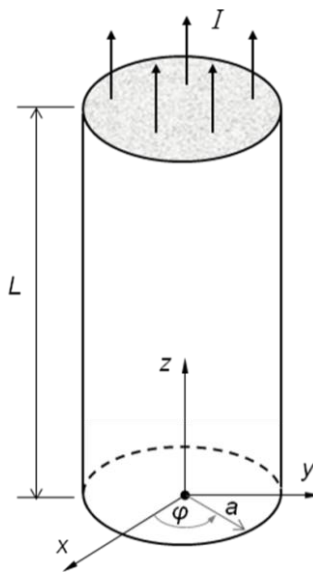


Fig. P3.5. Resistance cylinder

P3.6. The parameters of a simple circuit are given as shown in Fig. P3.6 (a). An ammeter is connected in one of the branches. Determine the current, I_b , flowing through the ammeter. Then, switch the position of the voltage source V_s and the ammeter, Fig. P3.6 (b). Calculate the new current in the meter. Compare the results of the two calculations.

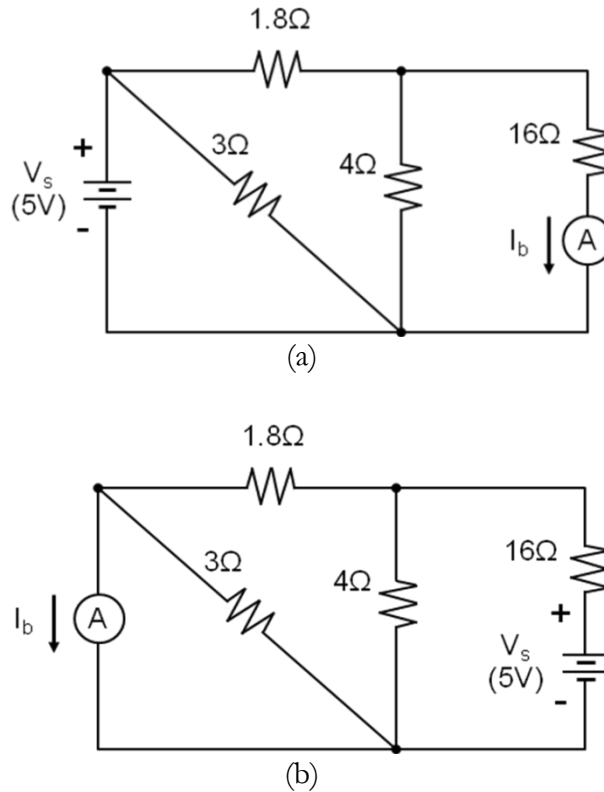


Fig. P3.6. Simple circuit to demonstrate the reciprocity theorem

3.10 References

- Balanis, C. A. 1989. *Advanced Engineering Electromagnetics*. Wiley, New York.
- Collin, R. E. 1991. *Field Theory of Guided Waves*, IEEE Press Series on Electromagnetic Wave Theory, Institute of Electrical and Electronics Engineers, Inc. New York.
- Dudley, D. G. 1994. *Mathematical Foundations for Electromagnetic Theory*, IEEE Press, New York.
- Harrington, R. F. 2001. *Time-Harmonic Electromagnetic Fields*. IEEE Press Series on Electromagnetic Wave Theory, Institute of Electrical and Electronics Engineers, Inc. New York.
- Hurd, R. 1976. "The Edge Condition in Electromagnetics," *IEEE Transactions on Antennas and Propagation*, Vol. AP-24. pp. 70-73. January.
- Smythe, W. R. 1968. *Static and Dynamic Electricity*, McGraw Hill, New York.

Stratton, J. A. 1941. *Electromagnetic Theory*. McGraw Hill, New York.

Weeks, W. L. 1968. *Antenna Theory*. McGraw Hill, New York.

Wen G., P. Jarmuszewski and Y. Qi. 2000. "The Foster Reactance Theorem for Antennas and Radiation Q," *IEEE Transactions on Antennas and Propagation*. Vol. APS-48, pp. 401 – 408, March

Chapter IV

Propagation on an Infinitely Long Single Conductor Transmission Line above Homogeneous Earth

4.1 Introduction

Problem definition

The purpose of this chapter is to review the exact mathematical theory for the problem illustrated in Fig. 4.1.1.

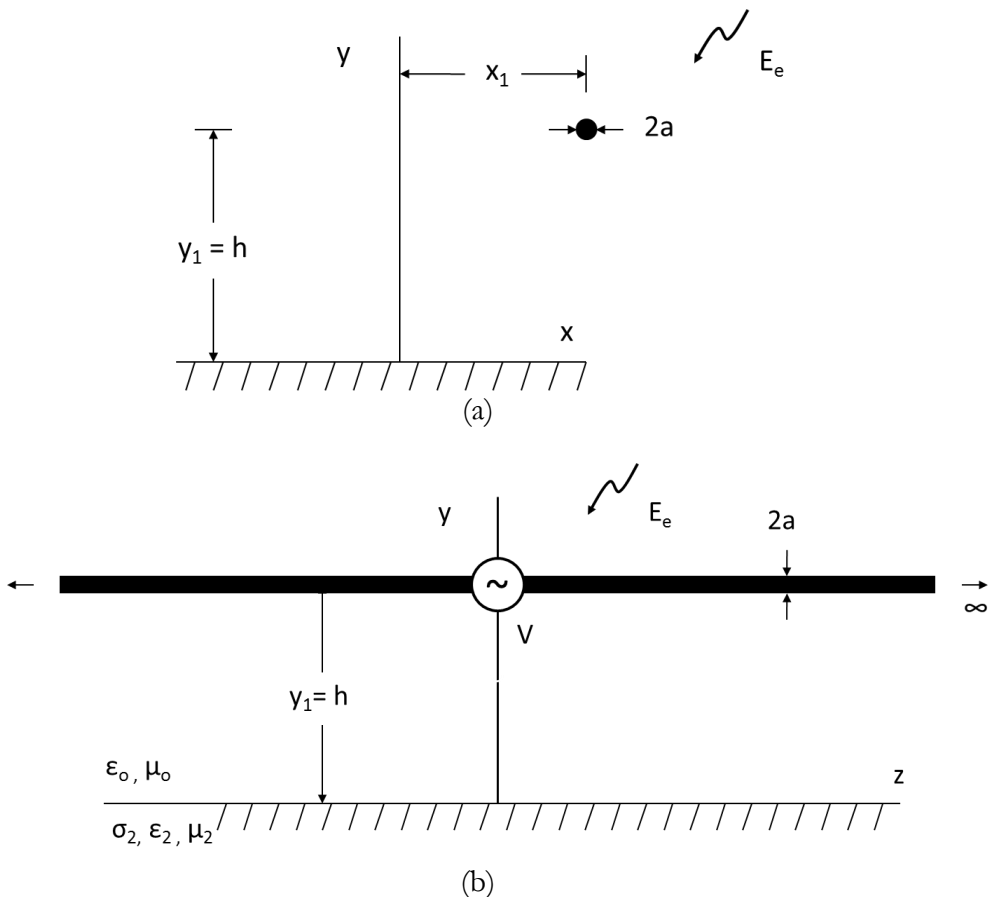


Fig. 4.1.1. a) end view and b) side view of the wire of radius “a” and height “ $y_1 = h$ ” above a linear, homogeneous isotropic lossy earth where V is a voltage source at its center and E_e is the electric field from an external source.

More specifically, the electric currents on a single infinitely long horizontal conductor located above a single-layer, linear, homogeneous, isotropic, lossy (i.e., non-zero conductivity) earth caused by a single frequency voltage source³⁷ at its center and/or an electromagnetic field (\bar{E}_e) from an external source will be found. This problem is the idealized problem described in Chapter 2, Section 2.3 for a single conductor.

Here, the z-oriented, horizontal conductor has radius a, and is located at a distance h above the earth and a distance x' from the y axis (Wait 1962; Kuester et. al. 1978). Standard International (SI) units are assumed. The upper half space (i.e., y > 0) is free space and is characterized by permittivity and permeability $\epsilon_1 = \epsilon_0$ and $\mu_1 = \mu_0$ respectively while the lower half space (i.e., y < 0) is a linear, homogeneous, isotropic lossy material characterized by conductivity, permittivity and permeability $\sigma_2, \epsilon_2 = \epsilon_{r2}\epsilon_0$ and $\mu_2 = \mu_{r2}\mu_0$ respectively. ϵ_{r2} and μ_{r2} are the relative permittivity and permeability of the half space respectively. The conductor is assumed to be non-magnetic (i.e., $\mu_w = \mu_0$) and to have a conductivity σ_w . The dielectric constant of the conductor is not needed since it is only used to calculate displacement currents and below optical frequencies these can always be neglected in the conductor. The conductor is driven by a voltage source of RMS magnitude V at z = 0 and by an electric field \bar{E}_e from some external source and it is assumed that all sources vary in time as $\exp(j\omega t)$. The external source could represent a man-made source such as a communications antenna or a natural source such as lightning or a corona discharge near a conductor.

Problem solution

The method by which the solution is found can be summarized as follows. First, an unknown current distribution $\hat{I}(z')$ is assumed to be carried by the conductor. Second, this current distribution is divided into infinitesimal lengths dz' and the axially directed electric field $\hat{E}_z(z, z')$ due to the short current element $\hat{I}(z')dz'$ is formally written (the specific formula for this will be determined later). Third, this result for $\hat{E}_z(z, z')$ is integrated over the entire conductor. The result is a formal expression for the axial electric field $\hat{E}_z(z)$ of the entire conductor current. Finally, an integral equation for the (as yet) unknown current distribution is obtained by setting $\hat{E}_z(z)$ plus the axial electric field of the external source (if any) equal to the axial electric field of the source voltage at $z = 0$ and an impedance boundary condition on the remainder of the conductor.

³⁷ It will be assumed that sinusoidal steady state sources and fields are phasors (e.g., \hat{A}) with RMS magnitudes and phases measured in radians. Hence the time variation can be found as $a(t) = \sqrt{2} \text{Re}(\hat{A} \exp(j\omega t))$.

The effect of the earth is taken into account when calculating the electromagnetic field of each short current element and is represented by Sommerfeld integrals (details are provided later). At lower frequencies, these integrals will be shown to produce expressions for the external inductance and capacitance per unit length of an equivalent transmission line for this system. The impedance boundary condition accounts for the distribution of current inside the conductor caused by the skin effect. At low frequency, this will be shown to produce expressions for the internal inductance and resistance per unit length of an equivalent transmission line. Details of the solution process are provided in Section 4.2. Once the integral equation has been set up, it is solved using Fourier Transform theory³⁸. Details of this are provided in Section 4.3.

Solution validity

The solution is formally valid at any frequency for which the conductor radius is small compared to a wavelength at the frequency of interest, for which the earth is represented by electrical constants appropriate to the frequency and for which the conductor can be represented by a surface impedance (generally at and below microwave frequencies). As a result, the solution can be used to study antenna problems at high frequency as well as power line propagation problems at low frequency. These two extremes are not separate issues and it is important that this not be forgotten. In fact, there are certain cases (such as for calculating electromagnetic interference from corona) for which general theory is needed even for analysis of power transmission lines.

Readers interested only in low frequency behavior

Given, however, that the interest of many readers is restricted to the behavior of power lines at lower frequencies (i.e., generally below 1 MHz), there is no need for these readers to spend a great deal of effort to understand the first few sections of this chapter. Rather, these readers can skip sections marked with a ◀ here and in the table of contents and proceed to Section 4.7 where a special introduction is written for readers who have skipped earlier sections.

In Section 4.7, systematic mathematical approximations to the exact solution will be made with care taken to list exactly the conditions under which each approximation is valid. These approximations include those that

³⁸ It is useful to note how the uniqueness theorem introduced in Chapter 3 applies to this problem. More specifically, if a solution to Maxwell's equations can be found that accounts for the source term (including the external electric field if any), satisfies the radiation condition as the distance from the center of conductor, $r \rightarrow \infty$ and for which the tangential electric and magnetic fields are continuous across the air-earth boundary and the air-conductor boundary, then this solution is the one and only solution to the problem.

lead in later sections to equivalent transmission line theory, circuit theory and quasi-static field calculations.

4.2 Setting up an Integral Equation for Conductor Current with Series Voltage and External Field Sources ◀

Strategy and approximations

The first step in finding the current on the wire shown in Fig 4.1.1 is write down a formal expression for the electric and magnetic fields of an infinitesimal element (i.e., length dz') of the wire at $(x_1, y_1 = h, z')$ that carries a current I . This current “element” is called a dipole with moment $I dz'$. The geometry for this problem is shown in Fig. 4.2.1

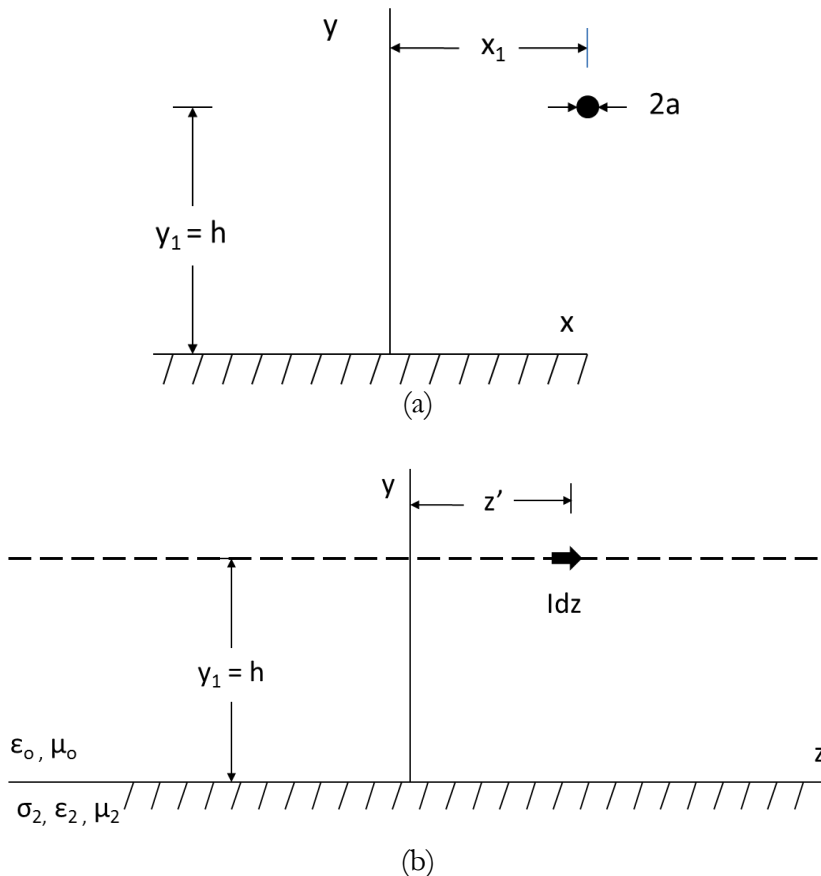


Fig. 4.2.1. a) end view and b) side view of the dipole height “h” above a lossy linear, homogeneous isotropic earth.

The electric and magnetic fields in medium 1 (i.e., $y \geq 0$) for the current element at $(x_1, y_1 = h, z')$ can be written down as (Baños 1966)

$$\begin{aligned} \hat{E}^1(x, y, z) = & g_{ex}^1(x - x_1, y, h, z - z')\hat{I}(z')dz' \bar{a}_x + \\ & g_{ey}^1(x - x_1, y, h, z - z')\hat{I}(z')dz' \bar{a}_y + g_{ez}^1(x - x_1, y, h, z - z')\hat{I}(z')dz' \bar{a}_z \end{aligned} \quad (4.2.1)$$

$$\begin{aligned} \hat{H}^1(x, y, z) = & g_{hx}^1(x - x_1, y, h, z - z')\hat{I}(z')dz' \bar{a}_x + \\ & g_{hy}^1(x - x_1, y, h, z - z')\hat{I}(z')dz' \bar{a}_y + g_{hz}^1(x - x_1, y, h, z - z')\hat{I}(z')dz' \bar{a}_z \end{aligned} \quad (4.2.2)$$

where it is assumed that all of the functions g_{ij} are selected to satisfy the appropriate boundary conditions at infinity and at the air-earth interface discussed earlier. Later in this chapter, it will be shown explicitly how this can be done. Note that the reason why y and h appear separately in (4.2.1) and (4.2.2) (unlike $x-x_1$ and $z-z'$) is due to the air-earth interface which makes the region inhomogeneous along any vertical line. Thus, the y variation of the field is not simply related to the difference $y-h$.

As mentioned earlier, the current on the wire ($\hat{I}(z)$) is yet unknown and is the object of the derivations in this section. As discussed earlier, this current can be found by setting up an integral equation on the surface of the wire. To do this, it is necessary to match appropriate boundary conditions on the wire surface. If the wire was perfectly conducting, then it would be sufficient to set the tangential component of the total electric field equal to zero on the wire surface (except at the voltage source where an electric field boundary condition that accounts for the difference in electric potential across the voltage source can be used). But, there are two problems with this approach. First, the wires of interest here are not perfect conductors and second, it is a laborious process to match boundary conditions at all points along the cross section of the conductor. Here the first of many approximations in this chapter will be made. More specifically, what is called the “thin wire” approximation will be made for which it is assumed that the electric field component along the direction of the wire is equal to the “intrinsic impedance per unit length” of the wire multiplied by the total current on the wire at one location on the cross-section of the wire. This approximation is valid under the condition (Pogorzelski and Chang 1977)

$$\left(\frac{a}{2h}\right) \ln\left(\frac{2h}{a}\right) \ll 1 \quad (4.2.3)$$

For the z directed non-magnetic wire considered here, the thin wire condition can be implemented as

$$\hat{E}_z^1(x_1 + a, h, z) = Z_{iw}(\omega) \hat{I}(z) \quad (4.2.4)$$

where it has been assumed that the boundary condition is matched on the side of the wire (i.e., more specifically at $(x_1 + a, h)$). In Appendix A, it is shown that (Weeks 1981)

$$Z_{iw}(\omega) = R_{dc} \left(\frac{k_w a}{2} \right) \frac{J_0(k_w a)}{J_1(k_w a)} \quad (4.2.5)$$

where

$$R_{dc} = \frac{1}{\sigma_w \pi a^2} \quad (4.2.6)$$

is the resistance per unit length of the wire at dc (i.e., zero frequency). σ_w is the wire conductivity, $k_w = (-j\omega\mu_0\sigma_w)^{1/2}$ and $J_0(k_w a)$ and $J_1(k_w a)$ are Bessel functions of argument q , and order zero and one respectively where the wire has been assumed to be non-magnetic since μ_w (the wire permeability) = μ_0 . Note that displacement currents in the wire can be neglected (i.e., $\epsilon_0\epsilon_{rw} \ll \sigma_w / \omega$). Hence it is not necessary to specify ϵ_w , the dielectric constant of the wire. If the frequency is low enough that $|k_w a| \ll 1$, then

$$Z_{iw}(\omega) \cong R_{dc} + j\omega \frac{\mu_0}{8\pi}, \quad |k_w a| \ll 1 \quad (4.2.7)$$

In this case, the current flows uniformly throughout the wire and “dc” calculations are accurate. The latter term of (4.2.7) represents the internal inductive reactance of the conductor and is equal to zero when $\omega = 0$ as expected.

If the frequency is high enough that $|k_w a| \gg 1$, then

$$Z_{iw}(\omega) \cong \left(\frac{\omega\mu_0}{2\sigma_w} \right)^{1/2} \frac{(1+j)}{2\pi a}, \quad |k_w a| \gg 1 \quad (4.2.8)$$

In this case, the current can be shown to flow primarily near the outside surface of the wire (i.e., the skin effect) where the thickness of this layer is roughly one skin depth

$$\delta = \sqrt{\frac{2}{\omega\mu_0\sigma}} \quad (4.2.9)$$

as shown in Fig. 4.2.2.

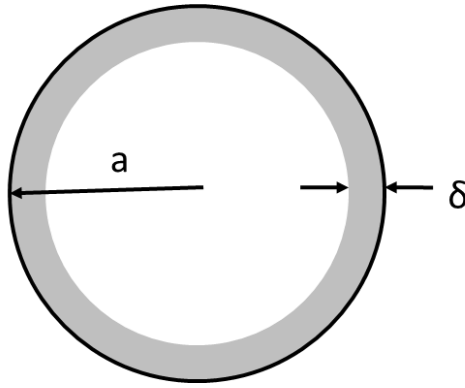


Fig. 4.2.2. Cross section of a round conductor. At high frequency, current flows in the “skin” (i.e., the shaded region of thickness δ) of a round conductor. The impedance per unit length is inversely proportional to the area $2\pi a\delta$.

As a result, the impedance is significantly larger than it is at lower frequencies. This is also why the impedance is proportional to the square root of ω . In fact, as a general rule, the smallest intrinsic impedance per unit length for a round conductor occurs at zero frequency. Since resistive losses are proportional to the real part of the intrinsic impedance, the smallest resistive losses are achieved by using the lowest frequency possible. This is the fundamental reason why dc power lines are more efficient (i.e., smaller resistive losses per unit length) than ac power lines. Generally, however, they are used only for relatively long distances because of the losses in transforming ac to dc and vice versa at the two ends of the transmission line.

The integral equation

If (as has been assumed) the boundary condition (4.2.4) is applied at the side of the conductor (i.e., at $(x_1 + a, h)$), then the total electric field (an integral over all sources plus the external source field) can be equated to the boundary condition on the surface of the conductor. The result is (Chang and Olsen 1975; Kuester et. al. 1978)

$$\int_{-\infty}^{\infty} g_{ez}^1(a, h, h, z - z') \hat{I}(z') dz' + \hat{E}_{ze}^1(x_1 + a, h, z) = -V\delta(z) + Z_{iw} \hat{I}(z), \quad -\infty < z < \infty \quad (4.2.10)$$

Here, $\delta(z)$ is the Dirac delta function which is zero everywhere except at $z = 0$ and has the property that any integral which includes $z = 0$ in its domain is equal to 1. Thus the term $-V\delta(z)$ represents a voltage source of RMS amplitude V on the wire at $z = 0$ since

$$-\int_{-\varepsilon}^{\varepsilon} \hat{\mathbf{E}} \cdot d\bar{\mathbf{l}} = -\int_{-\varepsilon}^{\varepsilon} (-V\delta(z))dz = V \quad (4.2.11)$$

where ε is an arbitrarily small number.

Equation 4.2.10 is a homogeneous Fredholm integral equation of the first kind for the current induced on the conductor by the voltage source and external sources.

4.3 Formal Solution to the Integral Equation for Conductor Current with Series Voltage and External Field Sources ◀

Explicit expressions for $\hat{\mathbf{E}}_{ze}^1(x_1 + a, h, z)$ can be (and will be later) found for sources such as plane waves and isolated dipoles above the earth (Olsen and Usta 1977; Olsen 1983). If in addition $g_{e\zeta}(a, b, b, \zeta - \zeta')$ is known, then it is (in principle) possible to solve (4.2.10) for the current distribution using numerical methods. But, this approach gives little insight into the solutions. Here, a formal solution for the current will be developed that is straightforward and elegant. It is based on the fact that the integral equation is valid over the entire range of ζ values from $-\infty$ to ∞ . The solution can be found by taking the spatial Fourier transform of both sides of (4.2.10). This transform and its inverse (i.e., $\tilde{F}(\gamma)$ and $\tilde{F}^{-1}(\gamma)$) used here are defined as

$$\tilde{F}(f(z)) = \tilde{F}(\gamma) = \int_{-\infty}^{\infty} f(z)e^{+j\gamma z} dz \quad (4.3.1)$$

$$\tilde{F}^{-1}(\tilde{F}(\gamma)) = f(z) = \frac{1}{2\pi} \int_{-\infty}^{\infty} \tilde{F}(\gamma)e^{-j\gamma z} d\gamma \quad (4.3.2)$$

The symbol \sim indicates a spatial Fourier transform with respect to the wire direction z that is dependent on the spatial Fourier transform variable γ .

Taking the Fourier transform of (4.2.10) using (4.3.1) and using the convolution identity

$$\tilde{F}(f(z))\tilde{H}(h(z)) = \tilde{F}(\gamma)\tilde{H}(\gamma) = \tilde{F} \left[\int_{-\infty}^{\infty} f(z')h(z-z')dz' \right] \quad (4.3.3)$$

results in the algebraic equation

$$\tilde{G}_{ez}^1(a, h, h, \gamma)\tilde{I}(\gamma) + \hat{\mathbf{E}}_{ze}^1(x_1 + a, h, \gamma) = -V + Z_{iw}\tilde{I}(\gamma) \quad (4.3.4)$$

where the axial electric field of the wire current is

$$\hat{E}_{zw}^1(x_1 + a, h, \gamma) = \tilde{G}_{ez}^1(a, h, h, \gamma) \hat{I}(\gamma) \quad (4.3.5)$$

If terms containing $\hat{I}(\gamma)$ are gathered, the equation can be solved for $\hat{I}(\gamma)$, resulting in

$$\hat{I}(\gamma) = \frac{-V - \hat{E}_{ze}^1(x_1, h - a, \gamma)}{\tilde{G}_{ez}^1(a, h, h, \gamma) - Z_{iw}} \quad (4.3.6)$$

Finally, an explicit expression (i.e., the formal solution to the integral equation) for the current as a function of position z can be written using the inverse Fourier transform as

$$\hat{I}(z) = \frac{-1}{2\pi} \int_{-\infty}^{\infty} \left(\frac{V + \hat{E}_{ze}^1(x_1 + a, h, \gamma)}{\tilde{G}_{ez}^1(a, h, h, \gamma) - Z_{iw}} \right) e^{-j\gamma z} d\gamma \quad (4.3.7)$$

Clearly, an explicit expression now exists for $\hat{I}(z)$ if an expression for $\tilde{G}_{ez}^1(a, h, h, \gamma)$ can be found.

Special case – no external sources

As the next step, it will be assumed that $\hat{E}_{ze}^1 = 0$ (i.e., no external incident fields). Hence, (Chang and Olsen 1975)

$$I(z) = -\frac{1}{2\pi} \int_{-\infty}^{\infty} \left(\frac{V}{\tilde{G}_{ez}^1(a, h, h, \gamma) - Z_{iw}} \right) e^{-j\gamma z} d\gamma \quad (4.3.8)$$

4.4 The Axial Electric Field of a Propagating Horizontal Current above Earth ◀

Introduction

In this section, an explicit expression for the term $\tilde{G}_{ez}^1(a, h, h, \gamma)$ in (4.3.6) and (4.3.7) will be found. This term represents the Fourier transform of the z -directed electric field due to a unit-amplitude impulse (in space) of current (i.e., an infinitesimal length dipole) at $z = z'$. Note that the spatial Fourier transform of an impulse at $z = z'$ is simply $\hat{I}(\gamma) = \exp(-j\gamma z')$. Hence, in the

transform domain, an infinitesimal current source at $z = z'$ becomes a line source carrying a current of the form $\exp(-j\gamma z')$. The fundamental issue that complicates the solution to this problem is the fact that the line current is above the earth and hence that appropriate boundary conditions have to be satisfied at the air-earth interface. This is done in the spatial Fourier transform domain as illustrated below.

It has been shown (in Chapter 3) that the electromagnetic field of this type of source can be derived from a set of electric and magnetic “potentials” (Wait, 1972). As mentioned in Chapter 3, these potentials are not used because it is necessary to do so, but rather because it provides a simpler formulation to the problem which (in turn) leads to a more elegant and simple representation of the result.

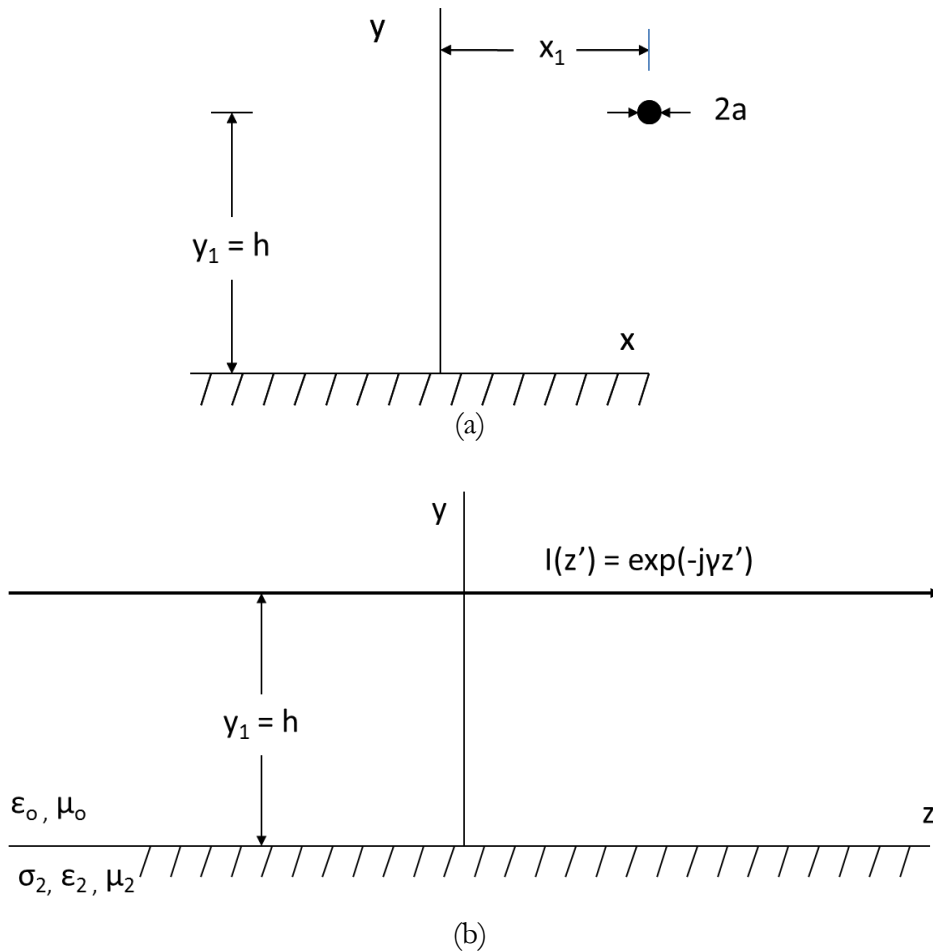


Fig. 4.4.1. a) end view and b) side view of the line current at (x_1, h) above a lossy linear, homogeneous isotropic earth carrying a current $\exp(-j\gamma z')$ (i.e., RMS current magnitude = 1).

Here, Hertzian electric and magnetic potentials will be used because it is possible to represent the entire set of electric and magnetic fields in terms of an axial (i.e., z directed) Hertzian electric and magnetic potential. The

“proof” of this is that if Π_z^e and Π_z^m are used, then it can be shown possible to find a solution to Maxwell’s equations that satisfies all required boundary conditions. By the uniqueness theorem, this must be the solution.

Consider next, the specific problem to be solved as shown in Fig. 4.4.1. This figure shows a line current of form $\hat{I}(\gamma) = \exp(-j\gamma z)$ above a homogeneous lossy earth as shown. As mentioned earlier, it is possible to use z directed electric and magnetic Hertzian potentials to solve for the electromagnetic fields of this source as shown below.

$\hat{G}_{ez}(a, h, h, \gamma)$ for a conductor in free space

Consider first only the source term (i.e., the earth is ignored for the moment). In this case, it is possible to represent the entire set of fields with a z-directed Hertzian electric potential. Since the vector potential must have the same z variation as the source, the wave equation for the potential can be written as

$$\left(\nabla^2 + k_0^2\right) \left(\hat{\Pi}_{ez}(x, y, \gamma) e^{-j\gamma z}\right) = \frac{j}{\omega \epsilon_0} e^{-j\gamma z} \delta(x - x_1) \delta(y - h) \quad (4.4.1)$$

where $k_1 = \omega \sqrt{\mu_1 \epsilon_1} = k_0 = \omega \sqrt{\mu_0 \epsilon_0}$, $\epsilon_1 = \epsilon_0$ and it has been assumed that the z variation of $\Pi_{ez}(x, y, z)$ is $e^{-j\gamma z}$ since (as mentioned above) the source current has this form.

A couple of comments about the source term in (4.4.1) are in order. Note first, that in (3.3.27) of Chapter 3, the source term for the electric Hertzian potential is $-P_0/\epsilon$ where P_0 is a “fixed” polarization that can be related to a current density (again, $\epsilon = \epsilon_1 = \epsilon_0$ in this case since the source that is in Region 1 is assumed to be free space). More specifically,

$$\bar{P}_0 = \frac{\bar{J}}{j\omega} = \frac{-j\bar{J}}{\omega} \quad (4.4.2)$$

where the line current’s current density (for a current with z variation $e^{-j\gamma z}$ can be written as

$$\bar{J} = I \delta(x - x_1) \delta(y - h) e^{-j\gamma z} \quad (4.4.3)$$

and I is the RMS amplitude of the current. Since $\hat{I}(\gamma) = \exp(-j\gamma z)$ in this case, the source term in (4.4.1) is

$$\frac{j}{\omega \epsilon_0} \delta(x - x_1) \delta(y - h) e^{-j\gamma z} \quad (4.4.4)$$

Now, since $\nabla^2 = \frac{\partial^2}{\partial x^2} + \frac{\partial^2}{\partial y^2} + \frac{\partial^2}{\partial z^2}$ and $\frac{\partial^2(e^{-j\gamma z})}{\partial z^2} = -\gamma^2 e^{-j\gamma z}$, (4.4.1)

can be written as

$$\left(\frac{\partial^2}{\partial x^2} + \frac{\partial^2}{\partial y^2} - \gamma^2 + k_0^2 \right) \hat{\Pi}_{ez}(x, y, \gamma) = \frac{j}{\omega \epsilon_0} \delta(x - x_1) \delta(y - h) \quad (4.4.5)$$

since the term $e^{-j\gamma z}$ is on both sides of the equation and cancels.

To solve (4.4.1), it is first transformed into the (κ, ξ) plane by using the Fourier transforms

$$F(f(x)) = F(\kappa) = \int_{-\infty}^{\infty} f(x) e^{+j\kappa x} dx \quad (4.4.6)$$

$$F(f(y)) = F(\xi) = \int_{-\infty}^{\infty} f(y) e^{+j\xi y} dy \quad (4.4.7)$$

in succession. The result is

$$(-\kappa^2 - \xi^2 - \gamma^2 + k_0^2) \hat{\Pi}_{ez}(\kappa, \xi, \gamma) = \frac{j}{\omega \epsilon_0} e^{+j\xi h} e^{j\kappa x_1} \quad (4.4.8)$$

so that

$$\hat{\Pi}_{ez}(\kappa, \xi, \gamma) = \frac{-j e^{j\xi h} e^{j\kappa x_1}}{\omega \epsilon_0 (\xi^2 + \kappa^2 + \gamma^2 - k_0^2)} \quad (4.4.9)$$

Using the inverse Fourier transforms corresponding to (4.4.6) and (4.4.7) (see (4.3.12), it is possible to write a formal solution for the Hertzian potential in the spatial domain as follows:

$$\hat{\Pi}_{ez}(x, y, \gamma) = \frac{-j}{(2\pi)^2 \omega \epsilon_0} \int_{-\infty}^{\infty} \int_{-\infty}^{\infty} \frac{e^{-j\kappa(x-x_1)} e^{-j\xi(y-h)}}{(\xi + ju_1)(\xi - ju_1)} d\xi d\kappa \quad (4.4.10)$$

where

$$u_1 = \sqrt{\kappa^2 + \gamma^2 - k_0^2}, \quad \text{Re}(u_1) \geq 0 \quad (4.4.11)$$

The ξ integration can be easily performed using the theory of residues (see Appendix B for details) by deforming the ξ contour into the lower infinite

semi-circle. If it is assumed that $\text{Re}(u_1) \geq 0$ ³⁹ so that $\text{Im}(ju_1) \geq 0$, and $(y-h) > 0$, then the integrand $\exp(-j\xi(y-h))$ goes exponentially to zero in the lower infinite semi-circle and the pole that occurs in the lower half plane is at $-ju_1$ (see Fig. 4.4.2).

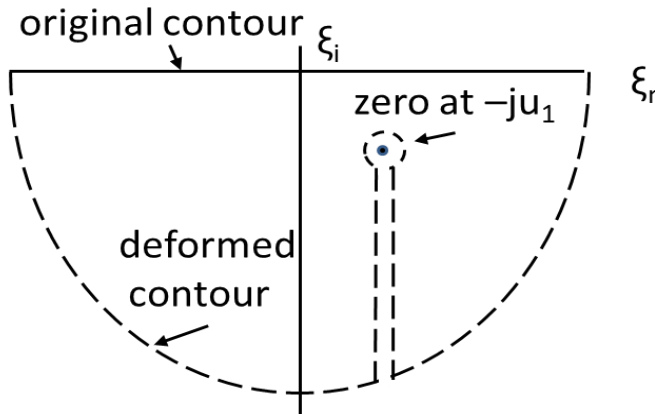


Fig. 4.4.2. Location of the pole at $-ju_1$ in the complex ξ plane.

The residue for the ξ integration (the portion of (4.4.10) in brackets) is

$$\frac{\pi e^{-j\kappa(x-x_1)} e^{-u_1(y-h)}}{u_1} \quad (4.4.12)$$

and the result is

$$\hat{\Pi}_{ez}(x, y, \gamma) = \frac{-j}{4\pi\omega\epsilon_0} \int_{-\infty}^{\infty} \frac{e^{-u_1|y-h|} e^{-j\kappa(x-x_1)}}{u_1} d\kappa \quad (4.4.13)$$

Where again, $\text{Re}(u_1) \geq 0$ and the absolute value sign has been used to combine the result with a similar integration for the case $(y-h) < 0$.

Before proceeding, it is useful to recognize the identity (Abramowitz and Stegun, 1972)

$$H_0^{(2)}\left(\left(k_0^2 - \gamma^2\right)^{1/2} \left[(x-x_1)^2 + (y-h)^2 \right]^{1/2}\right) = \frac{j}{\pi} \int_{-\infty}^{\infty} \frac{e^{-u_1|y-h|} e^{-j\kappa(x-x_1)}}{u_1} d\kappa \quad (4.4.14)$$

where $H_0^{(2)}(q)$ is the Hankel function of the second kind, order zero and argument q . In order to satisfy the radiation condition at infinity, $\text{Im}\left(\left(k_0^2 - \gamma^2\right)^{1/2}\right) \leq 0$ since the asymptotic expansion for the Hankel function is

³⁹ The choice is arbitrary. But, once made, all other operations must be consistent with this assumption.

$$H_0^{(2)}(q) \approx \sqrt{\frac{2}{\pi q}} e^{-j(q-j\pi/4)}, \quad |q| \rightarrow \infty$$

Given this result, 4.4.13 becomes

$$\hat{\Pi}_{ez}(x, y, \gamma) = \frac{-1}{4\omega\epsilon_0} H_0^{(2)}\left(\left(k_0^2 - \gamma^2\right)^{1/2} \left[(x-x_1)^2 + (y-h)^2\right]^{1/2}\right), \quad (4.4.15)$$

$$\text{Im}\left(\left(k_0^2 - \gamma^2\right)^{1/2}\right) \leq 0$$

Before proceeding, it is appropriate to illustrate how the result in (4.4.15) can be checked by integrating the magnetic field derived from (4.4.15) around a closed contour that just surrounds the current carrying conductor. Using cylindrical coordinates, the magnetic field can be expressed (for a current of the form $\exp(-j\gamma z)$ where this term is suppressed)

$$\begin{aligned} \hat{H}_\phi(r, \phi, \gamma) &= j\omega\epsilon_0 \nabla x \left(\hat{\Pi}_{ez} \bar{a}_z \right) \\ &= -j\omega\epsilon_0 \frac{\partial \hat{\Pi}_{ez}}{\partial \rho} \bar{a}_\phi \end{aligned} \quad (4.4.16)$$

Since $r = \left[(x-x_1)^2 + (y-h)^2\right]^{1/2}$ and for small arguments (Abramowitz and Stegun 1972)

$$H_0^{(2)}\left(\left(k_0^2 - \gamma^2\right)^{1/2} r\right) \cong \frac{-2j}{\pi} \ln\left(\left(k_0^2 - \gamma^2\right)^{1/2} r\right)$$

Hence,

$$\hat{H}_\phi(r, \phi, \gamma) = \frac{-j\omega\epsilon_0}{4\omega\epsilon_0} \frac{2j}{\pi} \frac{\partial}{\partial r} \left(\ln\left(\left(k_0^2 - \gamma^2\right)^{1/2} r\right) \right) = \frac{1}{2\pi r} \quad (4.4.17)$$

So that

$$\oint_C \hat{H} \cdot d\bar{l} = \int_0^{2\pi} \hat{H}_\phi r d\phi = 1 \quad (4.4.18)$$

where C is a contour that encircles the conductor. The result is as expected since the wire current amplitude was set equal to 1.

$\tilde{G}_{ez}^1(a, h, h, \gamma)$ for a conductor above a half-space

At this point, general expressions for the electric and magnetic fields in terms of the axial Hertzian potentials can be written (Wait 1972). Again, in all cases the current is of the form $\exp(-j\gamma z)$ where this term is suppressed.

The electric field related to the Hertzian electric vector potential in medium “1” is:

$$\begin{aligned}\hat{\hat{E}}^{ei}(x, y, \gamma) &= \nabla_x \nabla_x \left(\hat{\hat{\Pi}}_{ez}^i \bar{a}_z \right) = \nabla_x \left[\frac{\partial \hat{\hat{\Pi}}_{ez}^i}{\partial y} \bar{a}_x - \frac{\partial \hat{\hat{\Pi}}_{ez}^i}{\partial x} \bar{a}_y \right] \\ &= -j\gamma \frac{\partial \hat{\hat{\Pi}}_{ez}^i}{\partial x} \bar{a}_x - j\gamma \frac{\partial \hat{\hat{\Pi}}_{ez}^i}{\partial y} \bar{a}_y - \bar{a}_z \left(\frac{\partial^2 \hat{\hat{\Pi}}_{ez}^i}{\partial x^2} + \frac{\partial^2 \hat{\hat{\Pi}}_{ez}^i}{\partial y^2} \right)\end{aligned}\quad (4.4.19)$$

but from the wave equation (4.4.1) away from sources

$$\left(\frac{\partial^2}{\partial x^2} + \frac{\partial^2}{\partial y^2} - \gamma^2 + k_i^2 \right) \hat{\hat{\Pi}}_{ez}^i = 0$$

and

$$\begin{aligned}\hat{\hat{E}}^{ei}(x, y, \gamma) &= \nabla_x \nabla_x \left(\hat{\hat{\Pi}}_{ez}^i \bar{a}_z \right) = \\ &- j\gamma \left(\frac{\partial \hat{\hat{\Pi}}_{ez}^i}{\partial x} \bar{a}_x + \frac{\partial \hat{\hat{\Pi}}_{ez}^i}{\partial y} \bar{a}_y \right) - (\gamma^2 - k_i^2) \hat{\hat{\Pi}}_{ez}^i \bar{a}_z\end{aligned}\quad (4.4.20)$$

The electric field related to the Hertzian magnetic vector potential is:

$$\hat{\hat{E}}^{mi}(x, y, \gamma) = -j\omega\mu_i \nabla_x \hat{\hat{\Pi}}_{mz}^i = -j\omega\mu_i \left(\frac{\partial \hat{\hat{\Pi}}_{mz}^i}{\partial y} \bar{a}_x - \frac{\partial \hat{\hat{\Pi}}_{mz}^i}{\partial x} \bar{a}_y \right)\quad (4.4.21)$$

Similarly, the magnetic fields can be found as

$$\begin{aligned}\hat{\hat{H}}^{mi}(x, y, \gamma) &= \nabla_x \nabla_x \left(\hat{\hat{\Pi}}_{mz}^i \bar{a}_z \right) = \\ &- j\gamma \left(\frac{\partial \hat{\hat{\Pi}}_{mz}^i}{\partial x} \bar{a}_x + \frac{\partial \hat{\hat{\Pi}}_{mz}^i}{\partial y} \bar{a}_y \right) - (\gamma^2 - k_i^2) \hat{\hat{\Pi}}_{mz}^i \bar{a}_z\end{aligned}\quad (4.4.22)$$

and

$$\hat{H}^{ei}(x, y, \gamma) = j\omega\hat{\epsilon}_i \nabla_x \hat{\Pi}_{ez}^i = +j\omega\hat{\epsilon}_i \left(\frac{\partial \hat{\Pi}_{ez}^i}{\partial y} \bar{a}_x - \frac{\partial \hat{\Pi}_{ez}^i}{\partial x} \bar{a}_y \right) \quad (4.4.23)$$

where $\hat{\epsilon}_i = \epsilon_0 \epsilon_{ri} - j\sigma_i / \omega$ is the complex dielectric constant⁴⁰ and $k_i = \omega \sqrt{\mu_i \hat{\epsilon}_i}$ is the complex propagation constant of medium “ i ”. (4.4.19) – (4.4.23) will be used as the basis for calculating electric and magnetic field components other than \hat{E}_z in Chapter 5.

Given these results, the boundary conditions on the tangential components of the electric and magnetic field on a $y = \text{constant}$ plane (in this case $y = 0$) are:

For E_x

$$-j\gamma \frac{\partial \Pi_{ez}^1}{\partial x} - j\omega\mu_0 \frac{\partial \Pi_{mz}^1}{\partial y} = -j\gamma \frac{\partial \Pi_{ez}^2}{\partial x} - j\omega\mu_2 \frac{\partial \Pi_{mz}^2}{\partial y} \quad (4.4.24)$$

For E_z

$$(\gamma^2 - k_0^2) \Pi_{ez}^1 = (\gamma^2 - k_2^2) \Pi_{ez}^2 \quad (4.4.25)$$

For H_x

$$-j\gamma \frac{\partial \Pi_{mz}^1}{\partial x} + j\omega\epsilon_0 \frac{\partial \Pi_{ez}^1}{\partial y} = -j\gamma \frac{\partial \Pi_{mz}^2}{\partial x} + j\omega\epsilon_2 \frac{\partial \Pi_{ez}^2}{\partial y} \quad (4.4.26)$$

and for H_z

$$(\gamma^2 - k_0^2) \Pi_{mz}^1 = (\gamma^2 - k_2^2) \Pi_{mz}^2 \quad (4.4.27)$$

where $k_2 = \omega \sqrt{(\mu_2)(\epsilon_0 \epsilon_{r2} - j\sigma_2 / \omega)}$.

At this point, forms for the Hertz vector in each region will be set up. The particular forms will be selected in order to 1) match the source condition in Region 1 and 2) lead to results that will have simpler algebraic equations than otherwise might result. In each case, the result will be a spectral function which (when found and transformed back into the spatial domain) leads to an exact closed form expression for the respective vector potential.

It should be noted that there are only “down-going” waves in Region 2 (i.e., only an $\exp(u_2 y)$ term) and (aside from the source term which radiates in all directions) only “up-going” waves in Region 1 (i.e., only an $\exp(-u_1 y)$

⁴⁰ Here, the carat symbol over the dielectric constant $\hat{\epsilon}$ indicates a complex number, not a phasor.

term). These assumptions are consistent with the requirement of the uniqueness theorem that in “open” regions, there are no sources at infinity.

Appropriate expressions for the (yet unknown) Hertzian potentials are:

$$\hat{\Pi}_{ez}^1(x, y, \gamma) = A \int_{-\infty}^{\infty} \frac{\left(e^{-u_1|y-h|} + R(\kappa)e^{-u_1(y+h)} \right) e^{-j\kappa x}}{u_1} d\kappa \quad (4.4.28)$$

$$\hat{\Pi}_{mz}^1(x, y, \gamma) = A \int_{-\infty}^{\infty} \frac{M(\kappa)e^{-u_1(y+h)} e^{-j\kappa x}}{u_1} d\kappa \quad (4.4.29)$$

$$\hat{\Pi}_{ez}^2(x, y, \gamma) = A \int_{-\infty}^{\infty} \frac{e^{-u_1 h} T(\kappa) e^{u_2 y} e^{-j\kappa x}}{u_1} d\kappa \quad (4.4.30)$$

$$\hat{\Pi}_{mz}^2(x, y, \gamma) = A \int_{-\infty}^{\infty} \frac{e^{-u_1 h} N(\kappa) e^{u_2 y} e^{-j\kappa x}}{u_1} d\kappa \quad (4.4.31)$$

where $A = -j/(4\pi\omega\epsilon_0)$ and u_2 is defined as

$$u_2 = \sqrt{\kappa^2 + \gamma^2 - k_2^2} \quad \text{Re}(u_2) \geq 0 \quad (4.4.32)$$

Using the boundary conditions in (4.4.24) – 4.4.27), the following algebraic equations in the unknowns $R(\kappa)$, $M(\kappa)$, $T(\kappa)$ and $N(\kappa)$ can be written for each boundary condition. This results in four coupled linear equations in four unknowns that can be solved for $R(\kappa)$, $M(\kappa)$, $T(\kappa)$ and $N(\kappa)$ (Wait 1972).

For E_x

$$j\gamma\kappa(1 + R(\kappa)) + \omega\mu_1 u_1 M(\kappa) = j\gamma\kappa T(\kappa) - \omega\mu_2 u_2 N(\kappa) \quad (4.4.33)$$

For H_x

$$j\gamma\kappa M(\kappa) + \omega\epsilon_1 u_1 (1 - R(\kappa)) = j\gamma\kappa N(\kappa) + \omega\epsilon_2 u_2 T(\kappa) \quad (4.4.34)$$

For E_z

$$(k_1^2 - \gamma^2)(1 + R(\kappa)) = (k_2^2 - \gamma^2)T(\kappa) \quad (4.4.35)$$

and for H_z

$$(k_1^2 - \gamma^2)M(\kappa) = (k_2^2 - \gamma^2)N(\kappa) \quad (4.4.36)$$

The factor $K(\gamma)$ is defined as

$$K(\gamma) = \frac{N(\kappa)}{M(\kappa)} = \frac{(k_1^2 - \gamma^2)}{(k_2^2 - \gamma^2)} \quad (4.4.37)$$

After $T(\gamma)$ and $N(\gamma)$ have been eliminated by inserting (4.4.35). (4.4.36) and (4.4.37) into (4.4.33) and (4.4.34), (4.4.33) and (4.4.34) become

$$j\kappa\gamma(1 - K(\gamma))R(\kappa) + \omega(\mu_0 u_1 + K(\gamma)\mu_2 u_2)M(\kappa) = -j\kappa\gamma(1 - K(\gamma)) \quad (4.4.38)$$

And

$$j\kappa\gamma(1 - K(\gamma))M(\kappa) - \omega(\varepsilon_0 u_1 + K(\gamma)\varepsilon_2 u_2)R(\kappa) = -\omega(\varepsilon_0 u_1 - K(\gamma)\varepsilon_2 u_2) \quad (4.4.39)$$

These two equations can be rewritten as:

$$\begin{bmatrix} a_{11} & a_{12} \\ a_{21} & a_{22} \end{bmatrix} \begin{bmatrix} R(\kappa) \\ M(\kappa) \end{bmatrix} = \begin{bmatrix} -j\kappa\gamma(1 - K(\gamma)) \\ -\omega(\varepsilon_0 u_1 - K(\gamma)\varepsilon_2 u_2) \end{bmatrix} \quad (4.4.40)$$

where

$$a_{11} = a_{22} = j\kappa\gamma(1 - K(\gamma)) \quad (4.4.41)$$

$$a_{12} = \omega(\mu_0 u_1 + K(\gamma)\mu_2 u_2) \quad (4.4.42)$$

$$a_{21} = -\omega(\varepsilon_0 u_1 + K(\gamma)\varepsilon_2 u_2) \quad (4.4.43)$$

From the second equation in (4.4.40), it is possible to solve for $M(\gamma)$ to get

$$M(\kappa) = \frac{-\omega(\varepsilon_0 u_1 - K(\gamma)\varepsilon_2 u_2) - a_{21}R(\kappa)}{a_{22}} \quad (4.4.44)$$

Equation (4.4.44) can be inserted into the first equation in (4.4.40) to get

$$R(\kappa) = \frac{-j\kappa\gamma(1 - K(\gamma))a_{22} + a_{12}\omega(\varepsilon_0 u_1 - K(\gamma)\varepsilon_2 u_2)}{\Delta} \quad (4.4.45)$$

where $\Delta = a_{11}a_{22} - a_{12}a_{21}$. Expanding yields (Wait 1972)

$$R(\kappa) = \frac{\kappa^2 \gamma^2 (1 - K(\gamma))^2 + \omega^2 (\varepsilon_0 u_1 - K(\gamma)\varepsilon_2 u_2) (\mu_0 u_1 + K(\gamma)\mu_2 u_2)}{-\kappa^2 \gamma^2 (1 - K(\gamma))^2 + \omega^2 (\varepsilon_0 u_1 + K(\gamma)\varepsilon_2 u_2) (\mu_0 u_1 + K(\gamma)\mu_2 u_2)} \quad (4.4.46)$$

From these results, the other unknowns can be written as

$$M(\kappa) = \frac{-a_{11}R(\kappa) - j\kappa\gamma(1 - K(\gamma))}{a_{12}} \quad (4.4.47)$$

$$T(\kappa) = K(\gamma)(1 + R(\kappa)) \quad (4.4.48)$$

$$N(\kappa) = K(\gamma)M(\kappa) \quad (4.4.49)$$

Here, an alternative expression for $R(\kappa)$ is derived (under the condition that the earth is non-magnetic (i.e., $\mu_1 = \mu_2 = \mu_0$). Q is defined as Num/Den , where Num = the numerator of (4.4.46) and Den = the denominator of (4.4.46). If, in addition, $\mu_1 = \mu_2 = \mu_0$ then,

$$\begin{aligned} Num &= \kappa^2\gamma^2(1 - K(\gamma))^2 + (k_0^2u_1 - k_2^2u_2K(\gamma))(u_1 + u_2K(\gamma)) \\ Den &= -\kappa^2\gamma^2(1 - K(\gamma))^2 + (k_0^2u_1 + k_2^2u_2K(\gamma))(u_1 + u_2K(\gamma)) \end{aligned}$$

Now, Q can be written as

$$\frac{Num}{Den} = -1 + \frac{Num + Den}{Den} \quad (4.4.50)$$

where

$$\begin{aligned} Num + Den &= (k_0^2u_1 - k_2^2u_2K(\gamma))(u_1 + u_2K(\gamma)) + \\ &\quad (k_0^2u_1 + k_2^2u_2K(\gamma))(u_1 + u_2K(\gamma)) \\ &= 2k_0^2u_1(u_1 + u_2(K(\gamma))) \\ &= 2k_0^2u_1 \frac{[u_1(k_2^2 - \gamma^2) + u_2(k_0^2 - \gamma^2)]}{(k_2^2 - \gamma^2)} \\ &= \frac{2k_0^2u_1}{(k_2^2 - \gamma^2)} [u_1(\kappa^2 - u_2^2) + u_2(\kappa^2 - u_1^2)] \\ &= \frac{2k_0^2u_1}{(k_2^2 - \gamma^2)} [\kappa^2(u_1 + u_2) - u_1u_2((u_1 + u_2))] \\ &= \frac{2k_0^2u_1}{(k_2^2 - \gamma^2)} [(u_1 + u_2)(\kappa^2 - u_1u_2)] \end{aligned} \quad (4.4.51)$$

Next, substitute (4.4.37) into Den to get

(4.4.52)

$$\begin{aligned}
Den &= -\kappa^2 \gamma^2 \left(1 - \frac{(k_0^2 - \gamma^2)}{(k_2^2 - \gamma^2)} \right)^2 + \left[k_0^2 u_1 + k_2^2 u_2 \frac{(k_0^2 - \gamma^2)}{(k_2^2 - \gamma^2)} \right] \left[u_1 + u_2 \frac{(k_0^2 - \gamma^2)}{(k_2^2 - \gamma^2)} \right] \\
&= \frac{1}{(k_2^2 - \gamma^2)^2} \left[-\kappa^2 \gamma^2 \left((k_0^2 - \gamma^2)^2 - 2(k_0^2 - \gamma^2)(k_2^2 - \gamma^2) + (k_2^2 - \gamma^2)^2 \right) \right. \\
&\quad \left. + k_0^2 u_1^2 (k_2^2 - \gamma^2)^2 + k_2^2 u_2^2 (k_0^2 - \gamma^2)^2 + (k_0^2 u_1 u_2 + k_2^2 u_1 u_2)(k_0^2 - \gamma^2)(k_2^2 - \gamma^2) \right]
\end{aligned}$$

Collecting terms

(4.4.53)

$$\begin{aligned}
Den &= \frac{1}{(k_2^2 - \gamma^2)^2} \left[(-\kappa^2 \gamma^2 + k_0^2 u_1^2)(k_2^2 - \gamma^2)^2 + (-\kappa^2 \gamma^2 + k_2^2 u_2^2)(k_2^2 - \gamma^2)^2 \right. \\
&\quad \left. + (k_0^2 u_1 u_2 + k_2^2 u_1 u_2 + 2\kappa^2 \gamma^2)(k_0^2 - \gamma^2)(k_2^2 - \gamma^2) \right]
\end{aligned}$$

Next let

$$\begin{aligned}
A &= -\kappa^2 \gamma^2 + k_0^2 u_1^2 \\
&= -\kappa^2 (u_1^2 - \kappa^2 + k_0^2) + k_0^2 u_1^2 \\
&= (k_0^2 - \kappa^2)(u_1^2 - \kappa^2) \\
&= (\kappa^2 - k_0^2)(k_0^2 - \gamma^2)
\end{aligned} \tag{4.4.54}$$

Similarly

$$\begin{aligned}
B &= -\kappa^2 \gamma^2 + k_2^2 u_2^2 \\
&= (\kappa^2 - k_2^2)(k_2^2 - \gamma^2)
\end{aligned} \tag{4.4.55}$$

Inserting (4.4.54) and (4.4.55) into (4.4.53) and moving the common terms $(k_0^2 - \gamma^2)(k_2^2 - \gamma^2)$ out of the bracket results in

(4.4.56)

$$\begin{aligned}
Den &= \\
&\frac{(k_0^2 - \gamma^2)}{(k_2^2 - \gamma^2)} \left[(\kappa^2 - k_0^2)(k_2^2 - \gamma^2) + (\kappa^2 - k_2^2)(k_0^2 - \gamma^2) + ((k_0^2 + k_2^2)u_1 u_2 + 2\kappa^2 \gamma^2) \right] \\
&= \frac{(k_0^2 - \gamma^2)}{(k_2^2 - \gamma^2)} \left[\kappa^2 k_2^2 - k_0^2 k_2^2 - \kappa^2 \gamma^2 + k_0^2 \gamma^2 + \kappa^2 k_0^2 - k_0^2 k_2^2 - \kappa^2 \gamma^2 + k_2^2 \gamma^2 \right. \\
&\quad \left. + ((k_0^2 + k_2^2)u_1 u_2 + 2\kappa^2 \gamma^2) \right] \left[(u_1 + u_2)(k_0^2 u_2 + k_2^2 u_1) \right]
\end{aligned}$$

$$\begin{aligned}
&= \frac{(k_0^2 - \gamma^2)}{(k_2^2 - \gamma^2)} \left[k_0^2 (\kappa^2 + \gamma^2 - k_2^2) + k_2^2 (\kappa^2 + \gamma^2 - k_0^2) \right] (k_0^2 + k_2^2) u_1 u_2 \\
&= \frac{(k_0^2 - \gamma^2)}{(k_2^2 - \gamma^2)} \left[k_0^2 u_2^2 + k_2^2 u_1^2 + (k_0^2 + k_2^2) u_1 u_2 \right] \\
&= \frac{(k_0^2 - \gamma^2)}{(k_2^2 - \gamma^2)}
\end{aligned}$$

Finally, using (4.4.50) and (4.4.56)

$$R(\kappa) = -1 + \frac{2k_0^2 u_1 (\kappa^2 - u_1 u_2)}{(k_0^2 - \gamma^2) (k_0^2 u_2 + k_2^2 u_1)} \quad (4.4.57)$$

It can also be shown (here done backwards) that the factor

$$\frac{(\kappa^2 - u_1 u_2)}{(k_0^2 u_2 + k_2^2 u_1)} \quad (4.4.58)$$

is equal to

$$\frac{1}{u_1 + u_2} - \frac{\gamma^2}{(k_0^2 u_2 + k_2^2 u_1)} \quad (4.4.59)$$

This is done by 1) rewriting (4.4.59) with a common denominator and 2) multiplying numerator and denominator by $(u_1 - u_2)$. After writing u_1 and u_2 in terms of their definitions (i.e., 4.4.11 and 4.4.32) and collecting terms, (4.4.58) can be shown to be equal to (4.4.59). Hence

$$R(\kappa) = -1 + \frac{2k_0^2 u_1}{(k_0^2 - \gamma^2)} \left[\frac{1}{u_1 + u_2} - \frac{\gamma^2}{(k_0^2 u_2 + k_2^2 u_1)} \right] \quad (4.4.60)$$

Given this result, it is now possible to find an expression for the total axially (i.e., z) directed electric field anywhere. Using (4.4.20),

$$\hat{G}_{ez}^1(x - x_1, y, h, \gamma) = -(\gamma^2 - k_0^2) \hat{\Pi}_{ez}^1(x - x_1, y, h, \gamma) \bar{a}_z \quad (4.4.61)$$

where from (4.4.28),

$$\hat{\Pi}_{ez}^1(x - x_1, y, h, \gamma) = \frac{-j}{4\pi\omega\epsilon_0} \int_{-\infty}^{\infty} \frac{\left(e^{-u_1|y-h|} + R(\kappa) e^{-u_1(y+h)} \right) e^{-j\kappa(x-x_1)}}{u_1} d\kappa \quad (4.4.62)$$

so that

(4.4.63)

$$\hat{G}_{ez}^1(x-x_1, y, h, \gamma) = \frac{j(\gamma^2 - k_0^2)}{4\pi\omega\epsilon_0} \int_{-\infty}^{\infty} \frac{(e^{-u_1|y-h|} + R(\kappa)e^{-u_1(y+h)})e^{-j\kappa(x-x_1)}}{u_1} d\kappa$$

where $R(\gamma)$ is given by (4.4.57) or (4.4.60) (Wait 1972).

For the specific point $(x, y) = (x_1 + a, h)$ (i.e., at the side surface of the wire)

$$\hat{G}_{ez}^1(a, h, h, \gamma) = \frac{j(\gamma^2 - k_0^2)}{4\pi\omega\epsilon_0} \int_{-\infty}^{\infty} \frac{(1 + R(\kappa)e^{-u_1(2h)})e^{-j\kappa a}}{u_1} d\kappa \quad (4.4.64)$$

It is useful to note that (in some publications) (4.4.64) is written in an alternative form as

$$\hat{G}_{ez}^1(a, h, h, \gamma) = \frac{j(\gamma^2 - k_0^2)}{4\pi\omega\epsilon_0} \int_0^{\infty} \frac{(1 + R(\kappa)e^{-u_1(2h)})\cos(\kappa a)}{u_1} d\kappa \quad (4.4.65)$$

Finally, as discussed in Section 4.3, the electric field of the wire (for an arbitrary current) can be written explicitly as

$$\hat{E}_{zw}^1(x_1 + a, h, \gamma) = \tilde{G}_{ez}^1(a, h, h, \gamma) \hat{I}(\gamma) \quad (4.4.66)$$

4.5 Exact Modal Equation and General Expression for Current ◀

Introduction

Now that \tilde{G}_{ez}^1 is known, it is possible to use (4.3.8) to calculate the current on the wire. This equation is repeated here as (4.5.1)

$$\hat{I}(z) = -\frac{1}{2\pi} \int_{-\infty}^{\infty} \left(\frac{V}{\hat{G}_{ez}^1(a, h, h, \gamma) - Z_{iw}} \right) e^{-j\gamma z} d\gamma \quad (4.5.1)$$

This integral can be evaluated using the theory of residues for analytic functions in a manner similar to (4.4.10) (see also Appendix B). In that case the original contour of integration (i.e., the real γ axis from $-\infty$ to ∞) was deformed into the lower infinite semicircle of the complex plane. This can

also be done here for $z > 0$ since $e^{-\eta z} \rightarrow 0$ as $\text{Im}(\gamma) \rightarrow -\infty$. Since this is true, this semi-infinite integral is zero and the integral is simply the sum of residues of the poles of the integrand. More will be said about these for the case of (4.5.1) shortly.

There is, however, an additional complication in this case. According to Appendix B, a function of a complex variable is “analytic” in a specific domain D of the complex plane only if it is “single valued.” This requirement can be violated if the integrand involves multiple valued functions such as logarithms (i.e., $\ln(\gamma)$) or fractional powers (e.g., $\gamma^{1/2}$). In these cases branch cuts can be drawn between the branch points (they always occur in pairs – one of which may be at ∞). Branch cuts must not be crossed in order to preserve the single valued property of the integrand. An example of a function in the complex plane that contains a pair of branch points at 0 and $-j\infty$ along with vertical branch cut and a legitimate “deformed” contour of integration is shown in Fig. 4.5.1. In this case, the original contour must be deformed around the branch cut as shown in the figure. Thus the new integration (in addition to any residues that occur between the original and new contours) must include the integrations along $C_{\infty 1}$ and $C_{\infty 2}$ as well as those along C_{b1} and C_{b2} .

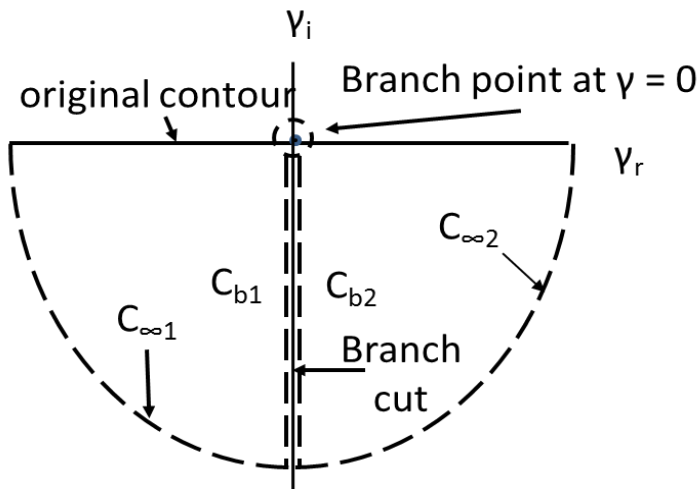


Fig. 4.5.1. The effect of a branch cut on permissible contour deformation.

In the next two sections, the simple poles of the integrand (i.e., simple zeros of the denominator) as well as the branch points and cuts of the integrand of (4.5.1) will be identified.

The exact modal equation – zeros of the denominator

The zeros of the denominator of (4.5.1) can be found by solving

$$\hat{G}_{ez}^1(a, h, h, \gamma) - Z_{iw} = 0 \tag{4.5.2}$$

Using (4.4.60) and (4.4.64), (4.5.2) can be expanded and written as

$$(4.5.3) \quad \frac{+(\gamma^2 - k_0^2)}{4\omega\epsilon_0} \left\{ \frac{j}{\pi} \int_{-\infty}^{\infty} \frac{e^{jk\alpha}}{u_1} d\kappa - \frac{j}{\pi} \int_{-\infty}^{\infty} \frac{e^{-2u_1 h} e^{jk\alpha}}{u_1} d\kappa \right. \\ \left. - \frac{2k_0^2}{(\gamma^2 - k_0^2)} \left(\frac{j}{\pi} \right) \int_{-\infty}^{\infty} \frac{e^{-2u_1 h} e^{ja}}{u_1 + u_2} d\kappa + \frac{2k_0^2 \gamma^2}{(\gamma^2 - k_0^2)} \left(\frac{j}{\pi} \right) \int_{-\infty}^{\infty} \frac{e^{-2u_1 h} e^{jk\alpha}}{k_2^2 u_1 + k_0^2 u_2} d\kappa \right\} - Z_{iw} = 0$$

Multiplying through by the initial factor $(\gamma^2 - k_0^2)$ and using the definition of the Hankel function in (4.4.14), (4.5.3) can be rewritten as

$$(4.5.4) \quad \frac{1}{4\omega\epsilon_0} \left\{ (\gamma^2 - k_0^2) \left[H_0^{(2)} \left((k_0^2 - \gamma^2)^{1/2} a \right) - H_0^{(2)} \left((k_0^2 - \gamma^2)^{1/2} \left((2h)^2 + a^2 \right)^{1/2} \right) \right] \right. \\ \left. - 2k_0^2 P(\gamma) + 2k_0^2 \gamma^2 Q(\gamma) \right\} - Z_{iw} = 0$$

where

$$P(\gamma) = \left(\frac{j}{\pi} \right) \int_{-\infty}^{\infty} \frac{e^{-2u_1 h} e^{jk\alpha}}{u_1 + u_2} d\kappa$$

and

$$Q(\gamma) = \left(\frac{j}{\pi} \right) \int_{-\infty}^{\infty} \frac{e^{-2u_1 h} e^{jk\alpha}}{k_2^2 u_1 + k_0^2 u_2} d\kappa$$

If next, terms multiplied by γ^2 are separated, then (4.5.4) becomes

$$(4.5.5) \quad \gamma^2 \left\{ \left(\frac{1}{4\omega\epsilon_0} \right) \left[H_0^{(2)} \left((k_0^2 - \gamma^2)^{1/2} a \right) - H_0^{(2)} \left((k_0^2 - \gamma^2)^{1/2} \left((2h)^2 + a^2 \right)^{1/2} \right) + 2k_0^2 Q(\gamma) \right] \right\} \\ + k_0^2 \left\{ \left(\frac{-1}{4\omega\epsilon_0} \right) \left[H_0^{(2)} \left((k_0^2 - \gamma^2)^{1/2} a \right) - H_0^{(2)} \left((k_0^2 - \gamma^2)^{1/2} \left((2h)^2 + a^2 \right)^{1/2} \right) + 2P(\gamma) \right] \right\} - Z_{iw} = 0$$

Equation (4.5.5) is the exact modal equation for a thin wire above the earth. It can be shown that discrete values of γ (i.e., γ_p) for which (4.5.5) is equal to zero represent different modes of current propagation on the conductor. The currents that correspond to each of these modes vary with z as

$$(4.5.6) \quad e^{-j\gamma_p z}$$

The exact modal equation – branch cuts and points

It can be shown that integrand of (4.5.1) has branch point pairs at $\pm k_0, -j\infty$ and $\pm k_2, -j\infty$ due to the existence of Hankel functions that behave as logarithmic functions close to k_0 and k_2 (Olsen, R. G. and D. C. Chang 1974a). The integration along these two branch cuts can be related to electromagnetic fields that radiate in the free space and the earth respectively. In addition there is another branch point pair with one branch point between the k_0 and k_2 and its pair at $-j\infty$. Integrations along this branch cut can be related to electromagnetic fields that radiate along the free space-earth interface. The locations of these three branch cuts are shown in Fig. 4.5.2.

Generalized impedance per unit length parameters for a wire above earth

The modal equation (4.5.5) can be recast in a form that leads naturally to identification of an equivalent transmission line with impedances and admittances per unit length. This can be achieved by defining

$$\hat{G}_{ez}^1(a, h, h, \gamma) - Z_{iw} = 0 = -(Z(\gamma) + \gamma^2 / Y(\gamma)) \quad (4.5.7)$$

where $Z(\gamma)$ and $Y(\gamma)$ are defined as

$$(4.5.8)$$

$$Z(\gamma) = \frac{\omega\mu_0}{4} \left[H_0^{(2)}\left(\left(\gamma^2 - k_0^2\right)^{1/2} a\right) - H_0^{(2)}\left(\left(\gamma^2 - k_0^2\right)^{1/2} \left((2h)^2 + a^2\right)^{1/2}\right) + 2P(\gamma) \right] + Z_{iw} \quad (4.5.9)$$

$$Y(\gamma) = -4\omega\epsilon_0 \left[H_0^{(2)}\left(\left(\gamma^2 - k_0^2\right)^{1/2} a\right) - H_0^{(2)}\left(\left(\gamma^2 - k_0^2\right)^{1/2} \left((2h)^2 + a^2\right)^{1/2}\right) + 2k_0^2 Q(\gamma) \right]^{-1} .$$

It will be evident later that

- $Z(\gamma)$ is the equivalent series transmission line impedance per unit length, and
- $Y(\gamma)$ is the equivalent shunt transmission line admittance per unit length.

Given this, the modal equation can be written as

$$\gamma = j\sqrt{Z(\gamma)Y(\gamma)} \quad (4.5.10)$$

where in this general case, $Z(\gamma)$ and $Y(\gamma)$ are functions of γ .

Although (4.5.8) – (4.5.10) look very much like the formula used for determining the propagation constant for a distributed parameter transmission line, the parameters are still complicated functions of the Fourier transform variable γ . In the low frequency case, however, these will

reduce to a form that is directly interpretable as an equivalent conventional distributed parameter transmission line with a single set of constant distributed parameter values. This will be done in the next section.

Given these definitions, 4.5.1 can be reformatted to look like

$$\hat{I}(z) = \frac{1}{2\pi} \int_{-\infty}^{\infty} \left(\frac{V}{Z(\gamma) + \gamma^2 / Y(\gamma)} \right) e^{-j\gamma z} d\gamma \quad (4.5.11)$$

which (given the denominator of the integral) begins to resemble a transmission line formulation (and this will become even more apparent later). As mentioned above, however, it is important to note again that $Z(\gamma)$ and $Y(\gamma)$ are functions of γ and have a fairly complicated set of singularities to be described further below (Olsen and Chang 1974a; Olsen and Chang 1974b; Olsen et. al. 1978).

General modal solution for the current

As mentioned above, for $z > 0$, the integral of (4.5.11) can be evaluated by closing the integration contour in the lower half of the complex γ plane. To keep the integral single-valued (or analytic) within and on the contour, the integral along the axis is deformed and set equal to the sum of several integrals each with its own physical significance. There are three types of these integrals: integrals about the various poles of the denominator of (4.5.11) (i.e., modal integrals), integrals along the various branch cuts of the denominator of (4.5.11) (i.e., radiation integrals) and an integral about the lower, infinitely extended semi-circle. This last contribution is zero by virtue of the radiation condition and the branch cut definitions, which specify that the real parts of the various multivalued functions be greater than zero. This specification defines the proper Riemann sheet. A detailed depiction of the deformed integration contour is shown in Fig. 4.5.2.

First, and most important (to power engineers) is the pole γ_{TL} (the transmission line or quasi-TEM zero) that is bound to the wire (i.e., the fields decay rapidly away from the wire) and will be seen later to be the dominant term for most power engineering applications. It is called quasi-TEM because as the earth conductivity becomes infinite, this mode becomes equivalent to the TEM mode on a perfectly conducting wire above a perfectly conducting ground plane. There is a second zero, γ_{SA} that is called a “surface attached” zero since it relates to a wave that travels along the wire, but is mostly bound to the interface between the air and the earth and which becomes less important at low frequencies. In addition, there are three branch points and associated branch cuts. The first one is at k_0 and the integration along its branch cut represents radiation away from the wire in all directions. The second one is at k_A and represents radiation that travels along the air-earth interface in all directions away from the wire. The third

occurs at k_2 and represents radiation away from the wire into the earth. This integration can usually be ignored for typical earth parameters.

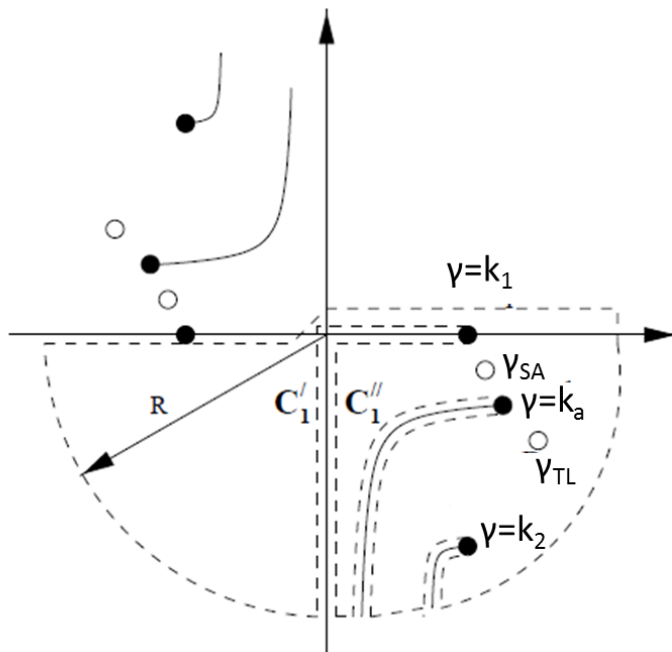


Fig 4.5.2. Spectrum of currents on the wire. The open dots represent zeros of the denominator and hence modal currents. The closed dots represent branch points of the denominator.

More specifically, it can be shown that the quasi-TEM modal current dominates the continuous spectrum currents if: 1) the wire height is small compared to the free-space wavelength and 2) the earth is a reasonably good conductor at the frequencies of interest. Since these conditions hold for many low-frequency systems, the quasi-TEM current can be, and has been assumed to be the total (or complete) current.

It is a reasonable question to ask whether the entire current can (in all cases) be represented by these components. One necessary (but not sufficient) condition for this is that the total current begin to approximate the (known) current on a wire in free space as the height of the wire above the earth becomes large compared to a wavelength (Olsen and Chang 1974). The results of such a calculation are shown in Fig. 4.5.3. More specifically, this represents an examination of the input conductance (i.e., current at $z = 0$ divided by the voltage of the source) of the wire. It is shown in Fig. 4.5.3 that the input conductance does (in fact) approach the correct result (i.e., 3.1 milli-siemens) when all terms mentioned above are included. Based on this result, an argument can be made that all significant spectral components of the current have been identified.

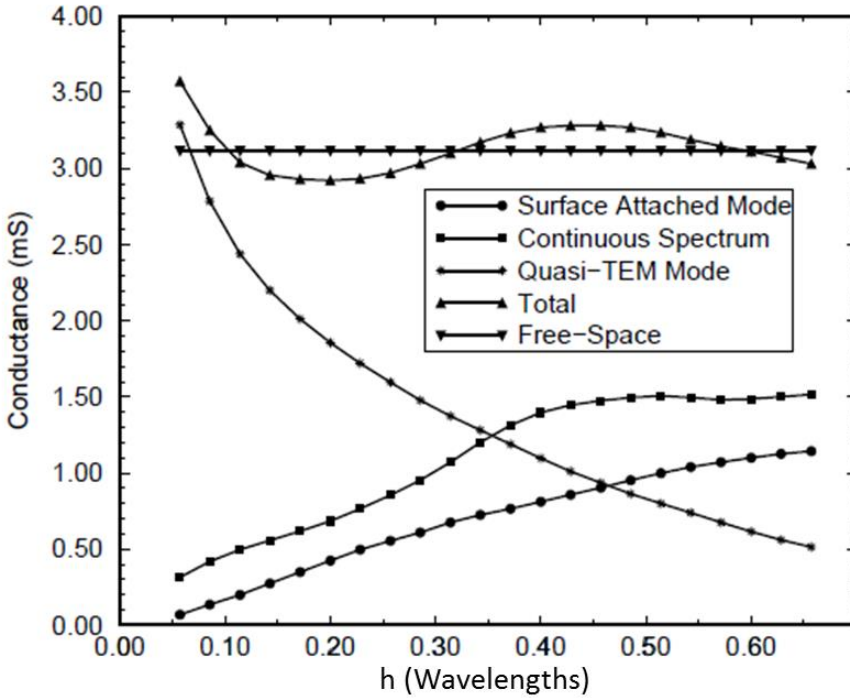


Fig. 4.5.3. Input conductance of the infinitely long wire. The individual contributions of modal and radiation terms are shown. The wire was assumed to be perfectly conducting.

As mentioned above, for small heights the transmission line (or quasi-TEM) component is dominant which agrees with the common assertion that the total current can be approximated as simply the quasi-TEM current. It is this current that will be considered when the low frequency approximation is discussed later.

4.6 Derivation of the Low-frequency Carson Approximation

Introduction

It has been shown in Sections 4.2 – 4.5 that an exact closed form solution for the conductor current can be written as

$$\hat{I}(z) = \frac{1}{2\pi} \int_{-\infty}^{\infty} \left(\frac{V}{Z(\gamma) + \gamma^2 / Y(\gamma)} \right) e^{-j\gamma z} d\gamma \quad (4.6.1)$$

For this result

(4.6.2)

$$Z(\gamma) = \frac{\omega\mu_0}{4} \left[H_0^{(2)}(\gamma^2 - k_0^2)^{1/2} a - H_0^{(2)}(\gamma^2 - k_0^2)^{1/2} ((2h)^2 + a^2)^{1/2} \right] + 2P(\gamma) + Z_{iw}$$

(4.6.3)

$$Y(\gamma) = -4\omega\varepsilon_0 \left[H_0^{(2)}(\gamma^2 - k_0^2)^{1/2} a - H_0^{(2)}(\gamma^2 - k_0^2)^{1/2} ((2h)^2 + a^2)^{1/2} \right] + 2k_1^2 Q(\gamma) \Big]^{-1}$$

where $H_0^{(2)}(q)$ is the Hankel function of the second kind, order zero and argument q (Abramowitz and Stegun, 1972),

$$P(\gamma) = \left(\frac{j}{\pi} \right) \int_{-\infty}^{\infty} \frac{e^{-2u_1 h} e^{j\kappa a}}{u_1 + u_2} d\kappa$$

and

$$Q(\gamma) = \left(\frac{j}{\pi} \right) \int_{-\infty}^{\infty} \frac{e^{-2u_1 h} e^{j\kappa a}}{k_2^2 u_1 + k_0^2 u_2} d\kappa.$$

where

$$u_1 = \sqrt{\kappa^2 + \gamma^2 - k_0^2} \quad \text{Re}(u_1) \geq 0$$

and

$$u_2 = \sqrt{\kappa^2 + \gamma^2 - k_2^2} \quad \text{Re}(u_2) \geq 0.$$

Finally,

$$k_0 = \omega \sqrt{\mu_0 \varepsilon_0},$$

$$k_2 = \omega \sqrt{(\mu_0)(\varepsilon_0 \varepsilon_{r2} - j\sigma_2 / \omega)} \cong \exp(-j\pi/4) \sqrt{\omega \mu_0 \sigma_2}, \quad \sigma_2 \gg \omega \varepsilon_0 \varepsilon_{r2}.$$

It is not important for the reader who has skipped Sections 4.2 – 4.5 to understand the details of (4.6.1) – (4.6.3). Rather, it is important only to recognize that this is an exact closed form solution that will be used in the next subsection to develop expressions that are very familiar to power engineers.

Approximations

According to Fig. 4.5.2, the “quasi-TEM” or “transmission line” mode is dominant for wire heights that are a small fraction of a wavelength ($\lambda = 3 \times 10^8 / f$ in meters where f is the frequency in Hertz). If 0.05λ is used as the criterion for “small,” then (at 60 Hz) h must be less than 250 km. Clearly, this condition is satisfied for all practical situations. In fact, if h is as much as 30 m, then the approximation that the total current is the “quasi-TEM” or

“transmission line” is valid up to approximately 0.5 MHz. In practice, it has been used to nearly 2 MHz.

When the wire height, h , is a small fraction of a wavelength and is much larger than the wire radius and the earth is a reasonably good conductor, then it can be generally assumed that

$$\begin{aligned}
 |a\sqrt{k_0^2 - \gamma^2}| &\ll 1 \\
 |2h\sqrt{k_0^2 - \gamma^2}| &\ll 1 \\
 a &\ll 2h \\
 |k_0 h| &\ll 1 \\
 |k_0^2 / k_2^2| &\ll 1
 \end{aligned} \tag{4.6.4}$$

Reduction to the Carson integral

Under these conditions, $Q(\gamma)$ is small compared to Λ and $P(\gamma)$ where

$$\Lambda = \frac{\omega\mu_0}{4} \left(H_0^{(2)} \left((\gamma^2 - k_0^2)^{1/2} a \right) - H_0^{(2)} \left((\gamma^2 - k_0^2)^{1/2} \left((2h)^2 + a^2 \right)^{1/2} \right) \right)$$

since Λ is independent of k_2 , $Q(\gamma)$ is proportional to $1/k_2^2$ and $P(\gamma)$ is proportional to $1/k_2$. (Wait 1972; Olsen and Pankaskie 1983)

Further,

$$H_0^{(2)}(q) \cong 1 - \frac{2j}{\pi} \ln(q/2) - \frac{2j\gamma_e}{\pi}, \quad q \ll 1$$

where $\gamma_e = 0.5772\dots$ is Euhler’s constant. Hence

$$\Lambda \cong \frac{j\omega\mu_0}{2\pi} \ln \left(\frac{\left((2h)^2 + a^2 \right)^{1/2}}{a} \right) \cong \frac{j\omega\mu_0}{2\pi} \ln \left(\frac{2h}{a} \right)$$

and

$$\begin{aligned}
 P(\gamma) &= \frac{j2}{\pi} \int_0^\infty \frac{(u_1 - u_2) e^{-2u_1 h}}{(u_1 - u_2)(u_1 + u_2)} \cos(\kappa a) d\kappa \\
 &\cong \frac{j2}{\pi} \int_0^\infty \frac{(\kappa - u_2) e^{-2u_1 h}}{(k_2^2 - k_0^2)} \cos(\kappa a) d\kappa \\
 &\cong -\frac{j2}{\pi k_2^2} \int_0^\infty (u - \kappa) e^{-2h\kappa} \cos(\kappa a) d\kappa
 \end{aligned} \tag{4.6.5}$$

where $u = \sqrt{\kappa^2 - k_2^2}$ and $u_1 \approx \kappa$ over most of the integration since $1/(2h) \gg \kappa_1$.

Low frequency equivalent per-unit length parameters

The result is that Z and Y can be considerably simplified and written as

$$Z \cong \frac{j\omega\mu_0}{2\pi} \{\ln(2h/a) - J_c(a, h, h)\} + Z_{iw} \quad (4.6.6)$$

where (in a more general form)

$$J_c(x - x_1, y, y_1) = \frac{2}{k_2^2} \int_0^\infty (u - \kappa) e^{-(y+y_1)\kappa} \cos(\kappa(x - x_1)) d\kappa \quad (4.6.7)$$

(4.6.7) is the ‘‘Carson’’ integral (Carson 1926)⁴¹. Finally,

$$Y \cong 2\pi j\omega\epsilon_0 \{\ln(2h/a)\}^{-1} = j\omega C \quad (4.6.8)$$

where

$$C = \frac{2\pi\epsilon_0}{\ln(2h/a)} \quad (4.6.9)$$

Of greatest importance here is that Z and Y are no longer functions of γ and hence, the set of singularities is much simpler than above. It will be shown later that ‘‘ C ’’ is the capacitance per unit length for a wire over a perfectly conducting earth and

$$L_e = \frac{\mu_0}{2\pi} \{\ln(2h/a) - \text{Re}(J_c(a, h, h))\}. \quad (4.6.10)$$

which is the external inductance per unit length where

$$J_c(a, h, h) = \frac{2}{k_2^2} \int_0^\infty (u - \kappa) e^{-2h\kappa} \cos(\kappa a) d\kappa \quad (4.6.11)$$

More will be said later in Chapter 7 about generalizing (4.6.9) and (4.6.10) to the case for a conductor bundle. The equivalent ‘‘external’’ resistance due to losses in the earth (R_e) can be written as

$$R_e = \frac{\omega\mu_0}{2\pi} \text{Im}(J_c(a, h, h)) \quad (4.6.12)$$

⁴¹ Note that the method used here to derive Carson’s integral is not the same as used by Carson in his original paper on this subject. Appendix C has been written to review the methodology used by Carson in his original paper.

while the equivalent resistance (R_i) and internal inductance (L_i) due to the conductor are:

$$R_i = \text{Re}(Z_{iw}) \quad (4.6.13)$$

and

$$L_i = \text{Im}(Z_{iw}) / \omega \quad (4.6.14)$$

Relationship to real conductor specifications

In handbooks used for specifying conductors used for high voltage transmission lines, the per-unit parameters introduced in the last section are presented in a different way. The purpose of this section is to relate the parameters presented here with those used to specify real conductors. Again, only the electrical properties of these conductors will be emphasized. For a more exhaustive discussion of conductor specifications, the reader is referred to (EPRI, 1982) and (Thrash et. al. 2007).

Conductor type and sizing

As mentioned in Chapter 2, transmission line conductors are generally stranded and constructed of aluminum strands. In many cases, there is a core of steel strands for strength. Nearly all conductors are 2.5 cm in diameter or larger. Most are “aluminum conductor steel reinforced” (ACSR) although there are a variety of other types such as “all aluminum conductor” (AAC) and “aluminum conductor alloy reinforced” (ACAR). More recently conductors with cores made of composite materials designed to operate at higher temperatures have become available.

Transmission line conductors are usually designated in tables by given names (usually birds such as Chukar or Pheasant). In addition to specifying the number of strands, the stranding pattern and outer diameter of the conductor (in millimeters or inches), it is common to specify the total cross sectional area of aluminum in the conductor since this represents the primary current carrying area of the conductor⁴². The cross sectional area is presented in either square millimeters or circular mils (the area of a circle that is 1 millimeter in diameter).

Resistance

In conductor tables, the resistance of the conductor at certain frequencies and temperatures is given. These will in general differ from the resistance given by the “internal” conductor resistance in (4.6.12) because the conductor is stranded rather than solid. The frequency correction is given because of the skin effect inherent in (4.6.12) and generally leads to higher resistances at higher frequencies. Since the component of resistance given in (4.6.11) is related to the overall transmission line geometry and the earth’s

⁴² The effect of considering currents in the steel core would reduce the resistance by 1 – 2%.

electrical properties, it is not considered in conductor tables. Rather, it must be considered separately when the overall transmission line is designed.

Capacitance

As shown earlier in (4.6.9), the capacitance per unit length of a conductor over earth (with the earth well approximated as a perfect conductor) is

$$C = \frac{2\pi\epsilon_0}{\ln(2h/a)} \quad \text{F/m} \quad (4.6.15)$$

Since this is a function of both a conductor parameter (i.e., the radius “a”) as well as a parameter that represents the overall geometry of the transmission line (i.e., the conductor height “h”), it is necessary to separate a portion that can be attributed to the conductor alone. This is done by first converting the capacitance per unit length into a capacitive reactance per unit length,

$$X_c = \frac{1}{\omega C} = \frac{\ln(2h/a)}{\omega 2\pi\epsilon_0} \quad \Omega/\text{m}. \quad (4.6.16)$$

This result is then split into two parts as

$$X_c = \frac{1}{\omega C} = X'_A + X'_D = \frac{\ln(1/a)}{\omega 2\pi\epsilon_0} + \frac{\ln(2h)}{\omega 2\pi\epsilon_0} \quad \Omega/\text{m}. \quad (4.6.17)$$

The first term of (4.6.17) (designated X'_A), is called the “conductor component” and represents the capacitive reactance “to one meter” (or one foot if English units are used)⁴³. The second term (designated X'_D), is sometimes tabulated and called the “separation component.” Usually, these are given in units of Ohms per km or Ohms per mile.

Inductance

As shown earlier in (4.6.10) and (4.6.14), the external and internal inductances per unit length of a conductor over earth are:

$$L = L_i + L_e = \text{Im}(Z_{iw})/\omega + \frac{\mu_0}{2\pi} \{ \ln(2h/a) - \text{Re}(J_c(a, h, h)) \} \quad \text{H/m}. \quad (4.6.18)$$

⁴³ Here the actual radius and height are used because the conductor is only a single conductor. In Chapter 7, this will be generalized to conductor bundles and “geometric mean radius” (GMR) and “geometric mean distance” (GMD) substituted for “a” and “h” respectively.

In conductor tables, this is first converted into inductive reactance by multiplying by ω as shown in (4.6.19)

(4.6.19)

$$X_L = \omega(L_i + L_e) = \text{Im}(Z_{iw}) + \frac{\omega\mu_0}{2\pi} \{\ln(2h/a) - \text{Re}(J_c(a, h, h))\} \Omega/\text{m}.$$

The next step is to separate the conductor component in a similar way as to that done for the capacitance term as shown in (4.6.20)

(4.6.20)

$$X_L = X_A + X_D = \left[\text{Im}(Z_{iw}) + \frac{\omega\mu_0}{2\pi} \ln(1/a) \right] + \left[\frac{\omega\mu_0}{2\pi} \{\ln(2h) - \text{Re}(J_c(a, h, h))\} \right] \Omega/\text{m}.$$

X_A represents the reactance of the conductor to one meter (or one foot if English units are used). X_D has sometimes been tabulated under the assumption that the earth is a perfect conductor, but as will be shown in Chapter 5, while this assumption is acceptable for capacitance, it is not for inductance. X_A is further simplified by selecting a fictitious distance “GMR” that is used to combine the two terms together. More specifically

$$X_A = \left[\text{Im}(Z_{iw}) + \frac{\omega\mu_0}{2\pi} \ln(1/a) \right] = \frac{\omega\mu_0}{2\pi} \ln(1/\text{GMR}) \quad (4.6.21)$$

In conductor tables the GMR refers to a radius called the geometric mean radius of a stranded conductor that is calculated by taking into account the geometry and material of the strands, the presence or absence of a steel core and the skin effect⁴⁴. More information about this calculation can be found in (EPRI, 1982). Typical values of GMR for stranded conductors range from 75% - 80% of the conductor radius. Usually, these are given in units of Ohms per km or mile.

Carson full series and first order approximation

Carson developed a full series expression for the integral that is given here in Appendix D (Carson 1926). If all terms that decay at least as fast as $\ln(k_2 r^i)(k_2 r^i)^2$ are dropped then

$$J_c(x - x_1, y, y_1) \cong \ln\left(j \frac{k_2 r^i}{2}\right) + 0.077 - j \frac{2}{3} k_2 (y + y_1) \quad (4.6.22)$$

⁴⁴ As indicated earlier with respect to the presentation of capacitive reactance GMR will be generalized in Chapter 7 for conductor bundles.

where

$$r^i = \sqrt{(y + y_1)^2 + (x - x_1)^2} \quad (4.6.23)$$

is the distance from the line current's image at $(x, y) = (x_1, -y_1)$ and it is assumed that $|k_2 r^i| < 0.25$ where

$$k_2 \cong \exp(-j\pi/4) \sqrt{\omega \mu_0 \sigma_2}, \quad \sigma_2 \gg \omega \epsilon_0 \epsilon_{r2}. \quad (4.6.24)$$

In the case for which $a = 0$ and $k_2 h \ll 1$, (4.6.22) reduces to

$$J_c(a, h, h) \cong \ln \left(j \frac{2h}{(2/k_2)} \right) \quad \text{if } k_2 h \ll 1. \quad (4.6.25)$$

This result can be shown to be nearly equivalent to an alternative expression for J_c developed in Section 5.4 that is interpreted as a complex image. If this result is used in (4.6.6), the series impedance of a wire above earth becomes

$$Z = Z_{iw} + \frac{j\omega\mu_0}{2\pi} \ln((2/jk_2)/a) \quad (4.6.26)$$

The last term of this formula has the interpretation of the series impedance of a wire in the presence of a “complex image” wire at a complex distance $2/(jk_2)$ meters below the source where the earth has been replaced by free space (Wait and Spies 1969). This very simple interpretation will be revisited later. Before finishing, however, it is interesting to note that the inductance L in (4.6.10) and (4.6.26) becomes infinite as $\omega \rightarrow 0$ since $k_2 \rightarrow 0$ as $\omega \rightarrow 0$. Thus, application of (4.6.24) to the “dc” case will require some additional thought (Bracken, 1982).

Transmission line equivalent

Again, repeating (4.6.1) with Z and Y written explicitly to indicate that after the “Carson” approximations they are no longer dependent on γ

$$I(z) = \frac{1}{2\pi} \int_{-\infty}^{\infty} \left(\frac{V}{Z + \gamma^2/Y} \right) e^{-j\gamma z} d\gamma = \frac{VY}{2\pi} \int_{-\infty}^{\infty} \left(\frac{V}{\gamma^2 - \gamma_{TL}^2} \right) e^{-j\gamma z} d\gamma \quad (4.6.27)$$

where there is a pair of zeros in the denominator at

$$\begin{aligned}\gamma = \gamma_{TL} &= \pm j\sqrt{ZY} \\ &= \pm \left(k_0^2 \left(1 - \frac{J_c(a, h, h)}{\ln(2h/a)} \right) - \frac{j2\pi\omega\epsilon_0 Z_{iw}}{\ln(2h/a)} \right)^{1/2}\end{aligned}\quad (4.6.28)$$

It will be assumed⁴⁵ that $\text{Im}(\gamma_{TL}) \leq 0$ which will be seen shortly to allow the original contour to be deformed in the lower half plane for $z > 0$. This zero represents the “quasi-TEM” or “transmission line” mode and can be represented by an equivalent transmission line with distributed parameters given by (4.6.6) and (4.6.8). Since this zero in the denominator represents a simple pole of the integrand, it becomes straightforward to evaluate (4.6.26) by residue theory. (4.6.26) becomes

$$I(z) = \frac{VY}{2\pi} \int_{-\infty}^{\infty} \left(\frac{1}{(\gamma + \gamma_{TL})(\gamma - \gamma_{TL})} \right) e^{-j\gamma z} d\gamma \quad (4.6.29)$$

If $z > 0$, then $e^{-j\gamma z} = e^{-j\beta z} e^{\alpha z}$ tends to zero for values of γ in the lower half of the complex γ plane and the integration along the real axis can be deformed as shown in Fig. 4.6.4 with the contribution of the infinite lower semi-circle (i.e., C_∞) is equal to zero. The only remaining contribution is that of the residue of the simple pole at γ_{TL} .

The contribution of the pole can be evaluated by using the transformation $\gamma \rightarrow \gamma_{TL} + re^{j\theta}$, $r \ll |\gamma_{TL}|$ where $d\gamma = jrd\theta e^{j\theta}$. The current becomes equal to the integral around the pole (i.e., the residue contribution) and is

$$\begin{aligned}\hat{I}(z) &= \frac{VY}{2\pi} \int_{-\infty}^{\infty} \left(\frac{1}{(\gamma + \gamma_{TL})(\gamma - \gamma_{TL})} \right) e^{-j\gamma z} d\gamma \\ &= -f(\gamma_{TL}) \int_{-\pi/2}^{3\pi/2} \frac{jre^{j\theta}}{re^{j\theta}} d\theta = -2\pi j f(\gamma_{TL})\end{aligned}\quad (4.6.30)$$

where

$$f(\gamma) = \frac{VY}{2\pi(\gamma + \gamma_{TL})} e^{-j\gamma z}$$

so that

$$\hat{I}(z) = \frac{-jVY}{2\gamma_{TL}} e^{-j\gamma_{TL}z} \quad (4.6.31)$$

⁴⁵ This is arbitrary, but once the assumption is made all other operations must be consistent with this assumption.

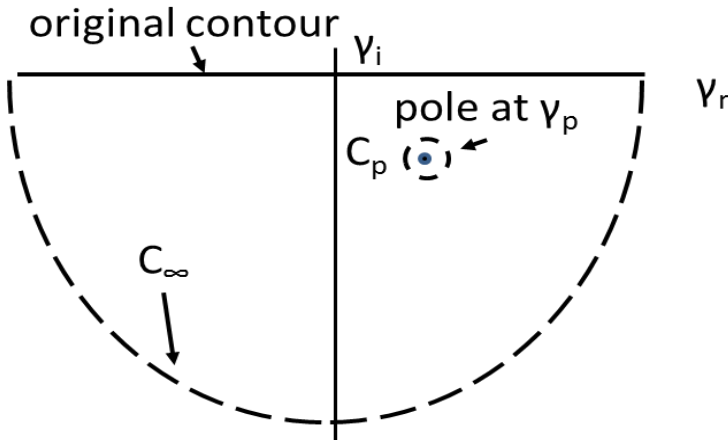


Fig. 4.6.4. contour integration for current on the wire

If $z < 0$, a similar derivation using the same reference direction for the current yields

$$\hat{I}(z) = \frac{jVY}{2\gamma_{TL}} e^{+j\gamma_{TL}z} \quad (4.6.32)$$

In the following section, this result will be interpreted using an equivalent distributed parameter transmission line that can be analyzed with all of the techniques that have been developed for analyzing transmission lines such as coaxial cable, parallel wire lines or microstrip.

4.7 Equivalent Transmission Line Theory

Approach

The first step in developing an equivalent transmission line theory is to recognize that, even though the conductor that was analyzed appears to be open circuited, it is also infinitely long. Hence the input current is not expected to be zero because the current never reaches the end of the conductor to “get the information” that the wire is open circuited.

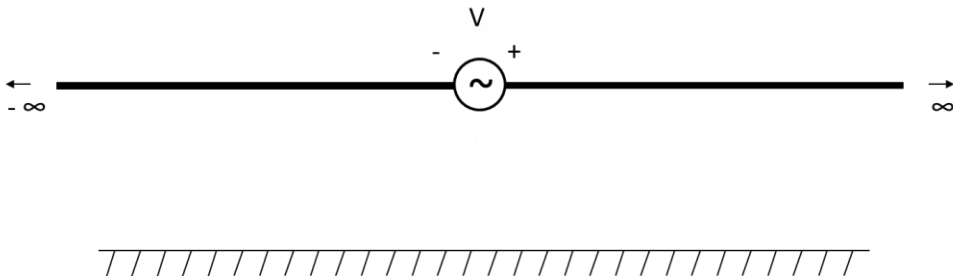


Fig. 4.7.1. The “voltage” in (4.7.23) as a source in series with the conductor.

The second step is to recognize that while the current $I(z)$ is the current that would be expected to appear in an equivalent transmission line theory for the conductor over the earth problem, the voltage V is not. First, the voltage V is due to a source in series with the conductor as shown in Fig. 4.7.1 rather than a voltage that is defined between two conductors as would be expected in transmission line theory. Second, V exists only at the origin. In the next section, the traditional transmission line “voltage” will be derived.

Identification of voltages

To identify a voltage that can be used to interpret (4.6.30) in terms of equivalent distributed parameter transmission line theory, it is helpful to refer to the two circuits shown in Fig. 4.7.2. **Given that all relevant cross sectional dimensions of the conductor over earth problem are small compared to a wavelength at power frequencies, and assuming that the electric potential at the center between the two voltages sources in a) is zero by symmetry, the circuit in b) is identical to that of a).** Further, it will be shown in Chapter 5 that (for the low frequencies usually associated with power transmission lines) the voltage V_{cg} (the conductor to ground voltage) can be uniquely defined as the potential difference between the conductor and any point on the earth that is in the same cross sectional plane.

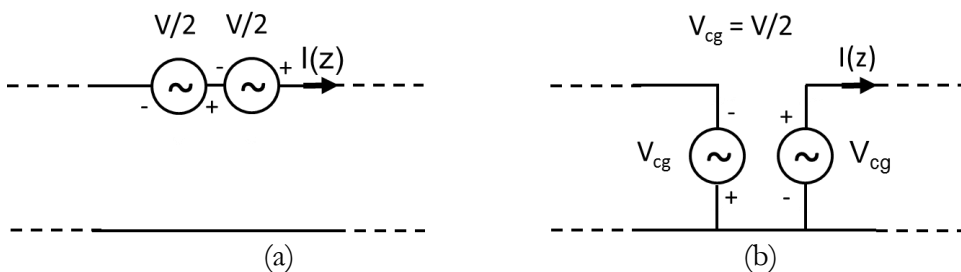


Fig. 4.7.2. a) circuit equivalent to Fig. 4.7.1 b) for the case that all cross sectional dimensions of the power line are small compared to a wavelength at the operating frequency.

Given this equivalence, it is now possible to write (4.6.30) in terms of the equivalent transmission line driving voltage V_{cg} where the subscript “cg” is read as “conductor to ground.” Given this, the “voltage” on the equivalent transmission line is the voltage measured between the conductor and any point on the earth in the same cross-sectional plane. In terms of this voltage

$$I(z) = \frac{-jV_{cg} Y}{\gamma_{TL}} e^{-j\beta_{TL}z} e^{-\alpha_{TL}z} \quad (4.7.1)$$

where (in addition) γ_{TL} has been written as $\beta_{TL} - j\alpha_{TL}$ to separate the propagation from the attenuation as often done in analyzing transmission lines.

Characteristic or surge impedance

The voltage along the power line can then be written as

$$V_{cg}(z) = Z_{OTL} I(z) = V_{cg} e^{-j\beta_{TL}z} e^{-\alpha_{TL}z} \quad z > 0 \quad (4.7.2)$$

where (using (4.6.19))

$$Z_{OTL} = (-jY/\gamma_{TL})^{-1} = j\gamma_{TL}/Y = \sqrt{\frac{Z}{Y}} \quad (4.7.3)$$

is called the “characteristic impedance” of the transmission line that is often referred to in the power engineering literature as the “surge impedance.”

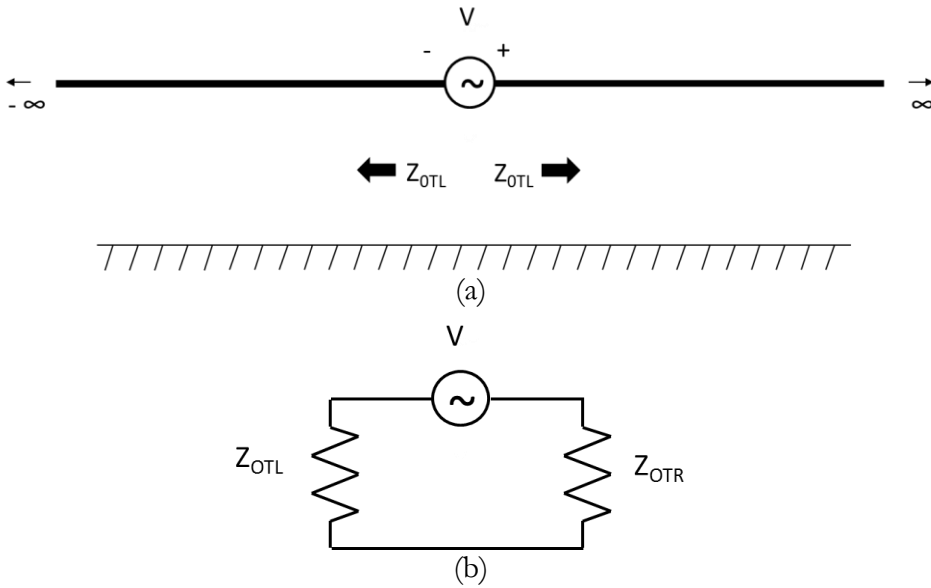


Fig. 4.7.3. a) Equivalent transmission line for an infinitely long power line. b) Equivalent input circuit

Given this (as shown in Fig. 4.7.3), an equivalent circuit can be developed to assist in understanding (4.7.2). The current into the transmission line can be written as

$$I(z=0) = \frac{V}{2Z_{OTL}} = \frac{V_{cg}}{Z_{OTL}} \quad (4.7.4)$$

Now that the voltage and current are defined, an equivalent transmission line distributed parameter system can be defined as shown in the “T equivalent” transmission line shown in Fig. 4.7.4 where in the limit, $\Delta l \rightarrow 0$.

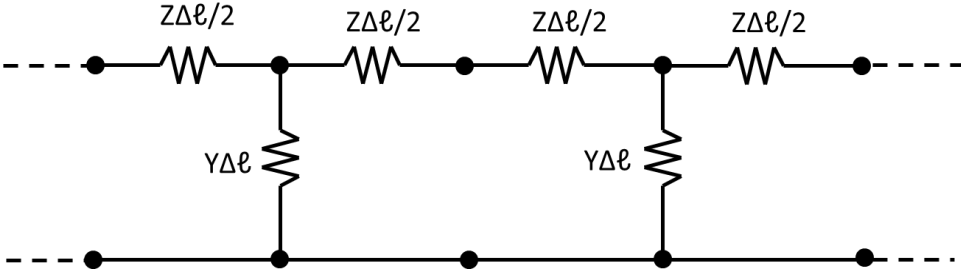


Fig. 4.7.4. Distributed parameter equivalent circuit of a power transmission line

Per unit length parameters of the equivalent system

Here, the parameters (i.e., Z and Y) of the distributed system are indicated. To review

$$Z = R_e + R_i + j\omega(L_e + L_i) \quad (4.7.5)$$

where R_e , R_i , L_e and L_i are defined by (4.6.11), (4.6.12), (4.6.10) and (4.6.13) respectively and

$$Y = j\omega C \quad (4.7.6)$$

where C is defined in (4.6.9). In the special case for a perfectly conducting conductor and earth, the propagation constant γ_{TL} and the characteristic impedance Z_{0TL} can be written as

$$\gamma_{TL} = -j\sqrt{ZY} \cong k_0 = \omega\sqrt{\mu_0\epsilon_0} \quad (4.7.7)$$

and

$$Z_{0TL} = \sqrt{\frac{Z}{Y}} \cong \eta_0 \frac{\ln(2h/a)}{2\pi} = \sqrt{\frac{\mu_0}{\epsilon_0}} \frac{\ln(2h/a)}{2\pi} \quad (4.7.8)$$

In the approximate forms of (4.7.7) and (4.7.8) both the conductor and the earth have been represented approximately as perfect conductors. This results in a propagation constant and characteristic impedance equivalent to that of a TEM transmission line.

Finite length transmission lines

Real power transmission lines are not infinitely long and, hence, it is important to consider the influence of the “end” (i.e., $z = \ell$) of a single wire power line. To do this, transmission line theory will be revisited (Ramo et al. 1965). This can be done by assuming that there is a terminating “load impedance” Z_L at a distance ℓ from the source V_g as shown in Fig. 4.7.5.

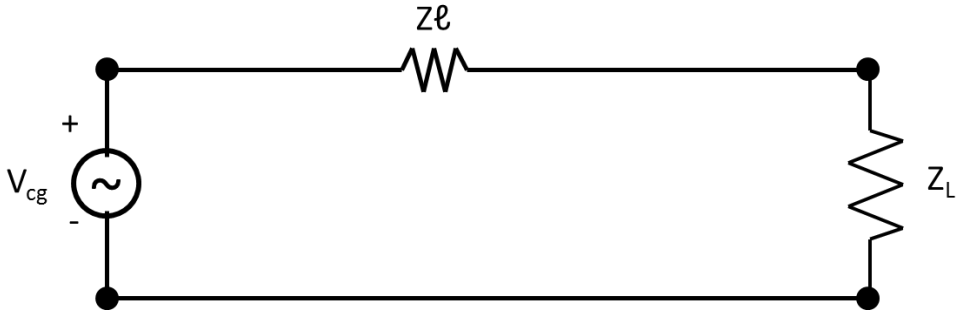


Fig. 4.7.5. Simple transmission line model for a “short” power line of length ℓ .

This impedance can be related to a reflection coefficient as

$$\Gamma = \frac{Z_L - Z_{0TL}}{Z_L + Z_{0TL}} \quad (4.7.9)$$

Hence, the voltage at some point z along the power line (with respect to earth) can be written as

$$V(z) = V^+ \left(e^{-j\gamma_{TL}(z-\ell)} + \Gamma e^{+j\gamma_{TL}(z-\ell)} \right) \quad (4.7.10)$$

where V^+ and $V^- = \Gamma V^+$ are the voltage amplitudes of the forward and reflected waves. Given that the voltage at $z = 0$ is V_{cg} , $V(z)$ can now be written as

$$V(z) = \frac{V_{cg}}{\left(e^{+j\gamma_{TL}\ell} + \Gamma e^{-j\gamma_{TL}\ell} \right)} \left(e^{-j\gamma_{TL}(z-\ell)} + \Gamma e^{+j\gamma_{TL}(z-\ell)} \right) \quad (4.7.11)$$

Similarly, the current distribution can be written as

$$I(z) = \frac{V_{cg}}{Z_{0TL} \left(e^{+j\gamma_{TL}\ell} + \Gamma e^{-j\gamma_{TL}\ell} \right)} \left(e^{-j\gamma_{TL}(z-\ell)} - \Gamma e^{+j\gamma_{TL}(z-\ell)} \right) \quad (4.7.12)$$

Note that this formulation in terms of forward and reflected waves is valid no matter what the length of the line. This is important because for “short” power lines the voltage and current are usually not discussed in terms of forward and reflected waves. Rather, only voltage and current are discussed. To understand why, it is useful to examine (4.7.11) and (4.7.12) under the condition that $\gamma_{TL}\ell \ll 1$ using the Taylor approximation $e^q \cong 1 + q$, $q \ll 1$.

Clearly $V(0) = V_{cg}$, but from (4.7.11)

$$V(\ell) \cong \frac{V_{cg}}{1 + j\gamma_{TL}\ell + \Gamma(1 - j\gamma_{TL}\ell)} (1 + \Gamma) = \frac{V_{cg} Z_L}{Z_L + Z\ell} \quad (4.7.13)$$

where (4.7.8) – (4.7.9) have been used to simplify the result. Clearly, this result is identical to the result obtained from the simplified power line model shown in Fig. 4.7.5 and justifies this simple model (Weeks 1981). It is also interesting to note that the simple model is equivalent to taking a single “T” circuit form Fig. 4.7.4 and assuming that $Y\ell$ is small enough to be ignored.

It is always permissible, however, to describe the voltage distribution on a short power line as a superposition of forward and reflected traveling waves. Taking the ratio of (4.7.11) and (4.7.12) at $z = 0$ yields

$$\frac{V(0)}{I(0)} = Z_{0TL} \frac{(e^{+j\gamma_{TL}\ell} - \Gamma e^{-j\gamma_{TL}\ell})}{(e^{+j\gamma_{TL}\ell} + \Gamma e^{-j\gamma_{TL}\ell})} \quad (4.7.14)$$

If Z_{0TL} is known and measurements of $V(0)$ and $I(0)$ (amplitude and phase) are known, then (4.7.14) can be solved for Γ and V_{cg} found from (4.7.11). Alternatively, if the forward and reflected wave amplitudes and phases are known, then the input voltage and current can be found.

4.8 Circuit Equivalents for Short Power Lines

The analysis at the end of Section 4.7 indicates that an electrically short (i.e., $\gamma_{TL}\ell \ll 1$) single conductor power line can be represented by an equivalent circuit. In this section this result will be generalized somewhat and more explicit circuits shown for short power lines. The most general circuit used for power lines is shown in Fig. 4.8.1. This is a pi network that consists of a series impedance that consists of resistive and inductive components and a pair of parallel capacitors at either end.

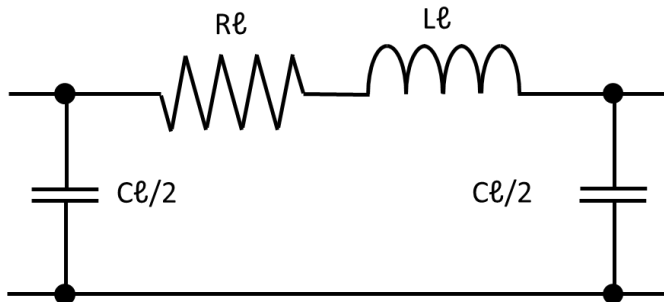


Fig. 4.8.1. Simple circuit equivalent for an electrically short power line of length ℓ

The value of each capacitance is

$$\frac{C\ell}{2} = \frac{\pi\epsilon_1\ell}{\ln(2h/a)}, \quad (4.8.1)$$

while the value of the inductor and resistor are respectively

$$L\ell = \frac{\mu_0}{2\pi} \{ \ln(2h/a) - \operatorname{Re}(J_c(a, h, h)) \} \ell + \operatorname{Im}(Z_{iw})\ell / \omega \quad (4.8.2)$$

and

$$R\ell = -\frac{\mu_0}{2\pi} \operatorname{Im}(J_c(a, h, h))\ell + \operatorname{Re}(Z_{iw})\ell . \quad (4.8.3)$$

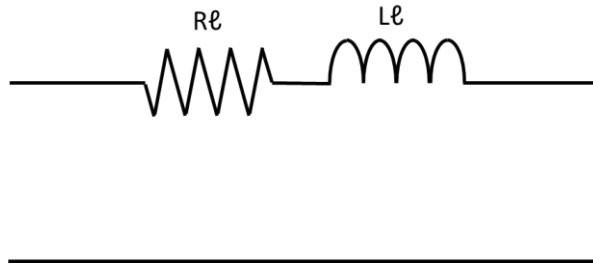


Fig. 4.8.2. Simple circuit equivalent for an electrically short power line ignoring capacitance

In many cases, the line is short enough that the capacitors at the end of the equivalent circuit can be ignored.⁴⁶ In this case, the equivalent circuit can be simplified to the one shown in Fig. 4.8.2.

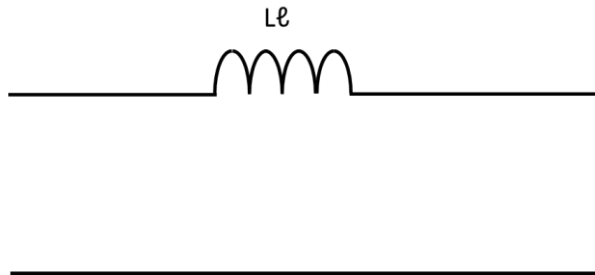


Fig. 4.8.3. Simple inductor circuit equivalent for an electrically short power line

⁴⁶ Because the capacitance per unit length of an underground cable is generally much larger than that for overhead lines it is usually not possible to ignore the capacitance for underground lines. In fact, the capacitance of underground cables is a limiting factor in the maximum length of underground ac cables because of the shunt current through the capacitance that is proportional to the length of the cable. Long underwater links are nearly always dc links because (except for initial transients) the capacitance can be ignored.

For many power system calculations the circuit of Fig. 4.8.2 is further simplified by ignoring the resistance per unit length since the impedance of this element is generally much smaller than that of the inductor at power frequencies of 50 or 60 Hertz. The resulting circuit is shown in Fig. 4.8.3

4.9 Limiting Case for DC Lines

It is tempting to apply the circuit of either Fig. 4.8.1 or Fig. 4.8.2 to the zero frequency (i.e., DC) case by simply allowing the frequency to go to zero for the circuit parameters. It would normally be assumed that (since inductive reactance is proportional to frequency and capacitive reactance is inversely proportional to frequency) the equivalent circuit is simply a series resistor and that its value is equal to (4.8.3). This value would be

$$R\ell = R_{dc}\ell = \ell/(\sigma_w \pi a^2) . \quad (4.9.1)$$

Unfortunately, more care must be used because in (4.6.11) the value of R_c approaches zero as $\omega \rightarrow 0$ (Bracken, 1982). This happens because as the frequency approaches zero, the skin depth of the earth approaches infinity and the current in the earth spreads out to an infinite depth. The result is that the earth resistance is zero despite the finite conductivity of the earth. This can be resolved by using a more realistic layered model of the earth that has a lower layer with zero conductivity.

4.10 Lumped Element Devices Along Lines – Line Compensation

Introduction

In Chapter 1, several lumped devices that are important to the successful operation of high voltage transmission lines were discussed. These included series capacitors, shunt reactors and surge arresters. The purpose of this section is to use the theory that has been developed in this chapter to examine the reasons why these devices are used and what can be accomplished by using them. While all of these devices are generally used on three phase transmission lines, the discussion here will be limited to the single phase case so that the fundamental ideas why they are used are not obscured by the relative complexity of three phase systems. Alternatively, the single phase solution here can be applied directly to balanced three phase systems that have a single phase equivalent.

Series compensation – series capacitors

Consider the use of a simple inductor model for a transmission line of inductance per unit length L and length $\Delta\ell$ that is used to connect two system busses with voltages of $V_{g1} = V_1 \angle \theta_1$ and $V_{g2} = V_2 \angle \theta_2$ respectively. A circuit that shows this arrangement is illustrated in Fig. 4.10.1.

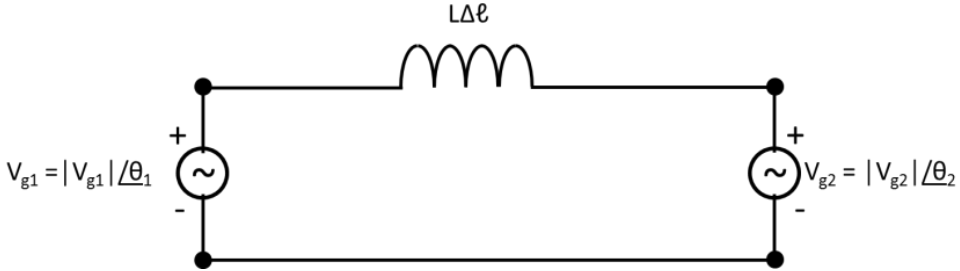


Fig. 4.10.1. Two voltage busses connected by a short transmission line.

It has been shown in Chapter 1 equations (1.3.20) and (1.3.21) that the real and imaginary power transferred from Bus #1 to Bus #2 are

$$P_{12} = \text{Re}(\hat{V}_{g2} \hat{I}_{g2}^*) = \text{Re}\left(\frac{\hat{V}_{g2}(\hat{V}_{g1}^* - \hat{V}_{g2}^*)}{-j\omega L\Delta\ell}\right) = \frac{|\hat{V}_{g1}| |\hat{V}_{g2}|}{\omega L\Delta\ell} \sin(\theta_1 - \theta_2) \quad (4.10.1)$$

$$(4.10.2)$$

$$Q_{12} = \text{Im}(\hat{V}_{g2} \hat{I}_{g2}^*) = \text{Im}\left(\frac{\hat{V}_{g2}(\hat{V}_{g1}^* - \hat{V}_{g2}^*)}{-j\omega L\Delta\ell}\right) = \frac{|\hat{V}_{g2}|}{\omega L\Delta\ell} \left(|\hat{V}_{g1}| \cos(\theta_1 - \theta_2) - |\hat{V}_{g2}| \right)$$

It is interesting to observe that (to first order in $(\theta_1 - \theta_2)$), Q_{12} is proportional to the difference in voltages between the busses. As a general rule, this means that minimizing the flow of reactive power will as a natural consequence reduce voltage differences within a power network. Hence controlling reactive power is an important tool for ensuring a high degree of uniformity in the voltage distribution.

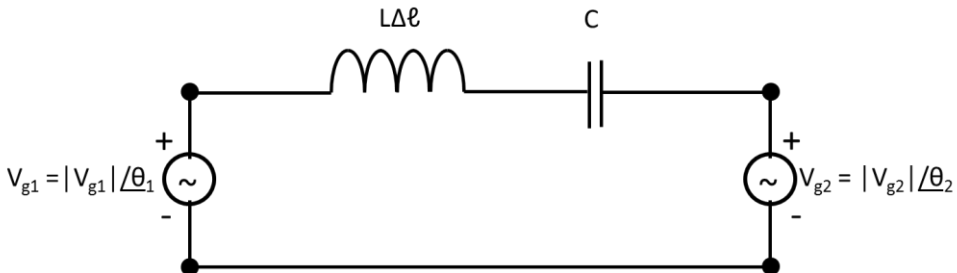


Fig.4.10.2. Two voltage busses connected by a short transmission line with a series capacitor inserted along the line.

Clearly, the real power transferred is limited by the reactance, $\omega L \Delta \ell$, of the transmission line. Given that (as will be demonstrated later in Chapter 8) it is not desirable to use large values of $(\theta_1 - \theta_2)$ it is useful to consider how this reactance can be reduced. This can be done by inserting a lumped capacitor of value C in series with the transmission line as shown in Fig. 4.10.2.

In this case, the power transferred from Bus #1 to Bus #2 can easily be shown to be

$$P_{12} = \frac{|V_{g1}| |V_{g2}|}{|\omega L \Delta \ell - 1/(\omega C)|} \sin(\theta_1 - \theta_2) \quad (4.10.3)$$

If the value of the capacitor's impedance is smaller than that of the transmission line's inductance, then the power flow can be larger for a given value of $(\theta_1 - \theta_2)$. This process is called series compensation. Of course, care must be used to select a capacitor that is capable of withstanding both the voltage across it and the current through it. A more general analysis of this problem for longer transmission lines can be found in (Weeks 1981).

Voltage regulation – series and shunt reactors

One criteria used to characterize the quality of a power line is changes in the voltage distribution along its length. More specifically, it is important that the voltage changes along the line be minimized in order that the power system performs properly. This is the subject of “voltage regulation.” To understand why these changes in voltage can occur, consider the model for a power line of length $\Delta \ell$ shown in Fig. 4.10.3. In this figure, resistive losses are neglected, the inductive and capacitive parameters of the transmission line are L Henries and C Farads per meter respectively and the line is driven by a voltage V_g and terminated with a load Z_ℓ .

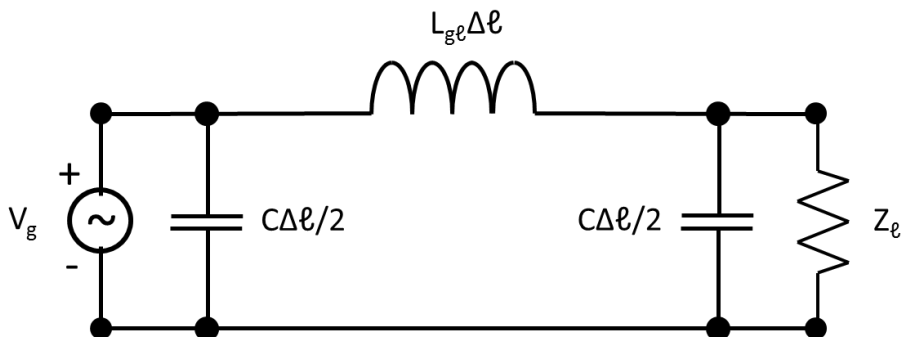


Fig. 4.10.3. Power line with load Z_ℓ

Two complementary approaches will be taken to solving this problem. The first is to use traditional linear circuit theory. The second will be to use the power flow analysis introduced in Chapter 1.

Linear circuit theory approach

The voltage across the load can easily be calculated to be

$$V_\ell = \frac{Z_\ell}{Z_\ell(1 - \omega^2 LC\Delta\ell^2/2) + j\omega L\Delta\ell} V_g \quad (4.10.4)$$

If the line is lightly loaded (i.e., Z_ℓ is large enough that the term $j\omega L\Delta\ell$ can be neglected) then (4.10.4) reduces to

$$V_\ell = \frac{1}{(1 - \omega^2 LC\Delta\ell^2/2)} V_g \quad (4.10.5)$$

It should be clear that the voltage at the load is larger than the input voltage and that the voltage rise is greater for longer line lengths. On transmission lines, this phenomenon is known as the “Ferranti effect” (Ibrahim and Dommel, 2005). Note that if the line is loaded normally (i.e., the $j\omega L\Delta\ell$ term cannot be neglected), the magnitude of (4.10.4) is

$$|V_\ell| = \frac{1}{\sqrt{\left[(1 - \omega^2 LC\Delta\ell^2/2) + (\omega L\Delta\ell X_\ell / (R_\ell^2 + X_\ell^2)) \right]^2 + \left[\omega L\Delta\ell R_\ell / (R_\ell^2 + X_\ell^2) \right]^2}} V_g \quad (4.10.6)$$

where R_ℓ and X_ℓ are respectively the real and imaginary components of the load impedance. Without going into details, the voltage regulation is much better in this case because the second term in the denominator adds to the denominator of (4.10.4) and (at least partially) mitigates the large changes in voltage along the transmission line during light loading. It is also useful to note that it is the reactance of the load that is responsible for this additional term. This is a first suggestion that a lumped element like a shunt reactor to be discussed shortly may be used in the same way.

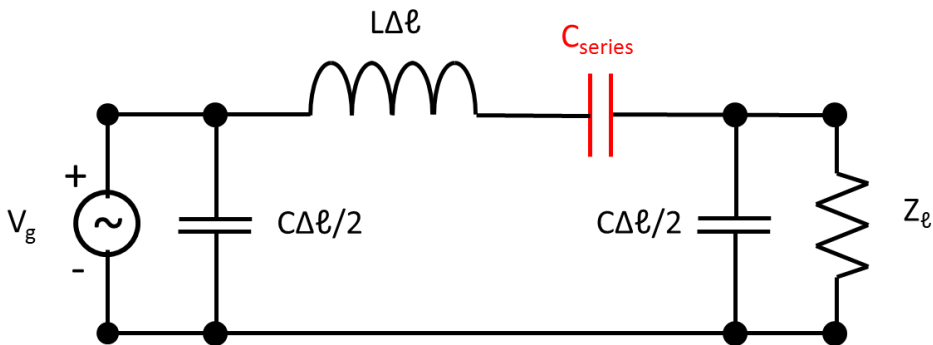


Fig. 4.10.4. The use of a series capacitor (reactor) to reduce voltage increases during light loads.

Fundamentally, there are two methods that have been used to compensate for this problem. The first is to use a capacitor in series with the inductance to reduce the voltage drop across the inductor as shown in Fig. 4.10.4.

Given the insertion of this series capacitor, L can be replaced with the term $L - 1/(\omega^2 C_{series})$ in (4.10.4) and the voltage across the load becomes

$$V_\ell = \frac{Z_\ell}{Z_\ell (1 - \omega^2 (L - 1/(\omega^2 C_{series})) C \Delta \ell^2 / 2) + j \omega L \Delta \ell} V_g \quad (4.10.7)$$

For large values of Z_ℓ (i.e., light loading) this becomes

$$V_\ell = \frac{1}{(1 - \omega^2 (L - 1/(\omega^2 C_{series})) C \Delta \ell^2 / 2)} V_\ell \quad (4.10.8)$$

It should be clear that the value of C_{series} can be selected to reduce the difference in voltage between the source and load ends of the transmission line and hence improve voltage regulation.

Another method to compensate for the Ferranti effect is to use an inductor in parallel with the load (i.e., a shunt reactor as shown in red) as illustrated in Fig. 4.10.5

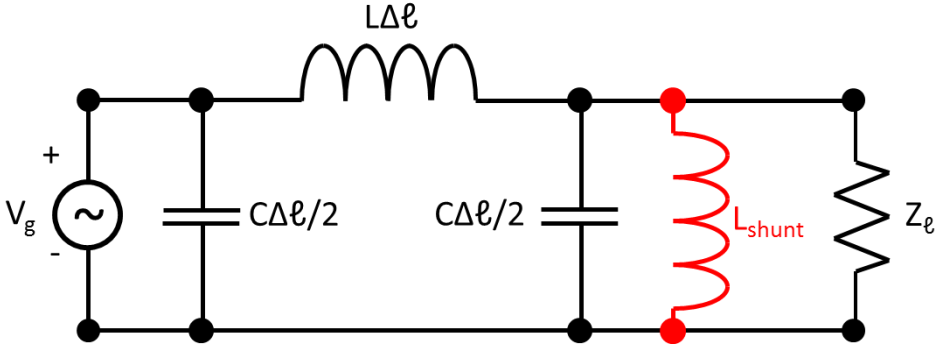


Fig. 4.10.5. Transmission line with a shunt reactor across the load.

Given the insertion of this shunt reactor, C can be replaced with the term

$$C \frac{(\omega^2 C \Delta \ell L_{shunt} / 2 - 1)}{\omega^2 C \Delta \ell L_{shunt} / 2}$$

in (4.10.4) and the voltage across the load becomes

$$V_\ell = \frac{Z_\ell}{Z_\ell \left(1 - \omega^2 C \left(\frac{\omega^2 C \Delta \ell L_{shunt} / 2 - 1}{\omega^2 C \Delta \ell L_{shunt} / 2} \right) L \Delta \ell^2 / 2 \right) + j \omega L \Delta \ell} V_g \quad (4.10.9)$$

For large values of Z_ℓ (i.e., light loading) this becomes

$$V_\ell = \frac{1}{\left(1 - \omega^2 L C \left(\frac{\omega^2 C \Delta \ell L_{shunt} / 2 - 1}{\omega^2 C \Delta \ell L_{shunt} / 2} \right) \Delta \ell^2 / 2 \right)} V_\ell \quad (4.10.10)$$

It should be clear that if L_{shunt} can be selected to reduce the difference in voltage between the source and load ends of the transmission line and again to improve the voltage regulation.

Power flow approach

In Chapter 1, the power flow equations have been set up and solved for the situation illustrated in Fig. 4.10.6 with $\Delta Q_\ell = 0$.

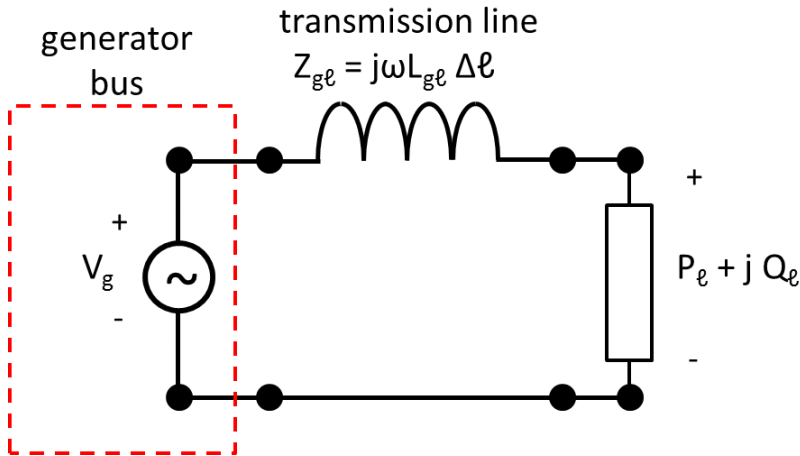


Fig. 4.10.6. Determining the power flow to an arbitrary load through a short transmission line.

While the transmission line model shown in Fig. 4.10.6 is not identical to the one shown in Fig. 4.10.3, the results for the analysis of power flow to the load and load voltage will be applicable for the following reasons. First, the “generator” power in Fig. 4.10.6 can be considered to be the combination of that from the actual generator as well as the reactive power from the parallel capacitor $C\Delta\ell/2$ in Fig. 4.10.3. The voltage across this combination remains V_g . Second, the reactive power supplied by the capacitor $C\Delta\ell/2$ in parallel with the load can be combined with that of the load. Hence $P_\ell + jQ_\ell$

includes the actual load plus the reactive power injected into the system by $C\Delta\ell/2$. Given these assumptions, it is possible to apply results for the system of Fig. 1.1.3 of Chapter 1 to that of Fig. 4.10.6 with $\Delta Q_\ell = 0$.

Using the standard assumption that the magnitude of the generator voltage is equal to 1, an expression for the voltage magnitude across the load was found in (1.3.28) which is repeated here as.

$$|\hat{V}_\ell|^2 = \frac{1 - 2\omega L_{g\ell}\Delta\ell Q_\ell \pm \sqrt{1 - 4\omega L_{g\ell}\Delta\ell Q_\ell - 4(\omega L_{g\ell}\Delta\ell)^2 P_\ell^2}}{2} \quad (4.10.11)$$

It is assumed here that Q_ℓ includes the reactive power supplied by the parallel capacitance of the transmission line, $C\Delta\ell/2$. Note that for most situations the physical solution of (4.10.11) corresponds to the + sign in the equation. This assumption will be made here. The effect of adding a shunt capacitor or inductor (reactor) across the load (ΔQ_ℓ in Fig. 4.10.6), the value of Q_ℓ will be changed to

$$Q'_\ell = Q_\ell + \Delta Q_\ell \quad (4.10.12)$$

To evaluate the effect of adding a shunt capacitor or inductor, the load voltage (4.10.11) will be expanded in a first order Taylor series with respect to Q'_ℓ around its value for $S_\ell = P_\ell + jQ_\ell$. An implicit derivative can be found by taking the derivative of both sides of (4.10.11) as

$$4|\hat{V}_\ell(S_\ell)| \frac{d|\hat{V}_\ell(S_\ell)|}{dQ_\ell} = -2\omega L_{g\ell}\Delta\ell + \frac{1}{2} \left(1 - 4\omega L_{g\ell}\Delta\ell Q_\ell - 4(\omega L_{g\ell}\Delta\ell)^2 P_\ell^2 \right)^{-\frac{1}{2}} (-4\omega L_{g\ell}\Delta\ell) \quad (4.10.13)$$

If, next it is assumed that the system is lightly loaded and hence

$$\left| 4\omega L_{g\ell}\Delta\ell Q_\ell + 4(\omega L_{g\ell}\Delta\ell)^2 P_\ell^2 \right| \ll 1,$$

the square root term in (4.10.13) can be represented as the first two terms of a Taylor series. The result is

$$(4.10.14)$$

$$4|\hat{V}_\ell(S_\ell)| \frac{d|\hat{V}_\ell(S_\ell)|}{dQ_\ell} \cong -2\omega L_{g\ell} \Delta\ell - 2\omega L_{g\ell} \Delta\ell \left(1 + 2\omega L_{g\ell} \Delta\ell Q_\ell + 2(\omega L_{g\ell} \Delta\ell)^2 P_\ell^2\right) \\ = -(4\omega L_{g\ell} \Delta\ell) \left(1 + \omega L_{g\ell} \Delta\ell Q_\ell + (\omega L_{g\ell} \Delta\ell)^2 P_\ell^2\right)$$

Given this result, the voltage after augmenting Q'_ℓ by ΔQ_ℓ is

$$|\hat{V}_\ell(S_\ell + j\Delta Q_\ell)| \cong |\hat{V}_\ell(S_\ell)| + \frac{d|\hat{V}_\ell(S_\ell)|}{dQ'_\ell} \Delta Q_\ell \\ \cong |\hat{V}_\ell(S_\ell)| - \frac{(\omega L_{g\ell} \Delta\ell)}{|\hat{V}_\ell(S_\ell)|} \left(1 + \omega L_{g\ell} \Delta\ell Q_\ell + (\omega L_{g\ell} \Delta\ell)^2 P_\ell^2\right) \Delta Q_\ell$$

Clearly, if a shunt capacitor is added at the load, the voltage at the load is increased since ΔQ_ℓ is a negative number. This would provide additional support to the voltage. Similarly, if a shunt inductor (reactor) is added at the load, the load voltage is decreased. This could be used to counteract the Ferranti effect as described above. Finally, the increase or decrease in voltage can be written as

$$\Delta|\hat{V}_\ell| \cong + \frac{d|\hat{V}_\ell(S_\ell)|}{dQ_\ell} \Delta Q_\ell = - \frac{(\omega L_{g\ell} \Delta\ell)^2}{|\hat{V}_\ell(S_\ell)|} \left(1 + \omega L_{g\ell} \Delta\ell Q_\ell + (\omega L_{g\ell} \Delta\ell)^2 P_\ell^2\right) \Delta Q_\ell$$

The calculation can be completed by recognizing that (according to (1.3.12), the “reactive power” supplied by a shunt capacitor of value C F/m is

$$\Delta Q_{C\ell} \cong -\omega C V_{\ell rms}^2 \quad (4.10.17)$$

Similarly, the “reactive power” absorbed by a shunt inductor of value L H/m is

$$\Delta Q_{L\ell} = \text{Im}(\hat{V}_\ell \hat{I}_\ell^*) = \frac{V_{\ell rms}^2}{\omega L} \quad (4.10.18)$$

In this section, two examples have been given about how the voltage distribution along the power line can be affected by adjusting the value of either a series capacitor or a shunt inductor.. Further studies of this idea for longer transmission lines can be found in Weeks (1981).

Nonlinear elements - surge arresters

As mentioned in Chapter 1, nonlinear lumped element devices called “surge arresters” are used on the power system to suppress surges that occur during switching operations. In order to understand how these elements work without obscuring the result in too much mathematics, it is appropriate to consider transmission lines under DC excitation. To this end, consider the problem illustrated in Fig. 4.10.7. This system consists of a DC source of voltage V_s and internal resistance R_s that drives a two wire lossless transmission line of length ℓ with propagation velocity c (the speed of light in free space) and surge (or characteristic) impedance Z_c . The transmission line is terminated in a resistor of value R_ℓ . A circuit breaker disconnects the load at time $t = 0$.

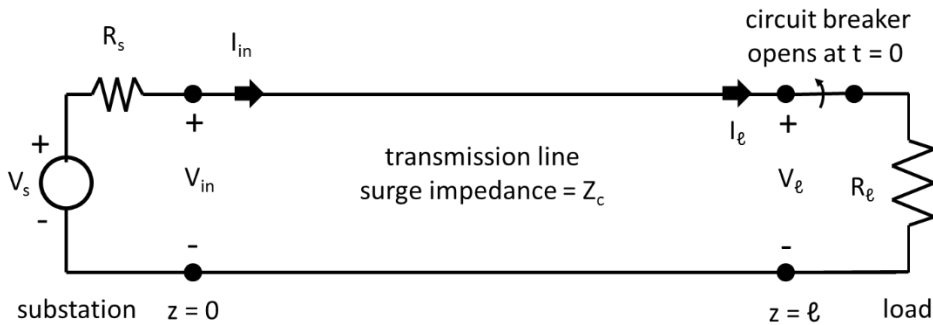


Fig. 4.10.7. Simple dc transmission line with a circuit breaker opening at $t = 0$.

Prior to $t = 0$, the operation of the transmission line can be described by dc circuit theory so that

$$V_{\ell 0} = V_{in0} = \frac{V_s R_\ell}{(R_s + R_\ell)} \quad (4.10.19)$$

and

$$I_{\ell 0} = I_{in0} = \frac{V_s}{(R_s + R_\ell)}. \quad (4.10.20)$$

The subscript “0” means the initial condition before $t = 0$. In terms of transmission line theory, it can be shown that the voltage and current on the line prior to $t = 0$ can be written as

$$V_{in0} = V_{\ell 0} = V_{f0} + V_{r0} = V_{f0}(1 + \Gamma_{\ell 0}) \quad (4.10.21)$$

where V_{f0} is the constant amplitude of a forward traveling wave⁴⁷, $V_{r0} = \Gamma_{\ell 0} V_{f0}$ is the amplitude of the reflected wave and

⁴⁷ Since the voltage source is constant in this case, traveling waves can be written in terms of the unit step function as $U(t + /-z/c)$. It is assumed in (4.10.19) that enough time has passed

$$\Gamma_{\ell 0} = \frac{(R_{\ell} - Z_c)}{(R_{\ell} + Z_c)} \quad (4.10.22)$$

is the reflection coefficient of the load where Z_c is the transmission line's surge (or characteristic) impedance. In a similar manner, the current can be written

$$I_{in0} = I_{\ell 0} = I_{f0} + I_{r0} = I_{f0}(1 - \Gamma_{\ell 0}) = \frac{V_{f0}}{Z_c}(1 - \Gamma_{\ell 0}) \quad (4.10.23)$$

From this information,

$$V_{f0} = V_{in0} \frac{(R_{\ell} + Z_c)}{2R_{\ell}} \quad (4.10.24)$$

and

$$V_{r0} = \Gamma V_{f0} = V_{in0} \frac{(R_{\ell} - Z_c)}{2R_{\ell}}. \quad (4.10.25)$$

Now, at $t = 0^+$, the forward traveling voltage and current do not change because they were generated at the source and hence cannot change until enough time has passed to allow a wave to travel to the source and back again to the load. The reflected traveling voltage and current can, however, change because they are generated at the load. They must change to reflect the changing conditions at the load (i.e. the total load current I_{ℓ} must instantaneously change from the value in (4.10.20) to zero since the circuit breaker has opened and the resistance of the load is now infinite (i.e., an open circuit). Here, to get a somewhat more general solution, the load resistance will be assumed to change to R_{ℓ}' . The total voltage and current at $z = \ell$ after $t = 0$ and until $t = 2\ell/c$ (because no changes take place at the load until a wave has time to travel to the source and back again to the load).

$$V_{\ell 1} = V_{f0} + V_{r1} = V_{f0}(1 + \Gamma_{\ell 1}) \quad 0 \leq t \leq 2\ell/c \quad (4.10.26)$$

and

$$I_{\ell 1} = I_{f0} + I_{r1} = \frac{V_{f0}}{Z_c}(1 - \Gamma_{\ell 1}), \quad 0 \leq t \leq 2\ell/c \quad (4.10.27)$$

for all the traveling waves to have completed their travel across the transmission line (i.e., steady state conditions). Hence the term $U(t+/-z/c) = 1$ and does not appear explicitly in (4.10.19).

where the minus sign in the expression for current occurs because a wave traveling in the $-z$ direction must have voltage and current related by a minus sign. The subscript “1” indicates the time after the first bounce at the load, but before the second. Since the ratio of total voltage to total current at the load must be R_ℓ' , (4.10.26) and (4.10.27) can be solved for $\Gamma_{\ell 1}$. The result is

$$\Gamma_{\ell 1} = \frac{(R_\ell' - Z_c)}{(R_\ell' + Z_c)} \quad (4.10.28)$$

From this result, it is possible to easily calculate the load voltage and current as

$$V_{\ell 1} = V_{f0} + V_{r1} = V_{f0}(1 + \Gamma_1) = V_{\ell 0} \left(\frac{R_\ell + Z_c}{R_\ell' + Z_c} \right) \left(\frac{R_\ell'}{R_\ell} \right), \quad 0 \leq t \leq 2\ell/c \quad (4.10.29)$$

and

$$I_{\ell 1} = I_{f0} + I_{r1} = \frac{V_{\ell 0}}{R_\ell} \left(\frac{R_\ell + Z_c}{R_\ell' + Z_c} \right) \quad 0 \leq t \leq 2\ell/c \quad (4.10.30)$$

Clearly, the voltage across the load can be significantly higher than the voltage prior to switching. In the case for which $R_\ell' \rightarrow \infty$, the voltage across the load is a factor of $(R_\ell + Z_c)/R_\ell$ greater than the voltage before switching. Voltages this much higher than operating voltages might lead to flashovers and (if the voltage is not suppressed) enough air insulation must be provided to withstand them. Note that the condition described above lasts only until the reflected wave has a chance to travel back to the source, reflect and return to the load (i.e., for a time equal to $2\ell/c$ where c is the speed of light). For a 150 km transmission line, this time is 1 mS, more than long enough for an arc to occur.

It is useful to specifically continue this process for one more bounce to examine what happens when the reflected wave reaches the source at $t = \ell/c$. In this case, the reflected wave must be constant during this event and a new forward wave with voltage amplitude V_{f2} is generated. The condition that must be satisfied at the source is

$$V_{in2} = (V_{f2} + V_{r1}) = V_s - I_{in2}R_s = V_s - \frac{R_s}{Z_c}(V_{f2} - V_{r1}) \quad (4.10.31)$$

Equation (4.10.31) can be solved for V_{f2} to get

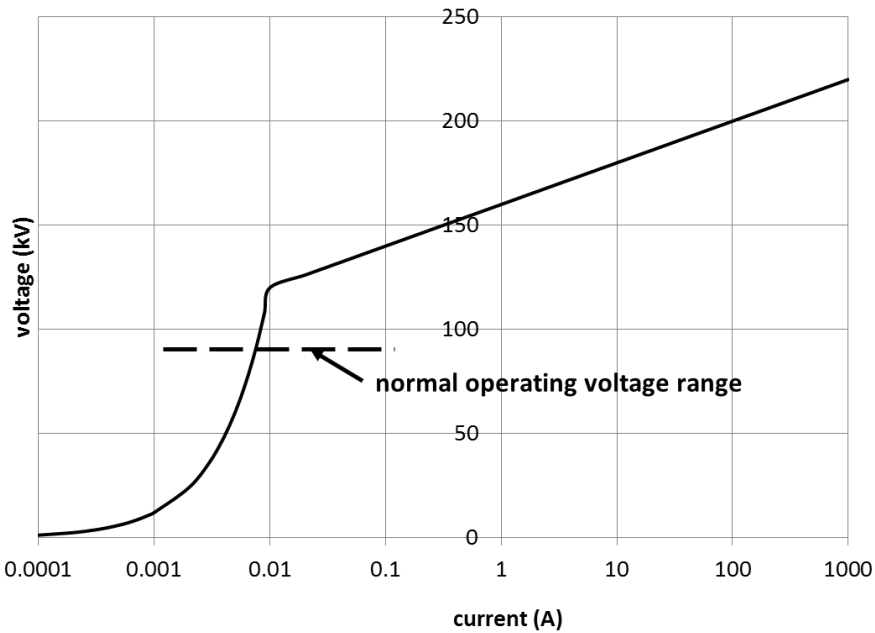


Fig. 4.10.9. Typical surge arrester characteristics.

For this particular surge arrester, the voltage (0 – 120 kV) is linear with current from 0 amps until 10 mA (it appears nonlinear due to the logarithmic scale). In this normal operating range, the current (hence the losses during normal operation) is small. Beyond 120 kV (and 0.01 A or 10 mA), however, the voltage increases only logarithmically with current. Effectively, this limits the voltage that can appear across the arrester.

Mathematically, this device's characteristics can be written as

$$V_{sa} = \frac{V_{sao}}{I_{sao}} I_{sa} = R_{sao} I_{sa} \quad , \quad 0 \leq I_{sa} \leq 0.01 \text{ A}$$

$$V_{sa} = V_{sac} + \Delta V_{sao} \log_{10} \left(\frac{I_{sa}}{I_{sao}} \right) \quad , \quad I_{sa} \geq 0.01 \text{ A}$$
(4.10.34)

If these VI characteristics are used in (4.10.26) – (4.10.27) instead of R_t , and the equations solved iteratively since the device is nonlinear, then it is possible to calculate the reflected wave from the surge arrester. A system that includes the surge arrester (shown in red) is illustrated in Fig. 4.10.10. For the arrester in this example, $V_{sao} = 120$ kV, $I_{sao} = 0.01$ A and $\Delta V_{sao} = 20$ kV. The response of the system to the opening circuit breaker is shown (in red) in Fig. 4.10.11 along with the response of the system without the surge arrester that was shown in Fig. 4.10.8.

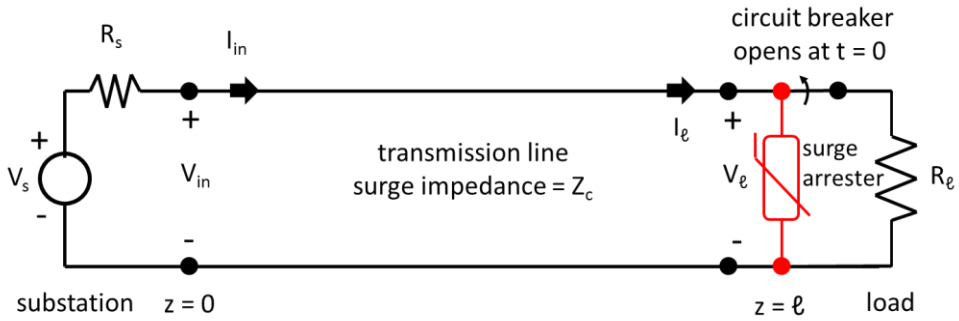


Fig. 4.10.10. simple dc transmission line with a circuit breaker opening at $t = 0$ and a surge arrester.

It is immediately clear that the surge arrester has had a significant impact on the system response. More specifically, the peak voltage has been reduced from approximately 480 kV to approximately 160 kV. This is a significant reduction and generally will justify the use of a surge arrester on economic grounds.

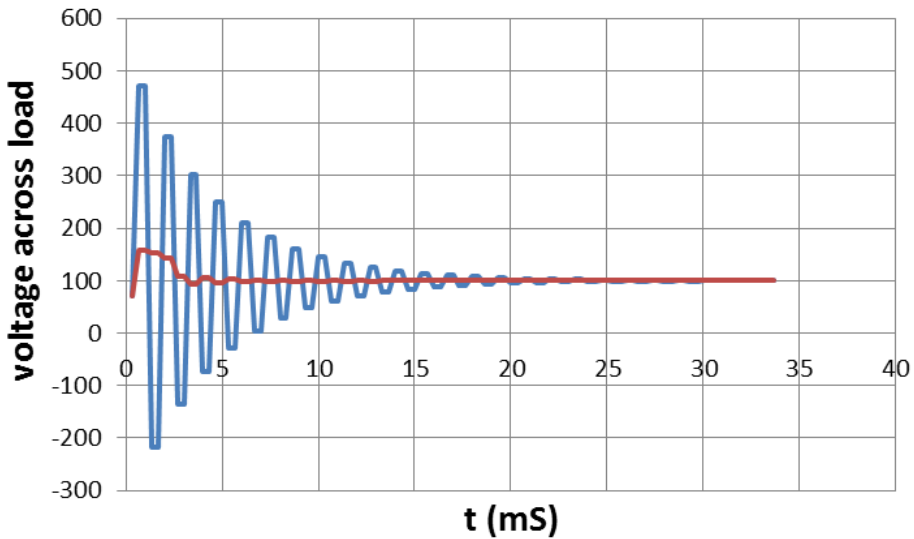


Fig. 4.10.11. Response of the system in Fig. 4.10.10 with (red) and without (blue) the surge arrester

This is, however, not done without penalty. During the initial reflections, not only is the voltage larger than the operating voltage, but the current as well. Hence, the surge arrester absorbs a considerable amount of energy during the surge and, hence, must be designed to withstand this overvoltage condition. Given this result, it is evident that a transmission line should be protected against voltages that are significantly larger than the operating voltage. The specific amount depends on the system in which the

transmission line is operated and should be investigated before the line is designed.

Natural surge arresters – earth and conductor losses and corona

In the model used in the last section to study switching surges, it was assumed that the transmission line was lossless. The attenuation of voltage and current waves traveling from one end of the transmission line to the other due to earth and phase conductor resistive losses were neglected. This attenuation can be relatively easily taken into account (albeit at some increased degree of complexity) and leads to smaller overvoltages than predicted by the lossless theory presented here. While the effect of these losses are well understood, there is another important (and much more complicated) phenomenon that must be considered when calculating the effects of voltage surges on high voltage overhead transmission lines (Wagner and Lloyd. 1955). This phenomenon is corona on the phase conductors that occurs when voltage is large enough that the electric field at the surface of the conductors exceeds some corona onset value. More about corona onset and other corona effects will be presented in Chapter 9. Here it will simply be stated that corona has an important influence in attenuating dynamic overvoltages and should therefore be modeled when studying the dynamic overvoltage stresses on a transmission line. Several models have been presented in the literature and while they are not perfect, they produce reasonable results when incorporated into programs designed to calculate transients on high voltage transmission lines (Suliciu, M.M. and I. Suliciu, I. 1981; Maruvada, et. al. 1989).

4.11 Problems

P4.1. The surface impedance of a conductor can be calculated by (4.2.5) of the text book. In this equation, the Bessel function of the first kind and order zero and one, J_0 and J_1 will be used. In fact, Bessel functions can be approximated by some simpler formulas when the arguments are either very small or very large. For small arguments $|q| \ll 1$,

$$J_0(q) \cong 1$$

and

$$J_1(q) \cong q/2$$

For large arguments $|q| \gg 1$,

$$J_0(q) \approx \sqrt{\frac{2}{\pi q}} \cos(q - \pi/4)$$

and

$$J_1(q) \approx \sqrt{\frac{2}{\pi q}} \cos(q - 3\pi/4)$$

Assume a long conductor wire has the radius of 0.01m and conductivity of $3.5 \times 10^7 \text{S/m}$. Its surface impedance is going to be calculated by different formulas. Let the frequency vary in this manner: from 10 to 90Hz with a 10Hz step and from 100 to 10,000Hz with a 100Hz step (the frequency array will be like [10, 20, 30, ..., 90, 100, 200, ..., 10,000], the total number of frequency points is 109). The permeability is $\mu_0 = 4\pi \times 10^{-7} \text{H/m}$.

a. Calculate the surface impedance Z_{iw} using the exact formula (4.2.5) and the small- and large-argument approximations of Bessel functions given before. Compare your results, plot the three curves in one figure, and make brief comments. The MATLAB functions to calculate $J_0(x)$ and $J_1(x)$ are “besselj(0,x)” and “besselj(1,x)”, respectively.

b. Calculate the surface impedance Z_{iw} using the approximations given in (4.2.6) and (4.2.7). Compare your results with those got in (a) using the small- and large-argument approximations of Bessel functions, respectively. Compare, plot, and make comments on the results.

P4.2. Suppose that a conductor wire, radius 0.01m and conductivity $3.5 \times 10^7 \text{S/m}$, is placed horizontally over the ground at a height of 10m, as shown in Fig. P4.2. The permittivity, permeability, and conductivity of the ground are $\epsilon_2 = 5\epsilon_0$ ($\epsilon_0 = 8.85 \times 10^{-12} \text{F/m}$), $\mu_2 = \mu_0 = 4\pi \times 10^{-7} \text{H/m}$, and $\sigma_2 = 0.01 \text{S/m}$, respectively. Let the frequency vary between 10Hz to 10,000Hz.

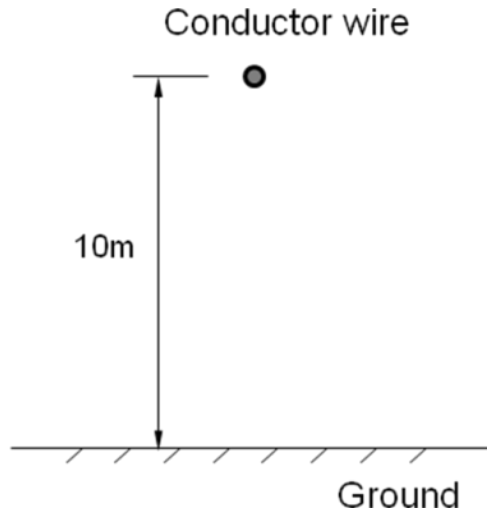


Fig. P4.2. A horizontal conductor wire above ground

a. Calculate the approximation of Carson’s integral by using (4.7.14) and (4.7.15), respectively. Compare and plot the results.

- b. Calculate the equivalent resistances due to the earth and the conductor by using (4.7.11) and (4.7.12), respectively. Which resistance dominates?
- c. Use any integration software/tools or write your own codes (in any language you prefer) to numerically evaluate the exact Carson's integral given by (4.7.7). Compare the results with that obtained in part (a) and plot the three curves in one figure.

P4.3. Use the same model and parameters given in Problem 8 except that now only consider the frequency at 60Hz.

a.) Calculate the transmission line propagation constants formulated by (4.7.18) and qualitatively indicate the position of the two roots in the complex plane. In fact, these two values are the poles of the integrand in (4.7.17).

b. According to the Cauchy integral theorem (http://en.wikipedia.org/wiki/Cauchy_integral_theorem) the integration in (4.7.17)

$$I(z) = -\frac{1}{2\pi} \int_{-\infty}^{+\infty} \left(\frac{V}{Z + \gamma^2 / Y} \right) e^{-j\gamma z} d\gamma$$

can be evaluated by deforming the integral contour from the real axis (C_{Re}) to the infinite lower semi-circle (C_{∞}), as shown in Fig. P4.3.

The contour C_{∞} is formed by 5 parts, $C_{\infty 1}$ to $C_{\infty 5}$. Part $C_{\infty 1}$ and $C_{\infty 5}$ are the infinite semi-circle. Part $C_{\infty 2}$ to $C_{\infty 4}$ are presented to exclude the pole, $\gamma_{TL(+)}$, out of the area enclosed by C_{Re} and C_{∞} . $C_{\infty 2}$ and $C_{\infty 4}$ are the vertical branches extending to infinity. $C_{\infty 3}$ is a circular contour encompassing the pole. Assume $z > 0$. Show that the integration in (4.7.17) equals to the integral only along the contour $C_{\infty 3}$ (Hint-1),

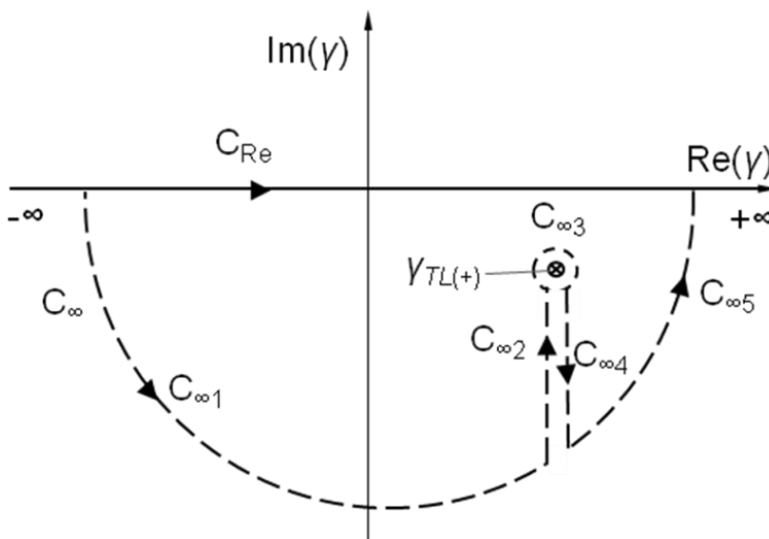


Fig. P4.3 Deformation of the integral contour for (4.7.17)

$$I(z) = -\frac{1}{2\pi} \int_{-\infty}^{\infty} \left(\frac{V}{Z + \gamma^2/Y} \right) e^{-j\gamma z} d\gamma = -\frac{1}{2\pi} \int_{C_{\infty 3}} \left(\frac{V}{Z + \gamma^2/Y} \right) e^{-j\gamma z} d\gamma$$

Then, evaluate the integration by using the residue theorem (Hint-2).

Hint-1: you need to show that the integrals along the other four parts ($C_{\infty 1}$, $C_{\infty 5}$ and $C_{\infty 2}$, $C_{\infty 4}$) have zero contributions. Note that $C_{\infty 2}$ and $C_{\infty 4}$ are in opposite directions.

Hint-2: the residue theorem: the integral for a complex variable function $f(\lambda)$ over an enclosed contour can be evaluated by its residues,

$$\oint_C f(\lambda) d\lambda = 2\pi j \sum_{\lambda=\lambda_{pi}} \text{Re } s(f(\lambda))$$

where λ_{pi} is the i^{th} pole of $f(\lambda)$. If $f(\lambda)$ only has simple pole (first order pole) λ_p and can be written as

$$f(\lambda) = \frac{g(\lambda)}{h(\lambda)} \quad \text{and} \quad h'(\lambda) \neq 0$$

the residue of $f(\lambda)$ at $\lambda = \lambda_p$ can be determined by $\lim_{\lambda \rightarrow \lambda_p} (\lambda - \lambda_p) f(\lambda) = \frac{g(\lambda)}{h'(\lambda)}$.

P4.4. The cross-linked Polyethylene (XLPE) coaxial cable is very commonly used in high-voltage transmission systems. However, high voltage cables are usually only used for short-range cases because of their much higher capacitances compared to overhead transmission lines used in the same voltage range. A typical 138kV XLPE coaxial cable, shown in Fig. P4.4, may have parameters as $d = 0.02\text{m}$, $D = 0.07\text{m}$, and $\epsilon_r = 2.5$, which are the diameter of the core conductor, diameter of the outer covering conductor, and permittivity (dielectric constant) of the XLPE filling, respectively.

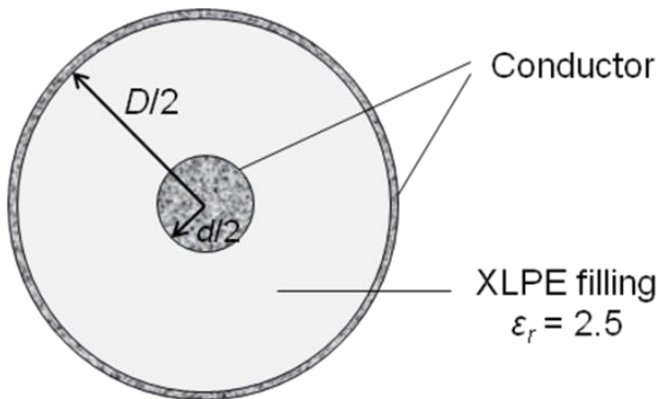


Fig. P4.4 Cross-sectional view of an XLPE cable

a. Calculate the per unit length capacitance of the cable.

$$C_b = \frac{5.56 \times 10^{-11} \epsilon_r}{\ln(D/d)} \quad (\text{F/m})$$

b. The single-wire overhead transmission line given in Problem 8 (radius 0.01m and 10m above the ground) can be used in the voltage range around 138kV. So, it is reasonable to compare its capacitance to the XLPE cable's. Calculate the per unit length capacitance and capacitive reactance ($X_{CTL} = 1/(\omega C_{TL})$) of the overhead line. Compare its capacitance to that of the XLPE cable.

c. Ignore the effect of the earth (Carson's term = 0). Calculate the per unit length inductance and inductive reactance ($X_{LTL} = \omega L_{TL}$) of the overhead line. In practice, the shunt capacitance is usually ignored. Based on your results, is it reasonable to do that?

P4.5. Consider a simple two-bus power system. Two generator buses, at voltage $V_1 \angle \delta_1$ and $V_2 \angle \delta_2$, are connected by a transmission line, characterized by its inductive reactance X (Ω), Fig. P4.5 (a). The resistance and shunt capacitance of the line have been ignored. To improve the power transfer capability of the transmission line, a capacitance, with reactance X_C , is connected in series with the line, Fig. P4.5 (b).

a. Determine the power transferred through the line before and after adding the series capacitance.

b. Assume the voltages at bus 1 and 2, respectively, are $V_1 \angle \delta_1 = 10 \angle 0^\circ$ (kV) and $V_2 \angle \delta_2 = 10.5 \angle -12^\circ$ (kV). The transmission line is 30 miles long with a per-unit length reactance of $0.5 \Omega/\text{mile}$. The value of the series capacitance is chosen by its portion to the transmission line's reactance, $X_C = kX$. When $k = 0, 0.2$ and 0.4 , determine the value of the series capacitance (in Farads) and the power transferred by the line.

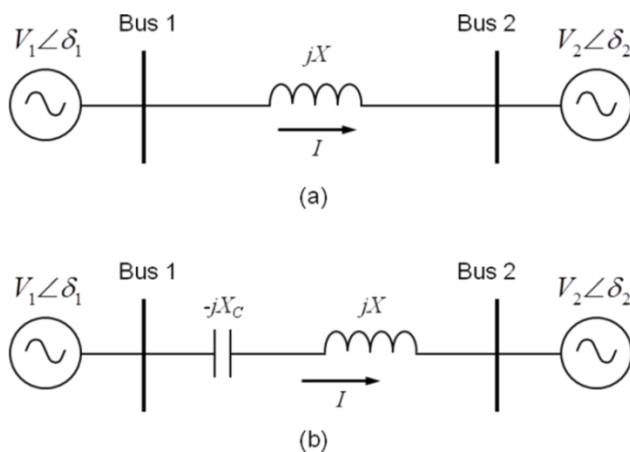


Fig. P4.5 Two-bus power system (a) without series capacitance, (b) with series capacitance

P4.6. A single-phase voltage source $V_s = 100\angle 0^\circ$ (V) (at 60Hz) is providing power to the load $Z_L = R_L + jX_L = 30 + j50(\Omega)$ through a 50km long single-wire transmission line, Fig. P4.6.

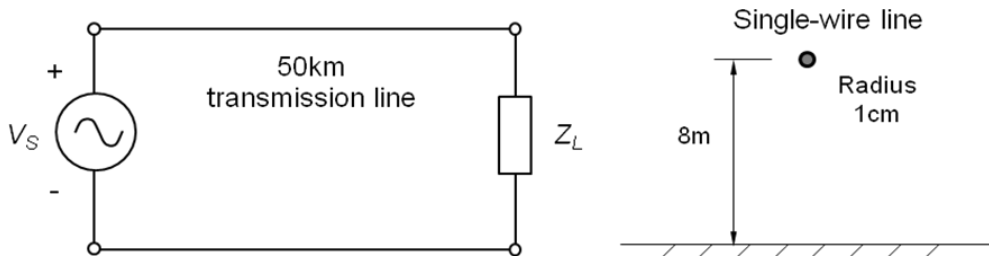


Fig. P4.6. System model for voltage regulation problem

The line conductor is 1cm in radius and 8m above the ground. Ignore the resistance and shunt capacitance of the line. Calculate the voltage on the line at 10km and 25km away from the source and the voltage at the load end.

P4.7 Show that at 60 Hz, the surface impedance of an “a” = 1 cm copper wire cannot be represented by either (4.2.7) or (4.2.8) but rather must be evaluated by the more complicated (4.2.5).

4.12 References

Abramowitz, M and I. A. Stegun. 1972. *Handbook of Mathematical Functions with Formulas, Graphs and Mathematical Tables*. Applied Mathematics Series 55, National Bureau of Standards, Washington DC.

Banos, A. 1966. *Dipole Radiation in the Presence of a Conducting Half-Space*. Pergamon. New York.

Bracken, T. D. 1982. “DC and Low Frequency Impedance for the Ground Return Mode of an Overhead HVDC Transmission Line.” Bonneville Power Administration (Portland OR., USA), Division of System Engineering Report No. 79-82 BP33228. July.

Carson, J. R. 1926. “Wave Propagation in Overhead Wires with a Ground Return.” *Bell System Technical Journal*. Vol. 5. pp. 539-554. October.

Chang, D. C. and R.G. Olsen. 1975. “Excitation of an Infinite Horizontal Wire above a Dissipative Earth,” *Radio Science*. Vol. 10. pp. 823-831. August-September

EPRI. 1982. *Transmission Line Reference Book: 345 kV and Above, Second Ed.* Electric Power Research Institute, Palo, Alto, CA.

Ibrahim, A. I. and H. W. Dommel. 2005. "A Knowledge Base for Switching Surge Transients," Paper No. IPST05 – 050, *International Conference on Power Systems Transients (IPST'05), Montreal, Canada.* June.

Kuester, E. F., D. C. Chang and R.G. Olsen. 1978. "Modal Theory of Long Horizontal Wire Structures Above the Earth, 1, Excitation," *Radio Science*. Vol. 13. pp. 605-613. July-August.

Maruvada, P.S., D.H. Nguyen and H. Hamadani-Zadeh. 1989. "Studies on Modeling Corona Attenuation of Dynamic Overvoltages." *IEEE Transactions on Power Delivery*. Vol. 4. pp. 1441-1449. April.

Olsen R. G. and M.A. Usta. 1977. "The Excitation of Current on an Infinite Horizontal Wire above Earth by a Vertical Electric Dipole." *IEEE Transactions on Antennas and Propagation*. Vol. AP-25. pp. 560-565. July.

Olsen, R. G. and D. C. Chang. 1974a. "New Modal Representation of Electromagnetic Waves Supported by a Horizontal Wire above Dissipative Earth," *Electronics Letters*, Vol. 10. pp. 92–94. 4 April.

Olsen, R. G. and D. C. Chang. 1974b. "Current Induced by a Plane Wave on a Thin Infinite Wire near the Earth," *IEEE Transactions on Antennas and Propagation*. Vol. AP-22. pp. 586–589. July.

Olsen, R. G., E. F. Kuester and D. C. Chang. 1978. "Modal Theory of Long Horizontal Wire Structures above the Earth, 2, Properties of Discrete Modes," *Radio Science*. Vol. 13. pp. 615–623. July-August.

Olsen, R. G., and A. Aburwein. 1980. "Current Induced on a Pair of Wires above Earth by a Vertical Electric Dipole for Grazing Angles of Incidence." *Radio Science*. Vol. 15. pp. 733–742, July-August.

Olsen, R. G. and T.A. Pankaskie. 1983. "On the Exact, Carson and Image Theories for Wires at or above the Earth's Interface." *IEEE Transactions on Power Apparatus and Systems*. Vol. PAS-102. pp. 769-774. March.

Olsen, R. G. 1983. "Radio Noise Fields Generated by Corona Streamers on a Power Line." *Radio Science*. Vol. 18. pp. 399–408. May-June.

Pogorzelski. R. J. and D. C. Chang. 1977. "On the Validity of the Thin Wire Approximation in Analysis of Wave Propagation Along a Wire Over a Ground." *Radio Science*. pp. 699-707. September/October.

Ramo, S., J. R. Whinnery and T. Van Duzer. 1965. *Fields and Waves in Communication Electronics*. Wiley. New York.

Suliciu, M.M. and I. Suliciu, I. 1981. "A Rate Type Constitutive Equation for the Description of the Corona Effect." *IEEE Transactions on Power Apparatus and Systems*, Vol. PAS-100. pp. 3681-3685. August.

Thrash, R, G., A. Murrah, M. Lancaster and K. Knuckles eds. 2007. *Overhead Conductor Manual (2nd Ed.)*. Southwire, Co. Carolton, GA.

Wait, J. R. 1962. *Electromagnetic Waves in Stratified Media*. Macmillan, New York.

Wait, J. R. and K.P. Spies. 1969. "On the Image Representation of the Quasi-Static Fields of a Line Current Source above Ground." *Canadian Journal of Physics*. Vol. 47. pp. 2731-2733. December.

Wait, J. R. 1972. "Theory of Wave Propagation along a Thin Wire Parallel to an Interface," *Radio Science*. Vol. 7. pp. 675-679. June.

Wagner, C.F. and B. L. Lloyd. 1955. "Effects of Corona on Traveling Waves." *AIEE Transactions on Power Apparatus and Systems*. Vol. 74, Part 111. pp. 858-872. October.

Weeks, W. L. 1981. *Transmission and Distribution of Electrical Energy*. Harper and Rowe. New York.

Chapter V

Electromagnetic Fields Surrounding an Infinitely Long Single Conductor Transmission Line above Homogeneous Earth

5.1 Introduction

In this chapter, expressions for the electromagnetic fields of the single wire power line described in Chapter 4 will be derived. More specifically, the electric and magnetic fields associated with an infinitely long z -oriented horizontal wire of radius a located at a distance h above a lossy earth and a distance x' from the y axis will be developed. The geometry for this problem is shown in Fig. 5.1.1.

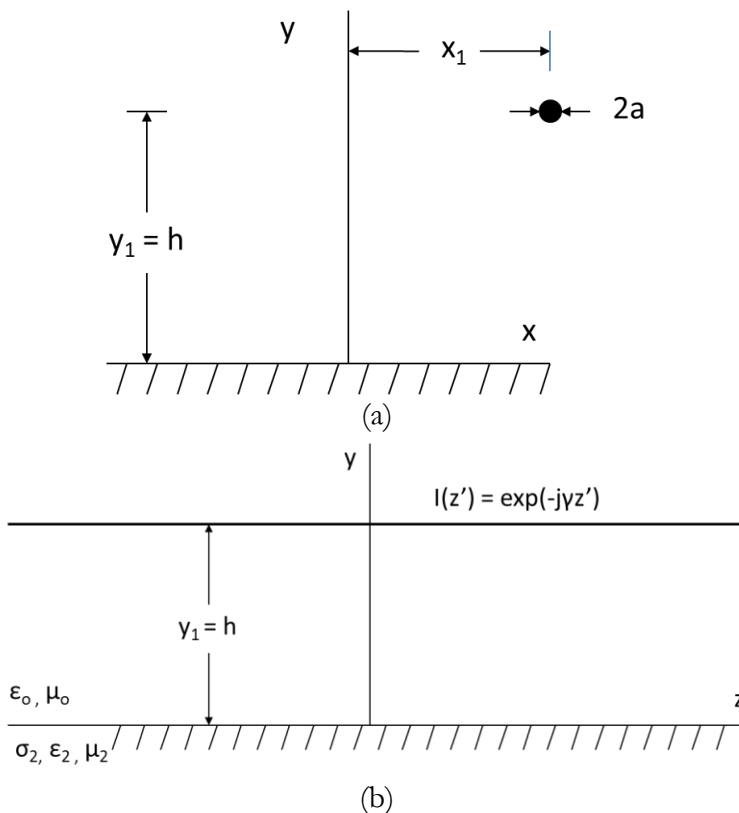


Fig. 5.1.1. a) end view and b) side view of the line current at (x', h) above a lossy linear, homogeneous isotropic earth carrying a current of $I(z') = \exp(-j\gamma z')$.

In this figure, the upper half space (i.e., $y > 0$) is free space and is characterized by permittivity and permeability $\epsilon_1 = \epsilon_0$ and $\mu_1 = \mu_0$ respectively while the lower half space (i.e., $y < 0$) is a linear, homogeneous isotropic lossy material characterized by conductivity, permittivity and permeability $\sigma_2, \epsilon_2 = \epsilon_{2r} \epsilon_0$ and $\mu_2 = \mu_{2r} \mu_0$ respectively. It is assumed here that the wire is carrying a current $\tilde{I}(\gamma) = \exp(-j\gamma z)$. The electric and magnetic fields associated with this current (where the explicit z variation $\exp(-j\gamma z)$ is suppressed) are labeled here as

\tilde{G}_{ei}^n (electric field in medium n ; the subscript “ i ” denotes the specific vector component)

\tilde{G}_{hi}^n (magnetic field in medium n ; the subscript “ i ” denotes the specific vector component)

The i th electric and magnetic field component for general currents in the spatial Fourier transform domain can be found by multiplying these functions by the spatially transformed current $\hat{I}(\gamma)$ as follows

$$\hat{E}_i^n = \tilde{G}_{ei}^n \hat{I}(\gamma) \quad (5.1.1)$$

$$\hat{H}_i^n = \tilde{G}_{hi}^n \hat{I}(\gamma) \quad (5.1.2)$$

These electric and magnetic fields can be found from (4.4.19) – (4.4.23). To use these results requires first that expressions for the z components of the Hertz Potential coefficients be found. This will be done in the next section.

5.2 Hertz Potential Coefficients Above and in the Earth ◀

Expressions for the z components of the electric and magnetic Hertz Potentials are found in (4.4.28) – (4.4.31). In Section 4.4, an explicit expression for the reflection coefficient $R(\kappa)$ was found so that \tilde{G}_{ez}^1 could be calculated. It is not possible, however, to write explicit expressions for field components unless the remaining coefficients in (4.4.28) – (4.4.31), $M(\kappa)$, $T(\kappa)$ and $N(\kappa)$ are found first. This will be done next.

Above the earth

To calculate the remaining components of the electric and magnetic fields above the earth (i.e., region 1), it is necessary to find an expression for $M(\kappa)$

From (4.4.47), using (4.4.41), (4.4.42) and the assumption $\mu_1 = \mu_2 = \mu_0$

$$M(\kappa) = \frac{-j\kappa\gamma(1-K(\gamma))(1+R(\kappa))}{\omega\mu_0(u_1 + K(\gamma)u_2)} \quad (5.2.1)$$

Equation (4.4.60) is repeated here as

$$R(\kappa) = -1 + \frac{2k_0^2u_1}{(k_0^2 - \gamma^2)} \left[\frac{1}{u_1 + u_2} - \frac{\gamma^2}{(k_0^2u_2 + k_2^2u_1)} \right] \quad (5.2.2)$$

These two results can be combined to obtain

$$M(\kappa) = \frac{-j\kappa\gamma(1-K(\gamma))}{\omega\mu_0(u_1 + K(\gamma)u_2)} \frac{2k_0^2u_1}{(k_0^2 - \gamma^2)} \left[\frac{1}{u_1 + u_2} - \frac{\gamma^2}{(k_0^2u_2 + k_2^2u_1)} \right] \quad (5.2.3)$$

This expression can be simplified by using the definitions of u_1, u_2 and $K(\gamma)$ in (4.4.11), (4.4.32) and (4.4.37), respectively and combining the two terms in the square brackets using a common denominator. The result of this is

$$M(\kappa) = \frac{-j2\kappa\gamma k_0^2(k_2^2 - k_0^2)u_1}{\omega\mu_0(k_0^2 - \gamma^2)} \left[\frac{1}{(u_1 + u_2)(k_0^2u_2 + k_2^2u_1)} \right] \quad (5.2.4)$$

Expanding the term in square brackets in a partial fraction expansion simplifies (5.2.4) to

$$M(\kappa) = \frac{-j2\kappa\gamma k_0^2}{\omega\mu_0(k_0^2 - \gamma^2)} \left[\frac{1}{(u_1 + u_2)} - \frac{k_0^2}{(k_0^2u_2 + k_2^2u_1)} \right] \quad (5.2.5)$$

This result (i.e., 5.2.5) can now be used with (4.4.20) – (4.4.23), (4.4.28) and (4.4.29) to find expressions for all field components in the upper medium (i.e., Medium 1).

In the earth

To calculate the remaining components of the electric and magnetic fields in the earth (i.e., region 2), it is necessary to find expressions for $T(\kappa)$ and $N(\kappa)$

From (4.4.35) – (4.4.36),

$$(k_0^2 - \gamma^2)(1 + R(\kappa)) = (k_2^2 - \gamma^2)T(\kappa) \quad (5.2.6)$$

$$(k_0^2 - \gamma^2)M(\kappa) = (k_2^2 - \gamma^2)N(\kappa) \quad (5.2.7)$$

where the factor $K(\gamma)$ is defined as

$$K(\gamma) = \frac{(k_0^2 - \gamma^2)}{(k_2^2 - \gamma^2)}. \quad (5.2.8)$$

Given that $R(\kappa)$ and $M(\kappa)$ are known as (5.2.2) and (5.2.5) these results

$$T(\kappa) = K(\gamma)(1 + R(\kappa)) = \frac{2k_0^2 u_1}{(k_2^2 - \gamma^2)} \left[\frac{1}{u_1 + u_2} - \frac{\gamma^2}{(k_0^2 u_2 + k_2^2 u_1)} \right] \quad (5.2.9)$$

and

$$N(\kappa) = K(\gamma)M(\kappa) = \frac{-j2\kappa\gamma k_0^2}{\omega\mu_0(k_2^2 - \gamma^2)} \left[\frac{1}{(u_1 + u_2)} - \frac{k_0^2}{(k_0^2 u_2 + k_2^2 u_1)} \right] \quad (5.2.10)$$

These last two results can now be used with (4.4.20) – (4.4.23), (4.4.30) and (4.4.31) to find expressions for all field components in the earth (i.e., Medium 2).

5.3 General Expressions for the Electric and Magnetic Fields at Arbitrary Frequency ◀

As shown in Chapter 4, formal expressions for the electric and magnetic fields in terms of the z -directed Hertzian potentials at arbitrary frequencies can be found. These are given in (4.4.19) – (4.4.23).

Fields above the earth

In the upper half space (i.e., Region 1), the expressions for the z directed Hertzian potentials are,

$$\Pi_{ez}^1 = A \int_{-\infty}^{\infty} \frac{(e^{-u_1|y-h|} + R(\kappa)e^{-u_1(y+h)})e^{-j\kappa(x-x_1)}}{u_1} d\kappa \quad (5.3.1)$$

and

$$\Pi_{mz}^1 = A \int_{-\infty}^{\infty} \frac{M(\kappa)e^{-u_1(y+h)}e^{-j\kappa(x-x_1)}}{u_1} d\kappa \quad (5.3.2)$$

where $A = -j/(4\pi\omega\epsilon_0)$ and u_2 is defined as

$$u_2 = \sqrt{\kappa^2 + \gamma^2 - k_2^2} . \quad (5.3.3)$$

In general, (i.e., including magnetic) media the coefficient $R(\kappa)$ is (from (4.4.46))

$$R(\kappa) = \frac{\kappa^2 \gamma^2 (1 - K(\gamma))^2 + \omega^2 (\epsilon_0 u_0 - K(\gamma) \epsilon_2 u_2) (\mu_0 u_0 + K(\gamma) \mu_2 u_2)}{-\kappa^2 \gamma^2 (1 - K(\gamma))^2 + \omega^2 (\epsilon_0 u_0 + K(\gamma) \epsilon_2 u_2) (\mu_0 u_0 + K(\gamma) \mu_2 u_2)} \quad (5.3.4)$$

A simpler expression for non-magnetic media is (from (4.4.60))

$$R(\kappa) = -1 + \frac{2k_0^2 u_1}{(k_0^2 - \gamma^2)} \left[\frac{1}{u_1 + u_2} - \frac{\gamma^2}{(k_0^2 u_2 + k_2^2 u_1)} \right] \quad (5.3.5)$$

$M(\kappa)$ was shown as (5.2.4). Given these results, expressions for all field components in the upper medium (i.e., Medium 1) can be found. The results are:

$$\tilde{G}_{ex}^1(x - x_1, y, h, \gamma) = -j\gamma \frac{\partial \Pi_{ez}^1}{\partial x} - j\omega \mu_0 \frac{\partial \Pi_{mz}^1}{\partial y} \quad (5.3.6)$$

$$\tilde{G}_{ey}^1(x - x_1, y, h, \gamma) = -j\gamma \frac{\partial \Pi_{ez}^1}{\partial y} + j\omega \mu_0 \frac{\partial \Pi_{mz}^1}{\partial x} \quad (5.3.7)$$

$$\tilde{G}_{ez}^1(x - x_1, y, h, \gamma) = -(\gamma^2 - k_0^2) \Pi_{ez}^1 \quad (5.3.8)$$

$$\tilde{G}_{hx}^1(x - x_1, y, h, \gamma) = -j\gamma \frac{\partial \Pi_{mz}^1}{\partial x} + j\omega \epsilon_0 \frac{\partial \Pi_{mz}^1}{\partial y} \quad (5.3.9)$$

$$\tilde{G}_{hy}^1(x - x_1, y, h, \gamma) = -j\gamma \frac{\partial \Pi_{mz}^1}{\partial y} - j\omega \epsilon_0 \frac{\partial \Pi_{mz}^1}{\partial x} \quad (5.3.10)$$

$$\tilde{G}_{hz}^1(x - x_1, y, h, \gamma) = -(\gamma^2 - k_0^2) \Pi_{mz}^1 \quad (5.3.11)$$

Repeating the result from Chapter 4, the axial electric field at any point in space is stated since that will be useful later. From (5.3.1) and (5.3.8)

$$\tilde{G}_{ez}^1(x - x_1, y, h, \gamma) = \frac{-j(k_0^2 - \gamma^2)}{4\pi\omega\epsilon_0} \int_{-\infty}^{\infty} \frac{(e^{-u_1|y-h|} + R(\kappa)e^{-u_1(y+h)}) e^{-j\kappa(x-x_1)}}{u_1} d\kappa \quad (5.3.12)$$

where $R(\kappa)$ is given by (5.3.5) so that

$$\begin{aligned} \tilde{G}_{ez}^1(x-x_1, y, h, \gamma) = & \frac{-j(k_0^2 - \gamma^2)}{4\pi\omega\epsilon_0} \int_{-\infty}^{\infty} \left\{ \frac{e^{-u_1|y-h|}}{u_1} - \frac{e^{-u_1(y+h)}}{u_1} \right. \\ & \left. + \frac{2k_0^2 e^{-u_1(y+h)}}{(k_0^2 - \gamma^2)} \left[\frac{1}{u_1 + u_2} - \frac{\gamma^2}{(k_0^2 u_2 + k_2^2 u_1)} \right] \right\} e^{-j\kappa(x-x_1)} d\kappa \end{aligned} \quad (5.3.13)$$

But, from (4.4.14)

$$H_0^{(2)}\left((k_0^2 - \gamma^2)^{1/2} r\right) = \frac{j}{\pi} \int_{-\infty}^{\infty} \frac{e^{-u_1|y-h|} e^{-j\kappa(x-x_1)}}{u_1} d\kappa, \quad \text{Im}(k_0^2 - \gamma^2)^{1/2} \leq 0 \quad (5.3.14)$$

where
so that

$$r = \left[(x-x_1)^2 + (y-h)^2 \right]^{1/2} \quad (5.3.15)$$

$$\begin{aligned} \tilde{G}_{ez}^1(x-x_1, y, h, \gamma) = & \frac{-1}{4\omega\epsilon_1} \left\{ (k_0^2 - \gamma^2) \left[H_0^{(2)}\left((k_0^2 - \gamma^2)^{1/2} r\right) - H_0^{(2)}\left((k_0^2 - \gamma^2)^{1/2} r^i\right) \right] \right. \\ & \left. + \frac{2jk_0^2}{\pi} \int_{-\infty}^{\infty} \left[\frac{1}{u_1 + u_2} \right] e^{-u_1(y+h)} e^{-j\kappa(x-x_1)} d\kappa - \frac{2jk_0^2}{\pi} \int_{-\infty}^{\infty} \left[\frac{\gamma^2}{(k_1^2 u_2 + k_2^2 u_1)} \right] e^{-u_1(y+h)} e^{-j\kappa(x-x_1)} d\kappa \right\} \end{aligned}$$

where $r^i = \left[(x-x_1)^2 + (y+h)^2 \right]^{1/2}$.

Next, general expressions will be found for the transverse electric and horizontal magnetic fields will be found. From (5.3.6) - (5.3.7) and (5.3.9) - (5.3.10), it is clear that the transverse derivatives of Π_{ez} and Π_{mz} are needed. These are

$$\begin{aligned} \frac{\partial \Pi_{ez}^1}{\partial x} = & \frac{-j}{4\pi\omega\epsilon_0} \left\{ \frac{\partial}{\partial x} \int_{-\infty}^{\infty} \left(\frac{e^{-u_1|y-h|} - e^{-u_1(y+h)}}{u_1} \right) e^{-j\kappa(x-x_1)} d\kappa \right. \\ & \left. + \frac{2k_0^2}{(k_0^2 - \gamma^2)} \frac{\partial}{\partial x} \int_{-\infty}^{\infty} \left(\frac{1}{(u_1 + u_2)} - \frac{\gamma^2}{(k_0^2 u_2 + k_2^2 u_1)} \right) e^{-u_1(y+h)} e^{-j\kappa(x-x_1)} d\kappa \right. \\ = & \frac{-j}{4\pi\omega\epsilon_0} \left\{ \left(\frac{\pi}{j} \right) \frac{\partial}{\partial x} \left[H_0^{(2)}\left((k_0^2 - \gamma^2)^{1/2} r\right) - H_0^{(2)}\left((k_0^2 - \gamma^2)^{1/2} r^i\right) \right] \right. \\ & \left. - \frac{2jk_0^2}{(k_0^2 - \gamma^2)} \int_{-\infty}^{\infty} \left(\frac{\kappa u_1}{(u_1 + u_2)} - \frac{\gamma^2 \kappa u_1}{(k_0^2 u_2 + k_2^2 u_1)} \right) \frac{e^{-u_1(y+h)} e^{-j\kappa(x-x_1)}}{u_1} d\kappa \right\} \end{aligned} \quad (5.3.16)$$

Similarly,

(5.3.17)

$$\frac{\partial \Pi_{ez}^1}{\partial y} = \frac{-j}{4\pi\omega\epsilon_0} \left\{ \left(\frac{\pi}{j} \right) \frac{\partial}{\partial y} \left[H_0^{(2)} \left((k_0^2 - \gamma^2)^{1/2} r \right) - H_0^{(2)} \left((k_0^2 - \gamma^2)^{1/2} r^i \right) \right] \right. \\ \left. - \frac{2k_0^2}{(k_0^2 - \gamma^2)} \int_{-\infty}^{\infty} \left(\frac{u_1^2}{(u_1 + u_2)} - \frac{\gamma^2 u_1^2}{(k_0^2 u_2 + k_2^2 u_1)} \right) \frac{e^{-u_1(y+h)} e^{-j\kappa(x-x_1)}}{u_1} d\kappa \right\}.$$

The derivatives of the magnetic potentials can be found from (5.3.2) and (5.2.4) as

(5.3.18)

$$\frac{\partial \Pi_{mz}^1}{\partial x} = \frac{-\gamma}{2\pi(k_0^2 - \gamma^2)} \frac{\partial}{\partial x} \int_{-\infty}^{\infty} \kappa \left(\frac{1}{(u_1 + u_2)} - \frac{k_0^2}{(k_0^2 u_2 + k_2^2 u_1)} \right) \frac{e^{-u_1(y+h)} e^{-j\kappa(x-x_1)}}{u_1} d\kappa \\ = \frac{j\gamma}{2\pi(k_0^2 - \gamma^2)} \int_{-\infty}^{\infty} \kappa^2 \left(\frac{1}{(u_1 + u_2)} - \frac{k_0^2}{(k_0^2 u_2 + k_2^2 u_1)} \right) \frac{e^{-u_1(y+h)} e^{-j\kappa(x-x_1)}}{u_1} d\kappa$$

and

(5.3.19)

$$\frac{\partial \Pi_{mz}^1}{\partial y} = \frac{-\gamma}{2\pi(k_0^2 - \gamma^2)} \frac{\partial}{\partial y} \int_{-\infty}^{\infty} \kappa \left(\frac{1}{(u_1 + u_2)} - \frac{k_0^2}{(k_0^2 u_2 + k_2^2 u_1)} \right) \frac{e^{-u_1(y+h)} e^{-j\kappa(x-x_1)}}{u_1} d\kappa \\ = \frac{\gamma}{2\pi(k_0^2 - \gamma^2)} \int_{-\infty}^{\infty} u_1 \kappa \left(\frac{1}{(u_1 + u_2)} - \frac{k_0^2}{(k_0^2 u_2 + k_2^2 u_1)} \right) \frac{e^{-u_1(y+h)} e^{-j\kappa(x-x_1)}}{u_1} d\kappa$$

Using (4.6.6) then

$$\tilde{G}_{ex}^1 = \frac{-j\gamma}{4\omega\epsilon_0} \left\{ \frac{\partial}{\partial x} \left[H_0^{(2)} \left((k_0^2 - \gamma^2)^{1/2} r \right) - H_0^{(2)} \left((k_0^2 - \gamma^2)^{1/2} r^i \right) \right] \right. \\ \left. + \frac{2k_0^2}{\pi} \int_{-\infty}^{\infty} \left(\frac{\kappa u_1}{(k_0^2 u_2 + k_2^2 u_1)} \right) \frac{e^{-u_1(y+h)} e^{-j\kappa(x-x_1)}}{u_1} d\kappa \right\} \quad (5.3.20)$$

and

(5.3.21)

$$\tilde{G}_{ey}^1 = \frac{+j\gamma}{4\omega\epsilon_0} \frac{\partial}{\partial y} \left[H_0^{(2)} \left((k_0^2 - \gamma^2)^{1/2} r \right) - H_0^{(2)} \left((k_0^2 - \gamma^2)^{1/2} r^i \right) \right] \\ + \frac{+\gamma\omega\mu_0}{2\pi(k_0^2 - \gamma^2)} \int_{-\infty}^{\infty} \left(\frac{u_1^2 - \kappa^2}{(u_1 + u_2)} - \frac{u_1^2 \gamma^2 - \kappa^2 k_0^2}{(k_0^2 u_2 + k_2^2 u_1)} \right) \frac{e^{-u_1(y+h)} e^{-j\kappa(x-x_1)}}{u_1} d\kappa$$

$$\begin{aligned}
&= \frac{+j\gamma}{4\omega\epsilon_0} \frac{\partial}{\partial y} \left[H_0^{(2)}\left(\left(k_0^2 - \gamma^2\right)^{1/2} r\right) - H_0^{(2)}\left(\left(k_0^2 - \gamma^2\right)^{1/2} r^i\right) \right] \\
&- \frac{\gamma\omega\mu_0}{2\pi} \int_{-\infty}^{\infty} \left(\frac{1}{(u_1 + u_2)} - \frac{\kappa^2 + \gamma^2}{(k_0^2 u_2 + k_2^2 u_1)} \right) \frac{e^{-u_1(y+h)} e^{-j\kappa(x-x_1)}}{u_1} d\kappa
\end{aligned}$$

Clearly, if $k_0 \rightarrow k_2$ the integrals in the last two equations become the negative of the second Hankel function term leaving only the source term as should occur. It will also be shown later that these results reduce to the well know wire above a perfectly conducting earth case for conditions that are commonly satisfied for electric power transmission lines at 60 Hz.

Similar calculations using (5.3.9) and (5.3.10) for \tilde{G}_{hx}^1 and \tilde{G}_{hy}^1 yield

$$\begin{aligned}
\tilde{G}_{hx}^1 &= \frac{-j}{4} \frac{\partial}{\partial y} \left[H_0^{(2)}\left(\left(k_0^2 - \gamma^2\right)^{1/2} r\right) - H_0^{(2)}\left(\left(k_0^2 - \gamma^2\right)^{1/2} r^i\right) \right] \\
&- \frac{1}{2\pi(k_0^2 - \gamma^2)} \int_{-\infty}^{\infty} \left(\frac{k_0^2 u_1^2 - \gamma^2 \kappa^2}{(u_1 + u_2)} - \frac{\gamma^2 k_0^2 (u_1^2 - \kappa^2)}{(k_0^2 u_2 + k_2^2 u_1)} \right) \frac{e^{-u_1(y+h)} e^{-j\kappa(x-x_1)}}{u_1} d\kappa \\
&= \frac{-j}{4} \frac{\partial}{\partial y} \left[H_0^{(2)}\left(\left(k_0^2 - \gamma^2\right)^{1/2} r\right) - H_0^{(2)}\left(\left(k_0^2 - \gamma^2\right)^{1/2} r^i\right) \right] \\
&- \frac{1}{2\pi} \int_{-\infty}^{\infty} \left(\frac{\kappa^2 - k_0^2}{(u_1 + u_2)} + \frac{k_0^2 \gamma^2}{(k_0^2 u_2 + k_2^2 u_1)} \right) \frac{e^{-u_1(y+h)} e^{-j\kappa(x-x_1)}}{u_1} d\kappa
\end{aligned} \tag{5.3.22}$$

and

$$\begin{aligned}
\tilde{G}_{hy}^1 &= \frac{j}{4} \frac{\partial}{\partial x} \left[H_0^{(2)}\left(\left(k_0^2 - \gamma^2\right)^{1/2} r\right) - H_0^{(2)}\left(\left(k_0^2 - \gamma^2\right)^{1/2} r^i\right) \right] \\
&+ \frac{j}{2\pi} \int_{-\infty}^{\infty} \left(\frac{u_1 \kappa}{(u_1 + u_2)} \right) \frac{e^{-u_1(y+h)} e^{-j\kappa(x-x_1)}}{u_1} d\kappa
\end{aligned} \tag{5.3.23}$$

Clearly, if $k_0 \rightarrow k_2$ the integrals in the last two equations become the negative of the second Hankel function term leaving only the source term as should occur. It will be shown later that these results reduce to the case for which the earth is essentially transparent for conditions normally satisfied for power transmission lines at 60 Hz.

To find expressions for the electric and magnetic field components in the space domain, it is necessary to multiply the appropriate component by the Fourier Transform of the current and take the inverse Fourier transform. Several examples of this will be given later.

Fields in the earth

The Hertzian electric and magnetic vector potentials in the earth are:

$$\Pi_{ez}^2(x, y) = A \int_{-\infty}^{\infty} \frac{T(\kappa) e^{-u_1 h} e^{u_2 y} e^{-j\kappa x}}{u_1} d\kappa \quad (5.3.24)$$

$$\Pi_{mz}^2(x, y) = A \int_{-\infty}^{\infty} \frac{N(\kappa) e^{-u_1 h} e^{u_2 y} e^{-j\kappa x}}{u_1} d\kappa \quad (5.3.25)$$

where

$$A = \frac{-j}{4\pi\omega\epsilon_0}, \quad u_1 = (\kappa^2 + \gamma^2 - k_0^2)^{1/2}$$

and

$$u_2 = (\kappa^2 + \gamma^2 - k_2^2)^{1/2}.$$

Inserting (5.2.9) and (5.2.10) into (5.3.24) and (5.3.25) results in

$$\Pi_{ez}^2(x, y) = \frac{-2jk_0^2}{4\pi\omega\epsilon_0(k_2^2 - \gamma^2)} \int_{-\infty}^{\infty} \left[\frac{1}{u_1 + u_2} - \frac{\gamma^2}{(k_0^2 u_2 + k_2^2 u_1)} \right] e^{-u_1 h} e^{u_2 y} e^{-j\kappa x} d\kappa \quad (5.3.26)$$

$$\Pi_{mz}^2(x, y) = \frac{-2j\gamma}{4\pi(k_2^2 - \gamma^2)} \int_{-\infty}^{\infty} \left[\frac{\kappa}{u_1(u_1 + u_2)} - \frac{\kappa k_0^2}{u_1(k_0^2 u_2 + k_2^2 u_1)} \right] e^{-u_1 h} e^{u_2 y} e^{-j\kappa x} d\kappa \quad (5.3.27)$$

The electric fields in the earth have previously been defined in (4.4.19) and (4.4.21) as

$$\tilde{G}_{ex}^2(x - x_1, y, h, \gamma) = -j\gamma \frac{\partial \Pi_{ez}^2}{\partial x} - j\omega\mu_2 \frac{\partial \Pi_{mz}^2}{\partial y} \quad (5.3.28)$$

$$\tilde{G}_{ey}^2(x - x_1, y, h, \gamma) = -j\gamma \frac{\partial \Pi_{ez}^2}{\partial y} - j\omega\mu_2 \frac{\partial \Pi_{mz}^2}{\partial x} \quad (5.3.29)$$

$$\tilde{G}_{ez}^2(x - x_1, y, h, \gamma) = -(\gamma^2 - k_2^2) \Pi_{ez}^2 \quad (5.3.30)$$

Substituting (5.3.26) and (5.3.27) into (5.3.28) yields

$$\tilde{G}_{ex}^2(x - x_1, y, h, \gamma) = \frac{j\gamma k_0^2}{2\pi\omega\epsilon_0} \int_{-\infty}^{\infty} \frac{\kappa e^{-u_1 h} e^{u_2 y} e^{-j\kappa(x-x_1)}}{(k_0^2 u_2 + k_2^2 u_1)} d\kappa \quad (5.3.31)$$

Similarly

$$\tilde{G}_{ey}^2(x-x_1, y, h, \gamma) = \frac{-jk_0^2}{2\pi\omega\epsilon_0} \int_{-\infty}^{\infty} \frac{u_1 e^{-u_1 h} e^{u_2 y} e^{-j\omega(x-x_1)}}{(k_0^2 u_2 + k_2^2 u_1)} d\kappa \quad (5.3.32)$$

Finally,

$$\tilde{G}_{ez}^2(x-x_1, y, h, \gamma) = \frac{-jk_0^2}{2\pi\omega\epsilon_0} \int_{-\infty}^{\infty} \left[\frac{1}{u_1 + u_2} - \frac{\gamma^2}{(k_0^2 u_2 + k_2^2 u_1)} \right] e^{-u_1 h} e^{u_2 y} e^{-j\kappa(x-x_1)} d\kappa \quad (5.3.33)$$

The derivation of the magnetic fields will be left as a homework problem. They can be obtained either by using (4.4.22), (4.4.23), (5.3.26) and (5.3.27) directly or by application of Maxwell's equations to (5.3.31) – (5.3.33).

5.4 Low Frequency Approximations for the Electric and Magnetic Fields

The electric field above the earth

For readers who have skipped Sections 5.2 and 5.3, only the results from that section will be noted here. Expressions for the axial and transverse electric fields above the earth are given in (5.3.15) and (5.3.20) – (5.3.21) respectively while expressions for the transverse magnetic fields above the earth are found in (5.3.22) – (5.3.23). In the earth, expressions for the axial and transverse electric fields are found in (5.3.31) – (5.3.33). It should be emphasized that these expressions hold for all frequencies as long as the conductor radius is small compared to a wavelength and that electrical parameters for the earth appropriate to the frequency of interest are used. Here, much simpler approximations that are appropriate for low frequencies will be derived from these results.

First, for small arguments, it has been shown that

$$H_0^{(2)}(q) \cong 1 - \frac{2j}{\pi} \ln(q/2) - \frac{2j\gamma_e}{\pi}, \quad q \ll 1 \quad (5.4.1)$$

and further the last integral in (5.3.15) can be neglected for typical earths at low frequencies so that

$$(5.4.2)$$

$$\tilde{G}_{ez}^1(x-x_1, y, h, \gamma) \cong \frac{-1}{4\omega\epsilon_0} \left\{ \frac{2j}{\pi} (k_0^2 - \gamma^2) \ln\left(\frac{r^i}{r}\right) + \frac{2jk_0^2}{\pi} \int_{-\infty}^{\infty} \frac{e^{-u_1(y+h)} e^{-j\kappa(x-x_1)}}{u_1 + u_2} d\kappa \right\}$$

where

$$r = \left((x - x_1)^2 + (y - h)^2 \right)^{1/2} \text{ and } r^i = \left((x - x_1)^2 + (y + h)^2 \right)^{1/2}.$$

But, as shown in (4.6.5) the integral $P(\gamma)$ can be approximated at low frequencies for typical values of earth conductivity to be

$$\begin{aligned} P(\gamma) &= \frac{j}{\pi} \int_{-\infty}^{\infty} \frac{e^{-u_1(y+h)} e^{-j\kappa(x-x_1)}}{u_1 + u_2} d\kappa = \frac{j2}{\pi} \int_0^{\infty} \frac{e^{-u_1(y+h)} \cos\kappa(x-x_1)}{u_1 + u_2} d\kappa \\ &\cong \frac{-j2}{\pi k_2^2} \int_0^{\infty} (u - \kappa) e^{-\kappa(y+h)} \cos\kappa(x-x_1) d\kappa = \frac{-j}{\pi} J_c(x-x_1, y, h) \end{aligned} \quad (5.4.3)$$

where

$$J_c(x-x_1, y, y_1) = \frac{2}{k_2^2} \int_0^{\infty} (u - \kappa) e^{-(y+y_1)\kappa} \cos(\kappa(x-x_1)) d\kappa \quad (5.4.4)$$

and

$$u = (\kappa^2 - k_2^2)^{1/2}.$$

Thus finally, for low frequencies⁴⁸

$$(5.4.5)$$

$$\begin{aligned} \tilde{G}_{ez}^1(x-x_1, y, h, \gamma) &\cong \frac{-j}{2\pi\omega\epsilon_0} \left\{ -\gamma^2 \ln\left(\frac{r^i}{r}\right) + k_0^2 \left[\ln\left(\frac{r^i}{r}\right) - J_c(x-x_1, y, h) \right] \right\} \\ &= \frac{j\gamma^2}{2\pi\omega\epsilon_0} \ln\left(\frac{r^i}{r}\right) - \frac{j\omega\mu_0}{2\pi} \left[\ln\left(\frac{r^i}{r}\right) - J_c(x-x_1, y, h) \right] \end{aligned}$$

This result can be written in more familiar form (using insight from (4.6.6 – 4.6.8) and assuming an arbitrary current $\hat{I}(\gamma)$) as

$$(5.4.6)$$

$$\hat{E}_z^1(x-x_1, y, h, \gamma) = \tilde{G}_{ez}^1(x-x_1, y, h, \gamma) \hat{I}(\gamma) \cong - \left(\frac{\gamma^2}{Y(x-x_1, y, h)} + Z(x-x_1, y, h) \right) \hat{I}(\gamma)$$

⁴⁸ If γ is set equal to zero as in the quasi-static approximation of Wait and Spies (1969) and J_c is approximated by the first term of (4.6.22), then this expression is equivalent to the complex image formulation for the magnetic field introduced later in this section.

where

$$Y(x-x_1, y, h) = \frac{j2\pi\omega\epsilon_0}{\ln\left(\frac{r^i}{r}\right)} \quad (5.4.7)$$

and

$$Z(x-x_1, y, h) = \frac{j\omega\mu_0}{2\pi} \left[\ln\left(\frac{r^i}{r}\right) - J_c(x-x_1, y, h) \right] \quad (5.4.8)$$

The case for calculation of the vertical electric field at low frequencies is significantly different. For $\hat{\tilde{E}}_z$ the Hankel functions in (5.3.15) were multiplied by the factor $(k_0^2 - \gamma^2)$. Since $\gamma \cong k_0$ for power applications at low frequencies, $(k_0^2 - \gamma^2)$ is small and the term $2k_0^2 P(\gamma)$ cannot be ignored even though $|k_2| \gg |k_0|$ and $2k_0^2 P(\gamma)$ is proportional to $1/|k_2|$. However, for $\hat{\tilde{E}}_y$ the Hankel function terms are not small and the infinite integral can be ignored compared to them. If again, the Hankel functions are replaced by small argument expansions (i.e., (5.4.1)), since $|(k_0^2 - \gamma^2)^{1/2} r| \ll 1$, the expression for the vertical electric field reduces to

$$\begin{aligned} \tilde{G}_{ey}^1 &\cong \frac{\gamma}{2\pi\omega\epsilon_0} \frac{\partial}{\partial y} \left[\ln\left((k_0^2 - \gamma^2)^{1/2} r\right) - \ln\left((k_0^2 - \gamma^2)^{1/2} r^i\right) \right] \\ &= \frac{\gamma}{2\pi\omega\epsilon_0} \left[\frac{(y-h)}{\left((x-x_1)^2 + (y-h)^2\right)} - \frac{(y+h)}{\left((x-x_1)^2 + (y+h)^2\right)} \right] \end{aligned} \quad (5.4.9)$$

Clearly, this is the electric field of the current source above a “perfectly conducting earth” and is the approximation commonly used for power engineering calculations at typical power frequencies. This should be no surprise since $\frac{\sigma}{\omega\epsilon_0\epsilon_r} \gg 1$ at low frequencies for typical earths and the earth can be treated as a perfect conductor.

The electric field for an arbitrary current $\hat{\tilde{I}}(\gamma)$ can be written as

$$\hat{\tilde{E}}_y^1(x-x_1, y, h, \gamma) = \tilde{G}_{ey}^1(x-x_1, y, h, \gamma) \hat{\tilde{I}}(\gamma) \quad (5.4.10)$$

In a manner similar to that above, it can be shown that

$$\tilde{G}_{ex}^1 \cong \frac{\gamma}{2\pi\omega\epsilon_0} \left[\frac{(x-x_1)}{\left((x-x_1)^2 + (y-h)^2\right)} - \frac{(x-x_1)}{\left((x-x_1)^2 + (y+h)^2\right)} \right] \quad (5.4.11)$$

and

$$\hat{E}_x^1(x-x_1, y, h, \gamma) = \tilde{G}_{ex}^1(x-x_1, y, h, \gamma) \hat{I}(\gamma) \quad (5.4.12)$$

Electric fields in the space domain

To recover the electric fields in the space domain, it is necessary to perform the inverse Fourier transform with respect to γ in order to see the explicit z dependence. The simplest way to do this is to assume that the current in the space domain is an exponential function of z (as in Section 4.8) that has the form in the γ domain

$$\hat{I}(\gamma) = \frac{2j\hat{I}_0\gamma_{TL}}{(\gamma + \gamma_{TL})(\gamma - \gamma_{TL})} \quad (5.4.13)$$

where $\gamma_{TL} = \pm j\sqrt{ZY}$ as in Section 4.6 and Z and Y are defined in (4.6.6) and (4.6.8) respectively. (5.4.13) corresponds to a current in the space domain of

$$\hat{I}(z) = \hat{I}_0 e^{\pm j\gamma_{TL}z} \quad (5.4.14)$$

where the “+” sign corresponds to $z < 0$ and the “-” sign to $z > 0$.

Given this result and applying it to (5.4.6), (5.4.10) and (5.4.12) results in

$$\hat{E}_z^1(x-x_1, y, h, \gamma) \cong - \left(\frac{\gamma^2}{Y(x-x_1, y, h)} + Z(x-x_1, y, h) \right) \frac{2j\hat{I}_0\gamma_{TL}}{(\gamma + \gamma_{TL})(\gamma - \gamma_{TL})} \quad (5.4.15)$$

$$\hat{E}_y^1(x-x_1, y, h, \gamma) \cong \frac{\gamma}{2\pi\omega\epsilon_0} \left[\frac{(y-h)}{\left((x-x_1)^2 + (y-h)^2\right)} - \frac{(y+h)}{\left((x-x_1)^2 + (y+h)^2\right)} \right] \frac{2j\hat{I}_0\gamma_{TL}}{(\gamma + \gamma_{TL})(\gamma - \gamma_{TL})} \quad (5.4.16)$$

$$\hat{E}_x^1(x-x_1, y, h, \gamma) \cong \frac{\gamma}{2\pi\omega\epsilon_0} \left[\frac{(x-x_1)}{\left((x-x_1)^2 + (y-h)^2\right)} - \frac{(x-x_1)}{\left((x-x_1)^2 + (y+h)^2\right)} \right] \frac{2j\hat{I}_0\gamma_{TL}}{(\gamma + \gamma_{TL})(\gamma - \gamma_{TL})} \quad (5.4.17)$$

After transformation to the space domain, these fields are

$$\hat{E}_z^1(x-x_1, y, h, z) \cong - \left(\frac{\gamma_{TL}^2}{Y(x-x_1, y, h)} + Z(x-x_1, y, h) \right) \hat{I}_0 e^{\pm j\gamma_{TL}z} \quad (5.4.18)$$

where again, the “+” sign corresponds to $z < 0$ and the “-” sign to $z > 0$.

$$\hat{E}_y^1(x-x_1, y, h, z) \cong \frac{\gamma_{TL}}{2\pi\omega\epsilon_0} \left[\frac{(y-h)}{\left((x-x_1)^2 + (y-h)^2\right)} - \frac{(y+h)}{\left((x-x_1)^2 + (y+h)^2\right)} \right] \hat{I}_0 e^{\pm j\gamma_{TL}z} \quad (5.4.19)$$

$$\hat{E}_x^1(x-x_1, y, h, z) \cong \frac{\gamma_{TL}}{2\pi\omega\epsilon_0} \left[\frac{(x-x_1)}{\left((x-x_1)^2 + (y-h)^2\right)} - \frac{(x-x_1)}{\left((x-x_1)^2 + (y+h)^2\right)} \right] \hat{I}_0 e^{\pm j\gamma_{TL}z} \quad (5.4.20)$$

Given that a derivative with respect to z (for $z > 0$) corresponds to a factor $-j\gamma_{TL}$, the z component of the field can be recast in a different form that will be useful later as

$$\hat{E}_z^1(x-x_1, y, h, z) \cong - \frac{\partial}{\partial z} \hat{V}_w(x-x_1, y, h) e^{\pm j\gamma_{TL}z} - Z(x-x_1, y, h) \hat{I}_0 e^{\pm j\gamma_{TL}z} \quad (5.4.21)$$

where

$$\hat{V}_w(x-x_1, y, h) = \frac{\gamma_{TL} \hat{I}_0}{2\pi\omega\epsilon_0} \ln\left(\frac{r^i}{r}\right) \quad (5.4.22)$$

is the space potential due to the wire above the earth and for convenience from (5.4.8) and (5.4.4)

$$Z(x-x_1, y, h) = \frac{j\omega\mu_0}{2\pi} \left[\ln\left(\frac{r^i}{r}\right) - J_c(x-x_1, y, h) \right]$$

$$J_c(x-x_1, y, y_1) = \frac{2}{k_2^2} \int_0^\infty (u - \kappa) e^{-(y+y_1)\kappa} \cos(\kappa(x-x_1)) d\kappa$$

Equivalence to electrostatic fields

Equations (5.4.19), (5.4.20) and the first part of (5.4.21) are identical to what would be obtained from electrostatic theory. This can be understood more clearly by using the one dimensional current continuity relationship

$$\frac{\partial \hat{I}(z)}{\partial z} = -j\omega \hat{\rho}_\ell(z) \quad (5.4.23)$$

where $\hat{\rho}_\ell(z) = \hat{\rho}_\ell e^{-j\lambda_{TL}z}$ is the line charge density along the conductor. Since $\hat{I}(z) = \hat{I}_0 e^{-j\gamma_{TL}z}$, using (5.4.23) results in

$$\hat{\rho}_\ell = \frac{\gamma_{TL} \hat{I}_0}{\omega} \quad (5.4.24)$$

and (for example) the vertical electric field becomes

$$\hat{E}_y^1 \cong \frac{\hat{\rho}_\ell}{2\pi\epsilon_0} \left[\frac{(y-h)}{\left((x-x_1)^2 + (y-h)^2\right)} - \frac{(y+h)}{\left((x-x_1)^2 + (y+h)^2\right)} \right] e^{-j\gamma_{TL}z} \quad (5.4.25)$$

This result is identical to that which would be obtained by calculating the electric field of a line charge with line charge density ρ_ℓ over a perfectly conducting half space. At the surface of the earth (i.e., $y = 0$)

$$\hat{E}_y^1 \cong \frac{-\hat{\rho}_\ell}{2\pi\epsilon_1} \frac{2h}{\left((x-x_1)^2 + h^2\right)} e^{-j\gamma_{TL}z} \quad (5.4.26)$$

Since the tangential component of electric field is zero at a perfect conductor, this is the total electric field at the earth's surface. It must be vertical because components tangential to the earth must be zero because the earth is approximated as a perfect conductor.

Equation (5.3.12) can be related to line voltage rather than line charge amplitude by calculating the voltage of the line relative to the earth (V_w) as follows.

$$\begin{aligned} \hat{V}_w &= \hat{V}(x_1, h-a) - \hat{V}(x_1, 0) = - \int_0^{h-a} \hat{E}_y(y) dy \\ &= \frac{\hat{\rho}_\ell}{2\pi\epsilon_0} \int_0^{h-a} \left[\frac{1}{(y-h)} + \frac{1}{(y+h)} \right] dy = \frac{\hat{\rho}_\ell}{2\pi\epsilon_0} \ln\left(\frac{2h}{a}\right) \end{aligned} \quad (5.4.27)$$

Given this result,

$$\hat{E}_y^1 \cong \frac{\hat{V}_w}{\ln\left(\frac{2h}{a}\right)} \left[\frac{(y-h)}{\left((x-x_1)^2 + (y-h)^2\right)} - \frac{(y+h)}{\left((x-x_1)^2 + (y+h)^2\right)} \right] e^{-j\gamma_{TL}z} \quad (5.4.28)$$

For completeness, the horizontal component of the electric field at low frequencies is

$$\hat{E}_x^1 \cong \frac{\tilde{V}_w}{\ln\left(\frac{2h}{a}\right)} \left[\frac{(x-x_1)}{\left((x-x_1)^2 + (y-h)^2\right)} - \frac{(x-x_1)}{\left((x-x_1)^2 + (y+h)^2\right)} \right] e^{-j\gamma_{TL}z} \quad (5.4.29)$$

The electric field at a point on the earth's surface just below the conductor (i.e.,) $x = x_1, y = 0$ is

$$\hat{E}_y^1 \cong \frac{-2\hat{V}_w}{h \ln\left(\frac{2h}{a}\right)} e^{-j\gamma_{TL}z} \quad (5.4.30)$$

Using the same result for vertical electric field, it is possible to calculate the electric field at the surface of the conductor (i.e., $x = x_1, y = h - a$). The result is

$$\hat{E}_y^1 \cong \frac{-\hat{V}_w}{a \ln\left(\frac{2h}{a}\right)} e^{-j\gamma_{TL}z} \quad (5.4.31)$$

Clearly, the electric field at the surface of the conductor is a factor $b/2a$ greater than the electric field at the surface of the earth. This is almost always significantly greater since $b \gg a$. Note that these results are extended to the multiconductor case in Chapter 7.

For completeness, the space potential can be found to be:

$$\hat{V}(x, y, z) \cong \frac{\hat{V}_w}{\ln\left(\frac{2h}{a}\right)} \ln\left(\frac{\left((x-x_1)^2 + (y+h)^2\right)^{1/2}}{\left((x-x_1)^2 + (y-h)^2\right)^{1/2}}\right) e^{-j\gamma_{TL}z} \quad (5.4.32)$$

For a point on the wire (i.e., $x = x_1, y = h - a$), $V(x_1, h - a, z) = V_w$ as expected.

Alternative low frequency expression for E_x – the complex image model

Consider first, the general expression for axial electric field from (5.3.13)

$$\tilde{E}_{ez}^1(x - x_1, y, h, \gamma) = \tilde{G}_{ez}^1(x - x_1, y, h, \gamma) \hat{I}(\gamma) \quad (5.4.33)$$

where

$$\begin{aligned} \tilde{G}_{ez}^1(x-x_1, y, h, \gamma) = & \frac{-j(k_0^2 - \gamma^2)}{4\pi\omega\epsilon_0} \int_{-\infty}^{\infty} \left\{ \frac{e^{-u_1|y-h|}}{u_1} - \frac{e^{-u_1(y+h)}}{u_1} \right. \\ & \left. + \frac{2k_0^2 e^{-u_1(y+h)}}{(k_0^2 - \gamma^2)} \left[\frac{1}{u_1 + u_2} - \frac{\gamma^2}{(k_0^2 u_2 + k_2^2 u_1)} \right] \right\} e^{-j\kappa(x-x_1)} d\kappa \end{aligned} \quad (5.4.34)$$

If, as above, the last integral is ignored for typical earths at low frequencies, and the identity

$$\begin{aligned} H_0^{(2)}\left(\left(k_0^2 - \gamma^2\right)^{1/2} \left[(x-x_1)^2 + (y-h)^2 \right]^{1/2}\right) = & \frac{j}{\pi} \int_{-\infty}^{\infty} \frac{e^{-u_1|y-h|} e^{-j\kappa(x-x_1)}}{u_1} d\kappa \quad (5.4.35) \\ \text{Im}\left(k_0^2 - \gamma^2\right)^{1/2} \leq & 0 \end{aligned}$$

is used for all of the first two integrals except the part of the second term multiplied by k_0^2 , then (5.4.34) becomes

$$\begin{aligned} \tilde{G}_{ez}^1(x-x_1, y, h, \gamma) = & \frac{\gamma^2}{4\omega\epsilon_0} \left[H_0^{(2)}\left(\left(k_0^2 - \gamma^2\right)^{1/2} r\right) - H_0^{(2)}\left(\left(k_0^2 - \gamma^2\right)^{1/2} r^i\right) \right] \\ & - \frac{\omega\mu_0}{4} \left[H_0^{(2)}\left(\left(k_0^2 - \gamma^2\right)^{1/2} r\right) \right. \\ & \left. + \frac{j}{\pi} \int_{-\infty}^{\infty} \left[-\frac{1}{u_1} + \frac{2}{u_1 + u_2} \right] e^{-u_1(y+h)} e^{-j\kappa(x-x_1)} d\kappa \right] \\ = & \frac{\gamma^2}{4\omega\epsilon_0} \left[H_0^{(2)}\left(\left(k_0^2 - \gamma^2\right)^{1/2} r\right) - H_0^{(2)}\left(\left(k_0^2 - \gamma^2\right)^{1/2} r^i\right) \right] \\ & - \frac{\omega\mu_0}{4} \left[H_0^{(2)}\left(\left(k_0^2 - \gamma^2\right)^{1/2} r\right) \right. \\ & \left. - \frac{j}{\pi} \int_{-\infty}^{\infty} \left[\frac{u_1 - u_2}{u_1(u_1 + u_2)} \right] e^{-u_1(y+h)} e^{-j\kappa(x-x_1)} d\kappa \right] \end{aligned} \quad (5.4.36)$$

where

$$r = \left[(x-x_1)^2 + (y-h)^2 \right]^{1/2}, \quad r^i = \left[(x-x_1)^2 + (y+h)^2 \right]^{1/2} \quad (5.4.37)$$

Next, recognizing that for low frequencies, $u_2 \cong u = (\kappa^2 - k_2^2)^{1/2}$ and $u_1 \cong \kappa$ over most of the integration path since $k_0(y+h) \ll 1$ and, hence the integral does not converge until $\kappa \gg k_0$,

$$\frac{u_1 - u_2}{u_1 + u_2} \cong \frac{\kappa - u}{\kappa + u} \cong e^{-\kappa\alpha} \quad (5.4.38)$$

where $\alpha = \frac{2}{k_2}$ and the final step has been shown by Wait and Spies (1969).

Using this result in (5.4.36) gives

$$\begin{aligned} \tilde{G}_{ez}^1(x-x_1, y, h, \gamma) &= \frac{\gamma^2}{4\omega\epsilon_0} \left[H_0^{(2)}\left(\left(k_0^2 - \gamma^2\right)^{1/2} r\right) - H_0^{(2)}\left(\left(k_0^2 - \gamma^2\right)^{1/2} r^i\right) \right] \\ &\quad - \frac{\omega\mu_0}{4} \left[H_0^{(2)}\left(\left(k_0^2 - \gamma^2\right)^{1/2} r\right) - \frac{j}{\pi} \int_{-\infty}^{\infty} \frac{e^{-u_1(y+h+\epsilon)} e^{-jk(x-x_1)}}{u_1} dk \right] \\ &= \frac{\gamma^2}{4\omega\epsilon_0} \left[H_0^{(2)}\left(\left(k_0^2 - \gamma^2\right)^{1/2} r\right) - H_0^{(2)}\left(\left(k_0^2 - \gamma^2\right)^{1/2} r^i\right) \right] \\ &\quad - \frac{\omega\mu_0}{4} \left[H_0^{(2)}\left(\left(k_0^2 - \gamma^2\right)^{1/2} r\right) - H_0^{(2)}\left(\left(k_0^2 - \gamma^2\right)^{1/2} \left((y+h+\alpha)^2 + (x-x_1)^2\right)^{1/2}\right) \right] \end{aligned} \quad (5.4.39)$$

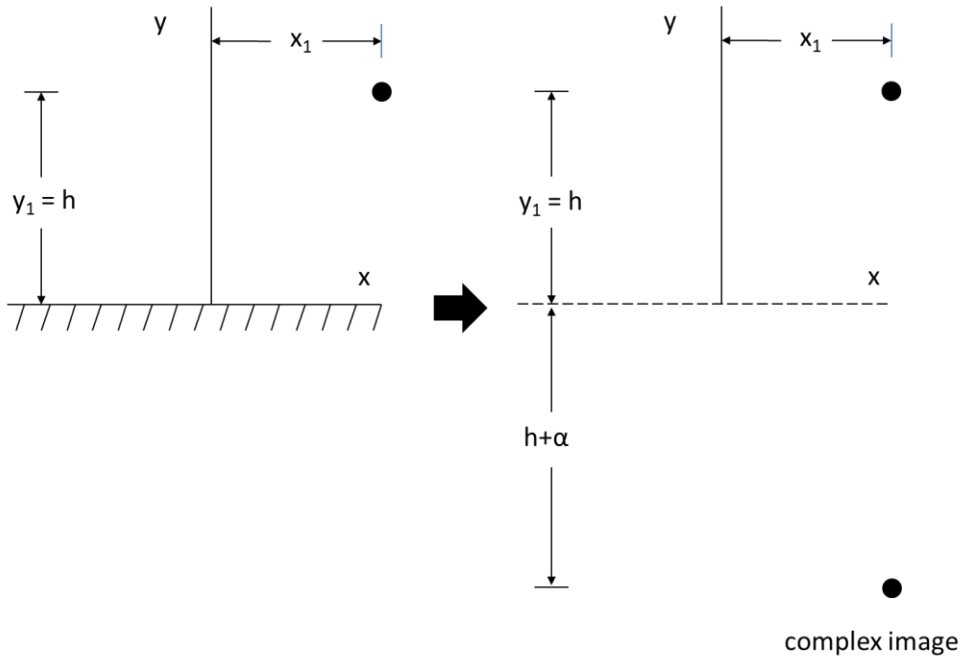


Fig. 5.4.1. Geometry for Complex Image formation

Since the approximations made limit this result to low frequencies, it is appropriate to use the small argument expansion for the Hankel functions to get (for the electric field)⁴⁹

$$\begin{aligned} \tilde{E}_{ez}^1(x-x_1, y, h, \gamma) &= \tilde{G}_{ez}^1(x-x_1, y, h, \gamma) \hat{I}(\gamma) \\ &= \left\{ \frac{j\gamma^2}{2\pi\omega\epsilon_0} \ln\left(\frac{r^i}{r}\right) - \frac{j\omega\mu_0}{2\pi} \ln\left(\frac{((y+h+\alpha)^2 + (x-x_1)^2)^{1/2}}{r}\right) \right\} \hat{I}(\gamma) \end{aligned} \quad (5.4.40)$$

where

$$\alpha = \frac{2}{k_0 \left[\frac{\epsilon_2}{\epsilon_0} \left(1 - j \frac{\sigma_2}{\omega\epsilon_2} \right) \right]^{1/2}} \cong \sqrt{2} \delta e^{+j\pi/4}$$

and

$$\delta = \frac{\sqrt{2}}{(\sigma_2 \mu_0 \omega)^{1/2}}$$

The physical interpretation of (5.3.40) is shown in Fig. 5.4.1. The second term of (5.4.40) is a “complex image” of the line current where $b+a$ is the complex depth of the image and δ is the “skin depth” of the earth. At 60 Hz, typical magnitudes for a are on the order of 1000 meters.

Following (5.4.13) – (5.4.20), the field in the space domain is

$$\begin{aligned} \tilde{E}_{ez}^1(x-x_1, y, h, z) &= F^{-1} \left[\tilde{G}_{ez}^1(x-x_1, y, h, \gamma) \hat{I}(\gamma) \right] \\ &= \left\{ \frac{j\gamma^2}{2\pi\omega\epsilon_0} \ln\left(\frac{r^i}{r}\right) - \frac{j\omega\mu_0}{2\pi} \ln\left(\frac{((y+h+\alpha)^2 + (x-x_1)^2)^{1/2}}{r}\right) \right\} \hat{I}_0 e^{\pm j\gamma\pi z} \end{aligned} \quad (5.4.41)$$

The magnetic field above the earth— the complex image model

It is also important to calculate the magnetic field above the earth since it is not as clear at the beginning what will happen at low frequencies. One issue is that the earth is assumed to be non-magnetic. Hence, one would expect that the earth would be “transparent” at $\omega = 0$ (and hence perhaps at very low frequencies). But, the earth is also a good conductor and it is possible that the source’s magnetic fields would be modified by magnetically induced eddy currents due to the time rate of change of the magnetic field in the earth. It turns out that this is an issue that needs to be considered. To see this, consider the horizontal magnetic field.

⁴⁹ See the comment about (5.4.5) on setting $\gamma = 0$ in this expression.

(5.4.42)

$$\begin{aligned} \tilde{G}_{hx}^1(x-x_1, y, h, \gamma) = & \frac{-j}{4} \frac{\partial}{\partial y} \left[H_0^{(2)}\left((k_0^2 - \gamma^2)^{1/2} r\right) - H_0^{(2)}\left((k_0^2 - \gamma^2)^{1/2} r^i\right) \right] \\ & - \frac{1}{2\pi} \int_{-\infty}^{\infty} \left(\frac{\kappa^2 - k_0^2}{(u_1 + u_2)} + \frac{k_0^2 \gamma^2}{(k_0^2 u_2 + k_2^2 u_1)} \right) \frac{e^{-u_1(y+h)} e^{-j\kappa(x-x_1)}}{u_1} d\kappa \end{aligned}$$

In order to proceed, it is appropriate to combine all terms of (5.4.42) that account for the influence of the earth (i.e., all terms except for the source term). This can be done (as was done in the last section on the axial electric field) by replacing the second Hankel function by its integral representation and combining all three integrands into one. The result is

$$\begin{aligned} \tilde{G}_{hx}^1(x-x_1, y, h, \gamma) = & \frac{-j}{4} \frac{\partial}{\partial y} H_0^{(2)}\left((k_0^2 - \gamma^2)^{1/2} r\right) \\ & + \frac{1}{4\pi} \int_{-\infty}^{\infty} \left(u_1 - \frac{2(\lambda^2 - k_0^2)}{(u_1 + u_2)} - \frac{2k_0^2 \gamma^2}{(k_0^2 u_2 + k_2^2 u_1)} \right) \frac{e^{-u_1(y+h)} e^{-j\kappa(x-x_1)}}{u_1} d\kappa \end{aligned} \quad (5.4.43)$$

Clearly, if $k_1 \rightarrow k_2$ the integrand of the integral becomes zero leaving only the source term as should occur.

At low frequencies, several approximations can be made to this result. First, the Hankel function can be replaced by its small argument expansion as shown in (5.4.1). Next, it can be assumed that the propagation constant, γ , equals zero. With these approximations and some manipulation of the integrand,

(5.4.44)

$$\begin{aligned} \tilde{G}_{hx}^1(x-x_1, y, h, \gamma) = & \\ & \frac{-1}{2\pi} \frac{\partial}{\partial y} \left[\frac{j\pi}{2} + \ln\left(\frac{(k_0 r)}{2}\right) + \gamma_e \right] + \frac{1}{4\pi} \int_{-\infty}^{\infty} \left(\frac{(k_0^2 - \lambda^2) + u_1 u_2}{(u_1 + u_2)} \right) \frac{e^{-u_1(y+h)} e^{-j\kappa(x-x_1)}}{u_1} d\kappa \end{aligned}$$

Next, taking the derivative and recognizing that for low frequencies, $u_2 \cong u = (\kappa^2 - k_2^2)^{1/2}$ and $u_1 \cong \kappa$ over most of the integration path since $k_0(y+h) \ll 1$ and, hence the integral does not converge until $\kappa \gg k_0$,

(5.4.45)

$$\tilde{G}_{hx}^1(x-x_1, y, h, \gamma) = \frac{-1}{2\pi} \frac{(y-h)}{(x-x_1)^2 + (y-h)^2} + \frac{1}{4\pi} \int_{-\infty}^{\infty} \left(\frac{u - \kappa}{(u + \kappa)} \right) e^{-\kappa(y+h)} e^{-j\kappa(x-x_1)} d\kappa$$

As introduced earlier, Wait and Spies (1969) showed that

$$\frac{(u - \kappa)}{(u + \kappa)} \cong e^{-\kappa\alpha}$$

where

$$\alpha = \frac{2}{k_2} \quad (5.4.46)$$

so that

$$\begin{aligned} \tilde{G}_{hx}^1(x - x_1, y, h, \gamma) &= \frac{-1}{2\pi} \frac{(y - h)}{(x - x_1)^2 + (y - h)^2} + \frac{1}{4\pi} \int_{-\infty}^{\infty} e^{-\kappa(y+h+\alpha)} e^{-j\kappa(x-x_1)} d\kappa \\ &= \frac{-1}{2\pi} \left[\frac{(y - h)}{(x - x_1)^2 + (y - h)^2} - \frac{(y + h + \alpha)}{(x - x_1)^2 + (y + h + \alpha)^2} \right] \end{aligned} \quad (5.4.47)$$

where

$$\alpha = \frac{2}{k_0 \left[\frac{\epsilon_2}{\epsilon_0} \left(1 - j \frac{\sigma_2}{\omega \epsilon_2} \right) \right]^{1/2}} \cong \sqrt{2} \delta e^{+j\pi/4}$$

and

$$\delta = \frac{\sqrt{2}}{(\sigma_2 \mu_0 \omega)^{1/2}}$$

Again, (5.4.47) is the “complex image” formation of the line current over the earth problem where $h+a$ is the complex depth of the image and δ is the “skin depth” of the earth as illustrated in Fig. 5.4.1. Again, at 60 Hz, typical magnitudes for a are on the order of 1000 meters. Hence, for field points reasonably close to the power line, the earth appears to be transparent unless the frequency is increased substantially beyond power frequencies. The complex image formulation has been used for calculation of power line magnetic fields (Olsen et. al. 1995).

For completeness, a similar derivation for the y component of the magnetic field above the earth will be given. The starting point for this derivation will be (5.3.23) which is repeated here as:

$$(5.4.48)$$

$$\begin{aligned} \tilde{G}_{hy}^1(x - x_1, y, h, \gamma) &= \frac{j}{4} \frac{\partial}{\partial x} \left[H_0^{(2)} \left((k_0^2 - \gamma^2)^{1/2} r \right) - H_0^{(2)} \left((k_0^2 - \gamma^2)^{1/2} r^i \right) \right] \\ &+ \frac{j}{2\pi} \int_{-\infty}^{\infty} \left(\frac{u_1 \kappa}{(u_1 + u_2)} \right) \frac{e^{-u_1(y+h)} e^{-j\kappa(x-x_1)}}{u_1} d\kappa \end{aligned}$$

Again, at low frequencies, several approximations can be made to this result. First, the Hankel function can be replaced by its small argument expansion as shown in (5.3.1). Next, it can be assumed that the propagation constant, γ , equals zero. With these approximations and some manipulation of the integrand:

$$\begin{aligned} \tilde{G}_{hy}^1(x-x_1, y, h, \gamma) &= \frac{1}{2\pi} \frac{\partial}{\partial x} \left(\frac{j\pi}{2} - \frac{2j}{\pi} \ln\left(\frac{k_0 r}{2}\right) + \gamma_e \right) \\ &+ \frac{j}{4\pi} \int_{-\infty}^{\infty} \kappa \frac{u_1 - u_2}{(u_1 + u_2)} \frac{e^{-u_1(y+h)} e^{-j\kappa(x-x_1)}}{u_1} d\kappa \end{aligned} \quad (5.4.49)$$

Next, taking the derivative and recognizing that for low frequencies, $u_2 \cong u = (k^2 - k_0^2)^{1/2}$ and $u_1 \cong \kappa$ for the term $(u_1 - u_2)/(u_1 + u_2)$ over most of the integration path since $k_0(y+h) \ll 1$ and, hence the integral does not converge until $\kappa \gg k_0$,

$$\tilde{G}_{hy}^1(x-x_1, y, h, \gamma) = \frac{1}{2\pi} \frac{(x-x_1)}{(x-x_1)^2 + (y-h)^2} - \frac{j}{4\pi} \int_{-\infty}^{\infty} \kappa \left(\frac{u-\kappa}{(u+\kappa)} \right) \frac{e^{-u_1(y+h)} e^{-j\kappa(x-x_1)}}{u_1} d\kappa \quad (5.4.50)$$

Finally, using 5.4.46, approximating κ by u_1 in the result and the fact that multiplication by $-j\kappa$ within the integrand of (5.4.50) is equivalent to taking the derivative with respect to x , (5.4.50) reduces to,

$$(5.4.51)$$

$$\begin{aligned} \tilde{G}_{hy}^1(x-x_1, y, h, \gamma) &= \frac{1}{2\pi} \frac{(x-x_1)}{(x-x_1)^2 + (y-h)^2} + \frac{1}{4\pi} \frac{\partial}{\partial x} \int_{-\infty}^{\infty} \frac{e^{-u_1(y+h+\alpha)} e^{-j\kappa(x-x_1)}}{u_1} d\kappa \\ &= \frac{1}{2\pi} \frac{(x-x_1)}{(x-x_1)^2 + (y-h)^2} - \frac{j}{4} \frac{\partial}{\partial x} H_0^{(2)} \left(k_0 \left((x-x_1)^2 + (y+h+\alpha)^2 \right)^{1/2} \right) \\ &\cong \frac{1}{2\pi} \frac{(x-x_1)}{(x-x_1)^2 + (y-h)^2} - \frac{1}{2\pi} \frac{\partial}{\partial x} \left(\frac{j\pi}{2} + \ln \left(k_0 \left((x-x_1)^2 + (y+h+\alpha)^2 \right)^{1/2} \right) + \gamma_e \right) \\ &\cong \frac{1}{2\pi} \left[\frac{(x-x_1)}{(x-x_1)^2 + (y-h)^2} - \frac{(x-x_1)}{(x-x_1)^2 + (y+h+\alpha)^2} \right] \end{aligned}$$

where α is defined in (5.4.47).

This result is consistent with complex image theory discussed above.

Magnetic fields in the space domain

To recover the magnetic fields in the space domain, it is again necessary to perform the inverse Fourier transform with respect to γ in order to see the

explicit z dependence. The simplest way to do this is to assume that the current in the space domain is an exponential function of z (as in Section 4.8) that has the form in the γ domain

$$\hat{\tilde{I}}(\gamma) = \frac{2j\hat{I}_0\gamma_{TL}}{(\gamma + \gamma_{TL})(\gamma - \gamma_{TL})} \quad (5.4.52)$$

where $\gamma_{TL} = \pm j\sqrt{ZY}$ as in Section 4.6 and Z and Y are defined in (4.6.6) and (4.6.8) respectively. (5.4.52) corresponds to a current in the space domain of

$$\hat{I}(z) = \hat{I}_0 e^{\pm j\gamma_{TL}z} \quad (5.4.53)$$

where the “+” sign corresponds to $z < 0$ and the “-” sign to $z > 0$.

Now, as with the electric fields,

$$\hat{\tilde{H}}_x^1(x - x_1, y, h, \gamma) = \tilde{G}_{hx}^1(x - x_1, y, h, \gamma) \hat{\tilde{I}}(\gamma) \quad (5.4.54)$$

and

$$\hat{\tilde{H}}_y^1(x - x_1, y, h, \gamma) = \tilde{G}_{hy}^1(x - x_1, y, h, \gamma) \hat{\tilde{I}}(\gamma) \quad (5.4.55)$$

Given these and taking the inverse Fourier transform to each using (5.4.52) results in

$$(5.4.56)$$

$$\hat{H}_x^1(x, y, z) = \frac{-I_0}{2\pi} \left[\frac{(y - h)}{(x - x_1)^2 + (y - h)^2} - \frac{(y + h + \alpha)}{(x - x_1)^2 + (y + h + \alpha)^2} \right] e^{-j\gamma_{TL}z}$$

and

$$(5.4.57)$$

$$\hat{H}_y^1(x, y, z) = \frac{I_0}{2\pi} \left[\frac{(x - x_1)}{(x - x_1)^2 + (y - h)^2} - \frac{(x - x_1)}{(x - x_1)^2 + (y + h + \alpha)^2} \right] e^{-j\gamma_{TL}z}$$

where

$$\alpha = \frac{2}{k_0 \left[\frac{\epsilon_2}{\epsilon_0} \left(1 - j \frac{\sigma_2}{\omega \epsilon_2} \right) \right]^{1/2}} \cong \sqrt{2} \delta e^{+j\pi/4}$$

and

$$\delta = \frac{\sqrt{2}}{(\sigma_2 \mu_0 \omega)^{1/2}}$$

Electric fields in the earth

At low frequencies, the x and y components of the electric field in the earth (i.e., (5.3.31) and (5.3.32) respectively) can be ignored compared to the z component (i.e., (5.3.33)) because $|k_2| \gg |k_0|$ and the integrals in (5.3.31) and (5.3.32) are proportional to (at least) $1/|k_2|$.

Hence,

$$\tilde{G}_{ex}^2(x-x_1, y, h, \gamma) \cong \tilde{G}_{ey}^2(x-x_1, y, h, \gamma) \cong 0 \quad (5.4.58)$$

For the z component of the field, the latter integral of (5.3.33) can be ignored compared to the first for the same reason and

$$\tilde{G}_{ez}^2(x-x_1, y, h, \gamma) \cong \frac{-jk_0^2}{2\pi\omega\epsilon_0} \int_{-\infty}^{\infty} \frac{e^{-u_1 h} e^{u_2 y} e^{-j\kappa(x-x_1)}}{u_1 + u_2} d\kappa, y < 0 \quad (5.4.59)$$

(5.4.59) can be approximated at low frequencies in a manner similar to that used in deriving Carson's integral in (4.6.5). The result becomes

$$\begin{aligned} \tilde{G}_{ez}^2(x-x_1, y, h, \gamma) &= \frac{-jk_0^2}{2\pi\omega\epsilon_0} \int_{-\infty}^{\infty} \frac{(u_1 - u_2) e^{-u_1 h} e^{u_2 y} e^{-j\kappa(x-x_1)}}{(u_1 - u_2)(u_1 + u_2)} d\kappa \\ &\cong \frac{-jk_0^2}{\pi\omega\epsilon_0} \int_0^{\infty} \frac{(\kappa - u_2) e^{-\kappa h} e^{u_2 y}}{(k_2^2 - k_0^2)} \cos(\kappa(x-x_1)) d\kappa \quad (5.4.60) \\ &\cong \frac{j\omega\mu_0}{\pi k_2^2} \int_0^{\infty} (u - \kappa) e^{-\kappa h} e^{u y} \cos(\kappa(x-x_1)) d\kappa \\ & \quad y < 0 \end{aligned}$$

where $u_1 \cong \kappa$ and $u_2 \cong u = \sqrt{\kappa^2 - k_2^2}$ over most of the integration since the integral converges when $\kappa h \gg 1$ and $k_2 h \ll 1$.

Next, if $k_2 y \ll 1$, then $e^{u y} \cong e^{\kappa y}$ since k_2 is an important part of u only when $e^{u y} \cong 1$. Hence

$$\begin{aligned} \tilde{G}_{ez}^2(x-x_1, y, h, \gamma) &\cong \frac{j\omega\mu_0}{\pi k_2^2} \int_0^{\infty} (u - \kappa) e^{-\kappa(h-y)} \cos(\kappa(x-x_1)) d\kappa = \frac{j\omega\mu_0}{2\pi} J_c(x-x_1, y, h), \\ & \quad y < 0 \end{aligned} \quad (5.4.61)$$

This result can be further simplified by using the first two dominant terms of the Carson Series as in (4.6.14). The result is

$$\hat{E}_z^2(x-x_1, y, h, \gamma) = \tilde{G}_{ez}^2(x-x_1, y, h, \gamma) \hat{I}(\gamma) \cong \frac{j\omega\mu_0}{2\pi} \ln\left(\frac{r}{(2/(jk_2))}\right) \hat{I}(\gamma) \quad (5.4.62)$$

$y < 0$

This result can be transformed to the space domain by assuming a current of the form

$$\hat{I}(z) = I_0 e^{-j\gamma_{TL}z} \quad (5.4.62)$$

that has the Fourier Transform

$$\hat{I}(\gamma) = \frac{-2j\hat{I}_0\gamma_{TL}}{(\gamma + \gamma_{TL})(\gamma - \gamma_{TL})} \quad (5.4.64)$$

Given this, the axial electric field in the spatial domain becomes

$$\begin{aligned} \hat{E}_z^2(x-x_1, y, h, z) &\cong \frac{j\omega\mu_0}{2\pi} \ln\left(\frac{r}{(2/(jk_2))}\right) \frac{2j\hat{I}_0\gamma_{TL}}{2\pi} \int_{-\infty}^{\infty} \frac{e^{-j\gamma z}}{(\gamma + \gamma_{TL})(\gamma - \gamma_{TL})} d\gamma \\ &= \frac{j\omega\mu_0}{2\pi} \ln\left(\frac{r}{(2/(jk_2))}\right) \hat{I}_0 e^{-j\gamma_{TL}z} \end{aligned} \quad (5.4.65)$$

$y < 0$

As a check on this result, it is known from Maxwell's equations that (assuming that both E_x and E_y are zero in the earth and reinserting the current into the expression for E_z)

$$-j\omega\mu_0 \hat{H}_x = \frac{\partial \hat{E}_z}{\partial y} = \frac{j\omega\mu_0}{2\pi} \frac{-(y-h)}{(y-h)^2 + (x-x_1)^2} \hat{I}_0 e^{-j\gamma_{TL}z}, \quad y < 0 \quad (5.4.66)$$

or (for a general $I(z)$)

$$\hat{H}_x = -\frac{\hat{I}(z)}{2\pi} \frac{(y-h)}{(y-h)^2 + (x-x_1)^2}, \quad y < 0 \quad (5.4.67)$$

This is the correct first order result for the magnetic field in the earth since the earth is non-magnetic.

5.5 Capacitance and Inductance Per Unit Length of a Conductor over Earth

In this section, the capacitance and inductance per unit length will be derived using earlier results. For capacitance, it is noted from (4.6.9) that the capacitance per unit length (C) of a wire over the earth is

$$C = \frac{\hat{\rho}_\ell}{\hat{V}_w} = \frac{2\pi\epsilon_0}{\ln\left(\frac{2h}{a}\right)} \quad (5.5.1)$$

This result is identical to the result obtained using electrostatic theory.

The derivation of the inductance per unit length requires a bit more thought. In (4.6.10) it was shown that the external inductance per unit length was

$$L_e = \frac{\mu_0}{2\pi} \{\ln(2h/a) - \text{Re}(J_c(a, h, h))\}. \quad (5.5.2)$$

But, given the simple one term series approximation for J_c

$$J_c(2h, a) \cong \ln\left(\frac{2h}{(2/k_2)}\right) \quad (5.5.3)$$

$$(5.5.4)$$

$$L_e \cong \frac{\mu_0}{2\pi} \left\{ \ln(2h/a) - \text{Re} \left(\ln \left(\frac{2h}{(2/k_2)} \right) \right) \right\} = \frac{\mu_0}{2\pi} \{ \text{Re}(\ln(2/k_2)) - \ln(a) \}$$

But, at the low frequencies for which Carson's equations are valid,

$$k_2 \cong \sqrt{\omega\mu_0\sigma_2} e^{-j\pi/4} \quad (5.5.5)$$

and hence

$$L_e \cong \frac{\mu_0}{2\pi} \{ \ln(2/\sqrt{\omega\mu_0\sigma_2}) - \ln(a) \} = \frac{\mu_0}{2\pi} \ln \left(\frac{2}{a\sqrt{\omega\mu_0\sigma_2}} \right) = \frac{\mu_0}{2\pi} \ln \left(\frac{d_i}{a} \right) \quad (5.5.6)$$

where d_i (the "distance" to the complex image) is equal to

$$d_i = \frac{2}{\sqrt{\omega\mu_0\sigma_2}} \quad (5.5.7)$$

and it has been assumed (as before) that the earth is non-magnetic.

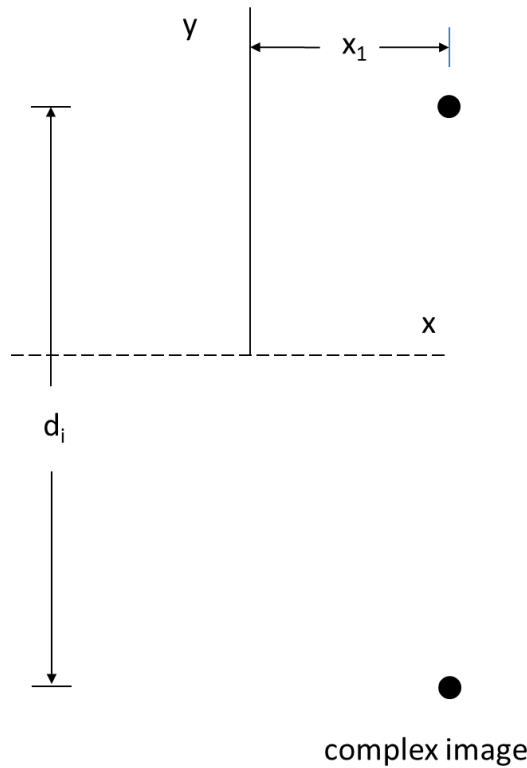


Fig. 5.5.1. Geometry for Calculation of the External Inductance of a Wire above Earth

The geometry, then, for calculating the inductance is shown in Fig. 5.5.1. The inductance per unit length can be calculated by integrating the flux generated by the current (I) and its return current located a distance (d_i) below over the region between the source conductor and the return conductor. This flux is

$$\phi = \frac{\mu_0 I}{2\pi} \int_a^{d_i} \left[\frac{1}{r} - \frac{1}{(r - d_i)} \right] dr = \frac{\mu_0 I}{2\pi} \ln \left(\frac{d_i}{a} \right) = \frac{\mu_0 I}{2\pi} \ln \left(\frac{2}{a\sqrt{\omega\mu_0\sigma_2}} \right) \quad (5.5.8)$$

Since the inductance is defined as the flux linkages per unit length divided by the loop current, the external inductance is

$$L_e = \frac{\mu_0}{2\pi} \ln \left(\frac{2}{a\sqrt{\omega\mu_0\sigma_2}} \right) \quad (5.5.9)$$

This result is identical to (5.4.6) that was derived from Carson's one term series. It should be no surprise that image theory and Carson's theory are

connected. It is interesting, however, to also note that the inductance becomes infinite as $\omega \rightarrow 0$.

5.6 Justification for Electrostatics

It should be clear from above that all of the electric field quantities (i.e., capacitance per unit length, and electric field near the conductor and the earth) could have been calculated using electrostatic theory for nearly all frequencies of interest to power engineers (i.e., frequencies low enough that $\ell \ll \lambda$ where ℓ is the largest significant dimension and λ is the free space wavelength). This is despite the fact that the length of the power line has been assumed to be infinite. This fact suggests that field calculations might be made using only the local geometry for which ℓ really is $\ll \lambda$. For example, consider the problem shown in Fig. 5.6.1. Here a finite length horizontal wire is energized to a voltage V_w and located above a perfectly conducting plane.

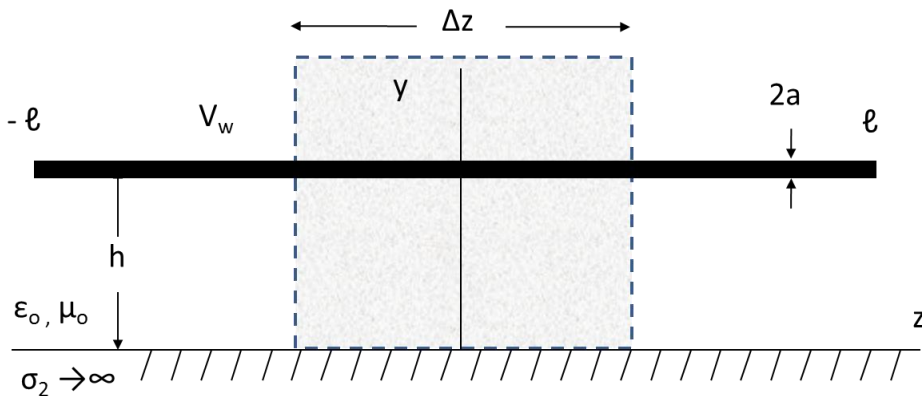


Fig. 5.6.1. Geometry illustrating how electrostatics can be used to simulate the fields of an infinitely long conductor with a finite length conductor

It can be shown that the electric fields in the shaded region of Fig. 5.6.1 are essentially equivalent to the fields near an infinitely long conductor carrying a propagating current as long as $\Delta z, h \ll \ell \ll \lambda$. Outside of the shaded region the two results would not be equivalent due to edge effects from the ends of the conductor.

The same result holds for problems that contain more geometrically complex regions such as insulators and hardware such as illustrated in Fig. 5.6.2. Here, a simulated potential transformer is located between the conductor and the perfectly conducting earth.

Problems such as that shown in Fig. 5.6.2 cannot generally be solved using closed form techniques such as the ones that have been introduced earlier in this manuscript. Rather, electrostatic approximations to Maxwell's equations are made first so that scalar theory rather than the more complex

vector theory required for the more general Maxwell's equations can be used. Then numerical techniques can be used to solve the problems that are otherwise intractable. In Chapter 6, several different types of numerical techniques in electrostatics will be introduced and some comments made on their utility.

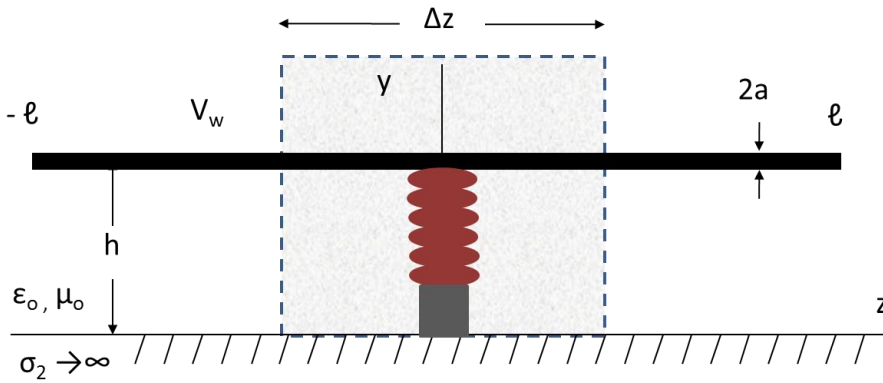


Fig. 5.6.2. More complicated geometry that can be solved using electrostatic techniques.

5.7 Problems

P5.1. (electric field above the earth) A horizontal long conductor, radius $a = 1.5\text{cm}$ and height $h = 12\text{m}$, is placed along the z -direction, as shown in Fig. 1. The line charge density, ρ , along the conductor is $1.2 \times 10^{-6}\text{ C/m}$. Assume $z = 0$.

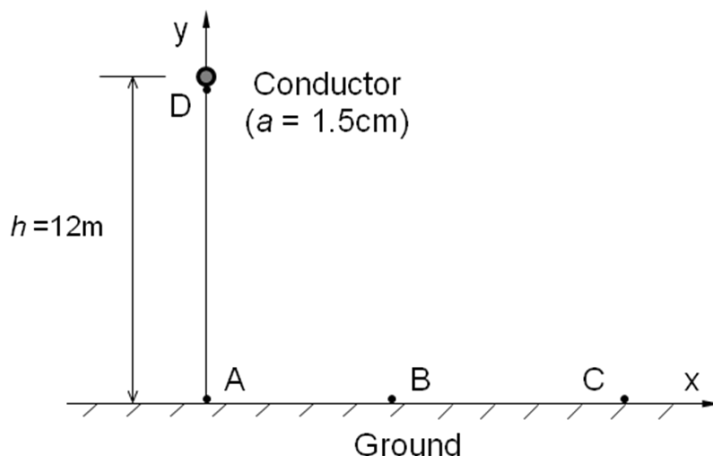


Fig. P5.1 Geometry of the model

a. Show that the x -component (E_x , tangential component) of the electric field at the ground surface ($y = 0$) is zero.

b. Find the decay rate of the y -component (E_y , normal component) of the electric field as a function of x for $y = 0$ and $x \gg b$. Calculate E_y at the three observation points A, B, and C, whose coordinates are $(0, 0)$, $(10, 0)$, and $(100, 0)$, respectively.

c. Calculate E_y at the point D, $(0, b - a)$, right on the bottom of the conductor. What happens to E_y if the radius of the conductor is increased to $2a$?

P5.2. (magnetic fields above the earth) Consider a single-conductor power line, radius $a = 1.5\text{cm}$ and height $h = 12\text{m}$, carrying a current $\bar{I} = I_0 e^{-j\gamma_{TL}z}$, as shown in Fig. P5.2. γ_{TL} is the propagation constant and $I_0 = 330\text{A}$. The ground has a dielectric constant $\epsilon_{r2} = 5$ (its permittivity $\epsilon_2 = \epsilon_{r2}\epsilon_0$, $\epsilon_0 = 8.85 \times 10^{-12}\text{F/m}$) and a conductivity $\sigma_2 = 0.01\text{S/m}$. Let the frequency of the current vary from 10 to 1000Hz. Assume $\mu_2 = \mu_0 = 4\pi \times 10^{-7}\text{H/m}$.

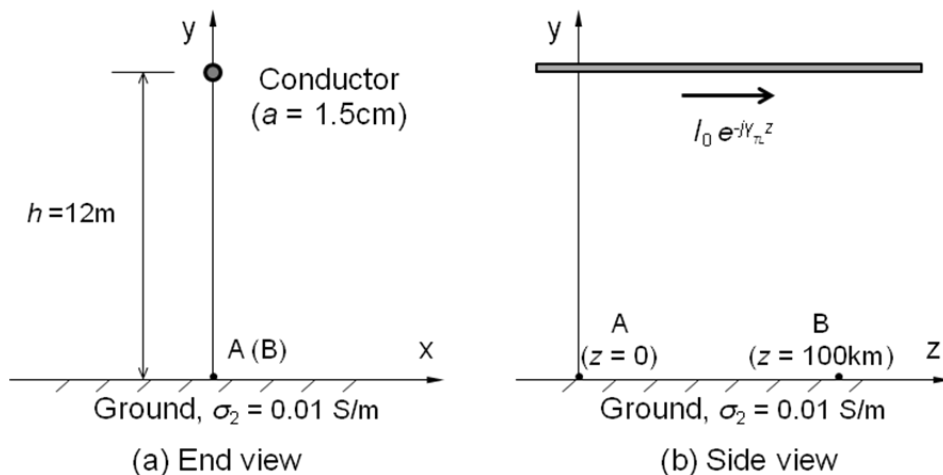


Fig. P5.2 Model of a single conductor power line for magnetic field calculation

Use the version of (5.4.47) that has been transformed into the space domain as

$$H_x^1 = \frac{-I_0}{2\pi} \left[\frac{(y-h)}{(x-x')^2 + (y-h)^2} - \frac{(y+h+\alpha)}{(x-x')^2 + (y+h+\alpha)^2} \right] e^{-j\gamma_{TL}z}$$

a. Determine the depth $(h + a)$ of the complex image (see (5.4.40)) at 60Hz. Compare the magnitude of $(h + a)$ with h .

b. There are two observation points, A and B, on the ground surface. They are both on the z -axis. A is at the origin, $(0, 0, 0)$, and B is 100 km down the z -axis, $(0, 0, 100,000)$. Calculate x -component H_x of the magnetic field at A and B over the frequency range 10 to 1000Hz. Plot the magnitude of H_x at each observation point vs. frequency.

c. How does your result change if $x = 100$ meters?

(Hint: find the propagation constant γ_{TL} by using (4.6.27) with $Z_{iw} = 0$. If you wish, you may use the approximation (4.6.24)

P5.3. (magnetic field in the earth) Derive expressions for the magnetic fields in the earth from a wire above earth carrying a current $\tilde{I}(\gamma) = \exp(-j\gamma z)$.

a. using (4.4.22), (4.4.23), (5.3.26) and (5.3.27) directly

b. by application of Maxwell's equations to (5.3.31) – (5.3.33)

Show that the two are equivalent.

5.8 References

Wait, J. R. and K.P. Spies. 1969. "On the Image Representation of the Quasi-Static Fields of a Line Current Source above Ground." *Canadian Journal of Physics*. Vol. 47. pp. 2731-2733. December.

Olsen, R. G., S.L. Backus and R.D. Stearns. 1995. "Development and Validation of Software for Predicting ELF Magnetic Fields near Power Lines." *IEEE Transactions on Power Delivery*. Vol. 10. pp. 1525-1534. July.

Chapter VI

Brief Overview of Numerical Techniques for Electrostatics

6.1 Introduction

Electrostatics

In the electrostatics case, $\omega = 0$ and according to (3.1.10)⁵⁰

$$\nabla \times \bar{E} = 0 \quad (6.1.1)$$

According to the Helmholtz theorem in (3.7.5), if $\nabla \times \bar{E} = 0$, then it is possible to write the electric field as

$$\bar{E} = -\nabla \psi \quad (6.1.2)$$

where $\psi(x, y, z)$ is a scalar potential. Further, since according to (3.1.14) $\nabla \cdot \bar{D} = \nabla \cdot \bar{E} = 0$ in a homogeneous, sourceless region, ψ satisfies

$$\nabla^2 \psi = 0 \quad (6.1.3)$$

which is Laplace's equation.

In rectangular coordinates, Laplace's equation is

$$\left(\frac{\partial^2}{\partial x^2} + \frac{\partial^2}{\partial y^2} + \frac{\partial^2}{\partial z^2} \right) \psi(x, y, z) = 0 \quad (6.1.4)$$

This equation will be given later in other coordinate systems as needed.

In solving electrostatics problems several boundary conditions will be used. On a conductor,

$$\psi(x, y, z) = V_B \quad (6.1.5)$$

⁵⁰ If $\omega = 0$, the RMS value of the field amplitude is the same as the peak value. Therefore, the electric field amplitude in this purely electrostatic case is the peak (i.e., constant) value and not a phasor.

where V_B is a specified boundary potential will be the condition used here.⁵¹ The charge density (ρ_s) on the surface of a conductor can be determined once the potential is known as

$$\rho_s = -\epsilon \bar{n} \cdot \nabla \psi = -\epsilon \frac{\partial \psi(x, y, z)}{\partial n} = \epsilon \bar{E} \cdot \bar{n} \quad (6.1.6)$$

where \bar{n} is the outward normal from the surface and $\epsilon = \epsilon_0 \epsilon_r$ is the dielectric constant of the material at the dielectric/conductor boundary. ϵ_0 is the permittivity of free space and ϵ_r is the relative dielectric constant.

At an interface between two dielectric materials, two continuity boundary conditions must be used. They are

$$\psi_i = \psi_j \quad \text{and} \quad \epsilon_i \frac{\partial \psi_i}{\partial n} = \epsilon_j \frac{\partial \psi_j}{\partial n} \quad (6.1.7)$$

where the two sides of the interface are indicated by “i” and “j” and the dielectric constants of each medium are ϵ_i and ϵ_j respectively.

Electroquasistatics

The terminology “electroquasistatics” is consistent with the definition in Haus and Melcher (1989). This generalization of electrostatics to non-zero frequencies is introduced because while the spatial behavior of the dominant electric fields at power frequencies satisfies Laplace’s equation (6.1.3), the behavior of materials can be enough different to warrant more care. More specifically, any conducting material is essentially a perfect conductor at DC because charges have the time to relax to their natural positions such that the electric field inside the material is zero. Only if a material is pure dielectric can it be characterized at zero frequency by its dielectric constant alone. For time varying fields, on the other hand, electric current flow (both conduction current and displacement or “capacitive” current) must be taken into account. More specifically, (assuming sinusoidal steady state at a radian frequency ω) the fields must satisfy

$$\nabla \times \hat{E} = 0 \quad (6.1.8)$$

and

⁵¹ This is the Dirichlet condition. It is also possible to use a Neuman condition in which case the derivative of the potential normal to the surface is used (Stratton 1941). If some combination of these boundary conditions is used on the entire boundary of the problem, the uniqueness theorem for electrostatics can be used to state that if a solution is found that satisfies both Laplace’s equation and these boundary conditions, it is the only solution possible.

$$\nabla \times \hat{H} = j\omega\epsilon_0\epsilon_r\hat{E} + \hat{J} = j\omega\epsilon_0\left(\epsilon_r - j\frac{\sigma}{\omega}\right)\hat{E} = j\omega\epsilon_0\hat{\epsilon}_r\hat{E} \quad (6.1.9)$$

where \hat{H} is the magnetic field intensity, the term $j\omega\epsilon_0\hat{\epsilon}_r\hat{E}$ represents displacement currents and the term $\hat{J} = \hat{\sigma}\hat{E}$ represents conduction currents⁵². Note that the source current \hat{J}_s has been assumed to be zero. The carat over the electric and magnetic fields now indicates that they are both phasors (with RMS amplitudes) while the “carat” over the dielectric constant indicates that it represents a “complex relative dielectric constant,” $\epsilon_r - j\sigma/\omega$, which includes both conduction and displacement currents. The most relevant fact here is that (6.1.9) can be used to determine whether a material behaves more like a conductor or more like an insulator.

For the problems discussed here, there are no free charge sources within the materials (i.e., all charges exist on the surfaces) so that

$$\nabla \bullet \hat{D} = \nabla \bullet \hat{E} = 0 \quad (6.1.10)$$

and, again the potential satisfies Laplace’s equation

$$\nabla^2 \hat{\psi} = 0 \quad (6.1.11)$$

In this case, the potential is a phasor and has an RMS amplitude. For the problems considered here, the magnetic field in (6.1.9) can generally be neglected. More detailed information about the validity of this electroquasistatic approximation is available in Haus and Melcher (1989).

Finally, again

$$\hat{E} = -\nabla \hat{\psi} \quad (6.1.12)$$

The boundary conditions that will be used here are generalizations of (6.1.5) – (6.1.7) where the dielectric constants in (6.1.7) are replaced with the complex dielectric constants.

There are many closed form solutions to Laplace’s equation for very simple geometries that are well known and introduced in undergraduate electromagnetics courses (e.g., point charge source, line charge source, coaxial cable, infinite parallel plate capacitor). These are useful for both understanding the nature of solutions to Laplace’s equation and as limiting cases to check the accuracy of numerical solutions. Many examples of problems with more complex geometries that still have analytical closed form

⁵² Here the carat symbol of the dielectric constant $\hat{\epsilon}$ indicates a complex number rather than a phasor.

solutions can be found in the literature (Schwab 1998). Several will be introduced here. However, for most complicated geometries, it is necessary to use numerical methods to solve Laplace's equation. In the final section of this chapter, short introductions to several numerical methods for solving Laplace's equation subject to simple boundary conditions will be given along with references for further study.

6.2 Analytical Solutions

Simple shapes (parallel planes, coaxial cylinders, sphere)

The simplest geometry in which to solve Laplace's equation is that of parallel conducting planes as shown in Fig. 6.2.1. Note that this is a one dimensional problem⁵³ given the symmetry in the x and z directions. Given this, it can be assumed that the solution to Laplace's equation does not vary with x or z.

Hence (6.1.4) expressed in rectangular coordinates can be written as

$$\left(\frac{\partial^2}{\partial x^2} + \frac{\partial^2}{\partial y^2} + \frac{\partial^2}{\partial z^2} \right) \hat{\psi}(x, y, z) = \frac{\partial^2}{\partial y^2} \hat{\psi}(y) = 0 \quad (6.2.1)$$

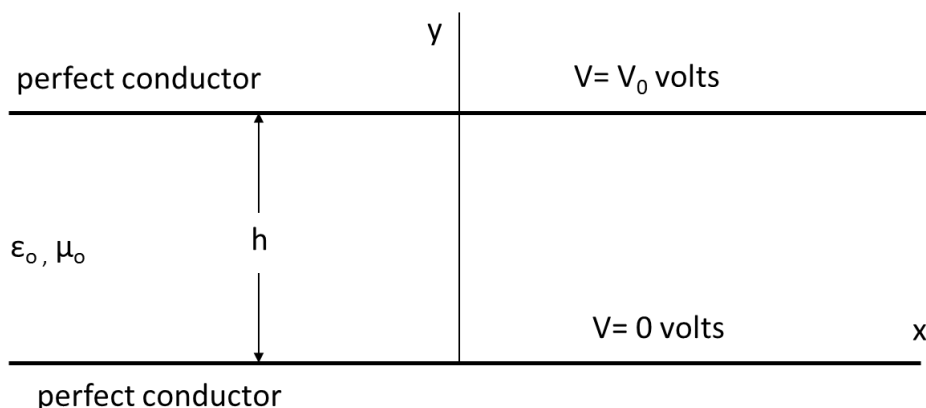


Fig. 6.2.1 The parallel plate geometry (the coordinate z is directed into the page).

Integrating this equation twice with respect to y yields

$$\hat{\psi}(y) = Ay + B \quad (6.2.2)$$

The application of the $V = 0$ boundary condition at $y = 0$ requires that $B = 0$. The remaining $V = 100$ volt boundary condition at $y = h$ requires that $A = 100/h$. The final result is

⁵³ Often one or two dimensional problems are useful approximations to real three dimensional problems in local regions for which the geometry is approximately one or two dimensional.

$$\hat{\psi}(y) = \frac{V_0 y}{h} \quad (6.2.3)$$

The electric field can be determined using (6.1.12) and is

$$\hat{E}_y = -\frac{\partial \hat{\psi}}{\partial y} = -\frac{V_0}{h} \quad (6.2.4)$$

Then, using (6.1.6) (generalized to time varying fields), the charge density on the top plate can be determined to be

$$\hat{\rho}_s = \epsilon_0 \hat{E}_y \cdot \bar{n} = \epsilon_0 \hat{E}_y \cdot (-\bar{a}_y) = \epsilon_0 \frac{V_0}{h} \quad (6.2.5)$$

Finally, the capacitance per unit area of this parallel plate capacitor can be found as

$$C_{pp} = \frac{\hat{\rho}_s}{\hat{\psi}(h)} = \frac{\epsilon_0}{h} \quad (6.2.6)$$

Another simple geometry in which Laplace's equation can easily be solved is that of coaxial conducting cylinders as shown in Fig. 6.2.2.

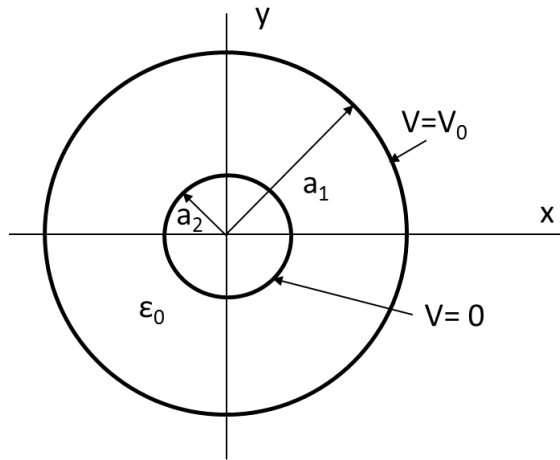


Fig. 6.2.2 The coaxial cylinder geometry (the coordinate z is directed into the page).

Since by symmetry it can be assumed that the solution to Laplace's equation does not vary with ϕ or z , (6.1.3) expressed in cylindrical coordinates can be written as

(6.2.7)

$$\left(\frac{1}{\rho} \frac{\partial}{\partial \rho} \left(\rho \frac{\partial}{\partial \rho} \right) + \frac{1}{\rho^2} \frac{\partial^2}{\partial \phi^2} + \frac{\partial^2}{\partial z^2} \right) \hat{\psi}(\rho, \phi, z) = \frac{1}{\rho} \frac{\partial}{\partial \rho} \left(\rho \frac{\partial}{\partial \rho} \right) \hat{\psi}(\rho) = 0$$

Multiplying (6.2.7) by ρ and integrating with respect to ρ yields

$$\left(\rho \frac{\partial}{\partial \rho} \right) \hat{\psi}(\rho) = A \quad (6.2.8)$$

Dividing by ρ and integrating again with respect to ρ yields

$$\hat{\psi}(\rho) = A \int \frac{d\rho}{\rho} = A \ln(\rho) + B \quad (6.2.9)$$

Matching the boundary condition at $\rho = a_2$ yields

$$B = -A \ln(a_2) \quad (6.2.10)$$

Finally, matching the boundary condition at $\rho = a_1$ yields

$$\hat{\psi}(\rho) = V_0 \frac{\ln(\rho/a_2)}{\ln(a_1/a_2)} \quad a_2 \leq \rho \leq a_1 \quad (6.2.11)$$

As before, it is possible to calculate the electric field as

$$\hat{E}_\rho = -\frac{\partial \hat{\psi}}{\partial \rho} = -\frac{V_0}{\rho \ln(a_1/a_2)} \quad (6.2.12)$$

The corresponding charge per unit length on the inner conductor (identical to that on the outer conductor) for this coaxial geometry is

$$\hat{\rho}_\ell = 2\pi a_2 \varepsilon_0 \hat{E}_\rho \cdot \bar{n} = 2\pi a_2 \varepsilon_0 \hat{E}_\rho \cdot \bar{a}_\rho = \varepsilon_0 \frac{2V_0 \pi}{\ln(a_1/a_2)} \quad (6.2.13)$$

Finally, the capacitance per unit length for this coaxial capacitor is

$$C_{\text{coax}} = \frac{\hat{\rho}_s}{\hat{\psi}(a_1)} = \varepsilon_0 \frac{2\pi}{\ln(a_1/a_2)} \quad (6.2.14)$$

A final simple example is that of a spherical capacitor as shown in Fig. 6.2.3

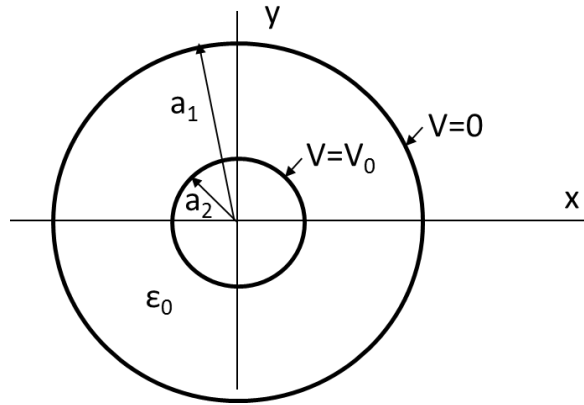


Fig. 6.2.3 The sphere geometry.

Since it can be assumed that the solution to Laplace's equation does not vary with θ or φ (6.1.3) expressed in spherical coordinates can be written as

(6.2.15)

$$\begin{aligned} & \left(\frac{1}{r^2} \frac{\partial}{\partial r} \left(r^2 \frac{\partial}{\partial r} \right) + \frac{1}{r^2 \sin(\theta)} \frac{\partial}{\partial \theta} \left(\sin(\theta) \frac{\partial}{\partial \theta} \right) + \frac{1}{r^2 \sin^2(\theta)} \frac{\partial^2}{\partial \varphi^2} \right) \hat{\psi}(r, \theta, \phi) \\ & = \frac{1}{r^2} \frac{\partial}{\partial r} \left(r^2 \frac{\partial}{\partial r} \right) \hat{\psi}(r) = 0 \end{aligned}$$

Multiplying (6.2.15) by r^2 and integrating yields

$$\left(r^2 \frac{\partial}{\partial r} \right) \hat{\psi}(r) = A \quad (6.2.16)$$

Dividing by r^2 and integrating again yields

$$\hat{\psi}(r) = A \int \frac{dr}{r^2} = \frac{A}{r} + B \quad (6.2.17)$$

Matching the boundary condition that the potential must be $= 0$ as $r \rightarrow a_1$ yields

$$B = -\frac{A}{a_1} \quad (6.2.18)$$

Finally, matching the boundary condition at $r = a_2$ yields

$$A = \frac{V_0 a_1 a_2}{a_1 - a_2} . \quad (6.2.19)$$

Thus,

$$\hat{\psi}(r) = V_0 \frac{a_1 a_2}{a_1 - a_2} \left(\frac{1}{r} - \frac{1}{a_1} \right) \quad (6.2.20)$$

The electric field is

$$\hat{E}_r = -\frac{\partial \hat{\psi}}{\partial r} = \left(\frac{V_0 a_1 a_2}{a_1 - a_2} \right) \frac{1}{r^2} \quad (6.2.21)$$

The total charge on the inner sphere (same as on the outer sphere) is

$$\hat{\rho}_{sphere} = 4\pi a_2^2 \epsilon_0 \hat{E}_r(a_2) = 4\pi \epsilon_0 \left(\frac{V_0 a_1 a_2}{a_1 - a_2} \right) \quad (6.2.22)$$

Finally, the capacitance of the spherical capacitor is

$$C_{sphere} = \frac{\hat{\rho}_{sphere}}{\hat{V}(a_2)} = 4\pi \epsilon_0 \left(\frac{a_1 a_2}{a_1 - a_2} \right) \quad (6.2.23)$$

A useful special case is the capacitance of an isolated sphere that is the limit as $a_1 \rightarrow \infty$. It is

$$C_{isolated\ sphere} = \frac{\hat{\rho}_{sphere}}{\hat{V}(a_2)} = 4\pi \epsilon_0 a_2 \quad (6.2.24)$$

Note that for all of these capacitances (i.e., parallel plate, coaxial and sphere), the capacitance for the case with free space replaced by a dielectric material can be solved by multiplying the solution by ϵ_r .

Imaging in conductors and dielectrics

A very convenient tool for electroquasistatics is image theory. This is illustrated by considering a point charge at a distance y_q above a perfectly conducting plane as illustrated in Fig. 6.2.4⁵⁴. It can be shown that the electric fields in the region $y > 0$ can be computed by replacing the conductor with a point charge of equal and opposite sign at $y = -y_q$. More specifically, this can be shown by calculating the tangential electric field at $y = 0$ from the

⁵⁴ By superposition of charges along the line $(x, y) = (0, y_q)$ with $-\infty < z < \infty$, the image theory results for a point charge can be extended to a line charge with line charge density q_l .

charge and its image and demonstrating that it is zero as required for a perfect conductor. By the uniqueness theorem, then, (since all necessary boundary conditions are satisfied) this is the only solution.

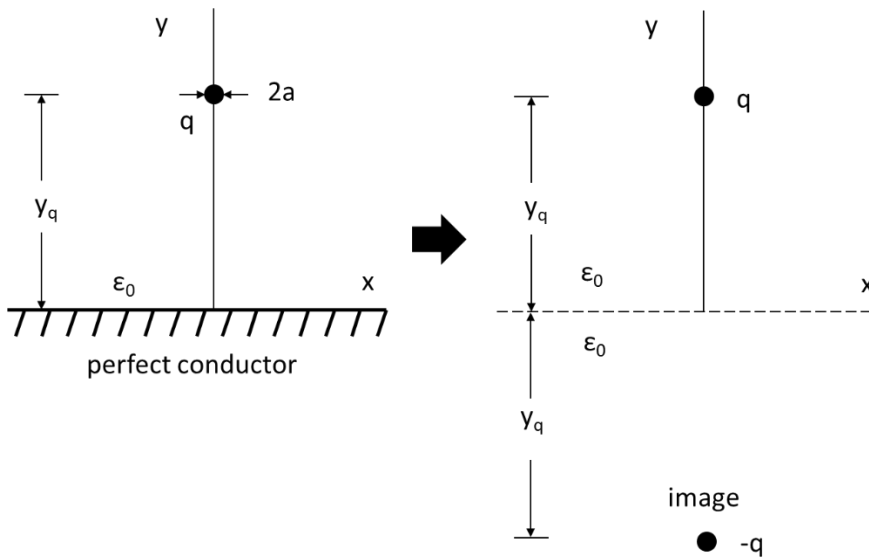


Fig. 6.2.4. Replacing a flat perfectly conducting interface with an image charge. The result is valid for $y > 0$.

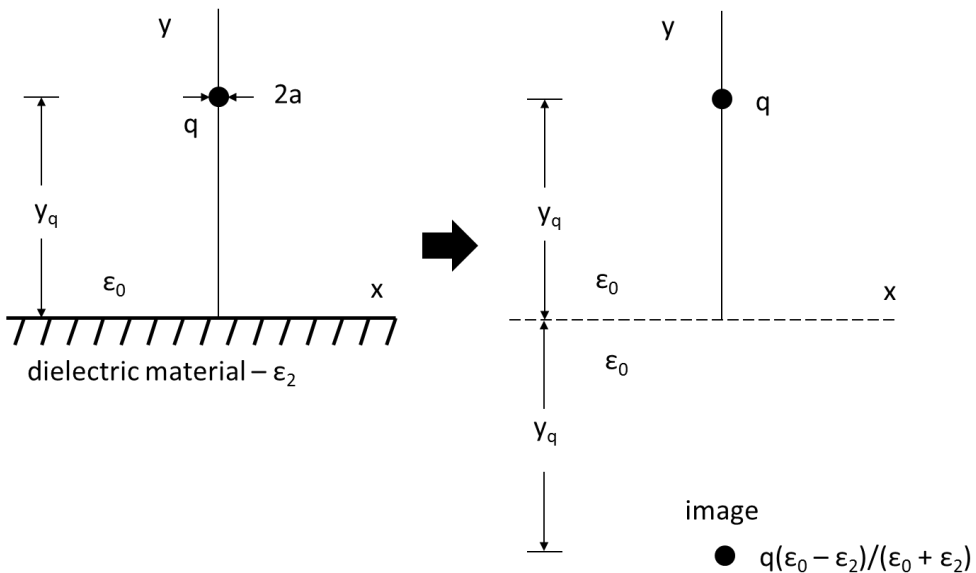


Fig. 6.2.5. Replacing a flat dielectric-dielectric interface with an image charge. The result is valid for $y > 0$. The material can be a pure dielectric as shown or a lossy material with a complex dielectric constant, $\epsilon_0 \hat{\epsilon}_r = \epsilon_0 \epsilon_r - j\sigma/(\omega\epsilon_0)$.

A similar result can be obtained for a charge in the presence of an infinite dielectric half space as illustrated in Fig. 6.2.5. The only difference is that the image now has a value that depends upon the dielectric constant.

The image charge is (for general lossy material)

$$\frac{(\epsilon_0 - \hat{\epsilon}_2)}{(\epsilon_0 + \hat{\epsilon}_2)} q \quad (6.2.25)$$

A similar result can be found that is valid for $y < 0$. This is illustrated in Fig. 6.2.6.

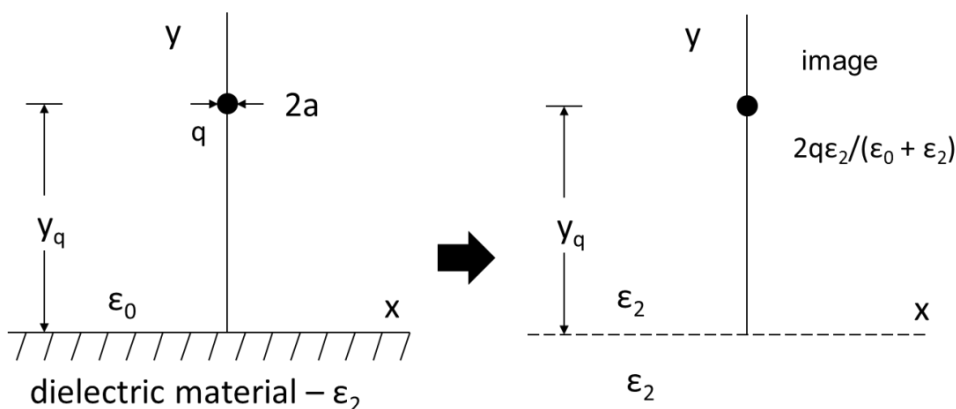


Fig. 6.2.6. Replacing a flat dielectric-dielectric interface with an image charge. The result is valid for $y < 0$. Again, the material can be a pure dielectric as shown or a lossy material with a complex dielectric constant, $\epsilon_0 \hat{\epsilon}_r = \epsilon_0 \epsilon_r - j\sigma/(\omega\epsilon_0)$.

The image charge for general lossy material is

$$\frac{2\hat{\epsilon}_2}{(\epsilon_0 + \hat{\epsilon}_2)} q \quad (6.2.26)$$

Again, this result can be proven by showing that the tangential electric field just above $y = 0$ in region 1 is identical to the tangential electric field just below $y = 0$ in region 2. By the uniqueness theorem, then, (since all necessary boundary conditions are satisfied) this is the only solution.

Spherical shell for quasi-electrostatic shielding

Consider the shell structure that is shown in Fig. 6.2.7. The shell is of inner and outer radius a_2 and a_1 , (i.e., a thickness $(a_1 - a_2)$) and a complex relative dielectric constant $\hat{\epsilon}_r$. The shell is immersed in a uniform vertical electric field of amplitude \hat{E}_0 .

Given the symmetry, the solution for the potential must be independent of ϕ . Given this, Laplace's equation (from 6.2.15) reduces to

$$\left(\frac{1}{r^2} \frac{\partial}{\partial r} \left(r^2 \frac{\partial}{\partial r} \right) + \frac{1}{r^2 \sin(\theta)} \frac{\partial}{\partial \theta} \left(\sin(\theta) \frac{\partial}{\partial \theta} \right) \right) \hat{\psi}(r, \theta) = 0 \quad (6.2.27)$$

Using separation of variables (Smythe 1968), it can be shown that a general solution to (6.2.27) is of the form (This result can be verified by direct substitution of (6.2.28) into (6.2.27).)

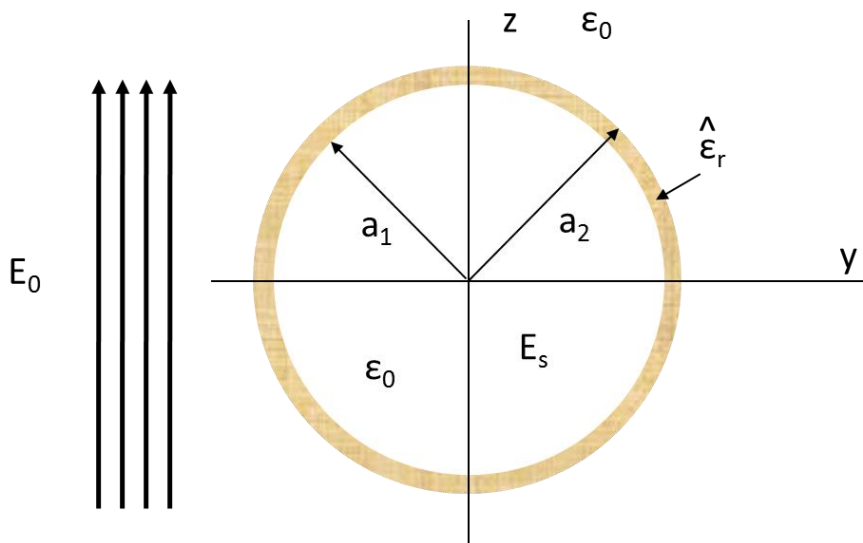


Fig. 6.2.7 A thin spherical shell immersed in a uniform electric field.

$$\hat{\psi}(r, \theta) = (Br + C/r^2) \cos(\theta) \quad (6.2.28)$$

Given this, solutions to Laplace's equation that are valid in each region of the problem are:

$$\begin{aligned} \hat{\psi}(r, \theta) &= Ar \cos(\theta), & r \leq a_1 \\ &= (Br + C/r^2) \cos(\theta), & a_1 \leq r \leq a_2 \\ &= (Dr + F/r^2) \cos(\theta), & a_2 \leq r \end{aligned} \quad (6.2.29)$$

Note that in the region, $r \leq a_1$, the term proportional to $1/r$ is dropped because it would result in a nonphysical singularity at $r = 0$. The constants A – F are to be determined by applying boundary conditions in (6.1.7) that are generalized to the electroquasistatics case. To do this, it is necessary to calculate the normal derivative of the potential (i.e., the electric field). This is

$$\begin{aligned}
\hat{E} &= -\nabla \hat{\psi} = -A(\bar{a}_R \cos\theta - \bar{a}_\theta \sin\theta) = -A\bar{a}_z, & r \leq a_1 \\
&= -(B - 2C/r^3)\cos\theta \bar{a}_R + (B + C/r^3)\sin\theta \bar{a}_\theta, & a_1 \leq r \leq a_2 \quad (6.2.30) \\
&= -(D - 2F/r^3)\cos\theta \bar{a}_R + (D + F/r^3)\sin\theta \bar{a}_\theta, & a_2 \leq r
\end{aligned}$$

To match the field for $r \gg a_2$,

$$D = -\hat{E}_0 \quad (6.2.31)$$

Applying the boundary conditions at a_1 and a_2 results in

$$\begin{vmatrix} a_1^3 & -a_1^3 & -1 & 0 \\ 0 & a_2^3 & 1 & -1 \\ a_1^3 & -\hat{\epsilon}_r a_1^3 & 2\hat{\epsilon}_r & 0 \\ 0 & \hat{\epsilon}_r a_2^3 & -2\hat{\epsilon}_r & 2 \end{vmatrix} \begin{vmatrix} A \\ B \\ C \\ F \end{vmatrix} = \begin{vmatrix} 0 \\ -\hat{E}_0 a_2^3 \\ 0 \\ -\hat{E}_0 a_2^3 \end{vmatrix} \quad (6.2.32)$$

These equations can be solved for A to get

$$A = \frac{-9\hat{\epsilon}_r E_0}{(2 + \hat{\epsilon}_r)(1 + 2\hat{\epsilon}_r) - 2(1 - \hat{\epsilon}_r)^2} \delta \quad (6.2.33)$$

where

$$\delta = \frac{a_1^3}{a_2^3} \quad (6.2.34)$$

Note that as $a_1 \rightarrow a_2$, $A \rightarrow -E_0$ as it should because for $\delta = 1$, no shell exists. Using (6.2.32) and (6.2.33),

$$B = \frac{(1 + 2\hat{\epsilon}_r)A}{3\hat{\epsilon}_r} = \frac{-3(1 + 2\hat{\epsilon}_r)E_0}{(2 + \hat{\epsilon}_r)(1 + 2\hat{\epsilon}_r) - 2(1 - \hat{\epsilon}_r)^2} \delta \quad (6.2.35)$$

If $a_1 \rightarrow 0$, the field inside the shell should reduce to that which is inside a solid dielectric sphere immersed in a uniform electric field. For this case, (i.e., $a_1 = 0$, $\delta \rightarrow 0$)⁵⁵

$$B = \frac{-3E_0}{(2 + \hat{\epsilon}_r)} \quad (6.2.36)$$

Hence the electric field in the center of the homogeneous sphere is

⁵⁵ In this case, C must equal zero. If not, then there would be a singularity in the electric field at $R = 0$.

$$\bar{E} = \frac{3E_0}{(2 + \hat{\epsilon}_r)} \hat{a}_z \quad (6.2.37)$$

This result is in agreement with that of (Zahn, 1979) and has (for example) been used to estimate the electric field shielding of a house. It is also interesting to note that the potential outside of the sphere is modified and can be written once an explicit expression for F is found.

Ring surrounding a conductor ◀

In some cases, it is useful to examine the effect of a tower window on the electrostatic fields of a power line conductor (Olsen 1999). One model that has been used to do this is shown in Fig. 6.2.8. Here a tower window is modeled by a conducting toroid of major radius b and minor radius c at zero potential (Smythe, 1968)⁵⁶. The phase conductor is modeled as a horizontal cylinder of radius a at a potential V_P in free space.

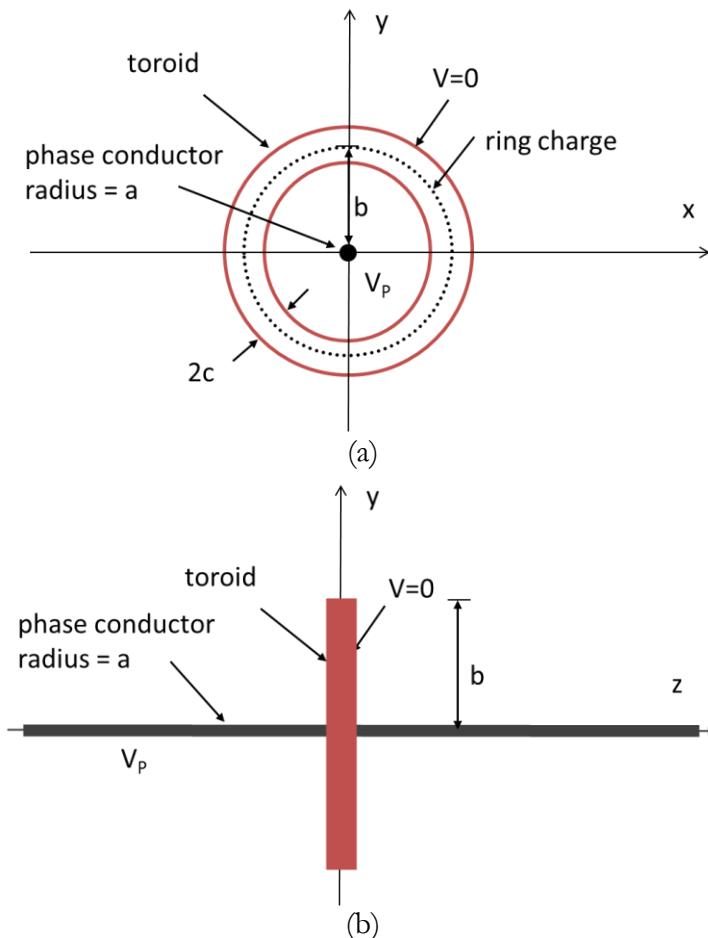


Fig. 6.2.8 Simple model of a tower window a) end view b) side view.

⁵⁶ In Olsen (1999) a perfectly conducting earth was added. Here, that is neglected in order to retain perfect symmetry.

The total scalar electric potential (a phasor) $\hat{\psi}(\rho, z)$, in space is independent of ϕ and is the superposition of that due to charge on the toroid plus that due to the charge distribution on the phase conductor. It will be assumed here that the potential outside the toroid can be approximated as that of a ring charge of radius b in the $\varepsilon = 0$ plane and centered at $\rho = 0$ as shown in Fig 6.2.8a. Similarly, it will be assumed that the potential of the phase conductor charge distribution can be represented as that of a line charge at the center of the ring. Thus, the total potential is

$$\hat{\psi}(\rho, z) = \hat{\psi}^{ring}(\rho, z) + \hat{\psi}^{line}(\rho, z) \quad (6.2.38)$$

It is convenient to solve this problem by spatially Fourier transforming the z dependence of the scalar potential. In the spatial Fourier transform domain (γ) the scalar potential of the ring charge is (for $\rho < b$) (Smythe 1968)

$$\hat{\Psi}^{ring}(\rho, \gamma) = \hat{q}_R b K_0(\gamma b) I_0(\gamma \rho) \quad \rho < (b-c) \quad (6.2.39)$$

where q_R is the magnitude of the ring charge density, $I_0(w)$ and $K_0(w)$ are respectively Modified Bessel functions of first and second kind of zero order and argument w (Abramowitz and Stegun 1964), and

$$\rho = \sqrt{x^2 + y^2} .$$

The Fourier Transform is defined as

$$\hat{\Psi}(\rho, \gamma) = \int_{-\infty}^{\infty} \hat{\psi}(\rho, z) \exp(-j\gamma z) dz . \quad (6.2.40)$$

It has been assumed here that the ring charge density is a constant due to symmetry.

In a similar way, the Fourier transformed scalar potential of a line charge parallel to the z axis and passing through $(x,y) = (0,0)$ with an unknown charge density distribution $q_L(z)$, for $\rho > a_p$ is:

$$\hat{\Psi}^{line}(\rho, \gamma) = \hat{Q}_L(\gamma) K_0(\gamma \rho) \quad (6.2.41)$$

where $\hat{Q}_L(\gamma)$ is the Fourier transform of $\hat{q}_L(z)$. Note that $\hat{q}_L(z)$ is not constant because of the presence of the tower. The total Fourier transformed scalar potential is then

$$\hat{\Psi}(\rho, \gamma) = \hat{\Psi}^{ring}(\rho, \gamma) + \hat{\Psi}^{line}(\rho, \gamma) \quad (6.2.42)$$

The inverse Fourier transform of (6.2.42) represents the total potential due to the conductor in the presence of a concentric toroidal conductor. The charge density of the line charge can be found in terms of the ring charge density by matching the electric potential boundary condition (i.e., $\hat{\psi}(z) = V_P$) at the surface of the wire. Assuming that the wire is thin, it is reasonable to do this at a single point. Thus,

$$\hat{\psi}(a, z) = \hat{\psi}^{ring}(a, z) + \hat{\psi}^{line}(a, z) = V_P \quad (6.2.43)$$

Taking the Fourier transform of (6.2.43) yields

$$\begin{aligned} \hat{\Psi}(a, \gamma) &= \hat{\Psi}^{ring}(a, \gamma) + \hat{\Psi}^{line}(a, \gamma) = V_P \delta(\gamma) \\ &= \hat{q}_R b K_0(\gamma b) I_0(\gamma a) + \hat{Q}_L(\gamma) K_0(\gamma a) = V_P \delta(\gamma) \end{aligned} \quad (6.2.44)$$

where $\delta(\gamma)$ is the Dirac delta function. Hence,

$$\hat{Q}_L(\gamma) = \frac{V_P \delta(\gamma)}{K_0(\gamma a)} - \frac{b K_0(\gamma b) I_0(\gamma a)}{K_0(\gamma a)} \hat{q}_R \quad (6.2.45)$$

so that

$$(6.2.46)$$

$$\hat{\Psi}(\rho, \gamma) = \hat{q}_R b K_0(\gamma b) \left[\frac{K_0(\gamma a) I_0(\gamma \rho) - I_0(\gamma a) K_0(\gamma \rho)}{K_0(\gamma a)} \right] + \frac{V_P K_0(\gamma \rho)}{K_0(\gamma a)} \delta(\gamma), \quad a < \rho < b-c$$

(6.2.46) can now be converted back into the spatial domain by taking the inverse Fourier transform to get

$$(6.2.47)$$

$$\hat{\psi}(\rho, z) = \frac{\hat{q}_R b}{2\pi} \int_{-\infty}^{\infty} \frac{K_0(\gamma b) [K_0(\gamma a) I_0(\gamma \rho) - I_0(\gamma a) K_0(\gamma \rho)]}{K_0(\gamma a)} \exp(j\gamma z) d\alpha + \frac{a V_P}{\rho}, \quad a < \rho < b-c$$

where $K_0(x) \cong -\ln(x)$, $x \ll 1$ and L'Hospital's rule was used to evaluate the limit of the ratio of the modified Bessel functions as $\gamma \rightarrow 0$. To complete the solution to the problem, the following boundary condition is applied in order to determine \hat{q}_R .

$$\psi(b - c, 0) = 0 \quad (6.2.48)$$

Using this boundary condition, the following simple closed form solution for the ring charge density can be written as.

$$\hat{q}_R = \frac{-2\pi V_p}{b \left[\int_{-\infty}^{\infty} \frac{K_0(\gamma b) [K_0(\gamma a) I_0(\gamma(b-c)) - I_0(\gamma a) K_0(\gamma(b-c))] d\gamma}{K_0(\gamma a)} \right]} \quad (6.2.49)$$

(6.2.49) can be used in (6.2.47) along with the gradient operation to calculate the z-directed electric field at any point for which $\rho < (b-c)$. This axial electric field can now be written as.

$$\hat{E}_z(\rho, z) = -\frac{\partial \hat{\psi}(\rho, z)}{\partial z} = \frac{j\hat{q}_R b}{2\pi} \int_{-\infty}^{\infty} \frac{\gamma K_0(\gamma b) [K_0(\gamma a) I_0(\gamma \rho) - I_0(\gamma a) K_0(\gamma \rho)]}{K_0(\gamma a)} \exp(j\gamma z) d\gamma \quad (6.2.50)$$

$\hat{E}_z(\rho, z)$ is negligible beyond $z \approx 4b$ since the tower window causes the non-zero axial field. This is approximately the distance beyond which the tower can be ignored when calculating electric field and for which a two dimensional approximation to the fields is reasonable.

By calculating the charge distribution on the conductor this result can also be used to find the excess capacitance due to the tower. If this capacitance is comparable to the capacitance per unit length of the transmission line multiplied by the distance between towers, then it would become an important part of the propagation model for a power line. It usually is not comparable and hence towers are usually ignored.

Non-infinite parallel plate capacitor ◀

Next, consider the case for a two dimensional parallel plate capacitor with plate spacing of $2b$ as shown in Fig. 6.2.9. The capacitor extends to infinity to the left but ends at $x = -b/\pi$. The upper conductor is held at a voltage V_0 and the lower at a voltage $-V_0$. Hence the axis $y = 0$ is at zero potential by symmetry.

This problem can be solved using conformal mapping methods (Schinzinger and Laura, 2003). Here, the approach will be to take the known solution and show that it satisfies the required boundary conditions. To this end, V_0 is set equal to π volts and two functions $u(x,y)$ and $v(x,y)$ are defined implicitly as

$$x(u, v) = \left(\frac{h}{\pi}\right)(u + e^u \cos v) \quad (6.2.51)$$

$$y(u, v) = \left(\frac{h}{\pi}\right)(v + e^u \sin v) \quad (6.2.52)$$

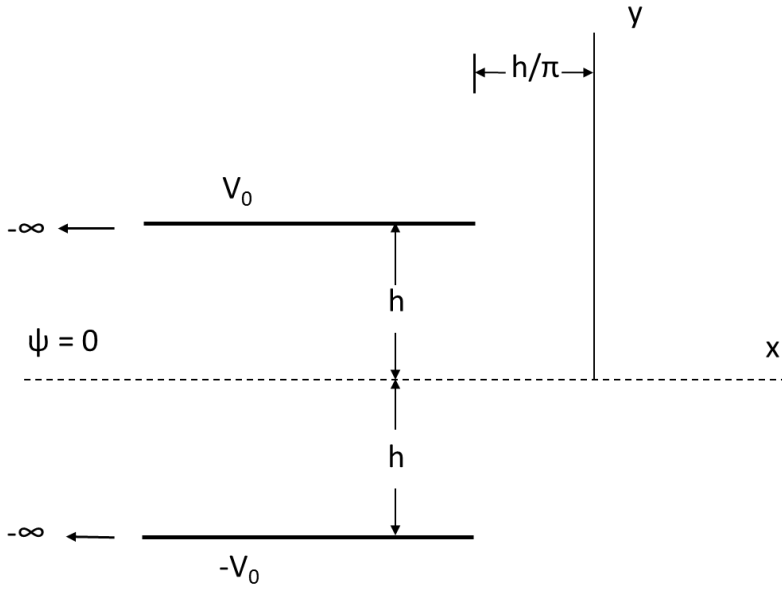


Fig. 6.2.9 Semi-infinite parallel plate capacitor with plate spacing of $2h$

In the next few steps, it will be shown that (6.2.51) and (6.2.52) are both solutions to Laplace's equation in two dimensions. To do this, partial derivatives can be taken with respect to x and y .

$$\frac{\partial(x)}{\partial x} = 1 = \left(\frac{h}{\pi}\right) \left[\frac{\partial u}{\partial x} + e^u \left(\frac{\partial u}{\partial x}\right) \cos v - e^u \left(\frac{\partial v}{\partial x}\right) \sin v \right] \quad (6.2.53)$$

$$\frac{\partial(x)}{\partial y} = 0 = \left(\frac{h}{\pi}\right) \left[\frac{\partial u}{\partial y} + e^u \left(\frac{\partial u}{\partial y}\right) \cos v - e^u \left(\frac{\partial v}{\partial y}\right) \sin v \right] \quad (6.2.54)$$

$$\frac{\partial(y)}{\partial x} = 0 = \left(\frac{h}{\pi}\right) \left[\frac{\partial v}{\partial x} + e^u \left(\frac{\partial u}{\partial x}\right) \sin v + e^u \left(\frac{\partial v}{\partial x}\right) \cos v \right] \quad (6.2.55)$$

$$\frac{\partial(y)}{\partial y} = 1 = \left(\frac{h}{\pi}\right) \left[\frac{\partial v}{\partial y} + e^u \left(\frac{\partial u}{\partial y}\right) \sin v + e^u \left(\frac{\partial v}{\partial y}\right) \cos v \right] \quad (6.2.56)$$

Now, adding (6.2.54) and (6.2.55) gives

$$\left(\frac{\partial u}{\partial y} + \frac{\partial v}{\partial x}\right)(1 + e^u \cos v) + \left(\frac{\partial u}{\partial x} - \frac{\partial v}{\partial y}\right)e^u \sin v = 0 \quad (6.2.57)$$

Subtracting (6.2.56) from (6.2.53) gives

$$\left(\frac{\partial u}{\partial x} - \frac{\partial v}{\partial y}\right)(1 + e^u \cos v) - \left(\frac{\partial u}{\partial y} + \frac{\partial v}{\partial x}\right)e^u \sin v = 0 \quad (6.2.58)$$

Multiplying (6.2.57) by $\left(\frac{\partial u}{\partial x} - \frac{\partial v}{\partial y}\right)$ yields

$$\left(\frac{\partial u}{\partial x} - \frac{\partial v}{\partial y}\right)\left(\frac{\partial u}{\partial y} + \frac{\partial v}{\partial x}\right)(1 + e^u \cos v) + \left(\frac{\partial u}{\partial x} - \frac{\partial v}{\partial y}\right)^2 e^u \sin v = 0 \quad (6.2.59)$$

Further, multiplying (6.2.58) by $\left(\frac{\partial u}{\partial y} + \frac{\partial v}{\partial x}\right)$ yields

$$\left(\frac{\partial u}{\partial x} - \frac{\partial v}{\partial y}\right)\left(\frac{\partial u}{\partial y} + \frac{\partial v}{\partial x}\right)(1 + e^u \cos v) - \left(\frac{\partial u}{\partial y} + \frac{\partial v}{\partial x}\right)^2 e^u \sin v = 0 \quad (6.2.60)$$

Next, (6.2.60) can be subtracted from (6.2.59) to get

$$\left[\left(\frac{\partial u}{\partial x} - \frac{\partial v}{\partial y}\right)^2 + \left(\frac{\partial u}{\partial y} + \frac{\partial v}{\partial x}\right)^2\right]e^u \sin v = 0 \quad (6.2.61)$$

Each term in the square bracket must be zero since (6.2.61) must be zero for all values of u and v and because each squared term is positive. Thus,

$$\frac{\partial u}{\partial x} = \frac{\partial v}{\partial y} \quad (6.2.62)$$

$$\frac{\partial u}{\partial y} = -\frac{\partial v}{\partial x} \quad (6.2.63)$$

(6.2.62) and (6.2.63) are the Cauchy-Riemann equations that are given in (C.18) and (C.19) of Appendix C. Given this, it is known that u and v must

be solutions of Laplace's equation as shown in (C.20) and (C.21) of Appendix C. Hence,

$$\frac{\partial^2 u}{\partial x^2} + \frac{\partial^2 u}{\partial y^2} = 0 \quad \text{or} \quad \nabla^2 u = 0 \quad (6.2.64)$$

$$\frac{\partial^2 v}{\partial x^2} + \frac{\partial^2 v}{\partial y^2} = 0 \quad \text{or} \quad \nabla^2 v = 0 \quad (6.2.65)$$

At this point, let

$$\psi(x, y) = V_0 v(x, y) / \pi \quad (6.2.66)$$

where $\psi(x, y)$ is the scalar potential in Fig. 6.2.9 and V_0 and $-V_0$ are the fixed potentials on the top and bottom plates respectively.

If ψ is set to zero in (6.2.66), then $v = 0$ in (6.2.52) and $y = 0$ for any value of u selected. This matches the known potential everywhere along $y = 0$ in Fig. 6.2.9. The value of x then becomes

$$x(u, v) = \left(\frac{h}{\pi} \right) (u + e^u) \quad (6.2.67)$$

Thus, every point $-\infty < u < \infty$ maps into a point on the $-\infty < x < \infty$ axis as shown in Fig. 6.2.10.

If now, v is set equal to π , then (6.2.52) gives $y = h$, but the value of x now becomes

$$x(u, v) = \left(\frac{h}{\pi} \right) (u - e^u) \quad (6.2.68)$$

so that over the range $-\infty < u < \infty$, x ranges from $-\infty$ to a maximum value of $-h/\pi$ and then returns to $-\infty$.

A plot of constant potential contour lines of ψ in (6.2.66) is shown in Fig. 6.2.10 for the top right quadrant of Fig. 6.2.9. It is assumed that the potential of the top and bottom plates are at the potentials V_0 and $-V_0$ respectively. A cursory examination of the equipotential lines in Fig. 6.2.10 indicates that as the spacing of the lines becomes closer, the closer the field point is to the edge at $(x, y) = (-h/\pi, h)$. Of course, the potential must approach V_0 in this case since that is the potential assigned to the electrode. But, the electric field is related to the "change" in potential over some distance. Given this, a closer examination of the electric field near this edge is warranted.

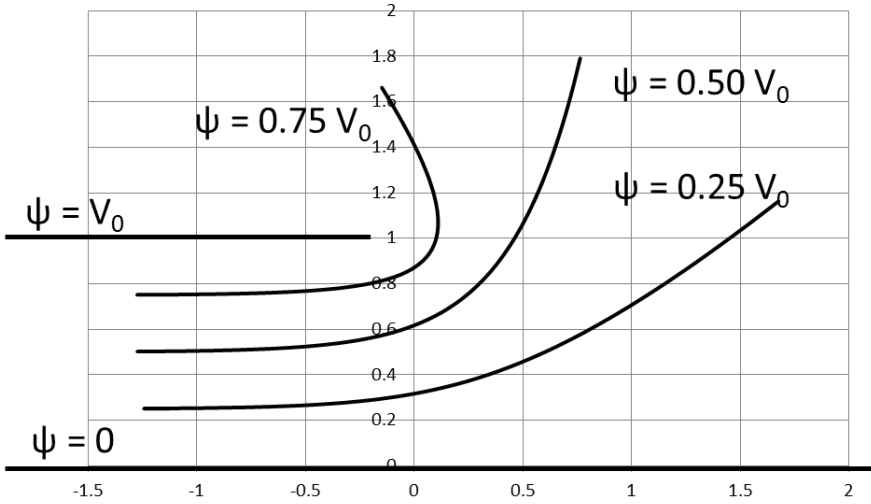


Fig. 6.2.10 Equipotential Lines for the top right hand quarter of Fig. 6.2.9.

Near the edge at $(x,y) = (-h/\pi,h)$, it will be assumed that $v(x,y) \cong V_0 - \varepsilon$ and $u(x,y) \cong \delta$ where $\varepsilon, \delta \ll 1$, (6.2.51) and (6.2.52) can be expanded to second order using Taylor series to get

$$\frac{2\pi}{h} [x(\varepsilon, \delta) + h/\pi] \cong \varepsilon^2 - \delta^2 \quad (6.2.69)$$

$$\frac{2\pi}{h} [y(\varepsilon, \delta) - h] = \varepsilon\delta \quad (6.2.70)$$

According to (6.2.70), δ must be equal to 0 along the line $y = h$ because the potential ψ has been assumed to have a first order variation, hence ε cannot be zero. Given this result, (6.2.69) can be solved to get

$$\varepsilon \cong \sqrt{\frac{2\pi}{h}} [x + h/\pi]^{1/2}. \quad (6.2.71)$$

Hence,

$$\psi(x,h) = \frac{V_0}{\pi} \left(\pi - \sqrt{\frac{2\pi}{h}} [x(\varepsilon,0) + h/\pi]^{1/2} \right) \quad (6.2.72)$$

Finally,

$$E_x(x) = -\frac{\partial}{\partial x} \psi(x,y) = V_0 \sqrt{\frac{1}{2\pi h}} [x + h/\pi]^{-1/2} \quad (6.2.73)$$

This result indicates that the electric field near this sharp edge is unbounded and is the reason why sharp edges are avoided near high voltage components. It is also useful to note here the comments on edge conditions

in the subsection entitled, “edge conditions” at the end of Section 3.6 on the uniqueness theorem. It is situations such as the one here that are relevant to the subject of edge conditions.

The equipotential lines in Fig. 6.2.10 define the shapes for Rogowski electrodes that are used in high voltage components to obtain constant normal electric field over the surface of the electrode (Trinh, 1980). This type of electrode is useful for minimizing the effect of corona.

Although the solution to the semi-infinite parallel plate capacitor problem is useful for illustrating the edge effect, it still represents a non-physical problem due to its infinite size. The solution for a square plate capacitor is only available via numerical computation, but it is useful for a number of reasons including the calibration of electric field meters and references will be given here to this work. More specifically, further work on this problem can found in Shih et. al. (1977), Thatcher (1976) and IEEE (2008).

Separation of variables – infinite series solution to Laplace’s equation in a two dimensional rectangular box

The last problem to be considered in this section is that of finding an “exact” solution of Laplace’s equation within the two dimensional rectangular region shown in Fig. 6.2.11. Part of the purpose for this exercise is to describe the method of separation of variables, a powerful tool that can be used to solve problems in several coordinate systems. Another part is the fact that the exact solution developed here can be used to check the numerical results that have been determined using the methods developed in the next section.

Starting with the two dimensional Laplace’s equation in rectangular coordinates,

$$\left(\frac{\partial^2}{\partial x^2} + \frac{\partial^2}{\partial y^2} \right) \psi(x, y) = 0 \tag{6.2.74}$$

It is assumed that the potential $\psi(x, y)$ can be written as an infinite sum of functions

$$\psi(x, y) = \sum_{n=1}^{\infty} \psi_n(x, y) \tag{6.2.75}$$

where the functions $\psi_n(x, y)$ are also solutions of Laplace’s equation. Next, it is assumed that each function $\psi_n(x, y)$ can be factored into a product of two functions, one a function of x only and the other a function of y only. This property can be written as

$$\psi_n(x, y) = X_n(x)Y_n(y) \tag{6.2.76}$$

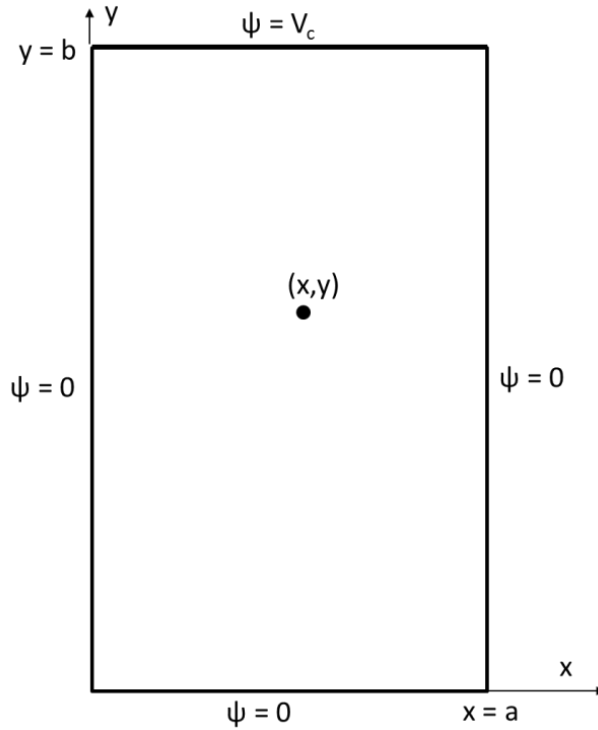


Fig. 6.2.11. Rectangular box of dimensions a and b with $\psi = 0$ on the right, left and bottom sides and $\psi = V_c$ on the top side.

Note that it may not be completely clear at this point why this assumption can be made. However, given that the requirements of the uniqueness theorem can be satisfied by the solution that results, the assumption can be justified a posteriori.

Given this assumption, Laplace's equation can be written as

$$Y_n(y) \frac{\partial^2 X_n(x)}{\partial x^2} + X_n(x) \frac{\partial^2 Y_n(y)}{\partial y^2} = 0 \quad (6.2.77)$$

Dividing both sides of (6.2.77) by $X_n(x)Y_n(y)$ results in

$$\frac{1}{X_n(x)} \frac{\partial^2 X_n(x)}{\partial x^2} = -\frac{1}{Y_n(y)} \frac{\partial^2 Y_n(y)}{\partial y^2} \quad (6.2.78)$$

Clearly, the left hand side of (6.2.78) is a function of x only while the right hand side is a function of y only. Since the equality must hold for all x and y in the domain, each side must be equal to a constant called the "separation" constant. Hence,

$$\frac{d^2 X_n(x)}{dx^2} + \alpha_n^2 X_n(x) = 0 \quad (6.2.79)$$

$$\frac{d^2 Y_n(x)}{dx^2} - \alpha_n^2 Y_n(x) = 0 \quad (6.2.80)$$

where α_n^2 is the separation constant. The solutions to (6.2.79) and (6.2.80) can easily be obtained by using elementary results from differential equations. They are:

$$X_n(x) = A_n \sin(\alpha_n x) + B_n \cos(\alpha_n x) \quad (6.2.81)$$

$$Y_n(x) = C_n \sinh(\alpha_n y) + D_n \cosh(\alpha_n y) \quad (6.2.82)$$

so that

$$(6.2.83)$$

$$\psi_n(x, y) = (A_n \sin(\alpha_n x) + B_n \cos(\alpha_n x))(C_n \sinh(\alpha_n y) + D_n \cosh(\alpha_n y))$$

Application of the boundary condition at $x = 0$ yields

$$(6.2.84)$$

$$\psi(x, y) = \sum_{n=1}^{\infty} B_n (C_n \sinh(\alpha_n y) + D_n \cosh(\alpha_n y)) \quad \text{for all } y \text{ in } [0, b]$$

The only non-trivial solution to this equation is $B_n = 0$ for all n . Now matching the boundary condition at $y = 0$ yields

$$\psi(x, y) = \sum_{n=1}^{\infty} A_n D_n \sin(\alpha_n y) \quad \text{for all } x \text{ in } [0, a] \quad (6.2.85)$$

The only nontrivial solution for this is to set $D_n = 0$. Thus, the remaining terms are:

$$\psi_n(x, y) = A_n \frac{\sin(\alpha_n x) \sinh(\alpha_n y)}{\sinh(\alpha_n b)} \quad (6.2.86)$$

where the separate constant C_n has been set equal to $1/(\sinh(\alpha_n b))$ since there is no need for two separate constants and this will turn out to be a convenient substitution. Thus,

$$\psi(x, y) = \sum_{n=1}^{\infty} A_n \sin(\alpha_n x) \frac{\sinh(\alpha_n y)}{\sinh(\alpha_n b)} \quad (6.2.87)$$

This formulation satisfies the boundary condition $\psi(a, y) = 0$ if $\alpha_n = n\pi/a$ where α_n is an eigenvalue of the differential equations (6.2.79) and (6.2.80) and the functions $\sin(n\pi x/a)$ and $\sinh(n\pi y/a)$ are eigenfunctions of the same equations respectively. The final boundary condition is satisfied at $y = b$ if

$$\psi(x, y) = V_C = \sum_{n=1}^{\infty} A_n \sin(n\pi x/a) \quad \text{for } 0 \leq x \leq a \quad (6.2.88)$$

The values of A_n required to satisfy this condition can be obtained by multiplying (6.2.88) by $\sin(m\pi x/a)$, integrating the result over the period $0 - a$ and using the orthogonality properties of the sine function. More specifically,

$$V_C \int_0^a \sin(m\pi x/a) dx = \sum_{n=1}^{\infty} A_n \int_0^a \sin(n\pi x/a) \sin(m\pi x/a) dx \quad (6.2.89)$$

$$\frac{aV_C}{m\pi} (1 - \cos(m\pi)) = \begin{cases} A_n a/2, & m = n \\ 0, & m \neq n \end{cases}$$

Hence

$$A_n = \frac{2V_C}{m\pi} (1 - \cos(m\pi)) \quad (6.2.90)$$

The final solution is

$$\psi(x, y) = \sum_{n=1}^{\infty} A_n \sin(n\pi x/a) \frac{\sinh(n\pi y/a)}{\sinh(n\pi b/a)} \quad (6.2.91)$$

with A_n given by (6.2.90). The validity of this solution can be verified using the uniqueness theorem (Chapter 3) because the potential satisfies Laplace's equation as well as the known potential (Dirichlet) boundary condition on all sides of the rectangle.

6.3 Numerical Solutions

Introduction

As mentioned in the introduction to this chapter, analytical techniques are useful for both insight and validation of numerical techniques. But, they are restricted to relatively simple geometries and, hence, numerical techniques will have to be used for most problems. The purpose of this section is to briefly introduce the reader to numerical techniques that have been used by the power engineering community to solve problems in electroquasistatics. These include techniques based on boundary source unknowns (i.e., boundary element method and charge simulation method) and field point unknowns (i.e. finite difference method, finite element method and Monte Carlo method). Each has its advantages and disadvantages as indicated throughout the section.

In each case, the numerical method will be introduced in the context of a two dimensional problem for which the computational domain is a finite area in space and involves only known electrical potential boundary conditions. More specifically, the computational domain will be identical to that shown in Fig. 6.2.11. While each of the methods can be extended to both infinite and three dimensional regions and more complicated boundary conditions, these extensions require a) discussions that are beyond the scope of this section and b) obfuscate the basic ideas behind each method.

The boundary element method⁵⁷

The Boundary Element Method (BEM) is designed to solve for the surface charges that are the sources of electrostatic fields (Daffe and Olsen 1979; Olsen 1986; Olsen and Einarsson 1987). Variations of this method have been referred to as the integral equation method, the moment method and the charge simulation method (the latter will be discussed in the following section).

In a two-dimensional homogeneous region of finite size with known potentials on its boundary, it is possible to write solutions of Laplace's equation for points within the region as

$$\hat{\psi}(x, y) = \frac{1}{2\pi\epsilon_0} \int_C \hat{\rho}_s(\ell) \ln\left(\sqrt{(x-x'(\ell))^2 + (y-y'(\ell))^2}\right) d\ell \quad (6.3.1)$$

where C is the perimeter of the region, (x, y) is the location of the field point, $(x'(\ell), y'(\ell))$ is the set of points along the perimeter that represents the locations of the electrical surface charge distribution $\hat{\rho}_s(\ell)$ that is the

⁵⁷ More specifically, the method presented here is called the "Indirect Boundary Element Method" (O'Brien, J. L. and T. L. Geers 1990)

“source” of the potential in the region. The geometry of the rectangular region to which the boundary element method will be applied is illustrated in Fig. 6.3.1.

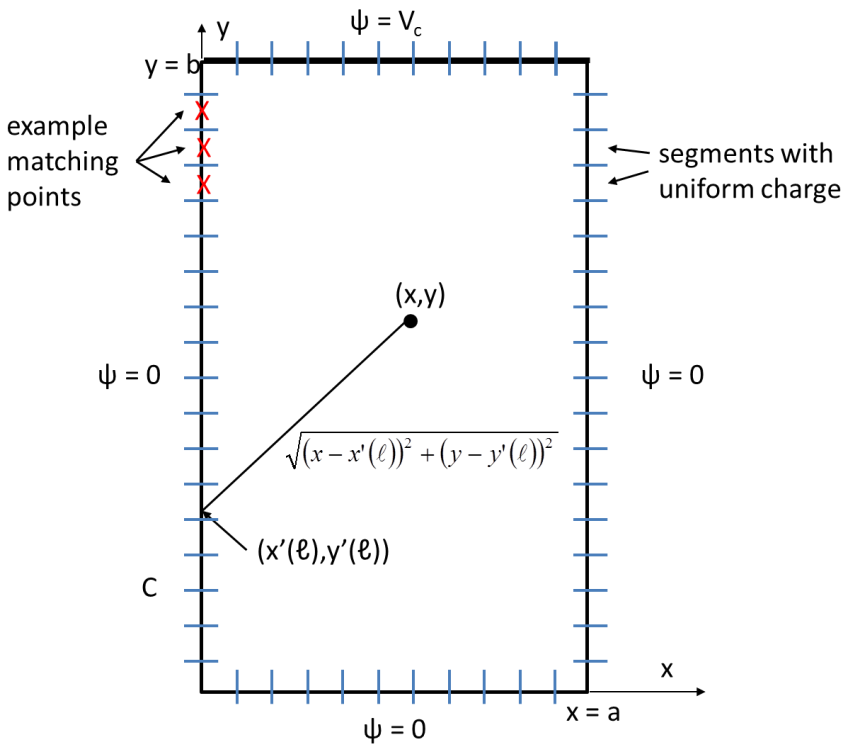


Fig. 6.3.1 Geometry for the boundary element method calculation

It is assumed next that the potential (i.e., voltage with respect to zero = V_B) is known everywhere on the boundary perimeter (C) so that

$$V_B = \frac{1}{2\pi\epsilon_0} \int_C \hat{\rho}_s(\ell) \ln\left(\sqrt{(x - x'(\ell))^2 + (y - y'(\ell))^2}\right) d\ell \quad (6.3.2)$$

where the point (x, y) is now constrained to be on the boundary surface. (6.3.2) is now an inhomogeneous Fredholm equation of the first kind for the unknown charge density on the boundary. An approximation to this charge distribution can be found by discretizing $\hat{\rho}_s(\ell)$ into a set of N unknown charges of constant value but finite extent along the total perimeter. A formula for each source can be written as

$$\hat{\rho}_{sn} f_n(\ell)$$

where $f_n(\ell)$ is equal to 1 on the patch of the perimeter C for which $\hat{q}_{\ell n}$ is the charge density there and the union of all functions $f_n(\ell)$ covers the entire perimeter C. Given this, (6.3.2) can be written

$$V_B = \frac{1}{2\pi\epsilon_0} \sum_{n=1}^N \hat{\rho}_{sn} \int_C f_n(\ell) \ln\left(\sqrt{(x-x'(\ell))^2 + (y-y'(\ell))^2}\right) d\ell \quad (6.3.3)$$

If the potential is “matched” at a distinct point on the surface (x_m, y_m) within each function $f_n(\ell)$, then (6.3.3) becomes

$$V_{Bn} = \frac{1}{2\pi\epsilon_0} \sum_{n=1}^N \hat{\rho}_{sn} \int_C f_n(\ell) \ln\left(\sqrt{(x_m-x'(\ell))^2 + (y_m-y'(\ell))^2}\right) d\ell \quad (6.3.4)$$

where V_{Bn} is the value of the boundary potential at (x_m, y_m) . (6.3.4) is a set of N algebraic equations in N unknowns that (in most cases) can be solved in a relatively straightforward manner. Once the charges are known, the potential at any point within the computational domain can be written using (6.3.1) and the electric field calculated from (6.1.2).

Note that one requirement for the simple implementation mentioned here is that the region be homogeneous. While this is a negative, the number of unknowns is proportional to the perimeter of the boundary and hence generally much smaller than the number of unknowns for field based methods such as the finite element method. While the number of equations is small, the matrix that represents the coefficients of the algebraic equations to be solved is completely filled or “dense.” Given this, techniques used to solve “sparse” matrices that result in field based methods such as the finite element method cannot be used. Another issue that must be considered when implementing the boundary element method is that the integrals in (6.3.4) have singular integrands. While these singularities are integrable, some care must be used when evaluating them.

The charge simulation method

As mentioned above, one problem with the boundary element method just described is that the integrals in (6.3.4) have a singularity in the integrand at points on the surface for which the integrand and matching point coincide. While such an integral can be evaluated, it requires some care.

An alternative approach to the boundary element method is to approximate the surface charges with a set of charges with simple forms but unknown amplitudes located outside the area for which the potential is to be calculated, but close to the surface (Singer et. al. 1974). In this case, line charges are placed just behind the perimeter C. The advantage is that field

calculations are simple and no singular integrals need be evaluated. This approach is called the “charge simulation method.”

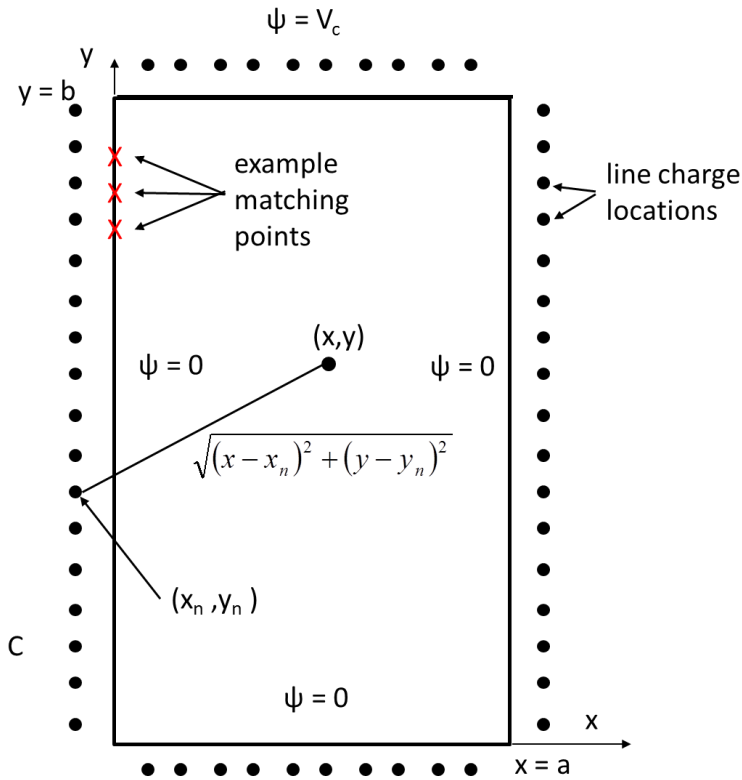


Fig. 6.3.2 The geometry used to illustrate the charge simulation method.

Consider the two dimensional problem shown in Fig. 6.3.2. The perimeter C surrounds the computational domain that extends to infinity in front of and behind the page. The perimeter is at a known potential (V_B) that may vary from point to point along the perimeter.

To implement the charge simulation method in this case, a large number (N) of line charges with amplitude ($\hat{\rho}_{ln}$) are located at (x_n, y_n) close to but behind the surface S . They are far enough away that their contribution to the potential on the nearby portion of the perimeter C can be reasonably constant, but close enough that the actual variation of potential on the surface is reasonably well matched. The electric potential at any point in space from these unknown charges is

$$\hat{\psi}(x, y) = \frac{1}{2\pi\epsilon_o} \sum_{n=1}^N \rho_{ln} \ln\left(\sqrt{(x-x_n)^2 + (y-y_n)^2}\right) \quad (6.3.5)$$

The values of the unknown charges are found by matching the potential on the surface at $M = N$ points (x_m, y_m) on the surface of the rectangle. Given this, N equations for the N unknown charges can be written as

$$(6.3.6)$$

$$\hat{\psi}(x_m, y_m) = V_B = \frac{1}{2\pi\epsilon_0} \sum_{n=1}^N \rho_{\ell n} \ln\left(\sqrt{(x_m - x_n)^2 + (y_m - y_n)^2}\right), \quad 1 \leq m \leq N$$

Once these equations have been solved for the unknown line charge amplitudes, (6.3.5) can be used to find the electric potential at any point in the rectangular computational domain. From this result, the electric field can be found using (6.1.2)

The finite difference method

Laplace's equation can be written in rectangular coordinates as

$$\nabla^2 \hat{\psi}(x, y) = \frac{\partial^2 \psi}{\partial x^2} + \frac{\partial^2 \psi}{\partial y^2} + \frac{\partial^2 \psi}{\partial z^2} = 0 \quad (6.3.7)$$

The partial derivative $\frac{\partial \psi}{\partial x}$ can be approximated as

$$\frac{\partial \psi}{\partial x} \cong \frac{\psi(x + \Delta x/2) - \psi(x - \Delta x/2)}{\Delta x} \quad (6.3.8)$$

where the geometry for (6.3.8) is shown in Fig. 6.3.3

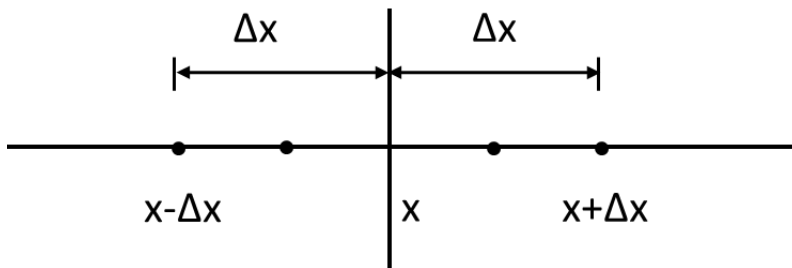


Fig. 6.3.3 Geometry for calculating the numerical derivative.

Using this result

$$\frac{\partial \psi(x - \Delta x/2)}{\partial x} \cong \frac{\psi(x) - \psi(x - \Delta x)}{\Delta x} \quad (6.3.9)$$

and

$$\frac{\partial \psi(x + \Delta x/2)}{\partial x} \cong \frac{\psi(x + \Delta x) - \psi(x)}{\Delta x} \quad (6.3.10)$$

(6.3.9) and (6.3.10) can be combined to yield

$$\frac{\partial^2 \psi}{\partial x^2} \cong \frac{\frac{\partial \psi(x + \Delta x/2)}{\partial x} - \frac{\partial \psi(x - \Delta x/2)}{\partial x}}{\Delta x} \cong \frac{\psi(x + \Delta x) + \psi(x - \Delta x) - 2\psi(x)}{(\Delta x)^2} \quad (6.3.11)$$

Similar expressions can be found for $\frac{\partial^2 \psi}{\partial y^2}$ and $\frac{\partial^2 \psi}{\partial z^2}$.

Next, these finite difference approximations will be applied to the “discretized” two-dimensional rectangular geometry shown in Fig. 6.3.4.

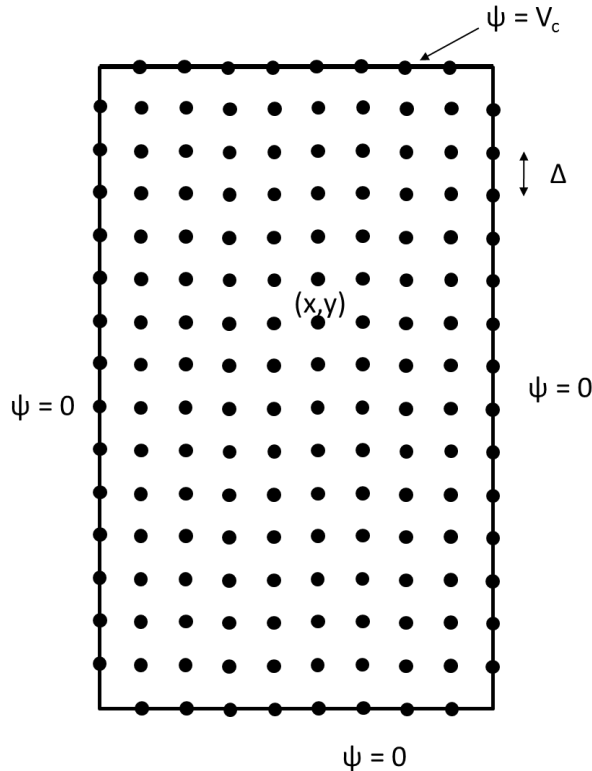


Fig. 6.3.4 Grid for application of the finite difference method.

In this grid, the potential on the top boundary surface is V_c while on the remaining boundary surfaces it is 0. It has also been assumed for the remainder of this derivation that $\Delta x = \Delta y = \Delta$.

At the point (x, y) , the two dimensional Laplace's equation can be written

(6.3.12)

$$\frac{\partial^2 \psi}{\partial x^2} + \frac{\partial^2 \psi}{\partial y^2} \cong \frac{1}{\Delta^2} \{ \psi(x + \Delta, y) + \psi(x - \Delta, y) + \psi(x, y + \Delta) + \psi(x, y - \Delta) - 4\psi(x, y) \} \cong 0$$

or

$$\psi(x, y) \cong \frac{1}{4} \{ \psi(x + \Delta, y) + \psi(x - \Delta, y) + \psi(x, y + \Delta) + \psi(x, y - \Delta) \} \quad (6.3.13)$$

(6.3.13) can be written for every point within the rectangular region in Fig. 6.3.4. For points next to the boundary surface one or more of these potentials is specified because it is on the boundary. A disadvantage of the method is that the number of unknowns is proportional to the area over which the solution is sought. This is in contrast to the two previous methods for which the number of unknowns is proportional to the perimeter of the area for which the solution is sought.

If there are N points at which (6.5.13) is applied, then the result is N algebraic equations in N unknowns. These equations can (usually) be solved in a relatively straightforward manner. Given that each equation refers to only 4 other points, many of the coefficients are zero and there are many methods to accelerate the solution. This partially compensates for the fact that the number of equations is proportional to the area of the rectangle rather than the perimeter.

Another issue with field based methods such as the finite difference method, is that there is an additional error in calculating the electric field. More specifically, to calculate the electric field from knowledge of the potential requires a numerical derivative. This process can introduce significant error. On the other hand, surface based methods such as the boundary element method calculate surface charge from which the electric field can be obtained without differentiation.

The Monte Carlo method

At first, the Monte Carlo method appears to be completely unrelated to the finite difference method, but it is related by the fact that in an electrostatic field the potential at the center of a sphere can be written as the average of the potential over the surface of the sphere (Pickles, 1977; Beasley et. al. 1979). In two dimensions, this is equivalent to the following mathematical statement,

$$V(x, y) = \frac{1}{2\pi a} \int_c V(x(\ell), y(\ell)) d\ell \quad (6.3.14)$$

where (x,y) is at the center of a circle of radius “ a ”, C is the perimeter of the circle and the entire circle is within a Laplacian field.

It is useful to note that (6.3.13) is a specific example of (6.3.14) in two dimensions. But, before making the connection, consider the same geometry as in Fig 6.3.4, but where the top side is assigned the value 1 and the remaining sides assigned the value 0. In a moment, the meanings of these will be described. This geometry is shown in Fig. 6.3.5.

Consider next a “random walk” beginning at (x,y) . Each step of the random walk is of length Δ and each step is in one of four directions; each with equal probability. These are up, right, down and left. The random walk shown in Fig. 6.3.5 eventually ends on the top surface. At the end of any walk that ends on the top, the number one is assigned to it and added to a sum. If, on the other hand, the walk ends on one of the other surfaces, it is assigned a zero and also added to the sum (of course, the sum is not changed by the addition of zero). After a large number of random walks, this sum (divided by the number of random walks) is an estimate of the probability that a random walk will end on the top surface. The larger the number of random walks, the more accurate the estimate.

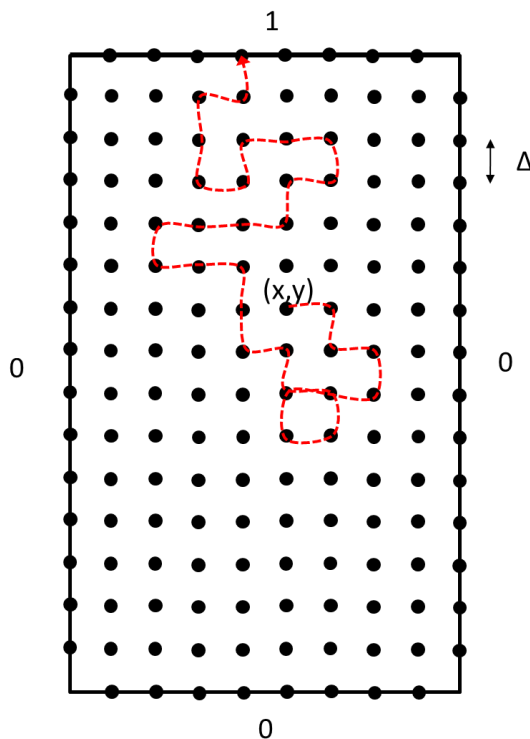


Fig. 6.3.5 A random walk from (x,y) to the top surface.

Now, there is another (and apparently completely different) way of calculating the probability that a random walk ends on the top surface. Consider the probability that a random walk starting at (x,y) ends up at $(x+\Delta,$

y) after the first step. Since by symmetry, it is equally probable that the walk will proceed in any one of the four directions, it can be said that

$$P(x + \Delta, y|x, y) = \frac{1}{4} \tag{6.3.15}$$

This notation is read as, the probability that the random walk which starts at (x,y) proceeds to (x+Δ, y) at the next step of the walk. Since there are only four initial steps that can be taken, and it is assumed that each step of the random walk is selected in a way that is independent of the others, it is possible to write an expression for the probability that the random walk ends on the top as

$$\tag{6.3.16}$$

$$P_{top}(x, y) = \frac{1}{4} \{P_{top}(x + \Delta, y) + P_{top}(x - \Delta, y) + P_{top}(x, y + \Delta) + P_{top}(x, y - \Delta)\}$$

This equation is read, “the probability that the random walk eventually hits the top is equal to the probability that it first goes to the right (i.e., 1/4) and then goes to the top from there plus the probability that it first goes to the left (i.e., 1/4) etc.” This equation holds for every starting point within the region.

What is interesting is that (6.3.16) has exactly the same form as (6.3.13). Hence, it is possible to calculate $P_{top}(x,y)$ by solving a set of linear equations. But, of course, this requires that one solve for all of the probabilities simultaneously. This may be a wasted effort if it is only desired to know the potential at one or a few points. To understand this is to discover the power of the Monte Carlo method. To estimate $P_{top}(x,y)$ using random walks, it is only necessary to calculate this probability at one point.

It can be shown that the error in the estimate of $P_{top}(x,y)$ is proportional to $1/\sqrt{N}$ where N is the number of random walks. Thus, time can be traded for accuracy.

Without going into details, it can be said that there are numerous ways to accelerate the random walk process including the so-called “floating random walk” method. These have been built in to programs to estimate potential in very complicated three-dimensional geometries. The method has been found to be useful when it is only necessary to find a reasonable estimate of the potential or electric field at a small number of points.

The finite element method ◀

As with the earlier summaries, the purpose of this discussion of the finite element method is not to replace the voluminous literature on this method (Zienkiewicz, 1971). Rather, it is to give an intuitive introduction to the method using the relatively simple problem shown in Fig. 6.2.11 of this chapter as context.

The finite element method for electrostatics usually involves a variational method (Zienkiewicz, 1971; Schwab 1988). This means that a “functional” is considered, where a functional is a function of a function (i.e., $F(f(x))$). Often it can be shown that a functional is minimized when the function is the solution of a differential equation such as Laplace’s equation. The functional usually used for identifying solutions to electrostatic problems is the potential energy stored in the field. This functional (in two dimensions to be consistent with the other numerical methods introduced here) is

$$W_A = \frac{1}{2} \epsilon_0 \iint_A |E(x, y)|^2 dx dy \quad (6.3.17)$$

where A is the area of interest and $\frac{1}{2} \epsilon_0 |E(x, y)|^2$ is the energy density at any point within the area of interest. When subjected to appropriate boundary conditions, minimizing this energy has been shown to be equivalent to solving Laplace’s equation (Stratton. 1941).

Since $\vec{E} = -\nabla(\psi)$ where ψ is a scalar potential,

$$W_A = \frac{1}{2} \epsilon_0 \iint_A \left(\left(\frac{d\psi}{dx} \right)^2 + \left(\frac{d\psi}{dy} \right)^2 \right) dx dy \quad (6.3.18)$$

At this point, the strategy is as follows:

1. The area of interest is discretized into individual “elements”
2. The potential (i.e., ψ) within each sub-area is approximated by a relatively simple function
3. A set of “element” equations is developed that forms a “system” of linear equations
4. A “system matrix” is assembled
5. Boundary conditions are introduced and the solution to the set of linear equations is found.

Discretization is generally done by subdividing the region into N_e elements of variable size and shape; usually triangles in two dimensions as shown in Fig. 6.3.6. The potential within the region is defined at the vertices of each triangle shown as the points in Fig. 6.36. The total number of points is $N_p = N_a + N_b$ where N_a is the number of points for which the potential is unknown and N_b is the number of points on the boundary with known potential.

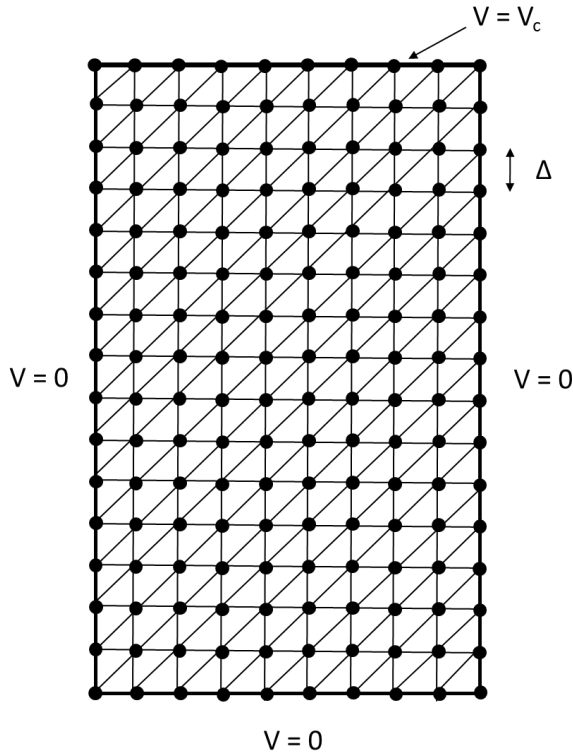


Fig. 6.3.6 Rectangular region discretized for application of the finite element method.

The functional in (6.3.18) is for the entire region of interest, but, of course, it is also possible to write the value of this functional for any of the elements within the region. For the n^{th} element with area ΔA_n , the functional becomes

$$W_{\Delta A_n} = \frac{1}{2} \varepsilon_0 \iint_{\Delta A_n} \left(\left(\frac{d\psi}{dx} \right)^2 + \left(\frac{d\psi}{dy} \right)^2 \right) dx dy \quad (6.3.19)$$

Over each element, the unknown potential is approximated by function that is characterized by unknown constants where the linear approximation is the simplest and is shown in (6.3.20)

$$\psi_{\Delta A_n}(x, y) \cong a_1 + a_2 x + a_3 y \quad (6.3.20)$$

where the constants a_1 , a_2 and a_3 are unknown constants. The constants can be determined in terms of the unknown potentials at the three vertices (i,j,k) of each triangle as:

$$\begin{aligned}
\psi(x_i, y_i) &\cong a_1 + a_2 x_i + a_3 y_i \\
\psi(x_j, y_j) &\cong a_1 + a_2 x_j + a_3 y_j \\
\psi(x_k, y_k) &\cong a_1 + a_2 x_k + a_3 y_k
\end{aligned}
\tag{6.3.21}$$

The set of equations (6.3.21) can be solved for the unknown coefficients in terms of the potentials at the locations of the vertices.

$$a_m = f(\psi_i, \psi_j, \psi_k, x_i, x_j, x_k, y_i, y_j, y_k) \quad m = 1, 2, 3 \tag{6.3.22}$$

Given these, it is possible to write an approximate expression for the potential within any particular element ΔA as

$$\psi_{\Delta A_n}(x, y) \cong N_{in}(x, y)\psi_i + N_{jn}(x, y)\psi_j + N_{kn}(x, y)\psi_k \tag{6.3.23}$$

where

$$N_{in}(x, y) = \frac{1}{2\Delta A_n} \left((x_j y_k - x_k y_j) + (y_j - y_k)x + (x_k - x_j)y \right) \tag{6.3.24}$$

where ΔA_n is the area of this n^{th} triangular element. The other functions $N_{jn}(x, y)$ and $N_{kn}(x, y)$ can be obtained by cyclically permuting the indices.

To set up the equations using the variational approach, the partial derivatives of the approximate potential functions in each sub-area with respect to x and y are taken. The result is

$$\frac{\partial \psi_{\Delta A_n}}{\partial x} = \frac{\partial N_{in}(x, y)}{\partial x} \psi_i + \frac{\partial N_{jn}(x, y)}{\partial x} \psi_j + \frac{\partial N_{kn}(x, y)}{\partial x} \psi_k \tag{6.3.25}$$

$$\frac{\partial \psi_{\Delta A_n}}{\partial y} = \frac{\partial N_{in}(x, y)}{\partial y} \psi_i + \frac{\partial N_{jn}(x, y)}{\partial y} \psi_j + \frac{\partial N_{kn}(x, y)}{\partial y} \psi_k$$

These derivatives can be substituted into (6.3.18) to get the functional for the total area. This result is

$$W_A = \frac{1}{2} \varepsilon_0 \sum_{n=1}^{N_e} \iint_{\Delta A_n} \left(\left(\frac{d\psi_{\Delta A_n}}{dx} \right)^2 + \left(\frac{d\psi_{\Delta A_n}}{dy} \right)^2 \right) dx dy \tag{6.3.26}$$

Given (6.3.25), and after performing the integrations, (6.3.26) can be written as

$$W_A = \frac{1}{2} \varepsilon_0 \sum_{i=1}^{N_p} \left(b_{ii} \psi_i^2 + \psi_i \sum_{\substack{j=1 \\ j \neq i}}^{N_p} b_{ij} \psi_j \right) \quad (6.3.27)$$

where most of the b_{ij} 's are equal to zero since they are only non-zero for adjacent points within the area.

To find the minimum energy of the functional, (6.3.27) can be differentiated with respect to each potential and the derivative then set to zero⁵⁸.

$$\frac{\partial W_A}{\partial \psi_i} = 0 \quad 1 \leq i \leq N_p \quad (6.3.28)$$

The result is

$$\frac{\partial W_A}{\partial \psi_i} = \sum_{i=1}^{N_p} \left(2b_{ii} \psi_i + \sum_{\substack{j=1 \\ j \neq i}}^{N_p} b_{ij} \psi_j \right) = 0 \quad 1 \leq i \leq N_p \quad (6.3.29)$$

which is a set of linear equations in ψ_i where $p_{ii} = \varepsilon_0 b_{ii}$ and $p_{ij} = \varepsilon_0 b_{ij} / 2$, $j \neq i$ that can be written in matrix form as

$$[P][\psi] = 0 \quad (6.3.30)$$

where $[P]$ is called the “permittivity” matrix and $[\psi]$ is the matrix of potentials. As mentioned earlier, however, this equation is not useful in this form because (while it is square) it involves equations developed assuming that the known boundary potentials can be varied. In addition, it can be shown to be a singular matrix (Schwab, 1988).

This issue can be resolved by partitioning the matrix into sub matrices that relate separately to the unknown potential within area A and the known boundary potentials. The result is

$$\begin{bmatrix} P_{AA} & P_{AB} \\ P_{BA} & P_{BB} \end{bmatrix} \begin{bmatrix} \psi_A \\ \psi_B \end{bmatrix} = 0 \quad (6.3.33)$$

Since the boundary potentials are known, the top equations can be rewritten as

⁵⁸ At this point, the derivative is taken with respect to all potentials included the known boundary potentials. Later the equations developed using these derivatives will be ignored since these potentials are known

$$[P_{AA}][\psi_A] + [P_{AB}][\psi_B] = 0 \quad (6.3.34)$$

Finally,

$$[P_{AA}][\psi_A] = -[P_{AB}][\psi_B] \quad (6.3.35)$$

This set of linear equations can be solved for the unknown potentials either by matrix solutions technique designed for sparse matrices or (often) by an iterative technique.

6.4 Problems

P6.1. For a material with a dielectric constant $\epsilon_r = 3$, find

- The capacitance per unit area for a parallel plate capacitor with a plate spacing of 1 mm.
- The capacitance per unit length for a coaxial capacitor with dimensions $a_1 = 2$ mm and $a_2 = 1$ mm.
- The capacitance of a spherical capacitor with $a_1 = 15$ cm and $a_2 = 10$ cm. What happens to the capacitance if $\epsilon_r = 1$ and $a_1 \rightarrow \infty$? This is the self capacitance of a spherical electrode in free space and is often useful in electromagnetic compatibility calculations.

P6.2. A conductor with a voltage $V = 1$ kV is located in free space at a distance $y_q = 1$ meter above an interface.

- Find the line charge per unit length ρ_ℓ assuming that the medium below the interface is a perfect conductor.
- For the medium in a), use image theory to calculate the vertical electric field E_y at $(x,y) = (0,0)$. Refer to Section 5.4 for background on the fields of line charges.
- If the perfect conductor is replaced with a dielectric with relative dielectric constant $\epsilon_r = 2$, but the charge density of the line charge remains the same as in a), calculate the vertical electric field E_y at $(x,y) = (0,\delta)$ as $\delta \rightarrow 0$. Then calculate E_y in the lower dielectric medium at $(x,y) = (0,-\delta)$ as $\delta \rightarrow 0$. Are the relevant boundary conditions satisfied?

P6.3. Calculate the electric fields E_x and E_y in the geometry of Fig. 6.2.9 at the given locations for the parameters $V_0 = 100$ kV and $h = 1$ meter.

- a. For $(x,y) = (-2, 0)$ meters calculate E_y . Assume that the field point is far enough into the capacitor for the parallel plate approximation to be valid.
- b. For $(x,y) = (-h/\pi + \delta, h)$ meters use (6.2.73) to calculate E_x where $\delta \ll h$. Compare this result with the result of part a).

P6.4. Determine an expression for F in (6.2.32).

P6.5. A small house is modeled as a hemispherical igloo (i.e., Using image theory, this is equivalent to half of the spherical shell shown in Fig. 6.2.7).

- a. Starting with (6.2.30) and (6.2.33), show that the shielding factor (SF) for $r < a_1$ (defined as E/E_0) is

$$\text{SF} = \frac{9\hat{\epsilon}_r(1-\Delta)}{9\hat{\epsilon}_r - (2 + \hat{\epsilon}_r)(1 + 2\hat{\epsilon}_r)\Delta} \quad \text{where } \Delta = (1 - 1/\delta)$$

- b. Note that in this form, it is more clear that the shielding factor $\rightarrow 1$ if the thickness of the wall becomes zero.
- c. Determine the 60 Hz electric field shielding factor for a house constructed of Douglas Fir with a 25% moisture content ($\hat{\epsilon}_r \approx 2.0 - j 4.3$), radius 5 meters and a thickness of 0.2 meters.

P6.6. Consider a 2-dimension problem. A rectangular region has a width $w = 4$ and a height $b = 8$. The potentials on the four boundaries of the region have been specified as that $V = V_0$ at the top boundary and $V = 0$ at the other three (left, right and bottom) boundaries. Let the lower left corner of the region to be the origin of the coordinates, the bottom boundary to be on x -axis and the left side boundary on y -axis, as shown in Fig. P.6.6.1

The region is divided into a grid with step size of 1. Set three observation points on the grid at $(2, 6)$, $(2, 4)$, and $(2, 2)$, whose potentials are assumed to be V_1 , V_2 , and V_3 , respectively. In this problem, four different methods will be applied to investigate the potentials at the observation points.

- a. Use the infinite series method of (6.2.91) and (6.2.90) to find the exact solution to the potential at the three points, $(x,y) = (2,2)$, $(2,4)$ and $(2,6)$ (i.e., V_1 , V_2 and V_3) in the region. Write a program (in any language you prefer) to calculate these potentials. If you wish, calculate the potential over the whole region and plot constant voltage contours for your results.

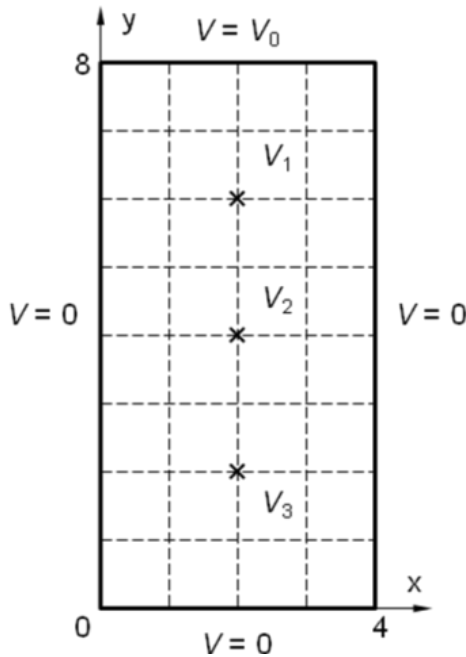


Fig. P6.6.1. A rectangular region with specified potentials on the boundaries

b. Apply the Monte Carlo method to find the potentials on the three observation points. Use at least ten random walks for each point if you do the calculation by hand. If you do not have a random number generator, you may generate random numbers using a 6 sided die and throwing it again if either the 5 or 6 come up. If you do this using a computer program, you can use a finer grid to do the simulation if you wish.

c. Use the grid with larger step size (step size of 2) shown in Fig. P.6.6.2. Apply the finite difference method to calculate V_1 , V_2 , and V_3 .

d) Apply the charge simulation method to set up equations for finding V_1 , V_2 , and V_3 (it is not necessary to solve these equations). Assume there is one equivalent line charge (with unknown line charge density) outside the center of each boundary where the distance between the line charge and its corresponding boundary is d , as shown in Fig. P.6.6.3. Assume $d = 0.5$ if you solve the problem by hand. Note that by symmetry, $\rho_L = \rho_R$. The equations can be found by matching boundary conditions at the center of each surface. It is only necessary to set up three equations since $\rho_L = \rho_R$.

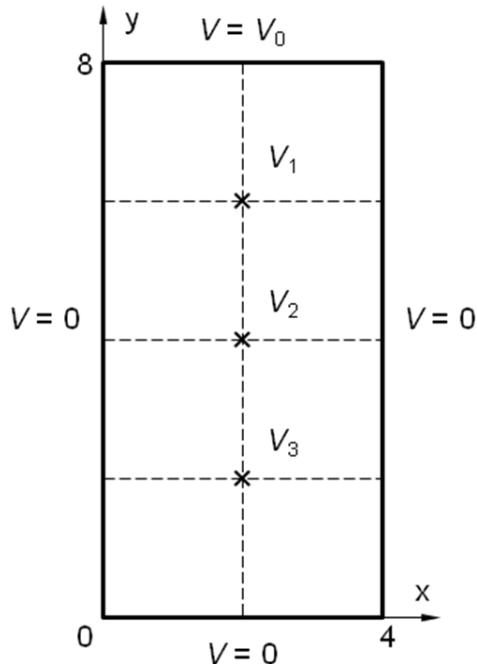


Fig. P6.6.2. Larger step size grid for finite difference method

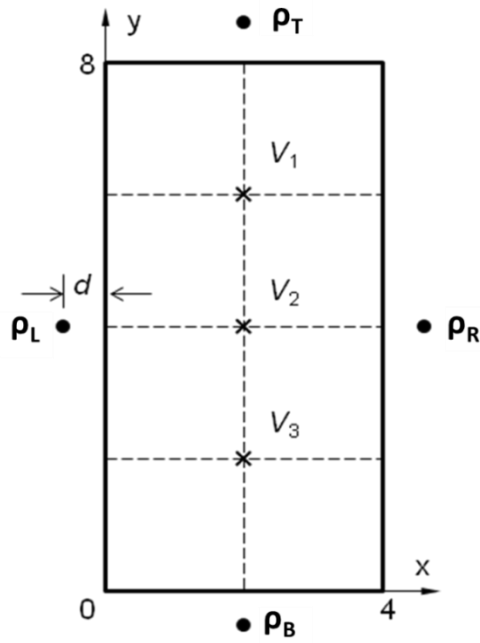


Fig. P6.6.3. Model for charge simulation method

6.5 References

- Abramowitz, M. and I. A. Stegun. 1964. *Handbook of Mathematical Functions*. National Bureau of Standards, Washington DC.
- Beasley, M. D. R., J. H. Pickles, G. d'Amico, L. Beretta, M. Fanelli, G. Giuseppetti, A. di Monaco, G. Gallet, J. P. Gregoire and M. Morin. 1979. "Comparative Study of Three Methods for Computing Electric Fields." *Proceedings of the IEE (London)*. Vol. 126. pp. 126 – 134. January.
- Daffe, J. and R. G. Olsen. 1979. "An Integral Equation Technique for Solving Rotationally Symmetric Electrostatic Problems in Conducting and Dielectric Material." *IEEE Transactions on Power Apparatus and Systems*. Vol. PAS-98. pp. 1609–1616. September/October.
- Haus, H. A., and J. R. Melcher. 1989. *Electromagnetic Fields and Energy*. Prentice Hall. Englewood Cliffs, NJ.
- IEEE. 2008. "IEEE Standard Procedures for Measurement of Power Frequency Electric and Magnetic Fields from AC Power Lines." IEEE Standard 644-1994 (Reaffirmed 2008). IEEE. New York, NY.
- O'Brien, J. L. and T. L. Geers. 1990. *Direct vs. Indirect Boundary Element Methods*. Springer – Verlag. Berlin.
- Olsen, R.G. 1986. "Integral Equations for Electrostatics Problems with Thin Dielectric or Conducting Layers." *IEEE Transactions on Electrical Insulation*. Vol. EI-21. pp. 565–573. August.
- Olsen, R. G. and O. Einarsson. 1987. "Boundary Element Methods for Weakly Three Dimensional Quasi-Electrostatics Problems." *IEEE Transactions on Power Delivery*. Vol. PRWD-2. pp. 1276–1284. October.
- Olsen, R. G. 1999. "An Improved Model for the Electromagnetic Compatibility of All Dielectric Self Supporting Fiber Optic Cable and High Voltage Power Lines," *IEEE Transactions on Electromagnetic Compatibility*. Vol. 41. pp. 180 – 192. August.
- Pickles, J. H. 1977. "Monte Carlo Field Calculations." *Proceedings of the IEE (London)*. Vol. 124. pp. 1271 – 1276. December.
- Schinzinger, R. and P. A. A. Laura. 2003. *Conformal Mapping: Methods and Applications*. Dover. Mineola, New York.
- Schwab, A. J. 1988. *Field Theory Concepts*. Springer-Verlag. Berlin.

Shih, C. H., DiPlacido, J., and Ware, B. J. 1977. "Analysis of Parallel Plate Simulation of Transmission Line Electric Field as Related to Biological Effects Laboratory Studies." *IEEE Transactions on Power Apparatus and Systems*. Vol. PAS-96. pp. 962–968. May/June.

Singer, H., H. Steinbigler and P. Weiss. 1974. "A Charge Simulation Method for the Calculation of High Voltage Fields." *IEEE Transactions on Power Apparatus and Systems*, Vol. PAS-93, pp. 1660 – 1668.

Smythe W. 1968. *Static and Dynamic Electricity*. McGraw Hill. New York

Stratton, J. A. 1941. *Electromagnetic Theory* (pp. 194-201). McGraw Hill. New York.

Thacher, P. D. 1976. "Fringing Fields in Kerr Cells - Sandia Report SLA-74-0302." *IEEE Transactions on Electrical Insulation*, Vol. EI-11. pp. 40–50. June.

Trinh, N. G. 1980. "Electrode Design for Testing in Uniform Field Gaps." *IEEE Transactions on Power Apparatus and Systems*. Vol. PAS-99. pp. 1235 – 1242. May/June.

Zahn, M. 1979. *Electromagnetic Field Theory* (pp. 284-297). Wiley, New York,

Zienkiewicz, O. C. 1971. *The Finite Element Method in Engineering Science*, McGraw Hill. New York.

Chapter VII

Propagation on an Infinitely Long Multiconductor Transmission Line above Homogeneous Earth

7.1 The Balanced Two Wire Line – Arbitrary Frequency

Introduction

A study of the case for two conductors adds some complexity to the problem because there are two unknown currents. As a result, there are not only “spectral” modes (i.e., transmission line, surface attached and radiation modes) similar to those discussed in Chapter 4 for the single wire line, but “geometric” modes or “components” that relate to the relative currents on each conductor of the transmission system. Here, care will be taken to be clear about which category (i.e., spectral modes or geometric modes/components) is the subject of the discussion.

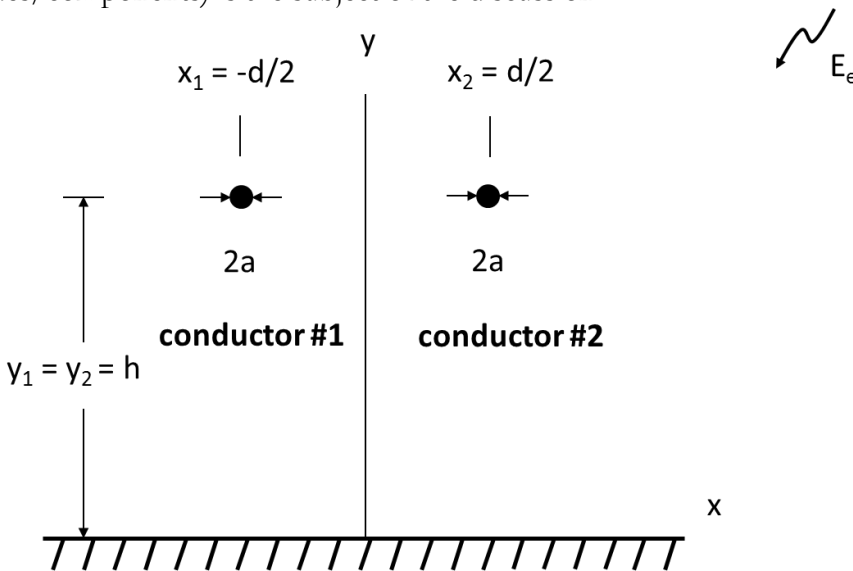


Fig. 7.1.1. Cross sectional geometry of a two wire transmission

The technique for solving for the propagation of currents on a single conductor can be readily extended to the case for multiple wires. Here, the case for two wires at identical heights above the earth is given because the additional steps in the process can be presented without obscuring the results

with excessive complication. Consider the case shown in Fig. 7.1.1 for two infinitely long parallel conductors at a height h above the earth and separated by a distance d , constructed of the same material and with the same radius, a . It has been assumed that there is an external source as shown in the figure and that each conductor is driven by a sinusoidal voltage source (different for each conductor but not shown in the figure) at $z = 0$. More about the case for external sources has been given by Olsen and Aburwein (1980) and by Wait (1977).

The method by which this problem can be solved is identical to that for the single wire case except that there is an additional source of field (i.e., the second conductor). Hence, there will be two coupled equations (one for each conductor boundary condition) rather than a single one as in Chapter 4. These equations will be expressed here in matrix form.

As with the general solution presented in Chapter 4, the solution to these equations is formally valid at any frequency for which the conductor radius a is small compared to other dimensions and the wavelength at the frequency of interest, for which the earth is represented by electrical constants appropriate to the frequency and for which the conductor is appropriately modeled by its conductance σ_w . As a result, the solution can be used to solve antenna problems at high frequency as well as power line propagation problems at low frequency. These two extremes are not separate issues and it is sometimes important that this not be forgotten. In fact, there are certain cases (such as for calculating electromagnetic interference from corona) for which general theory is needed even for analysis of power transmission lines.

Just as for Chapter 4, however, it is recognized that the interest of many readers is restricted to the behavior of power lines at lower frequencies (i.e., generally below 1 MHz). Thus, there is no need for these readers to spend a great deal of effort to understand the remainder of this first section of the chapter. Rather, these readers can skip topics marked with a ◀ here and in the table of contents and proceed to Section 7.2 where a special introduction is written for readers who have skipped earlier sections.

In the Section 7.2 systematic mathematical approximations to the exact solution will be made with care taken to list exactly the conditions under which each approximation is valid. These approximations include those that lead to equivalent transmission line theory. Following this is a section on mode coupling through reflection and non-symmetric transmission lines for which symmetric excitation do not produce symmetric currents. Finally, the theory is extended to transmission lines with an arbitrary number of conductors that may include shield wires.

Derivation for the general frequency case ◀

Using the previously derived result for the axially directed electric field of a conductor from (4.4.56), (4.4.50) and (4.4.19) two equations in the spatial

Fourier transform domain for the unknown currents on the two conductors can be obtained as⁵⁹

$$\tilde{G}_{ez}^{11}\hat{I}_1(\gamma) + \tilde{G}_{ez}^{12}\tilde{I}_2(\gamma) + \hat{E}_{ez}(-d/2, h-a, \gamma) = -\hat{V}_1 + Z_{iw}\hat{I}_1(\gamma) \quad (7.1.1)$$

$$\tilde{G}_{ez}^{21}\hat{I}_1(\gamma) + \tilde{G}_{ez}^{22}\tilde{I}_2(\gamma) + \hat{E}_{ez}(d/2, h-a, \gamma) = -\hat{V}_2 + Z_{iw}\hat{I}_2(\gamma) \quad (7.1.2)$$

where $\tilde{G}_{ez}^{11} = \tilde{G}_{ez}^{22} = \tilde{G}_{ez}(0, h-a, h, \gamma)$ and $\tilde{G}_{ez}^{12} = \tilde{G}_{ez}^{21} = \tilde{G}_{ez}(d, h-a, h, \gamma)$ while $\hat{E}_{ez}(-d/2, h-a, \gamma)$ and $\hat{E}_{ez}(d/2, h-a, \gamma)$ represent the axial electric field of the external source at each conductor. \hat{V}_1 and \hat{V}_2 represent the voltage at $z = 0$ of the source in series with each conductor.

Here (from (4.4.54) and (4.4.14)

(7.1.3)

$$\begin{aligned} \tilde{G}_{ez} \left(\begin{matrix} x - x_1 \\ 2 \\ y, h, \gamma \end{matrix} \right) = \\ \frac{1}{4\omega\epsilon_0} \left\{ (\gamma^2 - k_0^2) \left[H_0^{(2)} \left(\begin{matrix} (k_0^2 - \gamma^2)^{1/2} r_1 \\ 2 \end{matrix} \right) - H_0^{(2)} \left(\begin{matrix} (k_0^2 - \gamma^2)^{1/2} r_1^i \\ 2 \end{matrix} \right) \right] \right. \\ \left. - 2k_0^2 P(\gamma) + 2k_0^2 \gamma^2 Q(\gamma) \right\} \end{aligned}$$

where

$$\begin{aligned} r_1 &= \left(\left(\begin{matrix} x - x_1 \\ 2 \end{matrix} \right)^2 + (y - h)^2 \right)^{1/2} \\ r_1^i &= \left(\left(\begin{matrix} x - x_1 \\ 2 \end{matrix} \right)^2 + (y + h)^2 \right)^{1/2} \\ \text{Im}(k_0^2 - \gamma^2)^{1/2} &\leq 0 \end{aligned}$$

$$\tilde{P}(\gamma) = \left(\frac{j}{\pi} \right) \int_{-\infty}^{\infty} \frac{e^{-u_1(y+h)} e^{jk \begin{pmatrix} x-x_1 \\ 2 \end{pmatrix}}}{u_1 + u_2} d\kappa \quad (7.1.4)$$

and

⁵⁹ Note that the physical dimensions of E_{ez} and V are both “volts” in the Fourier transform domain.

$$\tilde{Q}(\gamma) = \left(\frac{j2}{\pi} \right) \int_{-\infty}^{\infty} \frac{e^{-u_1(y+h)} e^{jk \begin{pmatrix} x-x_1 \\ 2 \end{pmatrix}}}{k_2^2 u_1 + k_0^2 u_2} d\kappa. \quad (7.1.5)$$

$$u_1 = \sqrt{\kappa^2 + \gamma^2 - k_0^2} \quad \text{Re}(u_1) \geq 0$$

$$u_2 = \sqrt{\kappa^2 + \gamma^2 - k_2^2} \quad \text{Re}(u_2) \geq 0$$

Equations (7.1.1) and (7.1.2) can be written more compactly as

$$\begin{vmatrix} \tilde{G}_{ez}^{11} - Z_{iw} & \tilde{G}_{ez}^{12} \\ \tilde{G}_{ez}^{21} & \tilde{G}_{ez}^{22} - Z_{iw} \end{vmatrix} \begin{vmatrix} \hat{I}_1 \\ \hat{I}_2 \end{vmatrix} = \begin{vmatrix} -\hat{V}_1 - E_{ez}^1 \\ -\hat{V}_2 - E_{ez}^2 \end{vmatrix} \quad (7.1.6)$$

where (given symmetry and reciprocity) $\tilde{G}_{ez}^{11} - Z_{iw} = \tilde{G}_{ez}^{22} - Z_{iw}$ and $\tilde{G}_{ez}^{12} = \tilde{G}_{ez}^{21}$. \hat{E}_{ez}^1 and \hat{E}_{ez}^2 are, respectively, the axial electric fields of the external source evaluated at the bottom surfaces of conductor 1 and 2.

The matrix in (7.1.6) is a 2 x 2 matrix. It is known that if it has 2 distinct eigenvalues, then it has two distinct eigenvectors that are orthogonal with respect to it (Wiley 1966). It is also known that any two element vector (e.g., $\begin{vmatrix} \hat{I} \end{vmatrix}$) can be expanded in this set of eigenvectors so that

$$\begin{vmatrix} \hat{I} \end{vmatrix} = |\eta| \begin{vmatrix} \hat{I}_{gm} \end{vmatrix} \quad (7.1.7)$$

where $\begin{vmatrix} \hat{I}_{gm} \end{vmatrix}$ is the matrix of “geometric component” amplitudes (often referred to in the power engineering literature simply as “mode” amplitudes), and $|\eta|$ is the a square matrix (by columns) of normalized eigenvectors of the square matrix in (7.1.6). Since the matrix in (7.1.6) is symmetric, it can be written

$$\begin{vmatrix} A & B \\ B & A \end{vmatrix} \quad (7.1.8)$$

The eigenvalues of this matrix (λ)⁶⁰ are defined by

$$\begin{vmatrix} A & B \\ B & A \end{vmatrix} \begin{vmatrix} q_a \\ q_b \end{vmatrix} = \lambda \begin{vmatrix} q_a \\ q_b \end{vmatrix} \quad (7.1.9)$$

⁶⁰ Not to be confused with λ , used later to designate “wavelength”

where the vectors $\bar{q} = (q_a, q_b)$ are its eigenvectors⁶¹. Since (7.1.9) represents a homogeneous set of equations, it only has a solution if

$$\det \begin{vmatrix} A - \lambda & B \\ B & A - \lambda \end{vmatrix} = 0 \quad . \quad (7.1.10)$$

This occurs when the quadratic

$$\lambda^2 - 2A\lambda + (A^2 - B^2) = 0. \quad (7.1.11)$$

Hence the eigenvalues are

$$\lambda_1 = A \pm B = \tilde{G}_{ez}^{11} - Z_{iw} \pm \tilde{G}_{ez}^{12} \quad (7.1.12)$$

The eigenvectors can be found by inserting the eigenvalues into (7.1.9) as

$$\begin{vmatrix} \mp B & B \\ B & \mp B \end{vmatrix} \begin{vmatrix} q_a \\ q_b \end{vmatrix} = 0 \quad (7.1.13)$$

Given that the matrix in (7.1.13) is symmetric its eigenvectors are simply

$$\bar{q}_1 = a_1 \begin{vmatrix} 1 \\ 1 \end{vmatrix} \quad \text{and} \quad \bar{q}_2 = a_2 \begin{vmatrix} 1 \\ -1 \end{vmatrix} \quad (7.1.14)$$

where a_1 and a_2 are arbitrary constants. \bar{q}_1 represents the common component (again often called the “common mode”) which has equal currents on each conductor and \bar{q}_2 represents the differential component (again often called the “differential mode.”)

These eigenvectors can be written as a matrix of eigenvectors (by columns) that are normalized to a magnitude of 1 as

$$|\eta\rangle = \frac{1}{\sqrt{2}} \begin{vmatrix} 1 & 1 \\ 1 & -1 \end{vmatrix} \quad (7.1.15)$$

If the column matrix of conductor currents \hat{I}_1 and \hat{I}_2 is expanded in the eigenvectors of the symmetric matrix in (7.1.6), then

⁶¹ Not to be confused with q used later to represent charge

$$\begin{vmatrix} \hat{I}_1 \\ \hat{I}_2 \end{vmatrix} = |\eta| \begin{vmatrix} \hat{I}_{gm1} \\ \hat{I}_{gm2} \end{vmatrix} \quad (7.1.16)$$

where \hat{I}_{gm1} and \hat{I}_{gm2} are the “geometric mode” amplitudes.

If (7.1.16) is substituted into (7.1.6) and the entire equation pre-multiplied by the inverse matrix $|\eta|^{-1}$ which (in this case) is equal to $|\eta|$

$$\frac{1}{2} \begin{vmatrix} 1 & 1 \\ 1 & -1 \end{vmatrix} \begin{vmatrix} \tilde{G}_{ez}^{11} - Z_{iw} & \tilde{G}_{ez}^{12} \\ \tilde{G}_{ez}^{21} & \tilde{G}_{ez}^{22} - Z_{iw} \end{vmatrix} \begin{vmatrix} \hat{I}_{gm1} \\ \hat{I}_{gm2} \end{vmatrix} = \frac{1}{\sqrt{2}} \begin{vmatrix} 1 & 1 \\ 1 & -1 \end{vmatrix} \begin{vmatrix} -\hat{V}_1 - \hat{E}_{ze}^1 \\ -\hat{V}_2 - \hat{E}_{ze}^2 \end{vmatrix} \quad (7.1.17)$$

But, pre-multiplying and post-multiplying a matrix by a matrix of its eigenvectors results in a diagonalized matrix of eigenvalues as follows (Wiley 1966).

$$|\eta|^{-1} \begin{vmatrix} \tilde{G}_{ez}^{11} - Z_{iw} & \tilde{G}_{ez}^{12} \\ \tilde{G}_{ez}^{21} & \tilde{G}_{ez}^{22} - Z_{iw} \end{vmatrix} |\eta| = \frac{1}{2} \begin{vmatrix} \tilde{G}_{ez}^{11} - Z_{iw} + \tilde{G}_{ez}^{12} & 0 \\ 0 & \tilde{G}_{ez}^{22} - Z_{iw} - \tilde{G}_{ez}^{12} \end{vmatrix} \quad (7.1.18)$$

In addition, the right hand side of (7.1.17) becomes

$$\begin{vmatrix} 1 & 1 \\ 1 & -1 \end{vmatrix} \begin{vmatrix} -\hat{V}_1 - \hat{E}_{ze}^1 \\ -\hat{V}_2 - \hat{E}_{ze}^2 \end{vmatrix} = - \begin{vmatrix} \hat{V}_1 + \hat{V}_2 + \hat{E}_{ze}^1 + \hat{E}_{ze}^2 \\ \hat{V}_1 - \hat{V}_2 + \hat{E}_{ze}^1 - \hat{E}_{ze}^2 \end{vmatrix} \quad (7.1.19)$$

so that

$$\frac{1}{2} \begin{vmatrix} \tilde{G}_{ez}^{11} - Z_{iw} + \tilde{G}_{ez}^{12} & 0 \\ 0 & \tilde{G}_{ez}^{22} - Z_{iw} - \tilde{G}_{ez}^{12} \end{vmatrix} \begin{vmatrix} \hat{I}_{gm1} \\ \hat{I}_{gm2} \end{vmatrix} = \frac{-1}{\sqrt{2}} \begin{vmatrix} \hat{V}_1 + \hat{V}_2 + \hat{E}_{ze}^1 + \hat{E}_{ze}^2 \\ \hat{V}_1 - \hat{V}_2 + \hat{E}_{ze}^1 - \hat{E}_{ze}^2 \end{vmatrix} \quad (7.1.20)$$

Differential and common Modes ◀

Since the matrix is diagonalized, the solutions to this equation for the component amplitudes can be obtained by simple inspection as

$$\hat{I}_{gm1} = -\sqrt{2} \frac{\hat{V}_1 + \hat{V}_2 + \hat{E}_{ze}^1 + \hat{E}_{ze}^2}{\tilde{G}_{ez}^{11} - Z_{iw} + \tilde{G}_{ez}^{12}} \quad (7.1.21)$$

$$\hat{I}_{gm2} = -\sqrt{2} \frac{\hat{V}_1 - \hat{V}_2 + \hat{E}_{ez}^1 - \hat{E}_{ez}^2}{\tilde{G}_{ez}^{11} - Z_{iw} - \tilde{G}_{ez}^{12}} \quad (7.1.22)$$

From these results, it is trivial to find formal solutions for the actual conductor currents by using (7.1.16). If, for example, the external electric fields \hat{E}_{ez}^1 and \hat{E}_{ez}^2 are assumed to be zero, and $\hat{V}_1 = \hat{V} = -\hat{V}_2$, $\hat{I}_{gm1} = 0$ and only the differential geometric mode is excited. Given this,

$$\hat{I}_1 = -\hat{I}_2 = -\frac{2\hat{V}}{\tilde{G}_{ez}^{11} - Z_{iw} - \tilde{G}_{ez}^{12}} \quad (7.1.23)$$

Similarly (i.e., if, again, the external fields are zero), if $\hat{V}_1 = \hat{V} = \hat{V}_2$, $\hat{I}_{gm2} = 0$ and only the “common” geometric mode is excited. Given this,

$$\hat{I}_1 = \hat{I}_2 = -\frac{2\hat{V}}{\tilde{G}_{ez}^{11} - Z_{iw} + \tilde{G}_{ez}^{12}} \quad (7.1.24)$$

In general, however, both geometric modes will be excited but (as will be illustrated in the next section) each has a distinct propagation constant and the rate at which each geometric mode is attenuated as it propagates along the wires will be different.

It is now possible to calculate the inverse Fourier transform of (7.1.23) to calculate the currents in space using the methods of Chapter 4 (i.e., Section 4.7). However, because the frequency is still arbitrary, it is a difficult process because the singularities of $\tilde{G}_{ez}^{11} - Z_{iw} - \tilde{G}_{ez}^{12}$ are (in general) difficult to identify and this can obscure the process of finding currents on multiconductor transmission lines. For this reason, the material covered in Section 7.2 that includes a derivation of the currents in the space domain will be restricted to the low frequency case.

7.2 The balanced two wire line – low frequency

Introduction

It was shown in the last section that a matrix equation can be set up for the currents on parallel wires excited by a voltage source inserted in series with each wire at $z = 0$ and an external source of electric field. This equation is repeated here as

$$\begin{vmatrix} \tilde{G}_{ez}^{11} - Z_{iw} & \tilde{G}_{ez}^{12} \\ \tilde{G}_{ez}^{21} & \tilde{G}_{ez}^{22} - Z_{iw} \end{vmatrix} \begin{vmatrix} \hat{I}_1 \\ \hat{I}_2 \end{vmatrix} = \begin{vmatrix} -V_1 - E_{ez}^1 \\ -V_2 - E_{ez}^2 \end{vmatrix} \quad (7.2.1)$$

where $\tilde{G}_{ez}^{11} = \tilde{G}_{ez}^{22} = \tilde{G}_{ez}(0, h-a, h, \gamma)$ and $\tilde{G}_{ez}^{12} = \tilde{G}_{ez}^{21} = \tilde{G}_{ez}(d, h-a, h, \gamma)$. Given symmetry and reciprocity, $\tilde{G}_{ez}^{11} - Z_{iw} = \tilde{G}_{ez}^{22} - Z_{iw}$ and $\tilde{G}_{ez}^{12} = \tilde{G}_{ez}^{21} \cdot \hat{E}_{ez}^1$ and \hat{E}_{ez}^2 are, respectively, the external axial electric fields of the external source evaluated at the bottom surfaces of conductors 1 and 2.

For the reader who is beginning with this section, (7.1.3) – (7.1.5) are repeated here as

$$(7.2.2)$$

$$\tilde{G}_{ez} \left(\begin{matrix} x - x_1 \\ 2 \end{matrix}, y, h, \gamma \right) = \frac{1}{4\omega\epsilon_0} \left\{ (\gamma^2 - k_0^2) \left[H_0^{(2)} \left((k_0^2 - \gamma^2)^{1/2} r_1 \right) - H_0^{(2)} \left((k_0^2 - \gamma^2)^{1/2} r_1^i \right) \right] - 2k_0^2 P(\gamma) + 2k_0^2 \gamma^2 Q(\gamma) \right\}$$

where

$$\begin{aligned} r_1 &= \left(\left(\begin{matrix} x - x_1 \\ 2 \end{matrix} \right)^2 + (y - h)^2 \right)^{1/2} \\ r_1^i &= \left(\left(\begin{matrix} x - x_1 \\ 2 \end{matrix} \right)^2 + (y + h)^2 \right)^{1/2} \\ &, \\ \text{Im}(k_0^2 - \gamma^2)^{1/2} &\leq 0 \\ \tilde{P}(\gamma) &= \left(\frac{j}{\pi} \right) \int_{-\infty}^{\infty} \frac{e^{-u_1(y+h)} e^{j\kappa \left(\begin{matrix} x - x_1 \\ 2 \end{matrix} \right)}}{u_1 + u_2} d\kappa \end{aligned} \quad (7.2.3)$$

and

$$\tilde{Q}(\gamma) = \left(\frac{j2}{\pi} \right) \int_{-\infty}^{\infty} \frac{e^{-u_1(y+h)} e^{j\kappa \left(\begin{matrix} x - x_1 \\ 2 \end{matrix} \right)}}{k_2^2 u_1 + k_0^2 u_2} d\kappa. \quad (7.2.4)$$

$$\begin{aligned} u_1 &= \sqrt{k^2 + \gamma^2 - k_0^2} & \text{Re}(u_1) &\geq 0 \\ u_2 &= \sqrt{k^2 + \gamma^2 - k_2^2} & \text{Re}(u_2) &\geq 0 \end{aligned}$$

As was the case in Chapter 4, it is not important for the reader who has skipped most of Sections 7.1 to understand the details of (7.2.2) – (7.2.4). Rather, it is important only to recognize that they represent an exact closed form solution valid at nearly all frequencies and that will be used here to develop expressions that are very familiar to power engineers.

The low frequency approximation

In order to provide a better understanding of the process for finding currents on multiple conductor transmission lines, the first case studied will be limited to a two-conductor line that has a symmetrical geometry (i.e., Fig. 7.1.1) and is operated at “low” frequency.

At low frequencies, the terms containing the Hankel functions in (7.2.2) can be replaced by small argument expansions and are independent of k_0 , $\tilde{Q}(\gamma)$ is proportional to $1/k_2^2$ and $\tilde{P}(\gamma)$ is proportional to $1/k_2$. Thus, $\tilde{Q}(\gamma)$ can be ignored at low frequencies under most circumstances since $|k_2| \gg |k_0|$.

Given the small argument expansion for the Hankel function,

$$H_0^{(2)}(q) \cong -\frac{2j}{\pi} \ln(q/2) - \frac{2j\gamma_e}{\pi}$$

where γ_e is Euler’s constant, the first two terms of (7.2.2) become

$$\frac{j}{2\pi\omega\epsilon_0} (\gamma^2 - k_0^2) \ln \left(\frac{r_1^i}{r_1^2} / \frac{r_1^i}{r_1^2} \right). \quad (7.2.5)$$

In addition,

$$\begin{aligned} \tilde{P}(\gamma) &= \frac{2j}{\pi} \int_0^\infty \frac{(u_1 - u_2) e^{-u_1(y+h)}}{(u_1 - u_2)(u_1 + u_2)} \cos \left(\kappa \begin{pmatrix} x - x_1 \\ 2 \end{pmatrix} \right) d\kappa \\ &\cong \frac{2j}{\pi} \int_0^\infty \frac{(\lambda - u_2) e^{-u_1(y+h)}}{(k_2^2 - k_0^2)} \cos \left(\kappa \begin{pmatrix} x - x_1 \\ 2 \end{pmatrix} \right) d\kappa \\ &\cong -\frac{2j}{\pi k_2^2} \int_0^\infty (u - \kappa) e^{-\kappa(y+h)} \cos \left(\kappa \begin{pmatrix} x - x_1 \\ 2 \end{pmatrix} \right) d\kappa \end{aligned} \quad (7.2.6)$$

where $u = \sqrt{\kappa^2 - k_2^2}$, $\text{Re}(u) \geq 0$ and $u_1 \cong \kappa$ over most of the integration⁶² since $1/(2h) \gg k_0$. Note that (7.2.6) is essentially a generalization of Carson’s integral (i.e., (4.7.5) and (4.7.6)) to arbitrary locations in space.

⁶² this type of approximation is often called a “quasi-static” approximation.

Thus,

(7.2.7)

$$\tilde{G}_{ez} \left(\begin{matrix} x-x_1, y, h, \gamma \\ 2 \end{matrix} \right) \cong \frac{j}{2\pi\omega\epsilon_0} \left[(\gamma^2 - k_0^2) \ln \left(\begin{matrix} r_1^i / r_1 \\ 2 \quad 2 \end{matrix} \right) + k_0^2 J_c \left(\begin{matrix} x-x_1, y, h \\ 2 \end{matrix} \right) \right]$$

where

$$J_c \left(\begin{matrix} x-x_1, y, h \\ 2 \end{matrix} \right) = \frac{2}{k_2^2} \int_0^\infty (u - \kappa) e^{-\kappa(y+h)} \cos \left(\kappa \left(\begin{matrix} x-x_1 \\ 2 \end{matrix} \right) \right) d\kappa \quad (7.2.8)$$

and

$$u = \sqrt{\kappa^2 - k_2^2}.$$

As in Section 7.1, the currents on the conductors can be found by solving the following matrix equation

$$\begin{vmatrix} \tilde{G}_{ez}^{11} - Z_{iw} & \tilde{G}_{ez}^{12} \\ \tilde{G}_{ez}^{21} & \tilde{G}_{ez}^{22} - Z_{iw} \end{vmatrix} \begin{vmatrix} \hat{I}_1 \\ \hat{I}_2 \end{vmatrix} = \begin{vmatrix} -\hat{V}_1 - \hat{E}_{ez}^1 \\ -\hat{V}_2 - \hat{E}_{ez}^2 \end{vmatrix} \quad (7.2.9)$$

To facilitate solution of (7.2.9) at these low frequencies, G_{ez} is cast in the following form

$$\tilde{G}_{ez} \left(\begin{matrix} x-x_1, y, h, \gamma \\ 2 \end{matrix} \right) = - \left(Z \left(\begin{matrix} x-x_1, y, h \\ 2 \end{matrix} \right) + \frac{\gamma^2}{j\omega} A \left(\begin{matrix} x-x_1, y, h \\ 2 \end{matrix} \right) \right) \quad (7.2.10)$$

Where

$$Z \left(\begin{matrix} x-x_1, y, h \\ 2 \end{matrix} \right) = \frac{j\omega\mu_0}{2\pi} \left\{ \ln \left(\begin{matrix} r_1^i / r_1 \\ 2 \quad 2 \end{matrix} \right) - J_c \left(\begin{matrix} x-x_1, y, h \\ 2 \end{matrix} \right) \right\} \quad (7.2.11)$$

is a mutual impedance per unit length and

$$A \left(\begin{matrix} x-x_1, y, h \\ 2 \end{matrix} \right) = \frac{\ln \left(\begin{matrix} r_1^i / r_1 \\ 2 \quad 2 \end{matrix} \right)}{2\pi\epsilon_0} \quad (7.2.12)$$

where $A \left(\begin{matrix} x - x_1, y, h \\ 2 \end{matrix} \right)$ is the “potential coefficient” (i.e., the space potential at (x, y) for a line charge with unit amplitude at $\left(\begin{matrix} x_1, h \\ 2 \end{matrix} \right)$ and above a perfect ground plane.

Using these results in (7.2.9) yields

$$\begin{vmatrix} Z_{11} + Z_{iw} + \frac{\gamma^2}{j\omega} A_{11} & Z_{12} + \frac{\gamma^2}{j\omega} A_{12} \\ Z_{21} + \frac{\gamma^2}{j\omega} A_{21} & Z_{22} + Z_{iw} + \frac{\gamma^2}{j\omega} A_{22} \end{vmatrix} \begin{vmatrix} \hat{I}_1(\gamma) \\ \hat{I}_2(\gamma) \end{vmatrix} = \begin{vmatrix} \hat{V}_1 + \hat{E}_{ez}^1 \\ \hat{V}_2 + \hat{E}_{ez}^2 \end{vmatrix} \quad (7.2.13)$$

where

$$\begin{aligned} Z_{11} = Z_{22} = Z(0, h - a, h), \quad Z_{12} = Z_{21} = Z(d, h - a, h), \\ A_{11} = A_{22} = A(0, h - a, h), \quad A_{12} = A_{21} = A(d, h - a, h) \end{aligned}$$

Terms can be collected and (7.2.13) written as

$$\left\{ \begin{vmatrix} Z_{11} + Z_{iw} & Z_{12} \\ Z_{21} & Z_{22} + Z_{iw} \end{vmatrix} + \frac{\gamma^2}{j\omega} \begin{vmatrix} A_{11} & A_{12} \\ A_{21} & A_{22} \end{vmatrix} \right\} \begin{vmatrix} \hat{I}_1(\gamma) \\ \hat{I}_2(\gamma) \end{vmatrix} = \begin{vmatrix} \hat{V}_1 + \hat{E}_{ez}^1 \\ \hat{V}_2 + \hat{E}_{ez}^2 \end{vmatrix} \quad (7.2.14)$$

If the notation $|Z|$ is interpreted as the matrix of impedance elements in (7.2.14) and $|A|$ is interpreted as the matrix of potential coefficients, then

$$j\omega|A|^{-1} = j\omega|C| = |Y| \quad (7.2.15)$$

where $|Y|$ is the admittance matrix for the two conductors which is equal to $j\omega|C|$ where $|C|$ is the capacitance matrix for the conductors above a perfect earth⁶³.

If now, (7.2.14) is multiplied by $|Y|$

$$\left\{ |Y||Z| + \gamma^2 \right\} \hat{I} = |Y| \hat{V} + \hat{E} \quad (7.2.16)$$

⁶³ Some elements of $|C|$ are negative and do not represent physical capacitors. The relationship between $|C|$ and a network of equivalent capacitors between the conductors and the earth is discussed in Problem P7.2

where $\left| \hat{\mathbf{I}} \right|$ is the matrix of conductor currents and $\left| \hat{\mathbf{V}} + \hat{\mathbf{E}} \right|$ is the matrix of conductor source voltages and external fields.

Solving for the modes

In the balanced symmetrical two conductor case shown in Fig. 7.1.1, $\left| \mathbf{Y} \parallel \mathbf{Z} \right|$ can be written as

$$\left| \mathbf{Y} \parallel \mathbf{Z} \right| = \begin{vmatrix} (Z_{11} + Z_{iw})Y_{11} + Z_{12}Y_{12} & (Z_{11} + Z_{iw})Y_{12} + Z_{12}Y_{11} \\ Z_{12}Y_{11} + (Z_{11} + Z_{iw})Y_{12} & (Z_{11} + Z_{iw})Y_{11} + Z_{12}Y_{12} \end{vmatrix} \quad (7.2.17)$$

This matrix has the same form as the matrix in (7.1.6)

$$\begin{vmatrix} A & B \\ B & A \end{vmatrix} \quad (7.2.18)$$

as (7.1.6) and hence, the properties of this matrix developed earlier can be used again here.

As in Section 7.1, if $\left| \mathbf{Q}^2 \right| = \left| \mathbf{Y} \parallel \mathbf{Z} \right|$ is a 2 x 2 matrix and has 2 distinct eigenvalues, then it has two distinct eigenvectors that are orthogonal with respect to $\left| \mathbf{Q}^2 \right|$ (Wiley 1966). $\left| \eta \right|$ is the same square matrix (by columns) of normalized eigenvectors as shown in (7.1.19)

$$\left| \eta \right| = \frac{1}{\sqrt{2}} \begin{vmatrix} 1 & 1 \\ 1 & -1 \end{vmatrix} \quad (7.2.19)$$

Further, in this low frequency case, the eigenvalues can be written explicitly as⁶⁴

$$\lambda_1 = (Z_{11} + Z_{iw} + Z_{12})(Y_{11} + Y_{12}) \quad \text{and} \quad \lambda_2 = (Z_{11} + Z_{iw} - Z_{12})(Y_{11} - Y_{12}) \quad (7.2.20)$$

Then, any two component vector (e.g., $\left| \hat{\mathbf{I}} \right|$) can be expanded in this set of eigenvectors so that

$$\left| \hat{\mathbf{I}} \right| = \left| \eta \right| \left| \hat{\mathbf{I}}_{gm} \right| \quad (7.2.21)$$

⁶⁴ Again, λ is not to be confused with the wavelength that will be used later.

where $|\hat{\mathbf{I}}_{gm}|$ is the matrix of “geometric mode” amplitudes. Using the substitution (7.2.21), (7.2.16) becomes

$$\left\{ \mathbf{Q}^2 \left| |\boldsymbol{\eta}| + \gamma^2 |\boldsymbol{\eta}| \right. \right\} \hat{\mathbf{I}}_{cm} = |\mathbf{Y}| \mathbf{V} + \mathbf{E} \quad (7.2.22)$$

Now (as in Section 7.1) it can be shown that $|\boldsymbol{\eta}|^{-1} = |\boldsymbol{\eta}|$ and

$$|\boldsymbol{\eta}|^{-1} \mathbf{Q}^2 |\boldsymbol{\eta}| = \mathbf{Q}_d^2 \quad (7.2.23)$$

where $|\mathbf{Q}_d^2|$ is a diagonal matrix of the eigenvalues of $|\mathbf{Q}^2|$. Hence, premultiplying (7.2.22) by $|\boldsymbol{\eta}|^{-1}$ gives

$$\left\{ \mathbf{Q}_d^2 + \gamma^2 |\mathbf{U}| \right\} \hat{\mathbf{I}}_{gm} = |\boldsymbol{\eta}|^{-1} |\mathbf{Y}| \hat{\mathbf{V}} + \hat{\mathbf{E}} \quad (7.2.24)$$

where $|\mathbf{U}|$ is the unitary matrix.

Now, for the specific problem being considered here $|\mathbf{Q}_d^2|$ can be calculated in the following way

$$\frac{1}{\sqrt{2}} \begin{vmatrix} (\mathbf{Z}_{11} + \mathbf{Z}_{iw})\mathbf{Y}_{11} + \mathbf{Z}_{12}\mathbf{Y}_{12} & (\mathbf{Z}_{11} + \mathbf{Z}_{iw})\mathbf{Y}_{12} + \mathbf{Z}_{12}\mathbf{Y}_{11} \\ (\mathbf{Z}_{12}\mathbf{Y}_{11} + (\mathbf{Z}_{11} + \mathbf{Z}_{iw})\mathbf{Y}_{12}) & (\mathbf{Z}_{11} + \mathbf{Z}_{iw})\mathbf{Y}_{11} + \mathbf{Z}_{12}\mathbf{Y}_{12} \end{vmatrix} \begin{vmatrix} 1 & 1 \\ 1 & -1 \end{vmatrix} \quad (7.2.25)$$

$$= \frac{1}{\sqrt{2}} \begin{vmatrix} (\mathbf{Z}_{11} + \mathbf{Z}_{iw} + \mathbf{Z}_{12})(\mathbf{Y}_{11} + \mathbf{Y}_{12}) & (\mathbf{Z}_{11} + \mathbf{Z}_{iw} - \mathbf{Z}_{12})(\mathbf{Y}_{11} - \mathbf{Y}_{12}) \\ (\mathbf{Z}_{11} + \mathbf{Z}_{iw} + \mathbf{Z}_{12})(\mathbf{Y}_{11} + \mathbf{Y}_{12}) & -(\mathbf{Z}_{11} + \mathbf{Z}_{iw} - \mathbf{Z}_{12})(\mathbf{Y}_{11} - \mathbf{Y}_{12}) \end{vmatrix}$$

and

$$\frac{1}{\sqrt{2}} \begin{vmatrix} 1 & 1 \\ 1 & -1 \end{vmatrix} \frac{1}{\sqrt{2}} \begin{vmatrix} (\mathbf{Z}_{11} + \mathbf{Z}_{iw} + \mathbf{Z}_{12})(\mathbf{Y}_{11} + \mathbf{Y}_{12}) & (\mathbf{Z}_{11} + \mathbf{Z}_{iw} - \mathbf{Z}_{12})(\mathbf{Y}_{11} - \mathbf{Y}_{12}) \\ (\mathbf{Z}_{11} + \mathbf{Z}_{iw} + \mathbf{Z}_{12})(\mathbf{Y}_{11} + \mathbf{Y}_{12}) & -(\mathbf{Z}_{11} + \mathbf{Z}_{iw} - \mathbf{Z}_{12})(\mathbf{Y}_{11} - \mathbf{Y}_{12}) \end{vmatrix} = \begin{vmatrix} (\mathbf{Z}_{11} + \mathbf{Z}_{iw} + \mathbf{Z}_{12})(\mathbf{Y}_{11} + \mathbf{Y}_{12}) & 0 \\ 0 & (\mathbf{Z}_{11} + \mathbf{Z}_{iw} - \mathbf{Z}_{12})(\mathbf{Y}_{11} - \mathbf{Y}_{12}) \end{vmatrix} \quad (7.2.26)$$

Thus,

(7.2.27)

$$\left\{ \begin{array}{c} (Z_{11} + Z_{iw} + Z_{12})(Y_{11} + Y_{12}) \\ 0 \end{array} \right\} \begin{array}{c} 0 \\ (Z_{11} + Z_{iw} - Z_{12})(Y_{11} - Y_{12}) \end{array} \left| + \gamma^2 \begin{array}{c} 1 \quad 0 \\ 0 \quad 1 \end{array} \right\} \left| \begin{array}{c} \hat{I}_{gm1} \\ \hat{I}_{gm2} \end{array} \right|$$

$$= \frac{1}{\sqrt{2}} \left| \begin{array}{c} 1 \quad 1 \\ 1 \quad -1 \end{array} \right| \left| \begin{array}{c} Y_{11}(\hat{V}_1 + \hat{E}_{ez}^1) + Y_{12}(\hat{V}_2 + \hat{E}_{ez}^2) \\ Y_{12}(\hat{V}_1 + \hat{E}_{ez}^1) + Y_{11}(\hat{V}_2 + \hat{E}_{ez}^2) \end{array} \right| = \frac{1}{\sqrt{2}} \left| \begin{array}{c} (Y_{11} + Y_{12})(\hat{V}_1 + \hat{E}_{ez}^1 + \hat{V}_2 + \hat{E}_{ez}^2) \\ (Y_{11} - Y_{12})(\hat{V}_1 + \hat{E}_{ez}^1 - \hat{V}_2 - \hat{E}_{ez}^2) \end{array} \right|$$

Explicit solutions for differential and common modes

(7.2.27) can easily be solved to obtain

$$\hat{I}_{gm1}(\gamma) = \frac{(Y_{11} + Y_{12})(\hat{V}_1 + \hat{E}_{ez}^1 + \hat{V}_2 + \hat{E}_{ez}^2)}{\sqrt{2}[(Y_{11} + Y_{12})(Z_{11} + Z_{iw} + Z_{12}) + \gamma^2]} \quad (7.2.28)$$

(common geometric mode)

$$\hat{I}_{gm2}(\gamma) = \frac{(Y_{11} - Y_{12})(\hat{V}_1 - \hat{E}_{ez}^1 - \hat{V}_2 + \hat{E}_{ez}^2)}{\sqrt{2}[(Y_{11} - Y_{12})(Z_{11} + Z_{iw} - Z_{12}) + \gamma^2]} \quad (7.2.29)$$

(differential geometric mode)

These are the two geometric components of the current (again, often simply called “modes” in the power industry). The first is the amplitude of the common geometric component (or common mode or ground mode as used in power engineering terminology) and the second is the differential geometric component mode (or differential mode).

To complete these expressions for the current, explicit expressions for the impedances and admittances will be identified. Using (7.2.11) as the basis, the expression for the impedances in (7.2.28) and (7.2.29) are

(7.2.30)

$$Z_{11} + Z_{iw} \pm Z_{12} = \frac{j\omega\mu_0}{2\pi} \left\{ \ln\left(\frac{2h}{a}\right) \pm \ln\left(\frac{s}{d}\right) - J_c(0, h-a, h) \mp J_c(d, h-a, h) \right\} + Z_{iw}$$

where $s = [(2h)^2 + d^2]^{1/2}$ and it has been assumed that $a \ll d$. In each case, the log terms can be combined so that

(7.2.31)

$$Z_{11} + Z_{12} + Z_{iw} = \frac{j\omega\mu_0}{2\pi} \left\{ \ln\left(\frac{2hs}{ad}\right) - J_c(0, h-a, h) - J_c(d, h-a, h) \right\} + Z_{iw}$$

and

(7.2.32)

$$Z_{11} - Z_{12} + Z_{iw} = \frac{j\omega\mu_0}{2\pi} \left\{ \ln\left(\frac{2hd}{as}\right) - J_c(0, h-a, h) + J_c(d, h-a, h) \right\} + Z_{iw}$$

Calculation of the admittance term (i.e., $Y_{11} \pm Y_{12}$) is a bit more complicated because the inverse of the potential coefficient matrix must be evaluated first.

$$|A| = \frac{1}{2\pi\epsilon_0} \begin{vmatrix} \ln\left(\frac{2h}{a}\right) & \ln\left(\frac{s}{d}\right) \\ \ln\left(\frac{s}{d}\right) & \ln\left(\frac{2h}{a}\right) \end{vmatrix} \quad (7.2.33)$$

and its inverse can be shown to be

$$|A|^{-1} = \frac{2\pi\epsilon_0}{\ln^2\left(\frac{2h}{a}\right) - \ln^2\left(\frac{s}{d}\right)} \begin{vmatrix} \ln\left(\frac{2h}{a}\right) & -\ln\left(\frac{s}{d}\right) \\ -\ln\left(\frac{s}{d}\right) & \ln\left(\frac{2h}{a}\right) \end{vmatrix} \quad (7.2.34)$$

so that

$$Y_{11} = \frac{j2\pi\omega\epsilon_0}{\ln^2\left(\frac{2h}{a}\right) - \ln^2\left(\frac{s}{d}\right)} \ln\left(\frac{2h}{a}\right) \quad (7.2.35)$$

and

$$Y_{12} = \frac{-j2\pi\omega\epsilon_0}{\ln^2\left(\frac{2h}{a}\right) - \ln^2\left(\frac{s}{d}\right)} \ln\left(\frac{s}{d}\right) \quad (7.2.36)$$

so that (in general)

$$Y_{11} + Y_{12} = \frac{j2\pi\omega\epsilon_0}{\ln^2\left(\frac{2h}{a}\right) - \ln^2\left(\frac{s}{d}\right)} \left[\ln\left(\frac{2h}{a}\right) - \ln\left(\frac{s}{d}\right) \right] = \frac{j2\pi\omega\epsilon_0}{\ln\left(\frac{2hs}{ad}\right)} \quad (7.2.37)$$

and

$$Y_{11} - Y_{12} = \frac{j2\pi\omega\epsilon_0}{\ln^2\left(\frac{2h}{a}\right) - \ln^2\left(\frac{s}{d}\right)} \left[\ln\left(\frac{2h}{a}\right) + \ln\left(\frac{s}{d}\right) \right] = \frac{j2\pi\omega\epsilon_0}{\ln\left(\frac{2hd}{as}\right)} \quad (7.2.38)$$

Finally, the individual conductor currents (in the spatial transform domain) can be written as

$$\left| \hat{I} \right| = \frac{1}{\sqrt{2}} \begin{vmatrix} 1 & 1 \\ 1 & -1 \end{vmatrix} \left| \hat{I}_{gm} \right| \quad (7.2.39)$$

Thus, explicit expressions for the common and differential mode currents can be written respectively as

$$\hat{I}_1 = \hat{I}_2 = \frac{(Y_{11} + Y_{22}) \left(\hat{V}_1 + \hat{E}_{ez}^1 + \hat{V}_2 + \hat{E}_{ez}^2 \right)}{2(\gamma^2 - \gamma_c^2)} \quad (7.2.40)$$

(common geometric mode)

where

$$\gamma_c^2 = k_0^2 \left(1 - \frac{J_c(0, h-a, h) + J_c(d, h-a, h)}{\ln\left(\frac{2hs}{ad}\right)} \right) - (Y_{11} + Y_{12}) Z_{iw} \quad (7.2.41)$$

and

$$\hat{I}_1 = -\hat{I}_2 = \frac{(Y_{11} - Y_{12}) \left(\hat{V}_1 + \hat{E}_{ez}^1 - \hat{V}_2 - \hat{E}_{ez}^2 \right)}{2(\gamma^2 - \gamma_d^2)} \quad (7.2.42)$$

(differential geometric mode)

where

$$\gamma_d^2 = k_0^2 \left(1 - \frac{J_c(0, h-a, h) - J_c(d, h-a, h)}{\ln\left(\frac{2hd}{as}\right)} \right) - (Y_{11} - Y_{12}) Z_{iw} \quad (7.2.43)$$

These expressions can be transformed into the spatial domain using the inverse Fourier transform and same residue theory used in Section 4.7 More specifically, following (4.7.22) – (4.7.23)

$$\hat{I}_1(z) = \hat{I}_2(z) = \frac{-j(Y_{11} + Y_{12}) \left(\hat{V}_1 + \hat{E}_{ez}^1(\gamma_c) + \hat{V}_2 + \hat{E}_{ez}^2(\gamma_c) \right)}{4\gamma_c} e^{-j\gamma_c z} \quad (7.2.44)$$

for the common mode and for the differential mode

$$\hat{I}_1(z) = -\hat{I}_2(z) = \frac{-j(Y_{11} - Y_{12}) \left(\hat{V}_1 + \hat{E}_{ez}^1(\gamma_d) - \hat{V}_2 - \hat{E}_{ez}^2(\gamma_d) \right)}{4\gamma_d} e^{-j\gamma_d z}. \quad (7.2.45)$$

It has been assumed that $\text{Im}(\gamma_c), \text{Im}(\gamma_d) \leq 0$.

Special cases

Closely spaced conductors – differential mode

Consider the case for which the two wires are close to each other compared to the height above ground as shown in Fig. 7.2.1. Further, assume that the external source amplitude is zero and that the voltage sources are $\hat{V}_1 = \hat{V} = -\hat{V}_2$. In this case, the only currents excited are the differential currents given in (7.2.45).

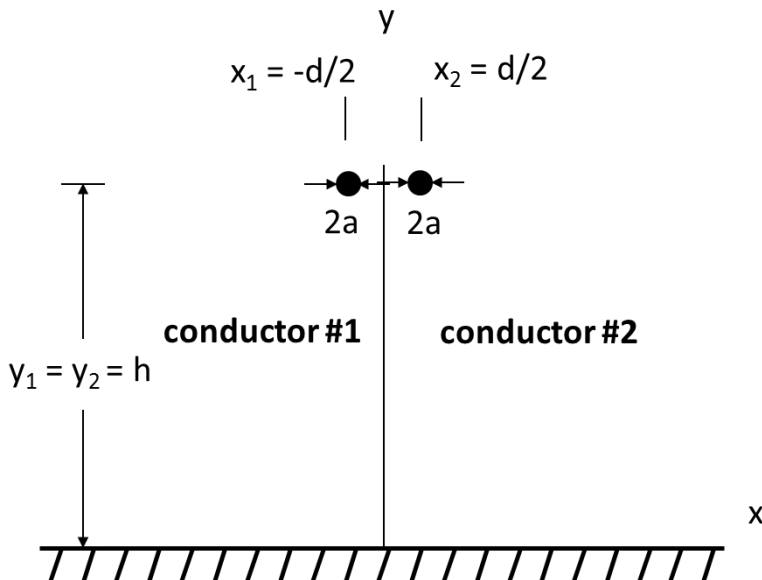


Fig. 7.2.1 Two closely spaced conductors over a lossy earth.

First, since $h \gg d$, it can be shown that

$$J_c(0, h - a, h) \cong J_c(d, h - a, h) \quad (7.2.46)$$

and

$$s = \sqrt{(2h)^2 + (d - a)^2} \cong 2h. \quad (7.2.47)$$

Hence

$$\hat{I}_1(z) = -\hat{I}_2(z) = \frac{-2\pi^2 \omega \epsilon_0 \hat{V}}{\ln\left(\frac{d}{a}\right) \gamma_d} e^{-j\gamma_d z} \quad (7.2.48)$$

where

$$\gamma_d^2 = k_0^2 - j \frac{2\pi \omega \epsilon_0 Z_{iw}}{\ln\left(\frac{d}{a}\right)} \quad (7.2.49)$$

In this case, the effect of the earth is negligible since the fields associated with the conductor currents are confined to points near the conductors. Also, the propagation constant is that for a transmission line mode on a pair of wires in free space as expected. Since high voltage transmission line conductors are relatively close to each other compared to their height above the earth, it can be expected that (at least for modes for which the sum of the currents is zero) the effect of the earth is relatively small. One practical consequence of this is that a power transmission line with conductors that are far from the earth suffers very little energy loss to the earth if it is driven in a balanced fashion so that only the differential component is excited. The only source of loss in (7.2.49) is Z_{iw} , the loss associated with the conductors.

Closely spaced conductors – common mode

Consider, again, the case for which the two wires are close to each other compared to the height above ground as shown in Fig. 7.2.1. Further, assume that the external source amplitude is zero and that the voltage sources are $V_1 = V = V_2$. In this case, the only currents excited are the common currents given in (7.2.44).

Again, (7.2.46) and (7.2.47) hold, so the common mode currents are

$$\hat{I}_{cm1}(z) = \hat{I}_{cm2}(z) = \frac{-\pi^2 \omega \epsilon_0 V}{\ln\left(\frac{2h}{\sqrt{ad}}\right) \gamma_c} e^{-j\gamma_c z} \quad (7.2.50)$$

where

$$\gamma_c^2 = k_0^2 \left(1 - \frac{J_c(0, h, h)}{\ln\left(\frac{2h}{\sqrt{ad}}\right)} - j \frac{\pi\omega\epsilon_0 Z_{iw}}{\ln\left(\frac{2h}{\sqrt{ad}}\right)} \right) \quad (7.2.51)$$

It is interesting to note that this result has almost the same form as that for a single conductor above earth as given in (4.7.20). The only differences are 1) that the radius of the single conductor is replaced by the factor \sqrt{ad} that is called the geomagnetic mean radius of the pair of conductors and 2) the deletion of the factor of 2 in the last term comes from the fact that having two wires in parallel decreases the impedance per unit length by a factor of 2. The factor \sqrt{ad} will surface again when conductor bundles are discussed in Section 7.11. The attenuation constant for the ground mode will generally be much larger than the attenuation constant for the transmission line mode because the return current flows in the lossy earth.

Unbalance due to unsymmetrical terminations

Clearly, there is a transmission line equivalent for each “mode” that can propagate on a two conductor transmission line. These are illustrated in Fig. 7.2.2 in the case for which there is no external source (i.e., $\mathbf{E}_{ze}^1 = \mathbf{E}_{ze}^2 = \mathbf{0}$).

The propagation constants have been given earlier in (7.2.41) and (7.2.43). The characteristic impedances for the “common” and “differential transmission line modes are defined respectively as

$$Z_{0C} = \sqrt{\frac{(Z_{11} + Z_{iw} + Z_{12})}{(Y_{11} + Y_{12})}} \cong \sqrt{\frac{(Z_{11} + Z_{12})}{(Y_{11} + Y_{12})}} \quad (7.2.52)$$

and

$$Z_{0D} = \sqrt{\frac{(Z_{11} + Z_{iw} - Z_{12})}{(Y_{11} - Y_{12})}} \cong \sqrt{\frac{(Z_{11} - Z_{12})}{(Y_{11} - Y_{12})}} \quad (7.2.53)$$

These transmission line modes can become “mixed” in two ways. First, as shown above, a source that is not completely symmetric or anti-symmetric will excite both common and differential modes. Thus, according to Fig. 7.2.2, if $V_1 \neq V_2$ or $V_1 \neq -V_2$, both common and differential modes will be excited and currents will be excited on both equivalent transmission lines. Second, if the transmission line is finite in length, then the terminations of the transmission line at its ends may (if the load is not perfectly symmetric or

anti-symmetric) cause reflections that consist of both modes even if only one is incident. Consider the impedance loading circuit illustrated in Fig. 7.2.3.

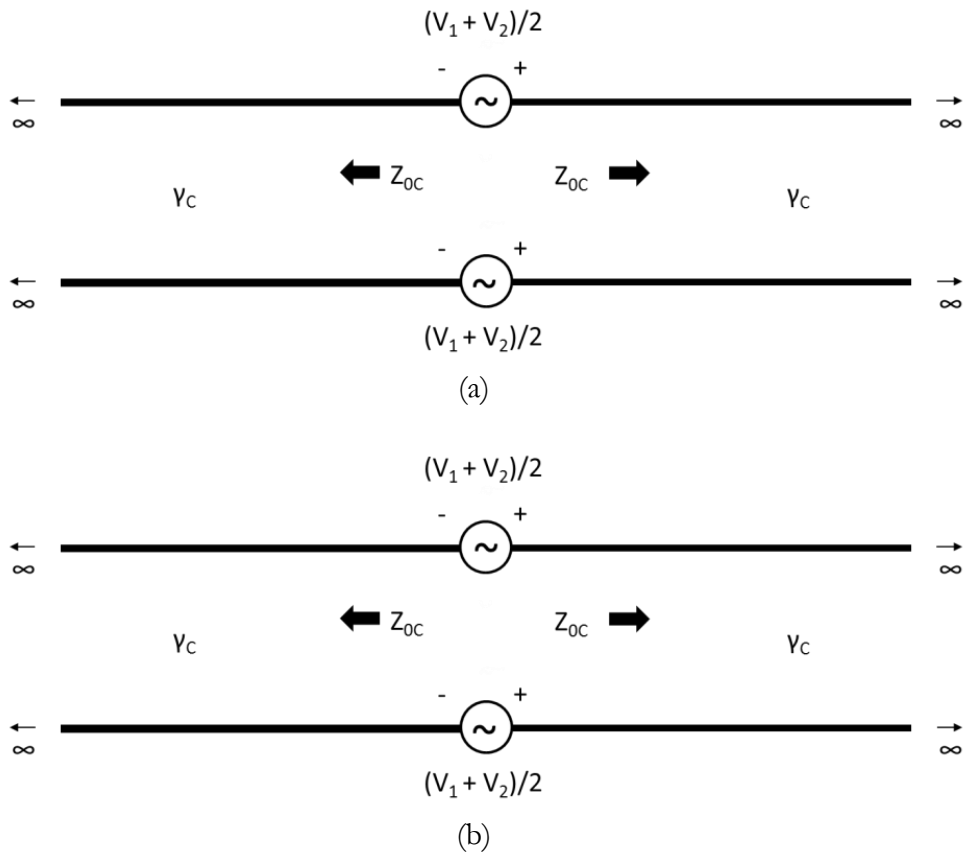


Fig. 7.2.2. Equivalent transmission lines for a symmetric two wire transmission line above the earth a) common mode b) differential mode

If symmetry is preserved at the terminations, so that $Z_{L1G} = Z_{L2G}$, then the reflection coefficients for incident common and differential modes respectively are

$$\Gamma_{cc} = \frac{Z_{L1G}/2 - Z_{0C}}{Z_{L1G}/2 + Z_{0C}}, \tag{7.2.54}$$

$$\Gamma_{dd} = \frac{\frac{2Z_{L1G}Z_{L12}}{Z_{L12} + 2Z_{L1G}} - Z_{0D}}{\frac{2Z_{L1G}Z_{L12}}{Z_{L12} + 2Z_{L1G}} + Z_{0D}} = \frac{2Z_{L1G}Z_{L12} - Z_{0D}(Z_{L12} + 2Z_{L1G})}{2Z_{L1G}Z_{L12} + Z_{0D}(Z_{L12} + 2Z_{L1G})} \tag{7.2.55}$$

If however, $Z_{L1G} \neq Z_{L2G}$, the reflected wave is a mixture of common and differential modes. The several pertinent reflection coefficients can be derived as follows.

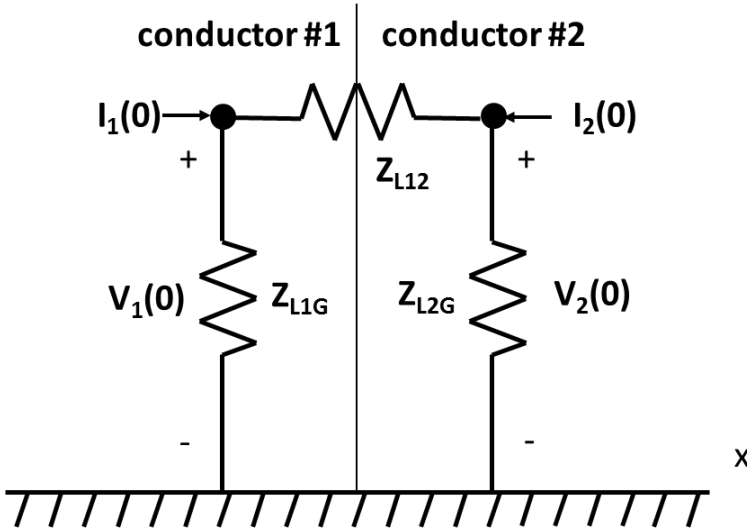


Fig. 7.2.3. Loads for a symmetric, two conductor transmission line at $z = \ell$.

Assume that the load is located at $z = 0$ and that the incident differential and common mode waves are $v_{df} e^{-j\gamma_d z}$ and $v_{cf} e^{-j\gamma_c z}$ respectively. In terms of these incident wave amplitudes (i.e. v_{df} and v_{cf}) and appropriate in-mode and cross-mode reflection coefficients, the voltages (with respect to perfect earth) and currents at $z = 0$ are

$$\begin{aligned}
 V_1(0) &= v_{df} (1 + \Gamma_{dd} + \Gamma_{dc}) / 2 + v_{cf} (1 + \Gamma_{cc} + \Gamma_{cd}) \\
 V_2(0) &= v_{df} (-1 - \Gamma_{dd} + \Gamma_{dc}) / 2 + v_{cf} (1 + \Gamma_{cc} - \Gamma_{cd}) \\
 I_1(0) &= v_{df} (Y_{0d} - Y_{0d} \Gamma_{dd} - Y_{0c} \Gamma_{dc}) + v_{cf} (Y_{0c} - Y_{0c} \Gamma_{cc} - Y_{0d} \Gamma_{cd}) \\
 I_2(0) &= v_{df} (-Y_{0d} + Y_{0d} \Gamma_{dd} - Y_{0c} \Gamma_{dc}) + v_{cf} (Y_{0c} - Y_{0c} \Gamma_{cc} + Y_{0d} \Gamma_{cd})
 \end{aligned} \tag{7.2.56}$$

Here note that v_{df} is the voltage between the two conductors and (given symmetry) the voltage between conductor 1 and 2 and ground is $v_{df} / 2$ and $-v_{df} / 2$, respectively, while v_{cf} is the voltage to ground of either conductor. In addition, the direction of the differential mode current for each conductor is opposite and, upon reflection, the current on either conductor changes sign.

Application of nodal analysis to the system in Fig. 7.2.3 yields another relationship between these voltages and currents

$$\begin{aligned}
I_1(0) &= V_1(0)(Y_{L1G} + Y_{L12}) - V_2(0)Y_{L12} \\
I_2(0) &= -V_1(0)Y_{L12} + V_2(0)(Y_{L2G} + Y_{L12})
\end{aligned} \tag{7.2.57}$$

The unknown reflection coefficients can be found by assuming (in succession) that the only incident wave is the differential (common) mode. In the first case, $v_{cf} = 0$ and equating the second two equations of (7.2.56) to the two equations in (7.2.57) and using the first two of (7.2.56) yields

$$\begin{aligned}
(Y_{0d} - Y_{0d}\Gamma_{dd} - Y_{0c}\Gamma_{dc}) &= \\
(Y_{L1G} + Y_{L12})(1 + \Gamma_{dd} + \Gamma_{dc})/2 - Y_{L12}(-1 - \Gamma_{dd} + \Gamma_{dc})/2 & \\
(-Y_{0d} + Y_{0d}\Gamma_{dd} - Y_{0c}\Gamma_{dc}) &= \\
-Y_{L12}(1 + \Gamma_{dd} + \Gamma_{dc})/2 + (Y_{L2G} + Y_{L12})(-1 - \Gamma_{dd} + \Gamma_{dc})/2 &
\end{aligned} \tag{7.2.58}$$

These can be rearranged in matrix form to give

$$\begin{vmatrix} Y_{0d} + Y_{L1G}/2 + Y_{L12} & Y_{0c} + Y_{L1G}/2 \\ Y_{0d} + Y_{L2G}/2 + Y_{L12} & -Y_{0c} - Y_{L2G}/2 \end{vmatrix} \begin{vmatrix} \Gamma_{dd} \\ \Gamma_{dc} \end{vmatrix} = \begin{vmatrix} Y_{0d} - Y_{L1G}/2 - Y_{L12} \\ Y_{0d} - Y_{L2G}/2 - Y_{L12} \end{vmatrix} \tag{7.2.59}$$

Equation (7.2.59) can be solved for Γ_{dd} and Γ_{dc} with the result

$$\begin{vmatrix} \Gamma_{dd} \\ \Gamma_{dc} \end{vmatrix} = \begin{vmatrix} Y_{0d} + Y_{L1G}/2 + Y_{L12} & Y_{0c} + Y_{L1G}/2 \\ Y_{0d} + Y_{L2G}/2 + Y_{L12} & -Y_{0c} - Y_{L2G}/2 \end{vmatrix}^{-1} \begin{vmatrix} Y_{0d} - Y_{L1G}/2 - Y_{L12} \\ Y_{0d} - Y_{L2G}/2 - Y_{L12} \end{vmatrix} \tag{7.2.60}$$

Clearly, in general, an incident differential mode wave causes both differential and common mode reflected waves. However, it can be determined by inspection that, if $Z_{L1G} = Z_{L2G}$, addition of the two equations of (7.2.59) results in

$$\Gamma_{dd} = \frac{Y_{0d} - Y_{L1G}/2 - Y_{L12}}{Y_{0d} + Y_{L1G}/2 + Y_{L12}}, \quad \Gamma_{dc} = 0 \tag{7.2.61}$$

which (after conversion to impedances) is identical to (7.2.55).

In the second case, $v_{df} = 0$ and equating the second two equations of (7.2.56) to the two equations in (7.2.57) and using the first two of (7.2.56) yields

$$\begin{aligned}
(Y_{0c} - Y_{0c}\Gamma_{cc} - Y_{0d}\Gamma_{cd}) &= (Y_{L1G} + Y_{L12})(1 + \Gamma_{cc} + \Gamma_{cd}) - Y_{L12}(1 + \Gamma_{cc} - \Gamma_{cd}) \\
(Y_{0c} - Y_{0c}\Gamma_{cc} + Y_{0d}\Gamma_{cd}) &= -Y_L(1 + \Gamma_{cc} + \Gamma_{cd}) + (Y_{2g} + Y_L)(1 + \Gamma_{cc} - \Gamma_{cd})
\end{aligned} \tag{7.2.62}$$

Again, these can be rearranged in matrix form to give

$$\begin{vmatrix} Y_{0c} + Y_{L1G} & Y_{0d} + Y_{L1G} + 2Y_{L12} \\ Y_{0c} + Y_{L2G} & -Y_{0d} - Y_{L2G} - 2Y_{L12} \end{vmatrix} \begin{vmatrix} \Gamma_{cc} \\ \Gamma_{cd} \end{vmatrix} = \begin{vmatrix} Y_{0c} - Y_{L1G} \\ Y_{0c} - Y_{L2G} \end{vmatrix} \quad (7.2.63)$$

Equation (7.2.63) can be solved for Γ_{cc} and Γ_{cd} .

$$\begin{vmatrix} \Gamma_{cc} \\ \Gamma_{cd} \end{vmatrix} = \begin{vmatrix} Y_{0c} + Y_{L1G} & Y_{0d} + Y_{L1G} + 2Y_{L12} \\ Y_{0c} + Y_{L2G} & -Y_{0d} - Y_{L2G} - 2Y_{L12} \end{vmatrix}^{-1} \begin{vmatrix} Y_{0c} - Y_{L1G} \\ Y_{0c} - Y_{L2G} \end{vmatrix} \quad (7.2.64)$$

Again, in general, an incident common mode wave causes both differential and common mode reflected waves. However, it can be determined by inspection that, if $Z_{L1G} = Z_{L2G}$, addition of the two equations of (7.2.59) results in

$$\Gamma_{cc} = \frac{Y_{0c} - Y_{L1G}}{Y_{0c} + Y_{L1G}}, \quad \Gamma_{cd} = 0 \quad (7.2.65)$$

which (after conversion to impedances) is identical to (7.2.54).

7.3 Examples of Coupling to Multiconductor Transmission Lines

Distant external field high frequency excitation (lightning)

Lightning strokes generate a significant amount of electromagnetic energy that can interact with and disrupt the operation of the electric power transmission and distribution system. In some cases (to be considered in more detail later) the lightning stroke current is directly injected into the power system. In others (the subject of this section), the effects are coupled to the power system electromagnetically. Lightning strokes may occur from cloud to ground or from cloud to cloud. While the purpose of this section is to develop an electromagnetic coupling model rather than to review specific lightning source models, it is appropriate to list a few examples of lightning source models. A comprehensive review of electromagnetic models for cloud to ground lightning has been given by Baba and Rakov (2007). Other models have been described by Delfino et. al. (2011) and Shoory et. al. (2005). Characteristics of Lightning in general as well as specific information about cloud to cloud discharges can be found in (Uman, M. A. 2001).

In all cases, the fundamental element of the lightning model is an elementary electric dipole. Here, this simple model will be used and further specialized to one that is vertical and (so that the essential physics will not be obscured by the mathematics) located in a vertical plane that contains the

center of the power line (i.e., the yz plane in Fig. 7.3.1) to which its energy is being coupled.

Consider again the case for which the two wires are close to each other compared to the height above ground as shown in Fig. 7.2.1. Further, assume that the voltage sources are zero, but there is an external field source. If the external source is distant and the spacing of the wires is small compared to a wavelength, then $\hat{E}_{ze}^1(\gamma) = \hat{E}_{ze}^2(\gamma) \cong \hat{E}_{ze}^2(\gamma)$ and only the common mode is excited. Hence, from (7.2.40) and (7.2.46),

$$\hat{I}_1(\gamma) = \hat{I}_2(\gamma) = \frac{(Y_{11} + Y_{22})\hat{E}_{ez}(\gamma)}{(\gamma^2 - \gamma_c^2)} \quad (7.3.1)$$

where

$$Y_{11} + Y_{12} = \frac{j2\pi\omega\epsilon_0}{\ln\left(\frac{2hs}{ad}\right)} \quad (7.3.2)$$

and

$$\gamma_c^2 = k_0^2 \left(1 - \frac{J_c(0, h, h)}{\ln\left(\frac{2h}{\sqrt{ad}}\right)} \right) - j \frac{\pi\omega\epsilon_0 Z_{iw}}{\ln\left(\frac{2h}{\sqrt{ad}}\right)} \quad (7.3.3)$$

Again, $\hat{E}_{ze}(\gamma)$ represents the spatial Fourier transform with respect to z of the incident electric field.

Using (7.3.1) and the inverse Fourier transform, the current in the space domain can be written as

$$\hat{I}_1(z) = \hat{I}(z) = \hat{I}_2(z) = \frac{j\omega\epsilon_0}{\ln\left(\frac{2hs}{ad}\right)} \int_{-\infty}^{\infty} \frac{\hat{E}_{ez}(\gamma)}{(\gamma^2 - \gamma_c^2)} e^{-j\gamma z} d\gamma \quad (7.3.4)$$

As mentioned above, the source is a distant vertical electric dipole source with dipole moment ($I_0\ell$) located in the yz plane at a distance R from the origin of coordinates as shown in Fig. 7.3.1.

If R is large compared to the wavelength (λ) in free space (i.e., $k_0R = 2\pi R/\lambda \gg 1$), the incident electric field in the yz plane as illustrated in Fig. 7.3.1 can be written as (Ulaby, 2001)

$$\hat{E}_{inc} = -j \frac{\omega\mu_0 I_0 \ell}{4\pi R} \sin(\theta_i) \exp(-jk_0 R) (\bar{a}_z \cos(\theta_i) + \bar{a}_y \sin(\theta_i)) \quad (7.3.5)$$

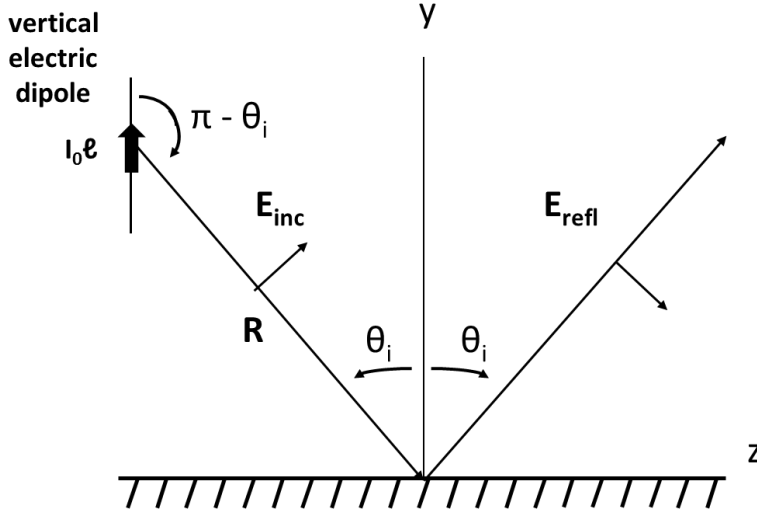


Fig. 7.3.1. A plane wave traveling in the $y z$ plane and incident on the earth at an angle θ_i

Near the earth's surface, this incident field can be approximated as a parallel polarized plane wave where "parallel" means that the electric field is parallel to the plane of incidence (i.e. the yz plane). Given this, the total incident field is that of the incident plane wave and its reflection that is required by the interface boundary conditions. The magnitude and phase of this reflected wave is determined by multiplying the incident wave amplitude by a Fresnel reflection coefficient appropriate to the polarization of the incident field (Ulaby, 2001)

In the space domain, the plane wave and its reflection can be written as (Ulaby 2001)

$$\hat{E}(y, z) = E_0 (\bar{a}_z \cos(\theta_i) + \bar{a}_y \sin(\theta_i)) \exp[-jk_0(z \sin(\theta_i) - y \cos(\theta_i))] + E_0 \Gamma_{par} (\bar{a}_z \cos(\theta_i) - \bar{a}_y \sin(\theta_i)) \exp[-jk_0(z \sin(\theta_i) + y \cos(\theta_i))] \quad (7.3.6)$$

where the Fresnel reflection coefficient can be written as

$$\Gamma_{par} = \frac{-k_2^2 \cos(\theta_i) + \sqrt{k_2^2 - k_0^2 \sin^2(\theta_i)}}{k_2^2 \cos(\theta_i) + \sqrt{k_2^2 - k_0^2 \sin^2(\theta_i)}} \quad (7.3.7)$$

and

$$E_0 = -j \frac{\omega \mu_0 I_0 \ell}{4\pi R} \sin(\theta_i) \exp(-jk_0 R) \quad (7.3.8)$$

Since only the z component is relevant to this derivation, it can be written as

$$\hat{\tilde{E}}_z(y, z) = E_0 \cos(\theta_i) \left[\exp[jk_0 y \cos(\theta_i)] + \Gamma_{par} \exp[-jk_0 y \cos(\theta_i)] \right] \cdot \exp[-jk_0(z \sin(\theta_i))] \quad (7.3.9)$$

The spatial Fourier transform of this expression with respect to z (see (4.3.1)) is

$$\hat{\tilde{E}}_z(y, \gamma) = 2\pi E_0 \cos(\theta_i) \left[\exp[jk_0 y \cos(\theta_i)] + \Gamma_{par} \exp[-jk_0 y \cos(\theta_i)] \right] \cdot \delta(\gamma - k_0 \sin(\theta_i)) \quad (7.3.10)$$

where $\delta(q)$ is the Dirac delta function of argument q .

Using this result, the final expression for the induced current is

$$\hat{i}(z, \omega) = \frac{j\pi\omega\epsilon_0 E_0 \cos(\theta_i)}{\ln\left(\frac{2h}{\sqrt{ad}}\right)} \cdot \frac{\left[\exp[jk_0 h \cos(\theta_i)] + \Gamma_{par} \exp[-jk_0 h \cos(\theta_i)] \right] \exp(-jk_0 z \sin(\theta_i))}{(k_0^2 \sin^2(\theta_i) - \gamma_c^2)} \quad (7.3.11)$$

This result has an interpretation that may not be obvious initially. First, the current has the same phase dependence with respect to z as that of the incident plane wave. This is to be expected. However, as θ_i approaches 90 degrees (i.e., grazing incidence), the amplitude of the induced current becomes quite large. This occurs because $(k_0^2 \sin^2(\theta_i) - \gamma_c^2) = k_0^2 \cos^2(\theta_i) + (\gamma_c^2 - k_0^2) \cong k_0^2 \cos^2(\theta_i)$ since $\gamma_c \approx k_0$. Hence the current is inversely proportional to $\cos(\theta_i)$ until θ_i is small enough that the term $(\gamma_c^2 - k_0^2)$ can no longer be neglected. This behavior has been noted in the literature and is related to the fact that long conductors carrying traveling wave currents radiate at grazing angles (Olsen and Usta, 1977; Olsen and Aburwein, 1980).

As mentioned at the beginning of this section, it is beyond the scope of this text to describe detailed electromagnetic models of lightning (Baba and Rakov 2007). However, it is useful to summarize here how the work described above can be used with lightning models to calculate the currents that are induced by lightning on high voltage transmission lines.

Generally cloud to ground lightning is modeled as a current $i_s(z, t)$ that travels between ground and cloud (for the return stroke) in a vertical channel as illustrated in Fig. 7.3.2.

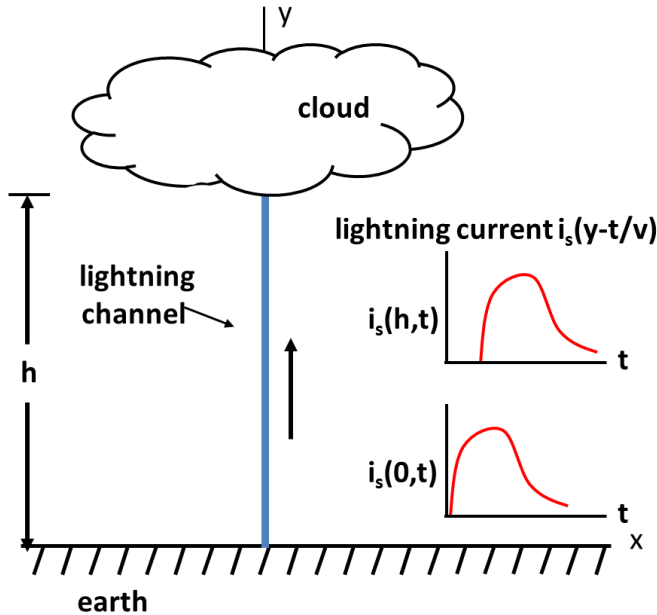


Fig. 7.3.2. A vertical cloud to ground lightning channel of height h carrying a return stroke current with a velocity v from the earth to the cloud.

The current induced on the transmission line due to this current can then be calculated by

- 1) Transforming the current to the frequency domain by taking the temporal Fourier transform using (7.3.12)

$$\tilde{F}(i_s(y,t)) = \tilde{I}_s(y,\omega) = \int_{-\infty}^{\infty} i_s(y,t) e^{-j\omega t} dt \quad (7.3.12)$$

- 2) Decomposing $\tilde{I}_s(y,\omega)$ into short “dipole” segments along the lightning channel shown in Fig. 7.3.2.
- 3) Calculating the induced current $\hat{I}(z,\omega)$ from each segment using (7.3.8) and (7.3.11) and summing to obtain the total induced current.
- 4) Transforming the induced current in the time domain using (7.3.13).

$$\tilde{F}^{-1}(\tilde{I}(z,\omega)) = i(z,t) = \frac{1}{2\pi} \int_{-\infty}^{\infty} \tilde{I}(z,\omega) e^{+j\omega t} d\omega \quad (7.3.13)$$

Distant external field low frequency excitation (geomagnetic induced currents)
 Electric power transmission systems have been designed to operate reliably under well-defined terrestrial weather conditions. However, space weather has also been shown to affect the operations of the transmission system (NASA 2003). More specifically, the sun emits a constant stream of charged

particles known as the solar wind that takes 4-5 days to reach the earth. This activity is cyclic in time and peaks during a relatively short period of an 11 year cycle. The charged particles of the solar wind constitute an electric current and interact with the earth's magnetic field to cause disturbances in the earth's magnetic field called "magnetic storms." Far from the earth's surface where the earth's magnetic field is weak, these currents distort the earth's field so that it appears as a paraboloid pointing at the sun. At closer distances where the earth's field is larger and essentially undistorted, the currents enter the ionosphere, flow along the magnetic field lines (in a more or less east – west direction) and then exit back out of the ionosphere. These ionospheric currents (called the "auroral electrojet") are largest in the northern regions of the earth and are responsible for the visible and very colorful aurora borealis. But the large quasi-DC (i.e., these currents vary on a scale of one to several minutes) electric currents in the ionosphere can also cause large unexpected geomagnetically induced currents (GICs) in high voltage transmission lines (parallel to the currents) and their grounding terminations (IEEE 2013). Absent sufficient warning and the use of appropriate countermeasures, these GICs can cause a severe impact on the transmission system (e.g, high harmonic levels due to saturation of transformer cores, generator reactive power output swings, voltage dips, negative sequence alarms and transformer failures) that can result in severe system disturbances.

In March of 1989 a blackout occurred on the Hydro Quebec transmission system that was attributed to the impact of geomagnetic disturbances caused by solar storm activity (NERC 1989). This incident and numerous other equipment malfunction and/or damage events in both North America and Europe demonstrated the need to account for reliability risks due to space weather and its resultant geomagnetically induced currents (Elovaara et. al. 1992).

As illustrated in Fig. 7.3.3, the quasi-DC ionospheric currents that cause these disturbances are often modeled as high altitude infinitely-long horizontal line currents although sometimes as infinitely-long finite-width sheet currents or finite length horizontal currents with vertical segments at the end to represent the entry and exit of currents from the ionosphere (Pirjola and Hakkinen, 1991). The current resides in the ionosphere at a height on the order of 100 km.

More specifically, Fig. 7.3.3 shows a high altitude auroral electrojet current modeled as a line current parallel to the z axis that intersects the (x, y) plane at (x_s, y_s) . It is assumed that the frequency of the electrojet current is ω_s and that it propagates with propagation constant γ_s (shortly the variation of the fields in time will be shown explicitly). Centered at $(x, y) = (0, h)$ is (for simplicity) a two conductor power line of length ℓ terminated at each end by a balanced transformer with a center tap that is grounded through an impedance of Z_{G2} at $z = 0$ and Z_{G1} at $z = \ell$. It will be assumed here that the current induced on the two conductors (the same holds for the set of three

conductors in a three phase system) are identical and can be replaced by a single conductor centered at $(0, h)$.

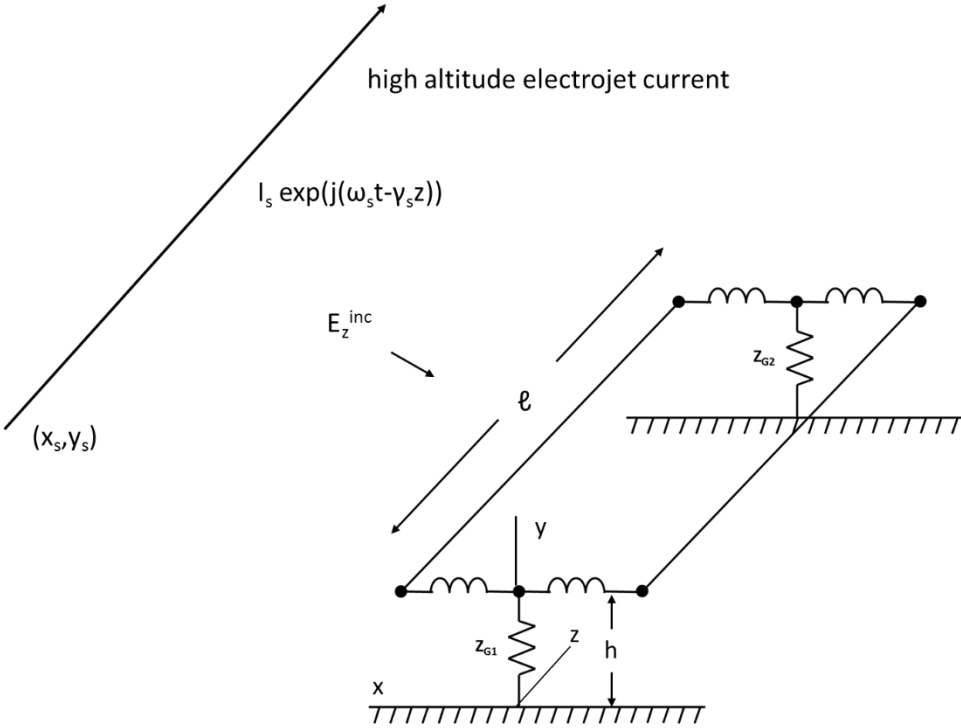


Fig. 7.3.3. High altitude auroral electrojet current above and parallel to a two conductor transmission line.

The auroral electrojet current generates an incident z directed electric field at a point (x, h) (see Section 5 for its derivation) that can be described as the field from the source in free space and a “complex image” that represents the effect of the earth⁶⁵

$$\begin{aligned}
 \tilde{E}_{ez}(x-x_s, h, y_s, z) &= \tilde{G}_{ez}(x-x_s, h, y_s, \gamma_s) \hat{I}_0 e^{-j\gamma_s z} \\
 &= \left\{ \frac{j\gamma_s^2}{2\pi\omega\epsilon_0} \ln\left(\frac{r_s^i}{r_s}\right) - \frac{j\omega\mu_0}{2\pi} \ln\left(\frac{(h+y_s+\alpha)^2 + (x-x_s)^2}{r_s}\right)^{1/2} \right\} \hat{I}_0 e^{-j\gamma_s z}
 \end{aligned}
 \tag{7.3.14}$$

where

⁶⁵ Note that this is not a divergence-less field as is often used in the GIC literature. Hence it is necessary to identify the vertical electric field that reduces to the quasi-static electric field. Its effect will be shown later to cancel out of the final expression so that the result is equivalent to that derived under the assumption of a divergence-less current.

$$\alpha = \frac{2}{k_0 \left[\frac{\epsilon_2}{\epsilon_0} \left(1 - j \frac{\sigma_2}{\omega \epsilon_2} \right) \right]^{1/2}} \cong \sqrt{2} \delta e^{+j\pi/4}$$

and

$$\delta = \frac{\sqrt{2}}{(\sigma_2 \mu_0 \omega)^{1/2}}$$

and

$$r_s = \left((x - x_s)^2 + (h - y_s)^2 \right)^{1/2}, \quad r_s^i = \left((x - x_s)^2 + (h + y_s)^2 \right)^{1/2}.$$

This interpretation (i.e., source plus “complex image”) is illustrated in Fig. 7.3.4. Here the line current source is located in free space at $(x, y) = (x_s, y_s)$ and its return current in the same free space at a complex depth $y_s + \alpha$.

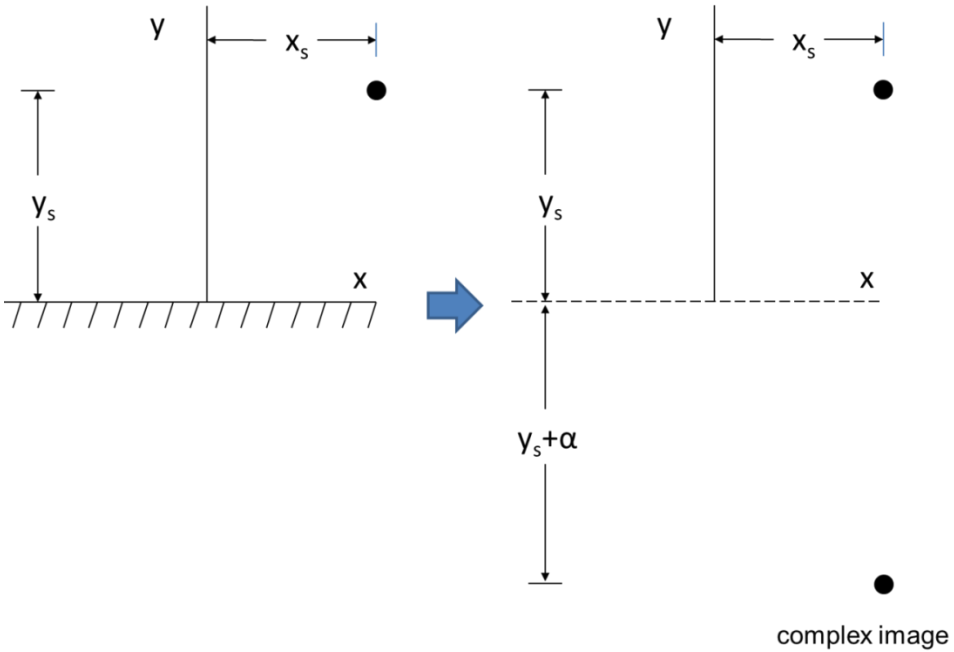


Fig. 7.3.4. Geometry for Complex Image formation of the source field

In the formulations used here, it is also necessary to have an expression for the vertical electric field which is

$$\hat{E}_y(x - x_s, h, y_s, z) \cong \frac{\gamma_s}{2\pi\omega\epsilon_0} \left[\frac{(h - y_s)}{(r_s)^2} - \frac{(h + y_s)}{(r_s^i)^2} \right] \hat{I}_0 e^{-j\gamma_s z} \quad (7.3.15)$$

It is shown in Section 10.3 of this text that for electrically short transmission lines (almost always the case at the frequencies of interest here)

the vertical electric field in (7.3.15) cancels a portion of the axial electric field in (7.3.14) when integrated around the loop. The remaining part of the axial electric field can be identified with inductive coupling between the electrojet current and the transmission line.

It has been assumed in this formulation of the problem that the earth is homogeneous and infinite in depth. This cannot always be assumed because the frequency content of auroral electrojet currents is very low (i.e., $\ll 1$ Hz). For this reason, many calculations of geomagnetically induced currents have assumed 4 or more layers for the earth (and also assumed that the electrical constants for these layers are known) (Erinmez et. al 2000; Boteler and Pirjola 1997).

This field (called \hat{E}_{ez}^{ind}) and an approximate form valid for $y_s \gg \alpha, h$, can be written as

(7.3.16)

$$\begin{aligned} \hat{E}_{ez}^{ind}(x-x_s, h, y_s, z) &= \left\{ -\frac{j\omega\mu_0}{2\pi} \ln \frac{\left((h+y_s+\alpha)^2 + (x-x_s)^2\right)^{1/2}}{r} \right\} \hat{I}_0 e^{-j\gamma_s z} \\ &\cong \left\{ -\frac{j\omega\mu_0}{4\pi} \ln \frac{(1+2y_s(h+\alpha))}{(1-2y_s h/r^2)} \right\} \hat{I}_0 e^{-j\gamma_s z} \\ &\cong -\frac{j\omega\mu_0}{2\pi} \frac{y_s(2h+\alpha)}{r^2} \hat{I}_0 e^{-j\gamma_s z} \cong -\frac{j\omega\mu_0}{2\pi} \frac{y_s\alpha}{r^2} \hat{I}_0 e^{-j\gamma_s z} \end{aligned}$$

since $\alpha \gg h$. To show the explicit dependence on frequency and conductivity, (7.3.16) can be written (using the approximation for α in (7.3.14)) as

$$\hat{E}_{ez}^{ind}(x-x_s, h, y_s, z) \cong -\frac{j(\omega\mu_0)^{1/2}}{\pi(\sigma_2)^{1/2}} \frac{y_s}{r^2} e^{+j\pi/4} \hat{I}_0 e^{-j\gamma_s z} \quad (7.3.17)$$

One thing evident at this point is that (for given values of grounding impedance) the currents induced are larger for a region with low conductivity (i.e., high resistivity).

Without going into details at this point, the current induced on the power line by an electrojet current directly above it is proportional to \hat{E}_{ez}^{ind} and the length of the transmission line ℓ and inversely proportional to the total quasi-DC impedance of the transmission line including the grounding impedances⁶⁶. The result is

⁶⁶ When the vertical electric field is integrated over the vertical end segments of the transmission line, it cancels the quasi-electrostatic portion of the horizontal electric field for

$$\tilde{I}_{ind}(z, \omega) = \tilde{H}'(z, \omega) \tilde{I}_s(\omega) \quad (7.3.18)$$

where the transfer function $\tilde{H}'(z, \omega)$ can be written as⁶⁷

$$\tilde{H}'(z, \omega) = \frac{j\sqrt{\omega\mu_0} e^{+j\pi/4} \ell}{\pi\sqrt{\sigma_2} (Z_{G1} + Z_{G2} + (2h + \ell)Z_{sw})} \frac{y_s}{r^2} e^{-j\gamma_s z} \quad (7.3.19)$$

Here $\tilde{I}_s(\omega)$ is the temporal Fourier transform of the electrojet current, $i_s(t)$, Z_{sw} is the self-impedance per unit length of the two parallel conductors, $2h + \ell$ is the total length of the transmission line including the vertical segments each of length h and the grounding impedances Z_{G1} and Z_{G2} include the resistance and inductance of the transformer windings (at the quasi-DC frequencies of interest here) through which the induced current flows.

Given this result, it is relatively straightforward to see how the time domain electric field can be calculated. The derivation begins with the definition of the temporal Fourier transform and its inverse that can be found in (7.3.12) and (7.3.13). Using the convolution identity, the inverse Fourier transform of the product $\tilde{F}(\omega)\tilde{H}(\omega)$ can be written as

$$(7.3.20)$$

$$\tilde{F}^{-1}[\tilde{F}(\omega)\tilde{H}'(\omega)] = \int_{-\infty}^{\infty} h'(t')f(t-t')dt' = \int_0^{\infty} h'(t')f(t-t')dt' = \int_{-\infty}^t h'(t-t')f(t')dt'$$

where the last steps can be taken because $h(t)$ is the response to an impulse at $t = 0$ and hence, $h'(t-t') = 0$ for $t' > t$.

For typical geomagnetic source currents, the induced current $\tilde{I}_{ind}(z, \omega)$ satisfies the conditions for its inverse transform to exist (Brigham, 1974). However, the inverse Fourier transform of $\tilde{H}'(z, \omega)$ does not exist because the function $\sqrt{\omega}$ is not integrable over the infinite range. To resolve this situation, the inverse Fourier transform of the temporal integral of the induced current will be found with the final result for the induced current being the time derivative of this result. This can easily be done since the following transform exists

electrically short transmission lines. The only remaining term is the “inductive coupling term.” This phenomenon is described more fully in Chapter 10, Section 3.

⁶⁷ The designation H' is given to the transfer function because as will be illustrated shortly, the inverse transform into the time domain will be done using the integral of H' in the frequency domain.

$$\tilde{F}\left(\int^t h'(t')dt'\right) = \frac{\tilde{H}'(\omega)}{j\omega} = \tilde{H}(\omega) \quad (7.3.21)$$

More specifically, the inverse Fourier transform of

$$\begin{aligned} \tilde{F}^{-1}\left[\frac{\tilde{I}_{ind}(z, \omega)}{j\omega}\right] &= \tilde{F}^{-1}\left[\frac{\tilde{H}'(z, \omega)}{j\omega}\tilde{I}_s(\omega)\right] = \\ \tilde{F}^{-1}\left[\tilde{H}(z, \omega)\tilde{I}_s(\omega)\right] &= \int_{-\infty}^t h(z, t-t')i_s(t')dt' \end{aligned} \quad (7.3.22)$$

will be found where

$$\tilde{H}(z, \omega) = \frac{\tilde{H}'(z, \omega)}{j\omega} = \frac{Ae^{j\theta_A}}{\sqrt{\omega}} \quad (7.3.23)$$

It has been assumed that the frequency is low enough that all impedances in (7.3.19) are purely resistive. Hence the only frequency dependence is the $1/\sqrt{\omega}$ term and A and θ_A are real constants. Next, it is known that

$$\frac{1}{\sqrt{t}} \Leftrightarrow \sqrt{\frac{2\pi}{\omega}} \quad (7.3.24)$$

represents a Fourier transform pair. Hence,

$$h(t) = \frac{A\cos(\theta_A)}{\sqrt{2\pi t}} \quad (7.3.25)$$

where A is the same constant defined above.

Finally, since the ultimate goal is to calculate the induced current which is the time derivative of the result just obtained,

$$i_{ind}(t) = \frac{A\cos(\theta_A)}{\sqrt{2\pi}} \frac{d}{dt} \left[\int_{-\infty}^t \frac{i_s(t')}{\sqrt{t-t'}} dt' \right] \quad (7.3.26)$$

Consider next an example of using this result for calculating induced currents in a power line. In this case, the normalized induced current

$$i_{normalized} = \frac{\sqrt{2\pi}i_{ind}(t)}{A\cos(\theta_A)} = \frac{d}{dt} \left[\int_{-\infty}^t \frac{i_s(t')}{\sqrt{t-t'}} dt' \right] \quad (7.3.27)$$

is calculated. The source current is assumed to be a linearly growing current for $T_0 = 200$ seconds that reaches 20 kA and then (unphysically) stops abruptly as shown in Fig. 7.3.5

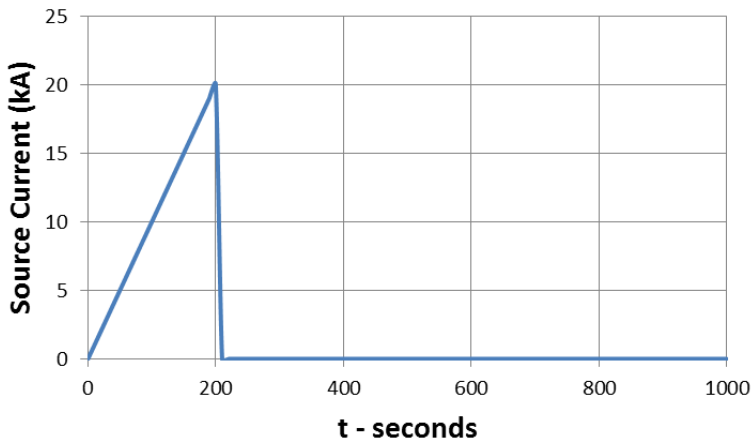


Fig. 7.3.5. Auroral Electrojet Source Current

Using integral tables from Gradshteyn and Ryzhik (2007), (7.3.27) can be evaluated to give

$$I_{normalized} = \begin{cases} 0.2\sqrt{t} & t \leq T_0 \\ 0.2 \left[\sqrt{t} - \frac{6t - 5T_0}{3\sqrt{t - T_0}} \right] & t > T_0 \end{cases} \quad (7.3.28)$$

where $T_0 = 200$ seconds. The normalized current is shown in Fig. 7.3.6.

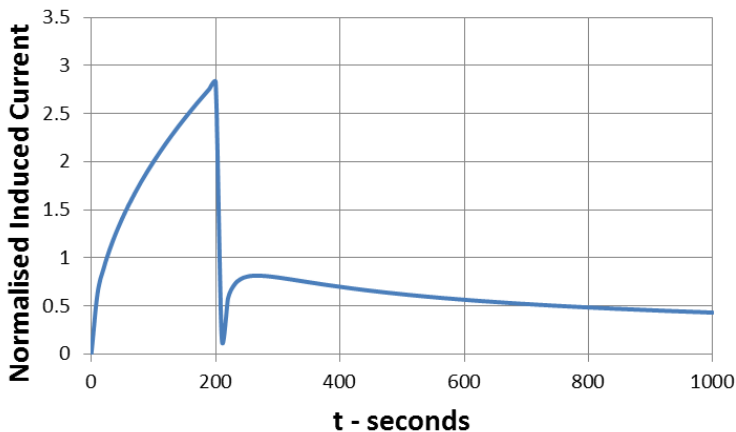


Fig. 7.3.6. Normalized current induced in a power line by the electrojet current shown in Fig. 7.3.5.

Because of the dispersive nature of the earth, the current increases as the square root of time and aside from a (nonphysical) spike due to the assumed abrupt current cutoff, decays very slowly towards zero after the source current becomes zero.

With respect to the time variation of the system voltages and currents, this geomagnetic induced current causes a nearly constant current (in the transformer windings). This current, in turn, creates a nearly constant flux through the cores of the transformers terminating the transmission line.

Now that the current induced on the transmission line has been found, the issue of its effect on the power system and its components will be addressed. More specifically, the effect of this quasi-dc current on the transformers that terminate the transmission line will be addressed.

The relationship between the voltage $v_w(t)$ across a transformer's winding terminals and the flux $\phi_c(t)$ in its core is (Chapman 2002)

$$\phi_c(t) = \frac{1}{N_w} \int v_w(t) dt \quad (7.3.29)$$

Hence, if the system voltage across the winding is

$$v_w(t) = V_m \cos(\omega t) \quad (7.3.30)$$

The flux passing through the transformer core is sinusoidal and equal to

$$\phi_c(t) = \frac{V_m}{\omega N_w} \sin(\omega t) \quad (7.3.31)$$

Now, the core of the transformer is generally made of nonlinear material so that the relationship between flux (or the magnetic flux density, B) and the current flowing in the winding (proportional to the magnetic field intensity, H) in the winding is also nonlinear. A somewhat idealized version of the relationship between flux and current is illustrated in Fig. 7.3.7.

In this case, the relationship between flux (or B) and current (or H) is linear (i.e., $i_w = \phi/10$) as long as the flux is less than 10 (unspecified units). However, if the total flux either exceeds 10 or is smaller than -10, the increase in i_w for a given increase in ϕ is markedly greater (i.e., $\Delta i_w = +/- 5.0\phi$).

Consider, first the transformer under normal operating conditions for which the transformer is approximately linear. In this case, the winding current is simply

$$i_w(t) = \frac{AV_m}{\omega N_w} \sin(\omega t) \quad (7.3.32)$$

where the constant A is determined by the characteristics of the core. If however, there is a quasi-DC geomagnetically induced flux ϕ_{gi} in the core, then the total flux in the core is now

$$\phi_c(t) = \phi_{gi} + \frac{V_m}{\omega N_w} \sin(\omega t) \quad (7.3.33)$$

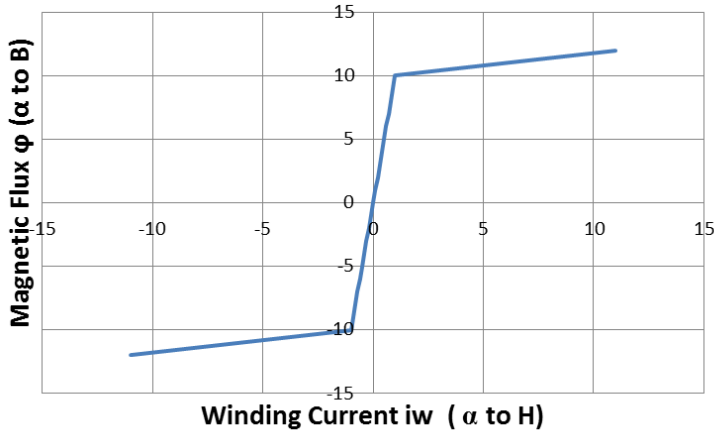


Fig. 7.3.7. Idealized transformer flux-current characteristic (no specific units).

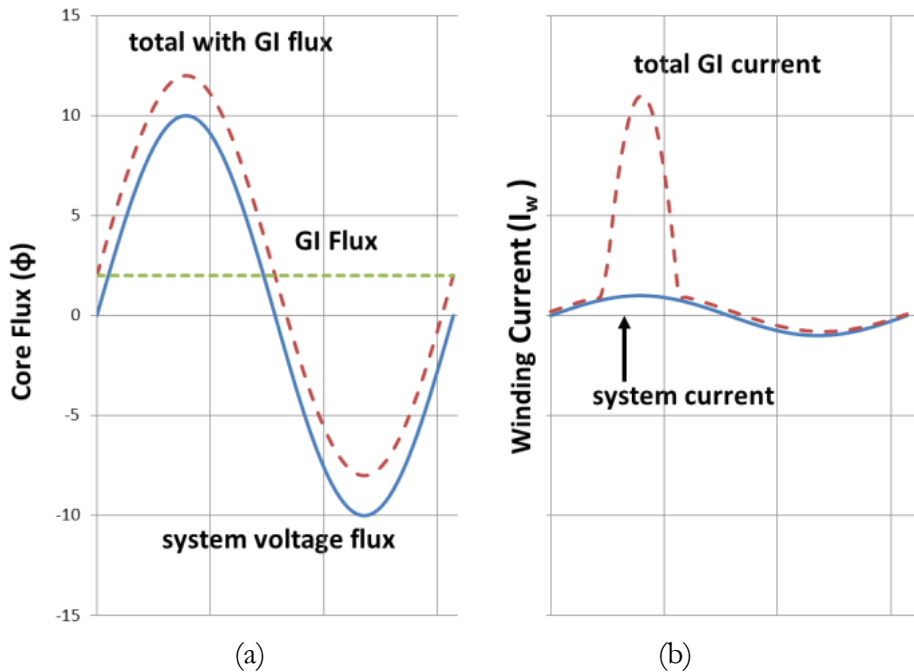


Fig. 7.3.8. a) Transformer core flux components (no specific units) and b) Total transformer winding current with and without the geomagnetically induced flux assuming the transformer characteristic given in Fig. 7.3.7 (no specific units).

The geomagnetically induced core flux ϕ_{gi} , the core flux without any geomagnetically induced flux (i.e., 7.3.31) and the total core flux (i.e., 7.3.33) are plotted in Fig. 7.3.8a. While under normal operating conditions, the core flux does not enter the saturation region, the total flux (including the geomagnetically induced flux) exceeds the level at which the core enters saturation at peak flux values (i.e., in this case those for which the total flux exceeds 10 units on the scale of Fig. 7.3.8a).

The transformer winding current is radically different during the half cycle for which the geomagnetically induced flux adds to the normal flux due to the fact that the transformer core saturates for values of flux greater than 10 (in this example). This winding current with and without the added quasi-DC flux is plotted in Fig. 7.3.8b. Clearly even small excursions of the total flux into the saturation region can cause very large increases in winding current for short periods of time during each cycle that can (as mentioned earlier) have significant consequences for the operation of the power system (IEEE 2013). These include transformer heating (although modeling and experience indicate that this is not a large problem), transformer shunt reactive loading that can cause voltage stability issues and the introduction of large harmonic currents that can lead to unintended relay tripping.

Unbalanced excitation of the transmission line (phase-to-ground fault current or lightning injection)

The purpose of this section is to find the current distribution on a two wire symmetric transmission line due to a current injected (or removed) at the center of the first conductor as shown in Fig. 7.3.9. This situation can occur when either there is a phase to ground fault or a lightning strike to the conductor.

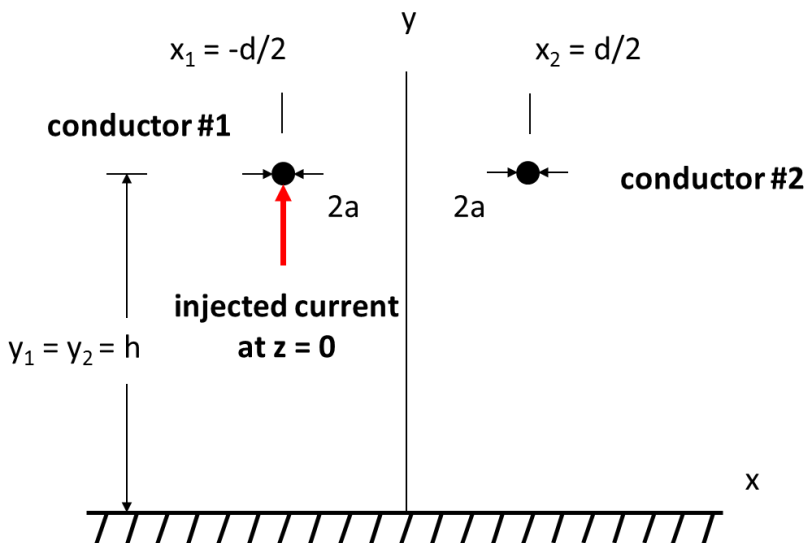


Fig. 7.3.9. A current injected into conductor #1 at $z = 0$.

At low frequencies, this problem can be solved using the existing solution for a voltage source on the conductor in the following way. Consider the set of two equal and opposite voltage sources on conductor #1 (with no sources on conductor #2) separated by a distance δ as illustrated in Fig. 7.3.9. Notice that the total voltage across the pair of sources is zero but there is a difference in current at $z = 0$ that is supplied by an injected current. This is characteristic of a current source driving the conductor at $z = 0$.

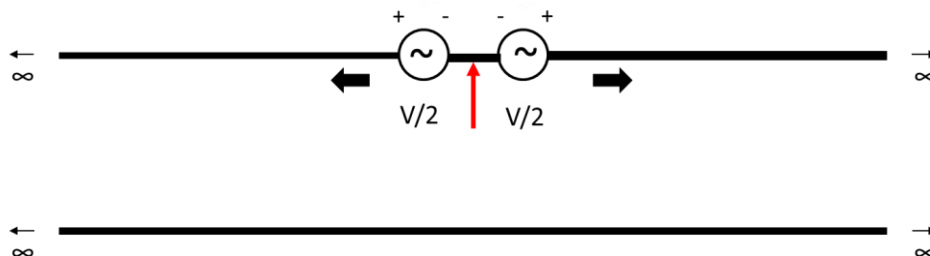


Fig. 7.3.10. Voltage sources with equal and opposite amplitudes separated by a distance δ on conductor #1 of a symmetric two conductor transmission line.

The current to the right can be calculated by superimposing the current from the two sources and assuming that the difference in currents at $z = 0$ is the injected current. Here, the current for $z > 0$ will be found; the current for $z < 0$ can be found in a similar way.

The fundamental result needed is that for the geometry shown in Fig. 7.1.1 with the external electric field set equal to zero. The starting point is Equations (7.2.44) and (7.2.45) for the common and differential mode currents with the respective propagation constants in (7.2.41) and (7.2.43).

The total currents for $z > \delta/2$ on conductors #1 and #2 respectively due to a single voltage source of amplitude $\hat{V}(\omega)/2$ at $z = \delta/2$ on conductor #1 is⁶⁸

$$\hat{I}_1(z) = \frac{-j(Y_{11} + Y_{12})\hat{V}(\omega)}{8\gamma_c} e^{-j\gamma_c|z-\delta/2|} - \frac{j(Y_{11} - Y_{12})\hat{V}(\omega)}{8\gamma_d} e^{-j\gamma_d|z-\delta/2|} \quad (7.3.34)$$

and

$$\hat{I}_2(z) = \frac{-j(Y_{11} + Y_{12})\hat{V}(\omega)}{8\gamma_c} e^{-j\gamma_c|z-\delta/2|} + \frac{j(Y_{11} - Y_{12})\hat{V}(\omega)}{8\gamma_d} e^{-j\gamma_d|z-\delta/2|} \quad (7.3.35)$$

Similarly, the currents for $z > \delta/2$ on conductors #1 and #2 respectively due to a single voltage source of amplitude $-\hat{V}(\omega)/2$ at $z = -\delta/2$ on conductor #1 is

⁶⁸ Of course this is a low frequency approximation, but should be valid to frequencies up to at least 1 MHz. The solutions for arbitrary frequencies can be found earlier in this chapter.

$$\hat{I}_1(z) = \frac{j(Y_{11} + Y_{12})\hat{V}(\omega)}{8\gamma_c} e^{-j\gamma_c|z+\delta/2|} + \frac{j(Y_{11} - Y_{12})\hat{V}(\omega)}{8\gamma_d} e^{-j\gamma_d|z+\delta/2|} \quad (7.3.36)$$

and

$$\hat{I}_1(z) = \frac{j(Y_{11} + Y_{12})\hat{V}(\omega)}{8\gamma_c} e^{-j\gamma_c|z+\delta/2|} + \frac{j(Y_{11} - Y_{12})\hat{V}(\omega)}{8\gamma_d} e^{-j\gamma_d|z+\delta/2|} \quad (7.3.37)$$

The total current on conductor #1 due to both sources (for $z > \delta/2$) is then

$$\begin{aligned} \hat{I}_1(z) = \frac{-j\hat{V}(\omega)}{8} \left\{ (Y_{11} + Y_{12})e^{-j\gamma_c z} \left(\frac{e^{j\gamma_c \delta/2} - e^{-j\gamma_c \delta/2}}{\gamma_c} \right) \right. \\ \left. + (Y_{11} - Y_{12})e^{-j\gamma_d z} \left(\frac{e^{j\gamma_d \delta/2} - e^{-j\gamma_d \delta/2}}{\gamma_d} \right) \right\} \end{aligned} \quad (7.3.38)$$

while the total current on conductor #2 from both sources (for $z > \delta/2$) is

$$\begin{aligned} \hat{I}_2(z) = \frac{-j\hat{V}(\omega)}{8} \left\{ (Y_{11} + Y_{12})e^{-j\gamma_c z} \left(\frac{e^{j\gamma_c \delta/2} - e^{-j\gamma_c \delta/2}}{\gamma_c} \right) \right. \\ \left. - (Y_{11} - Y_{12})e^{-j\gamma_d z} \left(\frac{e^{j\gamma_d \delta/2} - e^{-j\gamma_d \delta/2}}{\gamma_d} \right) \right\}. \end{aligned} \quad (7.3.39)$$

Now, $\gamma_c \delta/2, \gamma_d \delta/2 \ll 1$ because δ is assumed to be small compared to the wavelength of either mode, hence the terms involving δ in (7.3.38) and (7.3.39) can be simplified as

$$\left(\frac{e^{j\gamma_c \delta/2} - e^{-j\gamma_c \delta/2}}{\gamma_c} \right) = j2 \frac{\sin(\gamma_c \delta/2)}{\gamma_c} \cong j\delta \quad (7.3.40)$$

and

$$\left(\frac{e^{j\gamma_d \delta/2} - e^{-j\gamma_d \delta/2}}{\gamma_d} \right) = j2 \frac{\sin(\gamma_d \delta/2)}{\gamma_d} \cong j\delta \quad (7.3.41)$$

Hence, (7.3.38) and (7.3.39) become

$$\hat{I}_1(z) = \frac{\delta(Y_{11} + Y_{12})\hat{V}(\omega)}{8} e^{-j\gamma_c z} + \frac{\delta(Y_{11} - Y_{12})\hat{V}(\omega)}{8} e^{-j\gamma_d z}, \quad z > 0 \quad (7.3.42)$$

and

$$\hat{I}_2(z) = \frac{\delta(Y_{11} + Y_{12})\hat{V}(\omega)}{8} e^{-j\gamma_c z} - \frac{(Y_{11} - Y_{12})V(\omega)}{8} e^{-j\gamma_d z}, \quad z > 0 \quad (7.3.43)$$

These can be simplified further to

$$\hat{I}_1(z) = \frac{\delta\hat{V}(\omega)Y_{11}}{8} \left[\left(1 + \frac{Y_{12}}{Y_{11}}\right) e^{-j\gamma_c z} + \left(1 - \frac{Y_{12}}{Y_{11}}\right) e^{-j\gamma_d z} \right], \quad z > 0 \quad (7.3.44)$$

and

$$\hat{I}_2(z) = \frac{\delta\hat{V}(\omega)Y_{11}}{8} \left[\left(1 + \frac{Y_{12}}{Y_{11}}\right) e^{-j\gamma_c z} - \left(1 - \frac{Y_{12}}{Y_{11}}\right) e^{-j\gamma_d z} \right], \quad z > 0 \quad (7.3.45)$$

Now, from (7.2.35) and (7.2.36)

$$Y_{11} = \frac{j2\pi\omega\epsilon_0}{\ln^2\left(\frac{2h}{a}\right) - \ln^2\left(\frac{s}{d}\right)} \ln\left(\frac{2h}{a}\right) \quad (7.3.46)$$

and

$$Y_{12} = \frac{-j2\pi\omega\epsilon_0}{\ln^2\left(\frac{2h}{a}\right) - \ln^2\left(\frac{s}{d}\right)} \ln\left(\frac{s}{d}\right). \quad (7.3.47)$$

Hence

$$\frac{Y_{12}}{Y_{11}} = -\frac{\ln\left(\frac{s}{d}\right)}{\ln\left(\frac{2h}{a}\right)}. \quad (7.3.48)$$

Hence,

$$\hat{I}_1(z) = \frac{\delta\hat{V}(\omega)Y_{11}}{8} \left[\left(1 - \frac{\ln\left(\frac{s}{d}\right)}{\ln\left(\frac{2h}{a}\right)}\right) e^{-j\gamma_c z} + \left(1 + \frac{\ln\left(\frac{s}{d}\right)}{\ln\left(\frac{2h}{a}\right)}\right) e^{-j\gamma_d z} \right], \quad z > 0 \quad (7.3.49)$$

and

$$\hat{I}_2(z) = \frac{\delta\hat{V}(\omega)Y_{11}}{8} \left[\left(1 - \frac{\ln\left(\frac{s}{d}\right)}{\ln\left(\frac{2h}{a}\right)}\right) e^{-j\gamma_c z} - \left(1 + \frac{\ln\left(\frac{s}{d}\right)}{\ln\left(\frac{2h}{a}\right)}\right) e^{-j\gamma_d z} \right], \quad z > 0 \quad (7.3.50)$$

where from (7.2.41) and (7.2.43)

$$\gamma_c^2 = k_0^2 \left(1 - \frac{J_c(0, h-a, h) + J_c(d, h-a, h)}{\ln\left(\frac{2hs}{ad}\right)} \right) - (Y_{11} + Y_{12})Z_{iw} \quad (7.3.51)$$

and

$$\gamma_d^2 = k_0^2 \left(1 - \frac{J_c(0, h-a, h) - J_c(d, h-a, h)}{\ln\left(\frac{2hd}{as}\right)} \right) - (Y_{11} - Y_{12})Z_{iw}. \quad (7.3.52)$$

where $s = [(2h)^2 + d^2]^{1/2}$.

Now, γ_c and γ_d can be written as

$$\gamma_c = \frac{(\gamma_c + \gamma_d)}{2} + \frac{(\gamma_c - \gamma_d)}{2} \quad (7.3.53)$$

and

$$\gamma_d = \frac{(\gamma_c + \gamma_d)}{2} - \frac{(\gamma_c - \gamma_d)}{2} \quad (7.3.54)$$

With these substitutions the currents for $z > 0$, can be written as

$$\hat{I}_1(z) = \frac{\delta\hat{V}(\omega)Y_{11}}{4} e^{-j\frac{(\gamma_c + \gamma_d)}{2}z} \left[\left(\frac{e^{-j\frac{(\gamma_c - \gamma_d)}{2}z} + e^{+j\frac{(\gamma_c - \gamma_d)}{2}z}}{2} \right) - j \left(\frac{\ln\left(\frac{s}{d}\right)}{\ln\left(\frac{2h}{a}\right)} \right) \left(\frac{e^{-j\frac{(\gamma_c - \gamma_d)}{2}z} - e^{+j\frac{(\gamma_c - \gamma_d)}{2}z}}{2j} \right) \right] \quad (7.3.55)$$

and

$$\hat{I}_2(z) = \frac{\delta\hat{V}(\omega)Y_{11}}{4} e^{-j\frac{(\gamma_c + \gamma_d)}{2}z} \left[j \left(\frac{e^{-j\frac{(\gamma_c - \gamma_d)}{2}z} - e^{+j\frac{(\gamma_c - \gamma_d)}{2}z}}{2j} \right) - \left(\frac{\ln\left(\frac{s}{d}\right)}{\ln\left(\frac{2h}{a}\right)} \right) \left(\frac{e^{-j\frac{(\gamma_c - \gamma_d)}{2}z} + e^{+j\frac{(\gamma_c - \gamma_d)}{2}z}}{2} \right) \right] \quad (7.3.56)$$

Finally, using trigonometric substitutions

(7.3.57)

$$\hat{I}_1(z) = \frac{\delta \hat{V}(\omega) Y_{11}}{4} e^{-j \frac{(\gamma_c + \gamma_d)}{2} z} \left[\cos \frac{(\gamma_c - \gamma_d) z}{2} + j \frac{\left(\frac{\ln \left(\frac{s}{d} \right)}{\ln \left(\frac{2h}{a} \right)} \right)}{\left(\frac{\ln \left(\frac{2h}{a} \right)}{\ln \left(\frac{s}{d} \right)} \right)} \sin \frac{(\gamma_c - \gamma_d) z}{2} \right]$$

$z > 0$

and

(7.3.58)

$$\hat{I}_2(z) = \frac{\delta \hat{V}(\omega) Y_{11}}{4} e^{-j \frac{(\gamma_c + \gamma_d)}{2} z} \left[-j \sin \frac{(\gamma_c - \gamma_d) z}{2} - \frac{\left(\frac{\ln \left(\frac{s}{d} \right)}{\ln \left(\frac{2h}{a} \right)} \right)}{\left(\frac{\ln \left(\frac{2h}{a} \right)}{\ln \left(\frac{s}{d} \right)} \right)} \cos \frac{(\gamma_c - \gamma_d) z}{2} \right]$$

$z > 0$

Next,

$$(\gamma_c^2 - \gamma_d^2) = (\gamma_c + \gamma_d)(\gamma_c - \gamma_d) \quad (7.3.59)$$

Using the definitions of γ_c and γ_d ,

(7.3.60)

$$(\gamma_c^2 - \gamma_d^2) = 2k_0^2 \left[\frac{J_c(0, h-a, h) \ln(s/d) - J_c(d, h-a, h) \ln(2h/a)}{\ln^2 \left(\frac{2h}{a} \right) - \ln^2 \left(\frac{s}{d} \right)} \right] - 2Y_{12} Z_{iw}$$

Given this,

$$\frac{(\gamma_c - \gamma_d)}{2} = k_o^2 Q - \frac{Y_{12} Z_{iw}}{(\gamma_c + \gamma_d)} \quad (7.3.61)$$

where

$$Q = \left(\frac{J_c(0, h-a, h) \ln(s/d) - J_c(d, h-a, h) \ln(2h/a)}{(\gamma_c + \gamma_d) \left(\ln^2 \left(\frac{2h}{a} \right) - \ln^2 \left(\frac{s}{d} \right) \right)} \right), \quad (7.3.62)$$

Hence (for $z > 0$)

(7.3.63)

$$\hat{I}_1(z) = \frac{\delta\hat{V}(\omega)Y_{11}}{4} e^{-j\frac{(\gamma_c+\gamma_d)}{2}z}$$

$$\left[\cos\left\{\left[k_o^2Q - \frac{Y_{12}Z_{iw}}{(\gamma_c + \gamma_d)}\right]z\right\} + j\left(\frac{\ln\left(\frac{s}{d}\right)}{\ln\left(\frac{2h}{a}\right)}\right) \sin\left\{\left[k_o^2Q - \frac{Y_{12}Z_{iw}}{(\gamma_c + \gamma_d)}\right]z\right\} \right]$$

and

(7.3.64)

$$\hat{I}_2(z) = \frac{\delta\hat{V}(\omega)Y_{11}}{4} e^{-j\frac{(\gamma_c+\gamma_d)}{2}z}$$

$$\left[-j \sin\left\{\left[k_o^2Q - \frac{Y_{12}Z_{iw}}{(\gamma_c + \gamma_d)}\right]z\right\} - \left(\frac{\ln\left(\frac{s}{d}\right)}{\ln\left(\frac{2h}{a}\right)}\right) \cos\left\{\left[k_o^2Q - \frac{Y_{12}Z_{iw}}{(\gamma_c + \gamma_d)}\right]z\right\} \right]$$

The current at $z=0$ on conductor # 1 is

$$\hat{I}_1(0) = \frac{\delta\hat{V}(\omega)Y_{11}}{4} = \frac{\hat{I}_{fault}(\omega)}{2}$$

(7.3.65)

Hence (again for $z > 0$) (where, again, Q is defined in (7.3.62))

(7.3.66)

$$\hat{I}_1(z, \omega) = \frac{\hat{I}_{fault}(\omega)}{2} e^{-j\frac{(\gamma_c+\gamma_d)}{2}z}$$

$$\left[\cos\left\{\left[k_o^2Q - \frac{Y_{12}Z_{iw}}{(\gamma_c + \gamma_d)}\right]z\right\} + j\left(\frac{\ln\left(\frac{s}{d}\right)}{\ln\left(\frac{2h}{a}\right)}\right) \sin\left\{\left[k_o^2Q - \frac{Y_{12}Z_{iw}}{(\gamma_c + \gamma_d)}\right]z\right\} \right]$$

and

(7.3.67)

$$\hat{I}_2(z, \omega) = \frac{\hat{I}_{fault}(\omega)}{2} e^{-j\frac{(\gamma_c+\gamma_d)}{2}z}$$

$$\left[-j \sin\left\{\left[k_o^2Q - \frac{Y_{12}Z_{iw}}{(\gamma_c + \gamma_d)}\right]z\right\} - \left(\frac{\ln\left(\frac{s}{d}\right)}{\ln\left(\frac{2h}{a}\right)}\right) \cos\left\{\left[k_o^2Q - \frac{Y_{12}Z_{iw}}{(\gamma_c + \gamma_d)}\right]z\right\} \right]$$

Finally, if $|(\gamma_c - \gamma_d)/2|z \ll 1$ and $z > 0$,

$$\hat{I}_1(z) \cong \frac{\hat{I}_{fault}(\omega)}{2} e^{-j\frac{(\gamma_c + \gamma_d)}{2}z} \left[1 + j \frac{\ln\left(\frac{s}{d}\right)}{\ln\left(\frac{2h}{a}\right)} \left\{ k_o^2 Q - \frac{Y_{12} Z_{iw}}{(\gamma_c + \gamma_d)} \right\} z \right] \quad (7.3.68)$$

and

$$\hat{I}_2(z) \cong \frac{\hat{I}_{fault}(\omega)}{2} e^{-j\frac{(\gamma_c + \gamma_d)}{2}z} \left[-j \left\{ k_o^2 Q - \frac{Y_{12} Z_{iw}}{(\gamma_c + \gamma_d)} \right\} z - \frac{\ln\left(\frac{s}{d}\right)}{\ln\left(\frac{2h}{a}\right)} \right] \quad (7.3.69)$$

For typical values of parameters, $\ln\left(\frac{s}{d}\right) \ll \ln\left(\frac{2h}{a}\right)$. Hence, $\hat{I}_2(0) \ll \hat{I}_1(0)$ as expected.

Before interpreting this result further, it is useful to look more carefully at the current at $z = 0$ by examining the case for $\hat{I}_1(0)$ and $\hat{I}_2(0)$ before taking the limit as $\delta \rightarrow 0$.

These currents can be found by considering the sums (7.3.34) + (7.3.36) and (7.3.35) + (7.3.37). Since $|z - \delta/2| = \delta/2$ when $z = 0$,

$$\hat{I}_1(0) = \frac{-j\hat{V}(\omega)}{8} \left\{ \frac{(Y_{11} + Y_{12})}{\gamma_c} e^{-j\gamma_c \delta/2} + \frac{(Y_{11} - Y_{12})}{\gamma_d} e^{-j\gamma_d \delta/2} - \frac{(Y_{11} + Y_{12})}{\gamma_c} e^{-j\gamma_c \delta/2} - \frac{(Y_{11} - Y_{12})}{\gamma_d} e^{-j\gamma_d \delta/2} \right\} = 0 \quad (7.3.70)$$

and

$$\hat{I}_2(0) = \frac{-j\hat{V}(\omega)}{8} \left\{ \frac{(Y_{11} + Y_{12})}{\gamma_c} e^{-j\gamma_c \delta/2} - \frac{(Y_{11} - Y_{12})}{\gamma_d} e^{-j\gamma_d \delta/2} - \frac{(Y_{11} + Y_{12})}{\gamma_c} e^{-j\gamma_c \delta/2} + \frac{(Y_{11} - Y_{12})}{\gamma_d} e^{-j\gamma_d \delta/2} \right\} = 0 \quad (7.3.71)$$

Clearly, the current at $z = 0$ is equal to zero on both conductors as it should be by symmetry. But, on conductor #1, the current rises quickly to half the fault current on either side of the source area while on conductor #2,

the current rises to a fraction $Y_{12}/2Y_{11} = \ln(s/d)/2\ln(2h/a)$ of the fault current.

Interpretation of the Result

An examination of (7.3.68) and (7.3.69) reveals that one term in each increases algebraically with z . Clearly this behavior will be more evident in (7.3.69) because $\ln(s/d) \ll \ln(2h/a)$. Hence the linearly increasing term is the most important part of (7.3.69) but only a small part of (7.3.68). Ultimately, the current will no longer grow either because the argument of the sine in (7.3.68) will be large enough that $|(\gamma_c - \gamma_d)/2|z$ is no longer $\ll 1$ or because the exponential decay due to the term $\exp(-j(\gamma_c + \gamma_d)z/2)$ becomes important. Nevertheless, this is an unexpected enough result that it is worth some additional interpretation.

As mentioned above, the second term of each current in (7.3.68) and (7.3.69) is especially interesting because it grows linearly near the source. This behavior can be understood in the following way. Recall the problem of driving a circuit with a voltage source at its natural (i.e., resonant) frequency as shown in Fig. 7.3.10. It is assumed that the source is “turned on” at $t = 0$.

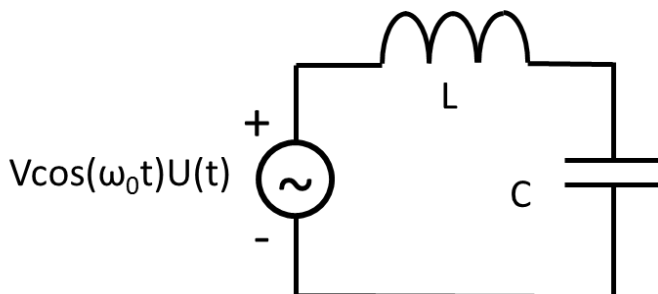


Fig. 7.3.11 A lossless LC circuit driven at its natural (i.e., resonant) frequency $\omega_0 = 1/\sqrt{LC}$

Clearly, in the steady state, the current that flows in this circuit is undefined because the impedance of the LC combination is $Z = j\omega_0 L - j/(\omega_0 C) = 0$. Hence, it is illustrative to study the circuit in the time domain for $t > 0$. It is well known that the differential equation for the current that flows in this circuit is

$$\frac{d^2 i(t)}{dt^2} + \frac{1}{LC} i(t) = -\omega V \sin(\omega_0 t), \quad t > 0 \quad (7.3.72)$$

The complementary solution $i_c(t)$ for this equation is of the form

$$i_c(t) = A \sin(\omega_0 t) + B \cos(\omega_0 t) \quad (7.3.73)$$

Given that the source frequency is ω_0 , the particular solution for this equation cannot take the form of either of complementary solutions. Rather, it must be of the form (Ford, 1955)

$$i_c(t) = At \sin(\omega_0 t) + Bt \cos(\omega_0 t) \quad (7.3.74)$$

Without going into the details of the solution which would require imposition of specific boundary conditions, it is simply worth noting that the current in this circuit will increase linearly with time until something about the circuit changes (e.g., the source current limit is reached or a circuit element becomes nonlinear).

By analogy to this time domain problem, conductor #2 in Fig. 7.3.7 is exposed to an incident field over its length that has natural spatial frequencies of $(\gamma_c + \gamma_d)/2$ and $(\gamma_c - \gamma_d)/2$. These are the same as the natural spatial frequencies of current on Conductor #2. Hence it is to be expected that the current induced on conductor #2 will have a component that is linearly growing along its length (Olsen, 1984). Of course, the current on conductor #2 eventually becomes large enough to influence the current on conductor #1 and the process is limited as indicated in (7.3.66) and (7.3.67). In addition it is limited by the exponential decay due to the term $\exp(-j(\gamma_c + \gamma_d)z/2)$.

Transform to the Time Domain

It is assumed that the source current has been transformed into the frequency domain using the Fourier transform

$$\hat{I}_{fault}(\omega) = \int_{-\infty}^{\infty} i_{fault}(t) e^{-j\omega t} dt \quad (7.3.75)$$

Hence, the current on conductors #1 and #2 can be found by evaluating the inverse Fourier transforms

$$i_1(z, t) = \frac{1}{2\pi} \int_{-\infty}^{\infty} \hat{I}_1(z, \omega) e^{+j\omega t} d\omega \quad (7.3.76)$$

and

$$i_2(z, t) = \frac{1}{2\pi} \int_{-\infty}^{\infty} \hat{I}_2(z, \omega) e^{+j\omega t} d\omega \quad (7.3.77)$$

using (7.3.66) and (7.3.67) as integrands in the respective inverse transforms. Given the complexity of (7.3.66) and (7.3.67), these transforms will be evaluated using the inverse Fast Fourier Transform (FFT) (Brigham, 1974).

For “large” values of z , $\hat{I}_1(z, \omega)$ and $\hat{I}_2(z, \omega)$ oscillate considerably in the ω domain. This behavior causes numerical difficulties for “large” z if the inverse FFT is applied directly to (7.3.66) and (7.3.67). To overcome this problem, it is helpful to recall the “time shift” theorem,

$$i'(z, t - t_0) = \frac{1}{2\pi} \int_{-\infty}^{\infty} \hat{I}'(z, \omega) e^{-j\omega t_0} e^{+j\omega t} d\omega \quad (7.3.78)$$

$$\hat{I}(z, \omega) = \hat{I}'(z, \omega) e^{-j\omega t_0} \quad (7.3.79)$$

and

$$i'(z, t) = \frac{1}{2\pi} \int_{-\infty}^{\infty} \hat{I}'(z, \omega) e^{+j\omega t} d\omega \quad (7.3.80)$$

Hence, if it is possible to separate out (at least most of) this oscillation in the form $e^{-j\omega t_0}$ it is only necessary to compute the inverse FFT of $\hat{I}'(z, \omega)$, which is much easier because it does not oscillate rapidly as a function of ω as does $\hat{I}(z, \omega)$.

The factor that contains most of the oscillation behavior of either (7.3.66) or (7.3.67) is

$$\exp(-j(\gamma_c + \gamma_d)z/2) \quad (7.3.81)$$

But, for most practical situations, $|\gamma_c - k_0|, |\gamma_d - k_0| \ll k_0$ and most of the oscillation can be taken out by separating out the factor $\exp(-jk_0 z) = \exp(-j\omega z/c)$ where $c = 1/\sqrt{\mu_0 \epsilon_0}$ is the speed of light in free space. Hence

$$(7.3.82)$$

$$\exp(-j(\gamma_c + \gamma_d)z/2) = [\exp(-j(\gamma_c + \gamma_d)z/2) \exp(+jk_0 z)] \exp(-j\omega t_0).$$

where $t_0 = z/c = z\sqrt{\mu_0 \epsilon_0}$ where the part in brackets oscillates much less rapidly than $\exp(-j\omega t_0)$. Then, if

$$\hat{I}_1(z, \omega) = \hat{I}_1'(z, \omega) e^{-j\omega t_0} \quad (7.3.83)$$

and

$$\hat{I}_2(z, \omega) = \hat{I}_2'(z, \omega) e^{-j\omega t_0}, \quad (7.3.84)$$

then,

$$i_1(z, t - z\sqrt{\mu_0 \epsilon_0}) = i_1'(z, t) = \frac{1}{2\pi} \int_{-\infty}^{\infty} \hat{I}_1'(z, \omega) e^{+j\omega t} d\omega \quad (7.3.85)$$

and

$$i_2(z, t - z\sqrt{\mu_0 \epsilon_0}) = i_2'(z, t) = \frac{1}{2\pi} \int_{-\infty}^{\infty} \hat{I}_2'(z, \omega) e^{+j\omega t} d\omega \quad (7.3.86)$$

To complete this derivation, it is necessary to define a pulse. A number of different pulses could be used, but here, the one used is

$$i_{fault}(t) = U(t) I_0 t e^{-at} \quad (7.3.87)$$

which has a Fourier transform

$$\hat{I}_{fault}(\omega) = \frac{I_0}{(\omega + ja)^2}. \quad (7.3.88)$$

Alternative method for very large values of z

If the method described above for removing the oscillatory term is not sufficient, a larger fraction of the oscillation can be eliminated by separating the currents into their component modes. More specifically, from (7.3.49) and (7.3.50),

$$\hat{I}_1(z, \omega) = \hat{I}_c(z, \omega) + \hat{I}_d(z, \omega) \quad (7.3.89)$$

where the component modes are

$$\hat{I}_c(z, \omega) = \frac{1}{4} \left(1 - \frac{\ln\left(\frac{s}{d}\right)}{\ln\left(\frac{2h}{a}\right)} \right) \hat{I}_{fault}(\omega) e^{-j\gamma_c z} \quad (7.3.90)$$

and

$$\hat{I}_d(z, \omega) = \frac{1}{4} \left(1 + \frac{\ln\left(\frac{s}{d}\right)}{\ln\left(\frac{2h}{a}\right)} \right) \hat{I}_{fault}(\omega) e^{-j\gamma_d z} \quad (7.3.91)$$

where (7.3.64) has been used. Similarly,

$$\hat{I}_2(z, \omega) = \hat{I}_c(z, \omega) - \hat{I}_d(z, \omega) \quad (7.3.92)$$

The pulse that will be used to represent the fault current is described in (7.3.87) and (7.3.88). From Parseval's theorem, roughly half the energy of the pulse is contained in frequencies below $\omega = a/2$. Hence, it is reasonable to write the first term of (7.3.90) as

(7.3.93)

$$\hat{I}_c(z, \omega) = \frac{1}{4} \left[\left(1 + \frac{\ln\left(\frac{s}{d}\right)}{\ln\left(\frac{2h}{a}\right)} \right) \hat{I}_{fault}(\omega) e^{-j\frac{2\text{Re}(\gamma_c(a/2))z}{a}\omega} e^{-j\left(\gamma_c - \frac{2\text{Re}(\gamma_c(a/2))}{a}\right)\omega} z \right]$$

Most of the integrand's oscillation is contained in the term $e^{-j\frac{2\text{Re}(\gamma_c(a/2))z}{a}\omega}$ which is in the form required to use the time shift theorem. Hence, a more stable form for calculating this component of the current is

$$i_c\left(z, t - \frac{2\text{Re}(\gamma_c(a/2))z}{a}\right) = \frac{1}{8\pi} \left(1 + \frac{\ln\left(\frac{s}{d}\right)}{\ln\left(\frac{2h}{a}\right)} \right) \int_{-\infty}^{\infty} \hat{I}_{fault}(\omega) e^{-j\left(\gamma_c - \frac{2\text{Re}(\gamma_c(a/2))}{a}\right)\omega} z} e^{j\omega t} d\omega \quad (7.3.94)$$

Similarly,

$$i_d\left(z, t - \frac{2\text{Re}(\gamma_d(a/2))z}{a}\right) = \frac{1}{8\pi} \left(1 - \frac{\ln\left(\frac{s}{d}\right)}{\ln\left(\frac{2h}{a}\right)} \right) \int_{-\infty}^{\infty} \hat{I}_{fault}(\omega) e^{-j\left(\gamma_d - \frac{2\text{Re}(\gamma_d(a/2))}{a}\right)\omega} z} e^{j\omega t} d\omega \quad (7.3.95)$$

Hence,

$$i_1(z, t) = i_c\left(z, t - \frac{2\text{Re}(\gamma_c(a/2))z}{a}\right) + i_d\left(z, t - \frac{2\text{Re}(\gamma_d(a/2))z}{a}\right) \quad (7.3.96)$$

and

$$i_2(z, t) = i_c\left(z, t - \frac{2\text{Re}(\gamma_c(a/2))z}{a}\right) - i_d\left(z, t - \frac{2\text{Re}(\gamma_d(a/2))z}{a}\right) \quad (7.3.97)$$

Note that the speeds of the two modes are approximately

$$v_c \cong \frac{a}{2 \operatorname{Re}(\gamma_c(a/2))} \text{ m/sec} \quad (7.3.98)$$

and

$$v_d \cong \frac{a}{2 \operatorname{Re}(\gamma_d(a/2))} \text{ m/sec} \quad (7.3.99)$$

respectively. Generally, the differential mode will be faster since it is not slowed down as much by electromagnetic fields in the earth.

Results

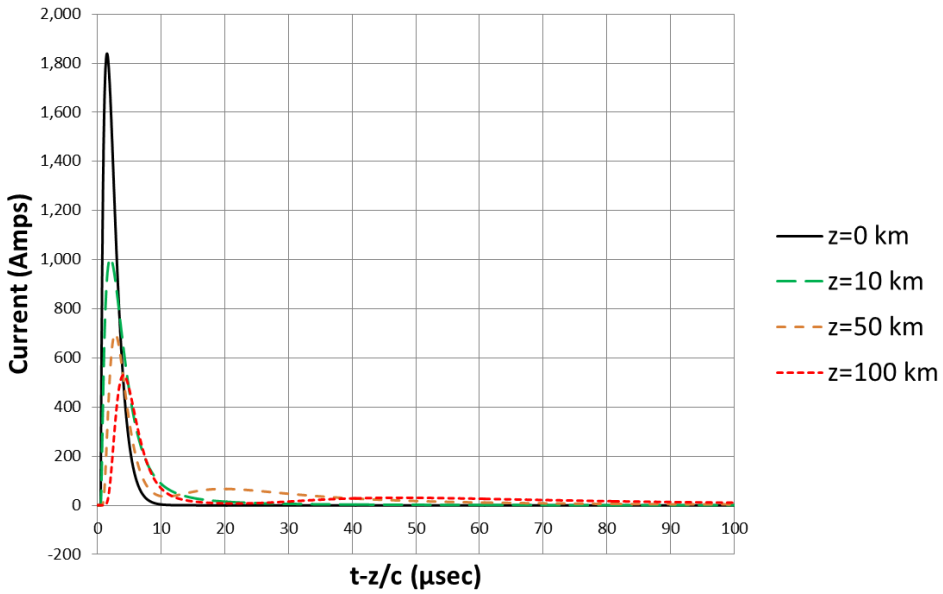
The currents $i_1(z, t)$ and $i_2(z, t)$ were determined for several relevant values of z using the geometry of Fig. 7.3.7, the expressions (7.3.85) and (7.2.86) and a fault current

$$i_{\text{fault}}(t) = U(t) 10^{10} t e^{-10^6 t} \quad (7.3.100)$$

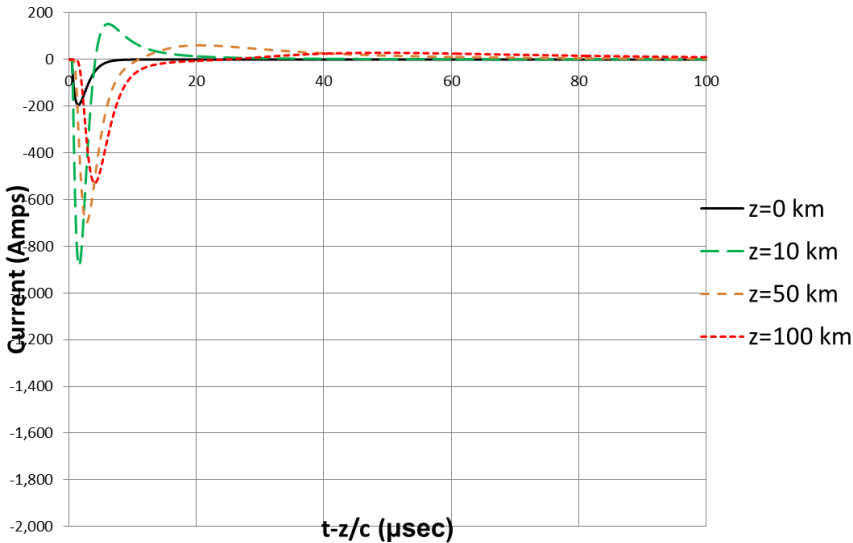
which has a (zero to peak) rise time of 1 μsec and a peak amplitude of 3678 amps at 1 μsec . The geometric parameters used were $a = 1 \text{ cm}$, $d = 10 \text{ m}$ and $h = 10 \text{ m}$ while the electrical parameters of the wire and earth were assumed to be $\sigma_w = 3.5 \times 10^7 \text{ S/m}$ (i.e., aluminum), $\sigma_2 = 0.01 \text{ S/m}$ and $\epsilon_{2r} = 5$.

In each case, the current is plotted with an advance of $t_0 = k_0 z$ so that the currents plotted for different values of z can easily be shown on the same plot. The inverse FFT used 2^{15} points with a sample rate in time of 32,768,000 per second. The frequency spectrum extended from 0 – 16.384 MHz. The results are shown in Fig. 7.3.11.

A number of things can be observed in these plots. First consider $i_1(t)$. At $z = 0$, the peak current is 1839 amps as expected since the total fault current of 3678 amps splits in half as it enters the conductor. As expected, and as observed for $z = 10 \text{ km}$, the current peak decays for larger values of z since there is attenuation of both modal currents due to losses in the conductor and the earth. At $z = 50 \text{ km}$, it is possible to observe the splitting of the differential mode (which occurs first at about 2 μsec since its speed is the faster of the two and has a larger peak due to lower earth losses) and the common mode (which occurs later at about 20 μsec since its speed is the slower of the two and has a smaller peak due to larger earth losses). Further, the common mode is more spread out more due to dispersion (i.e., frequency dependent speeds) from the earth. At $z = 100 \text{ km}$, the splitting of the two modes is essentially complete. The differential mode current is centered at approximately 4 μsec and the total current goes to zero by 20 μsec . Following this, the current increases again as the common mode current reaches $z = 100 \text{ km}$ at about 30 μsec .



(a)



(b)

Fig. 7.3.12. Currents (a) $i_1(z, t - z\sqrt{\mu_0\epsilon_0})$ and (b) $i_2(z, t - z\sqrt{\mu_0\epsilon_0})$ on conductors #1 and #2 respectively due to the fault current (7.3.95) at $z = 0$ on conductor #1 for several values of z .

Next consider $i_2(t)$. At $z = 0$, the peak current is approximately -200 amps. This occurs because the excitation amplitudes for the differential and common modes are slightly different according to (7.3.79) and (7.3.80). Since the differential mode amplitude is larger (and negative for conductor #2) and the total current on conductor #2 is the sum of the differential and common mode currents, the current is relatively small in the negative direction. Interestingly, the current peak increases for larger values of z (e.g.,

$z = 10$ km) since the common mode is delayed by its slower speed and attenuated, hence the sum of the two modal currents grows at smaller times because there is less cancellation between differential and common modes. This growth is consistent with the previous discussion about the current in the frequency domain. The total current actually becomes positive (e.g., $z = 10$ km) at later times because the differential mode has now passed while the delayed common mode arrives. Hence the common mode current is dominant for later times. At $z = 50$ km, the splitting of the negative differential mode current (which occurs first at about $2 \mu\text{sec}$ since its speed is the faster of the two and has a larger peak due to lower earth losses) and the positive common mode current (which occurs later at about $20 \mu\text{sec}$ since its speed is the slower of the two and has a smaller peak due to larger earth losses) becomes more obvious. Again, the common mode current is more spread out due to its larger dispersion. At $z = 100$ km, the splitting of the two modes is essentially complete. The differential mode current is centered around approximately $4 \mu\text{sec}$ and the total current goes to zero by $20 \mu\text{sec}$. It is interesting to note that $i_2(t) = -i_1(t)$ at short times as it should because the differential mode dominates, while $i_2(t) = i_1(t)$ at later times because the common mode dominates.

7.4 The Unbalanced Two Wire Line – Low Frequency

The results given in the last section are specific to the case for which the transmission line is symmetric with respect to the ground. For the more general case, an anti-symmetrical excitation (i.e., $V_2 = -V_1$) will not produce anti-symmetric currents. To illustrate how this happens, consider the problem solved here.

Derivation

Consider the case shown in Fig. 7.4.1. Here the two conductors are no longer at equal heights above the earth⁶⁹.

Again, (7.2.14) applies

$$\left\{ \begin{array}{cc} Z_{11} & Z_{12} \\ Z_{21} & Z_{22} \end{array} \right\} + \frac{\gamma^2}{j\omega} \left\{ \begin{array}{cc} A_{11} & A_{12} \\ A_{21} & A_{22} \end{array} \right\} \left\{ \begin{array}{c} \hat{I}_1(\gamma) \\ \hat{I}_2(\gamma) \end{array} \right\} = \left\{ \begin{array}{c} \hat{V}_1 \\ \hat{V}_2 \end{array} \right\} \quad (7.4.1)$$

Hence, the matrices $|Z|$ and $|A|$ are no longer symmetric as it was the case in Section 7.2. This difference, while seemingly subtle, has some important consequences.

⁶⁹ Again, for simplicity here, the conductor loss $Z_{iw} = 0$

Again $|Z|$ is the impedance matrix for this set of conductors and $|A|$ is the matrix of potential coefficients.

$$j\omega|A|^{-1} = j\omega|C| = |Y| \quad (7.4.2)$$

where $|Y|$ is the admittance matrix for the two conductors in the configuration of Fig. 7.4.1 and is equal to $j\omega|C|$ where $|C|$ is the capacitance matrix for this configuration.

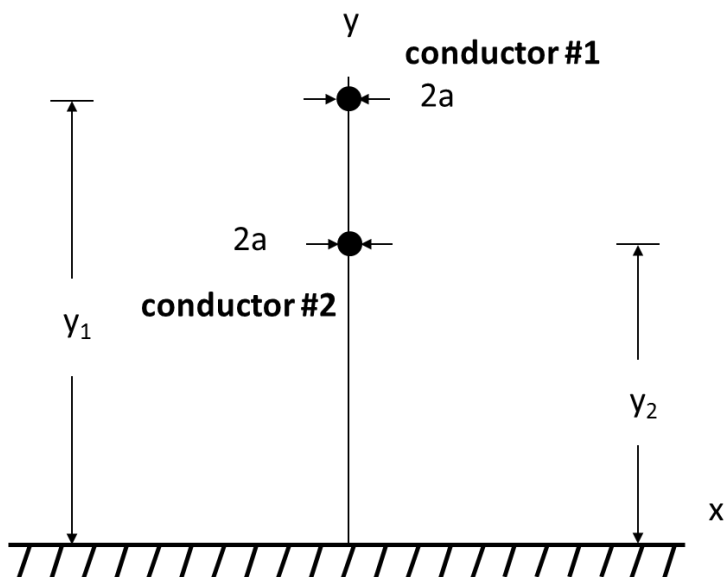


Fig. 7.4.1. An unbalanced two wire transmission line above the earth.

But in this case $Z_{11} \neq Z_{22}$, $Y_{11} \neq Y_{22}$. Instead, (with reference to 7.2.11 and 7.2.12)

$$\begin{aligned} Z_{11} &= Z(0, y_1 - a, h_{y1}), & Z_{22} &= Z(0, y_2 - a, y_2), & Z_{12} &= Z_{21} = Z(0, y_2 - a, y_1) \\ A_{11} &= A(0, y_1 - a, y_1), & A_{22} &= A(0, y_2 - a, y_2), & A_{12} &= A_{21} = A(0, y_2 - a, y_1) \end{aligned}$$

If, as before, (7.4.1) is pre-multiplied by $|Y|$

$$\{Y||Z| + \gamma^2\} \hat{I} = |Y| \hat{V} \quad (7.4.3)$$

where $|\hat{I}|$ is the matrix of conductor currents and $|\hat{V}|$ is the matrix of conductor source voltages.

Again, if $|\mathcal{Q}^2| = |\mathbf{Y}\|\mathbf{Z}|$ is a 2 x 2 matrix and has 2 distinct eigenvalues, then it has two distinct eigenvectors that are orthogonal with respect to $|\mathcal{Q}^2|$. Any two component vector (e.g., $|\hat{\mathbf{I}}|$) can be expanded in this set of eigenvectors so that

$$|\hat{\mathbf{I}}| = |\eta| |\hat{\mathbf{I}}_{gm}| \quad (7.4.4)$$

where $|\hat{\mathbf{I}}_{gm}|$ is the matrix of “component” amplitudes, and $|\eta|$ is a square matrix (by columns) of normalized eigenvectors of $|\mathcal{Q}^2| = |\mathbf{Y}\|\mathbf{Z}|$. The difference for the case of vertically oriented conductors is that the impedance and admittance matrices are no longer symmetric. The eigenvectors and eigenvalues can be found in the following way from the definition of eigenvectors. More specifically the eigenvalues of $|\mathcal{Q}^2|$ can be found from

$$\det\left\{|\mathcal{Q}_s^2| + |\Delta\mathcal{Q}^2| - (\lambda_s + \Delta\lambda)U\right\} = 0 \quad (7.4.5)$$

where $|\mathcal{Q}_s^2|$ and λ_s are the matrix and its eigenvalues for the symmetric case considered in Section 7.2, $|\Delta\mathcal{Q}^2|$ and $\Delta\lambda$ are the differences between the matrix and eigenvalues respectively for the symmetric and unsymmetric cases.

Given that the matrix is a 2 x 2 matrix, the determinant can be written explicitly as

$$(7.4.6)$$

$$\begin{aligned} & (\mathcal{Q}_{s11}^2 - \lambda)(\Delta\mathcal{Q}_{22}^2 - \Delta\lambda) + (\mathcal{Q}_{s22}^2 - \lambda)(\Delta\mathcal{Q}_{11}^2 - \Delta\lambda) + (\Delta\mathcal{Q}_{11}^2 - \Delta\lambda)(\Delta\mathcal{Q}_{22}^2 - \Delta\lambda) \\ & - \mathcal{Q}_{s21}^2 \Delta\mathcal{Q}_{12}^2 - \mathcal{Q}_{s12}^2 \Delta\mathcal{Q}_{21}^2 - \Delta\mathcal{Q}_{12}^2 \Delta\mathcal{Q}_{21}^2 = 0 \end{aligned}$$

where $(\mathcal{Q}_{s11}^2 - \lambda)(\mathcal{Q}_{s22}^2 - \lambda) - \mathcal{Q}_{s21}^2 \mathcal{Q}_{s12}^2 = 0$ since this is for the symmetrical case. (7.4.6) can be expanded in a quadratic expression in the variable $\Delta\lambda$ as

$$(7.4.7)$$

$$\begin{aligned} & (\Delta\lambda)^2 - \Delta\lambda(\mathcal{Q}_{s11}^2 + \mathcal{Q}_{s22}^2 - 2\lambda + \Delta\mathcal{Q}_{11}^2 + \Delta\mathcal{Q}_{22}^2) + (\mathcal{Q}_{s11}^2 - \lambda)(\Delta\mathcal{Q}_{22}^2) + \\ & (\mathcal{Q}_{s22}^2 - \lambda)(\Delta\mathcal{Q}_{11}^2) + (\Delta\mathcal{Q}_{11}^2)(\Delta\mathcal{Q}_{22}^2) - \mathcal{Q}_{s21}^2 \Delta\mathcal{Q}_{12}^2 - \mathcal{Q}_{s12}^2 \Delta\mathcal{Q}_{21}^2 - \Delta\mathcal{Q}_{12}^2 \Delta\mathcal{Q}_{21}^2 = 0 \end{aligned}$$

(7.4.7) can be expanded and solved explicitly for $\Delta\lambda_i$ as

$$\Delta\lambda_i = -\frac{b}{2} \pm \frac{1}{2} \sqrt{b^2 - 4c}, \quad i = 1, 2 \quad (7.4.8)$$

where

$$b = -(\mathcal{Q}_{s11}^2 + \mathcal{Q}_{s22}^2 - 2\lambda_i + \Delta\mathcal{Q}_{11}^2 + \Delta\mathcal{Q}_{22}^2)$$

and

$$c = (\mathcal{Q}_{s11}^2 - \lambda_i)(\Delta\mathcal{Q}_{22}^2) + (\mathcal{Q}_{s22}^2 - \lambda_i)(\Delta\mathcal{Q}_{11}^2) + (\Delta\mathcal{Q}_{11}^2)(\Delta\mathcal{Q}_{22}^2) - \mathcal{Q}_{s21}^2 \Delta\mathcal{Q}_{12}^2 - \mathcal{Q}_{s12}^2 \Delta\mathcal{Q}_{21}^2 - \Delta\mathcal{Q}_{12}^2 \Delta\mathcal{Q}_{21}^2$$

To first order (i.e., ignoring $(\Delta\lambda)^2$,

$$\Delta\lambda_i = \left[(\mathcal{Q}_{s11}^2 - \lambda_i)(\Delta\mathcal{Q}_{22}^2) + (\mathcal{Q}_{s22}^2 - \lambda_i)(\Delta\mathcal{Q}_{11}^2) + (\Delta\mathcal{Q}_{11}^2)(\Delta\mathcal{Q}_{22}^2) - \mathcal{Q}_{s21}^2 \Delta\mathcal{Q}_{12}^2 - \mathcal{Q}_{s12}^2 \Delta\mathcal{Q}_{21}^2 - \Delta\mathcal{Q}_{12}^2 \Delta\mathcal{Q}_{21}^2 \right] / (\mathcal{Q}_{s11}^2 + \mathcal{Q}_{s22}^2 - 2\lambda_i + \Delta\mathcal{Q}_{11}^2 + \Delta\mathcal{Q}_{22}^2) \quad (7.4.9)$$

The eigenvectors can be derived from this result by first writing

$$\begin{pmatrix} Y_{11} & Y_{12} \\ Y_{12} & Y_{11} + \Delta Y \end{pmatrix} \begin{vmatrix} Z_{11} + Z_{iw} & Z_{12} \\ Z_{12} & Z_{11} + \Delta Z + Z_{iw} \end{vmatrix} = \begin{vmatrix} (Z_{11} + Z_{iw})Y_{11} + Z_{12}Y_{12} & (Z_{11} + \Delta Z + Z_{iw})Y_{12} + Z_{12}Y_{11} \\ Z_{12}(Y_{11} + \Delta Y) + (Z_{11} + Z_{iw})Y_{12} & (Z_{11} + \Delta Z + Z_{iw})(Y_{11} + \Delta Y) + Z_{12}Y_{12} \end{vmatrix} \quad (7.4.10)$$

where $\Delta Y = Y_{22} - Y_{11}$, $\Delta Z = Z_{22} - Z_{11}$.

Now, the eigenvectors for the case $\Delta Y = \Delta Z = 0$ (since the matrix is symmetric) are

$$\bar{q}_1 = a_1 \begin{vmatrix} 1 \\ 1 \end{vmatrix} \quad \text{and} \quad \bar{q}_2 = a_2 \begin{vmatrix} 1 \\ -1 \end{vmatrix} \quad (7.4.11)$$

Hence, (for the eigenvector #1 case)

$$\begin{vmatrix} (Z_{11} + Z_{iw})Y_{11} + Z_{12}Y_{12} & (Z_{11} + Z_{iw})Y_{12} + Z_{12}Y_{11} \\ Z_{12}Y_{12} + (Z_{11} + Z_{iw})Y_{12} & (Z_{11} + Z_{iw})Y_{11} + Z_{12}Y_{12} \end{vmatrix} \begin{vmatrix} \Delta_{11} \\ \Delta_{12} \end{vmatrix} + \begin{vmatrix} 0 & Y_{12}\Delta Z \\ Z_{12}\Delta Y & (Z_{11} + Z_{iw})\Delta Y + Y_{11}\Delta Z \end{vmatrix} \begin{vmatrix} 1 \\ 1 \end{vmatrix} = \lambda_{s1} \begin{vmatrix} \Delta_{11} \\ \Delta_{12} \end{vmatrix} + \Delta\lambda_1 \begin{vmatrix} 1 \\ 1 \end{vmatrix} \quad (7.4.12)$$

which can be solved for Δ_{11} and Δ_{12} since $\Delta Y = Y_{22} - Y_{11}$, $\Delta Z = Z_{22} - Z_{11}$ are known, and λ_{s1} (the eigenvalue #1 in the symmetric case) is equal to $(Z_{11} + Z_{12})(Y_{11} + Y_{12})$ and $\Delta\lambda_i$ is the difference between the symmetric and unsymmetric case eigenvalues for $i = 1$.

Once the normalized eigenvectors are known, it is possible to solve for the modal currents from

$$\left\{ Q_d^2 + \gamma^2 |U| \right\} \hat{I}_{gm} = -|\eta|^{-1} |Y| \hat{V} \quad (7.4.13)$$

where $|U|$ is the unitary matrix, $|Q_d^2|$ is the diagonalized version of $|Q^2|$ and

$$|\eta|^{-1} |Q^2| |\eta| = |Q_d^2| \quad (7.4.14)$$

Here $|\eta|$ is the normalized matrix (by columns) of the eigenvectors in this case and $|\eta|^{-1}$ is its inverse. Since both $|Q_d^2|$ and $|U|$ are diagonal matrices (7.4.13) can be solved as individual equations to yield

$$\hat{I}_{gm1} = -\frac{(|\eta|^{-1} |Y| \hat{V})_1}{Q_{d11}^2 + \gamma^2} \quad (7.4.15)$$

and

$$\hat{I}_{gm2} = -\frac{(|\eta|^{-1} |Y| \hat{V})_2}{Q_{d22}^2 + \gamma^2} \quad (7.4.16)$$

A numerical study of (7.4.15) and (7.4.16) shows that these modes are no longer purely common or differential. This has consequences for the balance of transmission line currents as discussed in the next section.

Comment about balance

At this point, it is very important to point out a difference between the “unsymmetric” geometry case and the “symmetric” geometry case discussed in Section 7.2. In the symmetric geometry case an anti-symmetric source (i.e., $\hat{V}_1 = -\hat{V}_2$) excited only the component associated with the (1,-1) eigenvector and since the other component was never excited, only the anti-symmetric component will exist at arbitrary distances along the transmission line. Thus, if $\hat{V}_1 = -\hat{V}_2$, $\hat{I}_1 = -\hat{I}_2$ for all values of z ⁷⁰. This will generally not be

⁷⁰ Another reason for unbalanced currents is that the loads on each phase are not equal

the case for conductor configurations that are non-symmetric such as the one shown in Fig. 7.4.1. In these “unsymmetric” cases, an anti-symmetric excitation (i.e., $\hat{V}_1 = -\hat{V}_2$) will excite BOTH components. One result is that the currents at the input are no longer equal and opposite (i.e., $\hat{I}_1 \neq -\hat{I}_2$). In addition, because each component is attenuated at a different rate because each has its own (and generally different) propagation constant, the ratio of the currents at arbitrary distances down the transmission line will be different than at the input and (in general) will become even less balanced. Finally, as discussed in Section 7.2, non-symmetrical termination impedances (or junctions along the transmission line) can cause further unbalance in the currents.

7.5 The general multiconductor case – low frequency

Derivation

The solution for propagation of currents on a general number N_C ungrounded conductors above earth as shown in Fig. 7.5.1 will be summarized in this section. Only a summary will be given because even in the low frequency case, the solution is rather complex.

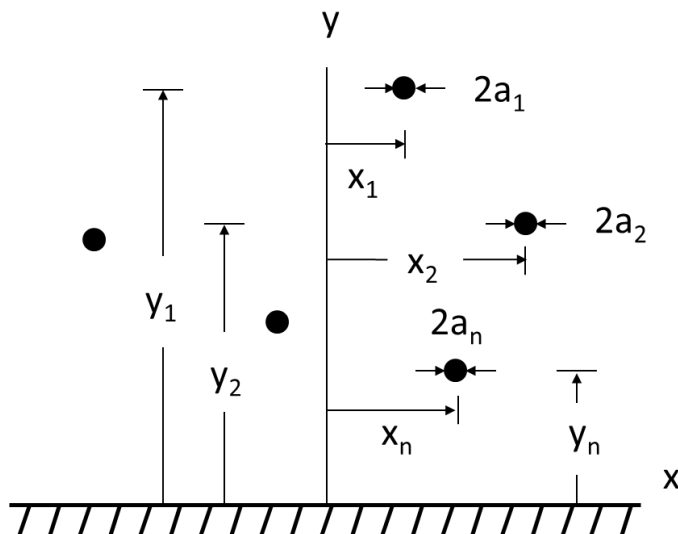


Fig. 7.5.1. Geometry for propagation on N_C conductors above earth.

Following the mathematical formulation of Section 7.2 but for N_C conductors

$$\left\{ \left| Z + \frac{\gamma^2}{j\omega} |A| \right\} \left| \hat{I}(\gamma) \right| = \left| \hat{V} \right| \quad (7.5.1)$$

where $|Z|$ and $|A|$ are $N_C \times N_C$ matrices of impedance and potential coefficients respectively, $|\hat{I}(\gamma)|$ is an $N_C \times 1$ column matrix of wire currents and $|\hat{V}|$ is an $N_C \times 1$ column matrix of voltage generators in series with the conductors at $z = 0$.

Here

$$Z(x_m - x_n, y_m, y_n) = \frac{j\omega\mu_0}{2\pi} \left\{ \ln\left(\frac{r_{mn}^i}{r_{mn}}\right) - J_c(x_m - x_n, y_m, y_n) \right\} \quad (7.5.2)$$

where

$$r_{mn} = \left((x_m - x_n)^2 + (y_m - y_n)^2 \right)^{1/2}, \quad r_{mn}^i = \left((x_m - x_n)^2 + (y_m + y_n)^2 \right)^{1/2}$$

and

$$J_c(x_m - x_n, y_m, y_n) = \frac{2}{k_2^2} \int_0^\infty (u - \kappa) e^{-\kappa(y_m + y_n)} \cos(\kappa(x_m - x_n)) d\kappa, \quad u = \sqrt{\kappa^2 - k_2^2} \quad (7.5.3)$$

is a mutual impedance per unit length. The potential coefficients are

$$A(x_m - x_n, y_m, y_n) = \frac{\ln\left(\frac{r_{mn}^i}{r_{mn}}\right)}{2\pi\epsilon_0} \quad (7.5.4)$$

As before, the admittance per unit length matrix $|Y|$ is related to the matrix of potential coefficients as

$$j\omega|A|^{-1} = |Y| \quad (7.5.5)$$

where $|Y|$ is an $N_C \times N_C$ matrix.

To solve for the currents, (7.5.1) is first pre-multiplied by $|Y|$ to get

$$\left\{ |Q^2| - \gamma^2 |U| \right\} |\hat{I}(\gamma)| = |Y| |\hat{V}| \quad (7.5.6)$$

where $|Q^2| = -|Y||Z|$ is an $N_C \times N_C$ matrix and $|U|$ is an $N_C \times N_C$ unit matrix. If it has N_C distinct eigenvalues, then it has N_C distinct eigenvectors that are

orthogonal with respect to $|\mathcal{Q}^2|$ and any n component vector (e.g., $|\hat{\mathbf{I}}(\gamma)|$) can be expanded in this set of eigenvectors so that

$$|\hat{\mathbf{I}}(\gamma)| = |\boldsymbol{\eta}| |\hat{\mathbf{I}}_{gm}(\gamma)| \quad (7.5.7)$$

where $|\hat{\mathbf{I}}_{gm}(\gamma)|$ is an $N_c \times 1$ column matrix of component amplitudes and $|\boldsymbol{\eta}|$ is an $N_c \times N_c$ matrix of normalized eigenvectors arranged by columns. Now, because $|\boldsymbol{\eta}|$ is a unitary matrix, it has the property that its inverse is equal to the complex conjugate of its transpose (i.e., its associate) so that

$$|\boldsymbol{\eta}|^{-1} = |\boldsymbol{\eta}|^{T*} \quad (7.5.8)$$

Further, because the eigenvectors are orthogonal with respect to $|\mathcal{Q}^2|$

$$|\boldsymbol{\eta}|^{-1} |\mathcal{Q}^2| |\boldsymbol{\eta}| = |\mathcal{Q}_d^2| \quad (7.5.9)$$

where $|\mathcal{Q}_d^2|$ is a diagonal matrix with elements equal to the eigenvalues of $|\mathcal{Q}^2|$

$$|\mathcal{Q}_d^2| = \begin{vmatrix} \gamma_1^2 & 0 & \bullet & 0 \\ 0 & \gamma_2^2 & \bullet & \bullet \\ \bullet & \bullet & \bullet & 0 \\ 0 & \bullet & 0 & \gamma_n^2 \end{vmatrix} \quad (7.5.10)$$

If (7.5.6) is pre-multiplied by $|\boldsymbol{\eta}|^{-1}$ and the above mentioned properties of $|\boldsymbol{\eta}|$ are used,

$$\{|\mathcal{Q}_d^2| - \gamma^2 |\mathbf{U}|\} |\hat{\mathbf{I}}_{gm}(\gamma)| = -|\boldsymbol{\eta}|^{-1} |\mathbf{Y}| |\hat{\mathbf{V}}| \quad (7.5.11)$$

The current component amplitudes can easily be determined from this equation. More specifically, since

$$\{|\mathcal{Q}_d^2| - \gamma^2 |\mathbf{U}|\}$$

is a diagonal matrix, its inverse may be obtained by inverting each term of the matrix. The result is

$$\left| \hat{\mathbf{I}}_{gm}(\gamma) \right| = - \left| \begin{array}{cccc} \frac{1}{Q_{d11}^2 - \gamma^2} & 0 & 0 & 0 \\ 0 & \bullet & 0 & 0 \\ 0 & 0 & \bullet & 0 \\ 0 & 0 & 0 & \frac{1}{Q_{dnn}^2 - \gamma^2} \end{array} \right| |\eta|^{-1} |\mathbf{Y}| |\hat{\mathbf{V}}| \quad (7.5.12)$$

The individual conductor currents can then be found from (7.5.7).

Currents in the space domain can be found using the inverse Fourier transform as illustrated in Section 4.6. More specifically, for $\hat{\mathbf{F}}(\gamma) = \mathbf{K}/(\gamma^2 - \gamma_p^2)$, where \mathbf{K} is an arbitrary constant.

$$f(z) = \frac{1}{2\pi} \int_{-\infty}^{\infty} \hat{\mathbf{F}}(\gamma) e^{-j\gamma z} d\gamma = \frac{\mathbf{K}}{2\pi} \int_{-\infty}^{\infty} \left(\frac{1}{\gamma^2 - \gamma_p^2} \right) e^{-j\gamma z} d\gamma = \frac{-j\mathbf{K}}{2\gamma_p} e^{-j\gamma_p z} \quad (7.5.13)$$

Hence,

$$\left| \hat{\mathbf{I}}(z) \right| = -\frac{j}{2} |\eta| \left| \begin{array}{cccc} \frac{e^{-jQ_{d11}z}}{Q_{d11}} & 0 & 0 & 0 \\ 0 & \bullet & 0 & 0 \\ 0 & 0 & \bullet & 0 \\ 0 & 0 & 0 & \frac{e^{-jQ_{dnn}z}}{Q_{dnn}} \end{array} \right| |\eta|^{-1} |\mathbf{Y}| |\hat{\mathbf{V}}| \quad (7.5.14)$$

The effect of shield wires

The derivation presented above can be applied to transmission lines that have grounded shield wires by modifying the impedance and admittance matrices $|\mathbf{Z}|$ and $|\mathbf{Y}|$ in the following way.

The impedance matrix

Consider a transmission line with N_C phase conductors and N_{sh} shield wires. According to (7.5.1) its impedance matrix satisfies the following equation for $\gamma \approx 0$ so that the effects of capacitance can be neglected.⁷¹

⁷¹ This corresponds to the case for which the current does not vary in the space domain. An alternative derivation can be done in the space domain using a short segment of transmission line (Anderson, 1973)

$$\begin{bmatrix} |Z_{pp}| \\ |Z_{gp}| \end{bmatrix} \begin{bmatrix} |Z_{pg}| \\ |Z_{gg}| \end{bmatrix} \begin{bmatrix} |\hat{I}_p| \\ |\hat{I}_g| \end{bmatrix} = \begin{bmatrix} |\hat{V}| \\ |0| \end{bmatrix} \quad (7.5.15)$$

where

$|Z_{pp}|$ is the $(N_C \times N_C)$ impedance matrix for the phase conductors only

$|Z_{gg}|$ is the $(N_{sh} \times N_{sh})$ impedance matrix for the shield wires only

$|Z_{pg}| = |Z_{gp}|^T$ (by reciprocity) is the $(N_{sh} \times N_C)$ matrix of mutual impedances between phase conductors and shield wires

$|\hat{I}_p|$ is the $1 \times N_C$ matrix of phase conductor currents

$|\hat{I}_g|$ is the $1 \times N_{sh}$ matrix of shield wire currents

$|\hat{V}|$ is the $1 \times N_C$ matrix of voltage sources in series with the phase conductors. As shown in Section 4.7, this corresponds to a line – ground voltages of $|\hat{V}|/2$.

$|0|$ is the $1 \times N_{sh}$ matrix of voltage generator amplitudes in series with the shield wires that are assumed to be zero.

The bottom set of equations of (7.5.15) can be separately solved to get

$$|\hat{I}_g| = -|Z_{gg}|^{-1} |Z_{gp}| |\hat{I}_p| \quad (7.5.16)$$

It is possible, then, to substitute (7.5.16) into the top set of equations of (7.5.15) to get

$$\left(|Z_{pp}| - |Z_{pg}| |Z_{gg}|^{-1} |Z_{gp}| \right) |\hat{I}_p| = |\hat{V}| \quad (7.5.17)$$

Hence the impedance matrix for an N_C conductor power line (with N_{sh} non-excited shield wires) can be written in terms of the phase currents only as (Anderson, 1973).

$$|Z'_{pp}| = |Z_{pp}| - |Z_{pg}| |Z_{gg}|^{-1} |Z_{gp}| \quad (7.5.18)$$

The admittance matrix

In the electrostatic case, the potential matrix (i.e., the inverse of the admittance matrix divided by $j\omega$ – see (7.5.5)) for a transmission line with N_C phase conductors and N_{sh} shield wires satisfies the following equation.

$$\begin{bmatrix} |A_{pp}| & |A_{pg}| \\ |A_{gp}| & |A_{gg}| \end{bmatrix} \begin{bmatrix} |\hat{\rho}_p| \\ |\hat{\rho}_g| \end{bmatrix} = \begin{bmatrix} |\hat{V}_p| \\ |0| \end{bmatrix} \quad (7.5.19)$$

where

$|A_{pp}|$ is the ($N_C \times N_C$) potential matrix for the phase conductors only

$|A_{gg}|$ is the ($N_{sh} \times N_{sh}$) potential matrix for the shield wires conductors only

$|A_{pg}| = |A_{gp}|^T$ (by reciprocity) is the ($N_{sh} \times N_C$) matrix of mutual potentials between phase conductors and shield wires

$|\hat{\rho}_p|$ is the $1 \times N_C$ matrix of phase conductor line charge densities
 $= (j / \omega) \partial I / \partial z$

$|\hat{\rho}_g|$ is the $1 \times N_{sh}$ matrix of shield wire line charge densities

$|\hat{V}_p|$ is the $1 \times N_C$ matrix of phase conductor voltages (i.e. voltages with respect to ground)

$|0|$ is the $1 \times N_{sh}$ matrix of shield wire voltages with respect to ground since they are assumed periodically grounded with spacing much less than a wavelength⁷²

In a similar way to the derivation for the impedance matrix, the bottom set of equations for (7.5.19) can be solved to get

$$|\hat{\rho}_g| = -|A_{gg}|^{-1} |A_{gp}| |\hat{\rho}_p| \quad (7.5.20)$$

It is possible, then, to substitute (7.5.20) into the top set of equations of (7.5.19) to get

$$\left[|A_{pp}| - |A_{pg}| |A_{gg}|^{-1} |A_{gp}| \right] |\hat{\rho}_p| = |\hat{V}_p| \quad (7.5.21)$$

Hence the potential matrix for an N_C conductor power line (with N_{sh} grounded shield wires) can be written in terms of the phase line current densities only as

$$|A'_{pp}| = |A_{pp}| - |A_{pg}| |A_{gg}|^{-1} |A_{gp}| \quad (7.5.22)$$

⁷² If the frequency is in the Megahertz range (such as for radio noise), this approximation is no longer generally valid.

Hence,

$$\left| \hat{\rho}_p \right| = \left| A'_{pp} \right|^{-1} \left| \hat{V}_p \right| = \left| C'_{pp} \right| \left| \hat{V}_p \right| \quad (7.5.23)$$

and

$$\left| Y'_{pp} \right| = j\omega \left| C'_{pp} \right| \quad (7.5.24)$$

Thus, as long as the shield wires are periodically grounded with spacing significantly smaller than a wavelength, the matrices $\left| Z'_{pp} \right|$ and $\left| Y'_{pp} \right|$ in (7.5.18) and (7.5.24) respectively can be substituted for the impedance and admittance matrices $\left| Z \right|$ and $\left| Y \right|$ in (7.5.1) to analyze high voltage transmission lines with shield wires.

Example results and interpretation

An example three phase transmission line for which individual phase conductor currents will be computed is shown in Fig. 7.5.2. For all results, the voltage V in series with each conductor is 100 kV which (since the line to ground voltage, V_{lg} , is $V/2$) results in a line-to-line voltage V_{ll} of 86.6 kV. The phasing of the line is as shown in the Figure with phases A, B and C equal to 0, -120 and 120 degrees respectively.

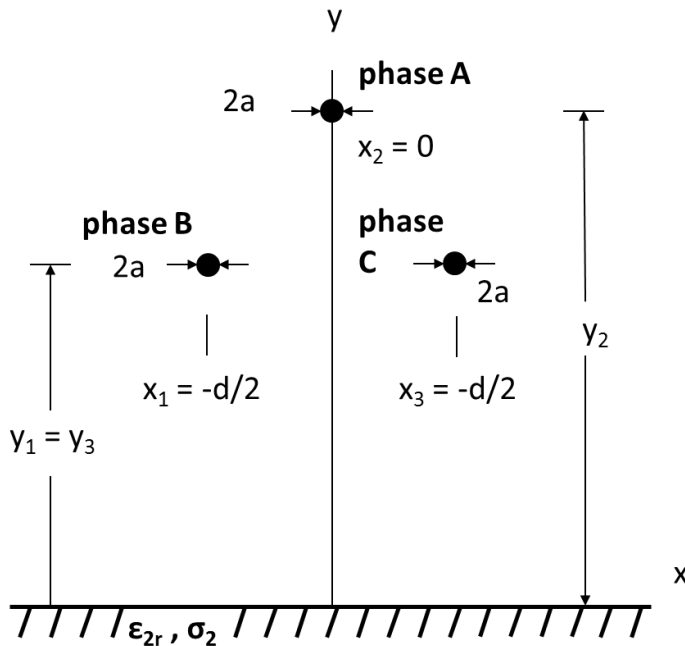


Fig. 7.5.2. The “generic” transmission line used for calculation of phase currents. For all examples given here, $a = 0.01$ meters and the earth relative dielectric constant ϵ_{r2} equals 5.

The “base case” is a horizontal transmission line with $y_1 = y_3$, $d/2$ and y_2 equal to 15, 5 and 15 meters respectively above an earth with conductivity $\sigma_2 = 0.01$ S/m. The results for this “base case” are shown in Fig. 7.5.3. At the input of the transmission line, the amplitudes of the three phase currents range from 123 to 134 amps, a spread of nearly 10% of the average input current. This spread in values occurs because the simple symmetry evident in the two conductor transmission line in Fig. 7.1.1 is complicated by the addition of a third conductor. However, while it is not surprising that the Phase A (i.e., center) current is different for the others, geometric symmetry and the fact that the voltages on phases B and C in the phasor domain have some symmetry, one might expect that the currents in phases B and C would have equal magnitudes. This issue will be examined in the next paragraphs.

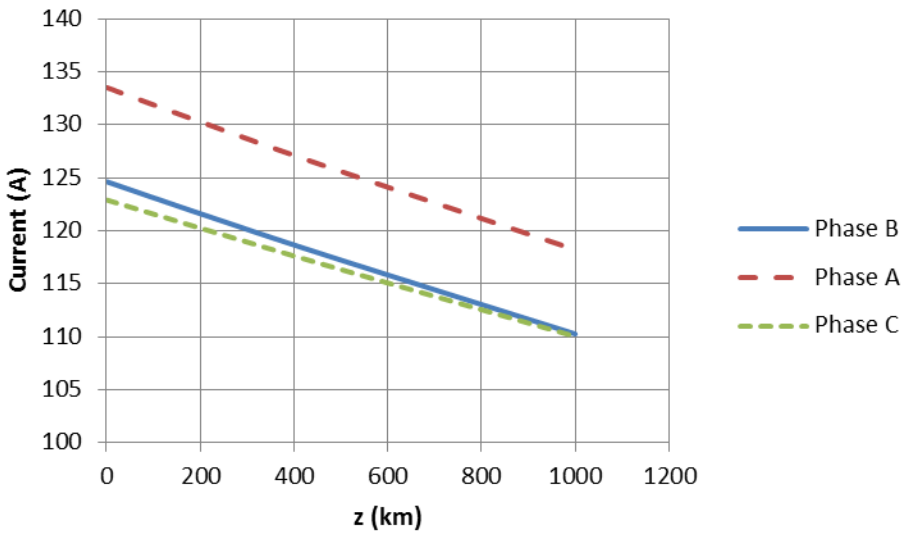


Fig. 7.5.3. Individual Phase Currents for the Case $y_1 = y_3 = 15$, $d/2 = 5$, $y_2 = 0$ meters, $\sigma_2 = 0.01$ S/m.

The vector of line to ground phasor voltages for each of the cases examined can be split into real and imaginary parts as shown in (7.5.25).

$$|V_{\ell g}| = |V_{\ell gr} + jV_{\ell gi}| = 50 \begin{bmatrix} -1/2 \\ +1 \\ +1/2 \end{bmatrix} + j50 \begin{bmatrix} -\sqrt{3}/2 \\ 0 \\ +\sqrt{3}/2 \end{bmatrix} \text{ kV} \quad (7.5.25)$$

It can be shown that the currents induced on the conductors by the real and imaginary parts of the line to ground voltage vector symmetric and anti-symmetric respectively. Hence, in each individual case, the currents on phases B and C have identical magnitudes.

The asymmetry in the current magnitudes for the sum of these currents results from the fact that the conductors and the earth are lossy and, hence,

the phases of the currents are no longer 0, -120 and 120 degrees respectively. Rather, they can be written (with the phase term “ j ” separated from the currents due to $|V_{\ell gi}|$) as

$$|I(V_{\ell gr})| = \begin{bmatrix} I_{Br}^{V_{\ell gr}} + jI_{Bi}^{V_{\ell gr}} \\ I_{Ar}^{V_{\ell gr}} + jI_{Ai}^{V_{\ell gr}} \\ I_{Br}^{V_{\ell gr}} + jI_{Bi}^{V_{\ell gr}} \end{bmatrix} \text{ and } |I(V_{\ell gi})| = j \begin{bmatrix} I_{Br}^{V_{\ell gi}} + jI_{Bi}^{V_{\ell gi}} \\ I_{Ar}^{V_{\ell gi}} + jI_{Ai}^{V_{\ell gi}} \\ -\left(I_{Br}^{V_{\ell gi}} + jI_{Bi}^{V_{\ell gi}}\right) \end{bmatrix} \quad (7.5.26)$$

If these currents are added, the results for phase currents B and C are

$$\begin{bmatrix} I_B \\ I_C \end{bmatrix} = I_{Br}^{V_{gr}} + jI_{Bi}^{V_{gr}} \pm j\left(I_{Br}^{V_{gi}} + jI_{Bi}^{V_{gi}}\right) = I_{Br}^{V_{gr}} \mp I_{Bi}^{V_{gi}} + j\left(\pm I_{Br}^{V_{gi}} + I_{Bi}^{V_{gr}}\right) \quad (7.5.27)$$

Clearly, if the currents in (7.5.26) had no imaginary parts, then the magnitudes of the phase B and C currents would be the same. However, since there is loss in the conductors and the earth, these imaginary parts are not zero and

$$\begin{bmatrix} |I_B| \\ |I_C| \end{bmatrix} = \sqrt{\left(I_{Br}^{V_{gr}}\right)^2 + \left(I_{Bi}^{V_{gi}}\right)^2 + \left(I_{Br}^{V_{gi}}\right)^2 + \left(I_{Bi}^{V_{gr}}\right)^2 \pm \left(2I_{Br}^{V_{gi}}I_{Bi}^{V_{gr}} - 2I_{Br}^{V_{gr}}I_{Bi}^{V_{gi}}\right)} \quad (7.5.28)$$

The last term of cross products is the term responsible for the fact that the phase B and C current magnitudes are not equal.

It is also clear from Fig. 7.5.3 that all currents decay as a function of distance along the transmission line because of losses in both the conductors and the earth. This is to be expected due to the fact that according to (7.5.14) each geometric mode decays exponentially with z , albeit with a different propagation constant Q_{dm} . For this transmission line, the current decay is somewhat more than 10% after 1000 km and appears to be a linear decay because $|\text{Im}(Q_{dm})z| \ll 1$ and $e^{-jQ_{dm}z} \cong e^{-j\text{Re}(Q_{dm})z} (1 - \text{Im}(Q_{dm})z)$. Finally, the current balance changes as the distance along the transmission line is increased. This is because each of the different modes of propagation has a different attenuation constant so that each current decays at a somewhat different rate. Thus, the ratio of the different current amplitudes will change with distance.

In the next sequence of figures, one parameter will be varied in each to illustrate its effect on the current excitation and propagation process. The first of these is shown in Fig. 7.5.4 in which the earth conductivity is changed to 0.001. It is clear from this figure that the change in the currents is minimal. In Fig. 7.5.5, y_2 is increased to 23.67 so that the transmission line becomes a “delta” configured transmission line. Two things can be noted

here. First, Phase currents B and C are essentially the same. It turns out that they are not identical, but the cross terms in (7.5.28) nearly cancel out. Second, the current magnitudes are more nearly the same. This is characteristic of transmission lines that have more symmetry such as the delta configuration. It is clear, however, that the balance changes with distance as with the horizontal configuration.

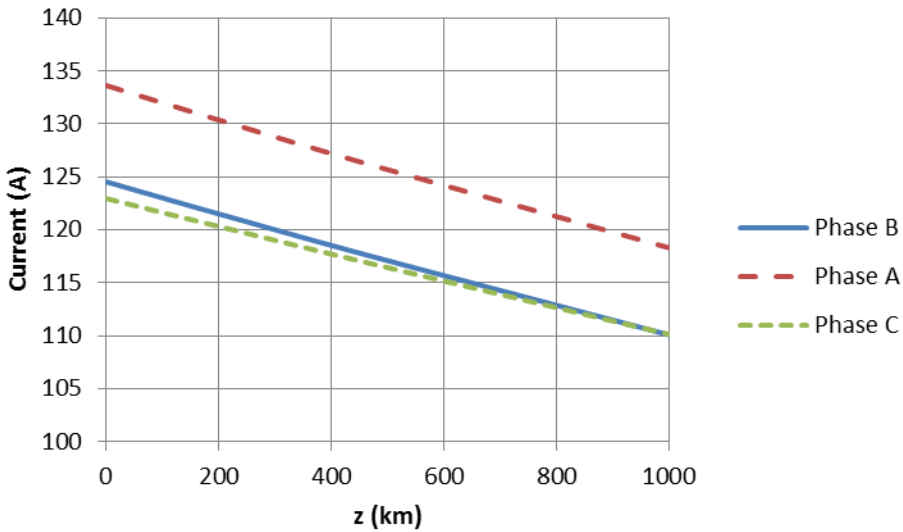


Fig. 7.5.4. Individual Phase Currents for an earth of lower conductivity ($y_1 = y_3 = 15$, $d/2 = 5$, $y_2 = 15$ meters, $\sigma_2 = 0.001$ S/m)

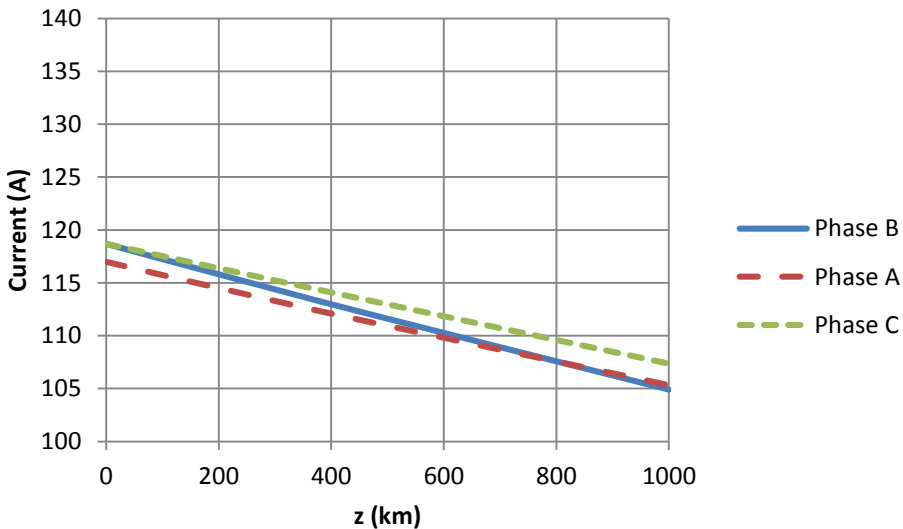


Fig. 7.5.5. Individual Phase Currents for a delta configured transmission line ($y_1 = y_3 = 15$, $d/2 = 5$, $y_2 = 23.67$ meters, $\sigma_2 = 0.01$ S/m)

In the next case, shown in Fig. 7.5.6, the height of the horizontal transmission line is decreased from 15 to 10 meters. This change appears to

have little effect on the currents induced or their rate of decay with distance. The final case is shown in Fig. 7.5.7. Here, the spacing between the phase conductors has been increased to 10 meters. One consequence is that the current induced on the transmission line is smaller. This reflects the fact that the inductance per unit length of this line is larger and, hence the surge impedance is higher. It can also be observed that the rate of decay for all three currents is roughly the same.

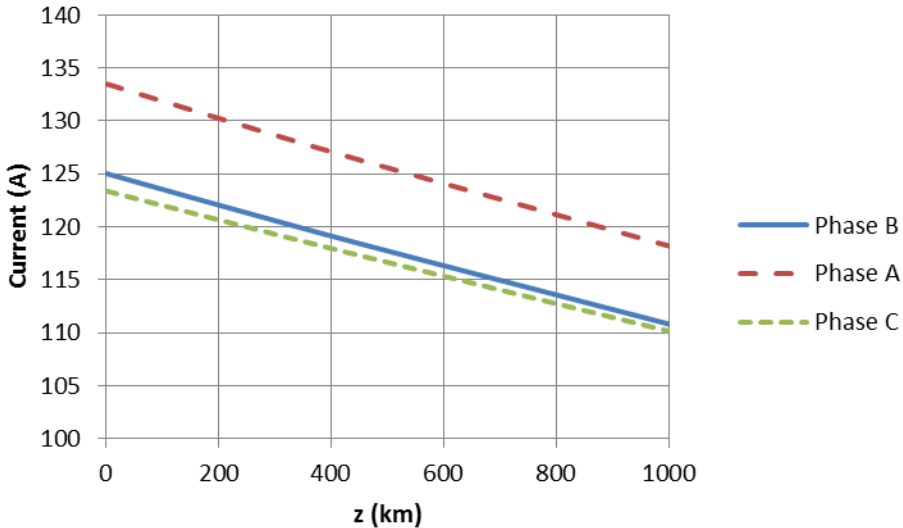


Fig. 7.5.6. Individual Phase Currents for a horizontal transmission line with a reduced height of 10 meters ($y_1 = y_3 = 10$, $d/2 = 5$, $y_2 = 10$ meters, $\sigma_2 = 0.01$ S/m).

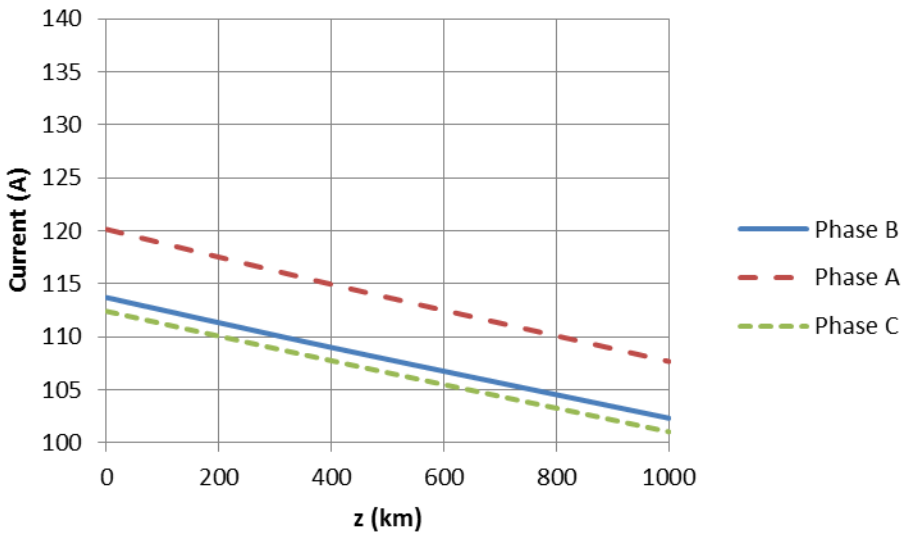


Fig. 7.5.7. Individual Phase Currents for a horizontal transmission line with an increased phase spacing of 10 meters ($y_1 = y_3 = 10$, $d/2 = 10$, $y_2 = 10$ meters, $\sigma_2 = 0.01$ S/m).

On the need for transposition

It was shown in section 7.4 that currents induced on transmission lines with unbalanced geometries with respect to the earth will generally exhibit unequal phase current magnitudes. This result was reinforced for the specific case for three phase transmission lines by the results shown in Figures 7.5.3 – 7.5.7. These results also illustrated the fact is that even if the excitation is balanced, the currents are generally unbalanced at the input and naturally become more unbalanced as they propagate down the line. For this reason, (at least some) utilities will “transpose” their power line conductors (i.e., change the positions of each conductor with respect to the earth at various distances along the power line). Such a tower is shown in Fig. 2.2.16.

While the issue of current unbalance is a real one, most analysis of power flow on transmission lines is carried out using analysis that assumes balanced currents. This is the subject covered in the next several sections. Later, this simplified theory for propagation using the approximate positive sequence component (and its single transmission line equivalent) will be compared to the complete theory developed in Sections 7.4 and 7.5. The comparison will shed light on both the amplitude of the individual phase currents compared to the “balanced” current as well as the change in unbalance with distance from the source along the transmission line.

7.6 Symmetrical Components

While the method described in Section 7.5 works in general for an arbitrary power line, it is complex and does not lead to much insight into the propagation process or answer the question about the conditions under which such a complex analysis is necessary. So, here, the process will be examined a bit further in the very important three-phase case.

If the results from Section 7.5 are written explicitly for the three conductor case, the result is

$$\left\{ \begin{array}{ccc} Z_{11} & Z_{12} & Z_{13} \\ Z_{21} & Z_{22} & Z_{23} \\ Z_{31} & Z_{32} & Z_{33} \end{array} \right\} + \frac{\gamma^2}{j\omega} \left\{ \begin{array}{ccc} A_{11} & A_{12} & A_{13} \\ A_{21} & A_{22} & A_{23} \\ A_{31} & A_{32} & A_{33} \end{array} \right\} \left\{ \begin{array}{c} \hat{I}_1 \\ \hat{I}_2 \\ \hat{I}_3 \end{array} \right\} = \left\{ \begin{array}{c} \hat{V}_1 \\ \hat{V}_2 \\ \hat{V}_3 \end{array} \right\} \quad (7.6.1)$$

where (as before) $Z_{ij} = Z_{ji}$ by reciprocity.

Again

$$j\omega|A|^{-1} = |Y| = j\omega|C| \quad (7.6.2)$$

(the admittance per unit length matrix for the conductors over earth). Multiplying (7.6.1) by $|Y|$ and then expanding the unknown current in the eigenvectors of $|Q^2| = |Y||Z|$ yields

$$\left\{ |\eta|^{-1} |Y||Z||\eta| + \gamma^2 |U| \right\} \hat{I}_c = |\eta|^{-1} |Y| \hat{V}$$

$$\left\{ |Q_d^2| + \gamma^2 |U| \right\} \hat{I}_c = |\eta|^{-1} |Y| \hat{V}$$
(7.6.3)

These equations could be solved for the natural modes as previously, but here it will be assumed (without justification at this time) that

$$Z_{ii} = Z_{jj} \quad i, j = 1, 3 \quad \text{and} \quad Z_{ij} = Z_{ji} \quad i \neq j$$

$$A_{ii} = A_{jj} \quad i, j = 1, 3 \quad \text{and} \quad A_{ij} = A_{ji} \quad i \neq j$$

These approximations are justified if the power line conductors are symmetrically located with respect to each other and very far from the earth. The approximations are also justified if a non-symmetric line is regularly transposed. But, also, it can be shown to be quite reasonable at 60 Hz for any realistic power line as will be demonstrated later in this chapter. Using this symmetry approximation

$$|Z| = \begin{vmatrix} Z_s & Z_m & Z_m \\ Z_m & Z_s & Z_m \\ Z_m & Z_m & Z_s \end{vmatrix}, \quad |Y| = \begin{vmatrix} Y_s & Y_m & Y_m \\ Y_m & Y_s & Y_m \\ Y_m & Y_m & Y_s \end{vmatrix}$$
(7.6.4)

so that

$$|Y||Z| = -|Q^2| = \begin{vmatrix} S & M & M \\ M & S & M \\ M & M & S \end{vmatrix}$$
(7.6.5)

Note that for a lossless earth, Y and Z are imaginary and hence the values of the matrix elements are negative. This is the reason for the “-“ sign.

In (7.6.5)

$$S = Z_s Y_s + 2Z_m Y_m \quad \text{and} \quad M = Z_m Y_m + Z_s Y_m + Z_m Y_s$$
(7.6.6)

Next, it will be shown that the eigenvectors and eigenvalues of $|Q^2|$ are respectively:

$$\begin{vmatrix} 1 \\ 1 \\ 1 \end{vmatrix} \quad \begin{vmatrix} 1 \\ e^{j2\pi/3} \\ e^{-j2\pi/3} \end{vmatrix} \quad \begin{vmatrix} 1 \\ e^{-j2\pi/3} \\ e^{j2\pi/3} \end{vmatrix} \quad (7.6.7)$$

and

$$S+2M \quad S-M \quad S-M \quad (7.6.8)$$

To prove this, consider that

$$\begin{vmatrix} S & M & M \\ M & S & M \\ M & M & S \end{vmatrix} \begin{vmatrix} 1 \\ 1 \\ 1 \end{vmatrix} = \begin{vmatrix} S+2M \\ S+2M \\ S+2M \end{vmatrix} = (S+2M) \begin{vmatrix} 1 \\ 1 \\ 1 \end{vmatrix} \quad (7.6.9)$$

for the first eigenvector. For the second,

$$\begin{vmatrix} S & M & M \\ M & S & M \\ M & M & S \end{vmatrix} \begin{vmatrix} 1 \\ e^{j2\pi/3} \\ e^{-j2\pi/3} \end{vmatrix} = \begin{vmatrix} S+M(e^{j2\pi/3} + e^{-j2\pi/3}) \\ Se^{j2\pi/3} + Me^{j2\pi/3}(e^{j2\pi/3} + e^{-j2\pi/3}) \\ Se^{-j2\pi/3} + Me^{-j2\pi/3}(e^{j2\pi/3} + e^{-j2\pi/3}) \end{vmatrix} \quad (7.6.10)$$

$$= \left[S+2M \cos\left(\frac{2\pi}{3}\right) \right] \begin{vmatrix} 1 \\ e^{j2\pi/3} \\ e^{-j2\pi/3} \end{vmatrix} = (S-M) \begin{vmatrix} 1 \\ e^{j2\pi/3} \\ e^{-j2\pi/3} \end{vmatrix}$$

The third proof is similar to the second.

This result means simply that the “components” for the symmetric case are simply the traditional symmetrical components that are commonly used in power systems analysis. These are the positive, negative and zero sequence components respectively.

To solve for the currents it is necessary to know the matrix of eigenvectors (arranged by columns) and its inverse. They are respectively

$$|\eta| = \frac{1}{\sqrt{3}} \begin{vmatrix} 1 & 1 & 1 \\ 1 & e^{j2\pi/3} & e^{-j2\pi/3} \\ 1 & e^{-j2\pi/3} & e^{j2\pi/3} \end{vmatrix} \quad (7.6.11)$$

and

$$|\eta|^{-1} = \frac{1}{\sqrt{3}} \begin{vmatrix} 1 & 1 & 1 \\ 1 & e^{-j2\pi/3} & e^{j2\pi/3} \\ 1 & e^{j2\pi/3} & e^{-j2\pi/3} \end{vmatrix} \quad (7.6.12)$$

These two matrices can be used to diagonalize $|\mathcal{Q}^2|$ using the identity, $|\eta|^{-1}|\mathcal{Q}^2||\eta| = |\mathcal{Q}_d^2|$. Carrying out the calculations results in

$$|\mathcal{Q}_d^2| = \begin{vmatrix} S + 2M & 0 & 0 \\ 0 & S - M & 0 \\ 0 & 0 & S - M \end{vmatrix} \quad (7.6.13)$$

A similar calculation for $|\eta|^{-1}|Y||\hat{V}|$ yields

$$|\eta|^{-1}|Y||\hat{V}| = \frac{1}{\sqrt{3}} \begin{vmatrix} (Y_s + 2Y_m)(\hat{V}_1 + \hat{V}_2 + \hat{V}_3) \\ (Y_s - Y_m)(\hat{V}_1 + \hat{V}_2 e^{-j2\pi/3} + \hat{V}_3 e^{j2\pi/3}) \\ (Y_s - Y_m)(\hat{V}_1 + \hat{V}_2 e^{j2\pi/3} + \hat{V}_3 e^{-j2\pi/3}) \end{vmatrix} \quad (7.6.14)$$

Given these results, (7.6.3) becomes explicitly

$$\left\{ \begin{array}{ccc|c} S + 2M & 0 & 0 & \\ 0 & S - M & 0 & \\ 0 & 0 & S - M & \end{array} \right\} + \gamma^2 \begin{vmatrix} 1 & 0 & 0 \\ 0 & 1 & 0 \\ 0 & 0 & 1 \end{vmatrix} \left\{ \begin{array}{c} \hat{I}_z \\ \hat{I}_p \\ \hat{I}_n \end{array} \right\} = \frac{1}{\sqrt{3}} \begin{vmatrix} (Y_s + 2Y_m)(\hat{V}_1 + \hat{V}_2 + \hat{V}_3) \\ (Y_s - Y_m)(\hat{V}_1 + \hat{V}_2 e^{-j2\pi/3} + \hat{V}_3 e^{j2\pi/3}) \\ (Y_s - Y_m)(\hat{V}_1 + \hat{V}_2 e^{j2\pi/3} + \hat{V}_3 e^{-j2\pi/3}) \end{vmatrix} \quad (7.6.15)$$

This is simple to solve because each equation is independent of the others. For example, the positive, negative and zero sequence currents are respectively

$$\hat{I}_p = \frac{(Y_s - Y_m)(\hat{V}_1 + \hat{V}_2 e^{j2\pi/3} + \hat{V}_3 e^{-j2\pi/3})}{\sqrt{3}[(Z_s - Z_m)(Y_s - Y_m) + \gamma^2]} \quad (7.6.16)$$

$$\hat{I}_n = \frac{(Y_s - Y_m)(\hat{V}_1 + \hat{V}_2 e^{-j2\pi/3} + \hat{V}_3 e^{j2\pi/3})}{\sqrt{3}[(Z_s - Z_m)(Y_s - Y_m) + \gamma^2]} \quad (7.6.17)$$

$$\hat{I}_z = \frac{(Y_s + 2Y_m)(\hat{V}_1 + \hat{V}_2 + \hat{V}_3)}{\sqrt{3}[(Z_s + Z_m)(Y_s + Y_m) + 2Z_m Y_m + \gamma^2]} \quad (7.6.18)$$

7.7 Per-Unit Length Parameters for an “Equivalent Symmetric” Transmission Line

Simplified method

The easiest way to calculate the “equivalent symmetric” parameters of a transmission line that is not long enough to become very unbalanced (or a transposed line) is to simply replace each diagonal (off-diagonal) element in the Z and Y matrices (i.e., (7.5.2) – (7.5.4) for transmission lines without shield wires with (7.5.18) and (7.5.22) for transmission lines with shield wires) with the average of the diagonal (off-diagonal) elements (Weeks, 1968). Using this method for a three phase transmission line,

$$\begin{aligned} Z_s &= \frac{1}{3} \sum_{n=1}^3 Z_{nn}} & Z_m &= \frac{1}{3} (Z_{12} + Z_{13} + Z_{23}) \\ Y_s &= \frac{1}{3} \sum_{n=1}^3 Y_{nn} & Y_m &= \frac{1}{3} (Y_{12} + Y_{13} + Y_{23}) \end{aligned} \quad (7.7.1)$$

Given this result, the positive and negative sequence impedance and admittance values (as shown in (7.6.16) are respectively

$$Z_{pos}, Z_{neg} = Z_s - Z_m, \quad Y_{pos}, Y_{neg} = Y_s - Y_m \quad (7.7.2)$$

and the zero sequence impedance and admittance values are

$$Z_{zero} = Z_s + 2Z_m, \quad Y_{zero} = Y_s + 2Y_m \quad (7.7.3)$$

More accurate method

A more common method for calculating the equivalent symmetric parameters begins by recognizing that a purely symmetric transmission line has impedance and admittance matrices that look like (7.6.4) or

$$|\mathbf{Z}| = \begin{vmatrix} Z_s & Z_m & Z_m \\ Z_m & Z_s & Z_m \\ Z_m & Z_m & Z_s \end{vmatrix}, \quad |\mathbf{Y}| = \begin{vmatrix} Y_s & Y_m & Y_m \\ Y_m & Y_s & Y_m \\ Y_m & Y_m & Y_s \end{vmatrix} \quad (7.7.4)$$

One property of this a matrix with this type of symmetry is that post-multiplying by $|\boldsymbol{\eta}|$ (a matrix of eigenvectors by columns) and pre-multiplying by $|\boldsymbol{\eta}|^{-1}$ where

$$|\boldsymbol{\eta}| = \frac{1}{\sqrt{3}} \begin{vmatrix} 1 & 1 & 1 \\ 1 & e^{j2\pi/3} & e^{-j2\pi/3} \\ 1 & e^{-j2\pi/3} & e^{j2\pi/3} \end{vmatrix} \quad (7.7.5)$$

and

$$|\boldsymbol{\eta}|^{-1} = \frac{1}{\sqrt{3}} \begin{vmatrix} 1 & 1 & 1 \\ 1 & e^{-j2\pi/3} & e^{j2\pi/3} \\ 1 & e^{j2\pi/3} & e^{-j2\pi/3} \end{vmatrix} \quad (7.7.6)$$

yields the diagonalized matrices,

$$|\mathbf{Z}_d| = \begin{vmatrix} Z_s + 2Z_m & 0 & 0 \\ 0 & Z_s - Z_m & 0 \\ 0 & 0 & Z_s - Z_m \end{vmatrix} \quad (7.7.7)$$

and

$$|\mathbf{Y}_d| = \begin{vmatrix} Y_s + 2Y_m & 0 & 0 \\ 0 & Y_s - Y_m & 0 \\ 0 & 0 & Y_s - Y_m \end{vmatrix} \quad (7.7.8)$$

where, as in Section 7.5, the positive and negative sequence impedance and admittance values are

$$\mathbf{Z}_{pos}, \mathbf{Z}_{neg} = Z_s - Z_m, \quad \mathbf{Y}_{pos}, \mathbf{Y}_{neg} = Y_s - Y_m \quad (7.7.9)$$

and the zero sequence impedance and admittance values are

$$\mathbf{Z}_{zero} = Z_s + 2Z_m, \quad \mathbf{Y}_{zero} = Y_s + 2Y_m \quad (7.7.10)$$

Using the same procedure for a transmission line that does not have perfect symmetry, but is close enough to symmetric, approximations to its equivalent “symmetric component” impedance” and admittance are:

$$|Z'_{ppd}| = |\eta|^{-1} |Z'_{pp}| |\eta| = \begin{vmatrix} Z_s + 2Z_m & \delta_{12} & \delta_{13} \\ \delta_{21} & Z_s - Z_m & \delta_{23} \\ \delta_{31} & \delta_{32} & Z_s - Z_m \end{vmatrix} \cong \begin{vmatrix} Z_s + 2Z_m & 0 & 0 \\ 0 & Z_s - Z_m & 0 \\ 0 & 0 & Z_s - Z_m \end{vmatrix} \quad (7.7.11)$$

and

$$|Y'_{ppd}| = |\eta|^{-1} |Y'_{pp}| |\eta| = \begin{vmatrix} Y_s + 2Y_m & \delta_{12} & \delta_{13} \\ \delta_{21} & Y_s - Y_m & \delta_{23} \\ \delta_{31} & \delta_{32} & Y_s - Y_m \end{vmatrix} \cong \begin{vmatrix} Y_s + 2Y_m & 0 & 0 \\ 0 & Y_s - Y_m & 0 \\ 0 & 0 & Y_s - Y_m \end{vmatrix} \quad (7.7.12)$$

where $|Z'_{pp}|$ and $|Y'_{pp}|$ can be found from (7.5.18) and (7.5.22) respectively⁷³.

Note that since $|\eta|$ does not represent the eigenvectors of $|Z'_{pp}|$ or $|Y'_{pp}|$, the matrices are not perfectly diagonalized. But, since the off-diagonal terms are assumed to be “small,” they have been neglected in the final result. In (7.7.11) and (7.7.12), $Z_s - Z_m$ and $Y_s - Y_m$ are the equivalent positive sequence impedance and admittance respectively.

Another approximate (but commonly used) method for calculating the positive sequence impedance and admittance can be found in Section 3.3 of EPRI (1982) or 2.4 of EPRI (2005). In this method, values of these parameters are derived using the geometric mean distance (GMD) of the transmission line conductors as well as the geometric mean radius of the phase conductor bundle.

Impedance per-unit length of a symmetrical transmission line

Consider the symmetrical transmission line above earth as illustrated in Fig. 7.7.1a. The impedance matrix for this power line is found from (7.5.1) – (7.5.3) as

$$\begin{bmatrix} Z_{11} & Z_{12} & Z_{13} \\ Z_{12} & Z_{22} & Z_{23} \\ Z_{13} & Z_{23} & Z_{33} \end{bmatrix} \cong -\frac{j\omega\mu_0}{2\pi} \begin{vmatrix} \ln(a) + \delta & \ln(s_{12}) + \delta & \ln(s_{12}) + \delta \\ \ln(s_{12}) + \delta & \ln(a) + \delta & \ln(s_{12}) + \delta \\ \ln(s_{12}) + \delta & \ln(s_{12}) + \delta & \ln(a) + \delta \end{vmatrix} \quad (7.7.13)$$

⁷³ If the transmission line has shield wires, it is first necessary to do a network reduction on the $3+N_s \times 3+N_s$ Z and Y matrices (where N_s is the number of shield wires and potential of each shield wire is assumed to be zero) to get an equivalent 3×3 system.

where by symmetry $s_{12} = s_{23} = s_{34}$ and the Carson integral has been approximated by (4.7.16) to be

$$J_c(x_m - x_n, y_m, y_n) \cong \ln\left(\frac{k_2 r_{mn}^i}{2}\right) + j\frac{\pi}{2}, \quad |k_2 r_{mn}^i| \ll 1 \quad (7.7.14)$$

Hence,

$$\delta = \ln(k_2 / 2) + j\pi / 2 \quad (7.7.15)$$

is independent of the geometry.

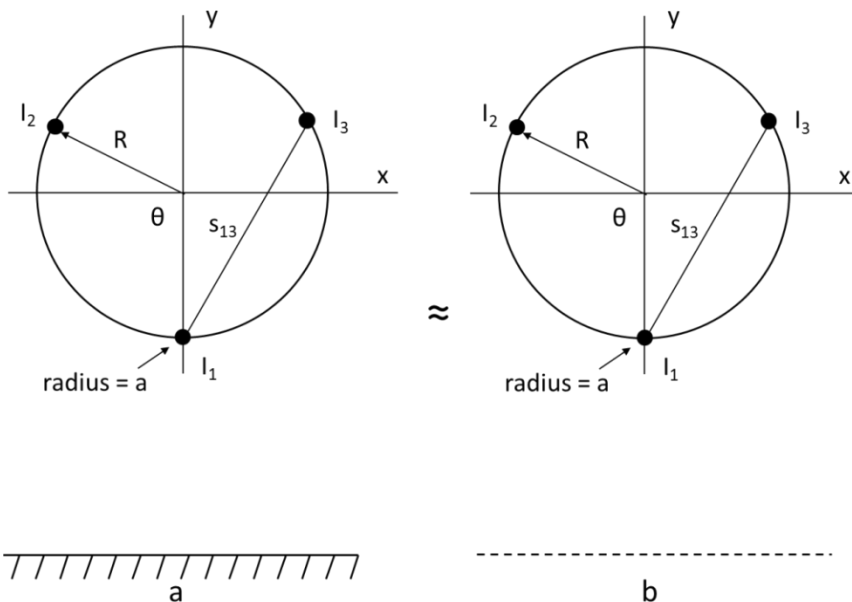


Fig. 7.7.1. A symmetrical three phase transmission line above earth. a) earth included b) earth neglected

If, next, (7.7.13) is matrix multiplied by a set of positive sequence currents then

$$\begin{aligned} & -\frac{j\omega\mu_0}{2\pi} \begin{vmatrix} \ln(a) + \delta & \ln(s_{12}) + \delta & \ln(s_{12}) + \delta \\ \ln(s_{12}) + \delta & \ln(a) + \delta & \ln(s_{12}) + \delta \\ \ln(s_{12}) + \delta & \ln(s_{12}) + \delta & \ln(a) + \delta \end{vmatrix} \begin{vmatrix} I \\ Ie^{-j2\pi/3} \\ Ie^{+j2\pi/3} \end{vmatrix} \\ & = \frac{j\omega\mu_0}{2\pi} \begin{vmatrix} (\ln(s_{12}/a))I \\ (\ln(s_{12}/a))Ie^{-j2\pi/3} \\ (\ln(s_{12}/a))Ie^{+j2\pi/3} \end{vmatrix} \end{aligned} \quad (7.7.16)$$

where the effect of the earth can now be neglected as illustrated in Fig. 7.7.1b. From this result, the zero sequence impedance for this balanced symmetrical transmission line can be written as

$$Z_{pos}^{sym} = \frac{j\omega\mu_0}{2\pi} \ln(s_{13}/a) \quad (7.7.17)$$

This result is identical to that derived in many textbooks using the theory of flux linkages (Bergen, 1986). A practical consequence of this is that a reduction in impedance can be had by either reducing the spacing between phases (i.e., a compact line) or increasing the conductor (or bundle) diameter.

7.8 Currents in the Space Domain

From 4.7.9, the inverse Fourier transform for calculating the current in the space domain can be written as

$$\hat{I}_p(z) = \frac{(Y_s - Y_m)(\hat{V}_1 + \hat{V}_2 e^{-j2\pi/3} + \hat{V}_3 e^{j2\pi/3})}{2\pi\sqrt{3}} \int_{-\infty}^{\infty} \left(\frac{1}{[(Z_s - Z_m)(Y_s - Y_m) + \gamma^2]} \right) e^{-j\gamma z} d\gamma \quad (7.8.2)$$

Since Z_s , Z_m , Y_s and Y_m are independent of γ , the only singularity of the denominator of (7.8.2) is the pair of zeros at

$$\gamma = \gamma_p = \pm j\sqrt{(Z_s - Z_m)(Y_s - Y_m)} \quad (7.8.3)$$

where it will be assumed that $\text{Im}(\gamma_p) \geq 0$. This zero represents the propagation constant of the positive sequence component. Since this zero in the denominator represents a simple pole of the integrand, it becomes straightforward to evaluate (7.8.2) by residue theory. Following (4.7.17) – (4.7.21), (7.8.2) becomes

$$\begin{aligned} \hat{I}_p(z) &= \frac{-j(Y_s - Y_m)(\hat{V}_1 + \hat{V}_2 e^{j2\pi/3} + \hat{V}_3 e^{-j2\pi/3})}{2\sqrt{3}\gamma_p} e^{-j\gamma_p z} \\ &= \frac{(\hat{V}_1 + \hat{V}_2 e^{j2\pi/3} + \hat{V}_3 e^{-j2\pi/3})}{2\sqrt{3}Z_{CP}} e^{-j\gamma_p z} \end{aligned} \quad (7.8.4)$$

where $Z_{CP} = \sqrt{(Z_s - Z_m)/(Y_s - Y_m)}$ is the positive sequence characteristic impedance.

Other components can be obtained in a similar manner.

7.9 The Single Line Approximation and Calculation of the Individual Currents

It is usually assumed for power flow calculations that the only component on the transmission line is the positive sequence voltage and current. If it is assumed that the transmission line is excited by a positive sequence voltage as in (7.9.1)

$$\begin{aligned}\hat{V}_1 &= \hat{V} \\ \hat{V}_2 &= \hat{V}e^{-j2\pi/3}, \\ \hat{V}_3 &= \hat{V}e^{j2\pi/3}\end{aligned}\quad (7.9.1)$$

where \hat{V} is the phase to ground voltage magnitude, then only the positive sequence current is excited and

$$\hat{I}_P(z) = \frac{-j(Y_s - Y_m)\sqrt{3}\hat{V}}{2\gamma_P} e^{-j\gamma_P z} \quad (7.9.2)$$

Further, it is now possible to determine the individual currents from (7.4.4)

$$\left| \hat{I}(\gamma) \right| = |\eta| \left| \hat{I}_{gm}(\gamma) \right| \quad (7.9.3)$$

and (7.6.11)

$$|\eta| = \frac{1}{3} \begin{vmatrix} 1 & 1 & 1 \\ 1 & e^{j2\pi/3} & e^{-j2\pi/3} \\ 1 & e^{-j2\pi/3} & e^{j2\pi/3} \end{vmatrix} \quad (7.9.4)$$

so that (since all other components are zero)

$$\hat{I}_1(z) = \frac{-j(Y_s - Y_m)\hat{V}}{2\gamma_P} e^{-j\gamma_P z} \quad (7.9.5)$$

Given the definition of γ_P in (7.8.3), (7.9.5) can be written as

$$I_1(z) = \frac{\hat{V}}{2Z_{PS}} e^{-j\gamma_P z} \quad (7.9.6)$$

where

$$Z_{PS} = \sqrt{\frac{(Z_s - Z_m)}{(Y_s - Y_m)}} \quad (7.9.7)$$

is the positive sequence characteristic impedance (often called “surge impedance”) of the transmission line. The reason for the factor of 2 in the denominator can be understood in the same way as in Chapter 4 where the voltage source in series with the line can be related to the “phase-to-ground” voltage V_{pg} as shown in Fig. 7.9.1



Fig. 7.9.1. a) circuit equivalent to a series source of voltage V b) equivalent phase to ground sources for the case that all cross sectional dimensions of the power line are small compared to a wavelength at the operating frequency.

Given this result, the current for $z > 0$ can be written as

$$I_1(z) = \frac{\hat{V}_{pg}}{Z_{PS}} e^{-j\gamma_P z} \quad (7.9.8)$$

Other components of the current can be obtained in a similar manner. More specifically,

$$\begin{aligned} \hat{I}_2(z) &= \hat{I}_1(z) e^{-j2\pi/3} \\ \hat{I}_3(z) &= \hat{I}_1(z) e^{+j2\pi/3} \end{aligned} \quad (7.9.9)$$

(7.9.8) and (7.9.9) are the basis for treating three phase systems carrying a balanced three phase positive sequence current as an equivalent single conductor line.

7.10 Comparison of the single line and general methods for calculating phase currents

In this section, a comparison will be made between the general results of Section 7.5 for currents induced on a transmission line and the simple approximations that have been made in the previous sections. More specifically, the magnitude of the individual positive sequence phase currents

of (7.9.8) where $V_{pg} = V_1/2$ using the simplified impedance and admittance parameters from (7.7.1) will be plotted in addition to the individual currents.

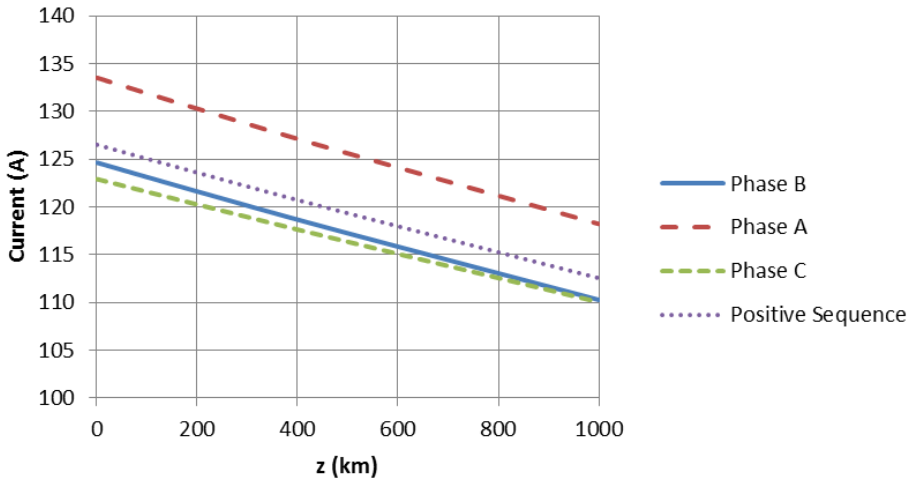


Fig. 7.10.1 Horizontal line of Fig. 7.5.3 with positive sequence current ($y_1 = y_3 = 15$, $d/2 = 5$, $y_2 = 15$ meters, $\sigma_2 = 0.01$ S/m)

In Fig. 7.10.1, the magnitude of the positive sequence currents is plotted for the horizontal configured transmission line base case along with the individual phase currents. As expected, the positive sequence current has a value at $z = 0$ that is roughly equal to the average of the three individual phase currents. In addition, the rate of decay is roughly the average for the three currents. Also, as expected, the current imbalance that varies with distance, is not captured by the positive sequence current.

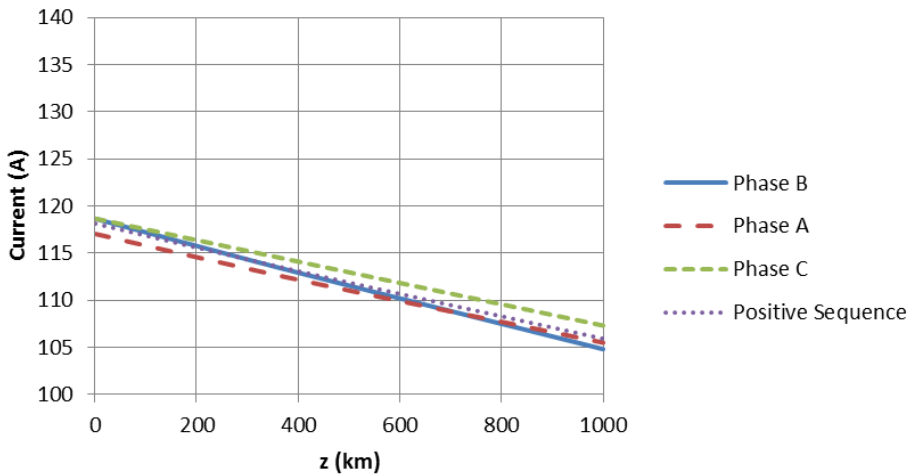


Fig. 7.10.2 Delta configured transmission line of Fig. 7.5.5 with positive sequence current ($y_1 = y_3 = 15$, $d/2 = 5$, $y_2 = 23.67$ meters, $\sigma_2 = 0.01$ S/m)

In Fig. 7.10.2, the magnitude of the positive sequence currents is plotted for the delta configured transmission line along with the individual phase currents. In this case, the agreement is much better because the individual currents are significantly closer. Nevertheless the current imbalance is, again, not captured.

7.11 Extension to conductor bundles

Introduction

A short introduction to the idea of a conductor bundle was given earlier in Section 7. 2. Here this idea will be examined more carefully in the case for two subconductors and then generalized to the case for an arbitrary number of subconductors. The effect of using conductor bundles on line parameters will then be discussed.

Two subconductors

Suppose that rather than a single wire above the earth, there are two parallel wires, each driven by an identical voltage source at $z = 0$, placed a distance d apart and at the same height, h , above a homogeneous earth (Olsen and Aburwein 1980). It is assumed here that $b \gg d \gg a$ and that $d \ll \lambda$. A cross sectional view of this problem is illustrated in Fig. 7.11.1.

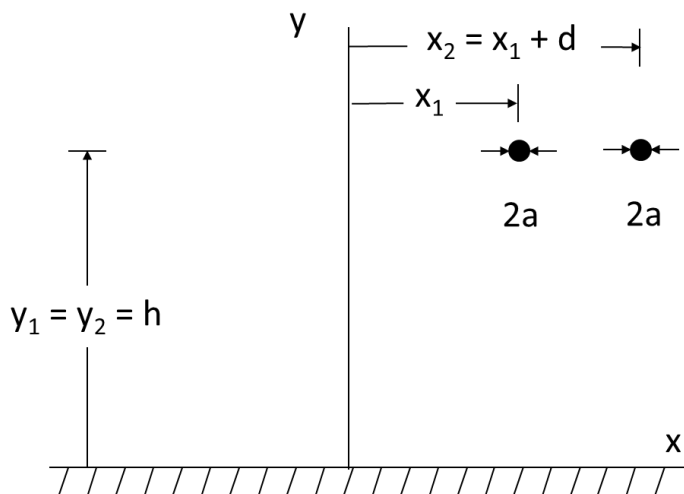


Fig. 7.11.1. Cross sectional view of a two conductor bundle. Each wire is driven by a sinusoidal voltage source with magnitude V at $z = 0$.

By symmetry, the current in each wire is the same. Hence, following (4.3.4) with $E_z = 0$ and assuming that the total axial electric field (due to

both sources) is zero at $(x, y) = \begin{pmatrix} x_1, h - a \\ 2 \end{pmatrix}$

$$(x, y) = \begin{pmatrix} x_1, h-a \\ 2 \end{pmatrix}$$

$$\tilde{G}_{ez}(0, h-a, h, \gamma) \hat{I}(\gamma) + \tilde{G}_{ez}(-d, h-a, h, \gamma) \hat{I}(\gamma) = -V + Z_{iw} \hat{I}(\gamma) \quad (7.11.1)$$

Note that only one equation is necessary here because (by symmetry) the electric field will automatically be zero at $(x, y) = (x_2, h-a)$. Given this, (7.11.1) can be solved for the total current (i.e., $2\hat{I}(\gamma)$) on the bundle. The result is

$$\hat{I}_{total}(\gamma) = \frac{-2V}{\tilde{G}_{ez}(0, h-a, h, \gamma) + \tilde{G}_{ez}(-d, h-a, h, \gamma) - Z_{iw}} \quad (7.11.2)$$

Now, from (4.4.64)

$$\tilde{G}_{ez} \begin{pmatrix} x - x_1, y, h, \gamma \\ 2 \end{pmatrix} = \tilde{G}_{ez}^s \begin{pmatrix} x - x_1, y, h, \gamma \\ 2 \end{pmatrix} + \tilde{G}_{ez}^r \begin{pmatrix} x - x_1, y, h, \gamma \\ 2 \end{pmatrix} \quad (7.11.3)$$

where

$$\tilde{G}_{ez}^s \begin{pmatrix} x - x_1, y, h, \gamma \\ 2 \end{pmatrix} = \frac{+(\gamma^2 - k_0^2)}{4\omega\epsilon_0} H_0^{(2)} \begin{pmatrix} (\gamma^2 - k_0^2)^{1/2} r_1 \\ 2 \end{pmatrix} \quad (7.11.4)$$

is the “source” term and

$$\tilde{G}_{ez}^r \begin{pmatrix} x - x_1, y, h, \gamma \\ 2 \end{pmatrix} = \frac{+(\gamma^2 - k_0^2)}{4\omega\epsilon_0} \left\{ -H_0^{(2)} \begin{pmatrix} (\gamma^2 - k_0^2)^{1/2} r_1^i \\ 2 \end{pmatrix} + \frac{j}{\pi} \int_{-\infty}^{\infty} \frac{(1 + R(\kappa)) e^{-u_1(y+h)} e^{-j\kappa(x-x_1)}}{u_1} d\kappa \right\} \quad (7.11.5)$$

is the earth “reflection” term.

Now, since $h \gg d \gg a$, $\tilde{G}_{ez}^s(0, h-a, h, \gamma)$ is substantially different from $\tilde{G}_{ez}^s(-d, h-a, h, \gamma)$ but $\tilde{G}_{ez}^r(0, h-a, h, \gamma) \cong \tilde{G}_{ez}^r(-d, h-a, h, \gamma)$. Thus, (7.11.2) can be written approximately as

$$\hat{I}_{total}(\gamma) = -2V / \left[\frac{(\gamma^2 - k_0^2)}{4\omega\epsilon_0} \left[H_0^{(2)}\left((\gamma^2 - k_0^2)^{1/2}(d^2 + a^2)^{1/2}\right) + H_0^{(2)}\left((\gamma^2 - k_0^2)^{1/2}a\right) \right] + 2\tilde{G}_{ez}^r(d/2, h, h, \gamma) - Z_{iw} \right] \quad (7.11.6)$$

Further, since

$$H_0^{(2)}(q) \cong 1 - \frac{2j}{\pi} \ln(q/2) - \frac{2j\gamma_e}{\pi}, \quad q \ll 1$$

where γ_e is Euhler's constant, (7.11.6) can be written

$$\hat{I}_{total}(\gamma) = \frac{-2V}{\frac{-j(\gamma^2 - k_0^2)}{2\pi\omega\epsilon_0} \left[\ln(d^2 + a^2)^{1/2} + \ln(a) \right] + 2\tilde{G}_{ez}^r(d/2, h, h, \gamma) - Z_{iw}} \quad (7.11.7)$$

and, by combining the log terms,

$$\hat{I}_{total}(\gamma) = \frac{-2V}{2\frac{-j(\gamma^2 - k_0^2)}{2\pi\omega\epsilon_0} \ln \left[\left(a(d^2 + a^2)^{1/2} \right)^{1/2} \right] + 2\tilde{G}_{ez}^r(d/2, h, h, \gamma) - Z_{iw}} \quad (7.11.8)$$

The term $\left(a(d^2 + a^2)^{1/2} \right)^{1/2} \cong (ad)^{1/2}$, $a \ll d$ is called the “effective radius” of the conductor and can be used to write the final result for the total current as (Weeks 1981)

$$\hat{I}_{total}(\gamma) = \frac{-V}{\tilde{G}_{ez}^r\left((ad)^{1/2}, h, h, \gamma\right) - Z_{iw}/2} \quad (7.11.9)$$

This is exactly the same result as for a single wire except that the radius of the single conductor is replaced by the geometric mean radius of the bundle and the internal impedance per unit length of the conductor is halved.

Arbitrary number of subconductors

It was shown above that two conductors held at the same potential and driven by the same voltage can be combined into an “equivalent” single “bundled” conductor with an equivalent radius. Here this result will be generalized to an N conductor “symmetric” bundle (i.e., even values of N). It will be assumed that the bundle dimensions are small compared to either the distance to the nearest other phase or shield conductor and the earth. Such a problem is shown in Fig. 7.11.2

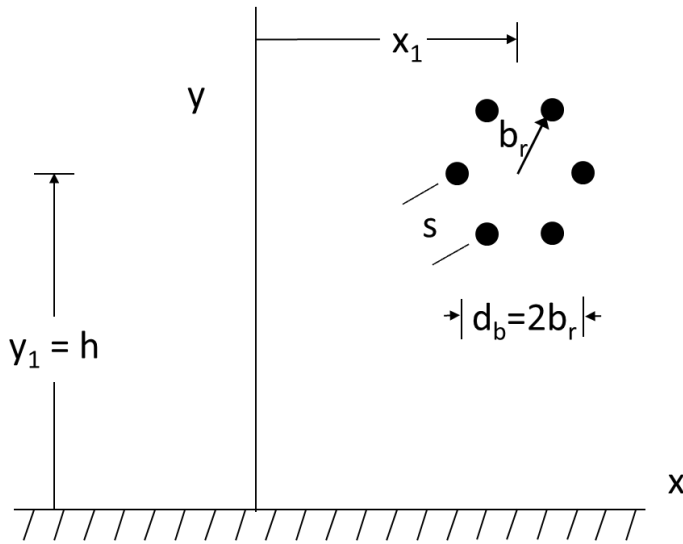


Fig. 7.11.2. Cross sectional view of an N conductor symmetric bundle of bundle diameter d_b , bundle radius b_r , and subconductor spacing s centered at (x_1, y_1) . Each subconductor is of radius a_{sub} and is driven by a sinusoidal voltage source with magnitude V at $z = 0$.

Assuming again that $a \ll d_b$, equation (7.11.8) can be generalized to the N conductor bundle shown in Fig. 7.11.2 and is given as (7.11.10) below (EPRI 1982)

$$\hat{I}_{total}(\gamma) = \frac{-V}{\frac{-j(\gamma^2 - k_0^2)}{2\pi\omega\epsilon_0} \ln \left[\left(N a_{sub} (b_r)^{N-1} \right)^{1/N} \right] + \tilde{G}_{ez}^r(d_b/2, h, h, \gamma) - Z_{iw}^{bundle}} \quad (7.11.10)$$

where the “effective radius” is

$$a_{eff} = \left(N a_{sub} (b_r)^{N-1} \right)^{1/N} \quad (7.11.11)$$

The relationship between the “bundle radius” and the “subconductor spacing” is

$$b_r = \frac{s}{2 \sin(\pi/N)} \quad (7.11.12)$$

The appropriate surface impedance to use for a conductor bundle is

$$Z_{iw}^{bundle} = Z_{iw} / N \quad (7.11.13)$$

where Z_{iw} is the surface impedance for an individual subconductor.

$$\hat{I}_{total}(\gamma) = \frac{-V}{\tilde{G}_{ez}(a_{eff}, h, h, \gamma) - Z_{iw} / N} \quad (7.11.14)$$

Again, this is exactly the same result as for a single wire case except that the radius of the single conductor is replaced by the effective radius of the bundle and the internal impedance per unit length of any subconductor is divided by N.

Effect of bundling on line parameters

Recall that the distributed capacitance and external inductance for a single conductor transmission line from (5.5.1) and (5.5.6) are respectively

$$C = \frac{2\pi\epsilon_0}{\ln\left(\frac{2h}{a}\right)} \quad (7.11.15)$$

and

$$L_e \cong \frac{\mu_0}{2\pi} \ln\left(\frac{d_i}{a}\right) \quad (7.11.16)$$

respectively, where a is the conductor radius. Hence, replacing the conductor radius a with the effective bundle radius a_{eff} (which is generally much larger than a even if the sub conductor radius is smaller than the original conductor) has the effect of increasing the capacitance per unit length of the equivalent power transmission line, and reducing the inductance per unit length of the equivalent transmission line. Since the inductance and capacitance are respectively proportional to and inversely proportional to the factor $\ln(\bullet/a)$, these changes occur logarithmically. According to (4.2.5) – (4.2.7), the behavior of the resistance is a bit more complicated. More specifically, since the resistance of a subconductor is proportional to something between a and a^2 , the total resistance of the bundle will be proportional to a factor between a/N and a^2/N where N is the number of subconductors. Thus, again, the resistance of the bundle is generally reduced compared to the original conductor even if the subconductor radius is smaller than the original conductor radius.

7.12 Problems

P7.1 Derive (7.2.14) starting with (7.2.9) – (7.2.10)

P7.2 a) Find an explicit expression for $|Y|$ and $|C|$ in (7.2.15) in terms of the individual elements of $|A|$ as defined in (7.2.12) and (7.2.14). Note that some elements of $|C|$ are negative, but this does not imply negative equivalent capacitances as shown in part b.

b) Consider Figure P 7.2 in which the cross section of a two conductor horizontal transmission line is shown along with a network of capacitors that accounts for the capacitive currents between conductors and between conductors and the earth. Using

$$\begin{bmatrix} \hat{I}_1 \\ \hat{I}_2 \end{bmatrix} = j\omega |C| \begin{bmatrix} \hat{V}_1 \\ \hat{V}_2 \end{bmatrix},$$

and the successive assumptions $V_1 = V_2$ and $V_1 = -V_2$, find explicit expressions for $C_{1g} = C_{2g}$ and C_{12} . Show that each of these has a positive value.

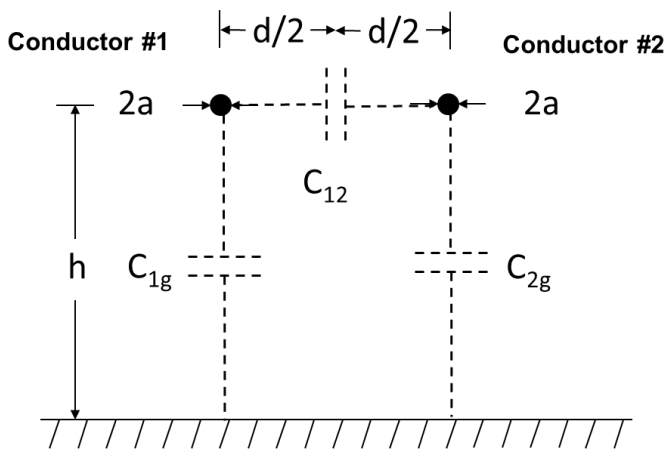


Fig. P7.2 Two conductors above earth with an array of capacitors used to calculate capacitive currents between conductors and between the conductors and the earth.

P7.3 Using (7.2.19), show explicitly that $|\eta|^{-1} |Q^2| |\eta| = |\eta|^{-1} |Y| |Z| |\eta|$ in (7.2.23) is a diagonal matrix and equal to (7.2.26) where $|Y| |Z|$ can be found in (7.2.17). Essentially this problem asks you to follow steps (7.2.25) through (7.2.26).

P7.4 Using (7.2.33) and (7.2.34) show explicitly that $|A|^{-1} |A| = |U|$, the unit matrix.

P7.5 Using the approximation for the Carson integral

$$J_c(x-x', y, y') \cong \ln\left(j \frac{k_2 r'}{2}\right) + 0.077 - j \frac{2}{3} k_2 (y + y')$$

where the last two terms can be ignored, calculate values of γ_c and γ_d . The formulas for these two propagation constants can be found in (7.2.41) and (7.2.43). Assume aluminum conductors (i.e., $\sigma_w = 3.5 \times 10^7$ S/m) and the parameters $f = 60$ Hz, $a = 0.01$ m, $h = 10$ m, $d = 5$ m and $\sigma_2 = 0.01$ S/m.

P7.6 Using the parameters of problem P7.5 except for the frequency, evaluate the attenuation constant (i.e., the imaginary part of the propagation constant) for γ_c and γ_d for the frequencies 100 Hz, 1 kHz, 10 kHz and 100 kHz. Does the loss from the conductors or the earth contribute the largest part of the attenuation?

P7.7 Assuming that conductors and the earth are both perfect conductors, calculate the characteristic impedances Z_{OC} and Z_{OD} in (7.2.52) and (7.2.53) for a pair conductors spaced 5 meters apart and located 10 meters above the earth. How do they compare? If $Z_{L1G} = 1000 \Omega$ and $Z_{L12} = Z_{LG2} \rightarrow \infty$, calculate the reflection coefficients $\Gamma_{dd}, \Gamma_{dc}, \Gamma_{cc}$ and Γ_{cd} .

P7.8 Given the propagation constant γ_c^2 in (7.3.3) and using the first term of the approximate Carson integral given in problem P7.5, show that the factor

$$\frac{k_0^2 \cos(\theta_i)}{(k_0^2 \sin^2(\theta_i) - \gamma_c^2)} \propto \hat{I}(z)$$

in (7.3.11) has a maximum value for some value of θ_i near $\pi/2$. For this calculation, assume that $Z_{iw} = 0$, that the frequency is 10 kHz and that $\sigma_2 = 0.01$ S/m, $d = 5$ meters, $b = 10$ meters and $a = 0.01$ meters. What does this result mean for induced currents on power lines from a lightning field at grazing incidence?

P7.9 A quasi-DC current of 100 A at a frequency of 0.01 Hz is induced in a 300 km long transmission line 20 meters above the earth by a parallel electrojet current that is 100 km directly above the transmission line. The earth conductivity is 0.01 S/m, the transmission line's quasi-DC resistance is 5Ω and the quasi-DC grounding impedance of each transformer is 5Ω . Using (7.3.18) and (7.3.19), determine the magnitude (i.e., not the phase) of the electrojet current.

P7.10 Assuming that $A \cos(\theta_A) = \sqrt{2\pi}$, and $i(t) = t \exp(-at)$ where $a = 0.01/\text{sec}$, find the geomagnetic induced current on a transmission line using (7.3.26) reproduced below.

$$i_{ind}(t) = \frac{A \cos(\theta_A)}{\sqrt{2\pi}} \int_{-\infty}^{\infty} \frac{i_s(t')}{\sqrt{t-t'}} dt'$$

Use whatever numerical technique you have available. Note that the singularity at $t = t'$ is integrable.

P7.11 For the transformer characteristics given in Fig. 7.3.7. and the flux given in

$$\phi(t) = 2 + 10 \sin(\omega t)$$

where $f = 60$ Hz and $\omega = 2\pi f$, plot the transformer current. Comment on the harmonic content of this current.

P7.12 Suppose you have a single wire transmission line 10 meters above earth with a single shield wire 2 meters above it. Write down the full impedances matrix as in (7.5.12) as well as its reduced form $|Z'_{pp}|$ that accounts for the shield wire. Also, write down the full admittance matrix as in (7.5.16) as well as its reduced form $|A'_{pp}|$ that accounts for the shield wire. Assume that the earth has a conductivity of 0.01 S/m, that the frequency is 60 Hz and that you can use the first term of the simplified Carson equation in P7.5. Also assume that $a_l = a_g = 0.01$ meters.

P7.13 Calculate the per-unit length impedance and admittance parameters (i.e., Z_{pos} , Z_{neg} , Z_{zero} , Y_{pos} , Y_{neg} and Y_{zero}) for an equivalent symmetric transmission line using the “simplified” and “more accurate” methods discussed in Section 7.6. Assume that the transmission line is a horizontal line at a height of 15 meters above ground and that the phase-phase spacing is 5 meters and that the radius of the conductor is 0.01 meters. Assume that the earth has a conductivity of 0.01 S/m, that the frequency is 60 Hz and that you can use the simplified Carson equation in P 7.5.

P7.14 Calculate the geometric mean radius for a four conductor bundle in a square configuration with a subconductor radius of 0.01 meters and a spacing of 0.5 meters.

P7.15 The geometries of a single-conductor power line and a bundle-conductor power line are shown in Fig. P7.15.1. The single conductor is solid, 1.75 centimeters in radius, and 14 meters above the ground. The four solid subconductors, each with radius of 1.75 centimeters and bundle

spacing, s of 45.72 centimeters, in the bundle are uniformly distributed on a circle contour. The center of the circle is 14 meters above the ground.

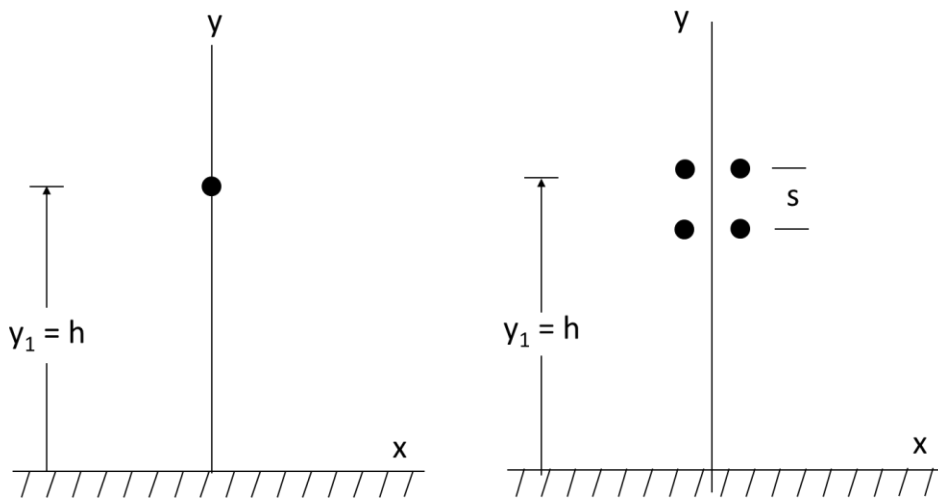


Fig. P7.15.1 Geometries of a single-conductor and a bundle-conductor power line

Find the effective radius of the conductor bundle. With the given information above and ignoring the effect due to the earth, calculate the per-unit length capacitance c and external inductance l_e of the single-conductor line and the bundle-conductor line. Compare the product of the capacitance and inductance ($c \times l$) for the two lines.

7.13 References

Anderson, P. A. 1973. *Analysis of Faulted Power Systems*. Iowa State University Press. Ames, Iowa.

Baba, Y. and V. A. Rakov. 2007. "Electromagnetic Models of the Lightning Return Stroke," *Journal of Geophysical Research*, Vol. 112, D04102, doi:[10.1029/2006JD007222](https://doi.org/10.1029/2006JD007222). February.

Bergen, A. R. 1986. *Power System Analysis*. Prentice Hall. Englewood Cliffs, NJ.

Boteler, D. H., and R. J. Rirjola. 1998. "The Complex-Image Method for Calculating the Magnetic and Electric Fields Produced at the Surface of the Earth by the Auroral Electrojet," *Geophysical Journal Int.* Vol 132. Pp.31-40.

Brigham, E. O. 1974. *The Fast Fourier Transform*. Prentice Hall. Englewood Cliffs, NJ.

Chapman, S. J. 2002. *Electric Machinery and Power System Fundamentals*. McGraw Hill. New York.

Delfino, F., R. Procopio, M. Rossi, A. Shoory, and F. Rachidi, 2011. Lightning Electromagnetic Radiation over a Stratified Conducting Ground: Formulation and Numerical Evaluation of the Electromagnetic Fields, *Journal of Geophysical Research*. Vol. 116, D04101, doi:10.1029/2010JD015077

Elovaara, J., P. Linblad, A. Viljanen, T. Makinen, R. Pirjola, S. Larsson, B. Kielen. 1992. "Geomagnetically Induced Currents in the Nordic Power System and their Effects on Equipment, Control, Protection and Operation." *CIGRE*. Paper 36-301.

EPRI. 1982. *Transmission Line Reference Book: 345 kV and Above, 2nd Ed.*, Electric Power Research Institute. Palo Alto, CA.

EPRI. 2005. *Transmission Line Reference Book: 200 kV and Above, 3rd Ed.* Electric Power Research Institute. Palo Alto, CA.

Erinmez, I. A., J. G. Kappenman and W. A. Radasky. 2000. "Management of the Geomagnetically Induced Current Risks on the National Grid Company's Electric Power Transmission System." *Journal of Atmospheric and Solar Terrestrial Physics*. Special Addition for NATO Space Weather Hazards Conference. June.

Ford, L. R. 1955. *Differential Equations*. McGraw Hill, New York

Gradshteyn, I. S. and I. M. Ryzhik (7th edition edited by A. Jeffrey and D. Zwillinger). 2007. *Table of Integrals, Series, and Products*. Academic Press. New York.

IEEE, Power & Energy Society Technical Council Task Force on Geomagnetic Disturbances. 2013. "Geomagnetic Disturbances." *IEEE Power and Energy Magazine*. pp. 71-78. July/August.

NASA. 2003. "The Exploration of the Earth's Magnetosphere." <http://www-istp.gsfc.nasa.gov/Education/Intro.html>

NERC. 1989. "The March 13, 1989 System Disturbances." NERC Disturbance Analysis Working Group Report pp. 8-9, 36-60.

Olsen, R. G., and M. A. Usta. 1977. "The Excitation of Current on an Infinite Horizontal Wire above Earth by a Vertical Electric Dipole." *IEEE Transactions on Antennas and Propagation*. Vol. AP-25. pp. 560-565. July.

Olsen, R. G. and A. Aburwejn. 1980. "Current Induced on a Pair of Wires Above Earth by a Vertical Electric Dipole for Grazing Angles of Incidence." *Radio Science*. Vol. 15. pp. 733–742. July/August.

Olsen, R. G. 1984. "A Simple Model for Weakly Coupled Lossy Transmission Lines of Finite Length," *IEEE Transactions on Electromagnetic Compatibility*. Vol. EMC-26. pp. 79–83, May.

Pirjola, R. 1982. "Electromagnetic Induction in the Earth by a Plane Wave or by Fields of Line Currents Harmonic in Time and Space," *Geophysica*. Vol. 18, pp. 1-161.

Pirjola, J. and L. T. V. Hakkinen. 1991. "Electrojet Field Caused by an Auroral Electrojet Current System Model," in Kikuchi, H., *Environmental and Space Electromagnetics*, Springer Verlag. Tokyo.

Shoory, A, R Moini, S. H. Hesam Sadeghi, and V. A. Rakov. 2005. "Analysis of Lightning-Radiated Electromagnetic Fields in the Vicinity of Lossy Ground." *IEEE Transaction on Electromagnetic Compatibility*. Vol 47. pp. 1341-146. February.

Ulaby, M. A. 2001. *Fundamentals of Applied Electromagnetics*. Prentice Hall. Upper Saddle River, NJ.

Uman, M. A. 2001. *The Lightning Discharge*. Dover. Toronto.

Wait, J. R. 1977. "Excitation of an Ensemble of J Parallel Cables by an External Dipole Over an M Layered Ground, *AEU*, Vol. 31. pp. 489-493. December.

Wiley, C. R. 1966. *Advanced Engineering Mathematics*. McGraw Hill. New York.

Weeks, W. L. 1968. *Transmission and Distribution of Electrical Energy*. Wiley. New York.

Appendix A

Wireless vs. Wired Transmission

It is shown in (7.2.45) that the differential mode current induced on two wires above the earth by either voltage sources or external fields is

$$\hat{I}_1(z) = -\hat{I}_2(z) = \frac{-j(Y_{11} - Y_{12}) \left(\hat{V}_1 + \hat{E}_{ez}^1(\gamma_d) - \hat{V}_2 - \hat{E}_{ez}^2(\gamma_d) \right)}{4\gamma_d} e^{-j\gamma_d z}. \quad (\text{A.1})$$

It is now assumed that 1) the voltage sources are set to zero, 2) the source of external fields is an electric dipole located between the two wires and oriented so that it points from one wire to another as shown in Fig. A.1 and that the earth is far enough away to be neglected.

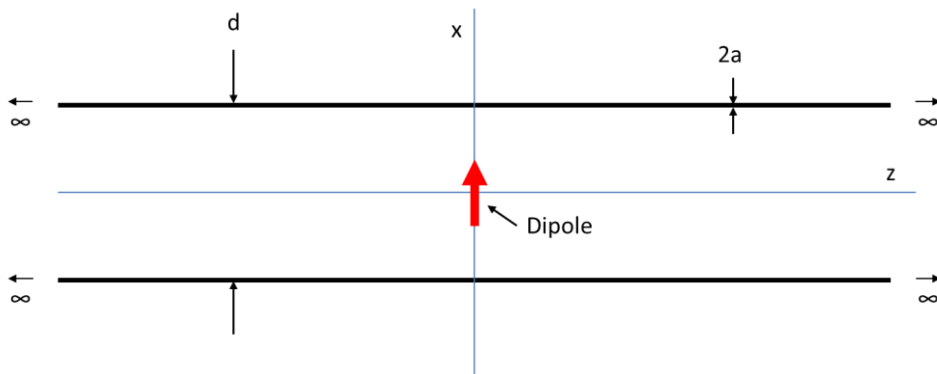


Fig. A.1 Two parallel wires in free space excited by a dipole between them

The result is shown in (A.2) – (A.3).

$$\hat{I}_1(z) = -\hat{I}_2(z) = \frac{-j(Y_{11} - Y_{12}) \left(\hat{E}_{ez}^1(\gamma_d) - \hat{E}_{ez}^2(\gamma_d) \right)}{4\gamma_d} e^{-j\gamma_d z}. \quad (\text{A.2})$$

where

$$\gamma_d^2 = k_0^2 - (Y_{11} - Y_{12})Z_{iw} \quad (\text{A.3})$$

and

$$Y_{11} - Y_{12} = \frac{j2\pi\omega\epsilon_0}{\ln\left(\frac{d}{a}\right)}, \quad Z_{iw}(\omega) = R_{dc} \left(\frac{k_w a}{2} \right) \frac{J_0(k_w a)}{J_1(k_w a)} \quad (\text{A.4})$$

Note that the common mode is not excited in this case because the excitation field has odd symmetry with respect to the x axis.

Further, at high enough frequencies that $|k_w a| \gg 1$

$$Z_{iw}(\omega) \cong \left(\frac{\omega\mu_o}{2\sigma_w} \right)^{1/2} \frac{(1+j)}{2\pi a}, \quad |k_w a| \gg 1 \quad (\text{A.5})$$

From (9.4.2), and assuming that $(k_0^2 - \gamma^2)^{1/2} d \ll 1$, the z component of the dipole fields in the spatial Fourier transform domain (i.e., as a function of γ) is

$$\hat{E}_{zs}(x-x', \gamma) \cong \frac{-\hat{I}h\gamma}{2\pi\omega\epsilon_0} \left\{ \frac{(x-x')}{r^2} \right\}. \quad (\text{A.6})$$

Hence, the induced current on each wire equals

$$\hat{I}_1(z) = -\hat{I}_2(z) = \frac{jIh(Y_{11} - Y_{12})}{2\pi\omega\epsilon_0 d} e^{-j\gamma_d z} = \frac{-Ih}{d \ln(d/a)} e^{-j\gamma_d z}. \quad (\text{A.7})$$

At large values of z, the magnetic field between the wires (at (x,y,z) = (0,0,z)) is

$$\hat{H}_y(0,0,z) = \frac{-2Ih}{\pi d^2 \ln(d/a)} e^{-j\gamma_d z} \quad (\text{A.8})$$

$$\gamma_d = k_0 \sqrt{1 - (Y_{11} - Y_{12})Z_{iw} / k_0^2} \quad (\text{A.9})$$

This compares to the magnetic field from the dipole without wires which is

$$\hat{H}_y(0,0,z) = \frac{Ihk_0^2}{4\pi} \left[\frac{j}{k_0 z} + \frac{1}{(k_0 z)^2} \right] \quad (\text{A.10})$$

Hence, (for $k_0 z \ll 1$ as is typical for 50/60 Hz) the ratio of the “guided” field to the free space field is

$$\hat{H}_y(\mathbf{0}, \mathbf{0}, z) = \frac{-8z^2}{d^2 \ln(d/a)} e^{-j\gamma_d z} \quad (\text{A.11})$$

Since $|\text{Im}(\gamma_p z)| \ll 1$, it is clear that for even moderate distances from the source, the “guided” field is significantly larger than the “free space” field.

Appendix B

Round Wire Impedance (Skin Effect)

Consider a solid round wire of radius “a” and conductivity σ_w as shown in Fig. B.1.

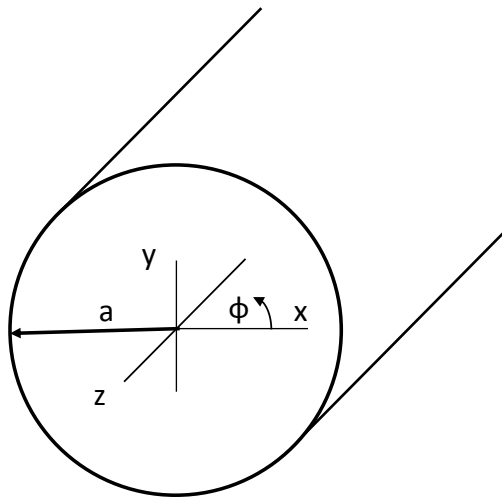


Fig. B.1. Solid Round conductor of radius a and conductivity σ_w .

The goal of this section is to determine the distribution of current flowing along z throughout the cross section of the conductor. The starting point will be Maxwell's equations in time harmonic form (with $J = \sigma_w E$) or

$$\nabla_x \bar{H} = j\omega\epsilon \bar{E} + \sigma \bar{E} = j\omega\epsilon \left(1 - j \frac{\sigma_w}{\omega\epsilon}\right) \bar{E} \quad (\text{B.1})$$

$$\nabla_x \bar{E} = -j\omega\mu \bar{H} \quad (\text{B.2})$$

In most metals σ is on the order of 10^7 S/m and hence, unless the radian frequency is on the order of 10^{14} Rad/s, $\frac{\sigma_w}{\omega\epsilon} \gg 1$ and Maxwell's equations reduce to

$$\nabla_x \bar{H} = \bar{J} \quad (\text{B.3})$$

$$\nabla_x \bar{J} = -j\omega\mu\sigma_w \bar{H} \quad (\text{B.4})$$

where the substitution $\mathbf{J} = \sigma\mathbf{E}$ has been made because the ultimate goal is to find the distribution of current. Taking the curl of (B.4), substituting (B.3) and using the vector identity

$$\nabla_x \nabla_x \bar{J} = \nabla(\nabla \cdot \bar{J}) - \nabla^2 \bar{J} \quad (\text{B.5})$$

where ∇^2 is the Laplacian operator results in

$$\nabla^2 \bar{J} = j\omega\mu\sigma_w \bar{J} \quad (\text{B.6})$$

If it is assumed that σ is constant throughout the conductor. Now, if it is assumed that the only component of current is in the z direction, then in cylindrical coordinates,

$$\nabla^2 \bar{J} = \frac{1}{\rho} \frac{\partial}{\partial \rho} \left(\rho \frac{\partial J_z}{\partial \rho} \right) + \frac{1}{\rho^2} \frac{\partial^2 J_z}{\partial \phi^2} + \frac{\partial^2 J_z}{\partial z^2} = j\omega\mu\sigma_w J_z \quad (\text{B.7})$$

The first simplification that can be made is that

$$\frac{\partial J_z}{\partial \phi} = 0 \quad (\text{B.8})$$

since it is assumed that the current distribution is independent of the angle ϕ . The remaining equation can be solved by a method called ‘‘Separation of Variables.’’ In this method, it is assumed that the unknown can be written as a product of a function of ρ only ($R(\rho)$) and a function of z only ($Z(z)$) so that

$$J_z(\rho, z) = R(\rho)Z(z) \quad (\text{B.9})$$

The justification for this assumption will come later. (B.7) can then be written as (after it has been divided by $J_z(\rho, \phi) = R(\rho)Z(z)$) as

$$\frac{1}{\rho R(\rho)} \frac{\partial}{\partial \rho} \left(\rho \frac{\partial R(\rho)}{\partial \rho} \right) - j\omega\mu\sigma_w + \frac{1}{Z(z)} \frac{\partial^2 Z(z)}{\partial z^2} = 0 \quad (\text{B.10})$$

Since the first two terms are a function of ρ only and the last a function of z only and the sum is a constant, each term must be a constant (a separation constant) that will be called here κ^2 . Given this,

$$\frac{1}{Z(z)} \frac{\partial^2 Z(z)}{\partial z^2} = \kappa^2 \quad (\text{B.11})$$

$$\frac{1}{\rho R(\rho)} \frac{\partial}{\partial \rho} \left(\rho \frac{\partial R(\rho)}{\partial \rho} \right) - j\omega\mu\sigma_w = -\kappa^2 \quad (\text{B.12})$$

The solution to the first equation is

$$Z(z) = A_f e^{-j\kappa z} + A_r e^{+j\kappa z} \quad (\text{B.13})$$

Since it will be show in Chapter 1 that currents that travel on power lines travel approximately as

$$e^{+/-jk_0 z} \quad (\text{B.14})$$

where $k_0 = \omega\sqrt{\mu_0\epsilon_0}$ and the fields inside the conductor must travel with the same factor, (B.12) can now be written

$$\frac{1}{\rho R(\rho)} \frac{\partial}{\partial \rho} \left(\rho \frac{\partial R(\rho)}{\partial \rho} \right) - j\omega\mu\sigma_w = -\omega^2 \mu_0 \epsilon_0 \cong 0 \quad (\text{B.15})$$

given the same assumption on frequency made between (B.1) and (B.3) (i.e., $\sigma_w / (\omega\epsilon_0) \gg 1$).

(B.15) can now be rewritten as

$$\begin{aligned} \frac{\partial}{\partial \rho} \left(\rho \frac{\partial R(\rho)}{\partial \rho} \right) - j\omega\mu\sigma_w \rho R(\rho) &= 0 \\ \rho \frac{\partial^2}{\partial \rho^2} R(\rho) + \frac{\partial R(\rho)}{\partial \rho} - j\omega\mu\sigma_w \rho R(\rho) &= 0 \\ \frac{\partial^2}{\partial \rho^2} R(\rho) + \frac{1}{\rho} \frac{\partial R(\rho)}{\partial \rho} - j\omega\mu\sigma_w R(\rho) &= 0 \end{aligned} \quad (\text{B.15})$$

This differential equation is known as Bessel's equation and is known to have a solution of the form

$$R(\rho) = AJ_0(\sqrt{-j\omega\mu\sigma_w}\rho) + BY_0(\sqrt{-j\omega\mu\sigma_w}\rho) \quad (\text{B.16})$$

where $J_0(x)$ is known as the Bessel function of first kind and order 0 and $Y_0(x)$ is known as the Bessel function of second kind and order 0. Now, $Y_0(x)$ cannot be a part of a physical solution because it is known to have a

singularity at $x = 0$ and the current density does not have a singularity there. Thus, the constant $B = 0$ and

$$R(\rho) = AJ_0(\sqrt{-j\omega\mu\sigma_w}\rho). \quad (\text{B.17})$$

The total current flowing on the conductor (I) is equal to

$$\begin{aligned} I &= \int_0^{2\pi a} \int_0^a J_z \rho d\rho d\phi = 2\pi A \int_0^a J_0(\sqrt{-j\omega\mu\sigma_w}\rho) d\rho \\ &= \frac{2\pi A}{v^2} \int_0^a J_0(k_w \rho)(k_w \rho) d(k_w \rho) \end{aligned} \quad (\text{B.18})$$

where $k_w = \sqrt{-j\omega\mu\sigma_w}$.

The last integral in (B.18) can be evaluated as follows

$$\begin{aligned} I &= \frac{2\pi A}{k_w^2} \int_0^a J_0(k_w \rho)(k_w \rho) d(k_w \rho) \\ &= \frac{2\pi A}{k_w^2} \int_0^{ka} J_0(x)(x) dx = \frac{2\pi A}{k_w^2} k_w a J_1(k_w a) \end{aligned} \quad (\text{B.19})$$

where $J_1(x)$ is known as the Bessel function of first kind and order 1. The current $I(z)$ can then be written as

$$I(z) = Ie^{+/-jk_0z} \quad (\text{B.20})$$

Using this result, it is possible to write the constant A in terms of the current and thus

$$R(\rho) = \frac{k_w I J_0(k_w \rho)}{2\pi a J_1(k_w a)} \quad (\text{B.21})$$

Hence,

$$J_z(\rho, z) = \frac{k_w I J_0(k_w \rho)}{2\pi a J_1(k_w a)} e^{+/-jk_0z} \quad (\text{B.22})$$

Given this result, the surface impedance Z_{iw} can be written as

$$Z_{iw}(\omega) = \frac{E_z(a, z)}{I(z)} = \frac{J_z(a, z)}{\sigma_w I(z)} = \frac{k_w}{2\pi\sigma_w a} \frac{J_0(k_w a)}{J_1(k_w a)} \quad (\text{B.23})$$

Where $k_w = \sqrt{-j\omega\mu\sigma_w}$. This can also be written in terms of the dc resistance per unit length of the wire as

$$Z_{iw}(\omega) = R_{dc} \left(\frac{k_w a}{2} \right) \frac{J_0(k_w a)}{J_1(k_w a)} \quad (\text{B.24})$$

where

$$R_{dc} = \frac{1}{\sigma_w \pi a^2} \quad (\text{B.25})$$

Appendix C

Essentials of Complex Variable Theory

It is appropriate here to provide some background about complex variables since relatively few of the readers of the text will have had a course in this area.

Consider the xy plane shown in Fig. C.1 below

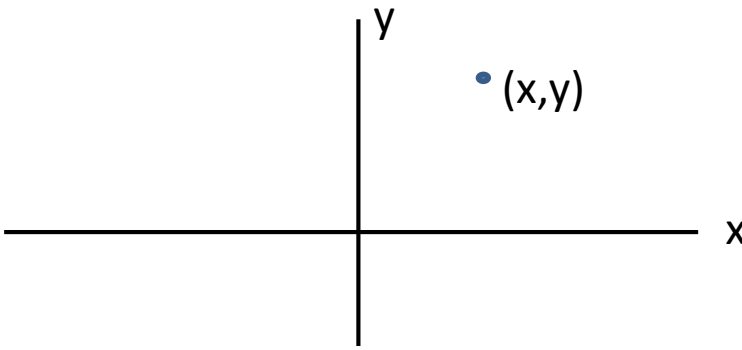


Fig. C.1 – the xy plane

It is possible to write an expression for a complex valued function of x and y as

$$w(x, y) = u(x, y) + jv(x, y) \quad (\text{C.1})$$

A point in the (x,y) plane can be described as

$$z = x + jy \quad (\text{C.2})$$

where z is a “complex variable.” (C.2) describes the values of x and y and can be used to find the value of the function $w(x,y)$. To carry out this process in general, the “complex conjugate” of z (i.e., \bar{z}) can be defined as

$$\bar{z} = x - jy \quad (\text{C.3})$$

so that $x = \frac{1}{2}(z + \bar{z})$ and $y = \frac{-j}{2}(z - \bar{z})$.

Thus, in general

$$w(x, y) = u\left(\frac{z + \bar{z}}{2}, -j\frac{z - \bar{z}}{2}\right) + jv\left(\frac{z + \bar{z}}{2}, -j\frac{z - \bar{z}}{2}\right) \quad (\text{C.4})$$

Now, it is clear that certain functions $w(x,y)$ can be written as a function of z alone (i.e., if x and y combine in just the right way). But that other functions $w(x,y)$ cannot be written in this way. For example,

$$w(x, y) = (x^2 - y^2) + j2xy = (x + jy)^2 = z^2 \quad (C.5)$$

$$w(x, y) = \frac{x}{x^2 + y^2} - j \frac{y}{x^2 + y^2} = \frac{1}{x + jy} = \frac{1}{z} \quad (C.6)$$

However,

$$\begin{aligned} w(x, y) &= 4x + j2y = 4(z + \bar{z})/2 + j2(-j(z - \bar{z})/2) \\ &= 2(z + \bar{z}) + 2(z - \bar{z}) = 3z + \bar{z} \end{aligned} \quad (C.7)$$

Functions which can be written as a function of z alone will be called analytic functions and will be shown to have the property that the methods of differential calculus for functions of a single real variable can be used. Prior to showing this, a few definitions will be given.

Continuity

A function f is continuous at a point z_0 if all of these following conditions are met.

$$\lim_{z \rightarrow z_0} f(z) \text{ exists} \quad (C.8)$$

$$f(z_0) \text{ exists} \quad (C.9)$$

$$\lim_{z \rightarrow z_0} f(z) = f(z_0) \quad (C.10)$$

A function of a complex variable is said to be continuous in a region R if it is continuous at every point in R . It should be noted that functions of both z and its complex conjugate may be continuous. For example, $f(z, \bar{z}) = \bar{z}$ is a continuous function.

Boundedness

If $f(z)$ is continuous in a region R which is closed and bounded, then f is "bounded" and $|f(z)|$ reaches a maximum value somewhere in R . To be precise, there exists a positive number M such that $|f(z)| \leq M$ for all z in R .

Differentiability

Let f be a function whose domain of definition contains a neighborhood of a point z_0 . The derivative of f at z_0 is written as $f'(z_0)$ and defined by

$$f'(z_0) = \lim_{z \rightarrow z_0} \frac{f(z) - f(z_0)}{z - z_0} = \lim_{\Delta z \rightarrow 0} \frac{f(z + \Delta z) - f(z_0)}{\Delta z} \quad (\text{C.11})$$

where $\Delta z = z - z_0$

If, further $\Delta w = f(z + \Delta z) - f(z)$, then

$$f'(z_0) = \frac{dw(z_0)}{dz} = \lim_{\Delta z \rightarrow 0} \frac{\Delta w}{\Delta z} \quad (\text{C.12})$$

Some examples will now be considered in order to solidify an understanding of the difference between analytic and non-analytic functions. Consider $f(z) = z^2$.

$$\lim_{\Delta z \rightarrow 0} \frac{\Delta w}{\Delta z} = \lim_{\Delta z \rightarrow 0} \frac{(z + \Delta z)^2 - z^2}{\Delta z} = \lim_{\Delta z \rightarrow 0} (2z + \Delta z) = 2z \quad (\text{C.13})$$

Hence, $f'(z) = 2z$.

Next consider, $f(z, \bar{z}) = z\bar{z} = |z|^2$

$$\lim_{\Delta z \rightarrow 0} \frac{\Delta w}{\Delta z} = \lim_{\Delta z \rightarrow 0} \frac{(z + \Delta z)(\bar{z} + \Delta \bar{z}) - z\bar{z}}{\Delta z} = \lim_{\Delta z \rightarrow 0} \left(\bar{z} + \Delta \bar{z} + z \frac{\Delta \bar{z}}{\Delta z} \right) \quad (\text{C.14})$$

If $z = 0$, $\frac{\Delta w}{\Delta z} = \Delta \bar{z}$, and $\frac{dw}{dz} = 0$.

If, however, $z \neq 0$, then the limit depends upon how Δz goes to zero. For example, if Δz approaches 0 through real values of z (i.e., $\Delta z = \Delta x$) then $\Delta \bar{z} = \Delta z$ and

$$\lim_{\Delta z \rightarrow 0} \left(\bar{z} + \Delta \bar{z} + z \frac{\Delta \bar{z}}{\Delta z} \right) = \bar{z} + z \quad (\text{C.15})$$

If Δz approaches 0 through pure imaginary values of z (i.e., $\Delta z = \Delta y$) then $\Delta \bar{z} = -\Delta z$ and

$$\lim_{\Delta z \rightarrow 0} \left(\bar{z} + \Delta \bar{z} + z \frac{\Delta \bar{z}}{\Delta z} \right) = \bar{z} - z \quad (\text{C.16})$$

Now since by definition any limit is unique, it is clear here that the limit does not exist. Consequently, $f'(z)$ exists only at the origin $z = 0$.

The real and imaginary parts of a complex function may have continuous partial derivatives of all orders and yet the function may not be differentiable.

It is, however, true that the existence of a derivative of a function at a point implies the continuity of the function there.

Analytic functions

If a function is single valued and differentiable at every point of a domain D , save possibly for a finite number of exceptional points, it can be said that it is analytic in D . The exceptional points are called the singular points or singularities of the function. If no point of D is a singularity, then it can be said that the function is regular in D . An entire function is one which is regular at each point in the entire complex plane. Consider next some specific examples of functions to examine their properties.

Polynomials

Consider the function z^n where n is an integer. This function can be shown to be regular in every bounded domain. It can be further shown that if $f(z)$ and $g(z)$ are regular, then $f(z) + g(z)$ is regular in the same domain. Thus any sum of terms z raised to an integer is a regular function in any bounded domain.

Thus, any polynomial is a regular function in any bounded domain.

For example,

$$f(z) = a(z - z_1)(z - z_2)(z - z_3) \cdots \text{ where the } z_i \text{ are constants is regular}$$

The function z^{-n} (where n is an integer) can be shown to be analytic in every bounded domain but has one singularity at the origin. This singularity is called a pole of order n .

The quotient of two polynomials is a rational function. A rational function is an analytic function with singularities at the zeros of the denominator. These singularities are called poles.

Power Series Representation

Consider the series $f(z) = \sum_{n=1}^{\infty} a_n z^n$.

This series converges absolutely when $\lim_{n \rightarrow \infty} |a_n z^n|^{1/n} < 1$ and diverges when $\lim_{n \rightarrow \infty} |a_n z^n|^{1/n} > 1$ by Cauchy's n th root test. Thus, if $\lim_{n \rightarrow \infty} |a_n|^{1/n} = R$, then the series is convergent when $|z| < R$ and divergent when $|z| > R$. R is called the radius of convergence.

It can be shown that the sum of a series with a non-zero radius of convergence is an analytic function regular within this circle of convergence. The converse can also be shown: that an analytic function regular in the neighborhood of a point z_0 can be expanded in a power series.

Cauchy-Riemann Equations

Consider a function

$$f(z) = u(x, y) + jv(x, y) \quad (\text{C.17})$$

It can be shown that if a function is analytic, then

$$\frac{\partial u}{\partial x} = \frac{\partial v}{\partial y} \quad (\text{C.18})$$

and

$$\frac{\partial u}{\partial y} = -\frac{\partial v}{\partial x} \quad (\text{C.19})$$

These are the **Cauchy-Reimann equations**.

Thus, for a function to be analytic, it is necessary that the four partial derivatives exist and that they satisfy the Cauchy-Riemann equations. For sufficient conditions, it can be said that

$f(z)$ is analytic, regular in D , if the function is single valued and if the four partial derivatives exist, are continuous and satisfy the Cauchy-Reimann equations at each point in D .

If the partial derivatives of (C.18) and (C.19) are taken with respect to x and y , respectively then added together, the result is

$$\frac{\partial^2 u}{\partial x^2} + \frac{\partial^2 u}{\partial y^2} = 0 \quad \text{or} \quad \nabla^2 u = 0 \quad (\text{C.20})$$

$$\frac{\partial^2 v}{\partial x^2} + \frac{\partial^2 v}{\partial y^2} = 0 \quad \text{or} \quad \nabla^2 v = 0 \quad (\text{C.21})$$

Thus, both the real and the imaginary parts of a regular function satisfy Laplace's equation. This property will be used again later.

One consequence of (C.20) and (C.21) is that a closed line integral of an analytic function around any path in the complex plane that does not enclose a singularity is zero. Hence

$$\oint_C f(z) = 0 \quad (\text{C.22})$$

There is another method for determining that a function is analytic. Consider the function

$$w(x, y) = u(x, y) + jv(x, y)$$

In terms of z and \bar{z} , w can be written (as earlier)

$$w(x, y) = u((z + \bar{z})/2, -j(z - \bar{z})/2) + jv((z + \bar{z})/2, -j(z - \bar{z})/2) \quad (\text{C.23})$$

It will now be shown that, if w is analytic, then w will not depend on \bar{z} .

To see this, the derivative $\frac{\partial w}{\partial \bar{z}}$ will be computed.

$$\begin{aligned} \frac{\partial w}{\partial \bar{z}} &= \frac{\partial(u + jv)}{\partial \bar{z}} = \frac{\partial u}{\partial \bar{z}} + j \frac{\partial v}{\partial \bar{z}} \\ &= \left(\frac{\partial u}{\partial x} \frac{\partial x}{\partial \bar{z}} + \frac{\partial u}{\partial y} \frac{\partial y}{\partial \bar{z}} \right) + j \left(\frac{\partial v}{\partial x} \frac{\partial x}{\partial \bar{z}} + \frac{\partial v}{\partial y} \frac{\partial y}{\partial \bar{z}} \right) \end{aligned} \quad (\text{C.24})$$

But, from the definitions

$$\frac{\partial x}{\partial \bar{z}} = \frac{1}{2} \quad \text{and} \quad \frac{\partial y}{\partial \bar{z}} = \frac{j}{2}$$

Thus,

$$\begin{aligned} \frac{\partial w}{\partial \bar{z}} &= \frac{1}{2} \left(\frac{\partial u}{\partial x} + \frac{\partial u}{\partial y} \right) + \frac{j}{2} \left(\frac{\partial v}{\partial x} + \frac{\partial v}{\partial y} \right) \\ &= \frac{1}{2} \left(\frac{\partial u}{\partial x} - \frac{\partial v}{\partial y} \right) + \frac{j}{2} \left(\frac{\partial u}{\partial y} + \frac{\partial v}{\partial x} \right) \\ &= 0 \end{aligned} \quad (\text{C.25})$$

since u and v satisfy the Cauchy Riemann equations because w was defined as analytic. Thus w must be a function of z alone.

The way that analytic functions will be used in this context is to begin with a function $f(x)$ defined on the real axis. x will then be replaced with z to extend the definition of $f(x)$ to the complex plane. The resulting function is analytic because it is a function of z alone. Strictly speaking this process has pitfalls that can be discussed in the context of analytic continuation, but the process works in nearly all cases.

Consider next some specific examples.

The exponential function

$$\exp(z) = 1 + \sum_{n=1}^{\infty} \frac{z^n}{n!} \quad (\text{C.26})$$

It can be shown that the radius of convergence of this series is infinite. Hence, the exponential function is an analytic function in any bounded domain of the z plane.

Trigonometric and Hyperbolic functions

Since trigonometric and hyperbolic functions are simply defined as sums of exponential functions, the same properties can be attributed to them as the above. Note also that

- $\sin(jz) = j \sinh(z)$
- $\sinh(jz) = j \sin(z)$
- $\cos(jz) = \cosh(z)$
- $\cosh(jz) = \cos(z)$

Next, the zeros of $\sin(z)$ and $\cos(z)$ will be examined.

$$\sin(z) = \sin(x+jy) = \sin(x) \cosh(y) + j \cos(x) \sinh(y) \quad (\text{C.27})$$

(C.27) vanishes if and only if

$$\sin(x) \cosh(y) = 0 \quad \text{and} \quad \cos(x) \sinh(y) = 0$$

Thus, the zeros of $\sin(z)$ are identical with the zeros of $\sin(x)$ and occur at $z = n\pi$.

The logarithmic function

If x is real and positive, $e^u = x$ has one solution which is called $u = \ln(x)$. But, the situation is more complicated if x is replaced with the complex variable $z = x + jy$. Then, u must also be replaced by the complex variable $w = u + jv$ resulting in

$$e^{(u+jv)} = e^u e^{jv} = z = |z| e^{j \arg(z)} \quad (\text{C.28})$$

where $\arg(z)$ is the angle from the $+x$ axis to the point z in the complex plane. To get equality, both magnitude and phase are equated so that

$$e^u = |z| \quad \text{and} \quad u = \ln(|z|) \quad \text{as before}$$

but $v = \arg(z)$, therefore

$$w = \log|z| + j \arg(z) \quad (\text{C.29})$$

There is a serious difficulty with the $\arg(z)$ function. This function must either be single valued and hence discontinuous across some angle θ (e.g., if

this line of discontinuity is $\theta = 0$, then the range of $\arg(z)$ is $0 \rightarrow 2\pi$ and it is discontinuous across the $\theta = 0$ line) or it is a multivalued function. In the latter case θ continues to increase as θ passes by 2π . In this latter case, $\arg(z)$ may take on values $\theta + 2n\pi$ where n is any integer.

The only way for w to be a single valued function is to define limits on θ and to recognize that w will be discontinuous (and hence non-analytic) along the constant θ boundary line. Each possible range of θ 's which result in single valuedness is called a branch or Riemann sheet. The line of discontinuity is called a branch cut.

An example branch cut for the log function is shown in Fig. C.2.

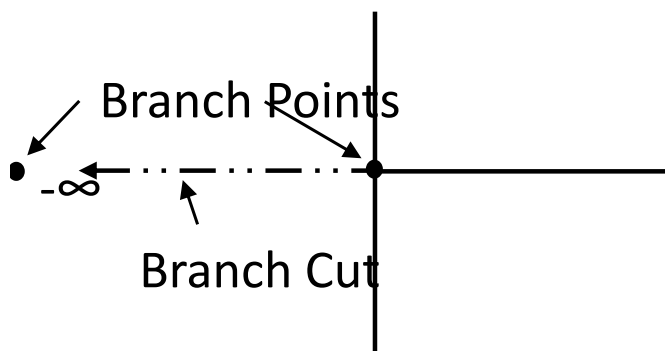


Fig. C.2. Possible branch cut and branch points for the logarithmic function.

In this case the definition of the branch is $-\pi < \theta < \pi$.

The branch cut is terminated at points called branch points which always occur in pairs. For the log function (and branch shown in Fig. C.2), the branch points occur at $z = 0$ and $z = -\infty$.

The final result is that if D is any bounded domain in the cut plane so that no point of the cut is in D (for continuity) $\log(z)$ is single valued and continuous (and regular) in D . It also has the derivative $1/z$.

The function z^α

Suppose $\alpha = p$ is an integer. Consider

$$\exp(p \log(z)) = \exp(\log(z^p)) = z^p \tag{C.30}$$

Recall that $\exp(z)$ is a periodic function since

$$\exp(z + j2n\pi) = \exp(z) \tag{C.31}$$

Thus, if p is an integer

$$\begin{aligned}
\exp(p \log(z)) &= \exp(p \log|z| + jp \arg(z) + j2\pi pn) \\
&= \exp(p \log|z| + jp \arg(z)) \\
&= |z|^p e^{jp \arg(z)}
\end{aligned} \tag{C.32}$$

where $\arg(z)$ is interpreted as being restricted to a specified branch (e.g., $-\pi < \theta < \pi$). Next consider

$$\begin{aligned}
\exp\left(\frac{p}{q} \log(z)\right) &= \exp\left(\frac{p}{q} \log|z| + j \frac{p}{q} \arg(z) + j2\pi \frac{p}{q} n\right) \\
&= |z|^{\frac{p}{q}} e^{j2pn \arg(z)/q}
\end{aligned} \tag{C.33}$$

There are several possible values of the function

$$|z|^{\frac{p}{q}} e^{j2k\pi/q} \tag{C.34}$$

for values $k = 0, 1, \dots, q-1$.

The value chosen depends upon which branch is specified. The branch chosen is usually called the principal branch and defines the meaning of $z^{p/q}$.

Example: $z^{1/2}$ has branch points at 0 and $-\infty$ if the branch cut is placed on the negative real axis. In this case, $z^{1/2}$ means

$$|z|^{1/2} e^{j \arg(z)/2} \tag{C.35}$$

where $-\pi < \arg(z) < \pi$.

Further properties of branch points and cuts

1. Branch points always occur in pairs and branch lines (i.e., cuts) join the branch points
2. To show the branch point at infinity for the function $f(z) = z^{1/2}$, use the transformation $z = 1/\xi$. Thus $z^{1/2}$ becomes $\xi^{-1/2}$ which is a multivalued function of ξ and has a branch point at $\xi = 0$ (or $z \rightarrow \infty$)
3. Branch cuts are not unique. They may be chosen in any convenient fashion. For example, for $z^{1/2}$, either the branch cut in Fig. C.3a or Fig. C.3b can be used.

Consider the example,

$$f(z) = (z^2 - 1)^{1/2} \tag{C.36}$$

This function can be shown to have branch points at $z = \pm 1$. Let $z = \pm 1 \mp \epsilon e^{j\theta}$. Then

$$\begin{aligned}
 f(z) &= (1 + \epsilon e^{j\theta} + \epsilon^2 e^{j2\theta} - 1)^{1/2} \\
 &\cong (\epsilon e^{j\theta})^{1/2} = \sqrt{\epsilon} e^{j\theta/2}
 \end{aligned}
 \tag{C.37}$$

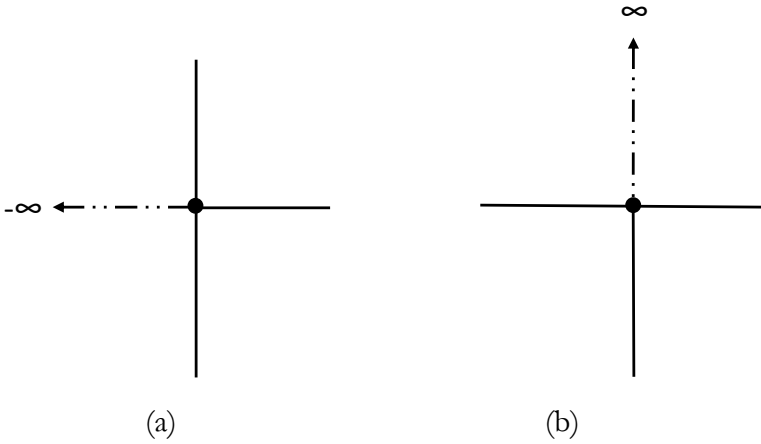


Fig. C.3 Possible branch cuts for $z^{1/2}$ a) horizontal to $-\infty$, b) vertical to ∞

(C.36) is multivalued no matter how small the value of ϵ . Note that there is no branch point at ∞ since if the transformation $z = 1/\xi$ is used,

$$\left(\frac{1}{\xi^2} - 1 \right)^{1/2} = \frac{(1 - \xi^2)^{1/2}}{\xi} \rightarrow \frac{1}{\xi} \text{ as } \xi \rightarrow 0 \text{ (i.e. as } z \rightarrow \infty)
 \tag{C.38}$$

This represents a simple pole behavior as $z \rightarrow \infty$. As mentioned above, the branch cuts are not unique and could be elected in a number of different ways. Two examples are shown in Fig. C.4 below.

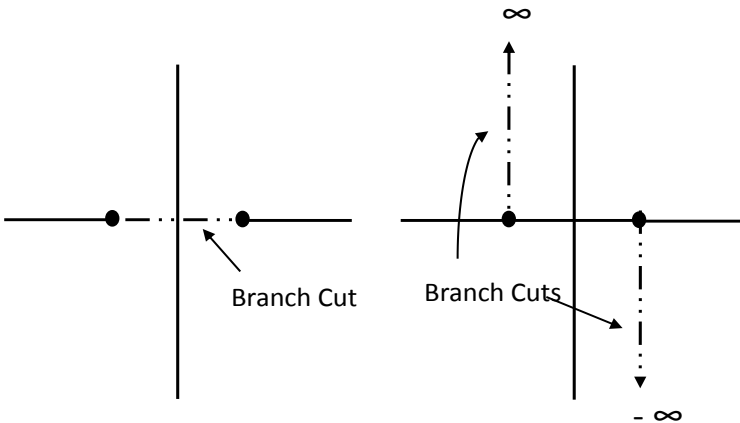


Fig. C.4 Two possible choices for branch cuts for the function $(z^2-1)^{1/2}$

Note that the fact that the branch cuts are arbitrary does not imply that there are no good reasons to select branch cuts in a certain way. For example, one way of selecting branch cuts may lead to a simpler result or another way might lead one that is easier to interpret physically.

Residue Theory for Calculating Integrals

Often in work related to transmission lines, integrals will appear that result from performing an inverse Fourier transform. In some cases, these can be solved easily by residue theory. An example is the one shown in (C.39). The denominator of the integrand contains a pair of zeros at $\pm \gamma_p$ which represent simple poles of the integrand. The numerator of the integrand is assumed to be regular (and hence to have no singularities in the plane except possibly at infinity).

$$I(z) = \int_{-\infty}^{\infty} \left(\frac{f(\gamma)}{(\gamma + \gamma_p)(\gamma - \gamma_p)} \right) e^{-j\gamma z} d\gamma \quad (C.39)$$

In this case the pole is chosen to have its imaginary part less than or equal to 0 (i.e., $\text{Im}(\gamma_p) = \text{Im}(\beta_p - j\alpha_p) \leq 0$ or $\text{Re}(\alpha_p) \geq 0$). Note that the opposite selection will lead eventually to an identical result. Since the integrand is analytic everywhere except at $\pm \gamma_p$, both its real and imaginary parts satisfy Laplace's equations according to (C.20) and (C.21). One consequence of this (as illustrated in (C.22)) is that any closed line integral that does not enclose singular points is zero. Hence,

$$\oint_C \left(\frac{f(\gamma)}{(\gamma + \gamma_p)(\gamma - \gamma_p)} \right) e^{-j\gamma z} d\gamma = 0 \quad (C.40)$$

for any contour C that does not enclose the singular points at $\pm \gamma_p$. Consider the contour $C = C_o$ (the original contour of integration) + $C_{\infty 2}$ + C_{b2} + C_p + C_{b1} + $C_{\infty 1}$ where the entire contour is defined in a clockwise direction. Since this contour does not enclose the pole at γ_p , the integral (C.37) is equal to zero and

$$\begin{aligned} I(z) &= \int_{C_o} \left(\frac{f(\gamma)}{(\gamma + \gamma_p)(\gamma - \gamma_p)} \right) e^{-j\gamma z} d\gamma \\ &= \int_{C_{\infty 1} + C_{b1} + C_p + C_{b2} + C_{\infty 2}} \left(\frac{f(\gamma)}{(\gamma + \gamma_p)(\gamma - \gamma_p)} \right) e^{-j\gamma z} d\gamma \end{aligned} \quad (C.41)$$

Note that the contour $C_{\infty 1} + C_{b1} + C_p + C_{b2} + C_{\infty 2}$ is now defined in the counter clockwise direction and accounted for by a change in sign of the

integral. If $z > 0$, then $e^{-j\gamma z} = e^{-j\gamma_r z} e^{\gamma_i z}$ (where $\gamma = \gamma_r + j\gamma_i$) tends to zero exponentially for values of γ in the lower half of the complex γ plane (i.e., $\gamma_i \leq 0$) and hence the integrations $C_{\infty 1}$ and $C_{\infty 2}$ are zero. In addition, since the integrations C_{b1} and C_{b2} are along the same line but in opposite directions their contributions cancel. The only remaining contribution is the integration C_p around the pole at γ_p (i.e. the residue due to the simple pole at γ_p).

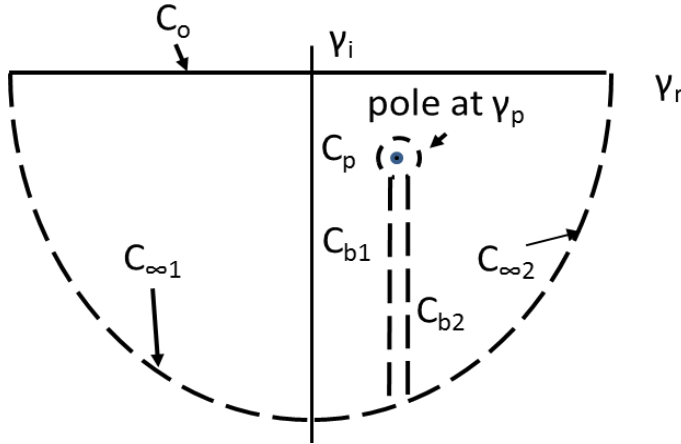


Fig. C.5 Deformation of contour leading to a residue integration

Therefore,

$$I(z) = \int_{C_p} \left(\frac{f(\gamma)}{(\gamma + \gamma_p)(\gamma - \gamma_p)} \right) e^{-j\gamma z} d\gamma \quad (C.42)$$

which is relatively simple to evaluate as follows.

The contribution of the pole can be evaluated by using the transformation

$$\gamma \rightarrow \gamma_p + \varepsilon e^{j\theta}, \quad \varepsilon \ll |\gamma_p|$$

where $d\gamma = j e^{j\theta} \varepsilon d\theta$.

The integral around the pole (i.e., the residue) then becomes

$$I(z) = f(\gamma_p) \int_{-\pi/2}^{3\pi/2} \frac{j \varepsilon e^{j\theta} e^{-j\gamma_p z}}{\varepsilon e^{j\theta} (2\gamma_p)} d\theta = \frac{f(\gamma_p) 2\pi j e^{-j\gamma_p z}}{2\gamma_p} = \frac{j\pi f(\gamma_p)}{\gamma_p} e^{-j\gamma_p z} \quad (C.43)$$

Note that if $\text{Im}(\gamma_p) \geq 0$, then the pole that is located in the lower half of the complex plane occurs at $-\gamma_p$, the transformation used is

$$\gamma \rightarrow -\gamma_p + \varepsilon e^{j\theta}, \quad \varepsilon \ll |\gamma_p|$$

and the residue becomes

$$\begin{aligned}
 I(z) &= f(-\gamma_p) \int_{-\pi/2}^{3\pi/2} \frac{j\epsilon e^{j\theta} e^{-j\gamma_p z}}{\epsilon e^{j\theta} (-2\gamma_p)} d\theta \\
 &= \frac{-f(-\gamma_p) 2\pi j e^{-j\gamma_p z}}{2\gamma_p} = \frac{-j\pi f(-\gamma_p)}{\gamma_p} e^{-j\gamma_p z}.
 \end{aligned} \tag{C.44}$$

Appendix D

Carson Integral and Series Derivation

D.1 Derivation of the Carson Integral

Problem Definition

The purpose of this Appendix is to review the methodology by which J. R. Carson in 1926 determined approximate expressions for the electric currents on and equivalent distributed parameters of an infinitely long horizontal conductor located above a single-layer linear, homogeneous, isotropic lossy (i.e., non-zero conductivity) earth. Here, the derivation will be repeated in SI units: the original was in cgs units. In addition, the arguments he used as well as the justification for the individual steps will be expanded to make the derivation easier to follow. The exact solution to this problem was discussed in great detail earlier in Chapter 4 and its geometry is shown again in Fig. D.1.1.

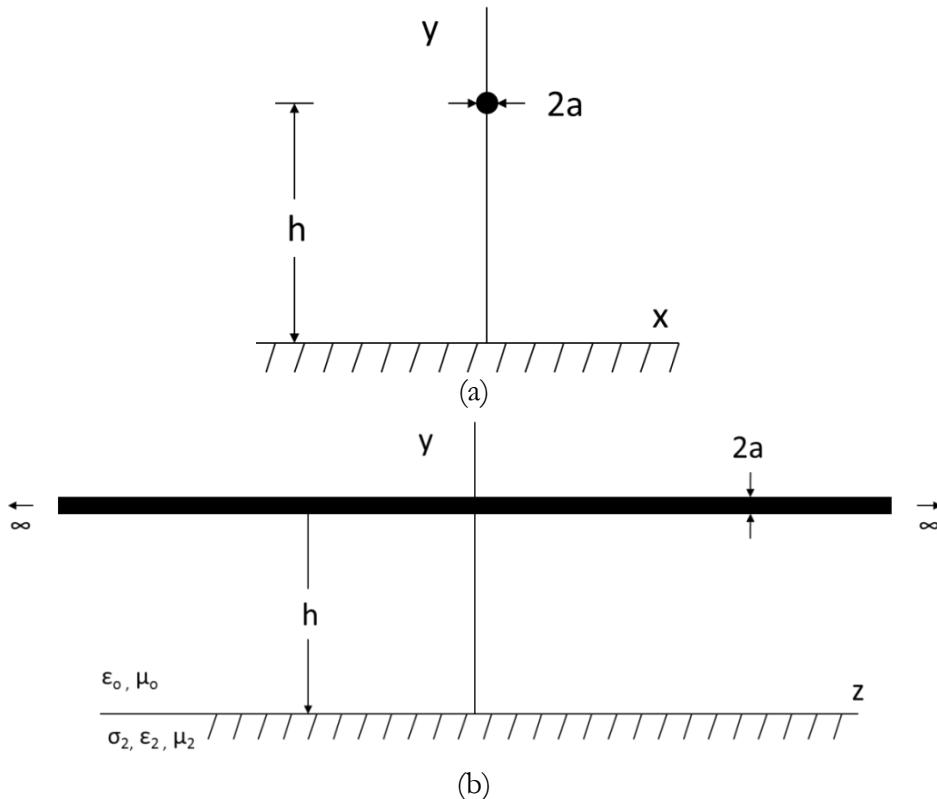


Fig. D.1.1 a) end view and b) side view of the infinitely long conductor of radius “ a ” and height “ h ” above a linear, homogeneous isotropic lossy earth.

As in Chapter 4, the z-oriented, horizontal conductor has radius a, and is located at a distance h above the earth but it is assumed here that it intersects the x axis at $x' = 0$ (Carson, 1926). The upper half space (i.e., $y > 0$) is free space and is characterized by permittivity and permeability $\epsilon_1 = \epsilon_0$ and $\mu_1 = \mu_0$ respectively while the lower half space (i.e., $y < 0$) is assumed to be a linear, homogeneous, isotropic lossy earth characterized by conductivity, permittivity and permeability $\sigma_2, \epsilon_2 = \epsilon_2 \epsilon_0$ and $\mu_2 = \mu_2 \mu_0$ respectively. ϵ_{2r} and μ_{2r} are the relative permittivity and permeability of the earth respectively. The conductor is assumed to be non-magnetic (i.e., $\mu_w = \mu_0$) and to have a conductivity σ_w . The dielectric constant of the conductor is not needed since it is only used to calculate displacement currents and (below optical frequencies) these can always be neglected in the conductor. It is assumed that all currents and fields vary in time as $\exp(j\omega t)$.

Problem Solution

The method by which the solution is found can be summarized as follows. First, a propagating current with unknown $\hat{I}(z) = \hat{I} \exp(-j\gamma z)$ is assumed to exist on the conductor. Given this, all fields have this same variation with z and hence can be suppressed; it can be added back by simply multiplying the current distribution or appropriate field expression by $\exp(-j\gamma z)$. As the derivation proceeds, a number of low frequency approximations will be made. These will be discussed in detail as they are made.

The first task addressed by Carson was to determine a general expression for the z-directed electric field in the earth (i.e., $y < 0$). To this end, the form of this expression was chosen to be one that is convenient for matching boundary conditions on a horizontal plane. This earth field must satisfy the homogeneous wave equation (3.3.4) because there are no primary sources in the earth (i.e., sources that do not depend on the electric and magnetic fields in the region such as earth currents that are equal to $\sigma_2 \hat{E}_z$).

Hence

$$\left(\frac{\partial^2}{\partial x^2} + \frac{\partial^2}{\partial y^2} - \gamma^2 + k_2^2 \right) \hat{E}_{2z}(x, y, \gamma) = 0, y < 0 \quad (\text{D.1.1})$$

where the subscript "2z" means the z component in the earth (i.e., region 2). As mentioned above, the field is assumed to vary as $\exp(-j\gamma z)$, hence the γ term in (D.1.1).

The spatial Fourier transform in the x direction and its inverse (i.e., $\tilde{Q}(\kappa)$ and $Q^{-1}(\kappa)$) used here are defined as

$$\tilde{Q}(f(x)) = \tilde{Q}(\kappa) = \int_{-\infty}^{\infty} q(x) e^{+j\kappa x} dx \quad (\text{D.1.2})$$

$$Q^{-1}(\tilde{Q}(\kappa)) = q(x) = \frac{1}{2\pi} \int_{-\infty}^{\infty} \tilde{Q}(\kappa) e^{-j\kappa x} d\kappa \quad (\text{D.1.3})$$

The symbol \sim indicates a spatial Fourier transform that is a function of the transform variable κ . If the spatial Fourier transform of (D.1.1) is taken, then (for all values of κ)

$$\left(-\kappa^2 + \frac{\partial^2}{\partial y^2} - \gamma^2 + k_2^2 \right) \hat{\tilde{E}}_{2z}(\kappa, y, \gamma) = 0, y < 0 \quad (\text{D.1.4})$$

It should be noted here that, given (D.1.2) and the even symmetry of the source and fields with respect to x , $\hat{\tilde{E}}_{2z}(\kappa, y, \gamma)$ must be an even function of κ . This property will be used later. The question now is, “Can a form be found for the y variation of the field that allows (D.1.4) to be satisfied for all values of κ ?” This can be done by assuming that

$$\hat{\tilde{E}}_{2z}(\kappa, y, \gamma) = \tilde{F}(\kappa) \exp(-j\xi(\kappa)y), y < 0 \quad (\text{D.1.5})$$

where $\text{Im}(\xi(\kappa)) > 0$ in order that the field decay as $y \rightarrow -\infty$ (i.e., the energy contained in the field is finite⁷⁴). In order that (D.1.4) be satisfied for all values of κ ,

$$(-\kappa^2 - \xi^2 - \gamma^2 + k_2^2) = 0 \quad (\text{D.1.6})$$

Hence,

$$\xi(\kappa) = \pm(-\kappa^2 - \gamma^2 + k_2^2)^{1/2} = 0 \text{ for all } \kappa \text{ where } \text{Im}(\xi(\kappa)) > 0. \quad (\text{D.1.7})$$

Given this result, the inverse Fourier transform of $\hat{\tilde{E}}_{2z}(\kappa, y, \gamma)$ can be taken using (D.1.3) and

$$\hat{E}_{2z}(x, y, \gamma) = \frac{1}{2\pi} \int_{-\infty}^{\infty} \tilde{F}(\kappa) \exp(-j\xi(\kappa)y) e^{-j\kappa x} d\kappa \quad (\text{D.1.8})$$

As noted earlier, this form has been selected because it is convenient to use for matching boundary conditions at the interface $y = 0$. Now

⁷⁴ The fact that this is the only possible answer can be determined by referring to the uniqueness theorem that is discussed in detail in Chapter 3. According to that theorem, a solution is unique if it satisfies Maxwell's equations, matches source conditions and satisfies certain boundary conditions at interfaces.

$$k_2 = \omega \sqrt{(\mu_0)(\epsilon_0 \epsilon_{r2} - j\sigma_2 / \omega)} \cong \exp(-j\pi/4) \sqrt{\omega \mu_0 \sigma_2} \gg k_0 \text{ if} \\ \omega \ll \sigma_2 / (\epsilon_0 \epsilon_{r2})$$

where it has been assumed that the earth is non-magnetic. In addition, given that values of γ will later be found to be relatively close to k_0 , γ can be ignored compared to k_2 in (D.1.6). Hence, after absorbing the factor j into $\xi(\kappa)$

$$\hat{E}_{2z}(x, y, \gamma) \cong \frac{1}{2\pi} \int_{-\infty}^{\infty} \tilde{F}(\kappa) \exp\left((\kappa^2 + j\omega\mu_0\sigma_2)^{1/2} y\right) e^{-j\kappa x} d\kappa \quad (D.1.9)$$

where

$$\text{Re}(\kappa^2 + j\omega\mu_0\sigma_2)^{1/2} > 0$$

If, in addition, it is recognized that $\xi(\kappa)$ and $\hat{E}_{2z}(\kappa, y, \gamma)$ are both even functions of κ , then the doubly infinite integral can be folded into an infinite integral as

$$\hat{E}_{2z}(x, y, \gamma) = \frac{1}{\pi} \int_0^{\infty} \tilde{F}(\kappa) \cos(\kappa x) \exp\left((\kappa^2 + j\omega\mu_0\sigma_2)^{1/2} y\right) d\kappa \quad (D.1.10)$$

Since $2\cos(\kappa x) = \exp(j\kappa x) + \exp(-j\kappa x)$, with the exception of the constants in front of the integral and inside the square root (a consequence of the different unit system used), (D.1.8) is identical to form of Equation (1) of Carson's 1926 paper (Carson, 1926).

At this point, Carson calculates the magnetic field in the earth. To this end, he used Faraday's law

$$\nabla_x \hat{E} + j\omega\mu_0 \hat{H} = 0, \quad (D.1.11)$$

where it has been assumed that the earth is non-magnetic. This equation is expressed in rectangular coordinates and it is assumed that the electric field components \hat{E}_x and \hat{E}_y are zero at low frequencies. The latter assumption can be made because as $\omega \rightarrow 0$ they reduced to the electrostatic fields of a line source above earth and the earth becomes a perfect conductor. Hence, these fields are zero in the earth. The same is not true for the axial component of the electric field because it is generated by the time varying magnetic field in the earth.

Hence,

$$-j\omega\mu_0\hat{H} = \nabla_x\hat{E} = \det \begin{vmatrix} \bar{a}_x & \bar{a}_y & \bar{a}_z \\ \frac{\partial}{\partial x} & \frac{\partial}{\partial y} & \frac{\partial}{\partial z} \\ 0 & 0 & E_z \end{vmatrix} = \bar{a}_x \frac{\partial}{\partial y} \hat{E}_z - \bar{a}_y \frac{\partial}{\partial x} \hat{E}_z \quad (\text{D.1.12})$$

Given this, the magnetic fields in the earth are

$$\hat{H}_{2x}(x, y, \gamma) = \frac{j}{\omega\mu_0\pi_0} \int_0^\infty (\kappa^2 + j\omega\mu_0\sigma_2)^{1/2} \tilde{F}(\kappa) \cos(\kappa x) \exp\left((\kappa^2 + j\omega\mu_0\sigma_2)^{1/2} y\right) d\kappa \quad (\text{D.1.13})$$

$$\hat{H}_{2y}(x, y, \gamma) = \frac{j}{\omega\mu_0\pi_0} \int_0^\infty \kappa \tilde{F}(\kappa) \sin(\kappa x) \exp\left((\kappa^2 + j\omega\mu_0\sigma_2)^{1/2} y\right) d\kappa \quad (\text{D.1.14})$$

Carson's next step was to calculate the magnetic fields in the free space medium $y > 0$. The first step in this process was to state the known magnetostatic solution for the magnetic fields of a z directed line source of current \hat{I} in free space at $(x,y) = (0,h)$. These are

$$\hat{H}_x^0 = -\frac{\hat{I}}{2\pi\sqrt{x^2 + (y-h)^2}} \sin\theta \quad (\text{D.1.15})$$

$$\hat{H}_y^0 = \frac{\hat{I}}{2\pi\sqrt{x^2 + (y-h)^2}} \cos\theta \quad (\text{D.1.16})$$

where θ is defined in Fig. D.2

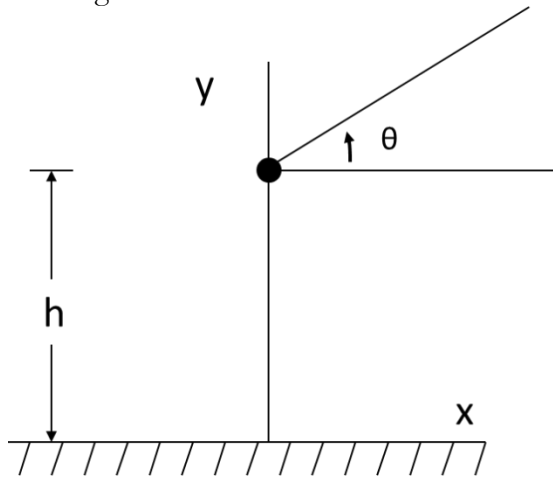


Fig. D.2 Definition of the angle θ (the z direction is out of the page)

The total magnetic field for $y > 0$ is then this source term plus terms due to induced currents in the earth. These can be expressed as

$$\hat{H}'_{1x} = \hat{H}'_x + \hat{H}'_{1x} \quad (\text{D.1.16})$$

$$\hat{H}'_{1y} = \hat{H}'_y + \hat{H}'_{1y} \quad (\text{D.1.17})$$

The magnetic field in the air due to distributed current sources in the earth is assumed to have the form

$$\hat{H}'_{1x}(x, y, \gamma) = \frac{1}{\pi} \int_0^{\infty} \tilde{\Phi}(\kappa) \cos(\kappa x) \exp(-\kappa y) d\kappa \quad y > 0 \quad (\text{D.1.18})$$

$$\hat{H}'_{1y}(x, y, \gamma) = -\frac{1}{\pi} \int_0^{\infty} \tilde{\Phi}(\kappa) \sin(\kappa x) \exp(-\kappa y) d\kappa \quad y > 0 \quad (\text{D.1.19})$$

Here, the sign of the exponent is negative in order that the field be properly behaved as $y \rightarrow \infty$. The relationship between the two field components is determined by the fact that the magnetic field in free space must satisfy the Maxwell equation

$$\nabla \cdot \hat{H} = 0 = \frac{\partial \hat{H}'_{1x}}{\partial x} + \frac{\partial \hat{H}'_{1y}}{\partial y} + \frac{\partial \hat{H}'_{1z}}{\partial z} \cong \frac{\partial \hat{H}'_{1x}}{\partial x} + \frac{\partial \hat{H}'_{1y}}{\partial y} = 0 \quad (\text{D.1.20})$$

Where \hat{H}'_{1z} is assumed to be zero given the nearly uniform z -directed source current.

Now, the source field can be expressed in a form that is useful for matching boundary conditions at $y = 0$. More specifically,

$$\hat{H}'_x(x, y, \gamma) = +\frac{I}{2\pi} \int_0^{\infty} \cos(\kappa x) \exp(\kappa(y-h)) d\kappa, \quad y < h \quad (\text{D.1.21})$$

$$\hat{H}'_y(x, y, \gamma) = +\frac{I}{2\pi} \int_0^{\infty} \sin(\kappa x) \exp(\kappa(y-h)) d\kappa, \quad y < h \quad (\text{D.1.22})$$

These can be proven by direct integration using the definitions of $\sin(\kappa x)$ and $\cos(\kappa x)$ in terms of exponentials and the result

$$\int_0^{\infty} \exp(+((y-h) \pm jx)\kappa) d\kappa = \frac{-1}{((y-h) \pm jx)}, \quad y < h \quad (\text{D.1.23})$$

Given these results, the boundary conditions (\bar{n} is a unit vector directed into region 1 from region 2.)

$$\bar{n}x(\bar{H}_1 - \bar{H}_2) = \bar{J}_s \quad (\text{D.1.24})$$

$$\bar{n} \bullet (\bar{B}_1 - \bar{B}_2) = 0 \quad (\text{D.1.25})$$

the facts that $J_s = 0$ on a dielectric-dielectric boundary and both materials are non-magnetic, both the x and y components of the magnetic field must be continuous across the boundary⁷⁵.

Hence (equating integrands)

$$\frac{+j}{\omega\mu_0} (\kappa^2 + j\omega\mu_0\sigma_2)^{1/2} \tilde{F}(\kappa) = \tilde{\Phi}(\kappa) + I \exp(-\kappa h) / 2 \quad (\text{D.1.26})$$

$$\frac{+j\kappa}{\omega\mu_0} \tilde{F}(\kappa) = -\tilde{\Phi}(\kappa) + I \exp(-\kappa h) / 2 \quad (\text{D.1.27})$$

If (D.1.26) and (D.1.27) are added, $\tilde{F}(\kappa)$ can easily be found as

$$\tilde{F}(\kappa) = \frac{-j\omega\mu_0 \hat{I} \exp(-\kappa h)}{(\kappa^2 + j\omega\mu_0\sigma_2)^{1/2} + \kappa} \quad (\text{D.1.28})$$

$\tilde{\Phi}(\kappa)$ can easily be found by using (D.1.28) in (D.1.27) as

$$\tilde{\Phi}(\kappa) = \frac{-\hat{I} \left((\kappa^2 + j\omega\mu_0\sigma_2)^{1/2} - \kappa \right) \exp(-\kappa h)}{2 \left((\kappa^2 + j\omega\mu_0\sigma_2)^{1/2} + \kappa \right)} \quad (\text{D.1.29})$$

Aside from constants due to the different unit system, (D.1.28) and (D.1.29) are equivalent to (11) and (12) of Carson (1926). Given this result, the electric field in the earth is

⁷⁵ In this case, the boundary conditions on normal and tangential magnetic field are applied. According to the uniqueness theorem, the boundary conditions on tangential electric and tangential magnetic fields should be applied. In this case, it can be shown that matching the normal magnetic field boundary condition is equivalent to matching the tangential electric field boundary condition.

(D.1.30)

$$\begin{aligned}\hat{E}_{2z}(x, y, \gamma) &= \\ &= \frac{-j\omega\mu_0\hat{I}}{\pi} \int_0^\infty \frac{\exp(-\kappa h)}{(\kappa^2 + j\omega\mu_0\sigma_2)^{1/2} + \kappa} \cos(\kappa x) \exp\left((\kappa^2 + j\omega\mu_0\sigma_2)^{1/2} y\right) d\kappa \\ &= \frac{-\hat{I}}{\pi\sigma_2} \int_0^\infty \left((\kappa^2 + j\omega\mu_0\sigma_2)^{1/2} - \kappa\right) \cos(\kappa x) \exp(-\kappa h) \exp\left((\kappa^2 + j\omega\mu_0\sigma_2)^{1/2} y\right) d\kappa\end{aligned}$$

after multiplying numerator and denominator by the factor $\left((\kappa^2 + j\omega\mu_0\sigma_2)^{1/2} - \kappa\right)$.

From Chapter 5 (5.3.40), the electric field in the earth is (for $x' = 0$ and $k_2^2 \cong j\omega\mu_0\sigma_2$) is

(D.1.31)

$$\tilde{G}_{ez}^2(x, y, h, \gamma) \cong \frac{-I}{\pi\sigma_2} \int_0^\infty (u - \kappa) \cos(\kappa x) \exp(-\kappa h) \exp\left((\kappa^2 + j\omega\mu_0\sigma_2)^{1/2} y\right) d\kappa$$

where $u = \sqrt{\kappa^2 - k_2^2} \cong \sqrt{\kappa^2 + j\omega\mu_0\sigma_2}$.

The equivalence of (D.1.29) and (D.1.30) is evident.

The axial electric field in the air can now be found as

$$E_{1z}(x, y, \gamma) = -j\omega A_{1z}(x, y) - \frac{\partial}{\partial z} V_1(x, y) \quad (D.1.32)$$

where $A_{1z}(x, y)$ and $V_1(x, y)$ are the vector and scalar potentials respectively.

Given this result, the axial electric field at a point (x, y) can be related to the field at a point directly below it on the surface at $y = 0$ as

$$\begin{aligned}E_{1z}(x, y, \gamma) - E_{1z}(x, 0, \gamma) \\ = -j\omega(A_{1z}(x, y) - A_{1z}(x, 0)) - \frac{\partial}{\partial z}(V_1(x, y) - V_1(x, 0))\end{aligned} \quad (D.1.33)$$

Now,

$$\begin{aligned}\hat{H}_x(x, y) &= \left(\frac{1}{\mu_0} \nabla_x \hat{A} \right)_x = \left(\frac{1}{\mu_0} \nabla_x \hat{A}_{1z} \right)_x \\ &= \left(\frac{1}{\mu_0} \det \begin{vmatrix} \bar{a}_x & \bar{a}_y & \bar{a}_z \\ \frac{\partial}{\partial x} & \frac{\partial}{\partial y} & \frac{\partial}{\partial z} \\ 0 & 0 & A_{1z} \end{vmatrix} \right)_x = \frac{1}{\mu_0} \frac{\partial}{\partial y} \hat{A}_{1z}(x, y)\end{aligned}\quad (D.1.34)$$

This result can be integrated along a vertical line to get

$$A_{1z}(x, y) - A_{1z}(x, 0) = \mu_0 \int_0^y \hat{H}_x(x, y) dy \quad (D.1.35)$$

Next, the scalar potential $V_1(x, y)$ is that of a line charge above a perfectly conducting earth. Hence, since by current continuity (3.1.14),

$$-j\gamma \hat{A} = -j\omega \rho_\ell$$

where ρ_ℓ is the line charge density (the exponential variation of current and charge has been suppressed).

With these results,

$$\begin{aligned}E_{1z}(x, y, \gamma) &= \\ E_{1z}(x, 0, \gamma) - j\omega \mu_0 \left(\int_0^y \hat{H}_x(x, y) dy \right) &+ j \frac{\gamma^2 \hat{I}}{\omega} \left(\frac{1}{2\pi \epsilon_0} \ln \left(\frac{\sqrt{(y+h)^2 + x^2}}{\sqrt{(y-h)^2 + x^2}} \right) \right)\end{aligned}\quad (D.1.36)$$

Consider next, the term

$$E_{1z}(x, 0, \gamma) - j\omega \mu_0 \left(\int_0^y \hat{H}_x(x, y) dy \right) \quad (D.1.37)$$

This is equal to

$$\begin{aligned}E_{1z}(x, 0, \gamma) &= -\frac{1}{\pi \sigma_2} \int_0^\infty \left((\kappa^2 + j\omega \mu_0 \sigma_2)^{1/2} - \kappa \right) \cos(\kappa x) \exp(-\kappa h) d\kappa \\ &- \frac{j\omega \mu_0 I}{2\pi} \int_0^\infty \exp(-\kappa h) \cos(\kappa x) \cdot \\ &\left(\int_0^y \exp(\kappa y) dy - \frac{(\kappa^2 + j\omega \mu_0 \sigma_2)^{1/2} - \kappa}{(\kappa^2 + j\omega \mu_0 \sigma_2)^{1/2} + \kappa} \int_0^y \exp(-\kappa y) dy \right) d\kappa\end{aligned}$$

$$\begin{aligned}
&= -\frac{1}{\pi\sigma_2} \int_0^\infty \left((\kappa^2 + j\omega\mu_0\sigma_2)^{1/2} - \kappa \right) \cos(\kappa x) \exp(-\kappa h) d\kappa \\
&\quad - \frac{j\omega\mu_0 I}{2\pi} \int_0^\infty \frac{\exp(-\kappa h) \cos(\kappa x)}{\kappa} \\
&\quad \left((\exp(\kappa y) - 1) + \frac{(\kappa^2 + j\omega\mu_0\sigma_2)^{1/2} - \kappa}{(\kappa^2 + j\omega\mu_0\sigma_2)^{1/2} + \kappa} (\exp(-\kappa y) - 1) \right) d\kappa
\end{aligned} \tag{D.1.38}$$

The terms in (D.1.38) that are independent of y can be gathered together as

$$\begin{aligned}
&-\frac{1}{\pi\sigma_2} \int_0^\infty \left((\kappa^2 + j\omega\mu_0\sigma_2)^{1/2} - \kappa \right) \cos(\kappa x) \exp(-\kappa h) d\kappa \\
&\quad + \frac{j\omega\mu_0 I}{2\pi} \int_0^\infty \frac{\exp(-\kappa h) \cos(\kappa x)}{\kappa} \left(1 + \frac{(\kappa^2 + j\omega\mu_0\sigma_2)^{1/2} - \kappa}{(\kappa^2 + j\omega\mu_0\sigma_2)^{1/2} + \kappa} \right) d\kappa \\
&= -\frac{1}{\pi\sigma_2} \int_0^\infty \left((\kappa^2 + j\omega\mu_0\sigma_2)^{1/2} - \kappa \right) \cos(\kappa x) \exp(-\kappa h) d\kappa \\
&\quad + \frac{j\omega\mu_0 I}{\pi} \int_0^\infty \frac{\exp(-\kappa h) \cos(\kappa x)}{(\kappa^2 + j\omega\mu_0\sigma_2)^{1/2} + \kappa} d\kappa \\
&= -\frac{1}{\pi\sigma_2} \int_0^\infty \left((\kappa^2 + j\omega\mu_0\sigma_2)^{1/2} - \kappa \right) \cos(\kappa x) \exp(-\kappa h) d\kappa \\
&\quad + \frac{j\omega\mu_0 I}{\pi} \int_0^\infty \frac{\left((\kappa^2 + j\omega\mu_0\sigma_2)^{1/2} - \kappa \right) \exp(-\kappa h) \cos(\kappa x)}{j\omega\mu_0\sigma_2} d\kappa = 0
\end{aligned} \tag{D.1.39}$$

The remaining terms of (D.1.36) are (aside from the scalar potential term)

$$\begin{aligned}
E_{1z}(x, y, \gamma) &= -\frac{j\omega\mu_0 I}{2\pi} \int_0^\infty \frac{\exp(-\kappa h) \cos(\kappa x)}{\kappa} \\
&\quad \left(\exp(\kappa y) + \frac{(\kappa^2 + j\omega\mu_0\sigma_2)^{1/2} - \kappa}{(\kappa^2 + j\omega\mu_0\sigma_2)^{1/2} + \kappa} \exp(-\kappa y) \right) d\kappa
\end{aligned} \tag{D.1.40}$$

The final term of (D.1.40) can be simplified by multiplying the numerator and denominator by the term $(\kappa^2 + j\omega\mu_0\sigma_2)^{1/2} - \kappa$. This results in

$$\begin{aligned}
E_{1z}(x, y, \gamma) &= -\frac{j\omega\mu_0 I}{2\pi} \int_0^\infty \frac{\exp(-\kappa h) \cos(\kappa x)}{\kappa} (\exp(\kappa y) \\
&\quad + \frac{2\kappa(\kappa - (\kappa^2 + j\omega\mu_0\sigma_2)^{1/2}) + j\omega\mu_0\sigma_2 \exp(-\kappa y)}{j\omega\mu_0\sigma_2}) d\kappa \\
&= -\frac{j\omega\mu_0 I}{2\pi} \int_0^\infty \frac{\cos(\kappa x)}{\kappa} (\exp(\kappa(y-h)) + \exp(-\kappa(y+h))) \\
&\quad + \frac{2\kappa(\kappa - (\kappa^2 + j\omega\mu_0\sigma_2)^{1/2})}{j\omega\mu_0\sigma_2} \exp(-\kappa(y+h)) d\kappa \tag{D.1.41} \\
&= -\frac{j\omega\mu_0 I}{2\pi} \int_0^\infty \frac{\cos(\kappa x)}{\kappa} (\exp(\kappa(y-h)) + \exp(-\kappa(y+h))) d\kappa \\
&\quad + \frac{I}{\pi\sigma_2} \int_0^\infty \cos(\kappa x) (\kappa - (\kappa^2 + j\omega\mu_0\sigma_2)^{1/2}) \exp(-\kappa(y+h)) d\kappa
\end{aligned}$$

The second to last term in (D.1.40) can be simplified by recognizing that

$$\begin{aligned}
&-\frac{j\omega\mu_0 I}{2\pi} \int_0^\infty \frac{\cos(\kappa x)}{\kappa} (\exp(\kappa(y-h)) + \exp(-\kappa(y+h))) d\kappa = \\
&-\frac{j\omega\mu_0 I}{2\pi} \int_0^y \int_0^\infty \cos(\kappa x) (\exp(\kappa(y-h)) + \exp(-\kappa(y+h))) d\kappa = \\
&-\frac{j\omega\mu_0 I}{2\pi} \ln \left(\frac{\sqrt{(y+h)^2 + x^2}}{\sqrt{(y-h)^2 + x^2}} \right)
\end{aligned}$$

Collecting all terms

$$\begin{aligned}
E_{1z}(x, y, \gamma) &= \\
&-\frac{j\omega\mu_0 I}{2\pi} \ln \left(\frac{\sqrt{(y+h)^2 + x^2}}{\sqrt{(y-h)^2 + x^2}} \right) + j \frac{\gamma^2 \hat{I}}{\omega} \left(\frac{1}{2\pi\epsilon_0} \ln \left(\frac{\sqrt{(y+h)^2 + x^2}}{\sqrt{(y-h)^2 + x^2}} \right) \right) \\
&\quad + \frac{I}{\pi\sigma_2} \int_0^\infty \cos(\kappa x) (\kappa - (\kappa^2 + j\omega\mu_0\sigma_2)^{1/2}) \exp(-\kappa(y+h)) d\kappa
\end{aligned}$$

$$\begin{aligned}
&= -\frac{j\hat{I}}{2\pi\omega\epsilon_0}(k_0^2 - \gamma^2) \ln \left(\frac{\sqrt{(y+h)^2 + x^2}}{\sqrt{(y-h)^2 + x^2}} \right) \\
&\quad + \frac{I}{\pi\sigma_2} \int_0^\infty \cos(\kappa x) \left(\kappa - (\kappa^2 + j\omega\mu_0\sigma_2)^{1/2} \right) \exp(-\kappa(y+h)) d\kappa
\end{aligned} \tag{D.1.42}$$

This result is identical to that developed in Chapter 5. To see this, note that (5.4.6) is

$$\begin{aligned}
\hat{\tilde{E}}_z(x-x', y, h, \gamma) &= \tilde{G}_{ez}(x-x', y, h, \gamma) \hat{\tilde{I}}(\gamma) \\
&\cong - \left(\frac{\gamma^2}{Y(x-x', y, h)} + Z(x-x', y, h) \right) \hat{\tilde{I}}(\gamma)
\end{aligned} \tag{D.1.43}$$

where

$$Y(x-x', y, h) = \frac{j2\pi\omega\epsilon_0}{\ln\left(\frac{R'}{R}\right)} \tag{D.1.44}$$

and

$$Z(x-x', y, h) = \frac{j\omega\mu_0}{2\pi} \left[\ln\left(\frac{R'}{R}\right) - J_c(y+h, x-x') \right] \tag{D.1.45}$$

D.2 The Full Carson Series

From Chapter 4, (4.6.7) Carson's integral (for $y' = h$) is given as

$$J_c(y+h, x-x') = \frac{2}{k_2^2} \int_0^\infty (u - \kappa) e^{-(y+h)u} \cos(\kappa(x-x')) d\kappa \tag{D.2.1}$$

where $u = \sqrt{\kappa^2 - k_2^2}$ and $k_2^2 = -j\omega\mu_0\sigma_2$.

Here this will be converted to the form that was originally presented by Carson and Carson's full series given. The first step is to change the integration variable by letting $\kappa = s\sqrt{\omega\mu_0\sigma_2}$ so that

$$\begin{aligned}
J_c &= \\
&= 2j \int_0^\infty \left(\sqrt{s^2 + j} - s \right) e^{-(y+h)\sqrt{\omega\mu_0\sigma_2}s} \cos\left(\sqrt{\omega\mu_0\sigma_2}(x-x')s\right) ds = 2jJ(p, q)
\end{aligned} \tag{D.2.2}$$

where $p = \sqrt{\omega\mu_0\sigma_2}(y+h)$ and $q = \sqrt{\omega\mu_0\sigma_2}(x-x')$. Hence

$$J(p, q) = \int_0^{\infty} \left(\sqrt{s^2 + j} - s \right) e^{-ps} \cos(qs) ds \quad (D.2.3)$$

which is the integral from Carson's equation (29).

Now, (D.2.3) can be evaluated by first evaluating an integral of the form

$$Int = \int_0^{\infty} \sqrt{\mu^2 + \alpha^2} e^{-\beta\mu} d\mu \quad (D.2.4)$$

This can be shown to be equal to

$$Int = \int_0^{\infty} \sqrt{\mu^2 + \alpha^2} e^{-\beta\mu} d\mu = \frac{\alpha}{\beta} (K_1(\alpha\beta) + G(\alpha\beta)) \quad (D.2.5)$$

where $K_1(x)$ is the Modified Bessel function of the second kind and $G(x)$ is the absolutely convergent series

$$G(x) = \frac{x^2}{3} - \frac{x^4}{3^2 \bullet 5} + \frac{x^6}{3^2 \bullet 5^2 \bullet 7} - \dots \quad (D.2.6)$$

Given these results, it is straightforward (though not simple) to develop the series that Carson derived for $J(p, q)$. It is

$$J(p, q) = P + jQ \quad (D.2.7)$$

where

$$P = \frac{\pi}{8}(1-s_4) + \frac{1}{2} \ln\left(\frac{2}{\gamma}\right) s_2 + \frac{1}{2} \theta s_2' - \frac{1}{\sqrt{2}} \sigma_1 + \frac{1}{2} \sigma_2 + \frac{1}{\sqrt{2}} \sigma_3 \quad (D.2.8)$$

and

$$Q = \frac{1}{4} + \frac{1}{2} \ln\left(\frac{2}{\gamma}\right) (1-s_4) - \frac{1}{2} \theta s_4' + \frac{1}{\sqrt{2}} \sigma_1 - \frac{\pi}{8} s_2 + \frac{1}{\sqrt{2}} \sigma_3 - \frac{1}{2} \sigma_4. \quad (D.2.9)$$

Here $r = \sqrt{p^2 + q^2}$, $\theta = \tan^{-1}(q/p)$, $\gamma = 1.7811$, $\ln\left(\frac{2}{\gamma}\right) = 0.11593$, $\ln(\gamma) = 0.57722$ and

$$s_2 = \frac{1}{1!2!} \left(\frac{r}{2}\right)^2 \cos(2\theta) - \frac{1}{3!4!} \left(\frac{r}{2}\right)^6 \cos(6\theta) + \dots \quad (\text{D.2.10})$$

$$s_4 = \frac{1}{2!3!} \left(\frac{r}{2}\right)^4 \cos(4\theta) - \frac{1}{4!5!} \left(\frac{r}{2}\right)^8 \cos(8\theta) + \dots \quad (\text{D.2.11})$$

$$s_4' = \frac{1}{2!3!} \left(\frac{r}{2}\right)^4 \sin(4\theta) - \frac{1}{4!5!} \left(\frac{r}{2}\right)^8 \sin(8\theta) + \dots \quad (\text{D.2.12})$$

$$\sigma_1 = \frac{r \cos(\theta)}{3} - \frac{r^5 \cos(5\theta)}{3^2 5^2 7} + \frac{r^9 \cos(9\theta)}{3^2 5^2 7^2 9^2 11} - \dots \quad (\text{D.2.13})$$

$$\sigma_3 = \frac{r^3 \cos(3\theta)}{3^2 5} - \frac{r^7 \cos(7\theta)}{3^2 5^2 7^2 9} + \frac{r^{11} \cos(11\theta)}{3^2 5^2 7^2 9^2 11^2 13} - \dots \quad (\text{D.2.14})$$

$$\sigma_2 = \left(1 + \frac{1}{2} - \frac{1}{4}\right) \frac{1}{1!2!} \left(\frac{r}{2}\right)^2 \cos(2\theta) \quad (\text{D.2.15})$$

$$- \left(1 + \frac{1}{2} + \frac{1}{3} + \frac{1}{4} - \frac{1}{8}\right) \frac{1}{3!4!} \left(\frac{r}{2}\right)^6 \cos(6\theta) + \dots \cong \frac{5}{4} s_2$$

$$\sigma_4 = \left(1 + \frac{1}{2} + \frac{1}{3} - \frac{1}{6}\right) \frac{1}{2!3!} \left(\frac{r}{2}\right)^4 \cos(4\theta) \quad (\text{D.2.16})$$

$$- \left(1 + \frac{1}{2} + \frac{1}{3} + \frac{1}{4} + \frac{1}{5} - \frac{1}{10}\right) \frac{1}{4!5!} \left(\frac{r}{2}\right)^8 \cos(8\theta) + \dots \cong \frac{5}{3} s_4$$

Index

- analytic functions 394
- antenna, dipole 9
- auroral electrojet 320
- boundary conditions 130
- branch cut 398
- branch point 398
- capacitance
 - effect of 22
 - per unit length 244
- capacitors, series 76
- Carson
 - approximations 181
 - integral 187, 404
 - series 187, 415
- Cauchy-Reimann equations 395
- characteristic impedance 192
- circuit breakers 79
- common mode 297
- conductor
 - bundle 62, 376
 - characteristics 185
 - heating 49
 - AAC 60
 - ASCR 61
 - sag 68
- constitutive relationships 126
- corona 48
- current continuity 38
- current, hidden paths 37
- differentiability 392
- differential mode 297
- distribution 59
- distribution underbuild 84
- double circuit 64
- earth, not equipotential 38
- earthquakes 90
- electric field
 - conductor bundle 102
 - terrain/vegetation 101
 - thin wire, axial 162
 - towers 103
 - single wire 219
- electromagnetic compatibility
 - optical fiber 81
 - pipeline 80
 - railroad 81
 - wireless communication 82
- electromagnetic potentials 137
- electrostatics
 - images 257
 - justification 246
 - simple shapes 253
 - theory 250
- exact solution, thin wire 175
- fault current excitation 329
- fire 89
- flashover, vegetation 71
- frequency, power system 15
- geomagnetic induced currents 89, 319
- gold standard 92
- grading ring 47
- grading ring 67
- grounding 37
 - tower 75
- hardware, environmental control 75
- high phase order transmission 51
- high voltage DC 50
- human occupancy 84
- ice 86
- image, complex
- inductance 21
 - effect of 21
 - per unit length 244
- insulator 47
 - contamination 68
 - post 67

suspension	67	impedance matrix	352
integral equation, single wire	157	admittance matrix	353
landslides	90	shunt reactor	78
lightning	87	single wire above earth	154
coupling from distant	315	arbitrary frequency	222
direct coupled	329	fields in earth	242
line compensation	197	low frequency	228
lumped circuit approximation	104	skin effect	386
magnetic field		snow	86
conductor sag	102	solution validity	100
single wire	219	spacer hardware	63
magnetic storm	320	spatially growing currents	337
marker ball	74	spherical shell	260
materials		splice	73
conducting	126	surge arresters	77, 205
dielectric	126	surge impedance	192
Maxwell's Equations	121	suspension clamp	67, 73
modal attenuation	342	symmetrical components	360
modal equation, thin wire	175	Tesla, Nikola	9
modal speeds	342	Thevenin equivalent	42
numerical solutions		thin wire	
boundary element method	274	approximation	158
charge simulation method	276	boundary condition	159
finite difference method	278	three phase	43
finite element method	282	tower	
Monte Carlo method	280	heavy angle	65
phase, leading vs. lagging	21	wood pole	65
phasor	16	transformer saturation	327
physical approximations	93,	transformers	79
97		transmission line	15
power factor	28	voltage	16
power flow	28	equivalent	190
power, complex	25	equivalent symmetric	364
Poynting's theorem	131	losses	17
rain	86	multiconductor, low frequency	
reactive power	26	349	
reciprocity		symmetric vs. actual	370
electromagnetic	142	finite length	193
electrostatic	147	short	195
residue theory	401	unbalanced	344
ring surrounding conductor	262	transposition	70
round wire impedance	386	transposition	360
rules of thumb	106	two wires above earth	293
separation of variables	270	arbitrary frequency	294
shield wires	64	closely spaced	309

low frequency	299	
uniqueness theorem	133	
unsymmetrical terminations	311	
vibration damper	67	
volcanoes	90	
voltage regulation	199	
voltages to earth	191	
wave equation	129	
wind	88	
windblown material	90	
wireless power transmission	9,	
	383	
wires, excitation of	11	